Palladium Catalyzed C–O Bond Activation

by

Gregory Gaube

B.Sc., Simon Fraser University, 2014

M.Sc., Université de Lille 1 and Universität Leipzig, 2019

A Dissertation Submitted for Fulfillment of the Requirements for the Degree of

DOCTOR OF PHILOSOPHY in the Department of Chemistry

Supervisory Committee

Palladium Catalyzed C–O Bond Activation

by

Gregory Gaube

B.Sc., Simon Fraser University, 2014

M.Sc., Université de Lille 1, 2019; M.Sc., Universität Leipzig, 2019

Supervisory Committee
Dr. David C. Leitch, Supervisor

Department of Chemistry

Dr. J. Scott Mclndoe, Departmental Member

Department of Chemistry

Dr. Heather L. Buckley, Departmental Member

Department of Chemistry

Dr. Jay T. Cullen, Outside Member

Department of Earth and Ocean Sciences

Dr. Timothy P. Brewster, External Examiner

Department of Chemistry, University of Memphis

Abstract

Carboxylate C–O bonds are atom-economical, robust in synthesis, and easily accessible, but have traditionally been ineffective synthetic handles for Pd catalysis. In this thesis the utility of these cross-coupling handles in Pd catalysis has been established. As global climate issues necessitate an alternative to oil-based processes, the development of Pd-catalyzed C–O bond activation chemistry, such as the chemistry explored in this thesis, has the potential to aid in biomass becoming a common future feedstock.

This thesis is divided into three research chapters. Firstly, we evaluated the mechanism of an air-stable, base-free, Pd-catalyzed cross coupling of enol carboxylates and aryl boronic acids that was first developed within the Leitch Lab. This experimental evaluation uncovered key intermediates that allowed us to propose a cationic Pd(II)-only mechanism. Secondly, the knowledge gained in evaluating the mechanism was applied to Miyaura borylation of various enol carboxylates. In this study we uncovered that the nature of the enol carboxylate and the boron source greatly impacted the reactivity in the initial synthesis as well as any future desired reactivity of the enol boronate. Finally, by identifying active pharmaceutical ingredients, specifically pyrido[1,2-a]pyrimidin-4-ones, that could be used in future C–O activation chemistry, we systematically approached their synthesis to create and characterize a library of substituted molecules. We demonstrated that we could functionalize these molecules with both pivalate and tosylate synthetic handles. Because the fundamental reactivity of these carboxylate C–O bonds is established, these three chapters have created myriad potential research projects that are discussed in Chapter 5.

Table of Contents

Table of Contents

Additional Information

When possible, the colours used in this thesis follow the IBM Design Library's colourblind palette.

List of Figures

List of Tables

List of Abbreviations

AAA	Asymmetric allylic alkylation
Ac	Acetate group
API	Active pharmaceutical ingredient
Ar	Aryl group
BDE	Bond dissociation energy
Bn	Benzyl group
BTCM	Bis(2,4,6-trichlorophenyl) malonate
CHPin	Cyclohexylpinacol
CID	Collision induced dissociation
CPME	Cyclopentyl methyl ether
CPPin	Cyclopentylpinacol
Cy	Cyclohexane group
DAB	Diaryldiazabutadiene
DBN	1,5-diazabicyclo[4.3.0]non-5-ene
DBU	1,8-diazabicyclo(5.4.0)undec-7-ene
DCID	Dichloroimidazolidinedione
DCM	Dichloromethane
DEM	Diethyl malonate
DFT	Density functional theory
DIPEA	N,N-diisopropylethylamine

DMAP 4-Dimethylaminopyridine

DMP Dimethylphenyl group

DMSO Dimethyl sulfoxide

dppp 1,3-bis(diphenylphosphino)propane

EArS Electrophilic aromatic substitution

EPin Ethylpinacol

ESI Electrospray ionization

Equiv Equivalent

FDA United States Food and Drug agency

GC Gas chromatography

HMBC Heteronuclear multiple bond correlation

HPLC High performance liquid chromatography

HRMS High-resolution mass spectrometry

HTE High-throughput experimentation

IR Infrared

KIE Kinetic isotope effect

MAH Maelic anhydride

MS Mass spectrometry

MW Microwave

NHC *N*-heterocyclic carbene

NMR Nuclear magnetic resonance

OAC Oxidative addition complex

OAc Acetoxy group

OPiv	Pivaloyloxy group
OTf	Triflate group
Ph	Phenyl group
Pin	Pinacol
Piv	Pivaloyl group
pK_a	acid dissociation constant
PPD	pyrido[1,2-α]pyramid-4-one
PPin	Propylpinacol
PSI	Pressurized sample injection
rt	Room temperature
S_NAr	Nucleophilic aromatic substitution
TFA	Trifluoroacetate
THF	Tetrahydrofuran
TMB	Trimethylboroxine
TON	Turnover number
t-Bu	*Tert*-butyl
UPLC	Ultra-high performance liquid chromatography
v/v	volume to volume ratio
VT	Variable temperature

Acknowledgements

I must begin with my supervisor and mentor Dr. David Leitch. Thank you for your guidance and support through these past five years. It has been a pleasure to be there for the beginning of what will undoubtably be an incredible independent career.

Dr. Scott McIndoe and Dr. Violeta Iosub, thank you both for supporting me throughout this time. Your help in navigating academia has been essential to my growth here at UVic. Dr. Tyler Trefz and Christopher Barr, I don't know what I would've done without you two, you both have made coming to work a pleasure and enabled much of the work within this thesis.

To the Leitch Group members, it's been enjoyable to work and learn alongside you. Thank you, Nahia, for being ever-present throughout my time here at UVic. Working together with you has been incredibly rewarding as we created something very special with our Strong-bond subgroup. To the undergrads I've had the pleasure of mentoring in that subgroup, if there's something I'm most proud of during my time here it's seeing you all develop into great scientists and even better people. Doug, Rowan, James, Sarah, Odhran, and Nelson, I can't wait to see what you all decide to do in this life. Lastly, thanks to Kushal for all the football chats, it was always welcome to have a non-chemistry conversation.

To the friends from past-lives to the friends I've made here, thank you for making this ride as enjoyable as possible. To the new friends here at UVic, we ruffled some feathers, but I think we made many long-lasting impacts both within the department and within the GSS.

Gilian, you came into my life when Ph.D. motivation was starting to wane, thank you for kicking my life into gear and reminding me that the mediocrity that surrounds us isn't the objective. You've been an essential support academically and personally throughout this time and I'm incredibly thankful for that. I'm excited to see where this life takes us.

Lastly, to my family. Thank you for your continued help throughout this time. I'm glad I was able to come back home. Whether it was river floats, concerts, or birthdays, it was great to be back. Mum and Dad, thanks for making all the sacrifices over the years for me to be able to pursue academia. Without your omnipresent support I wouldn't have made it this far.

It seems that the more places I see and experience, the bigger I realize the world to be. The more I become aware of, the more I realize how relatively little I know of it, how many places I have still to go, how much more there is to learn.

-Anthony Bourdain

Chapter 1: Introduction

1.1: Pd-Catalyzed Cross-Coupling Chemistry

1.1.1 History of Cross-coupling

Cross-coupling, the chemistry of covalently joining two distinct molecular entities through a reaction involving their respective synthetic handles,[1] can be seen throughout the chemical literature today. Although often thought of as transition metal-catalyzed,[2] these reactions can also be organo-catalyzed,[3,4] photo-redox catalyzed,[5,6] or even stoichiometrically metal mediated.[7,8] While all cross-coupling has utility, this thesis will focus on group 10 transition metal-catalyzed cross-coupling reactions.

Transition metal-catalyzed cross-coupling are generally thought of as the metal-catalyzed reactions of carbon-based nucleophiles and organo(pseudo-)halide electrophiles to form carbon-carbon and carbon-heteroatom bonds. Originating in the 1970's with seminal work from Kochi who reported the use of iron salts facilitating the combination of Grignard reagents and alkenyl halides.[9,10] This work was inspired by observations from the 1940's where first-row transition metal salts act as catalysts for homocoupling of Grignard reagents in the presence of aryl or alkyl halides.[11] Despite the small progression in those 30 years, the field of cross-coupling would soon balloon to be the considered one of the most important synthetic chemistry methods, being utilized in industrial quantities for production of pharmaceuticals,[12] agrochemicals,[13] and organic materials manufacturing.[14] While many metals have facilitated these reactions,[15–18] palladium (Pd), located in group 10 on the periodic table, quickly rose to prominence as the ease of use and high productivity surpassed other studied metals.[2] This is principally due to the well-behaved

two-electron organometallic reactivity of Pd that enables catalytic reaction mechanisms.[19] Pd is also reluctant to engage in radical one-electron processes which often complicate reliability and mechanism elucidation. The proliferation of these Pd-catalyzed reactions resulted in the just awarding of the Nobel prize to Richard Heck, Ei-ichi Negishi, and Akira Suzuki in 2010.[20]

Pd has become the catalysis workhorse of industrial chemistry. Although there has been considerable effort to divert production to more earth-abundant metals such as nickel,[21–23] iron,[24–26] cobalt,[27,28] and copper,[29–31] Pd continues to dominate the industrial and academic catalyst landscape as it continues to be ubiquitous in number of reactions. These include the Suzuki-Miyaura reaction,[32] Mizoroki-Heck reaction,[33,34] Sonogashira coupling,[35] Buchwald-Hartwig amination,[36–38] Miyaura borylation reaction,[39] Stille coupling,[40,41] Negishi coupling,[42] Kumada coupling,[43,44] Hiyama coupling,[45] and Murahashi coupling (Figure 1.1).[46] These cross-coupling reactions are defined by the synthetic handle they utilize to react with a suitable organo(pseudo-)halide reactant. For instance, the Suzuki reaction is when an organo(pseudo-)halide reacts with a boronic acid or ester to form a new carbon-carbon bond. Since Suzuki and Miyaura's discovery of this reaction in 1981, the reaction has become (as of 2014) the second most utilized reaction in medicinal chemistry as it can reliably add pre-functionalized aryl groups to a number of organo(pseudo-)halides.[47] This reliability has influenced molecular design, as the ease of use has prompted the addition of aryl groups to be used for convergent reaction design for a number of molecules.[48] Diversification of coupling partners is now being addressed by a number of groups as molecular designers create cross-coupling reactions for bioisosteres such as bicyclo-containing fragments.[49–51]

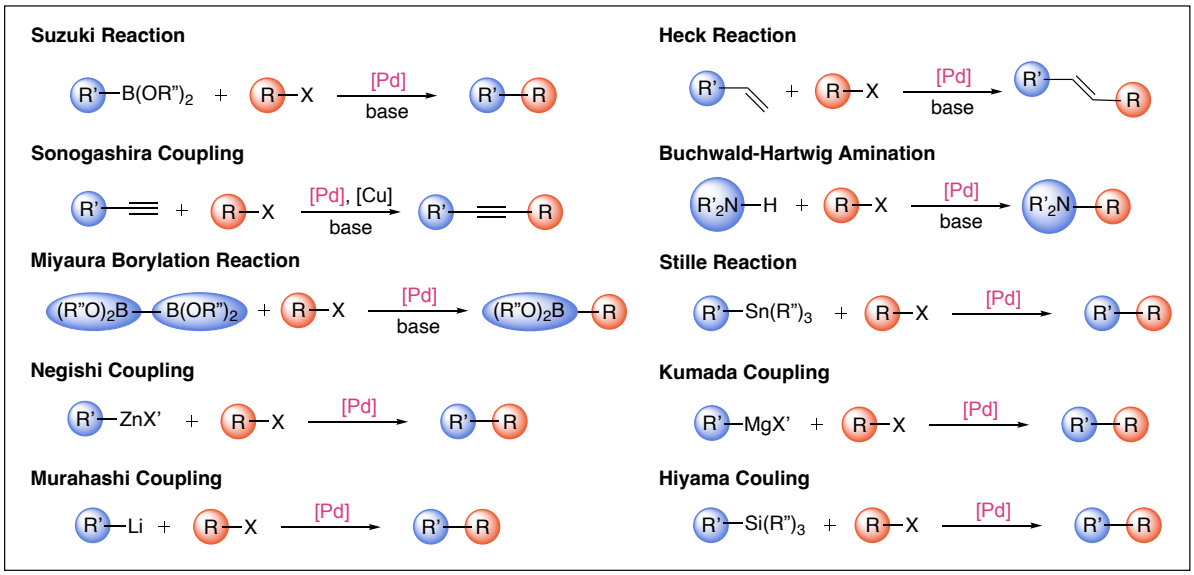

Figure 1.1: Common Pd-catalyzed cross-coupling reactions

1.1.2 Mechanisms of Pd-Catalyzed Cross-Coupling Reactions

Mechanisms of Pd-catalyzed cross-coupling reactions have been studied extensively throughout the literature.[52–57] Generally, once the precatalyst is initiated through an activation step, these catalytic reactions proceed through three fundamental organometallic steps: oxidative addition, transmetalation, and reductive elimination in a Pd(0)/Pd(II) catalytic cycle (Figure 1.2). The electrophile oxidatively adds to the unsaturated Pd(0) catalyst, followed by the nucleophile transmetalating, and finally reductively eliminating the product and regenerating the unsaturated Pd(0) catalyst.

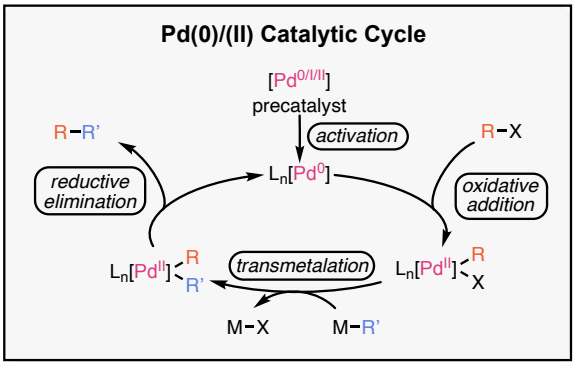

Figure 1.2: Common Pd(0)/(II) Catalytic Cycle involving oxidative addition, transmetalation, and reductive elimination

Oxidative addition plays a central role in many catalytic reactions.[58] Generally, the step involves the binding of two previously connected substituents to a metal complex, where the metal complex has a relatively low oxidation state.[59,60] The resulting complex has an oxidation state two units higher than before, the metal complex coordination number increases by two, and the metal's electron count increases by two. The electron count may increase by 0 or 1 while still being considered an oxidative addition.[61] Therefore, oxidative additions are favoured by metals that are coordinatively unsaturated and have a low oxidation state. A common example from introductory organic chemistry is the formation of Grignard reagents.[60] Mg(0) oxidatively adds to the aryl halide to create a Mg(II) centre connected to both an aryl group and the respective halide. Similarly, Pd(0) precursors often oxidatively add to aryl halides forming Pd(II) complexes in catalytic cycles. While a logical starting point for oxidative addition affinity is the bond dissociation enthalpy (BDE) of the respective carbon-(pseudo-)halogen bond,[62,63] the acid dissociation constant (pK_a) of the (pseudo-)halide partners have been found to be an equal contributor to the substrate's affinity for oxidative addition.[64,65] The lower pK_a alludes to a more stable conjugate, which can more effectively stabilize partial negative charge during the oxidative

addition. Both the ability of the metal centre and the affinity of the respective substrate can be tuned to increase or decrease the rate of oxidative addition. While oxidative addition and reductive elimination are often seen as equal and opposite processes, another intervening step is required to create a productive catalytic cycle.

Transmetalation is the process where substituents are exchanged between two metal centres.[66,67] Commonly, these reactions are thermodynamically driven as negatively charged ligands tend to prefer electropositive metals and alkyl/aryl groups tend to prefer larger metals.[60] These reactions can involve neutral metals, but a large subset of transmetalations are metathesis reactions, where one of those metals is bonded to a (pseudo-)halide. When these reactions generate a salt, they are called salt metathesis reactions. Transmetalations can proceed through a four-centered transition state,[60] but Denmark and coworkers have put considerable effort into identifying key short-lived intermediates in Suzuki chemistry that proceed through tri- or tetra-substituted boron complexes.[68–70]

Reductive eliminations are the opposite of oxidative addition reactions, where the oxidation state decreases by two units, the metal complex coordination number decreases by two, and the metal's electron count decreases by two.[60,71,72] Due to the principle of microscopic reversibility, the factors that affect reductive elimination are the same as oxidative addition, except now these factors have the opposite effect.

The key to creating a viable catalytic cycle is having a system where oxidative addition and reductive elimination are both viable.[73] If oxidative addition is too favoured, the catalyst may not effectively reductively eliminate, and *vice versa.* Therefore, the goal remains to create

systems that allow the catalytic cycle to effectively turn over through tailoring of the metal centre and substrates involved. Four cross-coupling reactions are of particular importance to this thesis, the Pd-catalyzed Suzuki reaction, oxidative Heck reaction, conjugate addition reaction, and Miyaura borylation reaction (Figure 1.3).

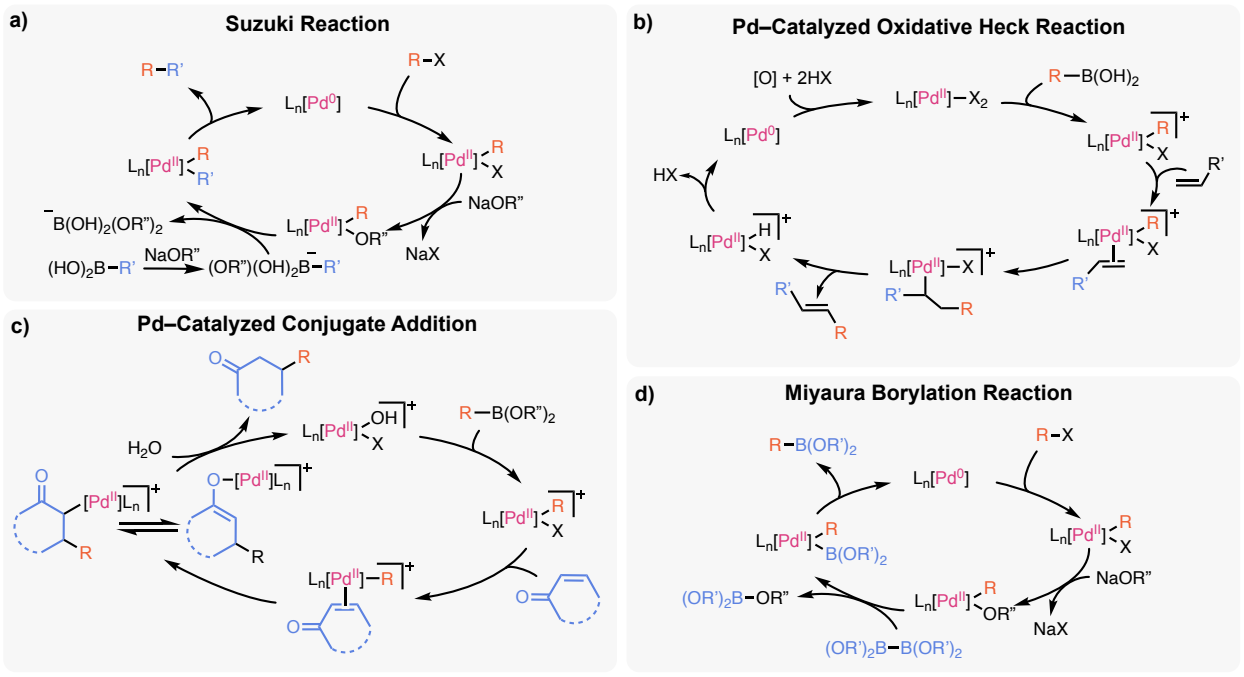

Figure 1.3: Pd-catalyzed cross-coupling mechanisms

The commonly accepted mechanism of the Suzuki reaction involves a Pd(0)/Pd(II) catalytic cycle (Figure 1.3a). Beginning with oxidative addition, a base then mediates a ligand substitution to create a Pd complex able to undergo transmetalation. It is in this transmetalation step where the base-activated boronic acid produces the desired Pd complex as well as a low energy boron-containing byproduct – an energetic driving force to this reaction step. The Pd complex with the two fragments then reductively eliminates to form the product and the starting catalyst. This reaction requires a base to turnover the catalytic cycle, and the necessary base has

also been found to accelerate the reductive elimination through a hydroxide bound Pd intermediate.[74]

The oxidative Heck reaction (Figure 1.3b) begins with a transmetalation of the boron containing species to the neutral Pd(II) centre, before binding the alkene in a migratory insertion.[75] At this point the cationic Pd(II) substrate *beta*-hydride eliminates to form the product and a neutral Pd(II) product. This Pd(II) product then reductively eliminates HX, before an external oxidant regenerates the active Pd(II) catalyst. Oxidants commonly used are silver salts,[76,77] copper salts,[78,79] and dioxygen,[80,81] while many other exist as well.[82–84]

Pd-catalyzed conjugate addition reactions (Figure 1.3c) begin similarly to the oxidative Heck in that they start with a transmetalation of the boron containing species to the Pd centre, but differ in that they utilize a cationic Pd species throughout the reaction. The alkene then performs a migratory insertion that, in this case, may be assisted via substrate association by the carbonyl.[85] The Pd-containing product is then in equilibrium between the C-bound and O-bound tautomer, where the O-bound tautomer can be protonated to form the product and the active on-cycle cationic Pd(II) catalyst.

Miyaura borylation reactions begin with an oxidative addition involving a Pd(0) source (Figure 1.3d). A ligand substitution by the base then creates a Pd(II) intermediate with a ligand that can undergo transmetalation with the diboron source.[86] This step may also involve an associative precomplexation of the diboron species.[87] The low energy boron byproduct formed again helps to drive the reaction forward. Once that boron handle is installed, the Pd reductively eliminates to give the desired product and the active Pd(0) catalyst.

These reactions share many of the same fundamental organometallic steps, while differing in order as well as the charge on the Pd centre with respect to the reactive components. Ultimately, they all achieve the goal of forming new carbon-carbon or carbon-heteroatom bonds through Pd-catalyzed cross-coupling reactions. Many of the seminal publications for these reactions began with investigations of coupling organohalides to other components, but economics, molecular-stability, and green chemistry principles have prompted chemists to search for suitable alternatives that are termed pseudohalides.[88]

1.2 C–O Bond Activation with Pd

1.2.1 Pseudohalides as Efficient, Green, and Economic Alternatives

Pseudohalides, as the name suggests, act in cross-coupling as an alternative to the well-studied halides. Unfortunately, many of these pseudohalides form toxic waste that would be ideal to avoid.[89] Specifically, fluorinated sulfonates, although often seen as a very reactive substitute, are the worst culprits for waste stream toxicity.[90] C–O bond activation has habitually been defined by reactions with triflates, but other groups such as nonaflates, fluorosulfonates, tosylates, and mesylates can also be referred to as pseudohalides.[90] These functional groups have been utilized catalytically with Pd and highlighted by a 2020 review by Zhou and Szostak.[90] Figure 1.4 summarizes the reactivity trends; notably, as of 2020 carboxylate esters were considered as "inert under Pd catalysis." Although the Leitch group had demonstrated oxidative addition of aryl C–O bonds was possible with Pd in 2020,[91] establishing broad reactivity had yet to be achieved and therefore became the subject of this thesis.

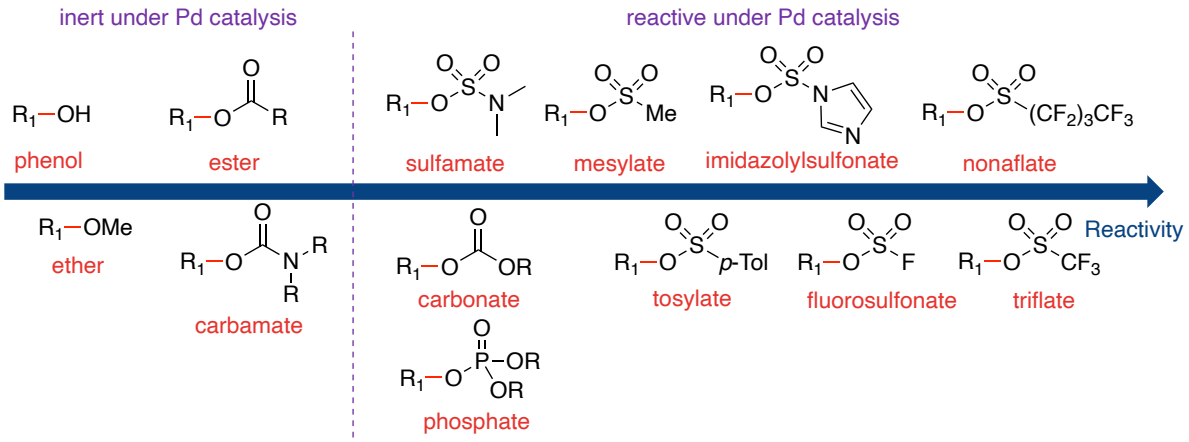

Figure 1.4: Pd reactivity of C–O bond containing pseudohalides, originally published in 2020.

As the world looks to replace petrochemicals, one sector that has been slow to adopt alternatives is the chemical production sector.[92,93] This is mostly due to the abundance of hydrocarbon byproducts that we can oxidize to generate useful feedstocks, which in turn drive synthetic chemistry in both academic and industrial labs. The reverse action of reducing heavily oxygenated compounds like cellulose, hemicellulose, and lignin, which make up the bulk of biomass,[94] remains an ongoing challenge. Activating and functionalizing the strong C–O bonds present in the alcohols, ethers, and esters that are widespread in these components of biomass will ultimately require considerable research.[93] The most commonly investigated catalysts for C–O bond activation are Ni-based,[2,95] although other first-row metals have been used.[96]

One notable C–O activation pathway that is not often discussed within the scope of C–O activation is Tsuji-Trost chemistry.[97,98] This reaction can utilize carboxylate functional groups to react a benzylic or allylic centre with a nucleophile in a cross-coupling reaction.[99,100] This reaction involves a Pd-allyl intermediate that stabilizes the generated charge. In addition, allylic or benzylic C–O bonds are significantly weaker, allowing the reaction to circumvent the large energetic

barrier to unactivated C–O cleavage. While this reactivity has been expanded thoroughly to react in an enantiospecific way, termed Asymmetric Allylic Alkylation (AAA chemistry),[101] this reaction is beyond the scope of this thesis and will not be reviewed.

Alkenyl carboxylates are a compelling subsection of C–O bonds, as they had been thought of as near unreactive in cross-coupling. However, alkenyl carboxylates – acetates and pivalates specifically – are an economic, less toxic, mass efficient source of non-aromatic functionality that can be easily accessible by O-acylation of ketones.[89,90,102] Some reactivity could be justified by the inherent electronic properties of the carboxylate substituent where the handle's carbonyl group would pull electron density away from the desired C–O bond. This can be quantified through the pK_a of the functional group's acid-conjugate which has been recently used as a significant indicator of affinity for oxidative addition,[64,103] and the carboxylate group's acid conjugate has a suitably comparable pK_a to other pseudohalides.

Several research groups have used alkenyl carboxylates in cross-coupling reactions; however, these reaction require sensitive organometallic nucleophiles or bases (Figure 1.5a).[104–107] To get around these procedural drawbacks, other groups began coupling alkenyl carboxylates with boron-based compounds with the aid of a base (Figure 1.5b).[108–110] The Larhed Group – with the help of high temperatures – and later the Leitch Group – at room temperature – explored this further using base-free conditions with palladium (Figure 1.5c).[102,111] The Leitch group had already demonstrated that the oxidative addition of palladium sources into these C–O bonds was possible, and selective.[91]

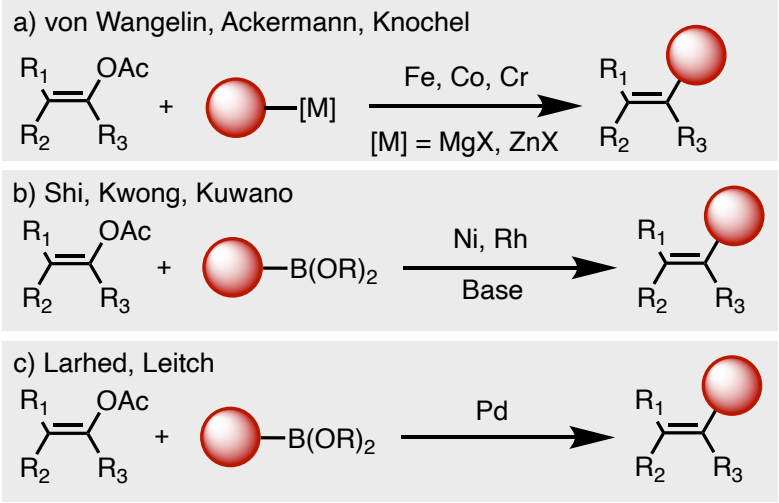

Figure 1.5: Previous methods of activation for carboxylate C–O bonds[102,104–111]

While reactivity with carboxylate synthetic handles was proven previously in the Leitch group, three questions emerged. The first concerned the operative mechanism. This initial cross-coupling was done at room temperature, without the use of a base. One would expect the oxidative addition of these compounds to require elevated temperatures,[91,112,113] and the well documented Suzuki reaction requires the use of a base.[86] The second question was whether this system, or a Pd-catalyzed system generally, could be applied to other types of cross-coupling. This led to our exploration in borylating alkenyl carboxylates and probing their respective stability and reactivity to create alternative series of novel products. The third question was whether a broader scope of electrophiles could be utilized to target current active pharmaceutical ingredients (APIs) through this chemistry.

However, while alkenyl carboxylates are the subject of this thesis, strategies to overcome the aforementioned difficulties can be gleaned from studying Pd-catalyzed C–O activation broadly. As previously mentioned, Zhou and Szostak conducted a thorough review of C–O bond activation with Pd that covers until June of 2020.[90] A brief literature review of Pd C–O activation

from June of 2020 to August of 2024 will therefore be conducted in order to demonstrate the position of this work within the academic literature.

1.2.2 Review of Recent Literature

C–O activation by Pd has been dominated by the use of the triflate functional group despite problems with its stability as well as notable downsides to its atom and fiscal economic costs.[114] Cross-coupling using triflate handles is a well-established field on its own,[115–121] as they have become ubiquitous substitutes for halides as their slight difference in reactivity allows for multi-functionalization of single aromatic rings.[122–124] Phenols or other alcohol derivatives are the natural precursor to these triflates,[125] which could be functionalized by a surplus of procedures to form less toxic, less fluorinated, and more stable cross-coupling handles.[126] The use of these other C–O handles such as phosphates, sulfamates, esters, and ethers in Ni catalyzed reactions is well established,[96,126–131] but these synthetic handles have not seen the immense spotlight in Pd chemistry.[90] This section will expand on the review done by Zhou and Szostak covering all Pd catalyzed C–O activation reactions applicable to this thesis: Suzuki, Heck, Buchwald-Hartwig, Sonogashira, and borylation chemistry for the period of June of 2020 to August of 2024. The review will be formatted by functional group handle (Figure 1.6).

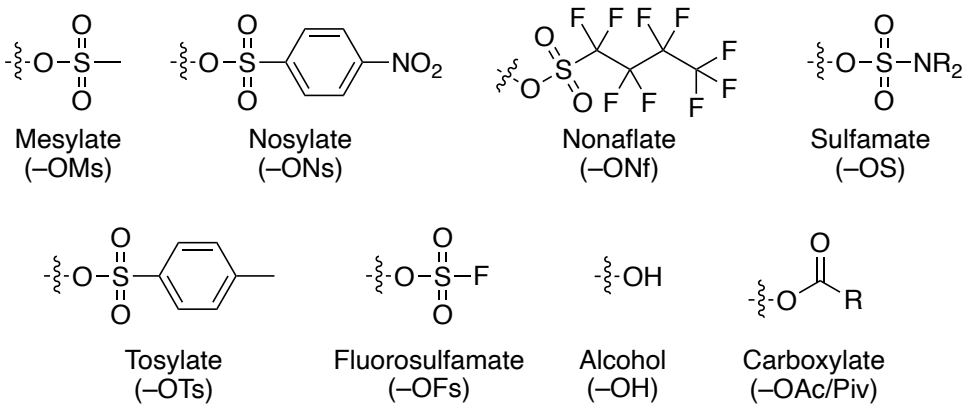

Figure 1.6: Functional groups discussed in this section

The mesylate functional group is an oxysulfone derivative that lacks a halide atom which are a common accompaniment to many of these sulfonate functional groups. This makes the mesylate handle an excellent green alternative, and also makes for a more atom-economic functional group for cross-coupling.[132] The stability this group offers is cited as the main reason for its relatively poor cross-coupling reactivity. They have not seen much utility in Pd catalysis in the previous four years, serving more as a scope example than the primary focus of any report. The Buchwald group has shown, with a single example, the utility of the mesylate handle in forming oxidative addition complexes (OAC) (Figure 1.7a).[133] They then perform a successful ligand exchange on this OAC. Blanc and Pale also demonstrated that an aryl mesylate performs as well as the tosyl, or halide counterparts in a microwave-assisted Suzuki reaction with phenylboronic acid and a single component $PdCl_2(XPhos)_2$ precatalyst (Figure 1.7b).

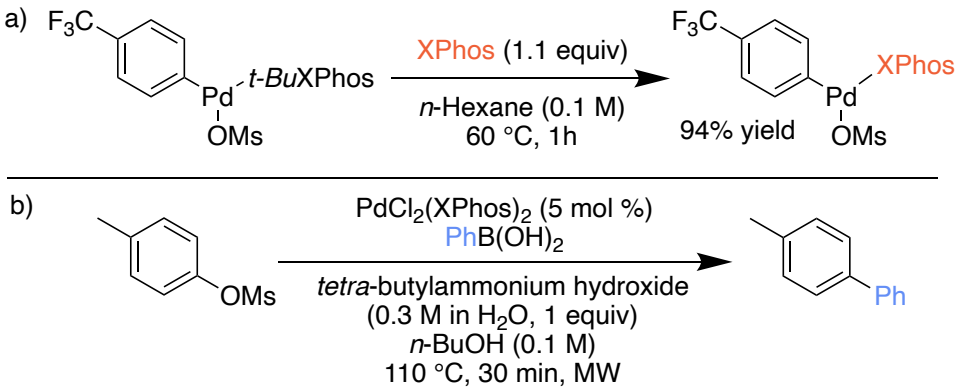

Figure 1.7: a) Ligand exchange reaction on mesylate containing OAC, b) Microwave assisted Suzuki coupling of aryl mesylate and phenylboronic acid.

Nosylates take the idea behind the electron withdrawing functionality of a triflate, and substitute the fluorinated methyl group with a 4-nitrophenyl group. Where this group lacks in atom economy, it benefits from lacking halogens and therefore is seen as a greener alternative that is easy to install.[134] Recently, Idorsia Pharmaceuticals Ltd. explored their use as an aryl Suzuki coupling partner with diethanolamine boronates (Figure 1.8a).[135] This novel coupling utilized a boronic ester functional group that lends itself to improved crystallizations, allowing the authors to circumvent typical isolation issues of boronic esters. This combined with the nosylate functional group which also exhibits a proclivity for crystallinity makes for an ideal combination on the preparatory side of the reaction. The authors functionalize both coupling partners to positive effects and include a robust procedure for capping aryl boronic acids with the diethanolamine handle used in this report. In contrast to the positive results of the Idorsia report, the Domínguez group evaluated four oxysulfone derivatives (tosylate (–OTs), triflate (-OTf), nonaflate (-ONf) and nosylate (-ONs)) for efficacy in a microwave-assisted Suzuki reaction between 4-pyrimidyl sulfonic esters and substituted aryl boronic acids in water (Figure 1.8b).[136] Under these conditions, of the handles evaluated, the nosylate group performed the poorest

across the scope evaluated, although modest yields were still achieved (27 – 74 %). The authors revealed incomplete reactions and homocoupling as the dominant issues of this functional group.

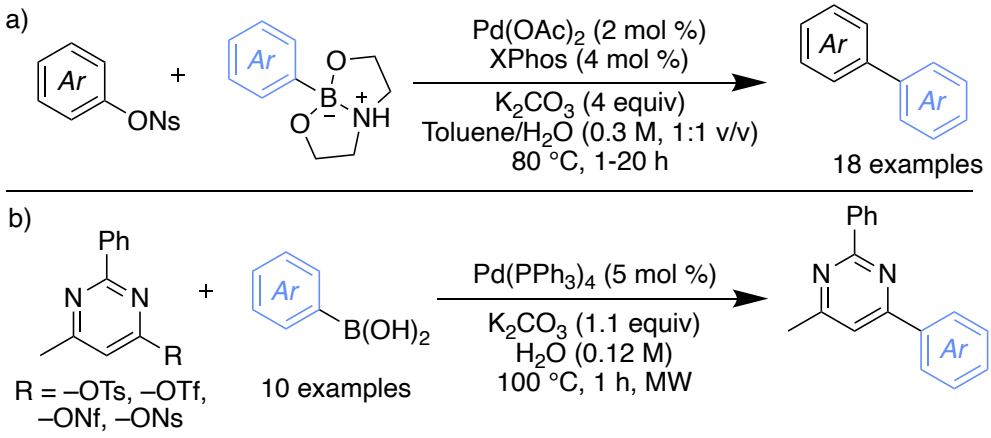

Figure 1.8: a) Novel Suzuki cross-coupling of aryl nosylates and phenyl diethanolamine boronates, b) Comparative reactivity of aryl oxysulfones when reacted in a Suzuki reaction with aryl boronic acids.

Nonaflates also featured in this work from the Domínguez group,[136] where they report that nonaflates performed better than their other oxysulfone counterparts in reactions with electron-poor boronic acids. Nonaflates were originally introduced as a less toxic alternative to other oxysulfone derivatives and also benefited from being column stable, as they are less prone to hydrolysis.[137,138] However, where they succeeded in these tasks, the nine fluorine atoms present in the handle is an excessive use of halogens in a time where many are looking to avoid their use entirely. Recently, the Manabe group has utilized aryl nonaflates as a replacement of aryl halides and aryl triflates in their recent publication detailing a combinatory C–H/C–O activation at the C3 position of indoles.[139]

Sulfamates have been used as directing groups for C–H activation,[140] and have been used sparingly as an effective cross-coupling handle in Pd-catalyzed Suzuki reactions.[141–143] The Arndt group has recently expanded this Suzuki reactivity to include oxazoles (Figure 1.9a).[144] They have

arylated the C5 position effectively with 16 unique aryl boronic acids using both the methyl and ethyl sulfamate derivatives and demonstrated that this is an effective methodology for late stage functionalization. In 2023, the Nicasio group expanded the sulfamate reactivity to Buchwald-Hartwig coupling using their recently reported Pd precatalyst (Figure 1.9b).[145,146] In their report they found that 1:1 (v/v) mixture of *t*-BuOH and H_2O was a necessary polar protic solvent system to achieve high yields. With this procedure they were able to couple aryl sulfamates to anilines, primary alkyl amines, primary amides, secondary amines, heteroaryl amines, and N-heterocycles. Using DFT studies they found the rate-limiting step to be the oxidative addition of the Pd source into the desired C–O bond, reaffirming that this synthetic handle has its limitations.

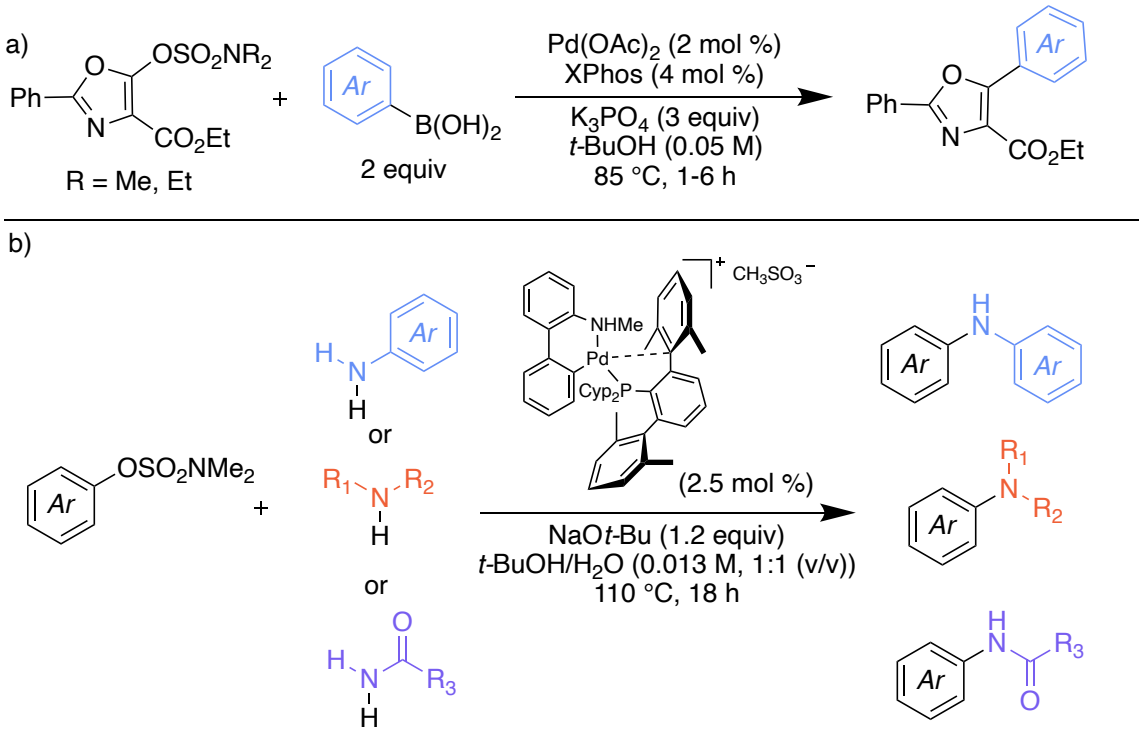

Figure 1.9: Expanded Suzuki reactivity to sulfamate functionalized oxazoles, b) Buchwald-Hartwig coupling of aryl sulfamates and anilines, aliphatic amines, and amides.

The tosylate functional group has been used extensively as a suitable pseudohalide because of its economic viability compared to other oxysulfone derivatives, along with its stability

towards hydrolysis.[147] Recent developments include a Suzuki method published by the Jeon group where 1-(*t*-butyldimethylsilyl)-2,2-difluoroethenyl tosylate or 1-aryl-2,2-difluoroethenyl tosylates, were reacted with substituted arylethenylboronic acids to produce aryl and fluorine substituted dienes.[148] Where work with this handle has expanded considerably in the recent past is with cross-electrophile, either tosylate/tosylate, or tosylate/triflate, coupling reactions facilitated by bimetallic Ni/Pd catalytic systems.[149–151] The Weix group in 2020 published a report detailing a cross-Ullmann coupling reaction where the Pd inserts into the triflate C–O bond and the Ni inserts on the tosylate C–O bond to create two separate catalytic systems connected through a Zn reductant cycle (Figure 1.10).[149] This was followed up in 2022 by Zhang and Lian who expanded the reactivity to include vinyl triflates and tosylates, again with both Ni and Pd with a Zn reductant.[150] Most recently Zhang and Lian have followed their previous work with an aryl/vinyl coupling reaction where in both cases the tosylate functional group is utilized.[151] Combining Pd catalysis with other transition metals that can more easily facilitate oxidative addition with difficult C–O bonds expands the scope of optimization for these reactions and thusly may be an attractive field in the future.

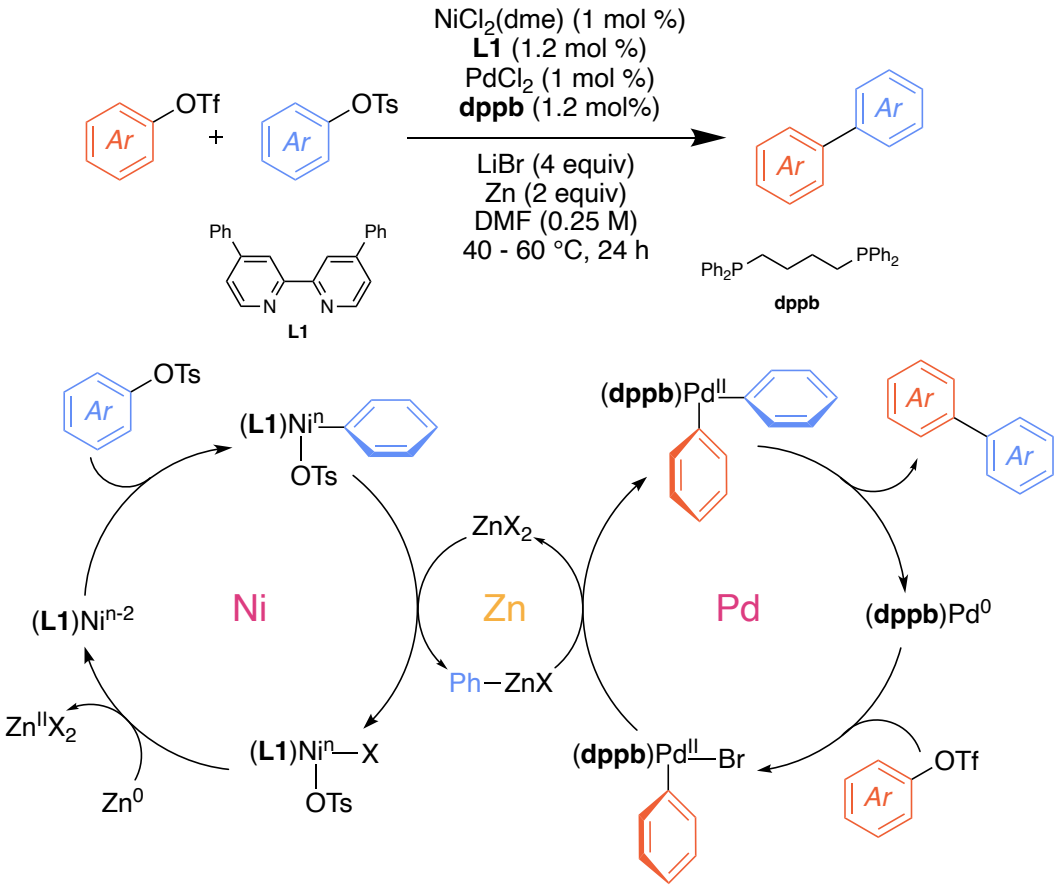

Figure 1.10: Bimetallic Pd/Ni cross-Ullman reaction of Aryl triflates and tosylates, hypothesized mechanism by Weix et al.

Another innovative facet of C–O activation is the incorporation of photochemistry into the field. In early 2024, the Maiti group used blue LEDs in their cross electrophile work.[152] While most of the work focused on halogenated electrophiles, triflates were also featured.

Perhaps the most abundant handle in recent Pd-catalyzed C–O activation literature is the fluorosulfonate. These functional groups have seen meteoric rise as their reactivity has been found to rival that of halides or triflates,[153,154] while being considerably more atom efficient than the triflates. Furthermore, their differing reactivity to the halides allows divergent functionalization. In 2022, the Szostak group developed a method for Suzuki coupling with fluorosulfonates using an *N*-heterocyclic carbene (NHC) Pd precatalyst dimer.[155] With 30

examples, the report details using both substituted aryl fluorosulfonates and substituted aryl boronic acids including gram scale reactions.

The Lipshutz group introduced a biodegradable surfactant synthesized from vitamin E and polysarcosine that they named Savie in 2023 that facilitates catalytic reactions in water.[156] They went on to use this recently to perform an aqueous Buchwald-Hartwig coupling reaction of aryl fluorosulfonates (Figure 1.11a).[157] In addition to 18 examples of substituted starting materials, they functionalized 9 natural products to confirm that this methodology is suitable for late-stage functionalization. Finally, they demonstrated the superiority of the fluorosulfonate handle to that of the triflate, bromine, or chlorine in this reaction.

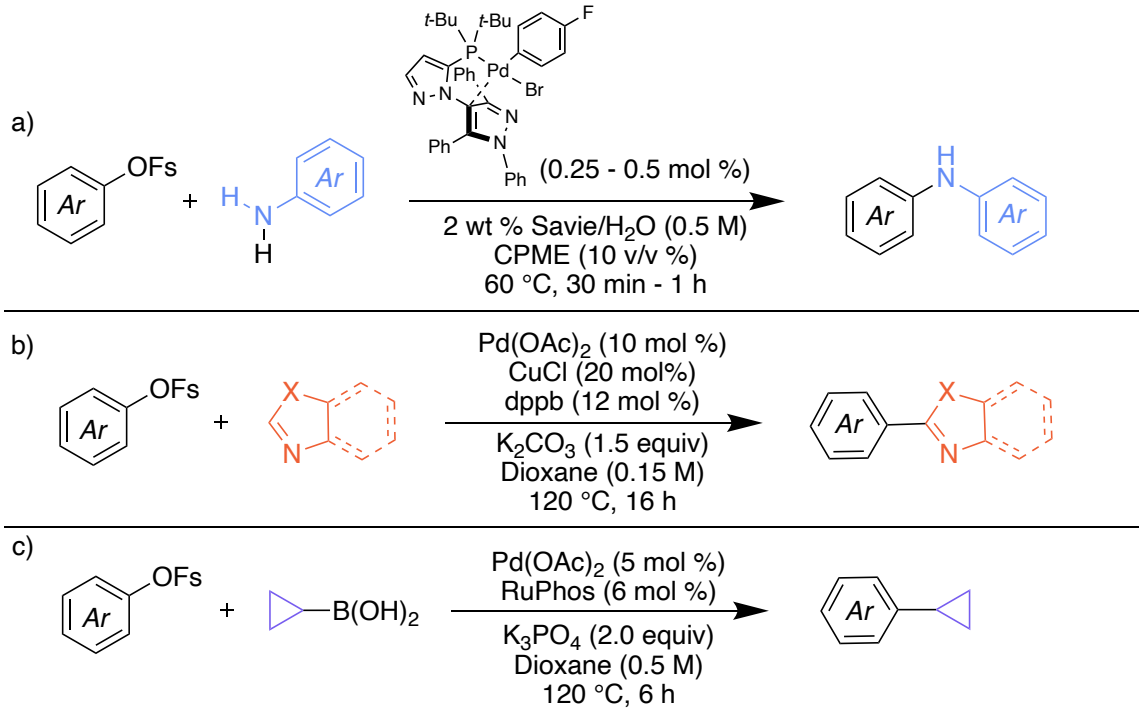

Figure 1.11: a) Buchwald-Hartwig coupling with aryl fluorosulfonates in water, b) Tandem C–O/C–H activation of aryl fluorosulfonates with benzoxazoles and other heterocycles, c) Cyclopropanation of aryl fluorosulfonates

The Ding group published two reports using fluorosulfonates in 2023.[158,159] The first report details a bimetallic Pd/Cu system combining C–O and C–H activation chemistry (Figure 1.11b).[159]

Using benzoxazoles, they optimized a reaction that was also suitable for coupling substituted phenylboronic acids with benzthiazole, benzimidazole, thiazole, and oxazole derivatives. They then applied Suzuki methodology to these aryl fluorosulfonates to develop a cyclopropanation reaction (Figure 1.11c).[158] In this report they detail an *in situ* method where a phenol is functionalized with the fluorosulfonate functional group before cyclopropanation in a one-pot method.

Conducting C–O activation with phenol derivatives has not yet been achieved with Pd. However, researchers are getting around this issue by functionalizing the alcohol group *in situ* and immediately coupling that newly formed group using Pd. The Ding group achieved this using sulfuryl fluoride and trimethylboroxine (TMB) to effectively deoxymethylate phenols (Figure 1.12a).[160] Other methylating agents did not yield product. In addition to a large scope of substituted aryl products, they also demonstrated the late-stage functionalization of this method with 18 natural products. The Yavari group conducted a Heck cross coupling using a similar idea,[161] instead of using a oxysulfone derivative they used dichloroimidazolidinedione (DCID) to create a novel handle for cross-coupling (Figure 1.12b). This handle offers some promise as non-sulfur containing C–O activations still remain rare, unfortunately the handle retains a chlorine atom and is very atom inefficient.

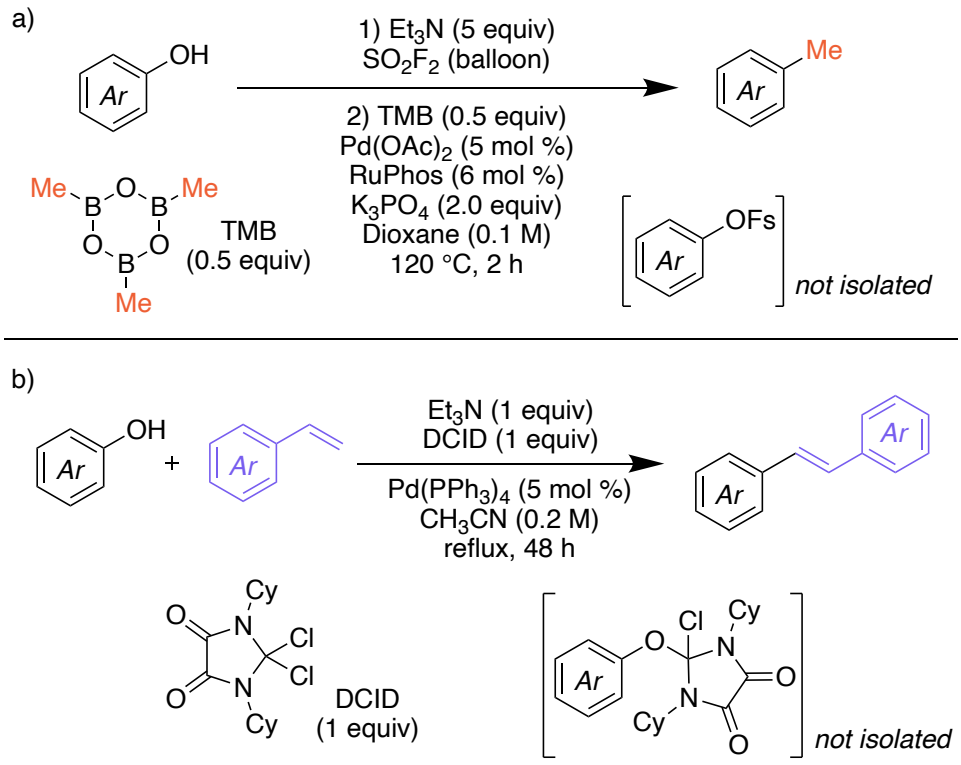

Figure 1.12: a) deoxymethylation of phenols through a fluorosulfonate intermediate, b) Heck coupling of phenols with alkenes through a DCID functionalized intermediate

This review has focused on activating C_{sp2}–O bonds, but another recent interesting methodology has been produced by the Morandi group where C_{sp3}–O alcohol bonds were prefunctionalized by carbodiimide group in order to arylate the benzylic carbon position with phenyl boronic acids.[162] The authors note that this methodology allows for reactions of base-sensitive boronic acids in addition to the already diverse scope.

The unique nature of carboxylate functional groups has been elaborated on in Section 1.2.1. There have been no other groups developing methods on Pd-catalyzed C–O activation of acetylated or pivalated starting materials. However, the Gunnoe group has been developing tandem C–H/C–H activation chemistry with $Cu(OAc)_2$ and/or $Cu(OPiv)_2$ to synthesize styrenes where the carboxylate group is essential to the chemistry. While they developed this chemistry

in 2019, they have gone on to elaborate on the mechanism in 2022,[163] and develop further precatalysts (Pd and Rh) for the reaction in 2023.[164] In their mechanism evaluation they utilize DFT to describe a multi-metal (Pd/Cu) active catalyst bridged through the acetoxy (μ–OAc) groups from the $Cu(OAc)_2$.

Considerable effort has gone into furthering the field of C–O activation chemistry in the past four years. Most of this work has focused on tailoring the oxysulfonate groups to improve atom economy, and to reduce halogenated waste. This review has highlighted that considerable investment into developing these methodologies is yet to be done, and there are multiple pathways forward when looking to develop C–O activation chemistry with Pd.

1.3 Analysis Techniques

1.3.1 Mass Spectrometry

Mass spectrometry (MS) has become essential for understanding numerous facets of chemistry, this is due to the ability of the technique to combine sensitive and accurate results with selective monitoring which can all be applied in a high-throughput manner.[165] Across these fields, MS has been applied to the discovery of new molecules, structural elucidation and reaction monitoring.[166] Electrospray ionization mass spectrometry (ESI-MS) in particular has been used successfully to monitor reactions in both online and offline modes.[167,168] ESI-MS is an ideal technique for monitoring metal-mediated catalytic processes.[169] Combining a soft ionization process with a fast, high sensitivity instrument with a high dynamic range lends itself extremely well to not only monitoring the formation and usage of small organic molecules, but also the heavy catalytic metal centered intermediates that are indispensable for the reaction.

In the offline mode, reactions proceed for a desired period of time and aliquots are taken as necessary.[170–172] These aliquots can be quenched, diluted and/or directly injected into the mass spectrometer. This technique has been used to discover new reaction intermediates for years; as pioneering work with is exemplified by Aliprantis and Canary, who in 1994 discovered previously unknown reaction intermediates in the Suzuki reaction using ESI-MS.[173] Since then, offline monitoring has remained an invaluable tool for discovering reaction intermediates.[174,175]

Reaction intermediates can be so short lived that offline monitoring can be inadequate for detection. Online ESI-MS facilitates the direct injection of the stirring reaction solution into the mass spectrometer.[176,177] Although undoubtedly useful, this methodology still remains less explored than its offline counterpart. Most notably, the McIndoe group at the University of Victoria has popularized using pressurized sample injection (PSI), a modified Schlenk flask that pushes the reaction solutions into the mass spectrometer using an inert gas.[179–181] This has proven extremely effective for the McIndoe group and others for monitoring reaction intermediates of metal catalyzed reactions.[176,177,182–187]

1.3.2 Nuclear Magnetic Resonance

Nuclear magnetic resonance (NMR) spectroscopy is an indispensable tool for the organic chemist. While 1D NMR (^{1}H, ^{13}C, ^{19}F, ^{31}P…) and standard 2D NMR (^{1}H-^{13}C) spectroscopies are ubiquitous throughout the literature, less common 2D experiments can serve an important role, especially in structure elucidation.[188–190] The most common of these 2D experiments is heteronuclear multiple bond correlation (HMBC). Developed in 1986 by Bax and Sommers,[191] these experiments exploit a pulse sequence that allow the user to see a correlation between spin-

active nuclei two, three and sometimes four bonds apart from each other.[192,193] While deciphering between these different bond distances is a hindrance to this method, it is still very useful when trying to establish how complexes have come together. In particular when using ^{1}H-^{31}P HMBC, correlations for phosphine ligands and nearby substituents on the original metal complex can be observed.[91,194]

1.3.2 High–Throughput Experimentation

High-throughput experimentation (HTE) is an invaluable tool to the synthetic chemist. The traditional approach to screening in chemical synthesis is to alter one variable at a time, fixing all other variables, until a desired reactivity is achieved. With this approach, much of the chemical space surrounding a reaction remains unprobed. HTE allows for multiple variables to be altered simultaneously, allowing for rapid development of a reactivity map of the system in question. This will reveal key trends across a large experimental space in a short period of time.

Apart from setting up the reaction arrays, the most time-demanding aspect of HTE is the analysis.[195] High- or ultra-high performance liquid chromatography (HP-LC, UP-LC) is often the preferred method because reliable quantification is achieved with fast analysis times (<3 minutes in most cases). While ^{1}H-NMR would also be suitable for this analysis, the time associated with loading an NMR tube and conducting the analysis (~5min), often makes it more time-intensive compared to HPLC or UPLC.

While commonplace in the industrial setting,[196] the cost associated to setting up a laboratory for these types of experiments have undoubtedly been an impediment.[197] However, modular, user-friendly, and cheaper systems have started being implemented into academic

labs.[198] This has allowed academic labs to behave as mini-industrial labs, leading to numerous academic-industry partnerships.[199] The Leitch Lab at the University of Victoria is now fully equipped to perform extensive HTE experimentation.

1.4 Thesis Objectives

As noted in the previous sections, every aspect in a cross-coupling reaction contributes to the efficiency of the desired transformation. The key to creating effective novel transformations is balancing these factors and critical to this is developing a thorough understanding. As we fixed one variable, the previously thought to be unreactive aryl/alkenyl C–O bond in carboxylates, other factors had to compensate and therefore required attention. Promoting the use of an unconventional functional group for catalysis opens opportunities in numerous fields, but specifically, the development of C–O activation chemistry is garnering attention as the world turns to biomass as a future common feedstock. In this context, the main objective of this thesis is to create a solid foundation as to how C–O activation of carboxylate groups can be understood.

This thesis is divided into three research chapters. Firstly Chapter 2 is a mechanistic evaluation of an air-stable, base-free, Pd-catalyzed cross-coupling reaction that was first developed within the Leitch Lab.[102] This would provide a solid base of understanding to activating C–O bonds of carboxylates. Chapter 3 will apply this mechanistic understanding to developing novel Pd-catalyzed borylation reactions with two boron-pinacol derivatives. In this chapter we exploited the unfortunate stability of the synthesized molecules or canonically reacted a modified version of these synthesized molecules. Lastly in Chapter 4, we have developed a series of

pharmaceutically-relevant molecules that include our studied C–O bond and provided the initial screening of its reactivity.

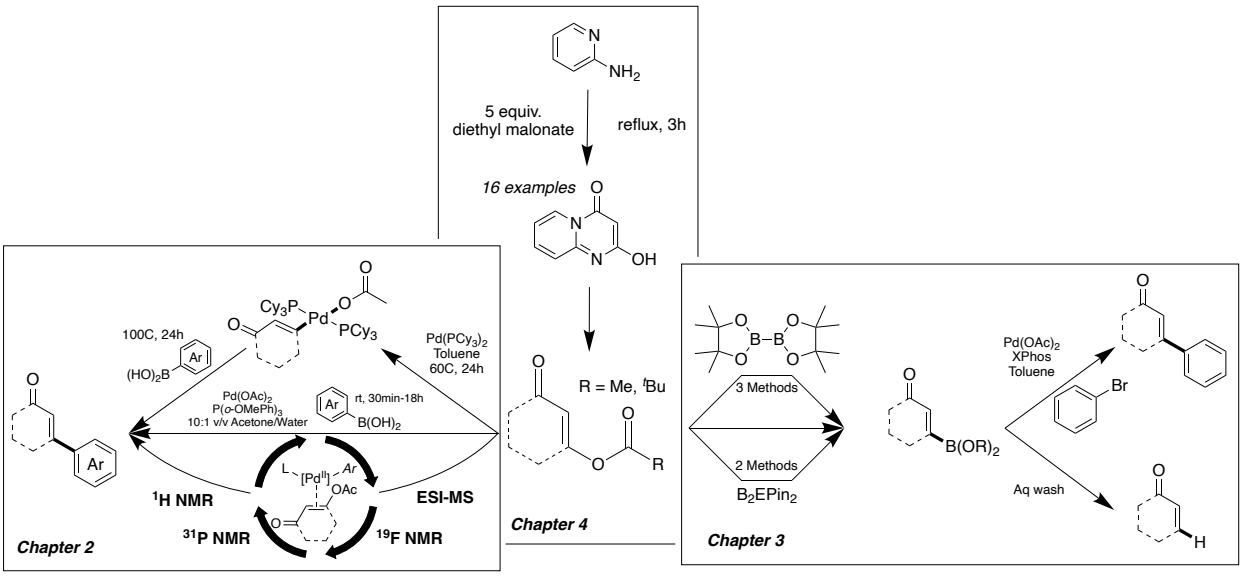

Figure 1.13: Summary of Chapters 2-4. Chapter 2: An experimental evaluation of an open to air, base-free, Pd-catalyzed reaction of enol carboxylates and aryl boronic acids. Chapter 3: Base-Free Palladium-Catalyzed Borylation of Enol Carboxylates and Further Reactivity Toward Deboronation and Cross-Coupling Chapter 4: The development of novel cross-coupling scaffolds for C–O activation chemistry.

As mentioned in Chapter 1.1, traditional Pd-cross-coupling reactions go through a series of fundamental steps, and Suzuki reactions typically react in the order of oxidative addition, salt metathesis, transmetalation, and reductive elimination (Figure 2). However, when looking at the Suzuki-like reaction developed by the Leitch Lab, 1) there was no halide for the salt metathesis, 2) there was no base present to conduct that salt metathesis, 3) the reaction proceeded at temperatures unfavourable to oxidation addition of the strong C–O bond, and 4) the reaction proceeded open to air – uncommon for this type of cross-coupling. Chapter 2 provides the understanding of how this reaction could get around these seemingly evident factors. This chapter provides the comprehension for utilizing these carboxylate groups in other cross-coupling

reactions. Hetereo- and proteo-nuclear NMR experiments allowed us to probe the species created within our reactions as well we monitor product formation with numerous Pd sources. ESI-MS granted us an ability to focus our view even smaller, and probe potential Pd intermediates. Together, these techniques allowed us to propose a mechanism that will educate future catalyst design.

When examining the established mechanism of the Miyaura borylation, comparisons to the Suzuki reaction are easy to ascertain as they both go through the same fundamental four steps (mentioned previously in Chapter 1.1.2). If the salt metathesis step could be avoided in the previous Suzuki-like reactivity with carboxylate functional groups, one could make the hypothesis that the same could occur if Miyaura borylation conditions were applied to the same starting materials. In Chapter 3, experimentally this was found this to be the case. With the help of high-throughput experimentation numerous optimized reaction conditions were established. The generated boronic pinacol ester derivatives proved to have varying levels of stability to base, where the BPin derivatives could be hydrolyzed with weak base to form the unsubstituted product and the BEPin derivatives could be arylated through basic (both in pH and simplicity) Suzuki chemistry. This chapter established that C–O bonds in carboxylates act as an effective handle for Pd-catalyzed borylation.

Recently, an important scaffold within pharmaceutical development has been the pyrido[1,2-α]pyramid-4-one (PPD) motif. In Chapter 4, a robust and solvent-free synthesis of substituted 2-hydroxy-PPDs was explored. This work complemented previous reports that, in our hands, provided inconsistent yields. Our optimized reaction synthesized 16 derivatives with

valuable alternative synthetic handles at four different positions within the structure. Model PPD substrates were then functionalized with carboxylates in preparation for future high-throughput screening for reactivity in Pd-catalyzed arylation.

Together this thesis tackles the development of a synthetic handle in Pd-catalyzed cross-coupling chemistry. From thoroughly studying it mechanistically, to applying this knowledge to develop novel transformations, and finally recognizing that this utility could be applied to react pharmaceutically active molecular fragments, this thesis culminates in Chapter 5 where potential future research will be explored.

1.5 References:

(1) Reimann, C. E.; Kim, K. E.; Rand, A. W.; Moghadam, F. A.; Stoltz, B. M. What Is a Cross-Coupling? An Argument for a Universal Definition. *Tetrahedron* **2023**, *130*, 133176. https://doi.org/10.1016/j.tet.2022.133176.

(2) Campeau, L.-C.; Hazari, N. Cross-Coupling and Related Reactions: Connecting Past Success to the Development of New Reactions for the Future. *Organometallics* **2019**, *38* (1), 3–35. https://doi.org/10.1021/acs.organomet.8b00720.

(3) Oliveira, V. da G.; Cardoso, M. F. do C.; Forezi, L. da S. M. Organocatalysis: A Brief Overview on Its Evolution and Applications. *Catalysts* **2018**, *8* (12), 605. https://doi.org/10.3390/catal8120605.

(4) García Mancheño, O.; Waser, M. Recent Developments and Trends in Asymmetric Organocatalysis. *Eur. J. Org. Chem.* **2023**, *26* (1), e202200950. https://doi.org/10.1002/ejoc.202200950.

(5) Matsui, J. K.; Lang, S. B.; Heitz, D. R.; Molander, G. A. Photoredox-Mediated Routes to Radicals: The Value of Catalytic Radical Generation in Synthetic Methods Development. *ACS Catal.* **2017**, *7* (4), 2563–2575. https://doi.org/10.1021/acscatal.7b00094.

(6) Twilton, J.; Le, C.; Zhang, P.; Shaw, M. H.; Evans, R. W.; MacMillan, D. W. C. The Merger of Transition Metal and Photocatalysis. *Nat. Rev. Chem.* **2017**, *1* (7), 1–19. https://doi.org/10.1038/s41570-017-0052.

(7) Peltzer, R. M.; Gauss, J.; Eisenstein, O.; Cascella, M. The Grignard Reaction – Unraveling a Chemical Puzzle. *J. Am. Chem. Soc.* **2020**, *142* (6), 2984–2994. https://doi.org/10.1021/jacs.9b11829.

(8) Bernoud, E.; Veillard, R.; Alayrac, C.; Gaumont, A.-C. Stoichiometric and Catalytic Synthesis of Alkynylphosphines. *Molecules* **2012**, *17* (12), 14573–14587. https://doi.org/10.3390/molecules171214573.

(9) Neumann, S. M.; Kochi, J. K. Synthesis of Olefins. Cross-Coupling of Alkenyl Halides and Grignard Reagents Catalyzed by Iron Complexes. *J. Org. Chem.* **1975**, *40* (5), 599–606. https://doi.org/10.1021/jo00893a013.

(10) Tamura, M.; Kochi, J. K. Vinylation of Grignard Reagents. Catalysis by Iron. *J. Am. Chem. Soc.* **1971**, *93* (6), 1487–1489. https://doi.org/10.1021/ja00735a030.

(11) Kharasch, M. S.; Reinmuth, O. *Grignard Reactions of Nonmetallic Substances*; Prentice-Hall Inc.: New York, 1954.

(12) Campos, K. R.; Coleman, P. J.; Alvarez, J. C.; Dreher, S. D.; Garbaccio, R. M.; Terrett, N. K.; Tillyer, R. D.; Truppo, M. D.; Parmee, E. R. The Importance of Synthetic Chemistry in the Pharmaceutical Industry. *Science* **2019**, *363* (6424), eaat0805. https://doi.org/10.1126/science.aat0805.

(13) Devendar, P.; Qu, R.-Y.; Kang, W.-M.; He, B.; Yang, G.-F. Palladium-Catalyzed Cross-Coupling Reactions: A Powerful Tool for the Synthesis of Agrochemicals. *J. Agric. Food Chem.* **2018**, *66* (34), 8914–8934. https://doi.org/10.1021/acs.jafc.8b03792.

(14) Barroso, R.; Valencia, R. A.; Cabal, M.-P.; Valdés, C. Pd-Catalyzed Autotandem C–C/C–C Bond-Forming Reactions with Tosylhydrazones: Synthesis of Spirocycles with Extended π-Conjugation. *Org. Lett.* **2014**, *16* (8), 2264–2267. https://doi.org/10.1021/ol500778u.

(15) Mesganaw, T.; Garg, N. K. Ni- and Fe-Catalyzed Cross-Coupling Reactions of Phenol Derivatives. *Org. Process Res. Dev.* **2013**, *17* (1), 29–39. https://doi.org/10.1021/op300236f.
(16) Aleena, M. B.; Philip, R. M.; Anilkumar, G. Advances in Non-Palladium-Catalysed Stille Couplings. *Appl. Organomet. Chem.* **2021**, *35* (12), e6430. https://doi.org/10.1002/aoc.6430.
(17) Zhou, J.; Fu, G. C. Suzuki Cross-Couplings of Unactivated Secondary Alkyl Bromides and Iodides. *J. Am. Chem. Soc.* **2004**, *126* (5), 1340–1341. https://doi.org/10.1021/ja039889k.
(18) Kabir, M. S.; Lorenz, M.; Namjoshi, O. A.; Cook, J. M. First Application of an Efficient and Versatile Ligand for Copper-Catalyzed Cross-Coupling Reactions of Vinyl Halides with N-Heterocycles and Phenols. *Org. Lett.* **2010**, *12* (3), 464–467. https://doi.org/10.1021/ol9026446.
(19) Gildner, P. G.; Colacot, T. J. Reactions of the 21st Century: Two Decades of Innovative Catalyst Design for Palladium-Catalyzed Cross-Couplings. *Organometallics* **2015**, *34* (23), 5497–5508. https://doi.org/10.1021/acs.organomet.5b00567.
(20) Johansson Seechurn, C. C. C.; Kitching, M. O.; Colacot, T. J.; Snieckus, V. Palladium-Catalyzed Cross-Coupling: A Historical Contextual Perspective to the 2010 Nobel Prize. *Angew. Chem. Int. Ed.* **2012**, *51* (21), 5062–5085. https://doi.org/10.1002/anie.201107017.
(21) Jose, J.; Diana, E. J.; Kanchana, U. S.; Mathew, T. V. Recent Advances in the Nickel-Catalysed Electrochemical Coupling Reactions with a Focus on the Type of Bond Formed. *Asian J. Org. Chem.* **2023**, *12* (2), e202200593. https://doi.org/10.1002/ajoc.202200593.
(22) Diccianni, J. B.; Diao, T. Mechanisms of Nickel-Catalyzed Cross-Coupling Reactions. *Trends Chem.* **2019**, *1* (9), 830–844. https://doi.org/10.1016/j.trechm.2019.08.004.
(23) Dawson, G. A.; Spielvogel, E. H.; Diao, T. Nickel-Catalyzed Radical Mechanisms: Informing Cross-Coupling for Synthesizing Non-Canonical Biomolecules. *Acc. Chem. Res.* **2023**, *56* (24), 3640–3653. https://doi.org/10.1021/acs.accounts.3c00588.
(24) Zhang, J.; Wang, S.; Zhang, Y.; Feng, Z. Iron-Catalyzed Cross-Coupling Reactions for the Construction of Carbon-Heteroatom Bonds. *Asian J. Org. Chem.* **2020**, *9* (10), 1519–1531. https://doi.org/10.1002/ajoc.202000334.
(25) Neidig, M. L.; Carpenter, S. H.; Curran, D. J.; DeMuth, J. C.; Fleischauer, V. E.; Iannuzzi, T. E.; Neate, P. G. N.; Sears, J. D.; Wolford, N. J. Development and Evolution of Mechanistic Understanding in Iron-Catalyzed Cross-Coupling. *Acc. Chem. Res.* **2019**, *52* (1), 140–150. https://doi.org/10.1021/acs.accounts.8b00519.
(26) Chen, P.; Chen, H.-N.; Wong, H. N. C.; Peng, X.-S. Recent Advances in Iron-Catalysed Coupling Reactions for the Construction of the C(Sp^2)–C(Sp^2) Bond. *Org. Biomol. Chem.* **2023**, *21* (30), 6083–6095. https://doi.org/10.1039/D3OB00824J.
(27) Gosmini, C.; Bégouin, J.-M.; Moncomble, A. Cobalt-Catalyzed Cross-Coupling Reactions. *Chem. Commun.* **2008**, No. 28, 3221–3233. https://doi.org/10.1039/B805142A.
(28) Cahiez, G.; Moyeux, A. Cobalt-Catalyzed Cross-Coupling Reactions. *Chem. Rev.* **2010**, *110* (3), 1435–1462. https://doi.org/10.1021/cr9000786.
(29) Evano, G.; Theunissen, C.; Pradal, A. Impact of Copper-Catalyzed Cross-Coupling Reactions in Natural Product Synthesis: The Emergence of New Retrosynthetic Paradigms. *Nat. Prod. Rep.* **2013**, *30* (12), 1467–1489. https://doi.org/10.1039/C3NP70071B.

(30) Thapa, S.; Shrestha, B.; Gurung, S. K.; Giri, R. Copper-Catalysed Cross-Coupling: An Untapped Potential. *Org. Biomol. Chem.* **2015**, *13* (17), 4816–4827. https://doi.org/10.1039/C5OB00200A.
(31) Beletskaya, I. P.; Cheprakov, A. V. Copper in Cross-Coupling Reactions: The Post-Ullmann Chemistry. *Coord. Chem. Rev.* **2004**, *248* (21), 2337–2364. https://doi.org/10.1016/j.ccr.2004.09.014.
(32) Miyaura, N.; Yamada, K.; Suzuki, A. A New Stereospecific Cross-Coupling by the Palladium-Catalyzed Reaction of 1-Alkenylboranes with 1-Alkenyl or 1-Alkynyl Halides. *Tetrahedron Lett.* **1979**, *20* (36), 3437–3440. https://doi.org/10.1016/S0040-4039(01)95429-2.
(33) Mizoroki, T.; Mori, K.; Ozaki, A. Arylation of Olefin with Aryl Iodide Catalyzed by Palladium. *Bull. Chem. Soc. Jpn.* **1971**, *44* (2), 581. https://doi.org/10.1246/bcsj.44.581.
(34) Heck, R. F.; Nolley, J. P. Palladium-Catalyzed Vinylic Hydrogen Substitution Reactions with Aryl, Benzyl, and Styryl Halides. *J. Org. Chem.* **1972**, *37* (14), 2320–2322. https://doi.org/10.1021/jo00979a024.
(35) Sonogashira, K.; Tohda, Y.; Hagihara, N. A Convenient Synthesis of Acetylenes: Catalytic Substitutions of Acetylenic Hydrogen with Bromoalkenes, Iodoarenes and Bromopyridines. *Tetrahedron Lett.* **1975**, *16* (50), 4467–4470.
(36) Kosugi, M.; Kameyama, M.; Migita, T. PALLADIUM-CATALYZED AROMATIC AMINATION OF ARYL BROMIDES WITH N,N-DI-ETHYLAMINO-TRIBUTYLTIN. *Chem. Lett.* **1983**, *12* (6), 927–928. https://doi.org/10.1246/cl.1983.927.
(37) Guram, A. S.; Buchwald, S. L. Palladium-Catalyzed Aromatic Aminations with in Situ Generated Aminostannanes. *J. Am. Chem. Soc.* **1994**, *116* (17), 7901–7902. https://doi.org/10.1021/ja00096a059.
(38) Paul, F.; Patt, J.; Hartwig, J. F. Palladium-Catalyzed Formation of Carbon-Nitrogen Bonds. Reaction Intermediates and Catalyst Improvements in the Hetero Cross-Coupling of Aryl Halides and Tin Amides. *J. Am. Chem. Soc.* **1994**, *116* (13), 5969–5970. https://doi.org/10.1021/ja00092a058.
(39) Ishiyama, T.; Murata, M.; Miyaura, N. Palladium(0)-Catalyzed Cross-Coupling Reaction of Alkoxydiboron with Haloarenes: A Direct Procedure for Arylboronic Esters. *J. Org. Chem.* **1995**, *60* (23), 7508–7510. https://doi.org/10.1021/jo00128a024.
(40) Kosugi, M.; Shimizu, Y.; Migita, T. ALKYLATION, ARYLATION, AND VINYLATION OF ACYL CHLORIDES BY MEANS OF ORGANOTIN COMPOUNDS IN THE PRESENCE OF CATALYTIC AMOUNTS OF TETRAKIS(TRIPHENYLPHOSPHINE)PALLADIUM(O). *Chem. Lett.* **1977**, *6* (12), 1423–1424. https://doi.org/10.1246/cl.1977.1423.
(41) Milstein, D.; Stille, J. K. A General, Selective, and Facile Method for Ketone Synthesis from Acid Chlorides and Organotin Compounds Catalyzed by Palladium. *J. Am. Chem. Soc.* **1978**, *100* (11), 3636–3638. https://doi.org/10.1021/ja00479a077.
(42) Negishi, E.; King, A. O.; Okukado, N. Selective Carbon-Carbon Bond Formation via Transition Metal Catalysis. 3. A Highly Selective Synthesis of Unsymmetrical Biaryls and Diarylmethanes by the Nickel- or Palladium-Catalyzed Reaction of Aryl- and Benzylzinc Derivatives with Aryl Halides. *J. Org. Chem.* **1977**, *42* (10), 1821–1823. https://doi.org/10.1021/jo00430a041.
(43) Tamao, K.; Sumitani, K.; Kumada, M. Selective Carbon-Carbon Bond Formation by Cross-Coupling of Grignard Reagents with Organic Halides. Catalysis by Nickel-Phosphine

Complexes. *J. Am. Chem. Soc.* **1972**, *94* (12), 4374–4376. https://doi.org/10.1021/ja00767a075.
(44) Corriu, R. J. P.; Masse, J. P. Activation of Grignard Reagents by Transition-Metal Complexes. A New and Simple Synthesis of Trans-Stilbenes and Polyphenyls. *J. Chem. Soc., Chem. Commun.* **1972**, No. 3, 144a–144a. https://doi.org/10.1039/C3972000144A.
(45) Hatanaka, Y.; Hiyama, T. Cross-Coupling of Organosilanes with Organic Halides Mediated by a Palladium Catalyst and Tris(Diethylamino)Sulfonium Difluorotrimethylsilicate. *J. Org. Chem.* **1988**, *53* (4), 918–920. https://doi.org/10.1021/jo00239a056.
(46) Murahashi, S.; Yamamura, M.; Yanagisawa, K.; Mita, N.; Kondo, K. Stereoselective Synthesis of Alkenes and Alkenyl Sulfides from Alkenyl Halides Using Palladium and Ruthenium Catalysts. *J. Org. Chem.* **1979**, *44* (14), 2408–2417. https://doi.org/10.1021/jo01328a016.
(47) Brown, D. G.; Boström, J. Analysis of Past and Present Synthetic Methodologies on Medicinal Chemistry: Where Have All the New Reactions Gone? *J. Med. Chem.* **2016**, *59* (10), 4443–4458. https://doi.org/10.1021/acs.jmedchem.5b01409.
(48) Lovering, F.; Bikker, J.; Humblet, C. Escape from Flatland: Increasing Saturation as an Approach to Improving Clinical Success. *J. Med. Chem.* **2009**, *52* (21), 6752–6756. https://doi.org/10.1021/jm901241e.
(49) McNamee, R. E.; Dasgupta, A.; Christensen, K. E.; Anderson, E. A. Bridge Cross-Coupling of Bicyclo[1.1.0]Butanes. *Org. Lett.* **2024**, *26* (1), 360–364. https://doi.org/10.1021/acs.orglett.3c04030.
(50) Shelp, R. A.; Ciro, A.; Pu, Y.; Merchant, R. R.; Hughes, J. M. E.; Walsh, P. J. Strain-Release 2-Azaallyl Anion Addition/Borylation of [1.1.1]Propellane: Synthesis and Functionalization of Benzylamine Bicyclo[1.1.1]Pentyl Boronates. *Chem. Sci.* **2021**, *12* (20), 7066–7072. https://doi.org/10.1039/D1SC01349A.
(51) Shire, B. R.; Anderson, E. A. Conquering the Synthesis and Functionalization of Bicyclo[1.1.1]Pentanes. *JACS Au* **2023**, *3* (6), 1539–1553. https://doi.org/10.1021/jacsau.3c00014.
(52) Firsan, S. J.; Sivakumar, V.; Colacot, T. J. Emerging Trends in Cross-Coupling: Twelve-Electron-Based L_1Pd(0) Catalysts, Their Mechanism of Action, and Selected Applications. *Chem. Rev.* **2022**, *122* (23), 16983–17027. https://doi.org/10.1021/acs.chemrev.2c00204.
(53) García-Melchor, M.; Braga, A. A. C.; Lledós, A.; Ujaque, G.; Maseras, F. Computational Perspective on Pd-Catalyzed C–C Cross-Coupling Reaction Mechanisms. *Acc. Chem. Res.* **2013**, *46* (11), 2626–2634. https://doi.org/10.1021/ar400080r.
(54) Xie, H.; Fan, T.; Lei, Q.; Fang, W. New Progress in Theoretical Studies on Palladium-Catalyzed C−C Bond-Forming Reaction Mechanisms. *Sci. China Chem.* **2016**, *59* (11), 1432–1447. https://doi.org/10.1007/s11426-016-0018-2.
(55) Biffis, A.; Centomo, P.; Del Zotto, A.; Zecca, M. Pd Metal Catalysts for Cross-Couplings and Related Reactions in the 21st Century: A Critical Review. *Chem. Rev.* **2018**, *118* (4), 2249–2295. https://doi.org/10.1021/acs.chemrev.7b00443.
(56) D'Alterio, M. C.; Casals-Cruañas, È.; Tzouras, N. V.; Talarico, G.; Nolan, S. P.; Poater, A. Mechanistic Aspects of the Palladium-Catalyzed Suzuki-Miyaura Cross-Coupling Reaction. *Chem. Eur. J.* **2021**, 27, 13481–13493. https://doi.org/10.1002/chem.202101880.

(57) Gazvoda, M.; Virant, M.; Pinter, B.; Košmrlj, J. Mechanism of Copper-Free Sonogashira Reaction Operates through Palladium-Palladium Transmetallation. *Nat Commun* **2018**, *9* (1), 4814. https://doi.org/10.1038/s41467-018-07081-5.
(58) Rio, J.; Liang, H.; Perrin, M.-E. L.; Perego, L. A.; Grimaud, L.; Payard, P.-A. We Already Know Everything about Oxidative Addition to Pd(0): Do We? *ACS Catal.* **2023**, *13* (17), 11399–11421. https://doi.org/10.1021/acscatal.3c01943.
(59) Astruc, D. *Organometallic Chemistry and Catalysis*; Springer-Verlag: Berlin Heidelberg, 2007.
(60) Spessard, G. O.; Miessler, G. L. *Organometallic Chemistry*, Third Ed.; Oxford University Press: New York, New York, 2016.
(61) Labinger, J. A. Tutorial on Oxidative Addition. *Organometallics* **2015**, *34* (20), 4784–4795. https://doi.org/10.1021/acs.organomet.5b00565.
(62) Longcake, A.; Lees, M. R.; Senn, M. S.; Chaplin, A. B. Oxidative Addition of C–Cl Bonds to a Rh(PONOP) Pincer Complex. *Organometallics* **2022**, *41* (23), 3557–3567. https://doi.org/10.1021/acs.organomet.2c00400.
(63) García-Rodeja, Y.; Bickelhaupt, F. M.; Fernández, I. Understanding the Oxidative Addition of σ-Bonds to Group 13 Compounds. *Chem. Eur. J.* **2016**, *22* (38), 13669–13676. https://doi.org/10.1002/chem.201602505.
(64) Lu, J.; Donnecke, S.; Paci, I.; Leitch, D. C. A Reactivity Model for Oxidative Addition to Palladium Enables Quantitative Predictions for Catalytic Cross-Coupling Reactions. *Chem. Sci.* **2022**, *13* (12), 3477–3488. https://doi.org/10.1039/D2SC00174H.
(65) Lu, J.; Celuszak, H.; Paci, I.; Leitch, D. Quantitative Reactivity Models for Oxidative Addition to L_2Pd(0): Additional Substrate Classes, Solvents, and Mechanistic Insights. *ChemRxiv* Preprint, June 12, 2024. https://doi.org/10.26434/chemrxiv-2024-v3q40.
(66) Rasmussen, S. C. Transmetalation: A Fundamental Organometallic Reaction Critical to Synthesis and Catalysis. *ChemTexts* **2021**, *7* (1), 1. https://doi.org/10.1007/s40828-020-00124-9.
(67) Partyka, D. V. Transmetalation of Unsaturated Carbon Nucleophiles from Boron-Containing Species to the Mid to Late d-Block Metals of Relevance to Catalytic C−X Coupling Reactions (X = C, F, N, O, Pb, S, Se, Te). *Chem. Rev.* **2011**, *111* (3), 1529–1595. https://doi.org/10.1021/cr1002276.
(68) Thomas, A. A.; Denmark, S. E. Pre-Transmetalation Intermediates in the Suzuki-Miyaura Reaction Revealed: The Missing Link. *Science* **2016**, *352* (6283), 329–332. https://doi.org/10.1126/science.aad6981.
(69) Thomas, A. A.; Wang, H.; Zahrt, A. F.; Denmark, S. E. Structural, Kinetic, and Computational Characterization of the Elusive Arylpalladium(II)Boronate Complexes in the Suzuki–Miyaura Reaction. *J. Am. Chem. Soc.* **2017**, *139* (10), 3805–3821. https://doi.org/10.1021/jacs.6b13384.
(70) Thomas, A. A.; Zahrt, A. F.; Delaney, C. P.; Denmark, S. E. Elucidating the Role of the Boronic Esters in the Suzuki–Miyaura Reaction: Structural, Kinetic, and Computational Investigations. *J. Am. Chem. Soc.* **2018**, *140* (12), 4401–4416. https://doi.org/10.1021/jacs.8b00400.

(71) Jiang, T.; Zhang, H.; Ding, Y.; Zou, S.; Chang, R.; Huang, H. Transition-Metal-Catalyzed Reactions Involving Reductive Elimination between Dative Ligands and Covalent Ligands. *Chem. Soc. Rev.* **2020**, *49* (5), 1487–1516. https://doi.org/10.1039/C9CS00539K.
(72) Hartwig, J. F. Electronic Effects on Reductive Elimination To Form Carbon−Carbon and Carbon−Heteroatom Bonds from Palladium(II) Complexes. *Inorg. Chem.* **2007**, *46* (6), 1936–1947. https://doi.org/10.1021/ic061926w.
(73) Protchenko, A. V.; Bates, J. I.; Saleh, L. M. A.; Blake, M. P.; Schwarz, A. D.; Kolychev, E. L.; Thompson, A. L.; Jones, C.; Mountford, P.; Aldridge, S. Enabling and Probing Oxidative Addition and Reductive Elimination at a Group 14 Metal Center: Cleavage and Functionalization of E–H Bonds by a Bis(Boryl)Stannylene. *J. Am. Chem. Soc.* **2016**, *138* (13), 4555–4564. https://doi.org/10.1021/jacs.6b00710.
(74) Amatore, C.; Jutand, A.; Le Duc, G. Kinetic Data for the Transmetalation/Reductive Elimination in Palladium-Catalyzed Suzuki–Miyaura Reactions: Unexpected Triple Role of Hydroxide Ions Used as Base. *Chem. Eur. J.* **2011**, *17* (8), 2492–2503. https://doi.org/10.1002/chem.201001911.
(75) Lee, A.-L. Enantioselective Oxidative Boron Heck Reactions. *Org. Biomol. Chem.* **2016**, *14* (24), 5357–5366. https://doi.org/10.1039/C5OB01984B.
(76) Zhang, Y.; Li, Z.; Liu, Z.-Q. Pd-Catalyzed Olefination of Furans and Thiophenes with Allyl Esters. *Org. Lett.* **2012**, *14* (1), 226–229. https://doi.org/10.1021/ol203013p.
(77) Su, Y.; Gao, S.; Huang, Y.; Lin, A.; Yao, H. Solvent-Controlled C2/C5-Regiodivergent Alkenylation of Pyrroles. *Chem. Eur. J.* **2015**, *21* (44), 15820–15825. https://doi.org/10.1002/chem.201502418.
(78) Wang, S.; Deng, G.; Gu, J.; Hua, W.; Jia, X.; Xi, K. In Site Preparation of Pd(II)–MoS_2 Complex: A New High-Efficiency Catalyst for Alkenylation of Heteroaromatics by Direct CH Bond Activation. *Appl. Cat. A: Gen.* **2015**, *508*, 80–85. https://doi.org/10.1016/j.apcata.2015.10.014.
(79) Laha, J. K.; Bhimpuria, R. A.; Mule, G. B. Site-Selective Oxidative C4 Alkenylation of (NH)-Pyrroles Bearing an Electron-Withdrawing C2 Group. *ChemCatChem* **2017**, *9* (6), 1092–1096. https://doi.org/10.1002/cctc.201601468.
(80) Zhu, B.; Li, Z.; Chen, F.; Xiong, W.; Tan, X.; Lei, M.; Wu, W.; Jiang, H. Palladium-Catalyzed Oxidative Heck Reaction of Non-Activated Alkenes Directed by Fluorinated Alcohol. *Chem. Commun.* **2022**, *58* (91), 12688–12691. https://doi.org/10.1039/D2CC04921J.
(81) Huang, L.; Qi, J.; Wu, X.; Wu, W.; Jiang, H. Aerobic Oxidative Coupling between Carbon Nucleophiles and Allylic Alcohols: A Strategy to Construct β-(Hetero)Aryl Ketones and Aldehydes through Hydrogen Migration. *Chem. Eur. J.* **2013**, *19* (46), 15462–15466. https://doi.org/10.1002/chem.201302962.
(82) Le Bras, J.; Muzart, J. Pd-Catalyzed Intermolecular Dehydrogenative Heck Reactions of Five-Membered Heteroarenes. *Catalysts* **2020**, *10* (5), 571. https://doi.org/10.3390/catal10050571.
(83) Dai, Q.; Zhao, B.; Yang, Y.; Shi, Y. Pd-Catalyzed Oxidative Heck Reaction of Grignard Reagents with Diaziridinone as Oxidant. *Org. Lett.* **2019**, *21* (13), 5157–5161. https://doi.org/10.1021/acs.orglett.9b01762.

(84) Karimi, B.; Behzadnia, H.; Elhamifar, D.; Akhavan, P.; Esfahani, F.; Zamani, A. Transition-Metal-Catalyzed Oxidative Heck Reactions. *Synthesis* **2010**, *2010* (09), 1399–1427. https://doi.org/10.1055/s-0029-1218748.
(85) Shockley, S. E.; Holder, J. C.; Stoltz, B. M. Palladium-Catalyzed Asymmetric Conjugate Addition of Arylboronic Acids to α,β-Unsaturated Cyclic Electrophiles. *Org. Process Res. Dev.* **2015**, *19* (8), 974–981. https://doi.org/10.1021/acs.oprd.5b00169.
(86) Miyaura, Norio.; Suzuki, Akira. Palladium-Catalyzed Cross-Coupling Reactions of Organoboron Compounds. *Chem. Rev.* **1995**, *95* (7), 2457–2483. https://doi.org/10.1021/cr00039a007.
(87) Barroso, S.; Joksch, M.; Puylaert, P.; Tin, S.; Bell, S. J.; Donnellan, L.; Duguid, S.; Muir, C.; Zhao, P.; Farina, V.; Tran, D. N.; de Vries, J. G. Improvement in the Palladium-Catalyzed Miyaura Borylation Reaction by Optimization of the Base: Scope and Mechanistic Study. *J. Org. Chem.* **2021**, *86* (1), 103–109. https://doi.org/10.1021/acs.joc.0c01758.
(88) Anastas, P. T.; Warner, J. C. Green Chemistry: Theory and Practice; Oxford University Press: New York, 1998; p 30.
(89) Kinuta, H.; Hasegawa, J.; Tobisu, M.; Chatani, N. Rhodium-Catalyzed Borylation of Aryl and Alkenyl Pivalates through the Cleavage of Carbon–Oxygen Bonds. *Chem. Lett.* **2015**, *44* (3), 366–368. https://doi.org/10.1246/cl.141084.
(90) Zhou, T.; Szostak, M. Palladium-Catalyzed Cross-Couplings by C–O Bond Activation. *Catal. Sci. Technol.* **2020**, *10* (17), 5702–5739. https://doi.org/10.1039/D0CY01159B.
(91) Becica, J.; Gaube, G.; A. Sabbers, W.; C. Leitch, D. Oxidative Addition of Activated Aryl-Carboxylates to Pd(0): Divergent Reactivity Dependant on Temperature and Structure. *Dalton Trans.* **2020**, *49* (45), 16067–16071. https://doi.org/10.1039/D0DT01119C.
(92) Fang, W.; Sixta, H. Advanced Biorefinery Based on the Fractionation of Biomass in γ-Valerolactone and Water. *ChemSusChem* **2015**, *8* (1), 73–76. https://doi.org/10.1002/cssc.201402821.
(93) Serrano-Ruiz, J. C.; Luque, R.; Sepúlveda-Escribano, A. Transformations of Biomass-Derived Platform Molecules: From High Added-Value Chemicals to Fuelsvia Aqueous-Phase Processing. *Chem. Soc. Rev.* **2011**, *40* (11), 5266–5281. https://doi.org/10.1039/C1CS15131B.
(94) Williams, C. L.; Emerson, R. M.; Tumuluru, J. S.; Williams, C. L.; Emerson, R. M.; Tumuluru, J. S. Biomass Compositional Analysis for Conversion to Renewable Fuels and Chemicals. In *Biomass Volume Estimation and Valorization for Energy*; IntechOpen, 2017.
(95) Takise, R.; Muto, K.; Yamaguchi, J. Cross-Coupling of Aromatic Esters and Amides. *Chem. Soc. Rev.* **2017**, *46* (19), 5864–5888. https://doi.org/10.1039/C7CS00182G.
(96) Boit, T. B.; Bulger, A. S.; Dander, J. E.; Garg, N. K. Activation of C–O and C–N Bonds Using Non-Precious-Metal Catalysis. *ACS Catal.* **2020**, *10* (20), 12109–12126. https://doi.org/10.1021/acscatal.0c03334.
(97) Tsuji, J.; Takahashi, H.; Morikawa, M. Organic Syntheses by Means of Noble Metal Compounds XVII. Reaction of π-Allylpalladium Chloride with Nucleophiles. *Tetrahedron Lett.* **1965**, *6* (49), 4387–4388. https://doi.org/10.1016/S0040-4039(00)71674-1.
(98) Trost, B. M.; Fullerton, T. J. New Synthetic Reactions. Allylic Alkylation. *J. Am. Chem. Soc.* **1973**, *95* (1), 292–294. https://doi.org/10.1021/ja00782a080.

(99) Zhao, G.; Li, W.; Zhang, J. Recent Advances in Palladium-Catalyzed Asymmetric Heck/Tsuji–Trost Reactions of 1,n-Dienes. *Chem. Eur. J.* **2024**, *30* (26), e202400076. https://doi.org/10.1002/chem.202400076.
(100) Pàmies, O.; Margalef, J.; Cañellas, S.; James, J.; Judge, E.; Guiry, P. J.; Moberg, C.; Bäckvall, J.-E.; Pfaltz, A.; Pericàs, M. A.; Diéguez, M. Recent Advances in Enantioselective Pd-Catalyzed Allylic Substitution: From Design to Applications. *Chem. Rev.* **2021**, *121* (8), 4373–4505. https://doi.org/10.1021/acs.chemrev.0c00736.
(101) Trost, B.; Schultz, J. Palladium-Catalyzed Asymmetric Allylic Alkylation Strategies for the Synthesis of Acyclic Tetrasubstituted Stereocenters. *Synthesis* **2019**, *51* (01), 1–30. https://doi.org/10.1055/s-0037-1610386.
(102) Becica, J.; Heath, O. R. J.; Zheng, C. H. M.; Leitch, D. C. Palladium-Catalyzed Cross-Coupling of Alkenyl Carboxylates. *Angew. Chem, Int. Ed.* **2020**, *59* (39), 17277–17281. https://doi.org/10.1002/anie.202006586.
(103) Kania, M. J.; Reyes, A.; Neufeldt, S. R. Oxidative Addition of (Hetero)Aryl (Pseudo)Halides at Palladium(0): Origin and Significance of Divergent Mechanisms. *J. Am. Chem. Soc.* **2024**, *146* (28), 19249–19260. https://doi.org/10.1021/jacs.4c04496.
(104) Li, J.; Knochel, P. Cobalt-Catalyzed Cross-Couplings between Alkenyl Acetates and Aryl or Alkenyl Zinc Pivalates. *Angew. Chem. Int. Ed.* **2018**, *57* (35), 11436–11440. https://doi.org/10.1002/anie.201805486.
(105) Li, J.; Ren, Q.; Cheng, X.; Karaghiosoff, K.; Knochel, P. Chromium(II)-Catalyzed Diastereoselective and Chemoselective Csp^2–Csp^3 Cross-Couplings Using Organomagnesium Reagents. *J. Am. Chem. Soc.* **2019**, *141* (45), 18127–18135. https://doi.org/10.1021/jacs.9b08586.
(106) Moselage, M.; Sauermann, N.; Richter, S. C.; Ackermann, L. C-H Alkenylations with Alkenyl Acetates, Phosphates, Carbonates, and Carbamates by Cobalt Catalysis at 23 °C. *Angew. Chem. Int. Ed.* **2015**, *54* (21), 6352–6355. https://doi.org/10.1002/anie.201412319.
(107) Gärtner, D.; Stein, A. L.; Grupe, S.; Arp, J.; Jacobi von Wangelin, A. Iron-Catalyzed Cross-Coupling of Alkenyl Acetates. *Angew. Chem. Int. Ed.* **2015**, *54* (36), 10545–10549. https://doi.org/10.1002/anie.201504524.
(108) Lee, H. W.; Kwong, F. Y. Rhodium-Catalyzed Cross-Coupling of Arylboronic Acids Using Vinyl Acetate as the Electrophilic Partner. *Synlett* **2009**, *2009* (19), 3151–3154. https://doi.org/10.1055/s-0029-1218283.
(109) Sun, C.-L.; Wang, Y.; Zhou, X.; Wu, Z.-H.; Li, B.-J.; Guan, B.-T.; Shi, Z.-J. Construction of Polysubstituted Olefins through Ni-Catalyzed Direct Activation of Alkenyl C-O of Substituted Alkenyl Acetates. *Chem. Eur. J.* **2010**, *16* (20), 5844–5847. https://doi.org/10.1002/chem.200902785.
(110) Yu, J.-Y.; Kuwano, R. Rhodium-Catalyzed Cross-Coupling of Organoboron Compounds with Vinyl Acetate. *Angew. Chem. Int. Ed.* **2009**, *48* (39), 7217–7220. https://doi.org/10.1002/anie.200903146.
(111) Lindh, J.; Sävmarker, J.; Nilsson, P.; Sjöberg, P. J. R.; Larhed, M. Synthesis of Styrenes by Palladium(II)-Catalyzed Vinylation of Arylboronic Acids and Aryltrifluoroborates by Using Vinyl Acetate. *Chem. Eur. J.* **2009**, *15* (18), 4630–4636. https://doi.org/10.1002/chem.200802744.

(112) Muto, K.; Yamaguchi, J.; Lei, A.; Itami, K. Isolation, Structure, and Reactivity of an Arylnickel(II) Pivalate Complex in Catalytic C–H/C–O Biaryl Coupling. *J. Am. Chem. Soc.* **2013**, *135* (44), 16384–16387. https://doi.org/10.1021/ja409803x.
(113) Tobisu, M.; Chatani, N. Nickel-Catalyzed Cross-Coupling Reactions of Unreactive Phenolic Electrophiles via C–O Bond Activation. *Top. Curr. Chem.* **2016**, *374* (4), 41. https://doi.org/10.1007/s41061-016-0043-1.
(114) Degli Innocenti, M.; Schreiner, T.; Breinbauer, R. Recent Advances in Pd-Catalyzed Suzuki-Miyaura Cross-Coupling Reactions with Triflates or Nonaflates. *Adv. Synth. Catal.* **2023**, *365* (23), 4086–4120. https://doi.org/10.1002/adsc.202301124.
(115) Louie, J.; Driver, M. S.; Hamann, B. C.; Hartwig, J. F. Palladium-Catalyzed Amination of Aryl Triflates and Importance of Triflate Addition Rate. *J. Org. Chem.* **1997**, *62* (5), 1268–1273. https://doi.org/10.1021/jo961930x.
(116) Wolfe, J. P.; Buchwald, S. L. Palladium-Catalyzed Amination of Aryl Triflates. *J. Org. Chem.* **1997**, *62* (5), 1264–1267. https://doi.org/10.1021/jo961915s.
(117) Åhman, J.; Buchwald, S. L. An Improved Method for the Palladium-Catalyzed Amination of Aryl Triflates. *Tetrahedron Lett.* **1997**, *38* (36), 6363–6366. https://doi.org/10.1016/S0040-4039(97)01464-0.
(118) Fors, B. P.; Buchwald, S. L. Pd-Catalyzed Conversion of Aryl Chlorides, Triflates, and Nonaflates to Nitroaromatics. *J. Am. Chem. Soc.* **2009**, *131* (36), 12898–12899. https://doi.org/10.1021/ja905768k.
(119) Littke, A. F.; Dai, C.; Fu, G. C. Versatile Catalysts for the Suzuki Cross-Coupling of Arylboronic Acids with Aryl and Vinyl Halides and Triflates under Mild Conditions. *J. Am. Chem. Soc.* **2000**, *122* (17), 4020–4028. https://doi.org/10.1021/ja0002058.
(120) So, C. M.; Yuen, O. Y.; Ng, S. S.; Chen, Z. General Chemoselective Suzuki–Miyaura Coupling of Polyhalogenated Aryl Triflates Enabled by an Alkyl-Heteroaryl-Based Phosphine Ligand. *ACS Catal.* **2021**, *11* (13), 7820–7827. https://doi.org/10.1021/acscatal.1c02146.
(121) Zhu, C.; Chu, H.; Li, G.; Ma, S.; Zhang, J. Pd-Catalyzed Enantioselective Heck Reaction of Aryl Triflates and Alkynes. *J. Am. Chem. Soc.* **2019**, *141* (49), 19246–19251. https://doi.org/10.1021/jacs.9b10883.
(122) Reeves, E. K.; Entz, E. D.; Neufeldt, S. R. Chemodivergence between Electrophiles in Cross-Coupling Reactions. *Chem. Eur. J.* **2021**, *27* (20), 6161–6177. https://doi.org/10.1002/chem.202004437.
(123) Ibsen, G. M.; Menezes da Silva, V. H.; Pettigrew, J. C.; Neufeldt, S. R. Triflate-Selective Suzuki Cross-Coupling of Chloro- and Bromoaryl Triflates Under Ligand-Free Conditions. *Chem. Asian J.* **2023**, *18* (9), e202300036. https://doi.org/10.1002/asia.202300036.
(124) Espino, G.; Kurbangalieva, A.; Brown, J. M. Aryl Bromide/Triflate Selectivities Reveal Mechanistic Divergence in Palladium-Catalysed Couplings; the Suzuki–Miyaura Anomaly. *Chem. Commun.* **2007**, No. 17, 1742–1744. https://doi.org/10.1039/B701517H.
(125) Gooßen, L. J.; Gooßen, K.; Stanciu, C. C(Aryl)-O Activation of Aryl Carboxylates in Nickel-Catalyzed Biaryl Syntheses. *Angew. Chem. Int. Ed.* **2009**, *48* (20), 3569–3571. https://doi.org/10.1002/anie.200900329.
(126) Li, Z.; Zhang, S.-L.; Fu, Y.; Guo, Q.-X.; Liu, L. Mechanism of Ni-Catalyzed Selective C−O Bond Activation in Cross-Coupling of Aryl Esters. *J. Am. Chem. Soc.* **2009**, *131* (25), 8815–8823. https://doi.org/10.1021/ja810157e.

(127) Yamaguchi, J.; Muto, K.; Itami, K. Recent Progress in Nickel-Catalyzed Biaryl Coupling. *Eur. J. Org. Chem.* **2013**, *2013* (1), 19–30. https://doi.org/10.1002/ejoc.201200914.
(128) Rosen, B. M.; Quasdorf, K. W.; Wilson, D. A.; Zhang, N.; Resmerita, A.-M.; Garg, N. K.; Percec, V. Nickel-Catalyzed Cross-Couplings Involving Carbon−Oxygen Bonds. *Chem. Rev.* **2011**, *111* (3), 1346–1416. https://doi.org/10.1021/cr100259t.
(129) Tobisu, M.; Chatani, N. Cross-Couplings Using Aryl Ethers via C–O Bond Activation Enabled by Nickel Catalysts. *Acc. Chem. Res.* **2015**, *48* (6), 1717–1726. https://doi.org/10.1021/acs.accounts.5b00051.
(130) Tollefson, E. J.; Hanna, L. E.; Jarvo, E. R. Stereospecific Nickel-Catalyzed Cross-Coupling Reactions of Benzylic Ethers and Esters. *Acc. Chem. Res.* **2015**, *48* (8), 2344–2353. https://doi.org/10.1021/acs.accounts.5b00223.
(131) Cornella, J.; Zarate, C.; Martin, R. Metal-Catalyzed Activation of Ethers via C–O Bond Cleavage: A New Strategy for Molecular Diversity. *Chem. Soc. Rev.* **2014**, *43* (23), 8081–8097. https://doi.org/10.1039/C4CS00206G.
(132) So, C. M.; Kwong, F. Y. Palladium-Catalyzed Cross-Coupling Reactions of Aryl Mesylates. *Chem. Soc. Rev.* **2011**, *40* (10), 4963. https://doi.org/10.1039/c1cs15114b.
(133) King, R. P.; Krska, S. W.; Buchwald, S. L. A Ligand Exchange Process for the Diversification of Palladium Oxidative Addition Complexes. *Org. Lett.* **2021**, *23* (15), 6030–6034. https://doi.org/10.1021/acs.orglett.1c02101.
(134) Dikova, A.; Cheval, N. P.; Blanc, A.; Weibel, J.-M.; Pale, P. Aryl and Heteroaryl Nosylates as Stable and Cheap Partners for Suzuki–Miyaura Cross-Coupling Reactions. *Tetrahedron* **2016**, *72* (16), 1960–1968. https://doi.org/10.1016/j.tet.2016.02.061.
(135) Kohler, P.; Perrin, T.; Schäfer, G. Suzuki–Miyaura Coupling of Aryl Nosylates with Diethanolamine Boronates. *Synthesis* **2023**, *55* (19), 3159–3171. https://doi.org/10.1055/a-2107-5307.
(136) Vidal, M.; Rodríguez-Aguilar, J.; Aburto, I.; Aliaga, C.; Domínguez, M. Reactivity of 4-Pyrimidyl Sulfonic Esters in Suzuki-Miyaura Cross-Coupling Reactions in Water Under Microwave Irradiation. *ChemistrySelect* **2021**, *6* (45), 12858–12861. https://doi.org/10.1002/slct.202103280.
(137) Rottländer, M.; Knochel, P. Palladium-Catalyzed Cross-Coupling Reactions with Aryl Nonaflates: A Practical Alternative to Aryl Triflates. *J. Org. Chem.* **1998**, *63* (1), 203–208. https://doi.org/10.1021/jo971636k.
(138) Anderson, K. W.; Mendez-Perez, M.; Priego, J.; Buchwald, S. L. Palladium-Catalyzed Amination of Aryl Nonaflates. *J. Org. Chem.* **2003**, *68* (25), 9563–9573. https://doi.org/10.1021/jo034962a.
(139) Yamaguchi, M.; Hagiwara, R.; Gayama, K.; Suzuki, K.; Sato, Y.; Konishi, H.; Manabe, K. Direct C3-Selective Arylation of N-Unsubstituted Indoles with Aryl Chlorides, Triflates, and Nonaflates Using a Palladium–Dihydroxyterphenylphosphine Catalyst. *J. Org. Chem.* **2020**, *85* (16), 10902–10912. https://doi.org/10.1021/acs.joc.0c01494.
(140) Macklin, T. K.; Snieckus, V. Directed Ortho Metalation Methodology. The N,N-Dialkyl Aryl O-Sulfamate as a New Directed Metalation Group and Cross-Coupling Partner for Grignard Reagents. *Org. Lett.* **2005**, *7* (13), 2519–2522. https://doi.org/10.1021/ol050393c.

(141) Melvin, P. R.; Hazari, N.; Beromi, M. M.; Shah, H. P.; Williams, M. J. Pd-Catalyzed Suzuki–Miyaura and Hiyama–Denmark Couplings of Aryl Sulfamates. *Org. Lett.* **2016**, *18* (22), 5784–5787. https://doi.org/10.1021/acs.orglett.6b02330.
(142) Molander, G. A.; Shin, I. Pd-Catalyzed Suzuki–Miyaura Cross-Coupling Reactions between Sulfamates and Potassium Boc-Protected Aminomethyltrifluoroborates. *Org. Lett.* **2013**, *15* (10), 2534–2537. https://doi.org/10.1021/ol401021x.
(143) Wang, Z.-Y.; Ma, Q.-N.; Li, R.-H.; Shao, L.-X. Palladium-Catalyzed Suzuki–Miyaura Coupling of Aryl Sulfamates with Arylboronic Acids. *Org. Biomol. Chem.* **2013**, *11* (45), 7899–7906. https://doi.org/10.1039/C3OB41382A.
(144) Oberheide, A.; Arndt, H.-D. Effective C5-Arylation of Peptide-Integrated Oxazoles: Almazole D. *Adv. Synth. Catal.* **2021**, *363* (4), 1132–1136. https://doi.org/10.1002/adsc.202001262.
(145) Monti, A.; López-Serrano, J.; Prieto, A.; Nicasio, M. C. Broad-Scope Amination of Aryl Sulfamates Catalyzed by a Palladium Phosphine Complex. *ACS Catal.* **2023**, *13* (16), 10945–10952. https://doi.org/10.1021/acscatal.3c03166.
(146) Monti, A.; Rama, R. J.; Gómez, B.; Maya, C.; Álvarez, E.; Carmona, E.; Nicasio, M. C. *N*-Substituted Aminobiphenyl Palladacycles Stabilized by Dialkylterphenyl Phosphanes: Preparation and Applications in CN Cross-Coupling Reactions. *Inorg. Chim. Acta* **2021**, *518*, 120214. https://doi.org/10.1016/j.ica.2020.120214.
(147) So, C. M.; Lau, C. P.; Chan, A. S. C.; Kwong, F. Y. Suzuki−Miyaura Coupling of Aryl Tosylates Catalyzed by an Array of Indolyl Phosphine−Palladium Catalysts. *J. Org. Chem.* **2008**, *73* (19), 7731–7734. https://doi.org/10.1021/jo8014819.
(148) Lee, S. H.; Ryu, H. G.; Jeon, S. L.; Jeong, I. H. Cross-Coupling Reactions of Sterically Hindered 2,2-Difluoro-1-(Aryl or Silyl)Ethenyl Tosylates with *(E)*-Arylethenylboronic Acids. *J. Fluor. Chem.* **2021**, *246*, 109784. https://doi.org/10.1016/j.jfluchem.2021.109784.
(149) Kang, K.; Huang, L.; Weix, D. J. Sulfonate Versus Sulfonate: Nickel and Palladium Multimetallic Cross-Electrophile Coupling of Aryl Triflates with Aryl Tosylates. *J. Am. Chem. Soc.* **2020**, *142* (24), 10634–10640. https://doi.org/10.1021/jacs.0c04670.
(150) Xiong, B.; Li, Y.; Zhang, J.; Liu, J.; Zhang, X.; Lian, Z. Cross-Electrophile Coupling between Aryl/Vinyl Triflates and Vinyl Tosylates for the Synthesis of Gem-Difluoroalkenes via Ni/Pd Cooperative Catalysis. *Adv. Synth. Catal.* **2022**, *364* (5), 1009–1015. https://doi.org/10.1002/adsc.202101388.
(151) Qu, R.; Zhang, J.; Lian, Z. Cross-Electrophile Coupling between Two Different Tosylates Enabled by Nickel/Palladium Cooperative Catalysis. *Eur. J. Org. Chem.* **2023**, *26* (40), e202300874. https://doi.org/10.1002/ejoc.202300874.
(152) Maiti, S.; Ghosh, P.; Raja, D.; Ghosh, S.; Chatterjee, S.; Sankar, V.; Roy, S.; Lahiri, G. K.; Maiti, D. Light-Induced Pd Catalyst Enables $C(Sp^2)$–$C(Sp^2)$ Cross-Electrophile Coupling Bypassing the Demand for Transmetalation. *Nat. Catal.* **2024**, *7* (3), 285–294. https://doi.org/10.1038/s41929-024-01109-4.
(153) Saraswat, S. K.; Seemaladinne, R.; Abdullah, M. N.; Zaini, H.; Ahmad, N.; Ahmad, N.; Vessally, E. Aryl Fluorosulfates: Powerful and Versatile Partners in Cross-Coupling Reactions. *RSC Adv.* **2023**, *13* (20), 13642–13654. https://doi.org/10.1039/D3RA01791E.

(154) Guan, C.; Qi, H.; Han, L.; Zhang, G.; Ding, C. (Hetero)Aryl Fluorosulfates ($ArOSO_2F$): Good Coupling Partners in Transition-Metal-Catalyzed Reactions. *Adv. Synth. Catal.* **2023**, *365* (23), 4068–4085. https://doi.org/10.1002/adsc.202301024.

(155) Yang, S.; Li, H.; Yu, X.; An, J.; Szostak, M. Suzuki–Miyaura Cross-Coupling of Aryl Fluorosulfonates Mediated by Air- and Moisture-Stable $[Pd(NHC)(\mu\text{-}Cl)Cl]_2$ Precatalysts: Broad Platform for C–O Cross-Coupling of Stable Phenolic Electrophiles. *J. Org. Chem.* **2022**, *87* (22), 15250–15260. https://doi.org/10.1021/acs.joc.2c01778.

(156) Kincaid, J. R. A.; Wong, M. J.; Akporji, N.; Gallou, F.; Fialho, D. M.; Lipshutz, B. H. Introducing Savie: A Biodegradable Surfactant Enabling Chemo- and Biocatalysis and Related Reactions in Recyclable Water. *J. Am. Chem. Soc.* **2023**, *145* (7), 4266–4278. https://doi.org/10.1021/jacs.2c13444.

(157) Iyer, K. S.; Dismuke Rodriguez, K. B.; Lammert, R. M.; Yirak, J. R.; Saunders, J. M.; Kavthe, R. D.; Aue, D. H.; Lipshutz, B. H. Rapid Aminations of Functionalized Aryl Fluorosulfates in Water. *Angew. Chem. Int. Ed.* **2024**, 63, e202411295. https://doi.org/10.1002/anie.202411295.

(158) Guan, C.; Qi, H.; Han, L.; Liu, M.; Wang, J.; Zhang, G.; Ding, C. Palladium-Catalyzed Cyclopropanation of Aryl/Heteroaryl Fluoro-Sulfonates. *ChemistrySelect* **2023**, *8* (10), e202300420. https://doi.org/10.1002/slct.202300420.

(159) Zhang, G.; Han, L.; Guan, C.; Qi, H.; Ding, C. Bimetallic Cooperatively Catalyzed Heteroarylation of Aryl Fluorosulfates. *Eur. J. Org. Chem.* **2023**, *26* (5), e202201352. https://doi.org/10.1002/ejoc.202201352.

(160) Zhang, G.; Guan, C.; Han, L.; Zhao, Y.; Ding, C. A Late-Stage Functionalization Tool: Sulfonyl Fluoride Mediated Deoxymethylation of Phenols. *Org. Biomol. Chem.* **2022**, *20* (38), 7640–7644. https://doi.org/10.1039/D2OB01523D.

(161) Hosseini, N.; Mokhtari, J.; Yavari, I. DCID-Mediated Heck Cross-Coupling of Phenols via C–O Bond Activation. *New J. Chem.* **2022**, *46* (12), 5588–5592. https://doi.org/10.1039/D1NJ06120H.

(162) Toupalas, G.; Thomann, G.; Schlemper, L.; Rivero-Crespo, M. A.; Schmitt, H. L.; Morandi, B. Pd-Catalyzed Direct Deoxygenative Arylation of Non-π-Extended Benzyl Alcohols with Boronic Acids via Transient Formation of Non-Innocent Isoureas. *ACS Catal.* **2022**, *12* (14), 8147–8154. https://doi.org/10.1021/acscatal.2c01858.

(163) Musgrave, C. B. I.; Bennett, M. T.; Ellena, J. F.; Dickie, D. A.; Gunnoe, T. B.; Goddard, W. A. I. Reaction Mechanism Underlying Pd(II)-Catalyzed Oxidative Coupling of Ethylene and Benzene to Form Styrene: Identification of a Cyclic Mono-Pd^{II} Bis-Cu^{II} Complex as the Active Catalyst. *Organometallics* **2022**, *41* (15), 1988–2000. https://doi.org/10.1021/acs.organomet.2c00183.

(164) Bennett, M. T.; Jia, X.; Musgrave, C. B. I.; Zhu, W.; Goddard, W. A. I.; Gunnoe, T. B. Pd(II) and Rh(I) Catalytic Precursors for Arene Alkenylation: Comparative Evaluation of Reactivity and Mechanism Based on Experimental and Computational Studies. *J. Am. Chem. Soc.* **2023**, *145* (28), 15507–15527. https://doi.org/10.1021/jacs.3c04295.

(165) Awad, H.; Khamis, M. M.; El-Aneed, A. Mass Spectrometry, Review of the Basics: Ionization. *Appl. Spectrosc. Rev.* **2015**, *50* (2), 158–175. https://doi.org/10.1080/05704928.2014.954046.

(166) Glish, G. L.; Vachet, R. W. The Basics of Mass Spectrometry in the Twenty-First Century. *Nat. Rev. Drug Discov.* **2003**, *2* (2), 140–150. https://doi.org/10.1038/nrd1011.
(167) Vikse, K. L.; Ahmadi, Z.; Scott McIndoe, J. The Application of Electrospray Ionization Mass Spectrometry to Homogeneous Catalysis. *Coord. Chem. Rev.* **2014**, *279*, 96–114. https://doi.org/10.1016/j.ccr.2014.06.012.
(168) Eberlin, M. N. Electrospray Ionization Mass Spectrometry: A Major Tool to Investigate Reaction Mechanisms in Both Solution and the Gas Phase. *Eur. J. Mass. Spectrom.* **2007**, *13* (1), 19–28. https://doi.org/10.1255/ejms.837.
(169) Yunker, L. P. E.; Stoddard, R. L.; McIndoe, J. S. Practical Approaches to the ESI-MS Analysis of Catalytic Reactions. *J. Mass Spectrom.* **2014**, *49* (1), 1–8. https://doi.org/10.1002/jms.3303.
(170) Norris, A. J.; Whitelegge, J. P.; Faull, K. F.; Toyokuni, T. Kinetic Characterization of Enzyme Inhibitors Using Electrospray-Ionization Mass Spectrometry Coupled with Multiple Reaction Monitoring. *Anal. Chem.* **2001**, *73* (24), 6024–6029. https://doi.org/10.1021/ac015574g.
(171) Norris, A. J.; Whitelegge, J. P.; Strouse, M. J.; Faull, K. F.; Toyokuni, T. Inhibition Kinetics of Carba- and C-Fucosyl Analogues of GDP-Fucose against Fucosyltransferase V: Implication for the Reaction Mechanism. *Bioorg. Med. Chem. Lett.* **2004**, *14* (3), 571–573. https://doi.org/10.1016/j.bmcl.2003.12.003.
(172) Zhuo, Q.; Deng, S.; Yang, B.; Huang, J.; Yu, G. Efficient Electrochemical Oxidation of Perfluorooctanoate Using a Ti/SnO_2 -Sb-Bi Anode. *Environ. Sci. Technol.* **2011**, *45* (7), 2973–2979. https://doi.org/10.1021/es1024542.
(173) Aliprantis, A. O.; Canary, J. W. Observation of Catalytic Intermediates in the Suzuki Reaction by Electrospray Mass Spectrometry. *J. Am. Chem. Soc.* **1994**, *116* (15), 6985–6986. https://doi.org/10.1021/ja00094a083.
(174) Davis, D. C.; Walker, K. L.; Hu, C.; Zare, R. N.; Waymouth, R. M.; Dai, M. Catalytic Carbonylative Spirolactonization of Hydroxycyclopropanols. *J. Am. Chem. Soc.* **2016**, *138* (33), 10693–10699. https://doi.org/10.1021/jacs.6b06573.
(175) Vicent, C.; Gusev, D. G. ESI-MS Insights into Acceptorless Dehydrogenative Coupling of Alcohols. *ACS Catal.* **2016**, *6* (5), 3301–3309. https://doi.org/10.1021/acscatal.6b00623.
(176) Yunker, L. P. E.; Ahmadi, Z.; Logan, J. R.; Wu, W.; Li, T.; Martindale, A.; Oliver, A. G.; McIndoe, J. S. Real-Time Mass Spectrometric Investigations into the Mechanism of the Suzuki–Miyaura Reaction. *Organometallics* **2018**, *37* (22), 4297–4308. https://doi.org/10.1021/acs.organomet.8b00705.
(177) Yan, X.; Sokol, E.; Li, X.; Li, G.; Xu, S.; Cooks, R. G. On-Line Reaction Monitoring and Mechanistic Studies by Mass Spectrometry: Negishi Cross-Coupling, Hydrogenolysis, and Reductive Amination. *Angew. Chem. Int. Ed.* **2014**, *53* (23), 5931–5935. https://doi.org/10.1002/anie.201310493.
(178) Chen, C.-C.; Lin, P.-C. Monitoring of Chemical Transformations by Mass Spectrometry. *Anal. Methods* **2015**, *7* (17), 6947–6959. https://doi.org/10.1039/C5AY00496A.
(179) Vikse, K. L.; Woods, M. P.; McIndoe, J. S. Pressurized Sample Infusion for the Continuous Analysis of Air- And Moisture-Sensitive Reactions Using Electrospray Ionization Mass Spectrometry. *Organometallics* **2010**, *29* (23), 6615–6618. https://doi.org/10.1021/om1008082.

(180) Vikse, K. L.; Ahmadi, Z.; Luo, J.; van der Wal, N.; Daze, K.; Taylor, N.; McIndoe, J. S. Pressurized Sample Infusion: An Easily Calibrated, Low Volume Pumping System for ESI-MS Analysis of Reactions. *Int. J. Mass Spectrom.* **2012**, *323–324*, 8–13. https://doi.org/10.1016/j.ijms.2012.03.007.
(181) Thomas, G. T.; MacGillivray, L.; Dean, N. L.; Stoddard, R. L.; Yunker, L. P. E.; McIndoe, J. S. Confounding Contaminants in Mass Spectrometric Reaction Monitoring. *Int. J. Mass Spectrom.* **2019**, *441*, 14–18. https://doi.org/10.1016/j.ijms.2019.04.001.
(182) Thomas, G. T.; Janusson, E.; Zijlstra, H. S.; McIndoe, J. S. Step-by-Step Real Time Monitoring of a Catalytic Amination Reaction. *Chem. Commun.* **2019**, *55* (78), 11727–11730. https://doi.org/10.1039/C9CC05076K.
(183) Luo, J.; Oliver, A. G.; McIndoe, J. S. A Detailed Kinetic Analysis of Rhodium-Catalyzed Alkyne Hydrogenation. *Dalton Trans.* **2013**, *42* (31), 11312–11318. https://doi.org/10.1039/C3DT51212F.
(184) Ingram, A. J.; Walker, K. L.; Zare, R. N.; Waymouth, R. M. Catalytic Role of Multinuclear Palladium–Oxygen Intermediates in Aerobic Oxidation Followed by Hydrogen Peroxide Disproportionation. *J. Am. Chem. Soc.* **2015**, *137* (42), 13632–13646. https://doi.org/10.1021/jacs.5b08719.
(185) Banerjee, S.; Sathyamoorthi, S.; Du Bois, J.; Zare, R. N. Mechanistic Analysis of a Copper-Catalyzed C–H Oxidative Cyclization of Carboxylic Acids. *Chem. Sci.* **2017**, *8* (10), 7003–7008. https://doi.org/10.1039/C7SC02240A.
(186) Chagunda, I. C.; Fisher, T.; Schierling, M.; McIndoe, J. S. Poisonous Truth about the Mercury Drop Test: The Effect of Elemental Mercury on Pd(0) and Pd(II)ArX Intermediates. *Organometallics* **2023**, *42* (19), 2938–2945. https://doi.org/10.1021/acs.organomet.3c00340.
(187) Dias, H. J.; Santos, W. H.; Filho, L. C. S.; Crevelin, E. J.; McIndoe, J. S.; Vessecchi, R.; Crotti, A. E. M. Electrospray Ionization Tandem Mass Spectrometry of 4-Aryl-3,4-Dihydrocoumarins. *J. Mass Spectrom.* **2024**, *59* (7), e5062. https://doi.org/10.1002/jms.5062.
(188) Furrer, J. A Comprehensive Discussion of HMBC Pulse Sequences, Part 1: The Classical HMBC. *Concepts Magn. Reson. A: Bridg. Educ. Res.* **2012**, *40A* (3), 101–127. https://doi.org/10.1002/cmr.a.21232.
(189) Furrer, J. A Comprehensive Discussion of HMBC Pulse Sequences. 2. Some Useful Variants. *Concepts Magn. Reson. A: Bridg. Educ. Res.* **2012**, *40A* (3), 146–169. https://doi.org/10.1002/cmr.a.21231.
(190) Furrer, J. A Comprehensive Discussion of HMBC Pulse Sequences. III. Solving the Problem of Missing and Weakly Observed Long-Range Correlations. *Concepts Magn. Reson. A: Bridg. Educ. Res.* **2014**, *43* (5), 177–206. https://doi.org/10.1002/cmr.a.21317.
(191) Bax, Ad.; Summers, M. F. Proton and Carbon-13 Assignments from Sensitivity-Enhanced Detection of Heteronuclear Multiple-Bond Connectivity by 2D Multiple Quantum NMR. *J. Am. Chem. Soc.* **1986**, *108* (8), 2093–2094. https://doi.org/10.1021/ja00268a061.
(192) Reynolds, W. F.; Burns, D. C. Getting the Most Out of HSQC and HMBC Spectra. In *Annual Reports on NMR Spectroscopy*; Elsevier, 2012; Vol. 76, pp 1–21.
(193) Reynolds, W. F.; Enríquez, R. G. Choosing the Best Pulse Sequences, Acquisition Parameters, Postacquisition Processing Strategies, and Probes for Natural Product

Structure Elucidation by NMR Spectroscopy. *J. Nat. Prod.* **2002**, *65* (2), 221–244. https://doi.org/10.1021/np010444o.
(194) Junge, J.; Engesser, T. A.; Krahmer, J.; Näther, C.; Tuczek, F. Rhodium(III) and Ruthenium(II) Complexes with a Pentadentate Tetrapodal Phosphine Ligand. *Z. Anorg. Allg. Chem.* **2021**, *647* (8), 822–831. https://doi.org/10.1002/zaac.202000455.
(195) Welch, C. J. High Throughput Analysis Enables High Throughput Experimentation in Pharmaceutical Process Research. *React. Chem. Eng.* **2019**, *4* (11), 1895–1911. https://doi.org/10.1039/C9RE00234K.
(196) Mennen, S. M.; Alhambra, C.; Allen, C. L.; Barberis, M.; Berritt, S.; Brandt, T. A.; Campbell, A. D.; Castañón, J.; Cherney, A. H.; Christensen, M.; Damon, D. B.; Eugenio de Diego, J.; García-Cerrada, S.; García-Losada, P.; Haro, R.; Janey, J.; Leitch, D. C.; Li, L.; Liu, F.; Lobben, P. C.; MacMillan, D. W. C.; Magano, J.; McInturff, E.; Monfette, S.; Post, R. J.; Schultz, D.; Sitter, B. J.; Stevens, J. M.; Strambeanu, I. I.; Twilton, J.; Wang, K.; Zajac, M. A. The Evolution of High-Throughput Experimentation in Pharmaceutical Development and Perspectives on the Future. *Org. Process Res. Dev.* **2019**, *23* (6), 1213–1242. https://doi.org/10.1021/acs.oprd.9b00140.
(197) Allen, C. L.; Leitch, D. C.; Anson, M. S.; Zajac, M. A. The Power and Accessibility of High-Throughput Methods for Catalysis Research. *Nat. Catal.* **2019**, *2* (1), 2–4. https://doi.org/10.1038/s41929-018-0220-4.
(198) Cook, A.; Clément, R.; Newman, S. G. Reaction Screening in Multiwell Plates: High-Throughput Optimization of a Buchwald–Hartwig Amination. *Nat. Protoc*. **2021**, *16* (2), 1152–1169. https://doi.org/10.1038/s41596-020-00452-7.
(199) Schultz, D.; Campeau, L.-C. Harder, Better, Faster. *Nat. Chem.* **2020**, *12* (8), 661–664. https://doi.org/10.1038/s41557-020-0510-8.

Chapter 2: An experimental evaluation of an open to air, base-free, Pd-catalyzed reaction of enol carboxylates and aryl boronic acids.

This chapter, excluding sections 2.1, and parts of 2.4.1 have been reproduced from a future publication coauthored by: Gaube, G.; Thomas, G.T.; McIndoe, J.S.; Leitch, D.C.

2.1: Preface

Dr. Gilian Thomas contributed ESI-MS data with help from Gregory Gaube. All other experimental and characterization work was conducted by Gregory Gaube.

2.2 Abstract

We report an experimental study of the Pd-catalyzed coupling of enol carboxylates with arylboronic acids, and propose a mechanism involving cationic Pd(II) intermediates. This reaction proceeds under mild conditions in the presence of O_2 and even reactive Pd(0) traps (phenyl triflate). Electrospray ionization mass spectrometry studies using a charge-tagged substrate revealed structural information on key intermediates. We propose an insertion/elimination mechanism operates under these conditions, analogous to oxidative Heck and conjugate addition reactions.

2.3 Introduction

Metal-catalyzed cross-coupling reactions were discovered over 50 years ago,[1] and now serve as one of the most important strategies for forming C–C bonds.[2–4] One of these reactions, the Suzuki-Miyaura coupling, is widely applied in synthesis, and was the subject of the Nobel prize in 2010.[5] This reaction involves the metal-mediated coupling of an organoboron nucleophile and an organohalide electrophile, usually in the presence of a base. Current work on further

developing this transformation focuses on expanding the scope of coupling partners, particularly new classes of electrophile.[6] Aryl and alkenyl carboxylates, based on acetoxy (-OAc) and pivaloyloxy (-OPiv) leaving groups, are of interest as alternatives to halide electrophiles to reduce our reliance on toxic/wasteful halogenation processes.[7] However, selectively activating the desired but stronger aryl or alkenyl C–O bond over the weaker acyl C–O bond has proven difficult.[8] If this hurdle can be overcome through catalyst development, these functional groups provide an economic, less-toxic, and mass efficient alternative that are easily accessible by O-acylation of ketones.[9]

In contrast to the well-established reactivity of allyl and benzyl carboxylates,[10–13] aryl or alkenyl carboxylates are typically considered unreactive in palladium-catalyzed cross-coupling reactions, leading to use of other transition metals.[6] Seminal work using Ni catalysts for aryl carboxylate coupling with organoboron nucleophiles was reported independently by the groups of Shi and Garg in 2008.[14,15] Since then, this methodology has been expanded to alkenyl carboxylates by Kuwano (Rh catalysis),[16] and Shi (Ni catalysis).[17] Alternatively, non-boron organometallics have been used in carboxylate couplings with Fe,[18] Co,[19,20] and Cr[21] based catalysts.

Despite the general notion that Pd catalysis is not suitable for C_{sp2}–O activation (other than with reactive pseudohalide leaving groups), there are several reports to the contrary. Larhead and co-workers disclosed a Pd-catalyzed coupling of vinyl acetate with aryl boronic acids in 2009, generating styrene derivatives through microwave heating.[22] In 2017, the Newman group reported Pd catalyzed synthesis of aryl ketones by coupling benzoate esters and aryl boronic acids, via C(acyl)–O activation.[23] Most recently, the Gunnoe group also used Pd to generate styrenes

through a C–O/C–H activation process.[24–26] Recent works from our group showed that palladium could selectively insert into aryl carboxylate C–O bonds,[8] and that Suzuki-like cross-coupling reactions are possible with a diverse scope of alkenyl carboxylates, even at room temperature open to air.[27] This reactivity was also expanded to Miyaura borylation (Chapter 3),[28,29] and tandem C–O/C–H cross-coupling.[30]

The generally accepted mechanism of the Suzuki reaction involves a Pd(0)/Pd(II) catalytic cycle, with oxidative addition, transmetallation, and reductive elimination steps. We evaluated this pathway for alkenyl carboxylate coupling in our initial publication,[27] isolating an oxidative addition intermediate using PCy_3 supporting ligands and demonstrating that it undergoes direct, base-free transmetallation/reductive elimination (Figure 2.1A). However, we observed oxidative addition requires elevated temperatures and proceeds slowly, which is inconsistent with catalytic conditions. Nevertheless, Zhao, Zhang, and Wang reported a computational study of a Pd(0)/(II) pathway, with catalyst activation through boronic acid-mediated reduction (Figure 2.1B) and turnover limiting oxidative addition.[30] Another recent computational report probed the possibility of Pd(0)/Pd(II) pathways, presenting two potential routes starting with Pd(0).[31]

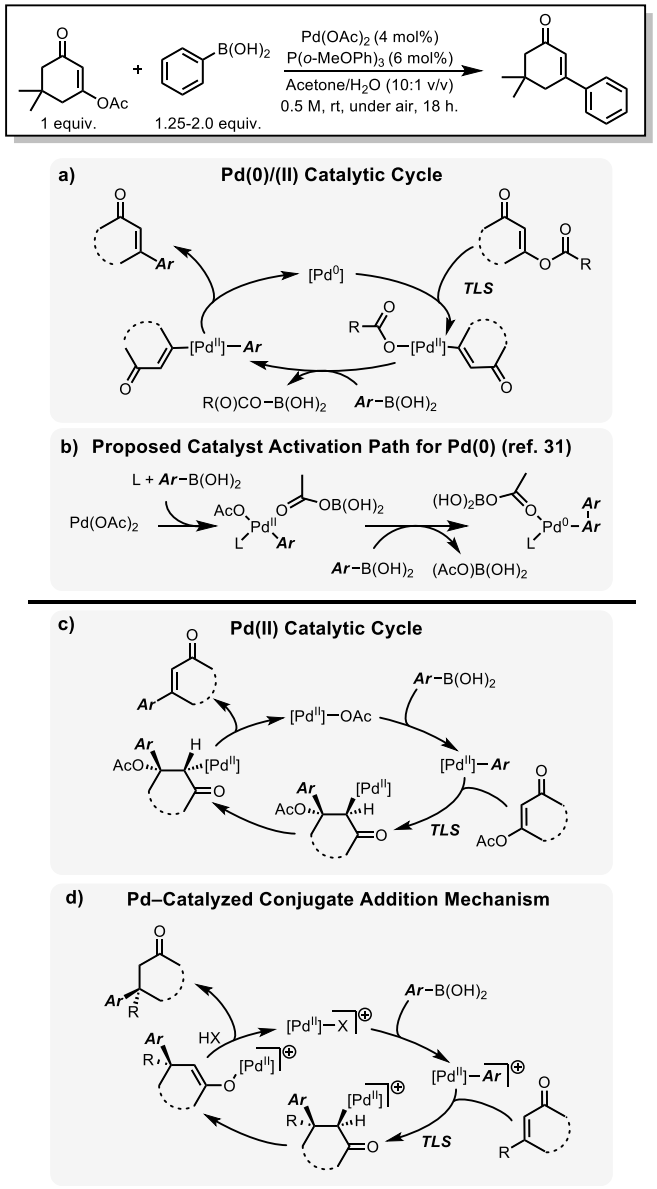

Figure 2.14: Alkenyl carboxylate coupling and potential mechanisms, A) 'Typical' Pd(0)/(II) pathway with turnover-limiting oxidative addition. B) Proposed reduction pathway for $Pd(OAc)_2$ involving double transmetallation and reductive elimination. C) Redox-neutral mechanism with turnover-limiting C=C insertion. D) Established Pd-catalyzed conjugate addition mechanism involving cationic Pd(II) intermediates.

Based on our initial observations, at the time we proposed a redox-neutral Pd(II) catalytic cycle (Figure 2.1C). This alternative pathway begins with transmetallation to generate a Pd(II) aryl species. *Syn*-carbopalladation with the alkenyl carboxylate then produces a Pd-enolate, which undergoes stereochemical inversion to bring the Pd and OAc group into a *syn* arrangement before

β-acetoxy elimination. While we did not speculate at the time, this proposed pathway could proceed through cationic Pd(II) intermediates, analogous to Pd-catalyzed oxidative Heck reactions,[32] and conjugate addition reactions (Figure 2.1D),[33] with the latter studied in detail by Houk, Stoltz, and co-workers.[34]

2.4 Results and Discussion

2.4.1 Preliminary Studies

Preliminary studies began with evaluating additional boronic acids outside the scope of the Leitch Lab's original publication (Figure 2.2).[27] We believed it was crucial to evaluate functional groups at all locations around the phenyl group of the boronic acid because the difference in electronic and steric nature could drastically affect reactivity. The reported reactions were found to be complete well before the 18 hour duration, therefore these reactions were monitored at three timepoints: 30 minutes, 2 hours, and 18 hours.

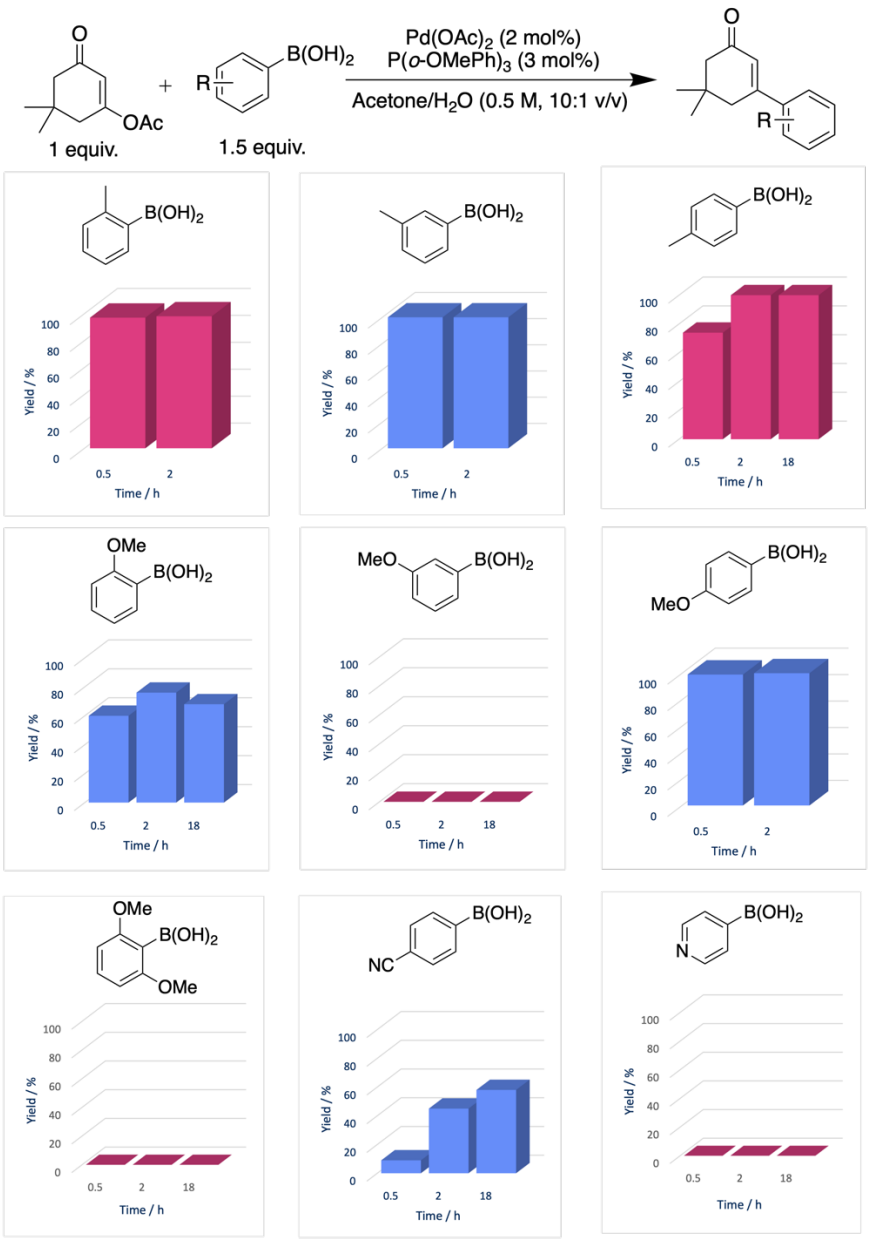

Figure 2.2: Monitoring of reactions between enol carboxylates and assorted aryl boronic acids. ^{1}H NMR solution yields determined using 1,3,5-trimethoxybenzene as internal standard.

Interestingly, the less sterically hindered *para*-tolylboronic acid was the slowest of the tolyl derivatives to finish reacting. The *ortho*- and *meta*- derivatives were essentially complete at the first time-point. For the methoxyphenyl boronic acids, the *para*-derivative was complete at the first time-point, the *ortho*-derivative plateaued without full conversion, and the *meta*-

derivative did not produce product at all. This strongly resonance donating functional group (an *ortho*/*para* director in EArS chemistry) may aid in the reaction when in the *ortho* or *para* position. But with unsuitable placement on the ring, the desired reactivity may be hindered because of the inductively electron-withdrawing ability of this functional group. The *ortho*-methoxyphenylboronic acid reactivity contrasted to the 2,6-dimethoxyphenylboronic acid, which did not produce product. The additional steric hindrance may have contributed to this reactivity pattern. Finally, nitrogen containing boronic acids were evaluated. *Para*-pyridineboronic acid yielded no product, which could be due to the lone pairs on the nitrogen competitively reacting with the metal center, or it could be due to the electron-poor nature of the aryl group. Finally, 4-cyanophenylboronic acid was slow to react, and we were able to monitor the reaction proceeding over 18 hours. The electron withdrawing nature of this functional group is the likely cause of the slow reactivity, consistent with the prior observations.

In our original report, a Pd : ligand ratio of 1 : 1.5 was used; this was empirically determined, and we sought to evaluate this ligand concentration in a similar manner as the nature of the boronic acid. Intriguingly, between 0.5 – 1.5 equivalents of ligand, the reaction was close to complete at the first time point evaluated (Figure 2.3). However, at 2 and 2.5 equivalents, the initial reactivity drops off substantially, but in both cases by 18 hours the overall reactivity is unperturbed. This may be due to phosphine oxide forming over time in the open-to-air system. The continuous generation of phosphine oxide will eventually lower the concentration of phosphine ligand accessible to the Pd center to the desired ligand ratio for reactivity. Without ligand this reaction is not productive, but under 2 equivalents (to Pd) we observe the desired

reactivity. These observations are consistent with a mono-phosphine Pd species as active, as we see detrimental reactivity under conditions that would favour a doubly ligated Pd center.

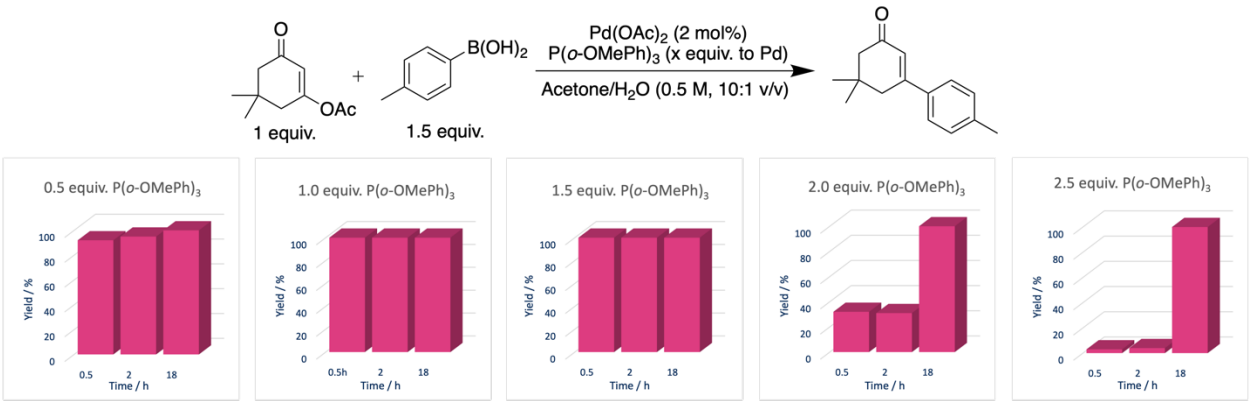

Figure 2.3: Monitoring of reactions between enol carboxylates and 4-tolylboronic acid with varying ligand concentrations. ^{1}H NMR solution yields determined using 1,3,5-trimethoxybenzene as internal standard.

As these reactions proceeded open to air, the nature of this relationship between atmosphere and Pd reactivity was then explored (Table 2.1). We found in all cases, regardless of solvent, reactions conducted open to air outperformed those under a N_2 atmosphere at room temperature. In reactions with $Pd(PCy_3)_2$, a Pd(0) source that readily oxidizes to Pd(II) when exposed to air, the same pattern was observed.

Table 2.1: Reactions between enol carboxylates and phenylboronic acid with varying solvents and atmospheres. ^1H NMR solution yields determined using 1,3,5-trimethoxybenzene as internal standard.

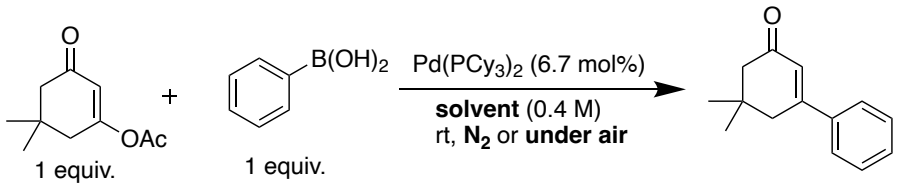

Entry	Solvent	Atmosphere	**a** yield / %
1	THF	N_2	33
2	THF	open	39
3	d-benzene	N_2	12
4	d-benzene	open	25
5	d-acetone	N_2	62
6	d-acetone	open	84

We then explored the possibility of aryl halides providing a competing reaction pathway. If this reaction indeed proceeded through a Pd(0)/Pd(II) reaction mechanism, one would expect competitive reactivity with aryl halides present within the system. Both the enol carboxylate and the phenylboronic acid were functionalized with a respective aryl halide. In reactions with or without a halogenated phenylboronic acid, the functionalized enol carboxylate still performed the desired reaction, albeit with lower yields (Table 2.2). Importantly, we observe no evidence of reaction at the Ar-X units. The previous report found improved isolated yields by utilizing an alternative solvent (toluene), but the reaction was still conducted open to air.[27]

Table 2.2: Reactions between functionalized enol carboxylate and phenylboronic acid or 3-chlorophenylboronic acid.

^{1}H NMR solution yields and conversion determined using 1,3,5-trimethoxybenzene as internal standard.

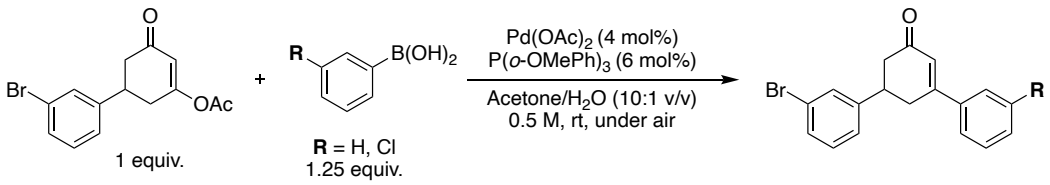

Entry	R	yield / %	conversion / %
1	H	17	39
2	Cl	29	54

Attention was then turned to address the nature of the Pd center. We hypothesized that an arylated Pd center would turn-over in the presence of the enol carboxylate to produce product. The arylated Pd center was produced by reacting phenyl triflate with $Pd(PCy_3)_2$ (Equation 2.1). This Pd center could also be produced by oxidative addition of $Pd(PCy_3)_2$ with bromobenzene followed by a ligand exchange using Ag(OTf) (Appendix A, Section A2). Our hypothesis proved false, as no product was produced when the enol carboxylate was introduced to the system containing the arylated Pd center. Interestingly though, with the addition of both enol carboxylate and phenylboronic acid, the reaction was productive. This leads us to believe that the boronic acid functional group is critical to this reaction. It could either serve as a reducing agent to generate Pd(0) in a traditional mechanism, or help to generate a Pd(II) cation by acting as a Lewis acid in a Pd(II)-only mechanism.

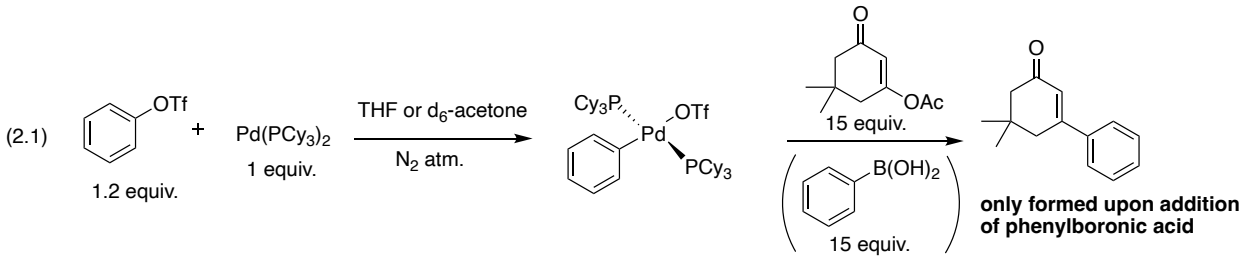

2.4.2 Analysis of Pd(II) vs Pd(0)/Pd(II) Mechanisms

Given the feasibility of both mechanistic types, especially in light of the reported computational studies,[30,31] and our own proposals of Pd(0)/(II) mechanisms in related reactions,[28,] we sought to assess the feasibility of a Pd(0) pathway. We assessed a number of catalyst systems for their ability to generate both the coupling product (**3a**) and biphenyl (**4**) as a byproduct (Table 2.3 – additional data in Appendix A, Table A1). Biphenyl, as proposed by Zhao, Zhang, and Wang, would be generated upon reduction of Pd(II), which may indicate a Pd(0)/(II) pathway. Reactions were conducted under previously reported conditions, open to air at room temperature in a mixed acetone/water solvent system.

Table 2.3: Reactions between an enol carboxylate, phenyl boronic acid and various Pd precatalysts.

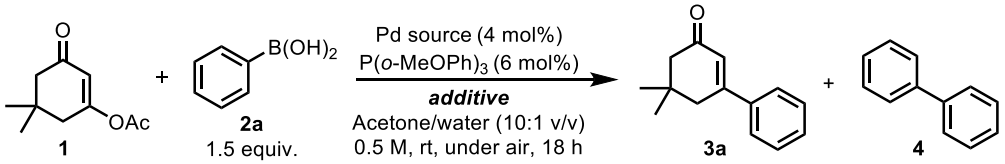

Entry	Pd Source	Additive	3a[a]	4[b]
1[c]	$Pd(OAc)_2$	-	29	3
2	$Pd(OAc)_2$	-	63	9
3	$Pd(OAc)_2$	PhOTf[d]	79	11
4	$[Pd(P(o\text{-}MeOPh)_3)(\mu\text{-}OAc)(Ph)]_2$	-	87	6
5	$Pd_2dba_3 \bullet CHCl_3$	-	66	13
6[d]	$Pd(OAc)_2$	-	0	5
7[e]	$Pd(OAc)_2$	-	-	7
8	none	-	0	0

*[a]Yields of **3a** are obtained by ^1H NMR spectroscopy by relative integration vs. internal standard, 1,3,5-trimethoxybenzene (TMB). [b]Yields of **4** are obtained by GCMS analysis by comparison to a calibration curve generated using authentic **4**. [c]1 hour reaction time. [d]No P(o-MeOPh)$_3$ added. [e]No **1** added.*

Under standard conditions, we observe the formation of **3a**, with 29% formed after 1 h and 63% after 18 h. Alongside this cross-coupling product, we do observe **4** in small but significant amounts (entries 1-2). This is consistent with reduction of Pd(II) by 2, generating **4** by oxidative homocoupling. To further probe the catalytic efficacy of an *in situ* generated Pd(0) species, we added 1 equiv of phenyl triflate (PhOTf) as a Pd(0) trapping reagent (entry 3). PhOTf should undergo rapid oxidative addition to Pd(0),[36] especially relative to the enol acetate, serving as a competitive inhibitor. This should slow/shut down the enol acetate cross-coupling, and/or produce significantly more biphenyl through competitive Suzuki coupling. To our surprise, PhOTf has essentially no effect, with both **3a** (79%) and **4** (11%) formed as observed with no PhOTf. We also tested the possibility of direct Suzuki coupling between **2** and PhOTf under the same reaction conditions, and observe <10% biphenyl. Furthermore, $[Pd(P(o\text{-}MeOPh)_3)(\mu\text{-}OAc)(Ph)]_2$,[37] which

has a bridging acetate X-type ligand, gives 87% of the cross-coupled product **3a**, along with ~6% of **4**.

The persistent formation of biphenyl as a byproduct led us to examine the use of a Pd(0) source. With $Pd_2dba_3 \bullet CHCl_3$ replacing $Pd(OAc)_2$, we observe essentially identical results, including the formation of biphenyl (entry 5), despite the fact that no oxidative homocoupling would be required to reduce Pd(II) to Pd(0). Notably, we also observe biphenyl as a byproduct when $Pd(OAc)_2$ is used without added phosphine, though there is no cross-coupling reactivity (entry 6). Biphenyl is also generated in the absence of enol acetate **1** (entry 7),[38] but neither **3a** or **4** are observed with no added Pd (entry 8).

While these experiments do confirm the presence of biphenyl, which is consistent with Pd(0) formation as proposed by Zhao, Zhang, and Wang,[30] the retention of catalytic activity in the presence of PhOTf led us to consider that a cationic Pd(II) mechanism could still be operative. Attempts to probe catalyst speciation by ^{31}P NMR spectroscopy were inconclusive; therefore, we used electrospray ionization mass spectrometry (ESI-MS) with a charge-tagged arylboronic acid to explore potential reaction intermediates.[39] This technique was chosen because it softly ionizes reaction intermediates resulting in minimal fragmentation. For these studies, a charge-tagged boronic acid was implemented to aid in the identification of low concentration species.

The reaction was probed both sequential addition and in a single pot method. However, specific speciation was elucidated through sequential addition. These studies were conducted in the order of Pd, ligand, boronic acid and alkenyl carboxylate (Full reaction scheme for ESI-MS experiments: Equation 2.2).

(2.2)

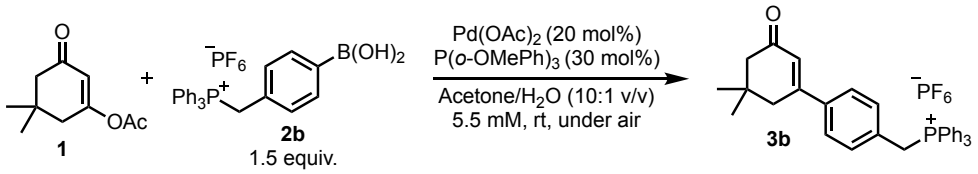

When $Pd(OAc)_2$ was mixed with 1.5 equivalents of P(*o*-OMePh)$_3$ in 10:1 (v/v) acetone/H_2O solution, we observed a singly-charged double-ligated Pd species with a single acetate (Figure 2.4).

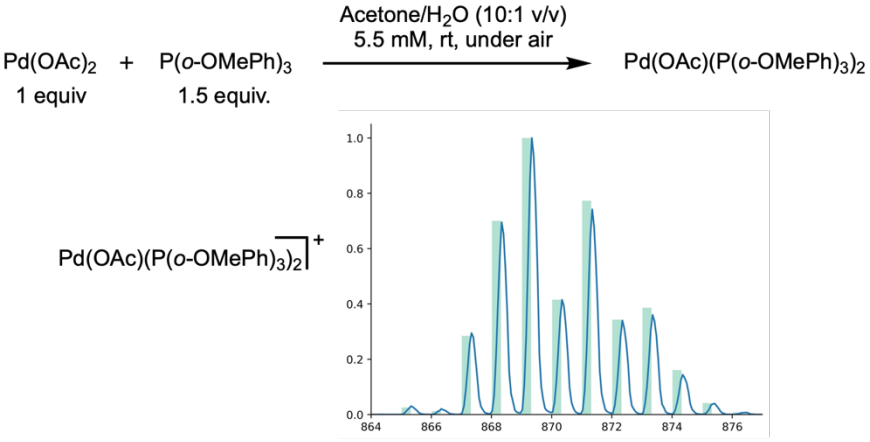

Figure 2.4: Sequential addition of P(o-OMePh)$_3$ to solution containing $Pd(OAc)_2$. Observed (trace) and calculated (bars) m/z isotope patterns.

Upon addition of the aryl boronic acid, the single acetate group was replaced with the aryl group producing a double charged Pd species (Figure 2.5), likely forming $(AcO)B(OH)_2$ as a result. When the boronic acid and alkenyl carboxylate were switched, we found that after the addition of alkenyl carboxylate the reaction did not proceed considerably, likely because an oxidative addition of these substrates have been seen to require elevated temperatures.[8] Only with the addition of the boronic acid did we observe a significant change in speciation.

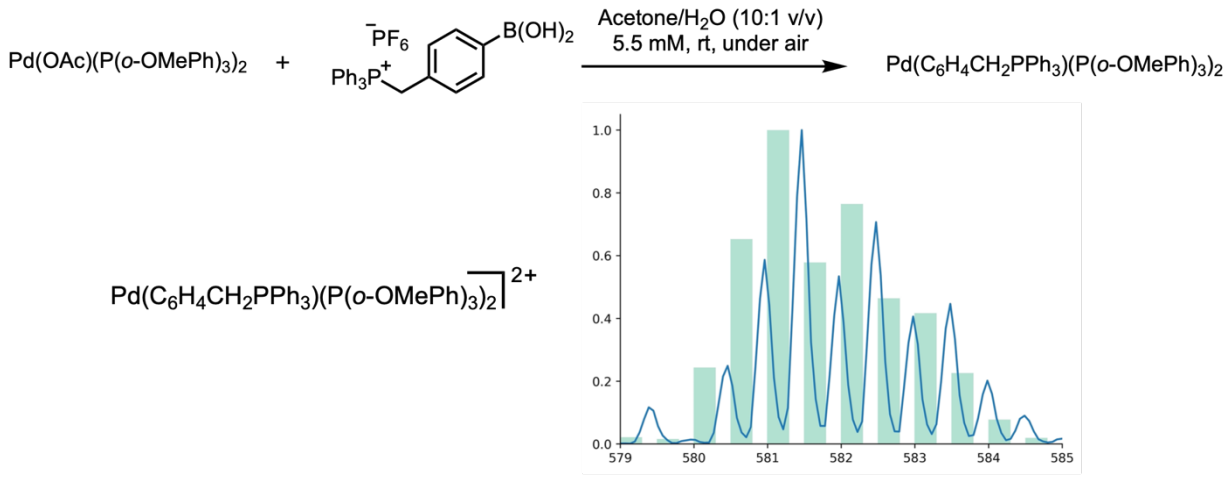

Figure 2.5: Sequential addition of a charge-tagged aryl boronic acid to a solution containing $Pd(OAc)_2$ and P(o-$OMePh)_3$. Observed (trace) and calculated (bars) m/z isotope patterns.

When the alkenyl carboxylate was added we observed the doubly charged singly-ligated Pd species bound to an alkenyl carboxylate and an aryl group (Figure 2.6a), we did not observe the single charged version of this complex. This structure was verified by using collision induced dissociation (CID) where a low voltage (5V) was applied. We observe dissociation of the alkenyl carboxylate to generate a doubly charged, mono-phosphine Pd aryl species (Figure 2.6b).

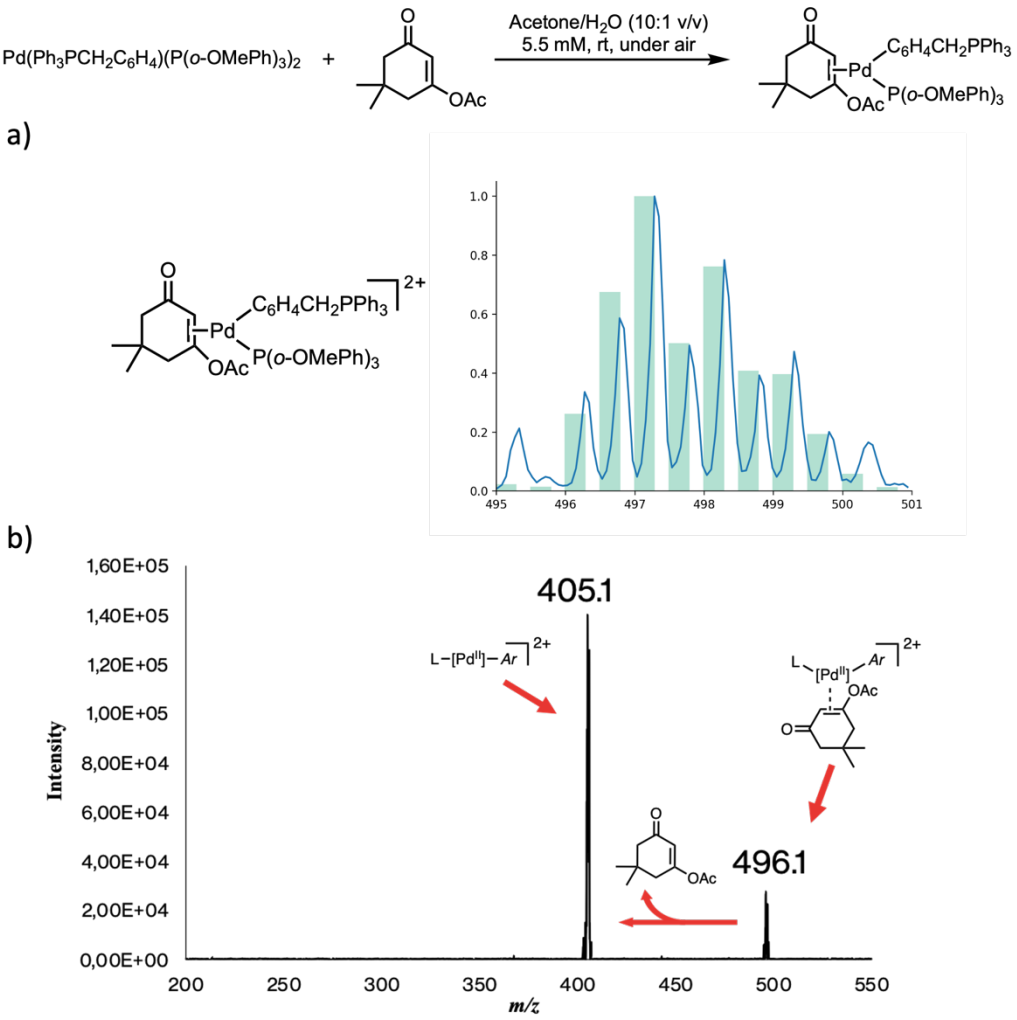

Figure 2.6: a) Sequential addition of an enol carboxylate to a solution containing $Pd(OAc)_2$, $P(o\text{-}OMePh)_3$, and a charge-tagged aryl boronic acid. Observed (trace) and calculated (bars) m/z isotope patterns. b) Collision induced dissociation of the formed intermediate.

These findings allow us to propose a new catalytic cycle (Figure 2.7) where $Pd(OAc)_2$ coordinates two phosphines, replacing a single acetate (**I.**), followed by the boronic acid transmetalating to remove the acetate (**II.**). This compound then coordinates to the alkene of the alkenyl carboxylate (**III.**), before *syn*-carbopalladation to produce a C-bound Pd-enolate (**IV.**). This then epimerizes to bring the Pd and OAc group into *syn* conformation (**IV'.**), which then eliminates to close the catalytic cycle. We believe that the turnover limiting steps are the coordination and

syn-carbopalladation to the alkene, because the short-lived species **IV** and **IV'** were not observed in the ESI-MS analysis.

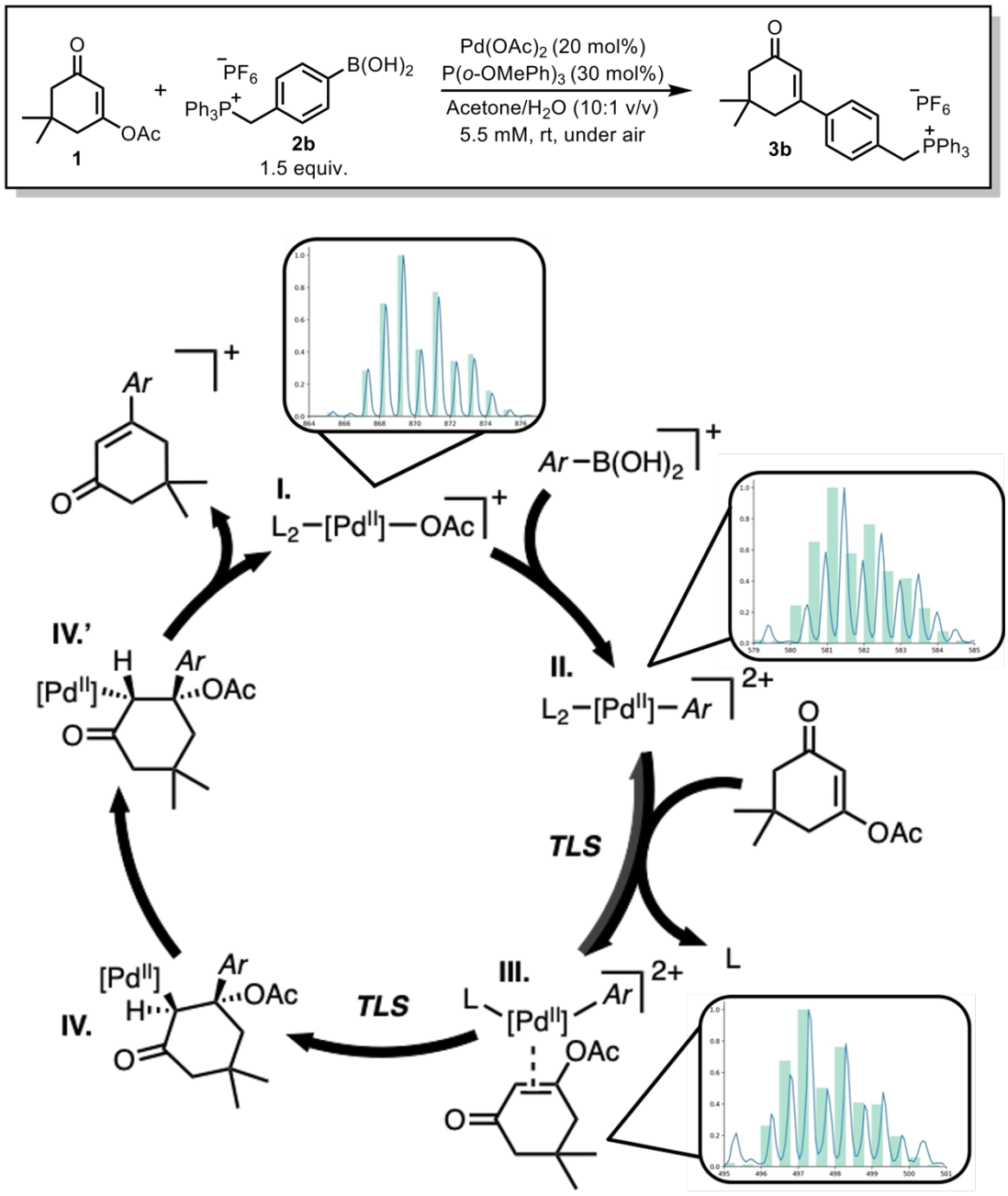

Figure 2.7: Proposed cationic Pd(II) cycle with observed (trace) and calculated (bars) m/z isotope patterns.

2.5 Conclusion

In conclusion, we have proposed a cationic Pd(II) only catalytic cycle for a base-free, open to air, palladium cross-coupling reaction through the use of hetero-nuclear NMR and *in situ* ESI-MS. While the computationally-proposed Pd(0)/(II) could be occurring,[30] we have shown experimental evidence of an alternative pathway that we believe dominates reactivity. Using this mechanistic information to guide decisions on expanding the substrate scope and designing new Pd catalysts is ongoing within our group.

2.6 Experimental

2.6.1 General Considerations

All solvents and common organic reagents were purchased from commercial suppliers and used without further purification. $Pd(OAc)_2$ and $Pd(PCy_3)_2$ was purchased from Strem Chemicals and used as received. PdPhBr(P(*o*-OMePh)$_3$) and [PdPh(μ-OAc)(P(*o*-OMePh)$_3$)]$_2$ were prepared according to literature.[37] Pd_2dba_3•$CHCl_3$ was prepared using the Zalesskiy and Ananikov method.[40] Phenyl trifluoromethanesulfonate was synthesized using literature procedures,[41] and characterized.[42] 5,5-dimethyl-3-oxocyclohex-1-en-1-yl acetate,[43] (4-Boronobenzyl)triphenylphosphonium hexafluorophosphate,[39] and 3'-bromo-5-oxo-1,2,5,6-tetrahydro-[1,1'-biphenyl]-3-yl acetate[27] were synthesized using literature procedures. All phosphine ligands were purchased from Strem Chemicals and used as received. Anhydrous solvents (SureSeal) were purchased from MilliporeSigma and used as received.

Isotope patterns were simulated using ChemCalc free-to-use software (chemcalc.org),[44] and were overlayed with the experimental data.

All air-free manipulations were performed under a dry nitrogen atmosphere using an MBraun glovebox.

All NMR spectra were acquired on either a Bruker AVANCE 300 MHz spectrometer or a Bruker AVANCE Neo 500 MHz spectrometer. All ^{1}H and ^{13}C NMR chemical shifts are calibrated to residual protio-solvents and all ^{31}P NMR chemical shifts are calibrated to external standards. All NMR spectroscopic data is processed using Bruker TopSpin 4.07.

Gas-Chromatography Mass-Spectrometry (GC-MS) analysis was conducted on a Finnigan Trace GC Ultra with DSQ mass spectrometer.

Electrospray-Ionization Mass-Spectrometry (ESI-MS) analysis was conducted on a Waters Acquity triple quadrupole detector. The capillary voltage was held at 3 kV, cone voltage at 13 V, extraction cone voltage at 2 V, and RF lens at 0.3 V. The desolvation gas flow rate 150 L/h, cone gas flow 150 L/h, source temperature 70 °C, desolvation temperature 150 °C. The mass range was set to *m/z* 50-1200; scan duration was 1 second; LM and HM resolution were set to 15.0. The mass range was narrowed and the LM and HM resolutions increased to 17.0 to obtain isotope pattern information.

2.6.2 Preliminary Studies

Monitoring of reactions with various arylboronic acids:

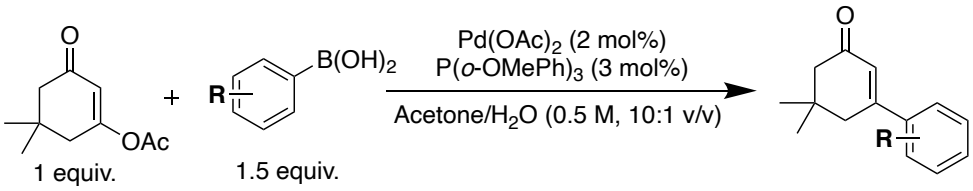

A 1-dram vial was charged with 5,5-dimethyl-3-oxocyclohex-1-en-1-yl acetate (0.60 mmol, 109.0 mg), aryl boronic acid (0.90 mmol), $Pd(OAc)_2$ (0.012 mmol, 2.7 mg), P(*o*-OMePh)$_3$ (0.018

mmol, 6.3 mg) and 1,3,5-trimethoxybenzene (0.06 mmol, 10.1 mg). 1.2 ml of 10:1 (v/v) Acetone/H_2O was added to each vial and the solution was allowed to stir (500 rpm) at room temperature. At 0.5 h, 2 h, and 18 h 0.4 ml of the reaction solution was removed to a separate vial and dried immediately using a Genevac EZ-2 (Aqueous setting, 45C). Yield was determined using ^{1}H-NMR in $CDCl_3$ with 1,3,5-trimethoxybenzene as an internal standard: 1-(2'-tolyl)-5,5-dimethylcyclohex-1-en-3-one,[45] 1-(3'-tolyl)-5,5-dimethylcyclohex-1-en-3-one,[45] 1-(4'-tolyl)-5,5-dimethylcyclohex-1-en-3-one,[45] 1-(2'-methoxyphenyl)-5,5-dimethylcyclohex-1-en-3-one,[27] 1-(3'-methoxyphenyl)-5,5-dimethylcyclohex-1-en-3-one,[45] 1-(4'-methoxyphenyl)-5,5-dimethylcyclohex-1-en-3-one.[45]

1-(4'-cyanophenyl)-5,5-dimethylcyclohex-1-en-3-one:

A 1-dram vial was charged with 5,5-dimethyl-3-oxocyclohex-1-en-1-yl acetate (0.64 mmol, 116.3 mg), 4-cyanophenyl boronic acid (0.96 mmol, 140.7 mg), $Pd(OAc)_2$ (0.013 mmol, 2.9 mg), and P(*o*-OMePh)$_3$ (0.019 mmol, 6.7 mg). 1.2 ml of 10:1 (v/v) Acetone/H_2O was added to the vial and the solution was allowed to stir (500 rpm) at room temperature overnight. The compound was isolated using a Biotage Selekt instrument with a hexanes/ethyl acetate gradient (0 – 40%, eluting at 30%).

^{1}H NMR (500 MHz, $CDCl_3$, 292 K, ppm): δ 7.69 – 7.65 (m, 2H), 7.61 – 7.56 (m, 2H), 6.38 (t, J = 1.5 Hz, 1H), 2.60 (d, J = 1.5 Hz, 2H), 2.33 (s, 2H), 1.11 (s, 6H). ^{13}C NMR (126 MHz, $CDCl_3$, 292 K, ppm): δ 199.48, 155.18, 143.56, 132.51, 126.80, 126.34, 118.32, 113.20, 50.85, 42.10, 33.83, 28.32. HRMS: Calc'd for $C_{15}H_{15}NO$ [M+H]+: 226.12264; found: 226.12270.

Monitoring of reaction with varying ligand concentrations:

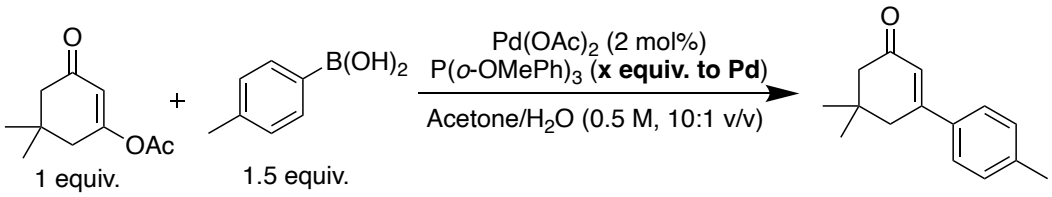

A 1-dram vial was charged with 5,5-dimethyl-3-oxocyclohex-1-en-1-yl acetate (0.60 mmol, 109.0 mg), 4-tolylboronic acid (0.90 mmol, 122.0 mg), $Pd(OAc)_2$ (0.012 mmol, 2.7 mg), P(*o*-OMePh)$_3$ (0.006 mmol, 2.1 mg; 0.012 mmol, 4.2 mg; 0.018 mmol, 6.3 mg; 0.024 mmol, 8.4 mg; or 0.030 mmol, 10.5 mg) and 1,3,5-trimethoxybenzene (0.06 mmol, 10.1 mg). 1.2 ml of 10:1 (v/v) Acetone/H_2O was added to each vial and the solution was allowed to stir (500 rpm) at room temperature. At 0.5 h, 2 h, and 18 h 0.4 ml of the reaction solution was removed to a separate vial and dried immediately using a Genevac EZ-2 (Aqueous setting, 45C). Yield was determined using ^{1}H-NMR in $CDCl_3$ with 1,3,5-trimethoxybenzene as an internal standard. [45]

Open to air vs inert atmosphere reactions:

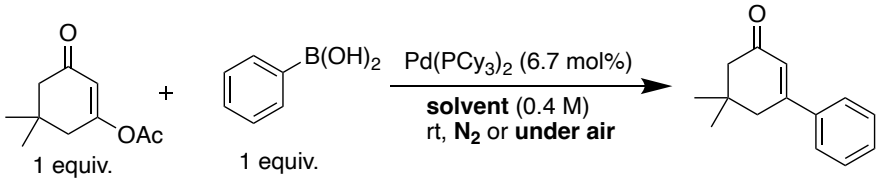

In an air-free environment a NMR tube* was charged with 5,5-dimethyl-3-oxocyclohex-1-en-1-yl acetate (41.0 mg, 0.22 mmol), phenyl boronic acid (27.4 mg, 0.22 mmol), $Pd(PCy_3)_2$ (10.0 mg, 0.015 mol, 6.7 mol%), and **solvent** (0.4 M) (Table 2.1). The tube was either sealed and brought out of the glovebox or brought out of the glovebox and opened to expose the contents to air (Table 2.1). After 18 hours, the yield was determined using ^{1}H-NMR in $CDCl_3$ with 1,3,5-trimethoxybenzene as an internal standard.[27]

*J-young tubes used for N_2 atmosphere reactions.

Competing oxidative addition pathways:

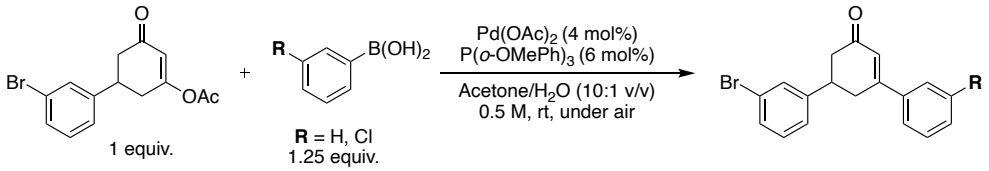

A 1-dram vial was charged with 3'-bromo-5-oxo-1,2,5,6-tetrahydro-[1,1'-biphenyl]-3-yl acetate (100.0 mg, 0.32 mmol), (3-chloro)phenyl boronic acid (0.40 mmol), $Pd(OAc)_2$ (2.9 mg, 0.013 mmol), P(*o*-OMePh)$_3$ (6.8 mg. 0.019 mmol), and 10:1 acetone/water (v/v) (0.5 M). The vial was capped and allowed to stir at room temperature for 18 h. The reaction was dried on a Genevac EZ-2 (Low BP, 30 °C) before yield was determined using ^{1}H-NMR in $CDCl_3$ with 1,3,5-trimethoxybenzene as an internal standard.[27]

Air-free chemistry:

All reactions were performed air-free, as detailed in Section 2.6.1.

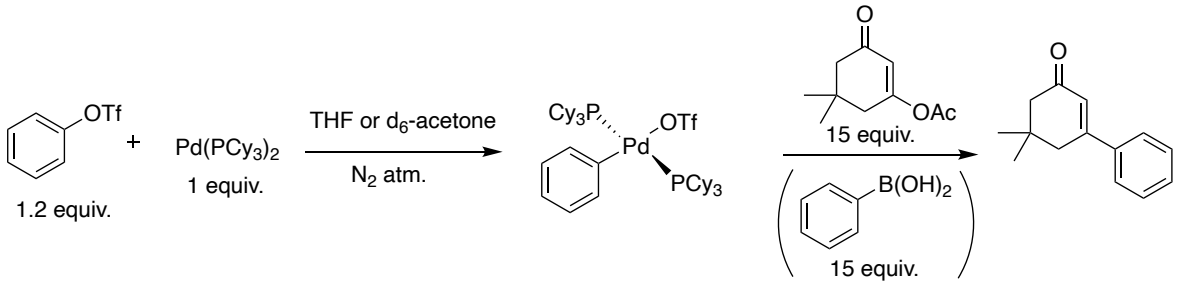

A J-young tube was charged with phenyl triflate (4.1 mg, 0.018 mol) and $Pd(PCy_3)_2$ (10.0 mg, 0.015 mol) in both THF and d-acetone (0.6 ml, 0.4 M). Subsequently 5,5-dimethyl-3-oxocyclohex-1-en-1-yl acetate (41.0 mg, 0.22 mol) and (if desired) phenyl boronic acid (27.4 mg, 0.22 mol) were added to the J-young tube in an air-free setting and monitored over 18 h. Product was only observed in reaction with phenyl boronic acid present.

2.6.3 Analysis of Pd(II) vs Pd(0)/Pd(II) Mechanisms

Monitoring of biphenyl (GC-MS):

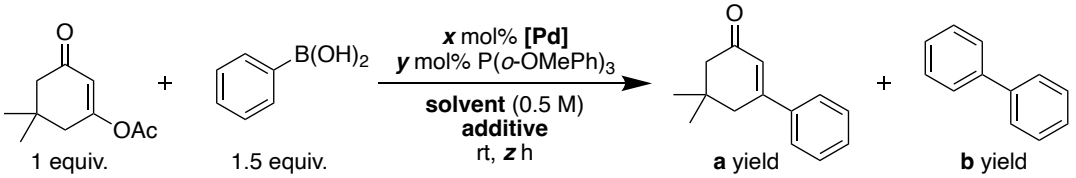

A 1-dram vial was charged with 5,5-dimethyl-3-oxocyclohex-1-en-1-yl acetate (50.0 mg, 0.27 mmol), phenyl boronic acid (50.2 mg, 0.41 mmol), [Palladium] (**x** mol%), P(*o*-OMePh)$_3$ (**y** mol%), **additive** and **solvent** (0.5 M). The vial was capped and allowed to stir for **z** h. At the appropriate time, an aliquot was taken for GC-MS analysis to determine the yield of **b** and the reaction was dried on a Genevac EZ-2 (Low BP, 30 °C) before yield of **a** was determined using ^{1}H-NMR in $CDCl_3$ with 1,3,5-trimethoxybenzene as an internal standard.

Electrospray Ionization Mass Spectrometry (ESI-MS):

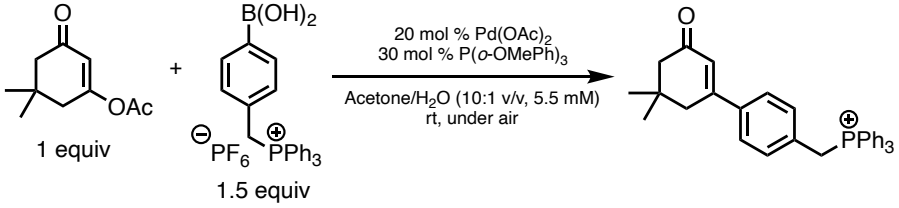

To a stirred solution of $Pd(OAc)_2$ (2.5 mg, 0.011 mmol) in 7.0 mL solvent (10:1 acetone/water (v/v)), sequentially the following was added: P(*o*-OMePh)$_3$ (5.8 mg, 0.017 mmol) in 1 mL solvent, (4-boronobenzyl)triphenylphosphonium hexafluorophosphate (44.6 mg, 0.082 mmol) in 1 mL solvent, and finally 5,5-dimethyl-3-oxocyclohex-1-en-1-yl acetate (10.0 mg, 0.055 mmol) in 1 mL solvent to obtain a final concentration of 5.5 mM in alkenyl carboxylate. Additions were only completed when new speciation formation had plateaued. Specific species (see

Appendix A, Figure A3 for example) were subject to collision induced dissociation (CID) to aid in identification.

2.7 References

(1) Campeau, L.-C.; Hazari, N. Cross-Coupling and Related Reactions: Connecting Past Success to the Development of New Reactions for the Future. *Organometallics* **2019**, *38* (1), 3–35. https://doi.org/10.1021/acs.organomet.8b00720.

(2) Magano, J.; Dunetz, J. R. Large-Scale Applications of Transition Metal-Catalyzed Couplings for the Synthesis of Pharmaceuticals. *Chem. Rev.* **2011**, *111* (3), 2177–2250. https://doi.org/10.1021/cr100346g.

(3) Gildner, P. G.; Colacot, T. J. Reactions of the 21st Century: Two Decades of Innovative Catalyst Design for Palladium-Catalyzed Cross-Couplings. *Organometallics* **2015**, *34* (23), 5497–5508. https://doi.org/10.1021/acs.organomet.5b00567.

(4) Firsan, S. J.; Sivakumar, V.; Colacot, T. J. Emerging Trends in Cross-Coupling: Twelve-Electron-Based L_1Pd(0) Catalysts, Their Mechanism of Action, and Selected Applications. *Chem. Rev.* **2022**, *122* (23), 16983–17027. https://doi.org/10.1021/acs.chemrev.2c00204.

(5) Johansson Seechurn, C. C. C.; Kitching, M. O.; Colacot, T. J.; Snieckus, V. Palladium-Catalyzed Cross-Coupling: A Historical Contextual Perspective to the 2010 Nobel Prize. *Angew. Chem Int. Ed.* **2012**, *51* (21), 5062–5085. https://doi.org/10.1002/anie.201107017.

(6) Zhou, T.; Szostak, M. Palladium-Catalyzed Cross-Couplings by C–O Bond Activation. *Catal. Sci. Technol.* **2020**, *10* (17), 5702–5739. https://doi.org/10.1039/D0CY01159B.

(7) Anastas, P. T.; Warner, J. C. Green Chemistry: Theory and Practice; Oxford University Press: New York, 1998; p 30.

(8) Becica, J.; Gaube, G.; A. Sabbers, W.; C. Leitch, D. Oxidative Addition of Activated Aryl-Carboxylates to Pd(0): Divergent Reactivity Dependant on Temperature and Structure. *Dalton Trans.* **2020**, *49* (45), 16067–16071. https://doi.org/10.1039/D0DT01119C.

(9) Kinuta, H.; Hasegawa, J.; Tobisu, M.; Chatani, N. Rhodium-Catalyzed Borylation of Aryl and Alkenyl Pivalates through the Cleavage of Carbon–Oxygen Bonds. *Chem. Lett.* **2015**, *44* (3), 366–368. https://doi.org/10.1246/cl.141084.

(10) Tsuji, J.; Takahashi, H.; Morikawa, M. Organic Syntheses by Means of Noble Metal Compounds XVII. Reaction of π-Allylpalladium Chloride with Nucleophiles. *Tetrahedron Lett.* **1965**, *6* (49), 4387–4388. https://doi.org/10.1016/S0040-4039(00)71674-1.

(11) Trost, B. M.; Fullerton, T. J. New Synthetic Reactions. Allylic Alkylation. *J. Am. Chem. Soc.* **1973**, *95* (1), 292–294. https://doi.org/10.1021/ja00782a080.

(12) Trost, B. M.; Van Vranken, D. L. Asymmetric Transition Metal-Catalyzed Allylic Alkylations. *Chem. Rev.* **1996**, *96* (1), 395–422. https://doi.org/10.1021/cr9409804.

(13) Trost, B. M.; Crawley, M. L. Asymmetric Transition-Metal-Catalyzed Allylic Alkylations: Applications in Total Synthesis. *Chem. Rev.* **2003**, *103* (8), 2921–2944. https://doi.org/10.1021/cr020027w.

(14) Quasdorf, K. W.; Tian, X.; Garg, N. K. Cross-Coupling Reactions of Aryl Pivalates with Boronic Acids. *J. Am. Chem. Soc.* **2008**, *130* (44), 14422–14423. https://doi.org/10.1021/ja806244b.

(15) Guan, B.-T.; Wang, Y.; Li, B.-J.; Yu, D.-G.; Shi, Z.-J. Biaryl Construction via Ni-Catalyzed C−O Activation of Phenolic Carboxylates. *J. Am. Chem. Soc.* **2008**, *130* (44), 14468–14470. https://doi.org/10.1021/ja8056503.

(16) Yu, J.-Y.; Kuwano, R. Rhodium-Catalyzed Cross-Coupling of Organoboron Compounds with Vinyl Acetate. *Angew. Chem. Int. Ed.* **2009**, *48* (39), 7217–7220. https://doi.org/10.1002/anie.200903146.
(17) Sun, C.-L.; Wang, Y.; Zhou, X.; Wu, Z.-H.; Li, B.-J.; Guan, B.-T.; Shi, Z.-J. Construction of Polysubstituted Olefins through Ni-Catalyzed Direct Activation of Alkenyl C-O of Substituted Alkenyl Acetates. *Chem. Eur. J.* **2010**, *16* (20), 5844–5847. https://doi.org/10.1002/chem.200902785.
(18) Gärtner, D.; Stein, A. L.; Grupe, S.; Arp, J.; Jacobi von Wangelin, A. Iron-Catalyzed Cross-Coupling of Alkenyl Acetates. *Angew. Chem. Int. Ed.* **2015**, *54* (36), 10545–10549. https://doi.org/10.1002/anie.201504524.
(19) Moselage, M.; Sauermann, N.; Richter, S. C.; Ackermann, L. C-H Alkenylations with Alkenyl Acetates, Phosphates, Carbonates, and Carbamates by Cobalt Catalysis at 23 °C. *Angew. Chem. Int. Ed.* **2015**, *54* (21), 6352–6355. https://doi.org/10.1002/anie.201412319.
(20) Li, J.; Knochel, P. Cobalt-Catalyzed Cross-Couplings between Alkenyl Acetates and Aryl or Alkenyl Zinc Pivalates. *Angew. Chem. Int. Ed.* **2018**, *57* (35), 11436–11440. https://doi.org/10.1002/anie.201805486.
(21) Li, J.; Ren, Q.; Cheng, X.; Karaghiosoff, K.; Knochel, P. Chromium(II)-Catalyzed Diastereoselective and Chemoselective Csp^2–Csp^3 Cross-Couplings Using Organomagnesium Reagents. *J. Am. Chem. Soc.* **2019**, *141* (45), 18127–18135. https://doi.org/10.1021/jacs.9b08586.
(22) Lindh, J.; Sävmarker, J.; Nilsson, P.; Sjöberg, P. J. R.; Larhed, M. Synthesis of Styrenes by Palladium(II)-Catalyzed Vinylation of Arylboronic Acids and Aryltrifluoroborates by Using Vinyl Acetate. *Chem. Eur. J.* **2009**, *15* (18), 4630–4636. https://doi.org/10.1002/chem.200802744.
(23) Ben Halima, T.; Zhang, W.; Yalaoui, I.; Hong, X.; Yang, Y.-F.; Houk, K. N.; Newman, S. G. Palladium-Catalyzed Suzuki–Miyaura Coupling of Aryl Esters. *J. Am. Chem. Soc.* **2017**, *139* (3), 1311–1318. https://doi.org/10.1021/jacs.6b12329.
(24) Jia, X.; Foley, A. M.; Liu, C.; Vaughan, B. A.; McKeown, B. A.; Zhang, S.; Gunnoe, T. B. Styrene Production from Benzene and Ethylene Catalyzed by Palladium(II): Enhancement of Selectivity toward Styrene via Temperature-Dependent Vinyl Ester Consumption. *Organometallics* **2019**, *38* (19), 3532–3541. https://doi.org/10.1021/acs.organomet.9b00349.
(25) Musgrave, C. B. I.; Bennett, M. T.; Ellena, J. F.; Dickie, D. A.; Gunnoe, T. B.; Goddard, W. A. I. Reaction Mechanism Underlying Pd(II)-Catalyzed Oxidative Coupling of Ethylene and Benzene to Form Styrene: Identification of a Cyclic Mono-Pd^{II} Bis-Cu^{II} Complex as the Active Catalyst. *Organometallics* **2022**, *41* (15), 1988–2000. https://doi.org/10.1021/acs.organomet.2c00183.
(26) Bennett, M. T.; Jia, X.; Musgrave, C. B. I.; Zhu, W.; Goddard, W. A. I.; Gunnoe, T. B. Pd(II) and Rh(I) Catalytic Precursors for Arene Alkenylation: Comparative Evaluation of Reactivity and Mechanism Based on Experimental and Computational Studies. *J. Am. Chem. Soc.* **2023**, *145* (28), 15507–15527. https://doi.org/10.1021/jacs.3c04295.
(27) Becica, J.; Heath, O. R. J.; Zheng, C. H. M.; Leitch, D. C. Palladium-Catalyzed Cross-Coupling of Alkenyl Carboxylates. *Angew. Chem. Int. Ed.* **2020**, *59* (39), 17277–17281. https://doi.org/10.1002/anie.202006586.

(28) Gaube, G.; Pipaon Fernandez, N.; Leitch, D. C. An Evaluation of Palladium-Based Catalysts for the Base-Free Borylation of Alkenyl Carboxylates. *New J. Chem.* **2021**, *45* (43), 20095–20098. https://doi.org/10.1039/D1NJ04008A.
(29) Gaube, G.; Miller, D.; McCallum, R.; Pipaon Fernandez, N.; Leitch, D. Base-Free Palladium-Catalyzed Borylation of Enol Carboxylates and Further Reactivity toward Deboronation and Cross-Coupling. *ChemRxiv,* Preprint, September 19, 2024. https://doi.org/10.26434/chemrxiv-2024-5mlml.
(30) Pipaon Fernandez, N.; Gaube, G.; Woelk, K.; Burns, M.; Hruszkewycz, D. P.; Leitch, D. Palladium-Catalyzed Direct C−H Alkenylation with Enol Pivalates Proceeds via Reversible C−O Oxidative Addition to Pd(0), *ACS Catal.* **2022**, 12, 6997–7003. https://doi.org/10.1021/acscatal.2c01305
(31) Zhao, X.; Zhang, D.; Wang, X. Unraveling the Mechanism of Palladium-Catalyzed Base-Free Cross-Coupling of Vinyl Carboxylates: Dual Role of Arylboronic Acids as a Reducing Agent and a Coupling Partner. *ACS Catal.* **2022**, *12* (3), 1809–1817. https://doi.org/10.1021/acscatal.1c00247.
(32) Wei, W.-M.; Xu, Y.-L.; Zheng, R.-H.; Fang, W.-J.; Zhao, T.-T. Theoretical Study of the Mechanism of Palladium-Catalyzed Arylation of Alkenyl Carboxylates. *Russ. J. Phys. Chem. B* **2023**, *17* (1), 68–95. https://doi.org/10.1134/S1990793123010293.
(33) Lee, A.-L. Enantioselective Oxidative Boron Heck Reactions. *Org. Biomol. Chem.* **2016**, *14* (24), 5357–5366. https://doi.org/10.1039/C5OB01984B.
(34) Shockley, S. E.; Holder, J. C.; Stoltz, B. M. Palladium-Catalyzed Asymmetric Conjugate Addition of Arylboronic Acids to α,β-Unsaturated Cyclic Electrophiles. *Org. Process Res. Dev.* **2015**, *19* (8), 974–981. https://doi.org/10.1021/acs.oprd.5b00169.
(35) Holder, J. C.; Zou, L.; Marziale, A. N.; Liu, P.; Lan, Y.; Gatti, M.; Kikushima, K.; Houk, K. N.; Stoltz, B. M. Mechanism and Enantioselectivity in Palladium-Catalyzed Conjugate Addition of Arylboronic Acids to β-Substituted Cyclic Enones: Insights from Computation and Experiment. *J. Am. Chem. Soc.* **2013**, *135* (40), 14996–15007. https://doi.org/10.1021/ja401713g.
(36) Jutand, A.; Mosleh, A. Rate and Mechanism of Oxidative Addition of Aryl Triflates to Zerovalent Palladium Complexes. Evidence for the Formation of Cationic (.Sigma.-Aryl)Palladium Complexes. *Organometallics* **1995**, *14* (4), 1810–1817. https://doi.org/10.1021/om00004a038.
(37) Wakioka, M.; Nakamura, Y.; Montgomery, M.; Ozawa, F. Remarkable Ligand Effect of P(2-$MeOC_6H_4)_3$ on Palladium-Catalyzed Direct Arylation. *Organometallics* **2015**, *34* (1), 198–205. https://doi.org/10.1021/om501052g.
(38) Moreno-Mañas, M.; Pérez, M.; Pleixats, R. Palladium-Catalyzed Suzuki-Type Self-Coupling of Arylboronic Acids. A Mechanistic Study. *J. Org. Chem.* **1996**, *61* (7), 2346–2351. https://doi.org/10.1021/jo9514329.
(39) Yunker, L. P. E.; Ahmadi, Z.; Logan, J. R.; Wu, W.; Li, T.; Martindale, A.; Oliver, A. G.; McIndoe, J. S. Real-Time Mass Spectrometric Investigations into the Mechanism of the Suzuki–Miyaura Reaction. *Organometallics* **2018**, *37* (22), 4297–4308. https://doi.org/10.1021/acs.organomet.8b00705.

(40) Zalesskiy, S. S.; Ananikov, V. P. Pd2(Dba)3 as a Precursor of Soluble Metal Complexes and Nanoparticles: Determination of Palladium Active Species for Catalysis and Synthesis. *Organometallics* **2012**, *31* (6), 2302–2309. https://doi.org/10.1021/om201217r.
(41) Thompson, Ca. L. S.; Kabalka, G. W.; Akula, M. R.; Huffman, J. W. The Conversion of Phenols to the Corresponding Aryl Halides Under Mild Conditions. *Synthesis* **2005**, 4, 547-550. https://doi.org/10.1055/s-2005-861791
(42) Gui, Y.-Y.; Liao, L.-L.; Sun, L.; Zhang, Z.; Ye, J.-H.; Shen, G.; Lu, Z.-P.; Zhou, W.-J.; Yu, D.-G. Coupling of C(Sp^3)–H Bonds with C(Sp^2)–O Electrophiles: Mild, General and Selective. *Chem. Commun.* **2017**, *53* (6), 1192–1195. https://doi.org/10.1039/C6CC09685A.
(43) Romanski, S.; Kraus, B.; Guttentag, M.; Schlundt, W.; Rücker, H.; Adler, A.; Neudörfl, J.-M.; Alberto, R.; Amslinger, S.; Schmalz, H.-G. Acyloxybutadiene Tricarbonyl Iron Complexes as Enzyme-Triggered CO-Releasing Molecules (ET-CORMs): A Structure–Activity Relationship Study. *Dalton Trans.* **2012**, *41* (45), 13862. https://doi.org/10.1039/c2dt30662j.
(44) Patiny, L.; Borel, A. ChemCalc: A Building Block for Tomorrow's Chemical Infrastructure. *J. Chem. Inf. Model.* **2013**, *53* (5), 1223–1228. https://doi.org/10.1021/ci300563h.
(45) Khatua, A.; Niyogi, S.; Bisai, V. Total Synthesis of (+)-Ar-Macrocarpene. *Org. Biomol. Chem.* **2019**, *17* (30), 7140–7143. https://doi.org/10.1039/C9OB01373C.

Chapter 3: Base-Free Palladium-Catalyzed Borylation of Enol Carboxylates and Further Reactivity Toward Deboronation and Cross-Coupling

This chapter, excluding section 3.1, have been reproduced from:

Gaube, G.; Fernandez, N.P.; Leitch, D.C., An Evaluation of Palladium-Based Catalysts for the Base-Free Borylation of Alkenyl Carboxylates, *New Journal of Chemistry,* **2021**, 45, 20095-20098, (DOI: 10.1039/D1NJ04008A), and Gaube, G.; Miller, D.L.; McCallum, R.A.; Fernandez, N.P.; Leitch, D.C., Base-Free Palladium-Catalyzed Borylation of Enol Carboxylates and Further Reactivity Toward Deboronation and Cross-Coupling, *ChemRxiv* **2024**, DOI: 10.26434/chemrxiv-2024-5mlml.

3.1 Preface

Contributions: Douglas L. Miller conducted catalyst screening with substrates **2e**-**2g**, aided in protodeboronation screening, and synthesized starting materials under supervision of Gregory Gaube. Rowan A. McCallum conducted catalyst screening with substrates **2b** and **2c**, synthesis optimization of 3,4-diethylhexane-3,4-diol, and reactions of **2b**-**2g** with B_2EPin_2 under supervision of Gregory Gaube. Nahiane Pipaon Fernandez conducted synthesis of **4e**-**4g**. All other experimental work and characterization was conducted by Gregory Gaube.

3.2 Abstract

A series of base-free Pd-catalyzed borylation procedures are reported for a number of alkenyl carboxylates. High-throughput experimentation was used to discover and optimize these reactions using *in situ* generated catalyst systems. With lactone or lactam substrates, the resulting alkenyl pinacol boronates are hydrolytically unstable, undergoing protodeboronation under acidic

and basic aqueous conditions. Optimization of this protodeboronation resulted in a mild, two-step reduction of the C–O bond, achieving net-deoxygenation while leaving the alkene intact. In contrast, use of an alternative tetraalkoxydiboron source – B_2EPin_2 – was successful in catalysis, and offered improved stability of the resulting organoboron species. This enables further reactivity, such as cross-coupling, without competing protodeboronation.

3.3 Introduction

Installation of boron-based functional groups is a valuable methodology, particularly in the context of metal-catalyzed cross-coupling.[1–7] Although numerous reactions utilize organoboron intermediates, Suzuki-Miyaura coupling is the most widespread, as it remains one of the most reliable methods for forming C–C bonds.[8–16] Accordingly, a plethora of methods to install a suitable boron-based unit are known.[17–21] Since seminal work from Miyaura,[22] Pd-catalyzed borylation of organohalides and *pseudo* halides (such as triflates) is often used achieve this,[23,24] typically with a tetraalkoxydiboron source (such as B_2Pin_2 or an alternative)[25] and a weak base (such as KOAc or other carboxylate bases)[26–28] to complete the catalytic cycle. Importantly, the vast majority of these reactions rely on the aforementioned halide or triflate electrophiles to accomplish this transformation.

Two ways to improve Pd-catalyzed borylation are to utilize alternative, non-halide electrophiles, and to eliminate the need for insoluble inorganic bases. For the former, simple oxygen based leaving groups such as alkoxyl or carboxyl are advantageous from an accessibility/installation standpoint;[29,30] however, the required C–O activation is kinetically difficult,[31] limiting the reported examples of C–O borylation to select systems based on Rh,[32–34] Ni,[35–39] and Fe (Figure 3.1a).[40,41] For the latter, conditions that use homogeneous bases, or no

base at all, would greatly improve reliability and scalability of these reactions, an important consideration in pharmaceutical process chemistry.[42–44]

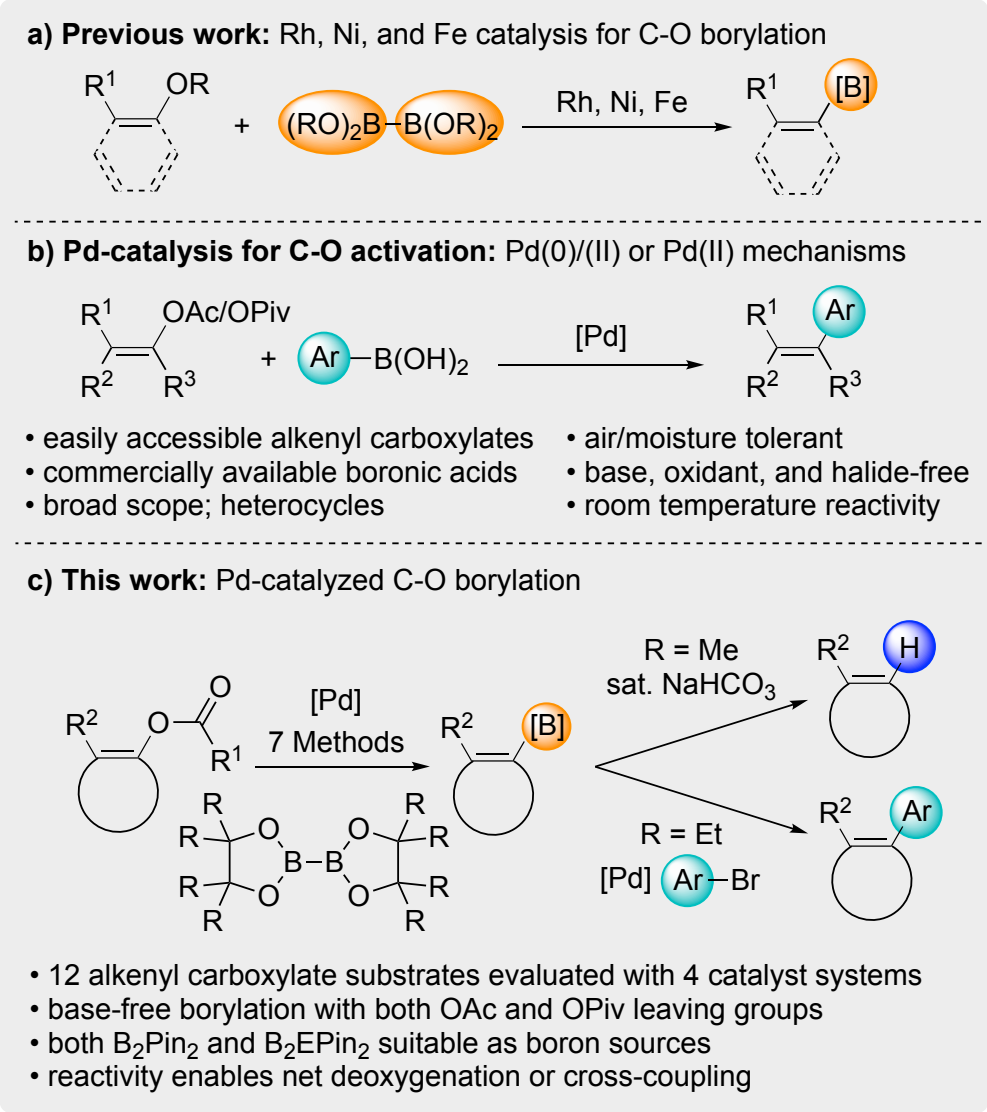

Figure 3.1: a) Prior catalytic strategies for C–O borylation; b) C–O activation in C–C bond formation with arylboronic acids; c) an evaluation of catalytic systems for borylation involving C–O activation, including comparable reactivity of two systems with both BPin and BEPin synthetic handles.

In both cases, carboxylate leaving groups offer several advantages.[45] They are easily installed by simple acylation, and the intermediacy of a Pd(II) carboxylate after C–O oxidative addition means that exogenous base should not be required. However, since carboxylates

contain two C–O bonds for Pd(0) to react with, an additional selectivity hurdle needs to be overcome. Accordingly, to the best of our knowledge there is a single, Rh-based catalytic system able to effect borylation with carboxylate-based electrophiles.[32]

While the Newman group has selectively activated the acyl C–O bond using Pd catalysis,[31] a 2020 publication by our lab has shown that Pd(0) can selectively insert into the desired aryl/alkenyl C–O bond in heteroaryl and alkenyl carboxylates.[46] This was then applied to Pd-catalyzed reactions of alkenyl carboxylates and phenyl boronic acids without the use of a base (Figure 3.1b).[47] We have since expanded this reactivity to tandem C–O/C–H activation for base-free direct alkenylation.[48]

We have investigated several methods of Pd-catalyzed Miyaura borylation of alkenyl carboxylates (Figure 3.1c), including using an air-stable Pd precatalyst (^{DMP}DAB–Pd–MAH) recently developed within our group.[49] We have also investigated the protodeboronation of alkenyl boronate esters derived from γ-lactones and γ-lactams. Using the standard BPin group, protodeboronation is readily achieved using biphasic hydrolysis under mildly basic conditions. Optimization of this deboronation results in a net reductive deoxygenation of the precursor enols, using conditions that leave the C=C bond intact. In contrast, use of the recently reported B_2EPin_2 under our catalytic conditions gives stable organoboron compounds that can be used further.[50]

3.4 Results and Discussion

3.4.1 Borylation Conditions for Multiple Substrate Classes

Our prior work on Pd-catalyzed Suzuki coupling with alkenyl carboxylates yielded two viable catalytic systems, both of which operate base-free.[47] One *in situ* system with $Pd(OAc)_2$ and tris(*ortho*-methoxyphenyl)phosphine functioned open to air, at room temperature, and in the presence of water, potentially through a redox-neutral Pd(II)-based mechanism.[51–53] The other system involves a single component Pd(0) catalyst, $Pd(PCy_3)_2$, which functioned at higher temperatures, through a more typical Pd(0)/(II) mechanism.[47] To determine if additional Pd/ligand combinations would yield product in a base-free Miyaura borylation, we conducted a series of microscale high-throughput screening experiments against multiple classes of alkenyl carboxylate electrophiles (Figure 3.2).

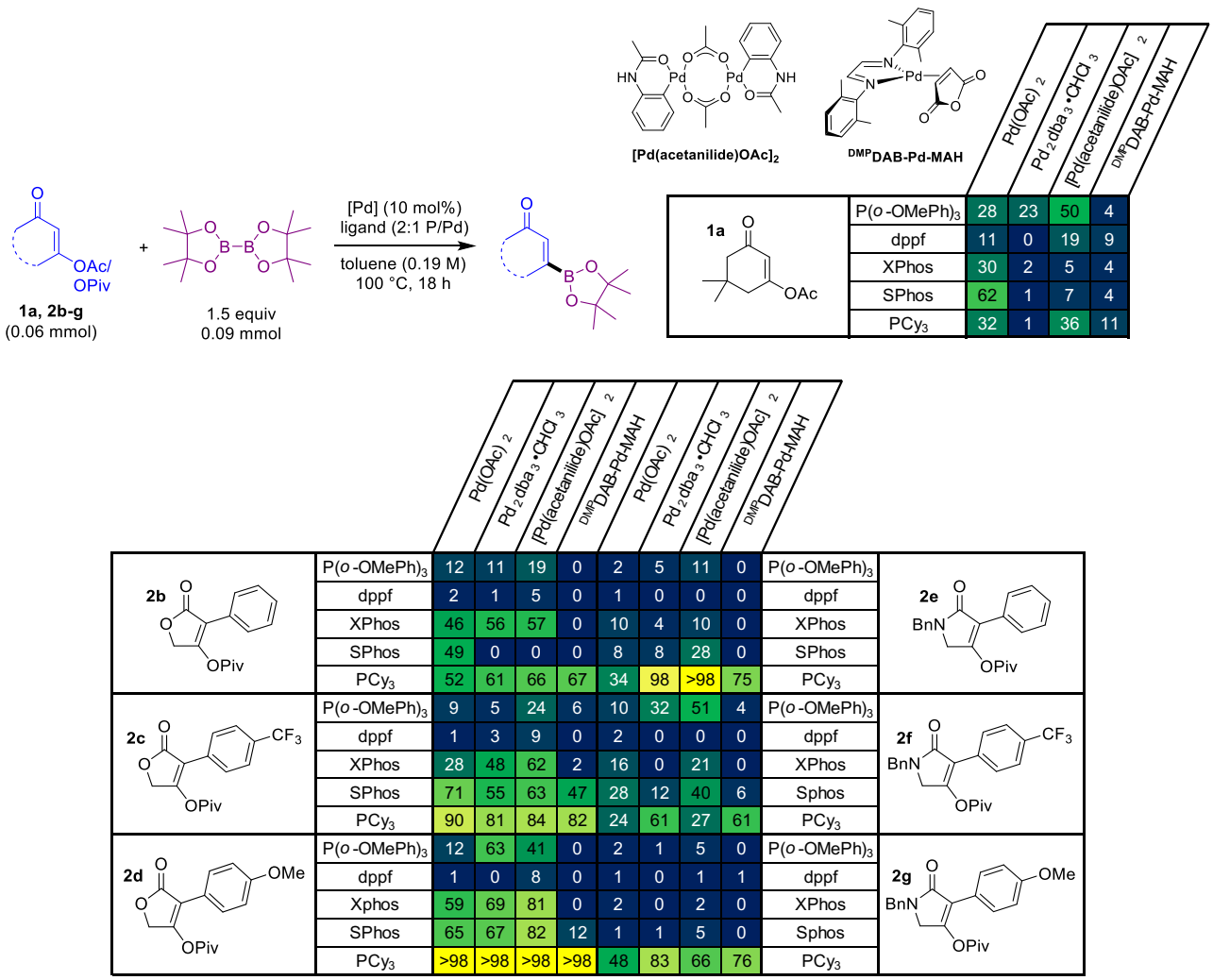

*Figure 3.2: Catalyst screening for the borylation of **1a**, **2b**-**2g**. Yield determined by ^{1}H NMR spectroscopy using 1,3,5-trimethoxybenzene internal standard.*

Our screening approach was two-pronged. First, dimedone-derived alkenyl acetate **1a** was reacted with B_2Pin_2 at elevated temperature with twenty *in situ* catalyst combinations involving four Pd precatalysts and five ligands. Of the 4 Pd sources, two were Pd(II), and two were Pd(0), including ^{DMP}DAB-Pd-MAH.[49] These precatalysts were assessed with five ligands: P(*o*-OMePh)$_3$ and PCy_3 (both successful in the prior Suzuki coupling method),[47] as well as SPhos, dppf and XPhos. Control experiments without Pd yielded no product (Appendix B: Figure B1). We also evaluated a single component Pd precatalyst, $Pd(PCy_3)_2$ (Figure B1).[54] Many combinations yielded

product, but generally Pd(II) sources outperformed Pd(0) sources. $Pd(OAc)_2$ and SPhos was the best *in situ* combination (62% solution yield), and was taken forward in further optimization. The single component $Pd(PCy_3)_2$ also yielded comparable product formation.

The second set of screens was done for six γ-lactone, and γ-lactam alkenyl pivalate substrates (**2b**-**2g**). The choice of pivalate as opposed to acetate was informed by further exploration of the dimedone-based system (*vide infra*). We opted to explore electronic effects by changing the *para* substituent on the phenyl ring at the α position. The aryl was either unsubstituted (-H) or substituted with an electron-withdrawing ($-CF_3$) or electron-donating (-OMe) group. The resulting 6 compounds were evaluated with the same twenty *in situ* combinations of Pd and ligands (Figure 3.2). Many combinations facilitated borylation; however, in contrast to **1a**, the lactone and lactam substrates generally preferred Pd(0) over Pd(II) sources. Control experiments with no catalyst again yielded no borylated product. With respect to ligand effects, every Pd source when combined with PCy_3 facilitated borylation to some extent. Notably, lactone substrates (**2b**-**d**) have generally higher reactivity than their lactam counterparts (**2e**-**g**): XPhos and SPhos performed reasonably well with the former set, but were generally ineffective for the latter set. Taken holistically, these results reveal that the combination of ^{DMP}DAB-Pd-MAH and PCy_3 performed well among all six substrates, with solution yields of the organoboron products between 61–98%.

Moving ahead, full factorial multivariate optimization was chosen to quickly obtain improved conditions for the $Pd(OAc)_2$/SPhos *in situ* system (Figure 3.3). Three variables were chosen for evaluation: concentration of Pd, concentration of ligand, and concentration of B_2Pin_2. Notably, excess ligand (3 equiv. to Pd) reduced yield with both the 4 and 10 mol% $Pd(OAc)_2$

reactions. This is consistent with a monoligated Pd(0) species as the active catalyst. In all cases, increasing the B_2Pin_2 in the reaction mixture improved yields of **3a**, while only marginally increasing the conversion; the mass balance is dimedone, formed by hydrolysis of **1a**. The best conditions are with 0.2 M **1a**, 10 mol% $Pd(OAc)_2$, 15 mol% SPhos, and 2 equiv B_2Pin_2, giving 71% solution yield, but only 89% conversion.

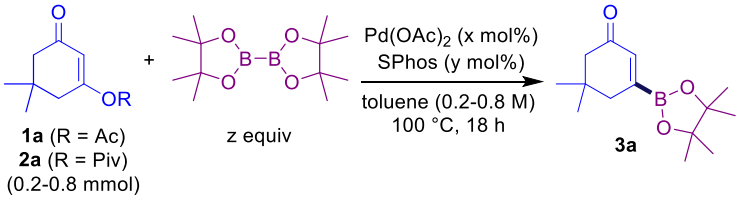

Substrate	[1] (M)	$Pd(OAc)_2$ loading (mol%)	SPhos equiv per Pd	B_2Pin_2 equiv	% Conv. **a**	% Yield **3a**	
1a	0.2	4.0	1.5	1.1	29	11	
				2.0	40	25	
			3.0	1.1	30	1	
				2.0	40	19	
		7.5	1.5	1.5	58	33	Centerpoint
		10.0	1.5	1.1	66	40	
				2.0	89	71	Maximum
			3.0	1.1	74	44	
				2.0	92	62	
1a	0.2	10.0	1.5	2.0	89	71	TON = 7
	0.4	5.0			>98	67	TON = 13
	0.6	3.3			>98	58	TON = 18
	0.8	2.5			>98	44	TON = 18
2a	0.8	2.5	1.5	2.0	>98	72	TON = 29

*Figure 3.3: Multivariate optimization of the borylation of **1a**. Conversion and yield determined by ^{1}H NMR spectroscopy using 1,3,5-trimethoxybenzene internal standard.*

While this result was satisfactory in yield, the high Pd loading and corresponding low

turnover number (TON = 7) and incomplete conversion were concerning. Furthermore, increasing [**1a**] while maintaining constant [catalyst] did lead to higher TON (up to 18), but also led to diminished yields of **3a** due to increased hydrolysis of **1a** to dimedone. To correct this, we evaluated the more sterically-hindered, electron-rich alkenyl pivalate derivate **2a** at a concentration of 0.8 M. This greatly improved the yield of **3a** (72% solution yield), the mass balance, and the TON (29).

Full factorial multivariate optimization was also performed for substrates **2b**-**g** with the ^{DMP}DAB-Pd-MAH/PCy_3 *in situ* system. A simplified 2 factor, 2 level design, in catalyst loading and B_2Pin_2 equivalents was conducted (Figure 3.4). The Pd:PCy_3 ratio was held steady at 2. We found that the best conditions are dependent on the motif. Consistent with initial screening, γ-lactams are less reactive, requiring both higher catalyst loading (5 mol%) and 2.0 equiv. B_2Pin_2 (92–98% solution yields) (Method **D**). In an effort to reduce B_2Pin_2, an additional data point (5 mol% [Pd] and 1.6 equiv. B_2Pin_2) was collected for **2e**-**g**; however, this resulted in reduced yield for **2f**. The γ-lactones **2b**-**d** had similar results with 2.0 mol% [Pd] and 2.0 equiv B_2Pin_2, and 3.5 mol% [Pd] and 1.6 equiv B_2Pin_2; the latter was chosen as Method **E** because excess B_2Pin_2 has been found to hamper purification in further steps.[55]

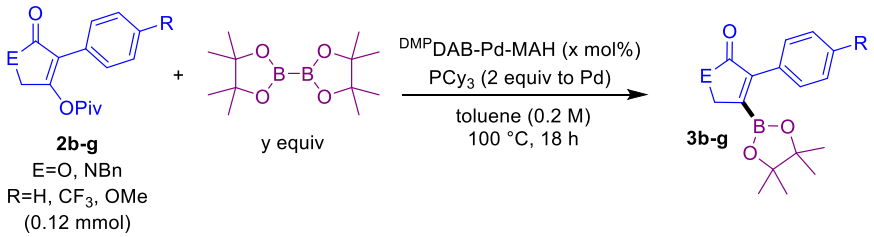

DMPDAB-Pd-MAH (mol%)	B_2Ph_2 equiv.	% Yield 3b	% Yield 3c	% Yield 3d	% Yield 3e	% Yield 3f	% Yield 3g
2	1.2	95	64	96	86	24	38
	2	>98	>98	95	97	33	73
3.5	1.6	>98	96	98	87	63	>98
5	1.2	>98	96	>98	81	91	>98
	1.6				>98	72	>98
	2	>98	95	97	>98	92	>98

*Figure 3.4: Full factorial optimization of the borylation of **2b**-**2g**. Yield was determined by ^{1}H NMR spectroscopy using 1,3,5-trimethoxybenzene internal standard. Grey cells indicate reactions not performed under these conditions.*

After these two targeted optimizations, we wanted to evaluate the utility of these procedures against the two methods our group had used previously for C–O activation in Suzuki coupling. For this assessment, we prepared twelve alkenyl carboxylates, including six main motifs with both acetate and pivalate leaving groups. Specifically, these are the previously described dimedone-derived substrates (**1**/**2a**), the γ-lactones (**1**/**2b**) and γ-lactams (**1**/**2e**), along with cyclopentanone derived substrates (**1**/**2h**), coumarins (**1**/**2i**) and pyrones (**1**/**2j**). These substrates were subjected to six reaction conditions, with Methods **A**-**D** shown in Figure 3.5 (two additional Methods **F** & **G** shown in Appendix B - Figure B2). Method **A** was previously used in Pd(II) catalyzed C–O activation cross-coupling, Method **B** is the $Pd(OAc)_2$/SPhos system optimized for **1/2a**,

Method **C** was previously used for Pd(0) catalyzed C–O activation cross-coupling, and Method **D** is the ^{DMP}DAB-Pd-MAH/PCy_3 system (5 mol% loading) optimized for **2e-2g**.

Overall, alkenyl pivalate substrates performed uniformly better than their alkenyl acetate counterparts, which points to product decomposition back to the corresponding enol being a significant issue with the acetate leaving group. Among the moderate yields that were obtained with an acetate leaving group, Pd(0) sources generally fared better than Pd(II) sources.

For the formation of **3a**, Method **B** proved to be best, which is consistent with our multivariate optimization; however, this method appears to be specific to the dimedone motif, as these conditions failed to borylate the similar cyclopentenone **1**/**2h**, and provided low yields for the other motifs. Method **D** proved to be best for the formation of **3b** and **3e** from the corresponding pivalates; however, Method **C** (which uses the same PCy_3 ligand) gave similar, albeit slightly lower yields with higher catalyst loading. Furthermore, while $Pd(PCy_3)_2$ is commercially available, its air sensitivity is a practical limitation; ^{DMP}DAB-Pd-MAH is air stable. For the formation of **3h** from the corresponding pivalate, Method **A** was best, which is again specific to this motif. Finally, formation of **3i** and **3j** was best using Method **C**. Given the success of PCy_3-based systems, we also evaluated $Pd(OAc)_2(PCy_3)_2$ as a single component Pd(II) source. This complex has been observed to reduce *in situ* to $Pd(PCy_3)_2$ in the presence of B_2Pin_2;[54] however, this ultimately proved inferior to $Pd(PCy_3)_2$ (Methods **F** & **G**, Appendix B - Figure B2).

Although the specific mechanistic reasons for the success/failure of these various methods for each substrate class are not yet clear, what *is* clear is the importance of including substrate identity as a variable when evaluating new synthetic methods.[56] Each of the alkenyl pinacol boronate compounds were characterized (NMR, HRMS) without purification, as attempts

to use column chromatography or selective extractions led to product decomposition (*vide infra*) and/or pinacol-containing impurities remaining; this latter issue is a known problem when synthesizing BPin-containing molecules.[1]

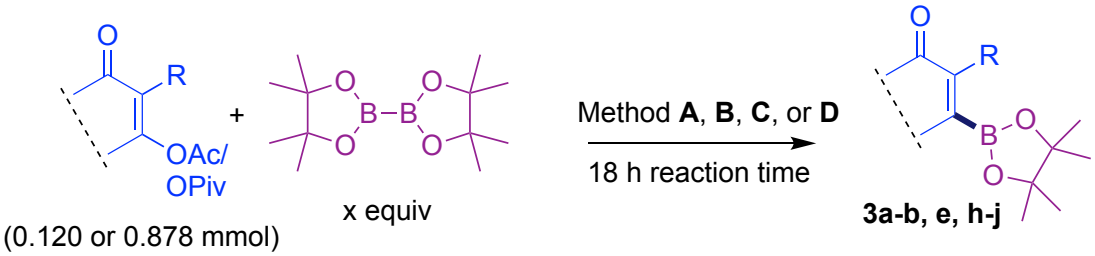

Method **A**: $Pd(OAc)_2$ (4 mol%) / P(*o*-OMePh)$_3$ (6 mol%), x = 1.1, acetone/water (10:1, 0.6 M), rt
Method **B**: $Pd(OAc)_2$ (2.5 mol%) / SPhos (3.8 mol%), x = 1.1, toluene (0.8 M), 100 °C
Method **C**: $Pd(PCy_3)_2$ (10 mol%), x = 1.1, toluene (0.2 M), 100 °C
Method **D**: ^{DMP}DAB-Pd-MAH (5 mol%) / PCy_3 (10 mol%), x = 2.0, toluene (0.2 M), 100 °C

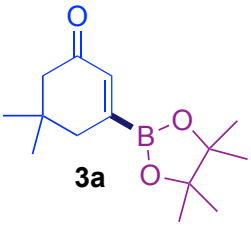

OAc: Method **A**: 28%
Method **B**: 38%
Method **C**: 33%
Method **D**: 24%
OPiv: Method **A**: 41%
Method **B**: **72%**
Method **C**: 43%
Method **D**: 14%

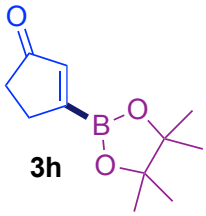

OAc: Method **A**: 9%
Method **B**: 0%
Method **C**: 0%
Method **D**: 0%
OPiv: Method **A**: **62%**
Method **B**: 0%
Method **C**: 0%
Method **D**: 0%

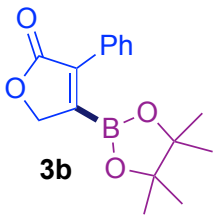

OAc: Method **A**: 0%
Method **B**: 0%
Method **C**: 43%
Method **D**: 50%
OPiv: Method **A**: 0%
Method **B**: 28%
Method **C**: 86%
Method **D**: **98%**

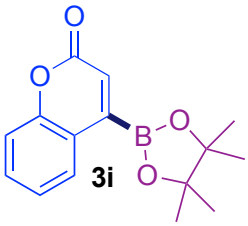

OAc: Method **A**: 32%
Method **B**: 0%
Method **C**: 46%
Method **D**: 20%
OPiv: Method **A**: 6%
Method **B**: 6%
Method **C**: **90%**
Method **D**: 4%

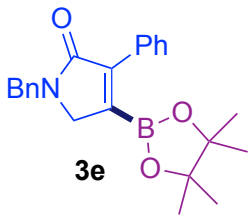

OAc: Method **A**: 0%
Method **B**: 0%
Method **C**: 32%
Method **D**: 0%
OPiv: Method **A**: 0%
Method **B**: 0%
Method **C**: 76%
Method **D**: **82%**

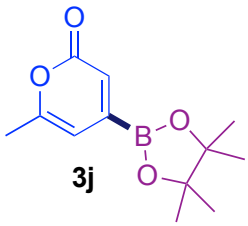

OAc: Method **A**: 0%
Method **B**: 0%
Method **C**: 66%
Method **D**: 22%
OPiv: Method **A**: 4%
Method **B**: 14%
Method **C**: **71%**
Method **D**: 25%

*Figure 3.5: Comparison of Pd-catalyzed methods for base-free Miyaura borylation of alkenyl acetate and pivalate substrates. Substrate loading: 0.12 mmol for Methods **A**, **C**-**D**, 0.88 mmol for Method **B**. Yields determined by ^{1}H NMR spectroscopy using 1,3,5-trimethoxybenzene*

As borylated compounds are usually targeted as synthetic intermediates, we chose to assess the newly formed alkenyl pinacol boronates in preparative scale Suzuki cross-coupling reactions. Enol pivalates **2a**, **b**, **e**, **h-j** were first borylated at a 1 mmol scale via the best Method from Figure 3.5 (**2b** and **2e** borylated using Method **C**) to obtain the respective organoboron compounds **3a**, **b**, **e**, **h-j**. These were then subject to a typical (and unoptimized) Suzuki cross-coupling protocol, allowing the isolation of the arylated product **5a**, **h-j** in moderate yields (Figure 3.6). However, coupling reactions with **3b** and **3e** resulted in low yields of the respective arylated products: coupling of **3b** resulted in a negligible yield (<2% isolated) and **4b** observed as the major product, and **3e** resulted as an inseparable mixture of arylated and deboronated products (49% yield of a 3.33 : 1 mixture of **5e** and **4e**).

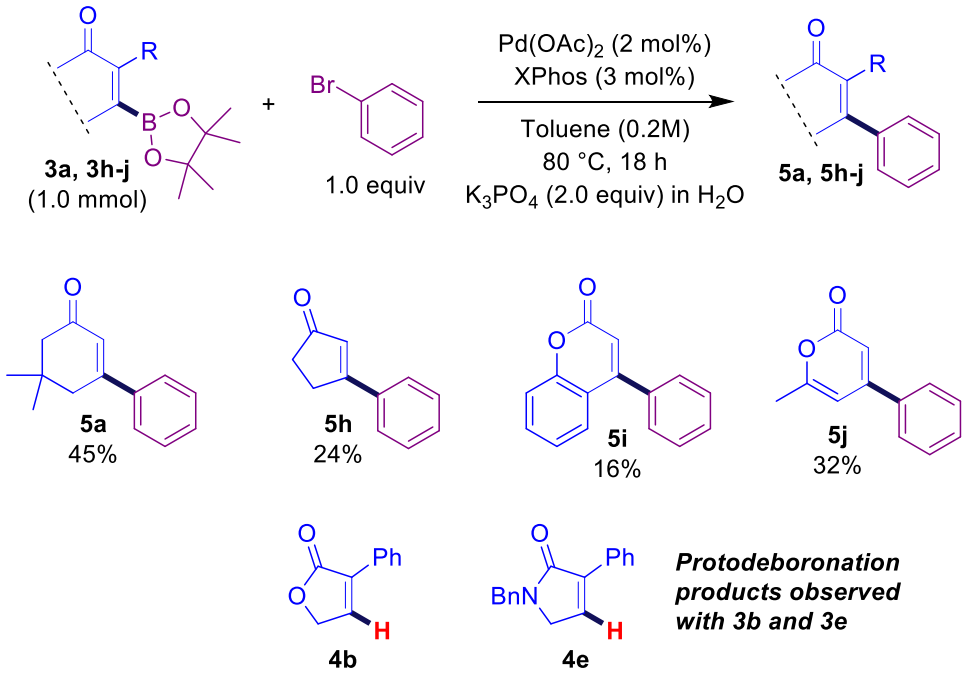

Figure 3.6: Suzuki cross-coupling of prepared alkenyl boronates. Yields are for isolated compounds over two steps after column chromatography.

3.4.2 Protodeboronation as a Means of Net-Deoxygenation

Observation of **4b** and **4e** led us to investigate the stability of the corresponding boronates **3b** and **3e** to simple aqueous work-up procedures. We discovered that these alkenyl boronates are extremely sensitive to even mild aqueous base, undergoing significant deboronation after a saturated $NaHCO_3$ wash. This is consistent with the deboronation observed during attempted Suzuki coupling, which uses an aqueous base.

Boronic ester functional groups are often used as a more robust alternative to the boronic acid.[57–60] The Lloyd-Jones group has completed a thorough investigation of the protodeboronation of (hetero)arylboronic esters, where they conclude that factors leading to deboronation are multi-faceted, with several operative mechanisms that depend on if the solution pH is close to the pK_a of the boronic ester.[57]

While the observed deboronation renders these compounds unsuitable for standard Suzuki cross-coupling, it does result in a net-deoxygenation process. Overall, the corresponding enol pivalates – readily generated by standard condensation chemistry – are acylated, borylated, and then deboronated to effectively replace –OH with –H. Furthermore, this reduction is selective, leaving other reducible groups (C=C and C=O) intact. After reviewing the literature for other cases where alkenyl carboxylates were deoxygenated, we identified a single report where a δ-lactone was deoxygenated through a process involving harsh acidic conditions and multiple steps.[61] Others have utilized the limited stability of boronic esters to deboronate selectively,[62] but use of deboronation as a desired synthetic method remains underdeveloped.

This led us to optimize the protodeboronation conditions for the set of six γ-lactone and γ-lactam boronates, as many biologically active molecules contain the γ-lactone and γ-lactam

motif.[63–66] Furthermore, the resulting deoxygenated γ-lactones would be valuable coupling partners in asymmetric allylic alkylation (AAA) chemistry,[67] while the unsubstituted γ-lactams have been used in Michael additions.[68]

Using Method **D** to borylate the **2b**-**g** to generate **3b-g**, five aqueous solutions of varying pH and ionic strength were tested for protodeboronation under biphasic conditions (toluene as the organic solvent) (Figure 3.7). The solutions were basic (saturated Na_2CO_3, saturated $NaHCO_3$), neutral (saturated NaCl, H_2O), and acidic (5% HCl). Very little deboronation was found to occur with the saturated NaCl and 5% HCl solutions, while neutral H_2O led to increased formation of **4b**-**g**. Under basic conditions, much higher extents of deboronation are observed, as measured by the ratio between **3** and **4** by NMR spectroscopy. However, when determining solution yields for all products with an internal standard, we observed a discrepancy with the mass balance. When using Na_2CO_3, the amount of product was significantly reduced for both the γ-lactones and lactams. Use of saturated $NaHCO_3$ led to missing mass balance specifically for the γ-lactones, which we suspected was due to product partitioning between the aqueous and organic phases. Acidification of the aqueous solutions and extraction with ethyl acetate confirmed this, as we recovered additional deboronated product. Accordingly, treatment with saturated $NaHCO_3$ was found to yield the best deboronation results for both γ-lactones and γ-lactams, but required a back extraction for the γ-lactones to achieve high yields.

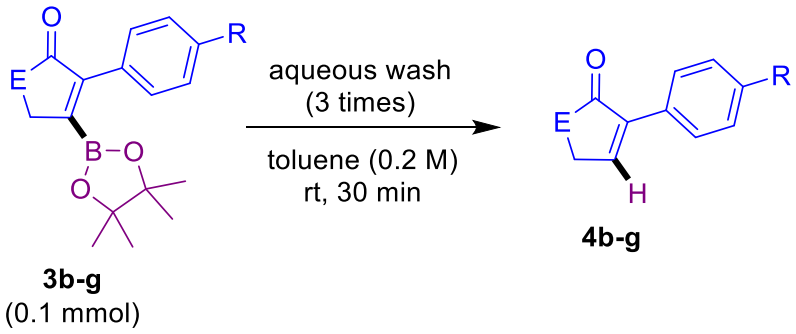

	% Yield	sat Na_2CO_3	sat $NaHCO_3$	sat NaCl	H_2O	5% HCl
4b	>98	>98	7	20	8	
4c	>98	81	7	12	7	
4d	>98	>98	9	34	10	
4e	47	69	12	40	22	
4f	46	41	19	45	21	
4g	77	85	11	61	12	

Figure 3.7: Protodeboronation of alkenyl boronates using aqueous solutions. Yields are represented as ratios of protodeboronated product : alkenyl boronate starting material, determined by ^1H NMR spectroscopy.

Upon scaling up this procedure, we observed incomplete deboronation, likely due to the decreased interfacial surface area to volume ratio in this biphasic reaction. We then decided to stir the biphasic solution overnight at 40 °C, which remedied this problem. This two-step method was then applied to a scope of γ-lactones and γ-lactams which resulted in moderate isolated yields for the γ-lactones (37–52%) and good isolated yields for the γ-lactams (75–82%) (Figure 3.8).

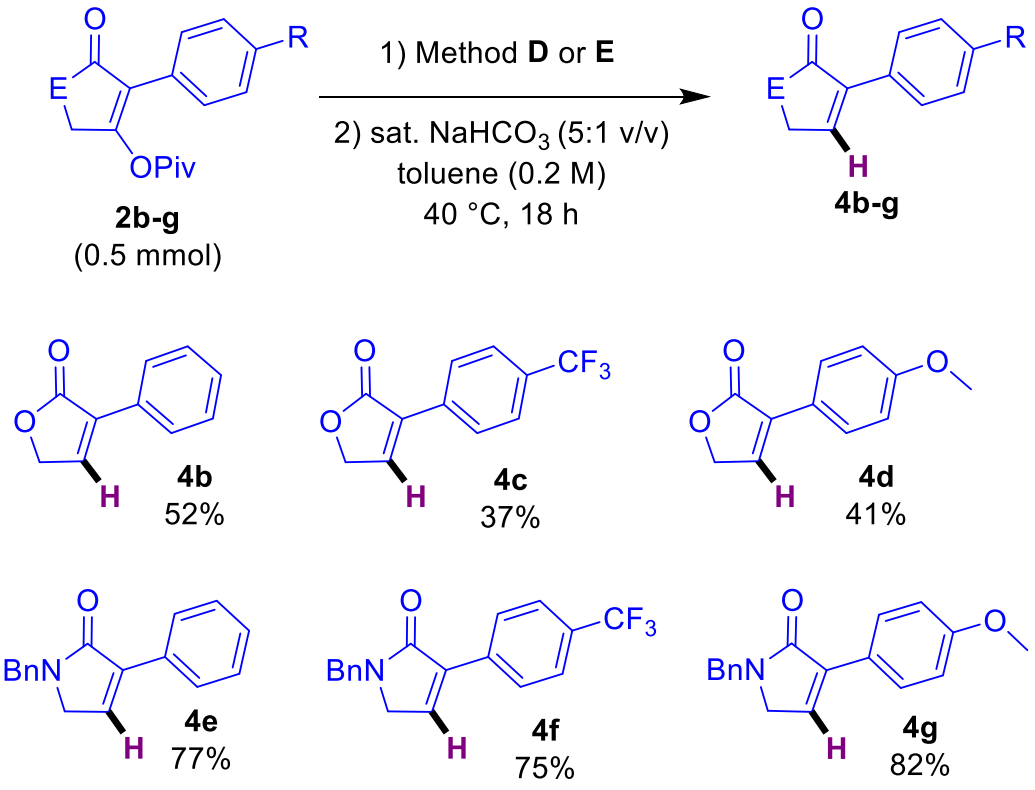

Figure 3.8: Protodeboronation of alkenyl pivalate substrates. Yields are for isolated compounds over two steps after column chromatography.

3.4.3 Achieving Stability with An Alternative Boronic Ester, B_2EPin_2

The instability of the boronates **3b**-**g**, while advantageous in the deoxygenation sequence, is clearly a liability for achieving other transformations of the organoboron group. To alleviate this, we sought alternative boronate groups that would be more robust toward protodeboronation. In particular, a recent account of arylboronic esters based on 3,4-diethyl-hexa-3,4-diol ("ethylpinacol" EPin)[50] caught our attention due to improved stability during column chromatography. The ethyl groups (which replace the methyls of the standard BPin) are hypothesized to sterically block the empty 2*p* orbital on the boron, reducing the likelihood of deboronation due to attack on the boron. Notably, while B_2EPin_2 is reported to function in a

standard Pd-catalyzed Miyaura borylation, its reactivity in more complex setting has yet to be evaluated.

We began by synthesizing B_2EPin_2, where we improved the reported literature yield with a revised work-up and isolation procedure for 3,4-diethyl-hexa-3,4-diol (See Appendix B). We then tested B_2EPin_2 as a drop-in replacement for B_2Pin_2 in our optimized borylation methods for γ-lactones and γ-lactams (**2b-g**) (Figure 3.9). In all cases, the desired product (**6b-g**) was generated in moderate to good solution yields. γ-Lactones **2b**-**d** gave comparable yields (80–81%) to their BPin counterparts; however γ-lactams saw an overall decrease in yield (48-83%, 65% average). Importantly, all six alkenyl-BEPin products are more stable to aqueous work-up, and to column chromatography, which is a marked improvement on their BPin counterparts. We do note that while protodeboronation is suppressed for these compounds, it is not completely eliminated (see Appendix B).

Finally, in an effort to test the reactivity of the BEPin group for cross-coupling, γ-lactone **6d** was subjected to Suzuki-Miyaura coupling using the same generic procedure from Figure 6 (eq. 1). This proved effective; however, two tetraethyl pinacol derived impurities remained in the crude reaction mixture. We found that treating the crude mixture with $B_2(OH)_4$ enabled removal of tetraethyl pinacol itself through re-forming B_2EPin_2, which is separable by chromatography. The second impurity, which we suspect is a different boron-complexed EPin species, partially coelutes during chromatography (resulting in a reduced isolated yield). Further efforts are underway to develop stable boron reagents that are compatible with this chemistry, while suppressing deboronation *and* enabling straightforward purification.

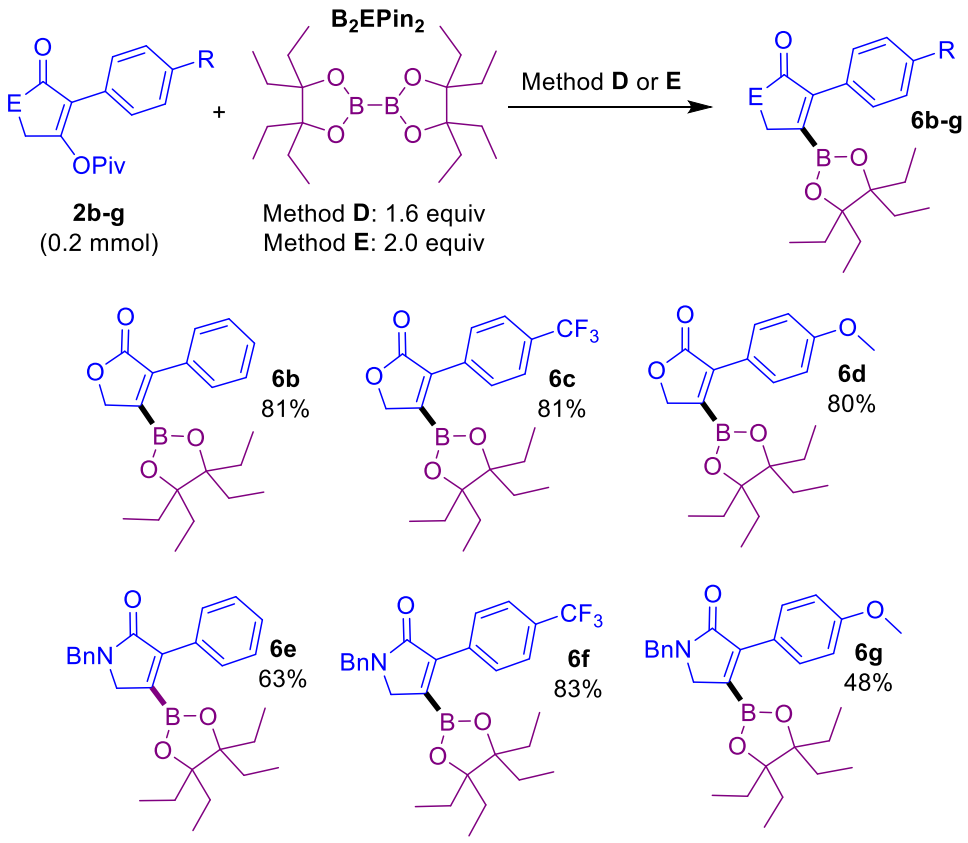

Figure 3.9: Base-free Miyaura borylation of alkenyl pivalates. Yields determined by ^{1}H NMR spectroscopy using 1,3,5-trimethoxybenzene as internal standard.

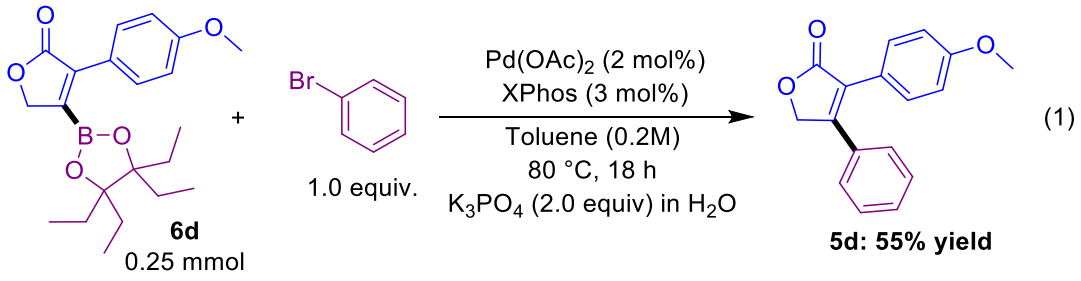

3.5 Conclusion

In summary, we have explored the base-free Pd-catalyzed borylation of several classes of alkenyl carboxylates. Depending on the substrate structure, different catalyst systems are required to achieve high yields. We also observe protodeboronation as a significant decomposition pathway for certain alkenyl boronates after even mild aqueous base treatment.

For γ-lactone and γ-lactam substrates, this can be exploited in a mild, net-deoxygenation of the precursor enols, leaving the C=C and C=O bonds intact. Using a more sterically-encumbered boron source – B_2EPin_2 – leads to greater stability, enabling downstream reactivity such as cross-coupling. Further investigations on the reactivity of these alkenyl boronates, and improved catalytic systems for C–O activation, are currently underway.

3.6 Experimental

3.6.1 General Considerations:

All solvents and chemicals were purchased from commercial suppliers and used without any further purification. All air-free manipulations were performed under a nitrogen atmosphere using an MBraun glovebox. Palladium (II) acetate, bis(tricyclohexylphosphine) palladium (0), Dichloro 1,1'-bis(diphenylphosphino)ferrocene palladium (II) dichloromethane, P(*o*-OMePh)$_3$, XPhos, SPhos, and dppf were purchased from Strem Chemicals and stored under inert atmosphere. B_2Pin_2 was purchased from AK Scientific and stored under inert atmosphere.

High-throughput screening experiments were performing using sealable aluminum reaction blocks obtained from Analytical Sales Inc. Heating/stirring was achieved using rare-earth magnetic tumble stirrers obtained from V&P Scientific.

All NMR spectra were acquired on either a Bruker AVANCE 300 MHz spectrometer or a Bruker AVANCE Neo 500 MHz spectrometer. All ^{1}H and ^{13}C chemical shifts are calibrated to residual protio-solvents. All data is processed using Bruker TopSpin 4.07. HRMS data was acquired on a Thermo Scientific Ultimate 3000 ESI-Orbitrap Exactive Plus.

3.6.2 Screening Procedures:

Catalyst Screening (Figure 3.2)

Pd catalyst dispensing: Catalyst precursors were added to 1 mL glass shell vials according to the screening design. $Pd(OAc)_2$ and $Pd_2(dba)_3 \bullet CHCl_3$ were dispensed as stock solutions (0.06 or 0.03 M respectively) in dichloromethane into 5 x 1 mL vials (1.3 mg, 0.0057 mmol and 2.6 mg, 0.0029 mmol respectively). ^{DMP}DAB-Pd-MAH and $[Pd(acetanilide)OAc]_2$ were dispensed as stock solutions (0.06 or 0.03 M respectively) in acetone into 5 x 1 mL vials (2.7 mg, 0.0057 mmol and 1.7 mg, 0.0029 mmol respectively). Solvent was then evaporated using a Genevac EZ-2 (Medium BP setting, no heat). These vials were then brought in the glovebox. $Pd(PCy_3)_2$ (3.8 mg, 0.0057 mmol) was added as a solid inside the glovebox.

Ligand, substrate, reagent, and standard dispensing: A 100 µL aliquot of toluene stock solutions of each ligand (P(*o*-OMePh)$_3$, SPhos and XPhos: 0.114 M, or dppf: 0.057 M) was dispensed to each vial as required. A 100 µL aliquot of toluene stock solutions containing substrate (one of **1a**, **2b**-**2g**) (0.57 M) and 1,3,5-trimethoxybenzene (0.057 M) was dispensed to each vial as required. A 100 µL aliquot of a toluene stock solution of B_2Pin_2 (0.90 M) was dispensed to each vial, followed by an additional 100 µL of toluene.

Therefore, the reactions are performed at 0.145 M in substrate (**1a**, **2b**-**2g**) and 0.218 M in B_2Pin_2, and (with respect to substrate **1a**, **2b**-**2g**) 10 mol% Pd,a 2:1 P to Pd ratio, and 10 mol% 1,3,5-trimethoxybenzene (internal standard) in 400 µL toluene.

The reaction plate was sealed, removed from the glovebox, and stirred for 18 hours at 100 °C. The yields are determined by ^{1}H NMR spectroscopy via relative peak integrations versus the internal standard. Additional control experiments can be found in Figure B1.

Full Factorial Screening 1a (Figure 3.3)

$Pd(OAc)_2$ was dispensed as a stock solution (0.08 M) in dichloromethane into 9 x 2 mL vials (1.8 mg, 0.008 mmol, or 3.4 mg, 0.015 mmol, or 4.6 mg, 0.02 mmol). Dichloromethane was then evaporated using a Genevac EZ-2 (Medium BP setting, no heat). These vials were then brought into the glovebox. A stock solution of SPhos (0.081 M, or 0.046 M) in toluene was dispensed to each plate (150, 300, 375, 750 µL or 500 µL respectively). A stock solution of **1a** (2.0 M) and 1,3,5-trimethoxybenzene (0.2 M, internal standard) in toluene was dispensed to each vial (100 µL). A stock solution of B_2Pin_2 (2.23 M, 1.52 M, or 1.62 M) in toluene was dispensed to each vial (100, 200, or 250 µL respectively) . Toluene was then dispensed to each vial to reach a total volume of 1.1 mL. The vials were sealed using Teflon-lined aluminum crimp caps, removed from the glovebox, and stirred for 18 hours at 100 °C. The conversion and yield are determined by ^1H NMR spectroscopy via relative peak integrations versus the internal standard.

Substrate Concentration Study 1a (Figure 3.3)

Inside the glovebox, 4 x 1 dram vials were charged with $Pd(OAc)_2$ (4.9 mg, 0.022 mmol) and SPhos (13.5 mg, 0.033 mmol). A separate set of 4 x 1 dram vials were charged with **1a** (40 mg, 0.22 mmol; 80 mg, 0.44 mmol; 120 mg, 0.66 mmol; or 160 mg, 0.88 mmol) and 1,3,5-trimethoxybenzene (internal standard; 3.7 mg, 0.022 mmol; 7.4 mg, 0.044 mmol; 11.1 mg, 0.066 mmol; 14.8 mg, 0.088 mmol). 4 x 2 mL vials were charged with B_2Pin_2 (111.5 mg, 0.44 mmol; 223.0 mg, 0.88 mmol; 334.5 mg, 1.32 mmol; or 445.9 mg, 1.76 mmol). The solids in the $Pd(OAc)_2$/SPhos vials were dissolved in 1.1 mL toluene, and transferred to the vials with **1a** and 1,3,5-trimethoxybenzene. Dissolution was ensured prior to transfer of these solutions to the 2 mL vials containing B_2Pin_2. Therefore, the reaction concentrations are 0.2 M, 0.4 M, 0.6 M, and 0.8

M with respect to **1a**, with 2.0 eq. B_2Pin_2, 0.1 equiv 1,3,5-trimethoxybenzene, $Pd(OAc)_2$ (2.5 mol%, 3.33 mol%, 5 mol%, and 10 mol%), and SPhos (3.75 mol%, 5.00 mol%, 7.5 mol% and 15 mol%). The reaction vials were sealed using Teflon-lined aluminum crimp caps, removed from the glovebox, and stirred for 18 hours at 100 °C. The conversion and yield are determined by ^{1}H NMR spectroscopy via relative peak integrations versus the internal standard.

Full Factorial Screening 2b-2g (Figure 3.4)

Under ambient atmosphere, for **2b** - **2d:** five 2 mL vials, and **2e** - **2g:** six 2 mL vials were charged with ^{DMP}DAB-Pd-MAH (2.0, 3.5, 5.0 mol%; 2.5, 4.3, 6.1 µmol; 1.2, 2.0, 2.9 mg respectively) by dispensing as an acetone solution (0.03 M). The solutions were evaporated to dryness using a Genevac EZ-2 (Low BP setting, no heat) before bringing the vials into the glovebox. Under N_2 atmosphere, vials were charged with 300 µL stock solution (pre-mixed: 6.5 equiv of 0.12 mmol substrate **2b** – **2g**, and 6.5 equiv of 0.012 mmol 1,3,5-trimethoxybenzene in 1.950 mL). For each B_2Pin_2 concentration level (1.2, 1.6, and 2.0 equiv; 0.15, 0.20, 0.25 mmol; 37.5, 50.0, 62.4 mg respectively) were dispensed as 200 µL stock solutions (0.75, 1.00, or 1.25 M respectively). Finally, PCy_3 (4.0, 7.0, 10.0 mol%; 5.0, 8.6, 12.2 µmol; 1.4, 2.4. 3.4 mg respectively) was dispensed as 100 µL stock solutions (0.05, 0.86, 1.22 M respectively). The vials were sealed with crimp caps, removed from N_2 atmosphere, and stirred for 18 hours at 100 °C. Final yields were determined by ^{1}H NMR via relative peak integrations versus the internal standard.

Evaluation of Methods A-G (Figure 3.5 and Figure B2)

Method A:

Under ambient atmosphere, a 1 dram vial was charged with the respective alkenyl carboxylate precursor (0.120 mmol), B_2Pin_2 (33.5 mg, 0.132 mmol), $Pd(OAc)_2$ (0.7 mg, 0.003

mmol), P(*o*-OMePh)$_3$ (1.6 mg, 0.005 mmol), 1,3,5-trimethoxybenzene (2.0 mg, 0.012 mmol), and 10:1 acetone:water (v/v) (0.6 M in alkenyl carboxylate). The reaction mixture was stirred at room temperature, open to air for 18 hours. The solutions were then evaporated to dryness, and NMR spectroscopic analysis conducted in $CDCl_3$ (0.6 mL).

Method B:

In the glovebox, a 2 mL vial was charged with the respective alkenyl carboxylate precursor (0.878 mmol), B_2Pin_2 (245.3 mg, 0.966 mmol), $Pd(OAc)_2$ (4.9 mg, 0.022 mmol), SPhos (13.5 mg, 0.033 mmol), 1,3,5-trimethoxybenzene (14.8 mg, 0.088 mmol), and toluene (0.8 M in alkenyl carboxylate). The reaction mixture was stirred at 100 °C for 18 hours. The solutions were then evaporated to dryness, and NMR spectroscopic analysis conducted in $CDCl_3$ (0.6 mL).

Method C:

In the glovebox, a J. Young NMR tube was charged with the respective vinyl carboxylate precursor (0.120 mmol), B_2Pin_2 (33.5 mg, 0.132 mmol), $Pd(PCy_3)_2$ (8.0 mg, 0.012 mmol), 1,3,5-trimethoxybenzene (2.0 mg, 0.012 mmol), and d_8-toluene (0.2 M in alkenyl carboxylate). The tubes were immersed in an oil bath set to 100 °C for 18 hours. ^{1}H NMR spectra were then obtained. These samples were then evaporated to dryness and NMR spectroscopic analysis was conducted in $CDCl_3$ (0.6 mL) for consistency with Methods A and B.

Method D:

In the glovebox, a 1 dram vial was charged with the respective alkenyl carboxylate precursor (0.120 mmol), B_2Pin_2 (60.9 mg, 0.240 mmol), ^{DMP}DAB-Pd-MAH (2.8 mg, 0.006 mmol), PCy_3 (3.4 mg, 0.012 mmol), 1,3,5-trimethoxybenzene (2.0 mg, 0.012 mmol), and toluene (0.6 M

in alkenyl carboxylate). The reaction mixture was stirred at 100 °C for 18 hours. The solutions were then evaporated to dryness, and NMR spectroscopic analysis conducted in $CDCl_3$ (0.6 mL).

Method F & **G**:

In the glovebox, a 1 dram vial was charged with $Pd(PCy_3)_2(OAc)_2$ (17.3 mg, 0.022 mmol), B_2Pin_2 (61.5 mg, 0.242 mmol) and toluene (1.1 mL, 0.2 M in alkenyl carboxylate). The vials were removed from the glovebox and stirred for 10 minutes at 100 °C (**Method F**), or 16 hours at 70°C (**Method G**). The vials were returned to the N_2 atmosphere and charged with the respective substrate (0.22 mmol) and 1,3,5-trimethoxybenzene (3.7 mg, 0.022 mmol). The vials were then removed from the glovebox and stirred for 18 hours at 100 °C. The conversion and yield are determined by ^1H NMR spectroscopy.

Protodeboronation Screening (Figure 3.7)

Compounds **2b**-**2g** were borylated at 0.5 mmol scale using the optimal borylation conditions detailed in Section 2.4. Only those with substrate conversions >95% were taken forward.

The alkenyl boronates were diluted in toluene (5.0 mL, 0.1 M), and 1.0 mL of the reaction solution was dispensed into 5 separate 1-dram vials. Into these vials 1.0 mL of either saturated Na_2CO_3, saturated $NaHCO_3$, saturated NaCl, H_2O, and 5% aqueous HCl were dispensed. These vials were sealed and stirred vigorously for 1 hour. The aqueous layer was removed using a Pasteur pipette, and the organic layer was dried with $MgSO_4$. The solutions were filtered and evaporated to dryness before ^1H NMR spectroscopy analysis conducted in $CDCl_3$. %Conversion is reported as [deboronated product] / [deboronated product + starting material] * 100%.

3.6.3 Synthesis of Starting Materials:

Starting Materials: Compounds prepared using literature procedures: **1a** (1-acetyloxy-5,5-dimethylcyclohex-1-en-3-one),[69] **1b** (5,5-dimethyl-3-oxocyclohex-1-en-1-yl pivalate),[69] **2i** (4-pivalyloxybenzopyran-2-one),[70]

General Synthesis 1: (Lactones)

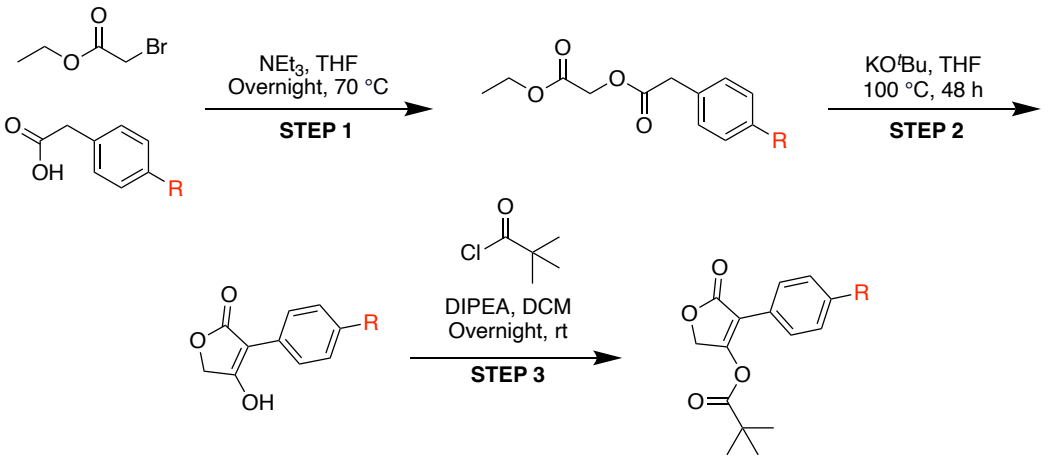

Figure 3.16: General Synthesis 1 (Lactones)

Step 1: A round bottom flask was charged with substituted phenyl acetic acid (1.0 equiv, [12.0 mmol]), triethyl amine (1.0 equiv, [1.22 g, 1.68 mL]), and THF (0.65 M [18.5 mL]). To the stirred solution ethyl bromoacetate (1.0 equiv, [2.01 g, 1.33 mL]) was added dropwise via syringe. The reaction was then stirred at 70 °C overnight. The reaction mixture was transferred to a separatory funnel and diluted with ethyl acetate (~2x (v/v) dilution [40 mL]), and H_2O (~2x (v/v) dilution [40 mL]). The organic phase is washed 3x with H_2O [40 mL]. The collected organic phase is dried with $MgSO_4$, filtered, and evaporated to dryness.

Step 2: *We found in order to optimize the yield of this reaction, that the maximum scale this step could be performed at was 3.5 mmol scale. Thusly this reaction was performed at larger scale in multiple 4-dram vials.* Potassium *tert*-butoxide (1.2 equiv) was evenly divided among the

appropriate number of 4-dram vials. THF (0.375 M) was dispensed into each vial. The esterification product synthesized in Step 1 was dissolved in THF (1/4 of previous amount in solution – net result is 0.3 M solution) and added dropwise evenly to the 4-dram vials. The 4-dram vials were sealed (with Teflon lined lids) and allowed to stir vigorously at 110 °C for 48 hours. The reaction mixtures were evaporated to dryness and resuspended in 1 M NaOH. The combined reaction mixtures were washed twice with hexanes. The aqueous phase was acidified slowly using 1 M HCl, until the product had fully precipitated out of solution. The product was collected by filtration, washing with hexanes. DMSO-d_6 used for ^{1}H NMR spectroscopy analysis.

Step 3: A round bottom flask was charged with the cyclized product from Step 2 (1.0 equiv), DIPEA (1.2 equiv), and DCM (0.3 M). Trimethylacetyl chloride (1.1 equiv) was added dropwise to the stirred solution and allowed to stir overnight at room temperature. The resulting organic phase was washed 3x with 1M HCl, 3x with saturated sodium bicarbonate, and dried with $MgSO_4$, before filtering and evaporating to dryness. The resulting oil was then triturated with hexanes to yield a colourless solid that can be analyzed by ^{1}H NMR spectroscopy in $CDCl_3$.

2b (4-pivalyloxy-3-phenylpyran-3-en-2-one)

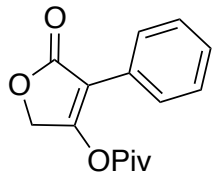

2b was synthesized using General Synthesis 1, detailed above. Step 1 was performed at 16.5 mmol scale [phenylacetic acid: 2.25 g], to produce 1.66 g, 39 % yield after Step 3.

^{1}H NMR (500 MHz, $CDCl_3$, 292 K, ppm): δ 7.84 (d, J=7.3 Hz, 2H), 7.46 (t, J=7.7 Hz, 2 H), 7.39 (t, J=7.6 Hz), 5.29 (s, 2H), 1.37 (s, 9H). ^{13}C NMR (126 MHz, $CDCl_3$, 292 K, ppm): δ 174.0, 170.8, 163.9, 128.7, 128.4, 128.2, 127.9, 110.6, 67.6, 39.6, 26.9. HRMS: Cal'd for $C_{15}H_{17}O_4$ $[M+H]^+$: 261.11269; found: 261.11212.

2c (4-pivalyloxy-3-(4-trifluoromethyl)phenylpyran-3-en-2-one)

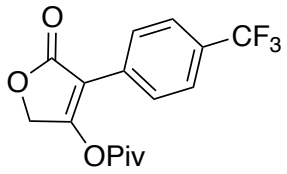

2c was synthesized using General Synthesis 1, detailed above. Step 1 was performed at 12.0 mmol scale [4-(trifluoromethyl)phenylacetic acid: 2.45 g], to produce 1.89 g, 48 % yield after Step 3.

^{1}H NMR (500 MHz, $CDCl_3$, 292 K, ppm): δ 7.95 (d, J = 8.2 Hz, 2H), 7.68 (d, J = 8.2 Hz, 2H), 5.31 (s, 2H), 1.35 (s, 9H).^{13}C NMR (126 MHz, $CDCl_3$, 292 K, ppm): δ 173.8, 170.4, 165.6, 131.6, 130.5 (q, J = 32.7 Hz), 128.6, 125.4 (q, 3.7 Hz), 124.0 (q, J = 272.7 Hz), 109.1, 67.8, 39.7, 26.9. ^{19}F NMR (282 MHz, $CDCl_3$, 292 K, ppm): δ -62.9. HRMS: Calc'd for $C_{16}H_{15}F_3O_4$ $[M+Na]^+$: 351.08146; found: 351.08148.

2d (3-(4-methoxyphenyl)-4-pivalyloxypyran-3-en-2-one)

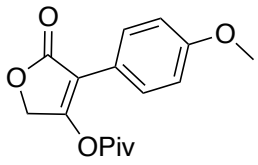

2d was synthesized using General Synthesis 1, detailed above. Step 1 was performed at 12.0 mmol scale [4-(methoxy)phenylacetic acid: 2.0 g], to produce 1.35 g, 39 % yield after Step 3.

^{1}H NMR (500 MHz, $CDCl_3$, 292 K, ppm): δ 7.66 (d, J = 8.9 Hz, 2H), 6.78 (d, J = 9.0 Hz, 2H), 5.01 (s, 2H), 3.63 (s, 3H), 1.20 (s, 9H). ^{13}C NMR (126 MHz, $CDCl_3$, 292 K, ppm): δ 173.8, 170.8, 162.6, 159.5, 129.3, 120.4, 113.6, 109.4, 67.3, 55.0, 39.3, 26.7. HRMS: Calc'd for $C_{16}H_{18}O_5$ $[M+Na]^+$: 313.10464; found: 313.10466.

General Synthesis 2: (Lactams)

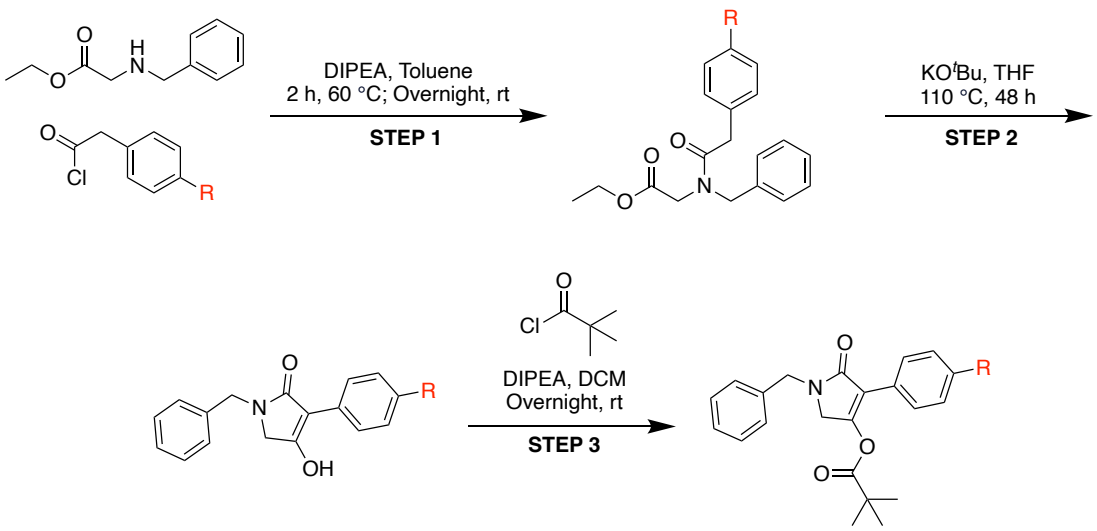

Figure 3.17: General Synthesis 2 (Lactams)

Step 1: A round bottom flask was charged with N-benzyl glycine ethyl ester (1.0 equiv [1.74 g, 1.64 mL]), DIPEA (1.5 equiv [1.74 g, 2.35 mL]), and toluene (0.5 M [18.0 mL]). The substituted phenylacetyl chloride (1.0 equiv [9.0 mmol]),[71] was dissolved in toluene (equal amount to what is previously in solution – net result is 0.25 M solution [18.0 mL]), and added dropwise to the stirred reaction. The stirred solution was then heated to 60 °C for 2 hours, then allowed to stir overnight at room temperature. The reaction mixture was washed with a solution of 50% saturated NH_4Cl and 50% H_2O [30 mL], then H_2O [30 mL], and then saturated aqueous

NaCl solution [30 mL]. The organic layer was dried with $MgSO_4$, filtered and evaporated to dryness. The crude product was taken forward in the next step.

Step 2: *We found in order to optimize the yield of this reaction, that the maximum scale this step could be performed at was 3.5 mmol scale. Thusly this reaction was performed at larger scale in multiple 4-dram vials.* Potassium *tert*-butoxide (1.2 equiv) was evenly divided among the appropriate number of 4-dram vials. THF (0.375 M) was dispensed into each vial. The alkylated amine synthesized in Step 1 was dissolved in THF (1/4 of previous amount in solution – net result is 0.3 M solution) and added dropwise evenly to the 4-dram vials. The 4-dram vials were sealed (with Teflon lined lids) and allowed to stir vigorously at 110 °C for 48 hours. The reaction mixtures were evaporated to dryness and resuspended in 1 M NaOH. The combined reaction mixtures were washed twice with hexanes. The aqueous phase was acidified slowly using 1 M HCl, until the product had fully precipitated out of solution. The product was collected by filtration, washing with hexanes. DMSO-d_6 used for ^{1}H NMR spectroscopy analysis.

Step 3: A round bottom flask was charged with the cyclized product from Step 2 (1.0 equiv), DIPEA (1.2 equiv), and DCM (0.3 M). Trimethylacetyl chloride (1.1 equiv) was added dropwise to the stirred solution and allowed to stir overnight at room temperature. The collected organic phase was washed 3x with 1M HCl, 3x with saturated sodium bicarbonate, and dried with $MgSO_4$, before filtering and evaporating to dryness. The resulting oil was then triturated with hexanes to yield a colourless solid that can be analyzed by ^{1}H NMR spectroscopy in $CDCl_3$.

2e(4-pivalyloxy-1-benzyl-3-phenylpyrrolidin-3-en-2-one)

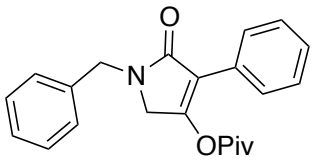

2e was synthesized using General Synthesis 2, detailed above. Step 1 was performed at 15.0 mmol scale [phenylacetyl chloride: 2.32 g], to produce 4.46 g, 63 % yield after Step 3.

^{1}H NMR (500 MHz, $CDCl_3$, 292 K, ppm): δ 7.83 (d, J=7.6 Hz, 2H), 7.46-7.29 (m, 8H), 4.73 (s, 2H), 4.27 (s, 2H), 1.30 (s, 9H). ^{13}C NMR (126 MHz, $CDCl_3$, 292 K, ppm): δ 174.8, 168.9, 157.1, 137.1, 129.4, 128.8, 128.6, 128.3, 128.2, 128.1, 127.7, 117.8, 49.2, 45.9, 39.4, 26.9. HRMS: Cal'd for $C_{22}H_{24}NO_3$ $[M+H]^+$: 350.17562; found: 350.17489.

2f (1-benzyl-4-pivalyloxy-3-(4-trifluoromethylphenyl)pyrrolidin-3-en-2-one)

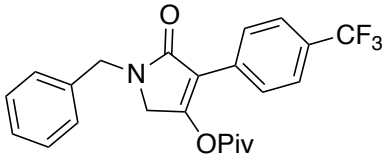

2f was synthesized using General Synthesis 2, detailed above. Step 1 was performed at 9.0 mmol scale [4-(trifluoromethyl)benzeneacetyl chloride: 2.0 g], to produce 1.65 g, 44 % yield after Step 3.

^{1}H NMR (500 MHz, CDCl3, 292 K, ppm): δ 7.96 (d, J = 8.2 Hz, 2H), 7.67 (d, J = 8.3 Hz, 2H), 7.33 (m, 5H), 4.71 (s, 2H), 4.30 (s, 2H), 1.29 (s, 9H). ^{13}C NMR (126 MHz, CDCl3, 292 K, ppm): δ 174.5, 168.4, 158.8, 136.9, 133.2, 129.9 (q, J = 32.6 Hz), 129.0, 128.9, 128.3, 127.9, 125.2 (q, J = 3.8 Hz), 124.2 (q, J = 272.3 Hz), 49.5, 46.0, 39.6, 27.0. ^{19}F NMR (282 MHz, CDCl3, 292 K, ppm): δ -62.7. HRMS: Calc'd for $C_{23}H_{22}F_3NO_3$ $[M+Na]^+$: 440.14440; found: 440.14441.

2g (1-benzyl-4-pivalyloxy-3-(4-methoxyphenyl)pyrrolidin-3-en-2-one)

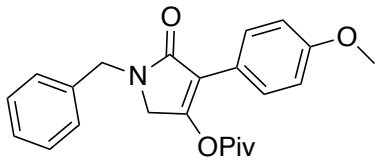

2g was synthesized using General Synthesis 2, detailed above. Step 1 was performed at 9.0 mmol scale[4-(methoxy)benzeneacetyl chloride: 1.66 g], to produce 2.13 g, 62 % yield after Step 3.

^{1}H NMR (500 MHz, $CDCl_3$, 292 K, ppm): δ 7.85 (d, J = 8.8 Hz, 2H), 7.27 (m, 5H), 6.95 (d, J = 8.8 Hz, 2H), 4.67 (s, 2H), 4.21 (s, 2H), 3.77 (s, 3H), 1.27 (s, 9H). ^{13}C NMR (126 MHz, $CDCl_3$, 292 K, ppm): δ 174.4, 168.9, 159.2, 155.8, 136.9, 129.7, 128.5, 127.9, 127.4, 121.8, 117.0, 113.4, 54.9, 48.9, 45.6, 39.1, 26.7. HRMS: Calc'd for $C_{23}H_{25}NO_4$ $[M+H]^+$: 380.18564; found: 380.18571.

2h 1-pivalyloxycyclopent-1-en-3-one:

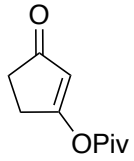

A 250 mL round bottom flask was charged with 1,3-cyclopentandione (3.0 g, 30.58 mmol), and DCM (60 mL). While stirring, DIPEA (10.65 mL, 61.16 mmol) was added. The round bottom flask was then submerged in an ice bath and trimethylacetyl chloride (3.84 mL, 31.19 mmol) was added dropwise over 20 minutes. The round bottom flask was removed from the ice bath and allowed to stir at room temperature overnight. The solution was filtered through a frit, washed three times with 1M HCl and reduced to dryness resulting in a brown oil. The crude product was then isolated by column chromatography using a hexanes/ethyl acetate solvent system on a

Biotage Selekt instrument. A dark orange oil was collected that solidified upon freezing. Dark orange oil (3.98 g, 73% yield).

^{1}H NMR (500 MHz, $CDCl_3$, 292 K, ppm): δ 6.23 (s, 1H), 2.80-2.76 (m, 2H), 2.50-2.46 (m, 2H), 1.33 (s, 9H). ^{13}C NMR (126 MHz, $CDCl_3$, 292 K, ppm): δ 206.8, 180.1, 174.0, 116.4, 39.6, 33.3, 28.7, 26.8. HRMS: Cal'd for $C_{10}H_{15}O_3$ $[M+H]^+$: 183.10212; found: 183.10157.

2j 4-pivalyloxy-6-methyl-2-pyrone:

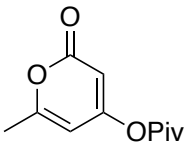

A 500 mL round bottom flask was charged with 6-methyl-4-hydroxypyrone (10 g, 79.3 mmol) and DCM (150 mL). While stirring, DIPEA (18.0 mL, 103 mmol) was added. The round bottom flask was then submerged in an ice bath and trimethylacetyl chloride (10.0 mL, 81.3 mmol) was added dropwise over 10 minutes. The round bottom flask was removed from the ice bath and allowed to stir at room temperature for two hours. The reaction mixture was washed with 1M HCl, dried using $MgSO_4$, filtered, and evaporated to dryness. A colourless oil was collected that solidified upon freezing. Colourless oil, (15.0 g, 90% yield).

^{1}H NMR (500 MHz, $CDCl_3$, 292 K, ppm): δ 5.93 (dd, J=2.0, 0.5, 1H), 5.86-5.84 (m, 1H), 2.19 (s, 3H), 1.25 (s, 9H). ^{13}C NMR (126 MHz, $CDCl_3$, 292 K, ppm): δ 174.7, 163.8, 163.6, 163.2, 101.4, 101.1, 39.5, 26.8, 20.1. HRMS: Cal'd for $C_{11}H_{15}O_4$ $[M+H]^+$: 211.09704; found: 211.09647.

3.6.4 Palladium Precatalysts

Compounds prepared using literature references: **$Pd_2(dba)_3 \cdot CHCl_3$**,[72] **^{DMP}DAB-Pd-MAH**,[49] **$Pd(PCy_3)_2(OAc)_2$**,[54] **$[Pd(acetanilide)OAc]_2$**.[73]

3.6.5 3,4-Diethylhexane-3,4-diol Synthesis

Caution: Read appropriate SDS before conducting this synthesis. Reaction should be performed in a fume hood. HCl gas is formed, the open neck of the flask should point towards the back of the fume hood.

This synthesis was adapted from literature,[74] with some modifications.

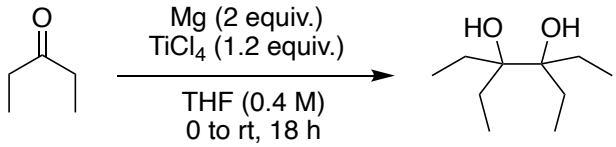

A two-necked round bottom flask was charged with Mg turnings (1.92 g, 78.95 mmol, 2 equiv), this was flushed with N_2 thoroughly before 60 mL anhydrous THF added to flask. The flask was then cooled to 0 °C. While under constant N_2 flow (through septum on one neck of flask – other neck of flask open and pointing into back of fume hood) $TiCl_4$ (5.2 mL, 47.37 mmol, 1.2 equiv) was added dropwise (through septum with N_2). Once complete, another 30 mL anhydrous THF was used to wash contents down in flask. After 30 mins, 0 °C was maintained, and 3-pentanone (4.2 mL, 39.48 mmol, 1 equiv) was added dropwise slowly. The reaction mixture was allowed to stir overnight and allowed to reach room temperature. The reaction was then quenched slowly with saturated Na_2CO_3 solution (~150 mL). Once gas evolving ceased, the reaction mixture was filtered through a pad of silica under vacuum. Dichloromethane (~400 mL)

was used to wash product through while constantly manually stirring with a spatula. The eluent was then extracted with diethyl ether, creating a triphasic mixture. Both organic layers were removed, dried with $MgSO_4$, filtered and evaporated to dryness to yield the final product (1.88g, 55% yield).

B_2EPin_2 was then synthesized according to the literature protocol.[50]

3.6.6 Synthesis of Alkenyl Pinacol Boronates

General Synthesis 3: (Borylation)

Method D:

In the glovebox, a 1 dram vial was charged with the respective lactam alkenyl carboxylate precursor (0.50 mmol), B_2Pin_2 (253.9 mg, 1.00 mmol), ^{DMP}DAB-Pd-MAH (11.7 mg, 0.025 mmol), PCy_3 (14.0 mg, 0.05 mmol), and toluene (2.5 mL, 0.2 M in alkenyl carboxylate). The reaction mixture was stirred at 100 °C for 18 hours. The solutions were then evaporated to dryness, and NMR spectroscopic analysis conducted in $CDCl_3$ (0.6 mL).

Method E:

In the glovebox, a 1 dram vial was charged with the respective lactone alkenyl carboxylate precursor (0.50 mmol), B_2Pin_2 (203.2 mg, 0.80 mmol), ^{DMP}DAB-Pd-MAH (8.2 mg, 0.018 mmol), PCy_3 (9.8 mg, 0.035 mmol), and toluene (2.5 mL, 0.2 M in alkenyl carboxylate). The reaction mixture was stirred at 100 °C for 18 hours. The solutions were then evaporated to dryness, and NMR spectroscopic analysis conducted in $CDCl_3$ (0.6 mL).

Characterization data

The following are known compounds; spectroscopic data matches previous reports:

3a (1-(4,4,5,5-tetramethyl-1,3,2- dioxaborolan-2-yl)-5,5-dimethylcyclohex-1-en-3-one)[75]

3h (1-(4,4,5,5-tetramethyl-1,3,2- dioxaborolan-2-yl)cyclop ent-1-en-3-one)[76]

The following were synthesized using **Methods C**, **D**, or **E**:

3b (4-(4,4,5,5-tetramethyl-1,3,2- dioxaborolan-2-yl)-3-phenylpyran-3-en-2-one):

Method C was performed.

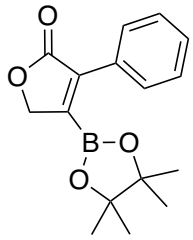

^{1}H NMR (500 MHz, $CDCl_3$, 292 K, ppm): δ 7.74-7.69 (m, 2H), 7.42-7.37 (m, 3H), 4.98 (s, 1H), 1.30 (s, 12H). ^{13}C NMR (126 MHz, $CDCl_3$, 292 K, ppm): δ 173.4, 144.4, 140.2, 130.5, 129.2, 127.9, 84.9, 72.8, 24.7. HRMS: Cal'd for $C_{16}H_{19}BO_4$ $[M+H]^+$: 287.14547; found: 287.14511.

3c (4-(4,4,5,5-tetramethyl-1,3,2-dioxaborolan-2-yl)-3-(4-(trifluoromethyl)phenyl)furan-2(5*H*)-one):

Method E was performed.

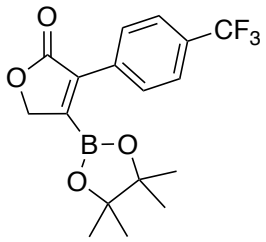

^{1}H NMR (500 MHz, $CDCl_3$, 292 K, ppm): δ 7.81 (d, J = 8.2 Hz, 2H), 7.63 (d, J = 8.3 Hz, 2H), 4.99 (s, 2H), 1.27 (s, 12H). ^{13}C NMR (126 MHz, $CDCl_3$, 292 K, ppm): δ 173.07, 139.20, 134.05, 131.09 (q, J = 32.6 Hz), 129.78, 126.75, 124.90 (q, J = 3.6 Hz) 85.24, 73.16, 24.78. ^{19}F NMR (282

MHz, $CDCl_3$, 292 K, ppm): δ -62.78. HRMS: Calc'd for $C_{17}H_{18}BF_3O_4$ $[M+H]^+$: 355.13230; found: 355.13223.

3d (3-(4-methoxyphenyl)-4-(4,4,5,5-tetramethyl-1,3,2-dioxaborolan-2-yl)furan-2(5*H*)-one)

Method E was performed.

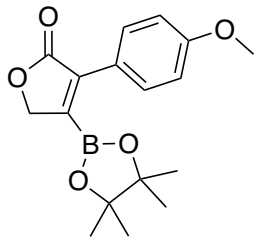

^{1}H NMR (500 MHz, $CDCl_3$, 292 K, ppm): δ 7.71 – 7.67 (m, 2H), 6.90 – 6.87 (m, 2H), 4.92 (s, 2H), 3.81 (s, 3H), 1.27 (s, 12H). ^{13}C NMR (126 MHz, $CDCl_3$, 292 K, ppm): δ 173.82, 139.68, 130.82, 128.40, 123.17, 113.42, 84.85, 72.86, 55.33, 24.78. HRMS: Calc'd for $C_{17}H_{21}BO_5$ $[M+H]^+$: 317.15548; found: 317.15528.

3e (4-(4,4,5,5-tetramethyl-1,3,2- dioxaborolan-2-yl)-1-benzyl-3-phenylpyrrolidin-3-en-2-one):

Method C was performed.

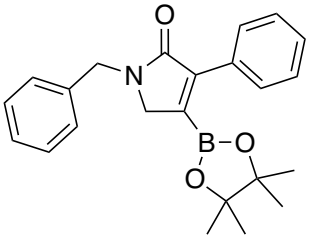

^{1}H NMR (500 MHz, $CDCl_3$, 292 K, ppm): δ 7.75-7.70 (m, 2H), 7.45-7.29 (m, 8H), 4.73 (s, 2H), 4.00 (s, 2H), 1.26 (s, 12H). ^{13}C NMR (126 MHz, $CDCl_3$, 292 K, ppm): 170.0, 137.4, 129.5,

128.7, 128.6, 128.4, 128.3, 128.1, 127.6, 127.0, 84.2, 53.1, 46.8, 24.6. HRMS: Cal'd for $C_{23}H_{27}BNO_3$ [M+H]: 376.20840; found: 376.20806.

3f (1-benzyl-4-(4,4,5,5-tetramethyl-1,3,2-dioxaborolan-2-yl)-3-(4-(trifluoromethyl)phenyl)-1,5-dihydro-2*H*-pyrrol-2-one):

Method D was performed.

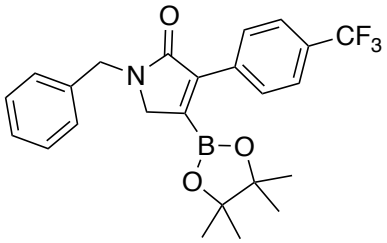

^{1}H NMR (500 MHz, $CDCl_3$, 292 K, ppm): δ 7.84 (d, J = 8.1 Hz, 2H), 7.64 (d, J = 8.2 Hz, 2H), 7.38 - 7.24 (m, 5H), 4.73 (s, 2H), 4.04 (s, 2H), 1.25 (s, 12H). ^{13}C NMR (126 MHz, $CDCl_3$, 292 K, ppm): δ 169.96, 146.26, 137.5, 137.12, 135.94, 130.37 (q, J = 32.3 Hz), 130.02, 128.87, 128.40, 127.78, 124.56 (q, J = 3.8 Hz), 84.58, 53.47, 46.93, 24.73. ^{19}F NMR (282 MHz, $CDCl_3$, 292 K, ppm): δ -62.59. HRMS: Calc'd for $C_{24}H_{28}BF_3NO_3$ $[M+H]^+$: 444.19524; found: 444.19512.

3g (1-benzyl-3-(4-methoxyphenyl)-4-(4,4,5,5-tetramethyl-1,3,2-dioxaborolan-2-yl)-1,5-dihydro-2*H*-pyrrol-2-one):

Method D was performed.

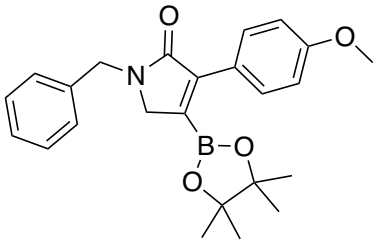

^{1}H NMR (500 MHz, $CDCl_3$, 292 K, ppm): δ 7.73 – 7.70 (m, 2H), 7.35 – 7.23 (m, 5H), 6.93 – 6.89 (m, 2H), 4.71 (s, 2H), 3.97 (s, 2H), 3.84 (s, 3H), 1.25 (s, 12H). ^{13}C NMR (126 MHz, $CDCl_3$, 292 K, ppm): δ 170.65, 137.37, 131.02, 128.78, 128.74, 128.33, 128.14, 127.58, 125.07, 113.12, 84.19, 55.27, 53.14, 46.83, 24.71. HRMS: Calc'd for $C_{24}H_{28}BNO_4$ $[M+H]^+$: 406.21842; found: 406.21816.

3i (4-(4,4,5,5-tetramethyl-1,3,2- dioxaborolan-2-yl)benzopyran-2-one):

Method C was performed.

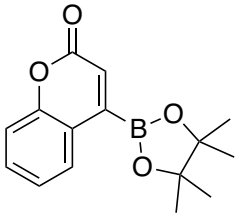

^{1}H NMR (500 MHz, $CDCl_3$, 292 K, ppm): δ 8.21 (dd, J=8.0, 0.7 Hz, 1H), 7.51 (t, J = 7.6 Hz 1H), 7.29 (q, J = 8.1 Hz, 2H), 6.91 (s, 1H), 1.41 (s, 12H). ^{13}C NMR (126 MHz, $CDCl_3$, 292 K, ppm): δ 160.2, 153.8, 131.3, 128.8, 125.5, 124.3, 120.6, 116.8, 85.1, 24.9. HRMS: Cal'd for $C_{15}H_{17}BO_4$ $[M+H]^+$: 273.12982; found: 273.12928.

3j (4-(4,4,5,5-tetramethyl-1,3,2- dioxaborolan-2-yl)-6-methyl-2H-pyran-2-one)**:**

Method C was performed.

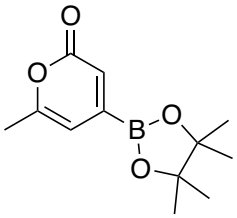

^{1}H NMR (500 MHz, $CDCl_3$, 292 K, ppm): δ 6.59 (s, 1H), 6.20 (s, 1H), 2.24 (s, 3H), 1.34 (s, 12H). ^{13}C NMR (126 MHz, $CDCl_3$, 292 K, ppm): δ 162.4, 161.3, 120.5, 105.8, 85.0, 24.5, 19.7. HRMS: Cal'd for $C_{12}H_{18}BO_4$ $[M+H]^+$: 237.12982; found: 237.12931.

3.6.7 Deboronation Products

General Synthesis 4: (Deboronation – Figure 3.8)

Method D or **E** (Section 3.4) was performed before the **Deboronation Procedure**:

Deboronation Procedure

The appropriate alkenyl boronate **3** (generated using Method **D** or **E**) was resuspended in a 4-dram vial with toluene (2.5 mL, 0.2 M in substrate). Saturated aqueous $NaHCO_3$ (2.5 mL, (1:1 v/v to toluene)) was dispensed into the vial. The reaction mixture was allowed to stir vigorously at 40 °C overnight. The reaction mixture was then transferred to a separatory funnel using toluene and H_2O. The aqueous phase was acidified using 5% HCl solution to pH = 2, extracted with ethyl acetate (~10 mL) twice. The combined organic fractions were dried using $MgSO_4$ and evaporated to dryness before column chromatography using Biotage Selekt instruments (details in Appendix B). Isolated yields are given in Figure 3.8.

Characterization data

The following are known compounds; spectroscopic data matches previous reports:

4b (3-phenyl-phenylfuran-2(5H)-one),[77]

4c (3-(4-trifluoromethyl)phenylfuran-2(5H)-one),[77]

4d (3-(4-methoxyphenyl)-phenylfuran-2(5H)-one),[77]

4e (1-benzyl-3-phenyl-1,5-dihydro-2H-pyrrol-2-one).[66]

4f (1-benzyl-3-(4-(trifluoromethyl)phenyl)-1,5-dihydro-2*H*-pyrrol-2-one):

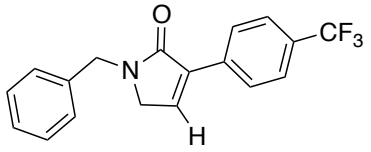

^{1}H NMR (500 MHz, $CDCl_3$, 292 K, ppm): δ 8.06 (d, J = 8.1 Hz, 2H), 7.67 (d, J = 8.2 Hz, 2H), 7.38 – 7.35 (m, 2H), 7.32 – 7.29 (m, 4H), 4.74 (s, 2H), 3.96 (d, J = 2.1 Hz, 2H). ^{13}C NMR (126 MHz, $CDCl_3$, 292 K, ppm): δ 169.48, 137.53, 137.14, 136.00, 135.30, 130.38 (q, J = 32.4 Hz), 128.94, 128.19, 127.82, 127.39, 125.44 (q, J = 3.8 Hz), 124.24 (q, J = 272.1 Hz), 50.02, 46.54. ^{19}F NMR (282 MHz, $CDCl_3$, 292 K, ppm): δ -62.65. HRMS: Calc'd for $C_{18}H_{14}F_3NO$ $[M+H]^+$: 318.11003; found: 318.10980.

4g (1-benzyl-3-(4-methoxyphenyl)-1,5-dihydro-2*H*-pyrrol-2-one):

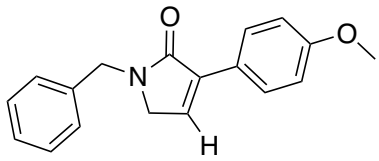

^{1}H NMR (500 MHz, $CDCl_3$, 292 K, ppm): δ 7.98 – 7.86 (m, 2H), 7.38 – 7.33 (m, 2H), 7.32 – 7.28 (m, 3H), 7.07 (t, J = 2.2 Hz, 1H), 6.97 – 6.91 (m, 2H), 4.73 (s, 2H), 3.88 (d, J = 2.2 Hz, 2H), 3.85 (s, 3H). ^{13}C NMR (126 MHz, $CDCl_3$, 292 K, ppm): δ 170.26, 159.90, 137.45, 136.27, 133.44,

128.81, 128.34, 128.13, 127.61, 124.60, 113.90, 55.35, 49.76, 46.44. HRMS: Calc'd for $C_{18}H_{17}NO_2$ $[M+Na]^+$: 302.11515; found: 302.11507.

3.6.8 Synthesis of Alkenyl Ethylpinacol Boronates

General Synthesis 5: (Ethylpinacol Borylation – Figure 3.9)

For isolation, **Method D** or **E** (Section 3.6.6) was performed, substituting B_2EPin_2 for B_2Pin_2 at 0.25 mmol scale. (**Method D**: B_2EPin_2: 183.9 mg, 0.50 mmol; **Method E**: B_2EPin_2: 147.1 mg, 0.40 mmol).

For yield (Figure 3.9), **Method D** or **E** (Section 3.6.6) was performed, substituting B_2EPin_2 for B_2Pin_2 at 0.20 mmol scale (**Method D**: B_2EPin_2: 147.1 mg, 0.40 mmol; **Method E**: B_2EPin_2: 117.7 mg, 0.32 mmol).

Products were isolated by column chromatography on Biotage Selekt instruments (chromatograms can be found in Appendix B). Single fractions were utilized to acquire characterization data as co-elution of starting material, deboronated product and ethylpinacol was a persistent issue. Further purification attempts led to deboronation.

Characterization data

6b (1-(4,4,5,5-tetraethyl-1,3,2- dioxaborolan-2-yl)-3-phenylpyran-3-en-2-one):

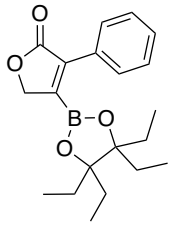

^{1}H NMR (500 MHz, $CDCl_3$, 292 K, ppm): δ 7.74 – 7.71 (m, 2H), 7.39 – 7.36 (m, 3H), 4.98 (s, 2H), 1.74 – 1.63 (m, 8H), 0.88 (t, J = 7.5 Hz, 12H). ^{13}C NMR (126 MHz, $CDCl_3$, 292 K, ppm): δ

173.69, 140.48, 130.78, 129.45, 129.27, 127.96, 90.15, 73.15, 26.34, 8.83. HRMS: Calc'd for $C_{20}H_{27}BO_4$ $[M+H]^+$: 343.29752; found: 343.29743.

6c (1-(4,4,5,5-tetraethyl-1,3,2- dioxaborolan-2-yl) -3-(4-trifluoromethyl)phenylpyran-3-en-2-one)**:**

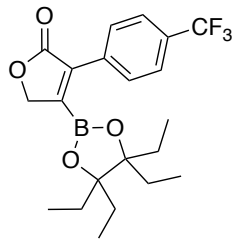

^{1}H NMR (500 MHz, $CDCl_3$, 292 K, ppm): δ 7.86 (d, J = 8.2 Hz, 2H), 7.64 (d, J = 8.3 Hz, 2H), 5.01 (s, 2H), 1.75 – 1.63 (m, 8H), 0.88 (t, J = 7.5 Hz, 12H). ^{13}C NMR (126 MHz, $CDCl_3$, 292 K, ppm): δ 173.17, 139.40, 134.21, 131.09 (q, J = 32.8 Hz) 129.91, 124.87 (q, J = 3.8 Hz), 124.18 (q, J = 271.9 Hz) 90.46, 73.34, 26.36, 8.82. ^{19}F NMR (282 MHz, $CDCl_3$, 292 K, ppm): δ -62.82. HRMS: Calc'd for $C_{21}H_{26}BF_3O_4$ $[M+H]^+$: 411.19490; found: 411.19477.

6d (1-(4,4,5,5-tetraethyl-1,3,2- dioxaborolan-2-yl) -3-(4-methoxy)phenylpyran-3-en-2-one)**:**

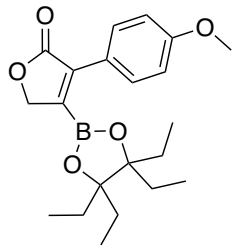

^{1}H NMR (500 MHz, $CDCl_3$, 292 K, ppm): δ 7.76 (d, J = 8.9 Hz, 2H), 6.89 (d, J = 8.9 Hz, 2H), 4.94 (s, 2H), 3.83 (s, 3H), 1.74 – 1.64 (m, 8H), 0.89 (t, J = 7.5 Hz, 12H). ^{13}C NMR (126 MHz, $CDCl_3$, 292 K, ppm): δ 174.01, 160.49, 139.78, 131.00, 123.37, 113.41, 90.06, 73.11, 55.43, 26.37, 8.88.

HRMS: Calc'd for $C_{21}H_{29}BO_5$ $[M+H]^+$: 373.21808; found: 373.21795.

6e (1-(4,4,5,5-tetraethyl-1,3,2- dioxaborolan-2-yl) -1-benzyl-3-phenylpyrrolidin-3-en-2-one):

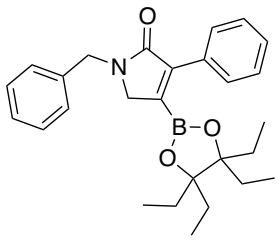

^{1}H NMR (500 MHz, $CDCl_3$, 292 K, ppm): δ 7.73 – 7.70 (m, 2H), 7.42 – 7.27 (m, 8H), 4.72 (s, 2H), 4.00 (s, 2H), 1.75 – 1.58 (m, 8H), 0.84 (t, J = 7.5 Hz, 12H). ^{13}C NMR (126 MHz, $CDCl_3$, 292 K, ppm): δ 170.59, 147.62, 137.58, 132.64, 129.71, 128.91, 128.54, 128.36, 127.66, 127.16, 89.47, 53.47, 46.89, 26.29, 8.85. HRMS: Calc'd for $C_{27}H_{34}BNO_3$ $[M+H]^+$: 432.27045; found: 432.27037.

6f (1-(4,4,5,5-tetraethyl-1,3,2- dioxaborolan-2-yl) -1-benzyl-3-(4-trifluoromethyl)phenylpyrrolidin-3-en-2-one):

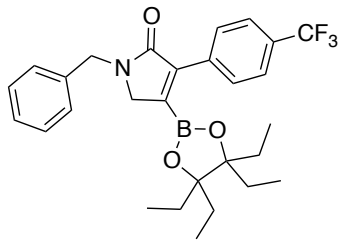

^{1}H NMR (500 MHz, $CDCl_3$, 292 K, ppm): δ 7.83 (d, J = 8.2 Hz, 2H), 7.61 (d, J = 8.3 Hz, 2H), 7.37 – 7.28 (m, 5H), 4.72 (s, 2H), 4.03 (s, 2H), 1.75 – 1.58 (m, 8H), 0.83 (t, J = 7.4 Hz, 12H). ^{13}C NMR (126 MHz, $CDCl_3$, 292 K, ppm): 170.10, 146.50, 137.32, 136.13, 130.33 (q, J = 32.4 Hz), 130.12, 128.92, 128.38, 127.78, 124.55 (q, J = 3.7 Hz), 124.4 (q, J = 271.9 Hz), 89.75, 53.64,

46.94, 26.30, 8.81. ^{19}F NMR (282 MHz, $CDCl_3$, 292 K, ppm): δ -62.67. HRMS: Calc'd for $C_{28}H_{33}BF_3NO_3$ $[M+H]^+$: 500.25784; found: 500.25744.

6g (1-(4,4,5,5-tetraethyl-1,3,2- dioxaborolan-2-yl) -1-benzyl-3-(4-methoxy)phenylpyrrolidin-3-en-2-one):

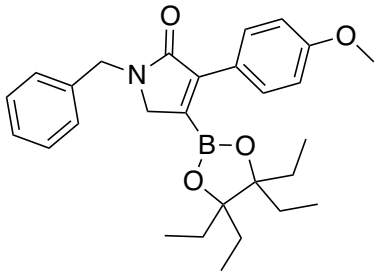

^{1}H NMR (500 MHz, $CDCl_3$, 292 K, ppm): δ 7.77 - 7.74 (m, 2H), 7.36 – 7.27 (m, 5H), 6.91 – 6.88 (m, 2H), 4.71 (s, 2H), 3.97 (s, 2H), 3.83 (s, 3H), 1.71 – 1.59 (m, 8H), 0.86 (t, J = 7.4 Hz, 12H). ^{13}C NMR (126 MHz, $CDCl_3$, 292 K, ppm): δ 170.84, 146.88, 137.61, 131.18, 130.03, 128.82, 128.42, 127.61, 125.32, 113.12, 89.37, 55.39, 53.40, 46.87, 26.31, 8.89. HRMS: Calc'd for $C_{28}H_{36}BNO_4$ $[M+H]^+$: 462.28102; found: 462.28077.

3.6.9 Suzuki Coupling

Suzuki Cross-Coupling of Alkenyl Boronates: (Figure 3.6)

Cross-coupling products were prepared by borylation using one of **Method A**, **B**, or **C** (1.0 mmol scale with respect to alkenyl pivalate precursor unless otherwise noted), followed by evaporating the reaction mixture to dryness, and then subjecting the crude product to **Arylation Procedure 1.**

Arylation Procedure 1:

The crude boronate ester was dissolved in toluene [10 ml], filtered through a pad of Celite, washed three times with saturated NaCl [10 ml], dried with $MgSO_4$, filtered, and then evaporated to dryness in a 20 mL vial with a septum cap. The vial was brought into the glovebox, and charged with $Pd(OAc)_2$ (4.5 mg, 0.02 mmol), XPhos (14.3 mg, 0.03 mmol), K_3PO_4 (425.7 mg, 2.0 mmol), bromobenzene (157.0 mg, 1.0 mmol) and toluene (5 mL, 0.2 M in alkenyl carboxylate). The vial was brought outside the glovebox, degassed H_2O [1 mL] was injected through the septum, and the reaction mixture stirred at 80 °C for 18 hours. The solution was then filtered through a pad of celite and evaporated to dryness. The crude product was then isolated by column chromatography using hexanes/ethyl acetate on a Biotage Selekt instrument (see Appendix B).

5a 1-phenyl-5,5-dimethylcyclohex-1-en-3-one

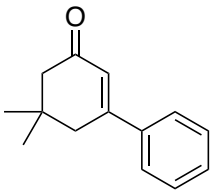

This product is prepared by borylation via **Method B** (3.3 mmol scale) followed by the cross-coupling procedure described above. NMR spectral data is consistent with that previously reported.[47] Yield: 297.8 mg (45%, yellow oil).

5h 1-phenylcyclopent-1-en-3-one

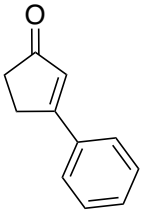

This product is prepared by borylation via **Method A** followed by the cross-coupling procedure described above. NMR spectral data is consistent with that previously reported.[47] Yield: 48.9 mg (24%, yellow solid).

5i 4-phenylbenzopyran-2-one

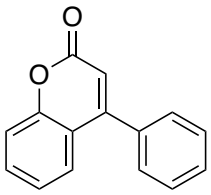

This product is prepared by borylation via **Method C** followed by the cross-coupling procedure described above. NMR spectral data is consistent with that previously reported.[47] Yield: 35.1 mg (16%, brown solid). The protodeboronation product (i.e. coumarin) was also obtained.[78] Yield: 46.7 mg (32%).

5j 4-phenyl-6-methyl-2*H*-pyran-2-one

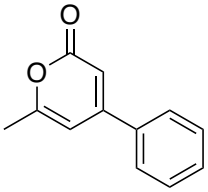

This product is prepared by borylation via **Method C** followed by the cross-coupling procedure described above. NMR spectral data is consistent with that previously reported.[79] Yield: 59.0 mg (32%, beige solid).

5e 4-phenyl-1-benzyl-3-phenylpyrrolidin-3-en-2-one

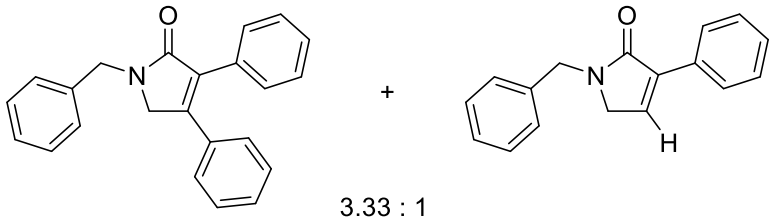

3.33 : 1

This product was attempted to be prepared by borylation via **Method C** followed by the cross-coupling procedure described above. Upon isolation using automated chromatography, we observe a 3.33 : 1 mixture of **5e** and **4e**. NMR spectral data for **5e** is consistent with that previously reported.[47] Yield: 151.7 mg (49% based on observed product ratio, yellow oil).

4b 3-phenylfuran-2(5H)-one

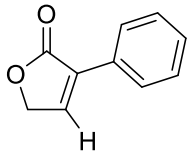

This product was prepared by borylation via **Method C** (0.500 mmol scale), followed by filtration of the crude reaction solution through Celite. The organic phase [5 mL total volume toluene] was then washed with 3 x 5 mL saturated $NaHCO_3$, and the organic layer dried over $MgSO_4$ before concentration in vacuo. The crude product was then isolated by column chromatography using hexanes/ethyl acetate on a Biotage Selekt instrument. NMR spectral data is consistent with that previously reported.[67] Yield: 52.8 mg (66%, yellow solid).

4e 1-benzyl-3-phenylpyrrolidin-3-en-2-one

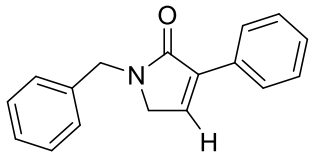

This product was prepared by borylation via **Method C** (0.500 mmol scale), followed by filtration of the crude reaction solution through Celite. The organic phase [5 mL total volume toluene] was then washed with 3 x 5 mL saturated $NaHCO_3$, and the organic layer dried over $MgSO_4$ before concentration in vacuo. The crude product was then isolated by column chromatography using hexanes/ethyl acetate on a Biotage Selekt instrument. NMR spectral data is consistent with that previously reported.[66] Yield: 53.9 mg (43%, yellow oil).

Synthesis of **5d** (Equation 1):

Method E (Section 3.4) was performed substituting B_2EPin_2 for B_2Pin_2 at 0.25 mmol scale (**Method E**: B_2EPin_2: 147.1 mg, 0.40 mmol), before the **Arylation Procedure 2**:

Arylation Procedure 2:

Under a N_2 atmosphere, a 1 dram vial was charged with the borylated (EPin) lactone from Methods **E**, $Pd(OAc)_2$ (1.1 mg, 0.005 mmol), XPhos (3.6 mg, 0.008 mmol), K_3PO_4 (106.9 mg, 0.50 mmol) and bromobenzene (39.4 mg, 26.8 µL, 0.25 mmol). Toluene (1.25 mL, 0.2 M) was dispensed into the vial and sealed with a septum cap. On the bench, 1.25 mL degassed H_2O was dispensed into the vial and the reaction mixture was allowed to stir vigorously at 80°C for 18 hours. The reaction mixture was then transferred to a separatory funnel using toluene and H_2O, the aqueous layer was extracted with toluene twice [10 mL]. The combined organic fractions were dried using $MgSO_4$, filtered, and evaporated to dryness. To remove the ethylpinacol generated in

this reaction, B_2EPin_2 was reformed by the crude product being combined with $B_2(OH)_4$ (18.0 mg, 0.20 mmol), NaOAc (18.5 mg, 0.23 mmol), and a scoop of sodium sulfate as a drying reagent in a 50 mL round bottom flask. Toluene (3.0 mL, 0.08 M) was used to resuspend the reaction mixture, and the round bottom flask was fitted with a condenser and swept with N_2. Under N_2, the reaction mixture was allowed to stir vigorously overnight at 120 °C. The reaction mixture was allowed to cool before filtering and evaporating to dryness before column chromatography using a Biotage Selekt instrument (chromatogram in Appendix B) to yield **5d** (36.7 mg, 55% yield). Spectroscopic data matches that previously reported.[80]

3.7 References

(1) Konowalchuk, D. J.; Schneider, O. M.; Hall, D. G. Saturated ($C(Sp^3)$ B) Boronic Acid Derivatives. In *Reference Module in Chemistry, Molecular Sciences and Chemical Engineering*; Elsevier, 2024; p B9780323960250000491.

(2) Schneider, O. M.; Konowalchuk, D. J.; Hall, D. G. Unsaturated ($C(Sp^2/Sp)$–B) Boronic Acid Derivatives. In *Reference Module in Chemistry, Molecular Sciences and Chemical Engineering*; Elsevier, 2024; p B9780323960250000508.

(3) Wang, M.; Shi, Z. Methodologies and Strategies for Selective Borylation of C–Het and C–C Bonds. *Chem. Rev.* **2020**, *120* (15), 7348–7398. https://doi.org/10.1021/acs.chemrev.9b00384.

(4) J. Geier, S.; M. Vogels, C.; A. Melanson, J.; A. Westcott, S. The Transition Metal-Catalysed Hydroboration Reaction. *Chem. Soc. Rev.* **2022**, *51* (21), 8877–8922. https://doi.org/10.1039/D2CS00344A.

(5) Guria, S.; Mahamudul Hassan, M. M.; Chattopadhyay, B. C–H Borylation: A Tool for Molecular Diversification. *Org. Chem. Front.* **2024**, *11* (3), 929–953. https://doi.org/10.1039/D3QO01931D.

(6) Yu, I. F.; Wilson, J. W.; Hartwig, J. F. Transition-Metal-Catalyzed Silylation and Borylation of C–H Bonds for the Synthesis and Functionalization of Complex Molecules. *Chem. Rev.* **2023**, *123* (19), 11619–11663. https://doi.org/10.1021/acs.chemrev.3c00207.

(7) Hassan, M. M. M.; Guria, S.; Dey, S.; Das, J.; Chattopadhyay, B. Transition Metal–Catalyzed Remote C–H Borylation: An Emerging Synthetic Tool. *Sci. Adv.* **2023**, *9* (16), eadg3311. https://doi.org/10.1126/sciadv.adg3311.

(8) Brown, D. G.; Boström, J. Analysis of Past and Present Synthetic Methodologies on Medicinal Chemistry: Where Have All the New Reactions Gone? *J. Med. Chem.* **2016**, *59* (10), 4443–4458. https://doi.org/10.1021/acs.jmedchem.5b01409.

(9) Mennen, S. M.; Alhambra, C.; Allen, C. L.; Barberis, M.; Berritt, S.; Brandt, T. A.; Campbell, A. D.; Castañón, J.; Cherney, A. H.; Christensen, M.; Damon, D. B.; Eugenio de Diego, J.; García-Cerrada, S.; García-Losada, P.; Haro, R.; Janey, J.; Leitch, D. C.; Li, L.; Liu, F.; Lobben, P. C.; MacMillan, D. W. C.; Magano, J.; McInturff, E.; Monfette, S.; Post, R. J.; Schultz, D.; Sitter, B. J.; Stevens, J. M.; Strambeanu, I. I.; Twilton, J.; Wang, K.; Zajac, M. A. The Evolution of High-Throughput Experimentation in Pharmaceutical Development and Perspectives on the Future. *Org. Process Res. Dev.* **2019**, *23* (6), 1213–1242. https://doi.org/10.1021/acs.oprd.9b00140.

(10) Miyaura, Norio.; Suzuki, Akira. Palladium-Catalyzed Cross-Coupling Reactions of Organoboron Compounds. *Chem. Rev.* **1995**, *95* (7), 2457–2483. https://doi.org/10.1021/cr00039a007.

(11) Martin, R.; Buchwald, S. L. Palladium-Catalyzed Suzuki−Miyaura Cross-Coupling Reactions Employing Dialkylbiaryl Phosphine Ligands. *Acc. Chem. Res.* **2008**, *41* (11), 1461–1473. https://doi.org/10.1021/ar800036s.

(12) Magano, J.; Dunetz, J. R. Large-Scale Applications of Transition Metal-Catalyzed Couplings for the Synthesis of Pharmaceuticals. *Chem. Rev.* **2011**, *111* (3), 2177–2250. https://doi.org/10.1021/cr100346g.

(13) D'Alterio, M. C.; Casals-Cruañas, È.; Tzouras, N. V.; Talarico, G.; Nolan, S. P.; Poater, A. Mechanistic Aspects of the Palladium-Catalyzed Suzuki-Miyaura Cross-Coupling Reaction. *Chem. Eur. J.* **2021**, *27* (54), 13481–13493. https://doi.org/10.1002/chem.202101880.
(14) Hooshmand, S. E.; Heidari, B.; Sedghi, R.; Varma, R. S. Recent Advances in the Suzuki–Miyaura Cross-Coupling Reaction Using Efficient Catalysts in Eco-Friendly Media. *Green Chem.* **2019**, *21* (3), 381–405. https://doi.org/10.1039/C8GC02860E.
(15) Farhang, M.; Akbarzadeh, A. R.; Rabbani, M.; Ghadiri, A. M. A Retrospective-Prospective Review of Suzuki–Miyaura Reaction: From Cross-Coupling Reaction to Pharmaceutical Industry Applications. *Polyhedron* **2022**, *227*, 116124. https://doi.org/10.1016/j.poly.2022.116124.
(16) Buskes, M. J.; Blanco, M.-J. Impact of Cross-Coupling Reactions in Drug Discovery and Development. *Molecules* **2020**, *25* (15), 3493. https://doi.org/10.3390/molecules25153493.
(17) Neeve, E. C.; Geier, S. J.; Mkhalid, I. A. I.; Westcott, S. A.; Marder, T. B. Diboron(4) Compounds: From Structural Curiosity to Synthetic Workhorse. *Chem. Rev.* **2016**, *116* (16), 9091–9161. https://doi.org/10.1021/acs.chemrev.6b00193.
(18) Carreras, J.; Caballero, A.; Pérez, P. J. Alkenyl Boronates: Synthesis and Applications. *Chem. Asian J.* **2019**, *14* (3), 329–343. https://doi.org/10.1002/asia.201801559.
(19) Nad, P.; Mukherjee, A. Metal-Free C–H Borylation and Hydroboration of Indoles. *ACS Omega* **2023**, *8* (41), 37623–37640. https://doi.org/10.1021/acsomega.3c05071.
(20) Rej, S.; Chatani, N. Regioselective Transition-Metal-Free C(Sp^2)−H Borylation: A Subject of Practical and Ongoing Interest in Synthetic Organic Chemistry. *Angew. Chem. Int. Ed.* **2022**, *61* (44), e202209539. https://doi.org/10.1002/anie.202209539.
(21) Nguyen, V. D.; Nguyen, V. T.; Jin, S.; Dang, H. T.; Larionov, O. V. Organoboron Chemistry Comes to Light: Recent Advances in Photoinduced Synthetic Approaches to Organoboron Compounds. *Tetrahedron* **2019**, *75* (5), 584–602. https://doi.org/10.1016/j.tet.2018.12.040.
(22) Ishiyama, T.; Murata, M.; Miyaura, N. Palladium(0)-Catalyzed Cross-Coupling Reaction of Alkoxydiboron with Haloarenes: A Direct Procedure for Arylboronic Esters. *J. Org. Chem.* **1995**, *60* (23), 7508–7510. https://doi.org/10.1021/jo00128a024.
(23) Munteanu, C.; Spiller, T. E.; Qiu, J.; DelMonte, A. J.; Wisniewski, S. R.; Simmons, E. M.; Frantz, D. E. Pd- and Ni-Based Systems for the Catalytic Borylation of Aryl (Pseudo)Halides with $B_2(OH)_4$. *J. Org. Chem.* **2020**, *85* (16), 10334–10349. https://doi.org/10.1021/acs.joc.0c00929.
(24) Chow, W. K.; Yuen, O. Y.; Choy, P. Y.; So, C. M.; Lau, C. P.; Wong, W. T.; Kwong, F. Y. A Decade Advancement of Transition Metal-Catalyzed Borylation of Aryl Halides and Sulfonates. *RSC Adv.* **2013**, *3* (31), 12518–12539. https://doi.org/10.1039/C3RA22905J.
(25) Fornwald, R. M.; Yadav, A.; Montero Bastidas, J. R.; Smith, M. R.; Maleczka, R. E. Simple and Green Preparation of Tetraalkoxydiborons and Diboron Diolates from Tetrahydroxydiboron. *J. Org. Chem.* **2024**, *89* (9), 6048–6052. https://doi.org/10.1021/acs.joc.3c02992.
(26) Arrington, K.; Barcan, G. A.; Calandra, N. A.; Erickson, G. A.; Li, L.; Liu, L.; Nilson, M. G.; Strambeanu, I. I.; VanGelder, K. F.; Woodard, J. L.; Xie, S.; Allen, C. L.; Kowalski, J. A.; Leitch, D. C. Convergent Synthesis of the NS5B Inhibitor GSK8175 Enabled by Transition Metal Catalysis. *J. Org. Chem.* **2019**, *84* (8), 4680–4694. https://doi.org/10.1021/acs.joc.8b02269.

(27) Ring, O. T.; Campbell, A. D.; Hayter, B. R.; Powell, L. Significant Rate Enhancement via Potassium Pivalate in a Miyaura Borylation Approach to Verinurad. *Tetrahedron Lett.* **2020**, *61* (10), 151589. https://doi.org/10.1016/j.tetlet.2019.151589.
(28) Barroso, S.; Joksch, M.; Puylaert, P.; Tin, S.; Bell, S. J.; Donnellan, L.; Duguid, S.; Muir, C.; Zhao, P.; Farina, V.; Tran, D. N.; de Vries, J. G. Improvement in the Palladium-Catalyzed Miyaura Borylation Reaction by Optimization of the Base: Scope and Mechanistic Study. *J. Org. Chem.* **2021**, *86* (1), 103–109. https://doi.org/10.1021/acs.joc.0c01758.
(29) Boit, T. B.; Bulger, A. S.; Dander, J. E.; Garg, N. K. Activation of C–O and C–N Bonds Using Non-Precious-Metal Catalysis. *ACS Catal.* **2020**, *10* (20), 12109–12126. https://doi.org/10.1021/acscatal.0c03334.
(30) Zhou, T.; Szostak, M. Palladium-Catalyzed Cross-Couplings by C–O Bond Activation. *Catal. Sci. Technol.* **2020**, *10* (17), 5702–5739. https://doi.org/10.1039/D0CY01159B.
(31) Ben Halima, T.; Zhang, W.; Yalaoui, I.; Hong, X.; Yang, Y.-F.; Houk, K. N.; Newman, S. G. Palladium-Catalyzed Suzuki–Miyaura Coupling of Aryl Esters. *J. Am. Chem. Soc.* **2017**, *139* (3), 1311–1318. https://doi.org/10.1021/jacs.6b12329.
(32) Kinuta, H.; Hasegawa, J.; Tobisu, M.; Chatani, N. Rhodium-Catalyzed Borylation of Aryl and Alkenyl Pivalates through the Cleavage of Carbon–Oxygen Bonds. *Chem. Lett.* **2015**, *44* (3), 366–368. https://doi.org/10.1246/cl.141084.
(33) Kinuta, H.; Tobisu, M.; Chatani, N. Rhodium-Catalyzed Borylation of Aryl 2-Pyridyl Ethers through Cleavage of the Carbon–Oxygen Bond: Borylative Removal of the Directing Group. *J. Am. Chem. Soc.* **2015**, *137* (4), 1593–1600. https://doi.org/10.1021/ja511622e.
(34) Seki, R.; Hara, N.; Saito, T.; Nakao, Y. Selective C–O Bond Reduction and Borylation of Aryl Ethers Catalyzed by a Rhodium–Aluminum Heterobimetallic Complex. *J. Am. Chem. Soc.* **2021**, *143* (17), 6388–6394. https://doi.org/10.1021/jacs.1c03038.
(35) Huang, K.; Yu, D.-G.; Zheng, S.-F.; Wu, Z.-H.; Shi, Z.-J. Borylation of Aryl and Alkenyl Carbamates through Ni-Catalyzed C-O Activation. *Chem. Eur. J.* **2011**, *17* (3), 786–791. https://doi.org/10.1002/chem.201001943.
(36) Zarate, C.; Manzano, R.; Martin, R. Ipso-Borylation of Aryl Ethers via Ni-Catalyzed C–OMe Cleavage. *J. Am. Chem. Soc.* **2015**, *137* (21), 6754–6757. https://doi.org/10.1021/jacs.5b03955.
(37) Nakamura, K.; Tobisu, M.; Chatani, N. Nickel-Catalyzed Formal Homocoupling of Methoxyarenes for the Synthesis of Symmetrical Biaryls via C–O Bond Cleavage. *Org. Lett.* **2015**, *17* (24), 6142–6145. https://doi.org/10.1021/acs.orglett.5b03151.
(38) Tobisu, M.; Zhao, J.; Kinuta, H.; Furukawa, T.; Igarashi, T.; Chatani, N. Nickel-Catalyzed Borylation of Aryl and Benzyl 2-Pyridyl Ethers: A Method for Converting a Robust Ortho-Directing Group. *Adv. Synth. Catal.* **2016**, *358* (15), 2417–2421. https://doi.org/10.1002/adsc.201600336.
(39) Pein, W. L.; Wiensch, E. M.; Montgomery, J. Nickel-Catalyzed Ipso-Borylation of Silyloxyarenes via C–O Bond Activation. *Org. Lett.* **2021**, *23* (12), 4588–4592. https://doi.org/10.1021/acs.orglett.1c01280.
(40) Zeng, X.; Zhang, Y.; Liu, Z.; Geng, S.; He, Y.; Feng, Z. Iron-Catalyzed Borylation of Aryl Ethers via Cleavage of C–O Bonds. *Org. Lett.* **2020**, *22* (8), 2950–2955. https://doi.org/10.1021/acs.orglett.0c00679.

(41) Geng, S.; Zhang, J.; Chen, S.; Liu, Z.; Zeng, X.; He, Y.; Feng, Z. Development and Mechanistic Studies of Iron-Catalyzed Construction of Csp^2–B Bonds via C–O Bond Activation. *Org. Lett.* **2020**, *22* (14), 5582–5588. https://doi.org/10.1021/acs.orglett.0c01937.
(42) Dennis, J. M.; White, N. A.; Liu, R. Y.; Buchwald, S. L. Pd-Catalyzed C–N Coupling Reactions Facilitated by Organic Bases: Mechanistic Investigation Leads to Enhanced Reactivity in the Arylation of Weakly Binding Amines. *ACS Catal.* **2019**, *9* (5), 3822–3830. https://doi.org/10.1021/acscatal.9b00981.
(43) Villatoro, R. S.; Belfield, J. R.; Arman, H. D.; Hernandez, L. W.; Simmons, E. M.; Garlets, Z. J.; Wisniewski, S. R.; Coombs, J. R.; Frantz, D. E. General Method for Ni-Catalyzed C–N Cross-Couplings of (Hetero)Aryl Chlorides with Anilines and Aliphatic Amines under Homogeneous Conditions Using a Dual-Base Strategy. *Organometallics* **2023**, *42* (21), 3164–3172. https://doi.org/10.1021/acs.organomet.3c00419.
(44) Goldfogel, M. J.; Guo, X.; Meléndez Matos, J. L.; Gurak, J. A. Jr.; Joannou, M. V.; Moffat, W. B.; Simmons, E. M.; Wisniewski, S. R. Advancing Base-Metal Catalysis: Development of a Screening Method for Nickel-Catalyzed Suzuki–Miyaura Reactions of Pharmaceutically Relevant Heterocycles. *Org. Process Res. Dev.* **2022**, *26* (3), 785–794. https://doi.org/10.1021/acs.oprd.1c00210.
(45) Becica, J.; Leitch, D. C. C–O Bond Activation as a Strategy in Palladium-Catalyzed Cross-Coupling. *Synlett* **2021**, *32* (7), 641–646. https://doi.org/10.1055/a-1306-3228.
(46) Becica, J.; Gaube, G.; A. Sabbers, W.; C. Leitch, D. Oxidative Addition of Activated Aryl-Carboxylates to Pd(0): Divergent Reactivity Dependant on Temperature and Structure. *Dalton Trans.* **2020**, *49* (45), 16067–16071. https://doi.org/10.1039/D0DT01119C.
(47) Becica, J.; Heath, O. R. J.; Zheng, C. H. M.; Leitch, D. C. Palladium-Catalyzed Cross-Coupling of Alkenyl Carboxylates. *Angew. Chem. Int. Ed.* **2020**, *59* (39), 17277–17281. https://doi.org/10.1002/anie.202006586.
(48) Pipaón Fernández, N.; Gaube, G.; Woelk, K. J.; Burns, M.; Hruszkewycz, D. P.; Leitch, D. C. Palladium-Catalyzed Direct C–H Alkenylation with Enol Pivalates Proceeds via Reversible C–O Oxidative Addition to Pd(0). *ACS Catal.* **2022**, *12* (12), 6997–7003. https://doi.org/10.1021/acscatal.2c01305.
(49) Huang, J.; Isaac, M.; Watt, R.; Becica, J.; Dennis, E.; Saidaminov, M. I.; Sabbers, W. A.; Leitch, D. C. ^{DMP}DAB–Pd–MAH: A Versatile Pd(0) Source for Precatalyst Formation, Reaction Screening, and Preparative-Scale Synthesis. *ACS Catal.* **2021**, *11* (9), 5636–5646. https://doi.org/10.1021/acscatal.1c00288.
(50) Oka, N.; Yamada, T.; Sajiki, H.; Akai, S.; Ikawa, T. Aryl Boronic Esters Are Stable on Silica Gel and Reactive under Suzuki–Miyaura Coupling Conditions. *Org. Lett.* **2022**, *24* (19), 3510–3514. https://doi.org/10.1021/acs.orglett.2c01174.
(51) Shockley, S. E.; Holder, J. C.; Stoltz, B. M. Palladium-Catalyzed Asymmetric Conjugate Addition of Arylboronic Acids to α,β-Unsaturated Cyclic Electrophiles. *Org. Process Res. Dev.* **2015**, *19* (8), 974–981. https://doi.org/10.1021/acs.oprd.5b00169.
(52) Lee, A.-L. Enantioselective Oxidative Boron Heck Reactions. *Org. Biomol. Chem.* **2016**, *14* (24), 5357–5366. https://doi.org/10.1039/C5OB01984B.
(53) Zhao, X.; Zhang, D.; Wang, X. Unraveling the Mechanism of Palladium-Catalyzed Base-Free Cross-Coupling of Vinyl Carboxylates: Dual Role of Arylboronic Acids as a Reducing Agent

and a Coupling Partner. *ACS Catal.* **2022**, *12* (3), 1809–1817. https://doi.org/10.1021/acscatal.1c00247.
(54) Wei, C. S.; Davies, G. H. M.; Soltani, O.; Albrecht, J.; Gao, Q.; Pathirana, C.; Hsiao, Y.; Tummala, S.; Eastgate, M. D. The Impact of Palladium(II) Reduction Pathways on the Structure and Activity of Palladium(0) Catalysts. *Angew. Chem. Int. Ed.* **2013**, *52* (22), 5822–5826. https://doi.org/10.1002/anie.201210252.
(55) Liu, Q. Synthesis of Alkylboronic Esters from Alkyl Iodides. *Org. Synth.* **2022**, *99*, 15–28. https://doi.org/10.15227/orgsyn.099.0015.
(56) Pipaón Fernández, N.; Cruise, O.; Easton, S. E. F.; Kaplan, J. M.; Woodard, J. L.; Hruszkewycz, D. P.; Leitch, D. C. Direct Heterocycle C–H Alkenylation via Dual Catalysis Using a Palladacycle Precatalyst: Multifactor Optimization and Scope Exploration Enabled by High-Throughput Experimentation. *J. Org. Chem.* **2024**. https://doi.org/10.1021/acs.joc.3c02311.
(57) Hayes, H. L. D.; Wei, R.; Assante, M.; Geogheghan, K. J.; Jin, N.; Tomasi, S.; Noonan, G.; Leach, A. G.; Lloyd-Jones, G. C. Protodeboronation of (Hetero)Arylboronic Esters: Direct versus Prehydrolytic Pathways and Self-/Auto-Catalysis. *J. Am. Chem. Soc.* **2021**, *143* (36), 14814–14826. https://doi.org/10.1021/jacs.1c06863.
(58) Matteson, D. S. Functional Group Compatibilities in Boronic Ester Chemistry. *J. Organomet. Chem.* **1999**, *581* (1), 51–65. https://doi.org/10.1016/S0022-328X(99)00064-9.
(59) Roy, C. D.; Brown, H. C. Stability of Boronic Esters – Structural Effects on the Relative Rates of Transesterification of 2-(Phenyl)-1,3,2-Dioxaborolane. *J. Org. Chem.* **2007**, *692* (4), 784–790. https://doi.org/10.1016/j.jorganchem.2006.10.013.
(60) García-Domínguez, A.; Leach, A. G.; Lloyd-Jones, G. C. *In Situ* Studies of Arylboronic Acids/Esters and R_3SiCF_3 Reagents: Kinetics, Speciation, and Dysfunction at the Carbanion–Ate Interface. *Acc. Chem. Res.* **2022**, *55* (9), 1324–1336. https://doi.org/10.1021/acs.accounts.2c00113.
(61) Ahluwalia, V. K.; Prakash, C.; Gupta, R. A Facile Synthesis of 3-Allylcoumarins. *Synthesis* **1980**, *1980* (1), 48–50. https://doi.org/10.1055/s-1980-28920.
(62) Bream, R. N.; Clark, H.; Edney, D.; Harsanyi, A.; Hayler, J.; Ironmonger, A.; Mc Cleary, N.; Phillips, N.; Priestley, C.; Roberts, A.; Rushworth, P.; Szeto, P.; Webb, M. R.; Wheelhouse, K. Application of C–H Functionalization in the Development of a Concise and Convergent Route to the Phosphatidylinositol-3-Kinase Delta Inhibitor Nemiralisib. *Org. Process Res. Dev.* **2021**, *25* (3), 529–540. https://doi.org/10.1021/acs.oprd.0c00486.
(63) Caruano, J.; Muccioli, G. G.; Robiette, R. Biologically Active γ-Lactams: Synthesis and Natural Sources. *Org. Biomol. Chem.* **2016**, *14* (43), 10134–10156. https://doi.org/10.1039/C6OB01349J.
(64) Chatterjee, S.; Sahoo, R.; Nanda, S. Recent Reports on the Synthesis of γ-Butenolide, γ-Alkylidenebutenolide Frameworks, and Related Natural Products. *Org. Biomol. Chem.* **2021**, *19* (34), 7298–7332. https://doi.org/10.1039/D1OB00875G.
(65) Rattray, B.; Nugent, D. J.; Young, G. Rofecoxib as Adjunctive Therapy for Haemophilic Arthropathy. *Haemophilia* **2005**, *11* (3), 240–244. https://doi.org/10.1111/j.1365-2516.2005.01087.x.

(66) Xie, J.; Xue, S.; Escudero-Adán, E. C.; Kleij, A. W. Domino Synthesis of α,β-Unsaturated γ-Lactams by Stereoselective Amination of α-Tertiary Allylic Alcohols. *Angew. Chem. Int. Ed.* **2018**, *57* (51), 16727–16731. https://doi.org/10.1002/anie.201810160.
(67) Aubert, S.; Katsina, T.; Arseniyadis, S. A Sequential Pd-AAA/Cross-Metathesis/Cope Rearrangement Strategy for the Stereoselective Synthesis of Chiral Butenolides. *Org. Lett.* **2019**, *21* (7), 2231–2235. https://doi.org/10.1021/acs.orglett.9b00521.
(68) Yan, J.; Zhang, W.; He, Q.; Hou, J.; Zeng, H.; Wei, H.; Xie, W. Enantioselective Direct Vinylogous Michael Addition for Constructing Enantioenriched γ,γ-Dialkyl Substituted Butyrolactams and Octahydroindoles. *Org. Biomol. Chem.* **2022**, *20* (12), 2387–2391. https://doi.org/10.1039/D2OB00112H.
(69) Romanski, S.; Kraus, B.; Guttentag, M.; Schlundt, W.; Rücker, H.; Adler, A.; Neudörfl, J.-M.; Alberto, R.; Amslinger, S.; Schmalz, H.-G. Acyloxybutadiene Tricarbonyl Iron Complexes as Enzyme-Triggered CO-Releasing Molecules (ET-CORMs): A Structure–Activity Relationship Study. *Dalton Trans.* **2012**, *41* (45), 13862. https://doi.org/10.1039/c2dt30662j.
(70) Li, B.-J.; Xu, L.; Wu, Z.-H.; Guan, B.-T.; Sun, C.-L.; Wang, B.-Q.; Shi, Z.-J. Cross-Coupling of Alkenyl/Aryl Carboxylates with Grignard Reagent via Fe-Catalyzed C−O Bond Activation. *J. Am. Chem. Soc.* **2009**, *131* (41), 14656–14657. https://doi.org/10.1021/ja907281f.
(71) Hoque, M. E.; Bisht, R.; Unnikrishnan, A.; Dey, S.; Mahamudul Hassan, M. M.; Guria, S.; Rai, R. N.; Sunoj, R. B.; Chattopadhyay, B. Iridium-Catalyzed Ligand-Controlled Remote *Para* -Selective C−H Activation and Borylation of Twisted Aromatic Amides. *Angew Chem Int Ed* **2022**, *61* (27), e202203539. https://doi.org/10.1002/anie.202203539.
(72) Zalesskiy, S. S.; Ananikov, V. P. Pd2(Dba)3 as a Precursor of Soluble Metal Complexes and Nanoparticles: Determination of Palladium Active Species for Catalysis and Synthesis. *Organometallics* **2012**, *31* (6), 2302–2309. https://doi.org/10.1021/om201217r.
(73) Mulligan, C. J.; Bagale, S. M.; Newton, O. J.; Parker, J. S.; Hii, K. K. M. Peracetic Acid: An Atom-Economical Reagent for Pd-Catalyzed Acetoxylation of C–H Bonds. *ACS Sustain. Chem. Eng.* **2019**, *7* (1), 1611–1615. https://doi.org/10.1021/acssuschemeng.8b05370.
(74) Villar, L.; Orlov, N. V.; Kondratyev, N. S.; Uria, U.; Vicario, J. L.; Malkov, A. V. Kinetic Resolution of Secondary Allyl Boronates and Their Application in the Synthesis of Homoallylic Amines. *Chem. Eur. J.* **2018**, *24* (61), 16262–16265. https://doi.org/10.1002/chem.201804395.
(75) Ishiyama, T.; Takagi, J.; Kamon, A.; Miyaura, N. Palladium-Catalyzed Cross-Coupling Reaction of Bis(Pinacolato)Diboron with Vinyl Triflates β-Substituted by a Carbonyl Group: Efficient Synthesis of β-Boryl-α,β-Unsaturated Carbonyl Compounds and Their Synthetic Utility. *J. Organomet. Chem.* **2003**, *687* (2), 284–290. https://doi.org/10.1016/S0022-328X(03)00611-9.
(76) Novartis AG; Azimioara, M.; Chen, B.; Epple, R.; Hardy, D.; Honda, A.; Lam, P.; Malik, H.A.; Meier, F.; Nguyen, T.N.; Okram, B.; Patel, S.; Rodriguez, R.; Shaw, D.; Shen, Y.; Wu, B. N-(Pyridine-2-Ylsulfonyl)Cyclopropanecarboxamide Derivatives and Their Use in the Treatment of a CFTR Mediated Disease. WO 2020/128768 A1, June 25, 2020.
(77) Nguyen, S. S.; Ferreira, A. J.; Long, Z. G.; Heiss, T. K.; Dorn, R. S.; Row, R. D.; Prescher, J. A. Butenolide Synthesis from Functionalized Cyclopropenones. *Org. Lett.* **2019**, *21* (21), 8695–8699. https://doi.org/10.1021/acs.orglett.9b03298.

(78) Zeitler, K.; Rose, C. A. An Efficient Carbene-Catalyzed Access to 3,4-Dihydrocoumarins. *J. Org. Chem.* **2009**, *74* (4), 1759–1762. https://doi.org/10.1021/jo802285r.
(79) Hu, Y.; Ding, Q.; Ye, S.; Peng, Y.; Wu, J. Rapid Access to 4-Substituted-Pyrones and 2(5H)-Furanones via a Palladium-Catalyzed C–OH Bond Activation. *Tetrahedron* **2011**, *67* (38), 7258–7262. https://doi.org/10.1016/j.tet.2011.07.048.
(80) Kang, Y.; Zhang, W.; Wang, T.; Liang, Y.; Zhang, Z. Two-Step Synthesis of π-Expanded Maleimides from 3,4-Diphenylfuran-2(5H)-Ones. *J. Org. Chem.* **2019**, *84* (19), 12387–12398. https://doi.org/10.1021/acs.joc.9b01792.

Chapter 4: The development of novel cross-coupling scaffolds for C–O activation chemistry

This chapter, excluding sections 4.1 and 4.5, have been reproduced from:

Gaube, G.; Mutter, J.; Leitch, D.C. A "Neat" Synthesis of Substituted 2-Hydroxy-pyrido[1,2-a]pyrimidin-4-ones, *Canadian Journal of Chemistry,* **2024**, 102, 206-213, (DOI: 10.1139/cjc-2023-0150), and adapted with permission from Canadian Science Publishing.

4.1: Preface

Contributions: James Mutter conducted initial evaluation of three methods as well as the synthesis of **2d** under supervision of Gregory Gaube. All other experimental work and characterization was conducted by Gregory Gaube.

4.2 Abstract

We report the synthesis of a series of substituted 2-hydroxy-pyrido[1,2-a]pyrimidin-4-ones through a condensation of 2-aminopyridines and diethyl malonate. This method is contrasted with three reported general procedures for the preparation of these compounds, revealing that simple, neat synthesis conditions are suitable for a number of derivatives, including halogenated compounds suitable for further functionalization. Environmental, safety, and economic factors were considered in exploring this effective and robust synthetic method.

4.3 Introduction

Nitrogen-containing heterocycles are an indispensable component of many functional organic compounds.[1–3] Both saturated and unsaturated nitrogen-containing heterocycles are not only ubiquitous in agrochemicals,[4] and natural products,[5] but they are critical moieties in many biologically active compounds for anticancer,[6] antibacterial,[7] and antiviral purposes,[8,9] conferring

significant pharmacological value.[10] This is reflected in the number of FDA approved small molecule pharmaceuticals that contain *N*-heterocycles. A 2014 review stated that 59% of FDA approved pharmaceuticals contained at least one *N*-heterocycle,[11] with a more recent 2020 review revealing a significant jump to 75%.[12] Thus, methods to prepare and functionalize *N*-heterocycles remain an important part of organic synthesis research.

Pyrido[1,2-a]pyrimidin-4-ones (PPDs) are a specific class of *N*-heterocycle, with an aromatic bicyclic structure containing nitrogens at the 1 and 5 positions, as well as a carbonyl at the 4 position. They were first synthesized in 1924,[13] but have only been recognized as an important scaffold more recently.[14–22] Specific examples of approved active pharmaceutical ingredients based on a PPD pharmacophore include permirolast,[23] an anti-allergen medication, and risdiplam,[24] a treatment for spinal muscular atrophy (Figure 4.1). Additional studies indicate PPDs have potential as compounds for cancer treatment,[25] and diabetes.[26]

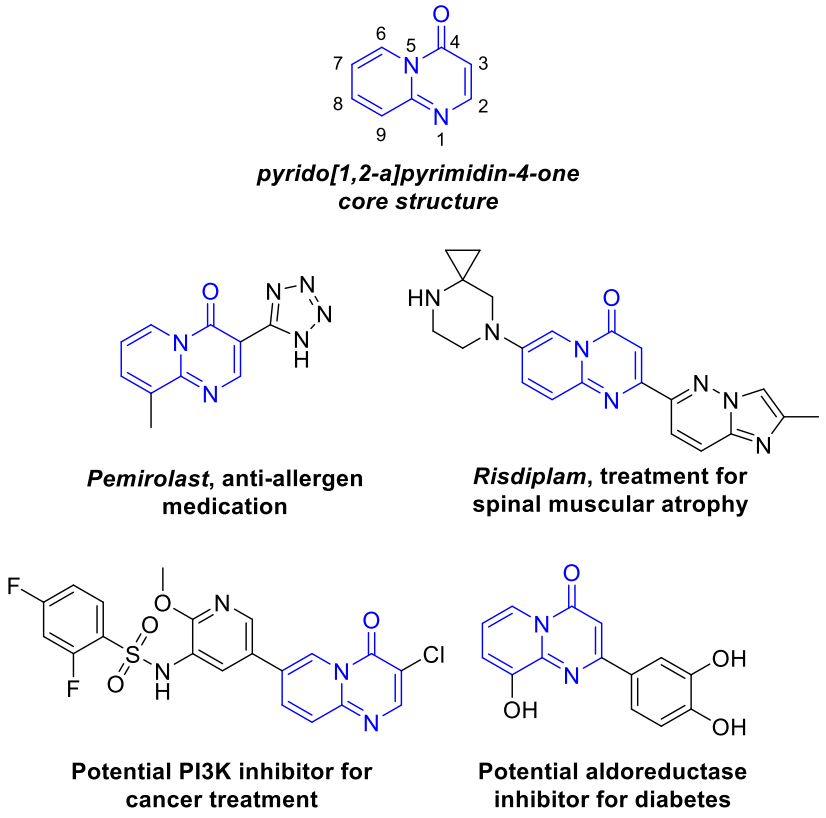

Figure 4.1: Current and potential active pharmaceutical ingredients containing a pyrido[1,2-a]pyrimidin-4-one subunit (highlighted in blue).[23–26]

Herein we evaluate three literature syntheses for substituted 2-hydroxy-PPDs, and report a simple and generally applicable neat synthesis of these compounds using commercially available substituted 2-aminopyridines and diethyl malonate without the need for chromatography. While numerous methods have been reported in the literature for a given target 2-hydroxy-PPD, there are relatively few reports detailing procedures applicable to the synthesis of multiple 2-hydroxy-PPD molecules. When we applied these literature syntheses to a series of substituted 2-aminopyridines, we found the product yields to be inconsistent. In addition, the poor solubility, high polarity, and high boiling points of these compounds means typical purification methods, such as recrystallization, column chromatography, and distillation, are often unsuitable. The method reported herein, building from specific prior reports of using neat diethyl

malonate,[13,19-21] proceeds without the need for such additional purification, relying instead on simple reslurrying of the isolated solid to dissolve soluble impurities. As a result, we have accessed various substituted 2-hydroxy-PPDs with potential for further functionalization.

4.4 Results and Discussion:

As part of our efforts to develop new catalytic methods for heterocycle functionalization, we sought a versatile and robust method to access various 2-hydroxy-PPDs. When synthesizing the otherwise unsubstituted 2-hydroxy-PPD **2a**, literature reports are consistent that using 2-aminopyridine and a malonate derivative to effect two successive amidation reactions is an efficient method.[25,28,30–33] However, in our hands we found yields to be inconsistent when we applied these methods to access 2-hydroxy-PPDs beyond the scope explored in the original reports, especially for substituted derivatives with potential for further functionalization through S_NAr and/or cross-coupling. With a goal to establish conditions that could be broadly applied to a library of commercially available 2-aminopyridine building blocks, we began by evaluating three methods (**A**-**C**) to access five 2-hydroxy-PPDs (**2a**-**c**, **2g**, **2i**; Figure 4.2).

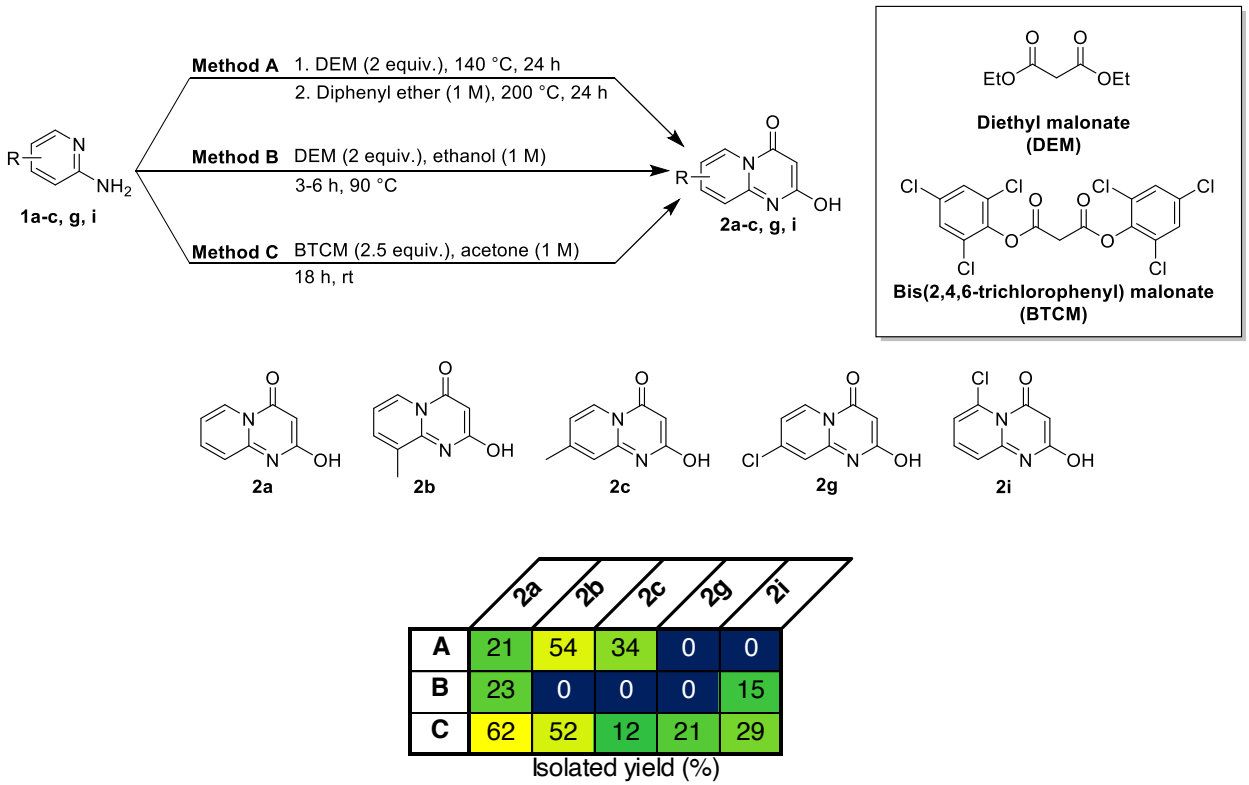

	2a	2b	2c	2g	2i
A	21	54	34	0	0
B	23	0	0	0	15
C	62	52	12	21	29

Isolated yield (%)

*Figure 4.2: Three reported methods (**A**-**C**) applied to the synthesis of five substituted 2-hydroxy-PPDs; reactions performed at 2.0 g scale (mass of 2-aminopyridine substrate).*

Initially, we explored a reported two-step method for the formation of **2a**, similar to **Method A** shown above (step 2 reaction temperature = 160 °C, and open to atmosphere);[28] however, we observed inconsistent results with respect to yield of desired product. A common issue when performing the second step is little/no cyclization to generate **2a**. To overcome this, we modified the procedure to run under N_2 (Appendix C – Figure C1) and then also at an elevated reaction temperature. We only observe appreciable cyclization when performing the second step ≥200 °C (Appendix C – Figure C2). With these modifications, **Method A** was then applied to convert all five 2-aminopyridines. While this method provided sufficient yield for the unsubstituted (**2a**) and tolyl derivatives (**2b**-**2c**), no halide containing species (**2g or 2i**) was

successfully synthesized using this method. Furthermore, the use of high-boiling diphenyl ether as solvent (b.p. = 258 °C) complicated isolation once the reaction was complete.

Method B, which uses ethanol as a polar protic solvent at reflux, was then attempted.[31] However, we again observed incomplete or no cyclization, with the initial monoamidation product as the major/sole species. While we were able to successfully isolate the unsubstituted (**2a**) and the 6-chloro product (**2i**), **Method B** was not able to furnish the other three 2-hydroxy-PPD products.

Method C, which employs a more elaborate malonate ester substrate bis(2,4,6-trichlorophenyl)malonate (BTCM), was the most broadly successful approach.[17] Originally reported by Kappe,[34] this procedure enables the difficult second amidation by replacing the ethyl esters with activated 2,4,6-trichlorophenol esters; the higher reactivity of BTCM also enables the cyclization to occur at room temperature. However, BTCM is considerably more expensive and mass inefficient compared to diethyl malonate. Its synthesis uses phosphorus oxychloride ($POCl_3$) to activate malonic acid. $POCl_3$ is highly hazardous, with safety incidents involving reaction quenching reported in the literature.[35] While **Method C** does provide the best results across the five 2-hydroxy-PPD targets, we sought a more economical and safe method to access these compounds that is consistent with the principles of green chemistry.[36] In particular, the reaction mass intensities ([mass of input reagents and solvents] / [mass of product]) for PPD formation of **Methods A-C** in our hands are 45, 36, and 18, respectively (note this does not include the synthesis of BTCM). Industry targets for step mass intensity are 10-30, with lower values being preferred. For a reaction mass intensity, which does not include the mass of solvents used for workup or purification, an ideal value is < 10.

Our experience with **Methods A**-**C** inspired us to explore an alternative pathway for preparation of 2-hydroxy-PPDs. With respect to **Method A**, elevated temperatures (>200 °C) and N_2 atmosphere were required to facilitate the second amidation. Rather than use diphenyl ether as a solvent for the second amidation, we simply used a larger excess of diethyl malonate (5 equiv) and directly heated the reaction mixture to high temperature. Notably, the original synthesis of **2a**, reported by Chichibabin, employed a similar approach of using malonate esters as both reactant and solvent.[13] More recent efforts have used neat reaction conditions to access specific PPD derivatives,[19-21] but there is no comprehensive assessment of this approach for a wide array of substituted derivatives.

With reactor block temperatures of 230 °C (diethyl malonate b.p. = 199 °C), we standardized the reaction time to 3 h to compare reactivity across the set of 2-aminopyridines (**1a**-**q**). This also enabled reaction set-up, execution, and clean-up to be completed within a single day, and avoided the need to run high temperature reactions unattended (i.e. overnight). Diethyl malonate proves to be an effective solvent as well as reactant, providing synthetically useful yields of 2-hydroxy-PPDs **2a**-**q** on (multi)gram scale (Figure 4.3). This includes halogenated derivatives **2f**-**q**, which provide synthetic handles for further functionalization via S_NAr or metal-catalyzed coupling. Notably, we do observe diminished yield in the case of **2e**, **2i**, and **2q**, all of which have a substituent at the 6-position. This is likely due to increased steric hindrance adjacent to the pyridyl nitrogen slowing the rate of cyclization. Importantly, on larger scale the excess diethyl malonate distilled at the end of the reaction can be reused in future experiments, significantly improving the overall mass efficiency of this process. We demonstrated this by synthesizing **2b** using recycled diethyl malonate without compromising the yield (Appendix C – Figure C4).

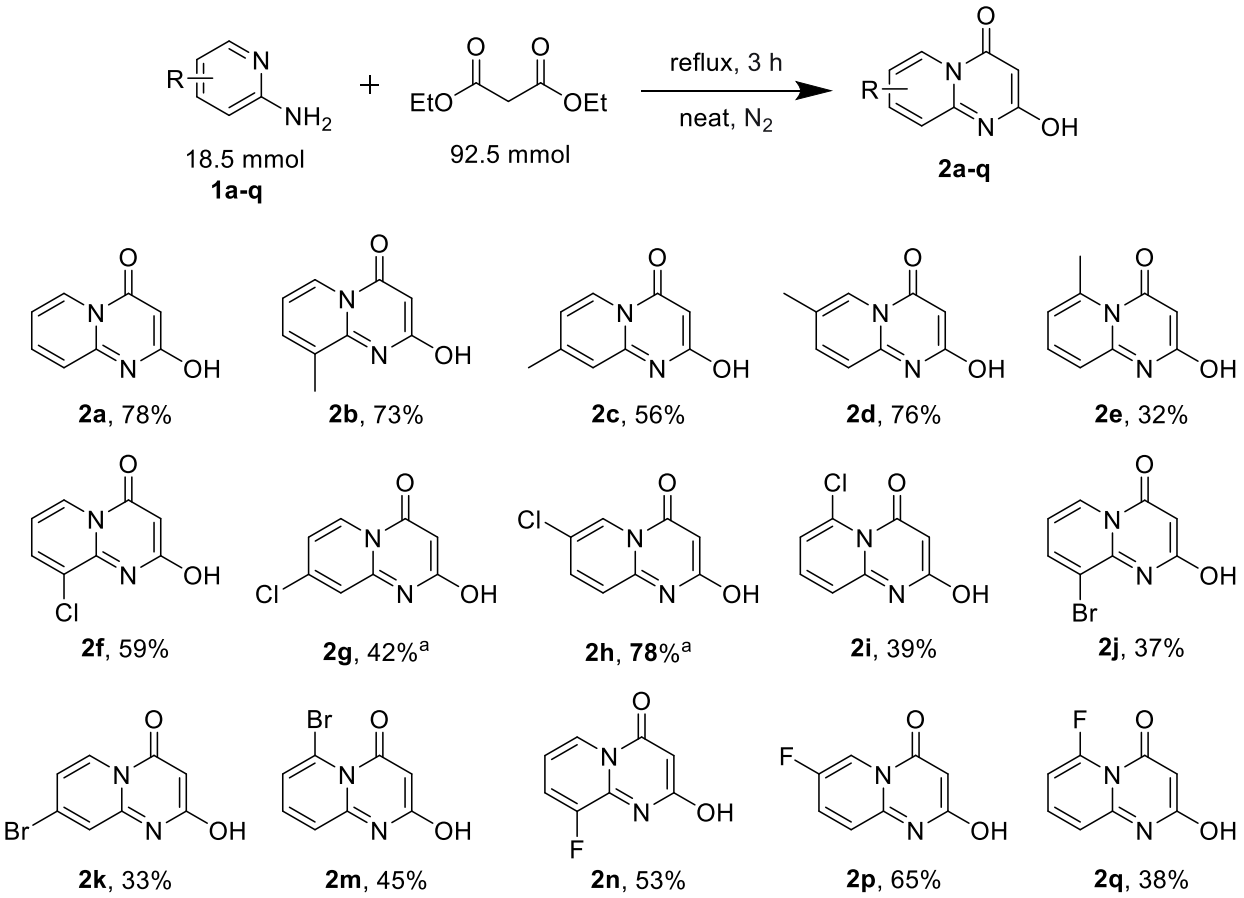

Figure 4.3: Synthesis of 2a-q (except 2l and 2o) from 1a-q using diethyl malonate. All reactions performed at 18.5 mmol scale relative to (substituted) 2-aminopyridine, isolated yields. [a]Open to air.

Finally, we do observe some limitations of the current method. Firstly, 8-fluoro-2-hydroxy-4H-pyrido[1,2-a]pyrimidin-4-one (**2o**) results in a complex mixture. We suspect the reason for this is that the starting material 2-amino-4-fluoropyridine (**1o**) is an excellent candidate for S_NAr chemistry; however, we note we can synthesize the analogous chloro (**2g**) and bromo (**2k**) products using the general procedure. Secondly, in an attempt to prepare 7-bromo-2-hydroxy-4*H*-pyrido[1,2-*a*]pyrimidin-4-one (**2l**) from the corresponding 2-amino-5-bromopyridine (**1l**), we observe a mixture containing **2l** (Appendix C – Figure C27 for ^{1}H NMR spectrum). Attempts to separate these materials via column chromatography were unsuccessful due to the poor solubility

and high polarity of **2l**. To circumvent these purification issues, we derivatized the generated **2l** with *p*-toluenesulfonyl chloride. A simple workup allowed us to remove the major impurity and isolate the desired tosylated product (**3l**) with 30% overall yield over two steps without the need for chromatography (Figure 4.4). Notably, the general method is successful in the synthesis of the analogous 5-chloro (**2h**) and fluoro (**2p**) products.

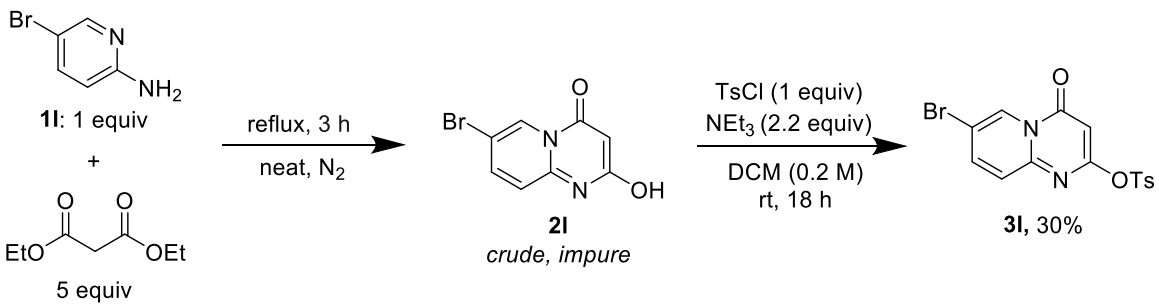

Figure 4.4: Synthesis of 2l from 1l using diethyl malonate and subsequent tosylation to yield 3l.

We also note that the low solubility and high melting points contributes to the limited characterization of the products. This has been evident in literature as characterization of any previously reported compounds is generally limited to ^{1}H NMR spectroscopy.[15,28,30,32] While we report ^{1}H NMR spectra for all compounds, we have had limited success acquiring ^{13}C NMR spectra (see SI, Section 4 for more details). These products also generally have melting points higher than standard melting point apparatuses can reach.[37] Despite these barriers, we report ^{1}H NMR spectra, and HR-MS data for all compounds synthesized, which includes 5 new compounds (**2g**, **2i**, **2k**, **2m**, **2q**).

4.5 Functionalization of PPDs

In order to evaluate the activity of these PPD compounds in Pd catalyzed C–O activation chemistry we needed to install the required functional groups for screening. Literature syntheses

of risdiplam utilize a tosylate functional group to functionalize the 2 position and then utilizes a halide to functionalize the backbone 7 position separately.[24] Future screening work on this motif should include the tosylated PPD structure, **3a,** with $Pd(OAc)_2$ and PCy_3 as a 1 : 2 *in situ* Pd catalyst system (with 2 equivalents K_2CO_3 base) as a positive control. We have demonstrated in Eq. 1 that **3a** can be synthesized at the gram scale. As carboxylates are the primary consideration of this thesis, it was imperative to demonstrate that these PPD motifs could be functionalized accordingly. Eq. 2 demonstrates that we were also able to synthesize the pivalated unsubstituted PPD **4a** at the gram scale. Both **3a** and **4a** are novel compounds, full characterization can be found in Section 4.7.

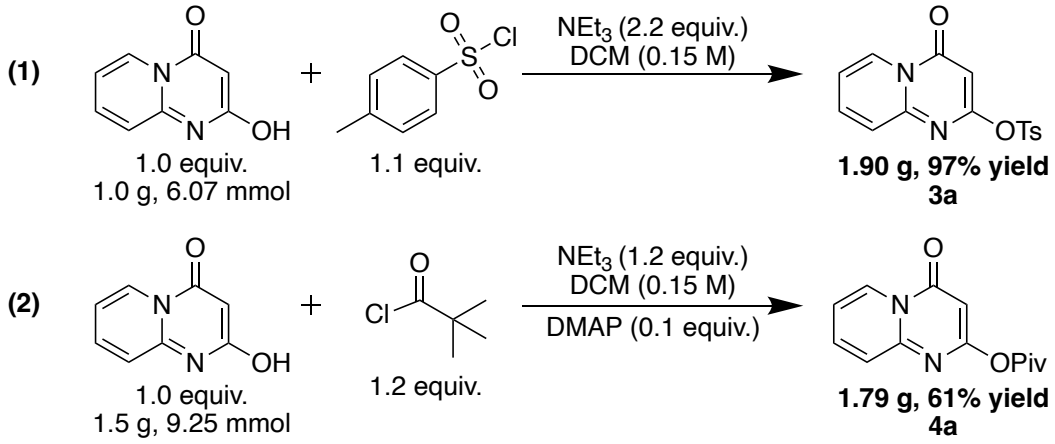

By synthesizing **3a** and **4a** we have demonstrated that the library of PPD molecules generated in Section 4.4 can be functionalized for screening in the future. **3a** and **4a** will provide the basis for initial screening experiments (detailed in Section 5.2.4).

4.6 Conclusions

By exploiting the use of diethyl malonate as both solvent and reactant, we have demonstrated the synthesis of substituted 2-hydroxy-PPDs, several of which are new compounds. By evaluating three reported methods and taking inspiration from Chichibabin's original

preparation, we have shown that neat reaction conditions are suitable as a generally applicable method. This procedure provides synthetically useful yields in a short turnaround time, with excellent mass efficiency (reaction mass intensity < 10) and a straightforward method to recover and reuse the unreacted diethyl malonate. We then demonstrated that these molecules could be functionalized in order to add them to our screening library. As the importance of nitrogen-containing heterocycles and PPDs in particular continues to grow, robust methods to access key scaffolds will remain critical.

4.7 Experimental

4.7.1 General Considerations:

Unless otherwise noted, all reactions were performed using standard Schlenk techniques under N_2. All starting materials were purchased from commercial suppliers and used without further purification. All NMR spectra were acquired on either a Bruker AVANCE 300 MHz spectrometer or a Bruker AVANCE Neo 500 MHz spectrometer. All ^{1}H and ^{13}C NMR chemical shifts are calibrated to residual protio-solvents (d_6-DMSO: 2.50 ppm, $CDCl_3$: 7.26 ppm). All NMR spectroscopic data is processed using Bruker TopSpin 4.10. High-resolution mass spectrometry (HRMS) were obtained using a Bruker maXis Impact Quadrupole Time-of-Flight LC/MS System, or Thermo Scientific Ultimate 3000 ESI-Orbitrap Exactive Plus. All spectra associated with this work can be found in Appendix C.

4.7.2 Method A-C Procedures:

Method A:

This procedure was adapted from the literature with modifications.[28] These reactions were run at 2.0 g scale relative to the (substituted) 2-aminopyridine, masses are shown below relative to the unsubstituted 2-aminopyridine (**1a**).

A round-bottom flask was charged with diethyl malonate (8.5 g, 8.1 ml, 53 mmol, 2.5 equiv) and 2-aminopyridine (2.0 g, 21.2 mmol, 1 equiv). The reaction was left to stir overnight at 140 °C for 24 h. The mixture was then cooled to room temperature and purified via flash chromatography. Diphenyl ether (22.5 g, 21.0 mL) was added to a round bottom flask along with the intermediate product to stir at 200 °C for 24 h. Diphenyl ether was removed via distillation under reduced pressure. The crude product was suspended in hot hexanes and then washed with diethyl ether to yield the cyclized product (0.722 g, 21% yield). Reaction mass intensity = [mass of input materials] / [mass of product] = 45.

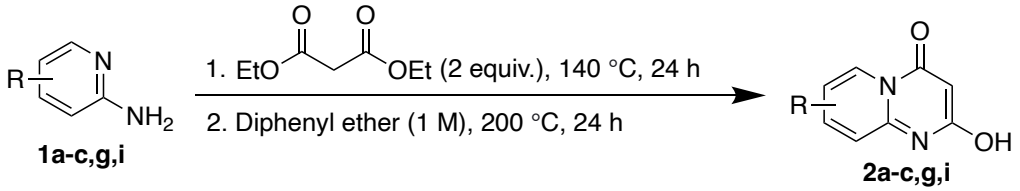

Figure 4.5: General reaction procedure for Method A

Method B:

This procedure was adapted from the literature.[31] These reactions were run at 2.0 g scale relative to the (substituted) 2-aminopyridine, masses are shown below relative to the unsubstituted 2-aminopyridine (**1a**).

An round bottom flask was charged with diethyl malonate (10.2 g, 9.7 ml, 63.6 mmol, 3 equiv) and 2-aminopyridine (2.0 g, 21.2 mmol, 1 equiv) and suspended in ethanol (16.6 g, 21.0 mL, 1 M). The reaction was fitted with a still head to continuously extract the ethanol and refluxed for 3 – 6 h. The mixture was then cooled to obtain the crude precipitate, which was washed with hexanes to yield the cyclized product (0.795 g, 23% yield). Reaction mass intensity = [mass of input materials] / [mass of product] = 36.

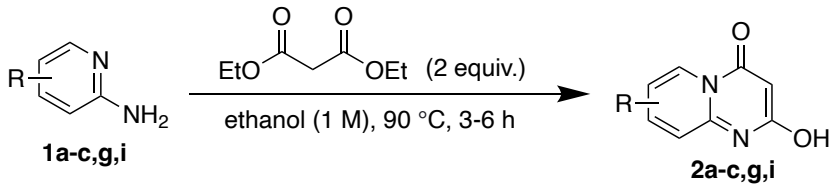

Figure 4.6: General reaction procedure for Method B

Method C:

This procedure was adapted from literature.[17] These reactions were run at 2.0 g scale relative to the (substituted) 2-aminopyridine, masses are shown below relative to the unsubstituted 2-aminopyridine (**1a**).

A round bottom flask was charged with bis(2,4,6-trichlorophenol)malonate (19.6 g, 42.4 mmol, 2 equiv), a (substituted) 2-aminopyridine (2.0 g, 21.2 mmol, 1 equiv), and acetone (16.5 g, 21.0 mL, 1 M). The solution was left to stir for 18 h at room temperature. Under reduced pressure, the solution was concentrated. The crude product was suspended in hot hexanes to yield the cyclized product (2.14 g, 62% yield). Reaction mass intensity = [mass of input materials] / [mass of product] = 18.

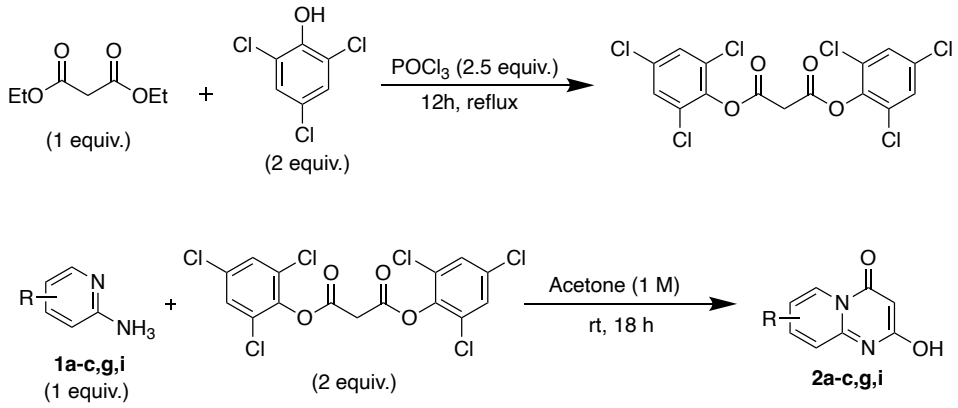

Figure 4.7: General reaction procedure for Method C

4.7.3: Synthesis of Substituted 2-hydroxy-PPDs

Caution: This procedure requires very high temperatures, please refrain from using oil-based heating as the temperatures required for this reaction exceed the flash point of standard oil-based heating mediums.

A round bottom flask was charged with diethyl malonate (5 equiv) and the desired 2-aminopyridine derivative (1 equiv). A condenser fitted to an N_2 line was attached to the reaction flask. The reaction mixture was then brought to reflux using an aluminum heat block (T_{block} = 230 °C) and stirred for 3 h. At this point, the reaction flask was removed from the aluminum heat block and allowed to cool below the boiling point of diethyl malonate. Once reflux had ceased, the condenser was replaced with a distillation apparatus, the reaction flask returned to the heat block, and excess diethyl malonate distilled from the flask at ambient pressure. The reaction mixture was then allowed to cool to room temperature. Once cool, hexanes was added to the reaction mass, and brought to reflux with vigorous stirring. The residual solid was suspended in refluxing hexanes for 1-18 h. The resulting solid was filtered, washed with diethyl ether, and dried

in vacuo, giving the desired 2-hydroxy-PPD product as a solid. All NMR spectroscopy on 2-hydroxy-PPDs was conducted in d_6-DMSO.

Poor solubility of these compounds hindered the acquisition of ^{13}C NMR spectra with acceptable signal-to-noise in several cases. Notably, this is a common issue with 2-hydroxy-PPDs, as to the best of our knowledge there is only one known compound with reported ^{13}C NMR chemical shifts.[27]

2-Hydroxy-4*H*-pyrido[1,2-*a*]pyrimidin-4-one (2a). 2-Aminopyridine **1a** (1.74 g, 18.5 mmol), was coupled with diethyl malonate (14.8 g, 14.0 mL, 92.5 mmol) using the general procedure to form **2a** as a beige solid. Isolated yield: 2.35 g, 78%.[28] ^1H NMR (300MHz, $(CD_3)_2SO$, 292 K, ppm): δ 12.03 (s, 1H), 8.93 (dd, *J* = 6.9, 0.7 Hz, 1H), 8.09 (dtd, *J* = 8.7, 6.9, 1.6 Hz, 1H), 7.41 (dt, *J* = 8.8, 1.3, 0.8 Hz, 1H), 7.33 (td, *J* = 6.9, 1.3 Hz, 1H), 4.97 (s, 1H).[28] HRMS: Calc'd for $C_8H_7N_2O_2$ $[M+H]^+$: 163.05020; found: 163.04973. Reaction mass intensity = [mass of input materials] / [mass of product] = 7.

2-Hydroxy-9-methyl-4*H*-pyrido[1,2-*a*]pyrimidin-4-one (2b). 2-Amino-3-methylpyridine **1b** (2.00 g, 18.5 mmol), was coupled with diethyl malonate (14.8 g, 14.0 mL, 92.5 mmol) using the general procedure to form **2b** as a pale yellow solid. Isolated yield: 2.39 g, 73%. ^1H NMR (500MHz, $(CD_3)_2SO$, 292 K, ppm): δ 11.48 (s, 1H), 8.80 (d, *J* = 7.0, 1.6 Hz, 1H), 7.84 (d, *J* = 6.9 Hz, 1H), 7.17 (t, *J* = 7.0 Hz, 1H), 5.40 (s, 1H), 2.44 (s, 3H). HRMS: Calc'd for $C_9H_9N_2O_2$ $[M+H]^+$: 177.06585; found: 177.06539.

2-Hydroxy-8-methyl-4*H*-pyrido[1,2-*a*]pyrimidin-4-one (2c). 2-Amino-4-methylpyridine **1c** (2.00 g, 18.5 mmol), was coupled with diethyl malonate (14.8 g, 14.0 mL, 92.5 mmol) using the general procedure to form **2c** as a beige solid. Isolated yield: 1.82 g, 56%.[29] ^1H NMR (300MHz,

$(CD_3)_2SO$, 292 K, ppm): δ 11.97 (s, 1H), 8.85 – 8.77 (d, 1H), 7.24 – 7.13 (m, 2H), 4.84 (s, 1H), 2.46 (s, 3H).[30] ^{13}C NMR (126 MHz, $(CD_3)_2SO$, 292 K, ppm): δ162.9, 155.8, 154.1, 147.3, 128.3, 117.7, 115.0, 80.8, 21.1. HRMS: Calc'd for $C_9H_9N_2O_2$ $[M+H]^+$: 177.06585; found: 177.06602.

2-Hydroxy-7-methyl-4*H*-pyrido[1,2-*a*]pyrimidin-4-one (2d). 2-Amino-5-methylpyridine **1c** (2.00 g, 18.5 mmol), was coupled with diethyl malonate (14.8 g, 14.0 mL, 92.5 mmol) using the general procedure to form **2c** as a pale yellow solid. Isolated yield: 2.49 g, 76%. ^1H NMR (300MHz, $(CD_3)_2SO$, 292 K, ppm): δ 11.92 (s, 1H), 8.77 (s, 1H), 7.97 (dd, J = 8.9, 2.1 Hz, 1H), 7.35 (d, J = 8.9 Hz, 1H), 4.95 (s, 1H), 2.37 (s, 3H). HRMS: Calc'd for $C_9H_9N_2O_2$ $[M+H]^+$: 177.06585; found: 177.06582.

2-Hydroxy-6-methyl-4*H*-pyrido[1,2-*a*]pyrimidin-4-one (2e). 2-amino-6-methylpyridine **1e** (2.00 g, 18.5 mmol), was coupled with diethyl malonate (14.8 g, 14.0 mL, 92.5 mmol) using the general procedure to form **2e** as a brown solid. Isolated yield: 1.05 g, 32%. ^1H NMR (300MHz, $(CD_3)_2SO$, 292 K, ppm): δ 10.59 (s, 1H), 7.88 (d, *J* = 8.2 Hz, 1H), 7.67 (t, *J* = 7.9 Hz, 1H), 6.98 (d, *J* = 7.4 Hz, 1H), 3.60 (s, 1H), 2.41 (s, 3H). HRMS: Calc'd for $C_9H_9N_2O_2$ $[M+H]^+$: 177.06585; found: 177.06559.

9-Chloro-2-hydroxy-4*H*-pyrido[1,2-*a*]pyrimidin-4-one (2f). 2-Amino-3-chloropyridine **1f** (2.38 g, 18.5 mmol), was coupled with diethyl malonate (14.8 g, 14.0 mL, 92.5 mmol) using the general procedure to form **2f** as a beige solid. Isolated yield: 2.13 g, 59%. ^1H NMR (300MHz, $(CD_3)_2SO$, 292 K, ppm): δ 11.90 (s, 1H), 8.85 (dd, *J* = 7.1, 1.5 Hz, 1H), 8.18 (dd, *J* = 7.4, 1.5 Hz, 1H), 7.19 (t, *J* = 7.3 Hz, 1H), 5.54 (s, 1H). HRMS: Calc'd for $C_8H_6ClN_2O_2$ $[M-H]^-$: 194.99668; found: 194.99669.

8-Chloro-2-hydroxy-4*H*-pyrido[1,2-*a*]pyrimidin-4-one (2g). 2-amino-4-chloropyridine **1g** (2.38 g, 18.5 mmol), was coupled with diethyl malonate (14.8 g, 14.0 mL, 92.5 mmol) using a modified general procedure (open to air instead of N_2 atmosphere) to form **2g** as a brown solid. Isolated yield: 1.53 g, 42%. ^{1}H NMR (300MHz, $(CD_3)_2SO$, 292 K, ppm): δ 12.02 (s, 1H), 8.87 (d, *J* = 7.5 Hz, 1H), 7.49 (d, *J* = 2.2 Hz, 1H), 7.36 (dd, *J* = 7.5, 2.3 Hz, 1H), 5.15 (s, 1H). ^{13}C NMR (126 MHz, $(CD_3)_2SO$, 292 K, ppm): δ 165.3, 156.5, 149.1, 145.4, 130.0, 118.3, 116.1, 82.3. HRMS: Calc'd for $C_8H_6ClN_2O_2$ $[M+H]^+$: 197.01123; found: 197.01035.

7-Chloro-2-hydroxy-4*H*-pyrido[1,2-*a*]pyrimidin-4-one (2h). 2-Amino-5-chloropyridine **1h** (2.38 g, 18.5 mmol), was coupled with diethyl malonate (14.8 g, 14.0 mL, 92.5 mmol) using a modified general procedure (open to air instead of N_2 atmosphere) to form **2h** as a pale yellow solid. Isolated yield: 2.83 g, 78%.[30] ^{1}H NMR (300MHz, $(CD_3)_2SO$, 292 K, ppm): δ 12.07 (s, 1H), 8.89 (d, J = 2.4 Hz, 1H), 8.10 (dd, J = 9.4, 2.5 Hz, 1H), 7.44 (dd, J = 9.4, 0.7 Hz, 1H), 5.19 (s, 1H). HRMS: Calc'd for $C_8H_6ClN_2O_2$ $[M+H]^+$: 197.01123; found: 197.01068.

6-Chloro-2-hydroxy-4*H*-pyrido[1,2-*a*]pyrimidin-4-one (2i). 2-Amino-6-chloropyridine **1i** (2.38 g, 18.5 mmol), was coupled with diethyl malonate (14.8 g, 14.0 mL, 92.5 mmol) using the general procedure to form **2i** as a brown solid. Isolated yield: 1.40 g, 39%. ^{1}H NMR (300MHz, $(CD_3)_2SO$, 292 K, ppm): δ 10.98 (s, 1H), 8.04 (d, *J* = 8.2 Hz, 1H), 7.86 (t, *J* = 8.0 Hz, 1H), 7.23 (dd, *J* = 7.8, 0.7 Hz, 1H), 3.63 (s, 1H). HRMS: Calc'd for $C_8H_6ClN_2O_2$ $[M+H]^+$: 197.01123; found: 197.01049.

9-Bromo-2-hydroxy-4*H*-pyrido[1,2-*a*]pyrimidin-4-one (2j). 2-amino-3-bromopyridine **1j** (3.20 g, 18.5 mmol), was coupled with diethyl malonate (14.8 g, 14.0 mL, 92.5 mmol) using the general procedure to form **2j** as a brown solid. Isolated yield: 1.64 g, 37%. ^{1}H NMR (300MHz,

$(CD_3)_2SO$, 292 K, ppm): δ 11.79 (s, 1H), 8.89 (d, J = 7.0 Hz, 1H), 8.34 (d, J = 7.3 Hz, 1H), 7.11 (t, J = 7.2 Hz, 1H), 5.53 (s, 1H). HRMS: Calc'd for $C_8H_6BrN_2O_2$ $[M-H]^-$: 238.94616; found: 238.94626 .

8-Bromo-2-hydroxy-4*H*-pyrido[1,2-*a*]pyrimidin-4-one (2k). 2-amino-4-bromopyridine **1k** (3.20 g, 18.5 mmol), was coupled with diethyl malonate (14.8 g, 14.0 mL, 92.5 mmol) using the general procedure to form **2k** as a beige solid. Isolated yield: 1.46 g, 33%. ^{1}H NMR (300MHz, $(CD_3)_2SO$, 292 K, ppm): δ 12.00 (s, 1H), 8.77 (d, *J* = 7.4 Hz, 1H), 7.64 (d, *J* = 2.1 Hz, 1H), 7.47 (dd, *J* = 7.4, 2.1 Hz, 1H), 5.15 (s, 1H). HRMS: Calc'd for $C_8H_6BrN_2O_2$ $[M+H]^+$: 240.96072; found: 240.96112.

6-Bromo-2-hydroxy-4*H*-pyrido[1,2-*a*]pyrimidin-4-one (2m). 2-amino-6-bromopyridine **1m** (3.20 g, 18.5 mmol), was coupled with diethyl malonate (14.8 g, 14.0 mL, 92.5 mmol) using the general procedure to form **2m** as a pale yellow solid. Isolated yield: 2.00 g, 45%. ^{1}H NMR (300MHz, $(CD_3)_2SO$, 292 K, ppm): δ 11.00 (s, 1H), 8.07 (d, J = 8.2 Hz, 1H), 7.75 (t, J = 7.9 Hz, 1H), 7.36 (d, J = 7.7 Hz, 1H), 3.63 (s, 1H). HRMS: Calc'd for $C_8H_6BrN_2O_2$ $[M-H]^-$: 238.94616; found: 238.94632.

9-Fluoro-2-hydroxy-4*H*-pyrido[1,2-*a*]pyrimidin-4-one (2n). 2-Amino-3-fluoropyridine **2n** (2.07 g, 18.5 mmol), was coupled with diethyl malonate (14.8 g, 14.0 mL, 92.5 mmol) using the general procedure to form **2n** as a beige solid. Isolated yield: 1.77 g, 53%. ^{1}H NMR (500MHz, $(CD_3)_2SO$, 292 K, ppm): δ 11.99 (s, 1H), 8.70 (d, J = 7.1 Hz, 1H), 7.87 (t, J = 8.7 Hz, 1H), 7.29 – 7.08 (m, 1H), 5.51 (s, 1H). ^{19}F-NMR (283 MHz, $(CD_3)_2SO$, 298 K) δ -126.7. HRMS: Calc'd for $C_8H_6FN_2O_2$ $[M+H]^+$: 181.04079; found: 181.04073.

7-Fluoro-2-hydroxy-4*H*-pyrido[1,2-*a*]pyrimidin-4-one (2p). 2-Amino-5-fluoropyridine **2p** (2.07 g, 18.5 mmol), was coupled with diethyl malonate (14.8 g, 14.0 mL, 92.5 mmol) using the

general procedure to form **2p** as a beige solid. Isolated yield: 2.07 g, 65%. ^{1}H NMR (500MHz, $(CD_3)_2SO$, 292 K, ppm): δ 11.97 (s, 1H), 8.92 – 8.87 (m, 1H), 8.19 – 8.11 (m, 1H), 7.49 (dd, J = 9.6, 5.0 Hz, 1H), 5.20 (s, 1H). ^{19}F-NMR (283 MHz, $(CD_3)_2SO$, 298 K) δ -135.1. HRMS: Calc'd for $C_8H_6FN_2O_2$ $[M+H]^+$: 181.04079; found: 181.04072.

6-Fluoro-2-hydroxy-4*H*-pyrido[1,2-*a*]pyrimidin-4-one (2q). 2-Amino-6-fluoropyridine **2q** (2.07 g, 18.5 mmol), was coupled with diethyl malonate (14.8 g, 14.0 mL, 92.5 mmol) using the general procedure to form **2q** as a beige solid. Isolated yield: 1.26 g, 38%. ^{1}H NMR (500MHz, $(CD_3)_2SO$, 292 K, ppm): δ 10.85 (s, 1H), 8.16 – 7.72 (m, 2H), 7.04 – 6.65 (m, 1H), 3.64 (s, 1H). ^{19}F-NMR (283 MHz, $(CD_3)_2SO$, 298 K) δ -69.5. HRMS: Calc'd for $C_8H_6FN_2O_2$ $[M+H]^+$: 181.04079 ; found: 181.04076.

4.7.4 Synthesis of Functionalized PPDs

Procedure for synthesis of 4-oxo-4H-pyrido[1,2-a]pyrimidin-2-yl 4-methylbenzenesulfonate (3a):

2-Hydroxy-4*H*-pyrido[1,2-*a*]pyrimidin-4-one (**2a**, 1g, 6.17 mmol) was charged in a round bottom flask with 30 mL DCM. Triethylamine (1.37 g, 1.89 mL, 13.57 mmol) was then added via syringe and the solution was allowed to stir. 4-Toluenesulfonyl chloride (1.29 g, 6.78 mmol) was dissolved in 10 mL DCM, and transferred to an addition funnel attached to the previously charged round bottom flask. The 4-toluenesulfonyl chloride solution was allowed to add dropwise, and the reaction was allowed to stir overnight at room temperature. The reaction was quenched with H_2O [20 mL], and the aqueous layer was extracted three time with DCM [20 mL]. The combined organic fractions were dried with $MgSO_4$ and filtered before evaporating to dryness. The resulting brown oil was then triturated with cold hexanes to yield a beige powder that was filtered and

washed again with cold hexanes [40 mL] to yield the final product **3a** (1.90 g, 97% yield). ^{1}H NMR (500MHz, $CDCl_3$, 292K, ppm): δ 9.04 (d, J = 7.0 Hz, 1H), 7.98 (d, J = 8.3 Hz, 2H), 7.86 – 7.81 (m, 1H), 7.57 (d, J = 8.6 Hz, 1H), 7.37 (d, J = 8.2 Hz, 2H) 7.22 (t, J = 7.0 Hz, 1H), 6.11 (s, 1H), 2.46 (s, 9H). ^{13}C NMR (126 MHz, ($CDCl_3$, 292 K, ppm): δ 162.15, 159.32, 150.50, 145.88, 138.21, 133.79, 129.90, 128.97, 128.06, 126.09, 116.39, 91.69, 21.91. HRMS: Calc'd for $C_{15}H_{12}N_2O_4S$ $[M+H]^+$: 317.05906; found: 317.05883.

Procedure for synthesis of 7-bromo-4-oxo-4H-pyrido[1,2-a]pyrimidin-2-yl 4-methylbenzenesulfonate (3l):

A mixture containing 7-bromo-2-hydroxy-4*H*-pyrido[1,2-*a*]pyrimidin-4-one was synthesized using the general procedure above for synthesis of substituted 2-hydroxy-PPDs. This was completed using 2-amino-4-bromopyridine **1l** (3.20 g, 18.5 mmol), and diethyl malonate (14.8 g, 14.0 mL, 92.5 mmol). The collected solid (2.58 g, see Appendix C: Figure C30 for ^{1}H NMR) was charged into a round bottom flask with 53 ml DCM and triethylamine (2.2 equiv, 3.31 mL) was added dropwise. 4-Toluenesulfonyl chloride (1.0 equiv, 2.04 g) was added slowly to the stirred solution and allowed to stir overnight. The solution was washed with H_2O and subsequently dried with $MgSO_4$ and dried *in vacuo*. The resulting solid was resuspended in toluene, and dried on a Genevac EZ-2 to produce a light-brown solid **3l** (2.20 g, 30% yield over two steps). ^{1}H NMR (500MHz, $CDCl_3$, 292K, ppm): δ 9.16 (d, J = 2.2 Hz, 1H), 8.01 – 7.92 (m, 2H), 7.85 (dd, J = 9.4, 2.2 Hz, 1H), 7.45 (d, J = 9.3 Hz, 1H), 7.38 (d, J = 8.1 Hz, 2H), 6.13 (s, 1H), 2.47 (s, 3H). ^{13}C NMR (126 MHz, ($CDCl_3$, 292 K, ppm): δ 162.2, 158.4, 149.1, 146.1, 141.6, 133.7, 130.1, 129.0, 128.3, 127.1, 111.8, 92.5, 22.0. HRMS: Calc'd for $C_{15}H_{11}BrN_2O_4S$ $[M+H]^+$: 394.96957; found: 394.96962.

Procedure for synthesis of 4-oxo-4H-pyrido[1,2-a]pyrimidin-2-yl pivalate (4a):

2-Hydroxy-4*H*-pyrido[1,2-*a*]pyrimidin-4-one (**2a**, 1.5 g, 9.25 mmol) was charged in a round bottom flask with 4-dimethylaminopyridine (113.0 mg, 0.925 mmol) and 70 mL DCM. Triethylamine (1.12 g, 1.55 mL, 11.1 mmol) was then added via syringe and the solution was allowed to stir. Pivaloyl chloride (1.34 g, 1.37 mL, 11.1 mmol) was then added slowly dropwise and the reaction was allowed to stir overnight at room temperature. The reaction was quenched with saturated sodium bisulfite [20 mL], washed with H_2O [40 mL], and the aqueous fractions were extracted three time with DCM [20 mL]. The combined organic fractions were dried with $MgSO_4$ and filtered before evaporating to dryness. The resulting brown oil was then triturated with cold hexanes to yield a colourless powder that was filtered and washed again with cold hexanes [40 mL] to yield the final product **4a** (1.79 g, 61% yield). ^{1}H NMR (500MHz, $CDCl_3$, 292K, ppm): δ 9.10 (d, J = 7.1 Hz, 1H), 7.86 – 7.82 (m, 1H), 7.68 (d, J = 8.8 Hz, 1H), 7.23 (dt, J = 0.9, 7.8 Hz, 1H), 6.19 (s, 1H), 1.41 (s, 9H). ^{13}C NMR (126 MHz, ($CDCl_3$, 292 K, ppm): δ 175.64, 163.94, 159.57, 150.94, 137.62, 127.99, 126.15, 116.00, 94.23, 39.55, 27.09. HRMS: Calc'd for $C_{13}H_{14}N_2O_3$ $[M+H]^+$: 247.10772; found: 247.10754.

4.8 References

(1) Shan, Y.; Su, L.; Zhao, Z.; Chen, D. The Construction of Nitrogen-Containing Heterocycles from Alkynyl Imines. *Adv. Synth. Catal.* **2021**, *363* (4), 906–923. https://doi.org/10.1002/adsc.202001283.

(2) Yu, H.; Xu, F. Advances in the Synthesis of Nitrogen-Containing Heterocyclic Compounds by in Situ Benzyne Cycloaddition. *RSC Adv.* **2023**, *13* (12), 8238–8253. https://doi.org/10.1039/D3RA00400G.

(3) Khan, I.; Ibrar, A.; Ahmed, W.; Saeed, A. Synthetic Approaches, Functionalization and Therapeutic Potential of Quinazoline and Quinazolinone Skeletons: The Advances Continue. *Eur. J. Med. Chem.* **2015**, *90*, 124–169. https://doi.org/10.1016/j.ejmech.2014.10.084.

(4) Lamberth, C. Heterocyclic Chemistry in Crop Protection. *Pest Manag. Sci.* **2013**, *69* (10), 1106–1114. https://doi.org/10.1002/ps.3615.

(5) Joule, J. A. Chapter Four - Natural Products Containing Nitrogen Heterocycles—Some Highlights 1990–2015. In *Advances in Heterocyclic Chemistry*; Scriven, E. F. V., Ramsden, C. A., Eds.; Heterocyclic Chemistry in the 21st Century; Academic Press, 2016; Vol. 119, 81–106.

(6) Kumar, A.; Singh, A. K.; Singh, H.; Vijayan, V.; Kumar, D.; Naik, J.; Thareja, S.; Yadav, J. P.; Pathak, P.; Grishina, M.; Verma, A.; Khalilullah, H.; Jaremko, M.; Emwas, A.-H.; Kumar, P. Nitrogen Containing Heterocycles as Anticancer Agents: A Medicinal Chemistry Perspective. *Pharmaceuticals* **2023**, *16* (2), 299. https://doi.org/10.3390/ph16020299.

(7) Aatif, M.; Raza, M. A.; Javed, K.; Nashre-ul-Islam, S. M.; Farhan, M.; Alam, M. W. Potential Nitrogen-Based Heterocyclic Compounds for Treating Infectious Diseases: A Literature Review. *Antibiotics* **2022**, *11* (12), 1750. https://doi.org/10.3390/antibiotics11121750.

(8) Mermer, A.; Keles, T.; Sirin, Y. Recent Studies of Nitrogen Containing Heterocyclic Compounds as Novel Antiviral Agents: A Review. *Bioorg. Chem.* **2021**, *114*, 105076. https://doi.org/10.1016/j.bioorg.2021.105076.

(9) Tran, T. N.; Henary, M. Synthesis and Applications of Nitrogen-Containing Heterocycles as Antiviral Agents. *Molecules* **2022**, *27* (9), 2700. https://doi.org/10.3390/molecules27092700.

(10) Heravi, M. M.; Zadsirjan, V. Prescribed Drugs Containing Nitrogen Heterocycles: An Overview. *RSC Adv.* **2020**, *10* (72), 44247–44311. https://doi.org/10.1039/D0RA09198G.

(11) Vitaku, E.; Smith, D. T.; Njardarson, J. T. Analysis of the Structural Diversity, Substitution Patterns, and Frequency of Nitrogen Heterocycles among U.S. FDA Approved Pharmaceuticals. *J. Med. Chem.* **2014**, *57* (24), 10257–10274. https://doi.org/10.1021/jm501100b.

(12) Kerru, N.; Gummidi, L.; Maddila, S.; Gangu, K. K.; Jonnalagadda, S. B. A Review on Recent Advances in Nitrogen-Containing Molecules and Their Biological Applications. *Molecules* **2020**, *25* (8), 1909. https://doi.org/10.3390/molecules25081909.

(13) Tschitschibabin, A. E. Tautomerie des α-Amino-pyridins, II: Über die Bildung von bicyclischen Derivaten des α-Amino-pyridins. *Ber. dtsch. Chem. Ges. A/B* **1924**, *57* (7), 1168–1172. https://doi.org/10.1002/cber.19240570723.

(14) Ibrahim, M. A.; El-Gohary, N. M. Chemical Behavior of 4,9-Dimethoxy-5-Oxo-5H-Furo[3,2-g]Chromene-6-Carboxaldehyde towards Carbon Nucleophilic Reagents. *J. Heterocycl. Chem.* **2020**, *57* (7), 2815–2830. https://doi.org/10.1002/jhet.3991.
(15) Urich, R.; Wishart, G.; Kiczun, M.; Richters, A.; Tidten-Luksch, N.; Rauh, D.; Sherborne, B.; Wyatt, P. G.; Brenk, R. De Novo Design of Protein Kinase Inhibitors by in Silico Identification of Hinge Region-Binding Fragments. *ACS Chem. Biol.* **2013**, *8* (5), 1044–1052. https://doi.org/10.1021/cb300729y.
(16) Priyadarshani, G.; Amrutkar, S.; Nayak, A.; Banerjee, U. C.; Kundu, C. N.; Guchhait, S. K. Scaffold-Hopping of Bioactive Flavonoids: Discovery of Aryl-Pyridopyrimidinones as Potent Anticancer Agents That Inhibit Catalytic Role of Topoisomerase IIα. *Eur. J. Med. Chem.* **2016**, *122*, 43–54. https://doi.org/10.1016/j.ejmech.2016.06.024.
(17) Park, D.-S.; Jo, E.; Choi, J.; Lee, M.; Kim, S.; Kim, H.-Y.; Nam, J.; Ahn, S.; Hwang, J. Y.; Windisch, M. P. Characterization and Structure-Activity Relationship Study of Iminodipyridinopyrimidines as Novel Hepatitis C Virus Inhibitor. *Eur. J. Med. Chem.* **2017**, *140*, 65–73. https://doi.org/10.1016/j.ejmech.2017.09.010.
(18) Bhawale, R. T.; Chillal, A. S.; Kshirsagar, U. A. 4H-Pyrido[1,2-a]Pyrimidin-4-One, Biologically Important Fused Heterocyclic Scaffold: Synthesis and Functionalization. *J. Heterocycl. Chem.* **2023**, *60* (8), 1356–1373. https://doi.org/10.1002/jhet.4637.
(19) Dong, Z.; Wang, Z.; Guo, Z.-Q.; Gong, S.; Zhang, T.; Liu, J.; Luo, C.; Jiang, H.; Yang, C.-G. Structure–Activity Relationship of SPOP Inhibitors against Kidney Cancer. *J. Med. Chem.* **2020**, *63* (9), 4849–4866. https://doi.org/10.1021/acs.jmedchem.0c00161.
(20) Sakurada, I.; Zhang, L. PYRIDMIDONES FOR TREATMENT OF POTASSIUM CHANNEL RELATED DISEASES. WO 2012/038850 A1, March 29, 2012.
(21) Bergman, H.; Buchanan, J. L.; Chakka, N.; Dimauro, E. F.; Gunaydin, H.; Guzman Perez, A.; Hua, Z.; Huang, X. QUINAZOLINONE COMPOUNDS AND DERIVATIVES THEREOF. WO/2014/036022, March 6, 2014.
(22) Guchhait, S. K.; Priyadarshani, G. Synthesis of 2-Arylpyridopyrimidinones, 6-Aryluracils, and Tri- and Tetrasubstituted Conjugated Alkenes via Pd-Catalyzed Enolic C–O Bond Activation–Arylation. *J. Org. Chem.* **2015**, *80* (12), 6342–6349. https://doi.org/10.1021/acs.joc.5b00771.
(23) Shulman, D. G.; Amdahl, L.; Washington, C.; Graves, A. A Combined Analysis of Two Studies Assessing the Ocular Comfort of Antiallergy Ophthalmic Agents. *Clin. Ther.* **2003**, *25* (4), 1096–1106. https://doi.org/10.1016/S0149-2918(03)80069-3.
(24) Moessner, C.; Hoffmann-Emery, F.; Adam, J.-M.; Fantasia, S.; Fishlock, D.; Meier, R.; Wuitschik, G.; Ratni, H. Development and Optimization of the Manufacturing Process for RNA-Splicing Modifier Risdiplam RG7916. In *Complete Accounts of Integrated Drug Discovery and Development: Recent Examples from the Pharmaceutical Industry. Volume 4*; ACS Symposium Series; American Chemical Society, 2022; Vol. 1423, 301–332.
(25) Yu, T.; Li, N.; Wu, C.; Guan, A.; Li, Y.; Peng, Z.; He, M.; Li, J.; Gong, Z.; Huang, L.; Gao, B.; Hao, D.; Sun, J.; Pan, Y.; Shen, L.; Chan, C.; Lu, X.; Yuan, H.; Li, Y.; Li, J.; Chen, S. Discovery of Pyridopyrimidinones as Potent and Orally Active Dual Inhibitors of PI3K/mTOR. *ACS Med. Chem. Lett.* **2018**, *9* (3), 256–261. https://doi.org/10.1021/acsmedchemlett.8b00002.
(26) La Motta, C.; Sartini, S.; Mugnaini, L.; Simorini, F.; Taliani, S.; Salerno, S.; Marini, A. M.; Da Settimo, F.; Lavecchia, A.; Novellino, E.; Cantore, M.; Failli, P.; Ciuffi, M. Pyrido[1,2-

a]Pyrimidin-4-One Derivatives as a Novel Class of Selective Aldose Reductase Inhibitors Exhibiting Antioxidant Activity. *J. Med. Chem.* **2007**, *50* (20), 4917–4927. https://doi.org/10.1021/jm070398a.
(27) Gawale, Y.; Jadhav, A.; Sekar, N. Azo Acid Dyes Based on 2H-Pyrido[1,2-a]Pyrimidine-2,4(3H)-Dione with Good Tinctorial Power and Wetfastness - Synthesis, Photophysical Properties, and Dyeing Studies. *Fibers Polym.* **2018**, *19* (8), 1678–1686. https://doi.org/10.1007/s12221-018-7522-7.
(28) Roy, A.; Kundu, M.; Dhar, P.; Chakraborty, A.; Mukherjee, S.; Naskar, J.; Rarhi, C.; Barik, R.; Mondal, S. K.; Wani, M. A.; Gajbhiye, R.; Roy, K. K.; Maiti, A.; Manna, P.; Adhikari, S. Novel Pyrimidinone Derivatives Show Anticancer Activity and Induce Apoptosis: Synthesis, SAR and Putative Binding Mode. *ChemistrySelect,* **2020**, *5* (15), 4559–4566. https://doi.org/10.1002/slct.202000208.
(29) Jannati, S.; Esmaeili, A. A. An Efficient One-Pot Synthesis of Highly Functionalized Benzylpyrazolyl Pyrido[1,2-a]Pyrimidine Derivatives Using $CuFe_2O_4$ Nanoparticles under Solvent-Free Conditions. *Res. Chem. Intermed.* **2017**, *43* (12), 6817–6833. https://doi.org/10.1007/s11164-017-3022-4.
(30) Yalduz, S.; Yilmaz, M. Microwave Assisted Synthesis of 2,3-Dihydro-4H- Furo[2,3-d]Pyrido[1,2-a]Pyrimidin-4-Ones and Furo[2,3-d]Pyrido[1,2-a]Pyrimidin-4-One. *ChemistrySelect,* **2023**, *8* (10), e202204260. https://doi.org/10.1002/slct.202204260.
(31) Alwan, S. M. Synthesis and Preliminary Antimicrobial Activity of New Schiff Bases of Pyrido [1,2-A] Pyrimidine Derivatives with Certain Amino Acids. *Med. Chem.* **2014**, *4* (9) 635-639. https://doi.org/10.4172/2161-0444.1000206.
(32) Stepan, A. F.; Claffey, M. M.; Reese, M. R.; Balan, G.; Barreiro, G.; Barricklow, J.; Bohanon, M. J.; Boscoe, B. P.; Cappon, G. D.; Chenard, L. K.; Cianfrogna, J.; Chen, L.; Coffman, K. J.; Drozda, S. E.; Dunetz, J. R.; Ghosh, S.; Hou, X.; Houle, C.; Karki, K.; Lazzaro, J. T.; Mancuso, J. Y.; Marcek, J. M.; Miller, E. L.; Moen, M. A.; O'Neil, S.; Sakurada, I.; Skaddan, M.; Parikh, V.; Smith, D. L.; Trapa, P.; Tuttle, J. B.; Verhoest, P. R.; Walker, D. P.; Won, A.; Wright, A. S.; Whritenour, J.; Zasadny, K.; Zaleska, M. M.; Zhang, L.; Shaffer, C. L. Discovery and Characterization of (R)-6-Neopentyl-2-(Pyridin-2-Ylmethoxy)-6,7-Dihydropyrimido[2,1-c][1,4]Oxazin-4(9H)-One (PF-06462894), an Alkyne-Lacking Metabotropic Glutamate Receptor 5 Negative Allosteric Modulator Profiled in Both Rat and Nonhuman Primates. *J. Med. Chem.* **2017**, *60* (18), 7764–7780. https://doi.org/10.1021/acs.jmedchem.7b00604.
(33) Abass, M.; Mayas, A. S. Substituted Pyridopyrimidinones, 1: Convenient PTC Alkylation and Halogenation of 2-Hydroxy-4H-Pyrido[1,2-a]Pyrimidin-4-One. *Heteroat. Chem.* **2007**, *18* (1), 19–27. https://doi.org/10.1002/hc.20245.
(34) Kappe, Th.; Lube, W. Zur Synthese mesomerer Pyrimidinbetaine. *Monatsh. Chem.* **1971**, *102* (3), 781–787. https://doi.org/10.1007/BF01167260.
(35) Achmatowicz, M. M.; Thiel, O. R.; Colyer, J. T.; Hu, J.; Elipe, M. V. S.; Tomaskevitch, J.; Tedrow, J. S.; Larsen, R. D. Hydrolysis of Phosphoryl Trichloride (POCl3): Characterization, in Situ Detection, and Safe Quenching of Energetic Metastable Intermediates. *Org. Process Res. Dev.* **2010**, *14* (6), 1490–1500. https://doi.org/10.1021/op1001484.
(36) Anastas, P. T.; Warner, J. C. Green Chemistry: Theory and Practice; Oxford University Press: New York, 1998; p 30.

(37) Lappin, G. R.; Petersen, Q. R.; Wheeler, C. E. CYCLIZATION OF 2-AMINOPYRIDINE DERIVATIVES. II. THE REACTION OF SUBSTITUTED 2-AMINOPYRIDINES WITH ETHYL MALONATE1. *J. Org. Chem.* **1950**, *15* (2), 377–380. https://doi.org/10.1021/jo01148a023.

Chapter 5: Conclusions and Future Outlook

5.1: Conclusions

The objective of this thesis was to create a foundational understanding of C–O activation of carboxylates with Pd. Alkenyl carboxylates served as a suitable starting point for these studies as they are less toxic, mass efficient and economic sources of non-aromatic functionality that can be easily accessible by O-acylation of ketones. As every aspect of a reaction affects the efficiency of a desired outcome, this thesis tackled this problem via three routes. Firstly, in Chapter 2, I investigated the mechanism behind a Suzuki-like reaction previously reported by the Leitch Lab. Pd sources, ligation, and solvents were all found to alter the outcome of the reaction. Specifically, through this multi-pronged investigation previously unseen intermediates were identified. A singly ligated Pd centre bound to the alkene of the substrate was uncovered, leading to a proposed hypothetical mechanism. This chapter provides the blueprint as to how future reactions with alkenyl carboxylates can be developed.

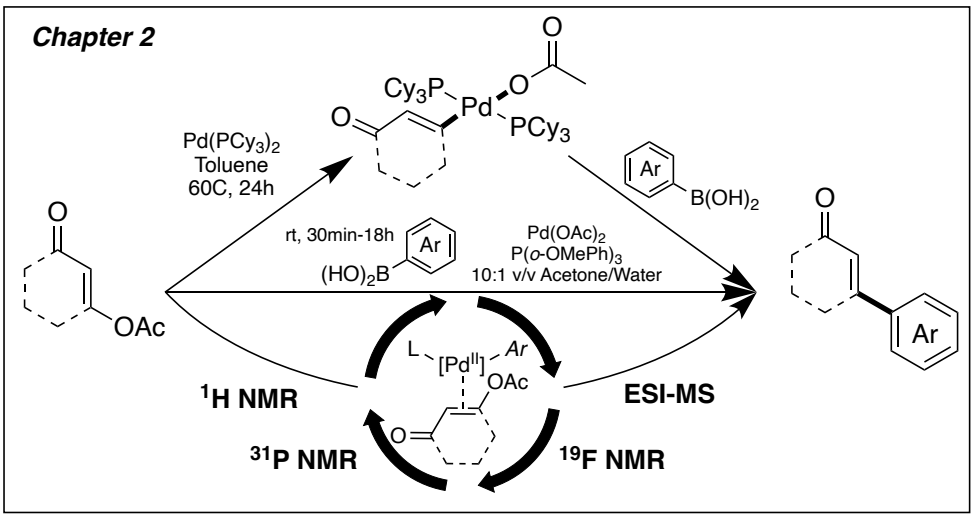

Figure 5.1: Graphical abstract for Chapter 2 - An Experimental Evaluation of a Base-Free, Open to Air, Pd Cross-Coupling Reaction

Secondly, Chapter 3 expanded on this known reactivity of alkenyl carboxylates, taking inspiration from the work developed in Chapter 2. Mechanistically, Miyaura borylation was a rational next phase in C–O activation chemistry as many of the same fundamental steps are shared with the Suzuki-like chemistry developed by the Leitch Lab. This proved fruitful, and several borylation reactions were developed and optimized using high-throughput experimentation. The generated alkenyl pinacol boronates proved to be variably stable and therefore undependable coupling partners. This was taken advantage of to develop a two-step deoxygenation procedure through this borylation chemistry. By altering the pinacol ester used, this stability issue could be overcome, which allowed for the reactivity one would desire from a boron substituent (such as cross-coupling).

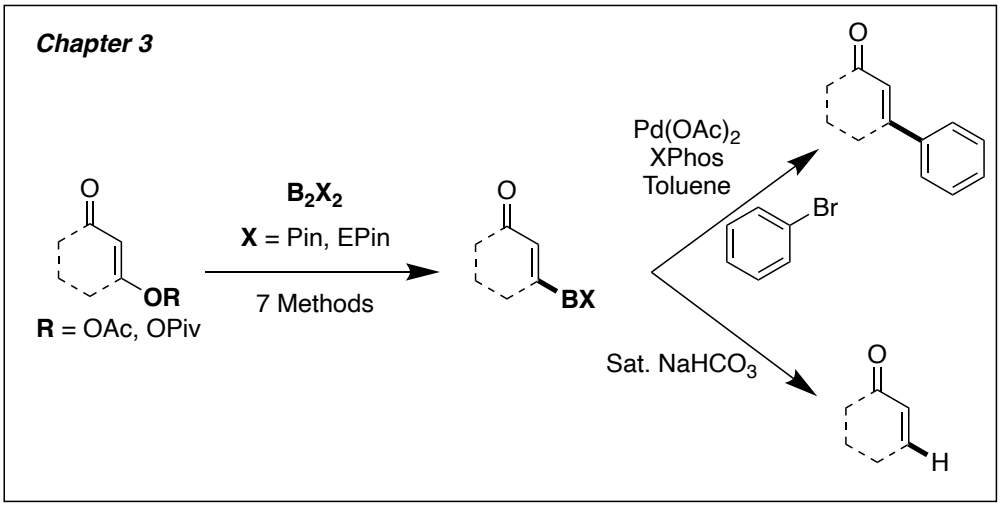

Figure 5.2: Graphical Abstract for Chapter 3 - Base-Free Palladium-Catalyzed Borylation of Enol Carboxylates and Further Reactivity Toward Deboronation and Cross-Coupling

Lastly, Chapter 4 focussed on the synthesis of substituted pyrido[1,2-α]pyramid-4-one (PPD) molecules. As literature methods proved to be unreliable when expanded beyond the scope initially conceived for, we developed a robust and solvent-free procedure to access these molecules. This reaction produced 16 unique PPD molecules, with CH_3, Cl, Br, and F handles in

four different positions within the structure. As these molecules demonstrate solubility issues, non-standard ^{1}H and ^{13}C NMR settings were utilized to characterize these molecules. The unsubstituted PPD molecule was then successfully functionalized as a critical first step towards using this motif as a model structure to demonstrate C–O activation chemistry with Pd.

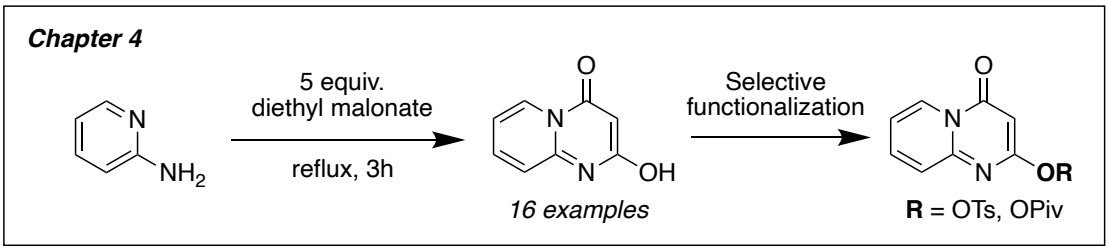

Figure 5.3: Graphical Abstract for Chapter 4 - The Development of Novel Cross-Coupling Scaffolds for C–O Activation Chemistry

Overall, this thesis has furthered the development of C–O activation of carboxylates in Pd-catalyzed cross-coupling chemistry. This thesis provides fundamental mechanistic insights into how to activate these strong C–O bonds, which then allowed for the development of alternative reactions, and finally, novel substrates were synthesized that could be utilized in all the previously mentioned chemistry. While all these chapters are unique in their approach, they all serve as essential legs in the metaphorical chair that is C–O activation with Pd chemistry. One leg does not make up this field, but all together they provide a suitable seat from where to begin examination of the next steps.

5.2 Future Directions

5.2.1 Suzuki Like Chemistry

After our experimental evaluation of the Suzuki-like chemistry created by the Leitch Lab, the next step in understanding this reaction would be to compute our hypothesized mechanism. Computations are often used as an additional point of validation for mechanistic studies;[1–5] however we were unable to complete these as they require a trained user. Special care would need to be taken in order to incorporate solvation effects as the co-solvent system (acetone/water) is experimentally a key feature of this reaction.

In addition to recreating our mechanism, one would also like to see specific experiments computed. As the main issue with this reaction is that it is exceptionally quick, examining specific steps in isolation would allow for a more complete understanding. One such example would be deuterium incorporation at the α position of the dimedone substrate. This would likely cause a change visible through a secondary kinetic isotope effect (KIE),[6,7] as we hypothesize that the either of the changes in hybridization from sp^2 to sp^3 and then back to sp^2 (Figure 5.4) would likely be the principal factor causing a change in rate. Isolation of the deuterated dimedone substrate proved to be an elusive task, but something a future researcher could execute. Comparison of observed to calculated KIE values would help support our proposed mechanism.

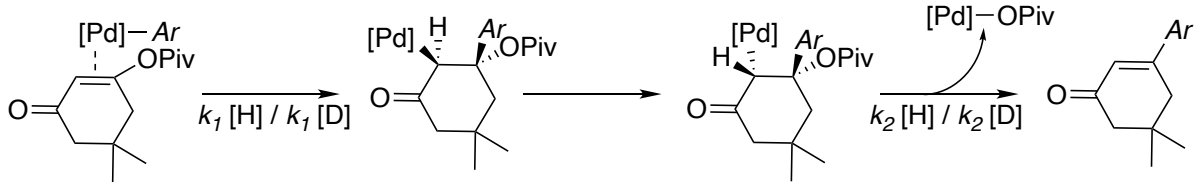

Figure 5.4: Addition of Pd to alkenyl carboxylate resulting in sp^2 to sp^3 hybridization: k_1 [H] / k_1 [D], epimerization, then hybridization from sp^3 to sp^2: k_2 [H] / k_2 [D].

In addition to computational studies, further synthetic experiments could be performed. One specifically is the alteration from the *in situ* $Pd(OAc)_2$ and P(*o*-OMePh)$_3$ (1 : 1.5 equiv.) combination to a single component $Pd(P(o\text{-}OMePh)_3)_2$ source (Figure 5.5). This Pd precatalyst is not currently available commercially; however, a recent publication from MilliporeSigma detailed the synthesis of a series of doubly ligated Pd(0) complexes,[8] all of which contain phosphine based ligands. While the P(*o*-OMePh)$_3$ complex was not detailed, P*t*Bu$_3$, PCy$_3$, and P(*o*-tol)$_3$ complexes were synthesized - leading one to believe that this could be an adequate starting point for this synthesis. The change in equivalents of Pd and ligand may affect the reaction outcome detrimentally as we found in Chapter 2, however if the yield is only minorly perturbed in favour of a single-component catalyst, that may prove acceptable.

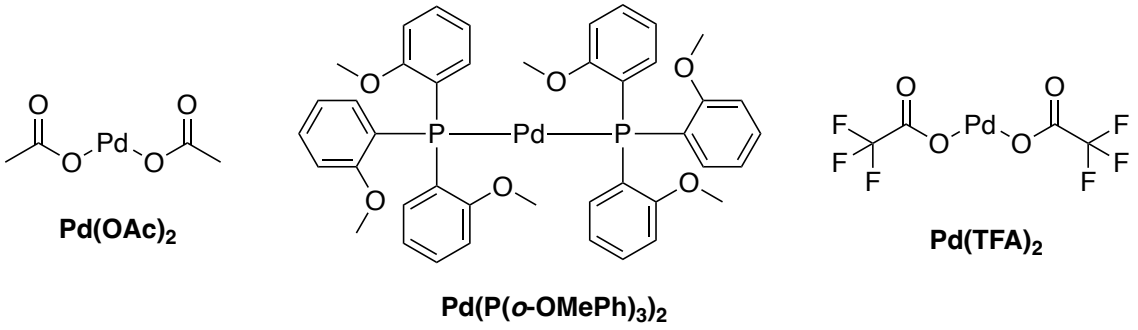

Figure 5.5: $Pd(OAc)_2$, $Pd(P(o\text{-}OMePh)_3)_2$, and $Pd(TFA)_2$

Another complex that is worthwhile exploring for this chemistry is Pd(trifluoroacetate)$_2$ ($Pd(TFA)_2$). This commercially available Pd precatalyst should work similarly to $Pd(OAc)_2$, as our hypothesized mechanism requires the substitution of the OAc ligand for the P(*o*-OMePh)$_3$ ligand. One would postulate that the additional F present in the TFA would improve stability of the dissociated anionic ligand, allowing for a less energetically hindered substitution. The additional

F present would also allow for supplementary ^{19}F NMR studies that may help to uncover decomposition pathways or unknown by-products.

5.2.2 Oxidative Addition of Alkenyl Carboxylates

One route in understanding mechanisms is to break down the mechanism into single steps, studying each step individually, before piecing together the complete picture. Much work has gone into understanding fundamental organometallic steps,[9–15] and oxidative addition is an accessible reaction to address as we often begin our reactions with this step. During work with Dr. Nahiane Pipaon Fernandez, it was discovered that the oxidative addition of an alkenyl carboxylate and $Pd(PCy_3)_2$ was reversible (Figure 5.6).[16] This spurred efforts to synthesize the oxidative addition products of numerous alkenyl carboxylates.

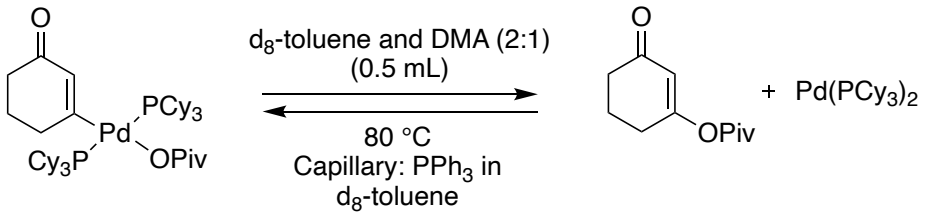

Figure 5.6: Reversible oxidative addition of alkenyl carboxylate and $Pd(PCy_3)_2$.

The following compounds were monitored for oxidative addition activity with $Pd(PCy_3)_2$ in d_8-toluene, and/or C_6D_6: 1-pivalyloxycyclopent-1-en-3-one (**1a**),[17] 3-oxocyclohex-1-en-1-yl pivalate (**1b**),[18] 5,5-dimethyl-3- oxocyclohex-1-en-1-yl pivalate (**1c**),[18] 4-pivalyloxy-3-phenylpyran-3-en-2-one (**1d**),[17] 4-pivalyloxy-1-benzyl-3-phenylpyrrolidin-3-en-2-one (**1e**),[17] 4-pivalyloxy-6-methyl-2-pyrone (**1f**),[17] 2-oxo-2*H*-chromen-4-yl pivalate (**1g**).[19] These reactions were conducted in J-Young tubes and monitored for up to seven days by ^{31}P NMR (Section 5.3.1).

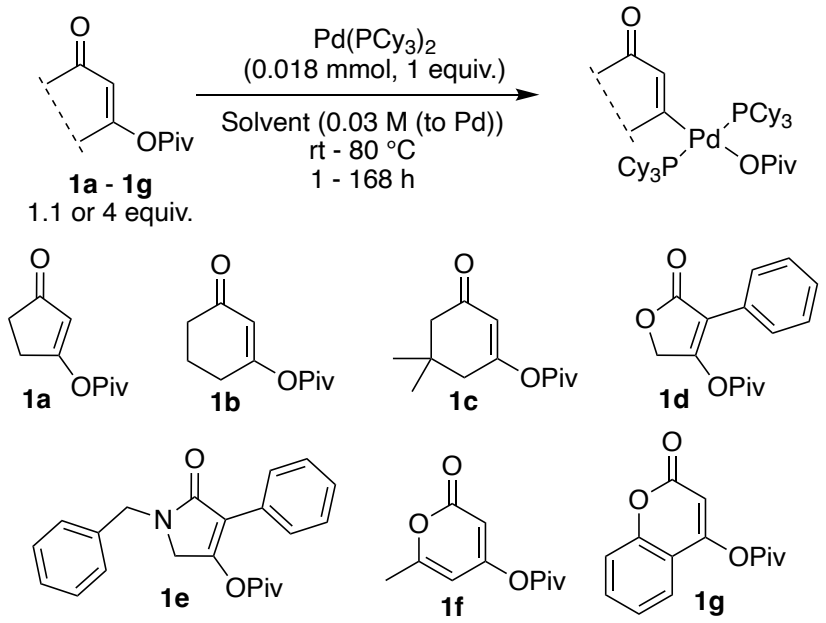

Figure 5.7: Oxidative addition experiments conducted using $Pd(PCy_3)_2$ on a series of alkenyl carboxylates. Reactions were monitored using ^{31}P NMR.

Because the species generated were only monitored by ^{31}P NMR the verification of each of these oxidative addition complexes remains to be completed. However, ^{31}P NMR has confirmed that in all cases, conditions were found where a single phosphorus-containing species was formed. Attempts to crystallize the resulting reaction mixtures yielded one compound suitable for X-ray diffraction analysis: the oxidative addition complex with 4-pivalyloxy-3-phenylpyran-3-en-2-one (Figure 5.8).

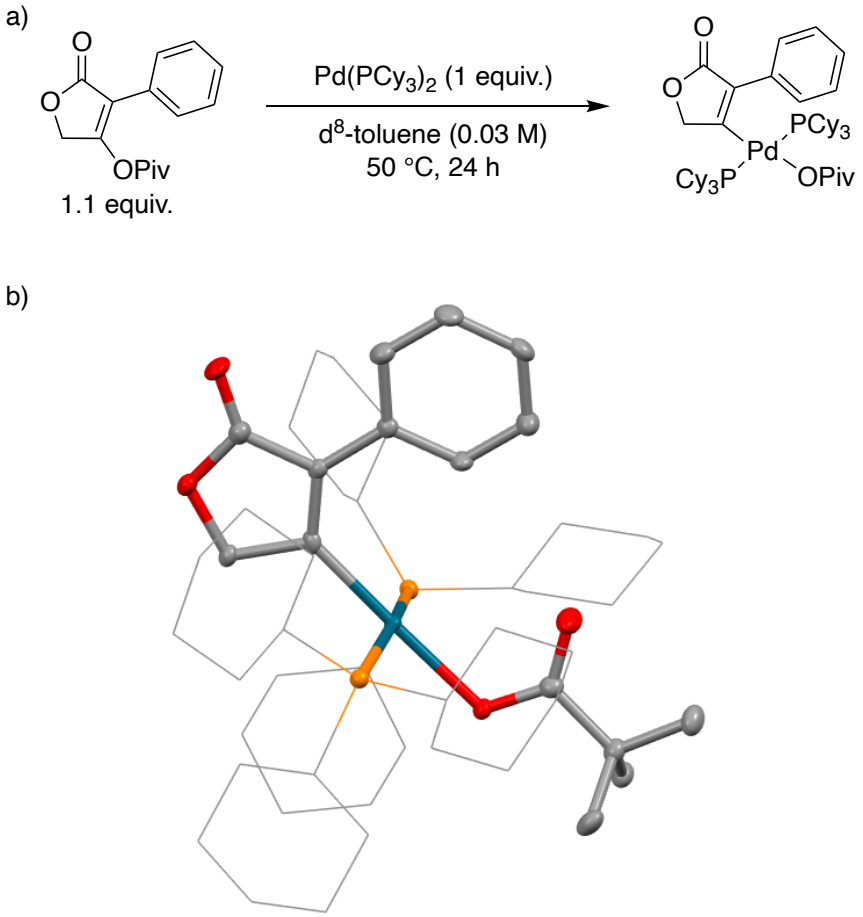

Figure 5.8: a) Oxidative addition conditions for 4-pivalyloxy-3-phenylpyran-3-en-2-one with $Pd(PCy_3)_2$ in d^8-toluene. b) Solid-state molecular structure of lactone oxidative addition complex. Ellipsoids plotted at 50% probability (cyclohexyls shown as wireframe). Hydrogens and toluene solvate not shown for clarity.

Next steps in this project would be to further characterize these compounds and seek to isolate them at a scale that would allow for reversibility studies to be conducted. By viewing this reversibility through the lens of multiple alkenyl carboxylates, the generality of this Pd C–O bond activation could be unveiled. These experiments could be monitored by variable temperature (VT) NMR; however issues with solubility with deuterated solvents were present when previously attempted. Pressurized sample infusion (PSI) electrospray ionization (ESI) mass spectrometry could also be performed to allow for online monitoring. Continuous monitoring through flow infrared (IR) spectroscopy could also be attempted as the change in C–O bonding would likely be

diagnostic. Finally, determining whether these formed compounds were all catalytically active in Suzuki chemistry, and at what temperatures, would also aid in verifying a more-traditional Pd(0) / Pd(II) pathway that these compounds may promote.

5.2.3 Borylation of Alkenyl Carboxylates

The dominant issue in borylation chemistry, as uncovered in Chapter 3, is that the boron handle that is essential for cross-coupling often becomes an impediment during isolation. While cross-coupling with new boron handles such as B_2EPin_2 is successful,[20] these isolation issues persist and form a logical next step in this project; namely, designing new B_2X_2-type compounds for Miyaura borylation. One solution is to attempt to synthesize a B_2PPin_2, B_2CPPin_2, and/or B_2CHPin_2 (Figure 5.9). For all cases, where ethyl pinacol was reacted with tetrahydroxydiboron to make B_2EPin_2,[20] the propyl, cyclopentyl, or cyclohexyl pinacol derivatives,[21] would be reacted instead. These pinacol derivatives are all known compounds, and their synthesis does not deviate from what was conducted for the ethyl pinacol in B_2EPin_2. B_2PPin_2, and B_2CHPin_2 are unreported compounds. B_2CPPin_2 has been reported;[22] however, its use as a B_2Pin_2 replacement in Miyaura borylation has not been reported (to the best of my knowledge).

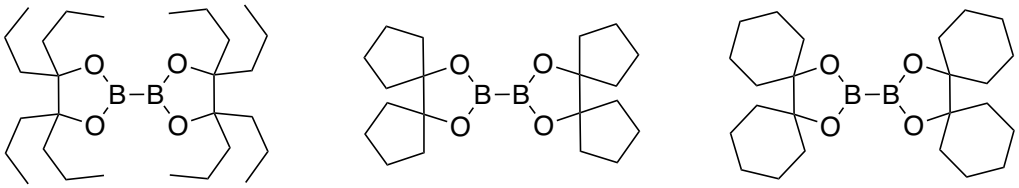

Figure 5.9: Potential B_2X_2 compounds to synthesize: B_2PPin_2, B_2CPPin_2, B_2CHPin_2.

B_2PPin_2 would have the similar or better propensity to block the open p orbital of the boron of B_2EPin_2 – often the cause of deboronation. This extended chain on the propyl pinacol

could alter where the problematic by-product eluted for column chromatography, however one could anticipate streaking on the column as a persistent issue. B_2CPPin_2 and B_2CHPin_2 would be bulky alternatives to B_2EPin_2, however without the linear alkyl chains, the tendency to block the open p-orbital of the boron may be diminished. However, these may be more suitable to overcome the coelution issue. Not only would one think that this difference of a closed chain would alter the elution on the column, but diminished solubility may enable removal by filtration.

We have successfully synthesized B_2CHPin_2 using literature precedent.[20] We have isolated the compound at gram scale. Full characterization can be found in Section 5.3.2. We have also confirmed its structure by X-ray crystallography (Figure 5.10).

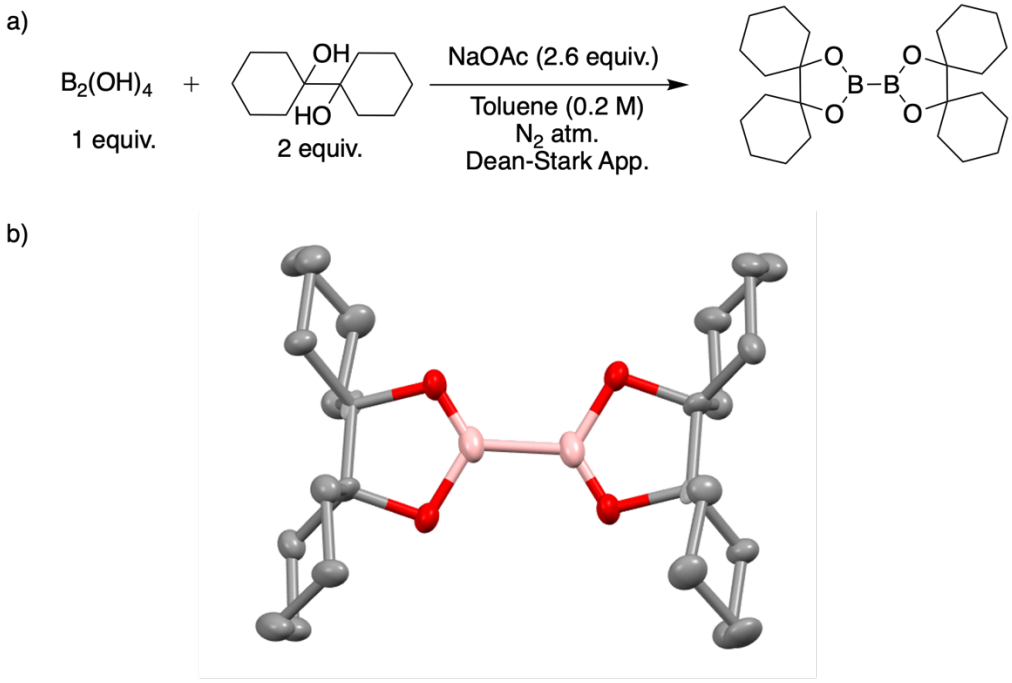

Figure 5.10: a) Synthesis of B_2CHPin_2, a novel B_2X_2 compound, b) Solid-state molecular structure of B_2CHPin_2. Ellipsoids plotted at 50% probability. One of two disordered rotational orientations shown. Hydrogens not shown for clarity.

Once these B_2X_2 compounds are synthesized, catalytic reactions would need to be performed. The ^{DMP}DAB-Pd-MAH and PCy_3 *in situ* system (detailed in Chapter 3) would be a clear place to begin catalytic studies, as this system has been amenable to two B_2X_2 compounds so far.

5.2.4 High Throughput Screening of Pivalated PPD for Suzuki Reactivity

Chapter 4 concludes with the synthesis of unsubstituted PPD molecules functionalized with tosylate and pivalate groups. These molecules could serve as an initial platform for expanding the Leitch Lab's C–O activation of carboxylate chemistry. As these molecules can be considered aromatic, initial screening should focus more on the 100 °C reactivity highlighted in the Leitch Lab's initial report.[23] This is likely due to these compounds undergoing coupling through a more traditional Pd(0) / Pd(II) Suzuki catalytic cycle, with the oxidative addition of these aromatic C–O carboxylate bonds requiring higher temperatures.[24] The arylated product of the unsubstituted PPD scaffold is a known structure,[25] and could be accessed via the chemistry used to synthesize risdiplam from the tosylated structure,[26] or from the unfunctionalized starting material as well.[25] $Pd(OAc)_2$ and PCy_3 that are used to synthesize risdiplam would likely be screening candidates, but expanding the screened ligand scope would be favourable. One particular set of ligands that we have under screened in previous years is the phenanthroline ligands (Figure 5.11). The Larhed group have utilized these phenanthroline ligands for oxidative Heck chemistry,[27–29] but they have also completed some mass spectrometry work that highlights that diphosphine ligands (such as dppp – Figure 5.11), as well as the aforementioned phenanthroline ligands, are capable of forming cationic Pd complexes in the presence of alkenes and pseudo-halides.[30] These ligands are often di-substituted typically at the 2, 9 positions or the 4, 7 positions, offering tunability of these nitrogen based ligands. These phenanthroline ligands,

along with mono- (such as tri(o-tolyl)phosphine – Figure 5.11) and diphosphine ligands would make an excellent start for a screening ligand set.

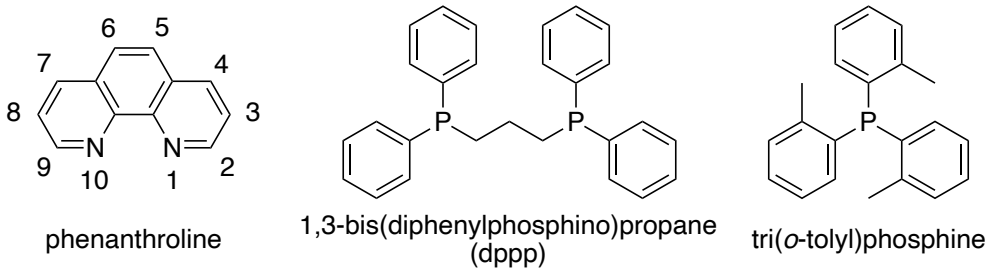

Figure 5.11: Unsubstituted phenanthroline ligand, 1,3-bis(diphenylphosphino)propane - a diphosphine ligand, and tri(o-tolyl)phosphine a monophosphine ligand.

5.2.5 Sonogashira Coupling

After Miyaura borylation, we sought other reactions where C–O activation of carboxylates could be feasible. One option is Sonogashira coupling,[31–33] where if oxidative addition to the correct C–O bond could be ensured, the rest of the reaction mechanisms could be viable. However, complicating this was the two different types of Sonogashira coupling, either with, or without a Cu source (Figure 5.12a and b).[34]

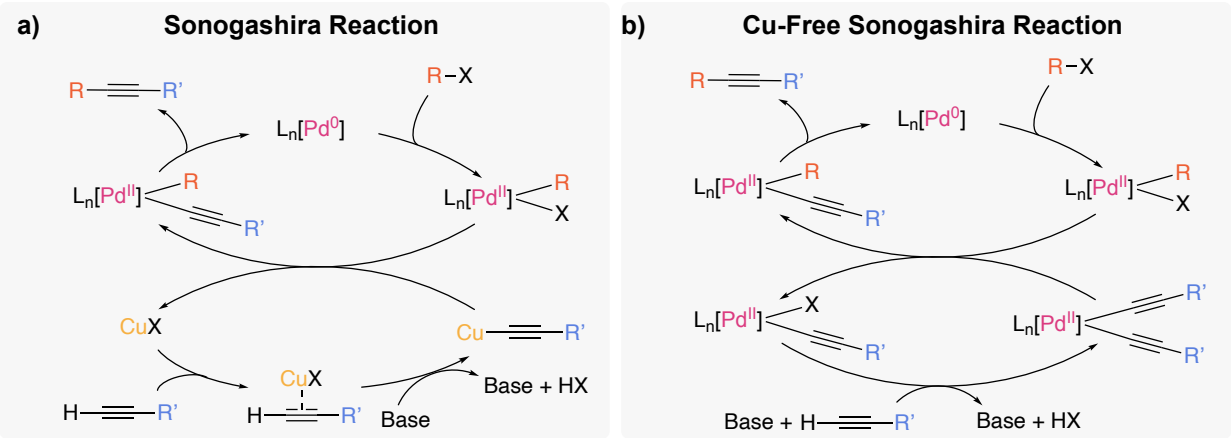

Figure 5.12: a) Sonogashira reaction mechanism with Cu, b) Sonogashira reaction mechanism without Cu

Based on both these mechanisms, initial screening should start with either temperatures high enough to ensure the required oxidative addition, or an oxidative addition complex where a ligated Pd source is already part of the starting material. While the Leitch Lab has used the cyclohexanone oxidative addition product because of its ease of use,[16,24] perhaps a product that strictly reacted under more traditional Pd(0) / Pd(II) conditions in the Suzuki-like chemistry, such as the substituted γ-lactone (isolated in Section 5.2.2), would be a more suitable choice.

One issue with this reaction would be choosing a base. Since the carboxylate handle has a built-in leaving group, the bases tested must not be nucleophilic. Amine bases also have a number of side reactivity issues that will need to be outcompeted if chosen.[35] This will limit the toolbox of the bases used in traditional Sonogashira coupling, likely causing us to turn to bases such as N,N-diisopropylethylamine (DIPEA), 1,8-diazabicyclo(5.4.0)undec-7-ene (DBU) or 1,5-diazabicyclo[4.3.0]non-5-ene (DBN).

J-Young tube experiments could be an accessible place to start with this reaction combining alkynes, bases, copper sources and the aforementioned oxidative addition complex. One could also use high throughput experimentation to screen for product formation, altering many factors at the same time in order to find a suitable combination.

5.2.6 Expansion of Suzuki-like Chemistry

Expanding the Suzuki-like reactivity that the Leitch Lab uncovered in 2020 to alternative alkenyl carboxylate electrophiles would be an excellent addition to this chemistry. Through Chapter 2 we have demonstrated that at room temperature this reaction likely goes through a cationic Pd(II) only mechanism. At elevated temperatures a more traditional Pd(0) / Pd(II) catalytic cycle is more likely. Both types of reactivity are valid and require evaluation. With this in mind, a

screening project was designed with multiple electrophiles that may exhibit different reactivity to the electrophiles detailed in that seminal paper. Two classes of electrophiles were created to group electrophiles with similar structures within the scope. Those two categories are: 1) acyclic electrophiles which either have a terminal or linear alkene or 2) cyclic electrophiles which have an internal alkene in a ring (Figure 5.13). These starting materials have all been sourced or synthesized (Section 5.3.3).

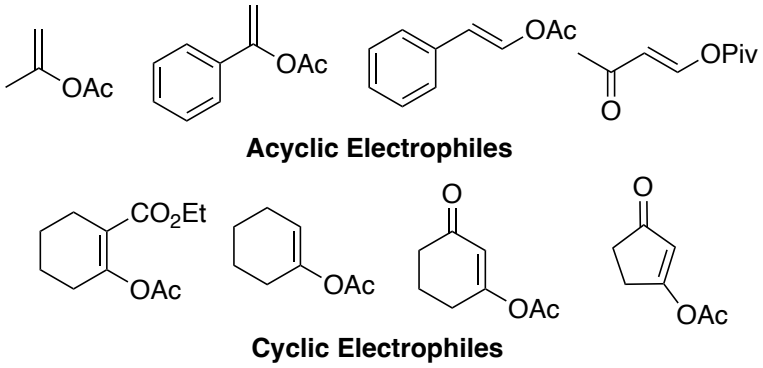

Figure 5.13: Acyclic and cyclic electrophiles sourced or synthesized for future screening project

To explore the effect of ligand structure on catalysis, a series of both phosphorus and nitrogen-based ligands that will stabilize a cationic Pd(II) center are suggested. While our previous studies indicate that monodentate phosphines are effective,[23] the Larhed group observed reactivity with both bidentate and nitrogen-containing ligands.[30,36] A key aspect of this multivariate design is that we can correlate ligand identity to successful reactions with our multiple electrophiles. With this knowledge we hope to be able to correlate class selectivity between variables.

5.3 Experimental

5.3.1 Oxidative Addition of Alkenyl Carboxylates

All air-free manipulations for this section were performed in a nitrogen-atmosphere using a MBraun Glovebox. $Pd(PCy_3)_2$ was purchased from Strem Chemicals and stored under inert atmosphere at -30 °C. Solvents were purchased from Sigma-Aldrich. All NMR spectra were acquired on a Bruker AVANCE Neo 500 MHz spectrometer. All applicable NMR spectra for this section can be found in Appendix D.

General Procedure:

An alkenyl carboxylate (0.020 mmol or 0.072 mmol – see table 5.1 for specific masses) was charged into a 1 dram vial and brought into the glovebox. The same vial was charged with $Pd(PCy_3)_2$ (12.0 mg, 0.018 mmol) and 0.6 mL (0.03 M) of either d_8-toluene or C_6D_6. The reaction mixture was transferred to a J-Young tube, sealed and brought out of the glovebox. A ^{1}H and ^{31}P NMR was acquired at time = 0, as well as every 24 hours for up to 7 days. Between analysis the J-Young tube was submerged in an oil bath set to the desired temperature.

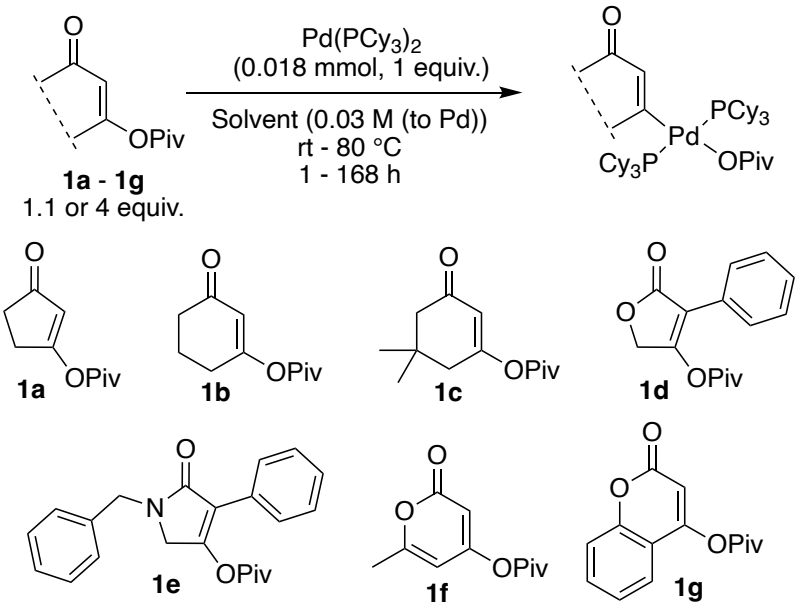

Entry	Alkenyl carboxylate	Alkenyl Carboxylate /mmol	Alkenyl Carboxylate /mg	Solvent	Temperature	Experiment Duration /days
1	**1a**	0.072	13.1	d-Tol	rt - 80 °C	5
2	**1a**	0.020	3.3	d-Tol	rt - 80 °C	6
3	**1a**	0.072	13.1	d-Tol	rt	5
4	**1a**	0.072	13.1	C_6D_6	rt - 100 °C	7
5	**1a**	0.020	3.3	C_6D_6	rt - 100 °C	7
6	**1b**	0.072	14.1	d-Tol	rt - 80 °C	5
7	**1c**	0.072	16.1	d-Tol	rt - 80 °C	5
8	**1c**	0.020	4.0	d-Tol	rt - 80 °C	7
9	**1d**	0.072	18.7	d-Tol	rt - 80 °C	5
10	**1d**	0.020	5.1	d-Tol	rt - 80 °C	5
11	**1d**	0.072	18.7	d-Tol	rt	5
12	**1e**	0.072	26.1	d-Tol	rt - 80 °C	5
13	**1e**	0.020	7.2	d-Tol	rt - 80 °C	5
14	**1f**	0.072	15.1	d-Tol	rt - 80 °C	5
15	**1g**	0.072	17.7	d-Tol	rt - 80 °C	5
16	**1g**	0.020	4.4	d-Tol	rt - 80 °C	6
17	**1g**	0.072	17.7	d-Tol	rt	6

Table 5.1: Reaction conditions for oxidative addition monitoring experiments

5.3.2 Borylation of Alkenyl Carboxylates

1-(1-hydroxycyclohexyl)cyclohexan-1-ol was synthesized according to the procedure detailed in Section 3.6.5 from cyclohexanone (3.86 g, 39.33 mmol) and characterized according to literature.[37]

Synthesis of B_2CHPin_2:

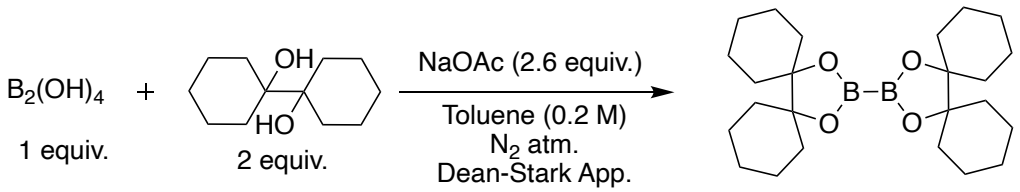

A round bottom flask was charged with 1-(1-hydroxycyclohexyl)cyclohexan-1-ol (1.6 g, 8.1 mmol), tetrahydroxydiboron (362.9 mg, 4.05 mmol), sodium acetate (863.5 mg, 10.53 mmol), and 40 mL toluene. The round bottom flask was fitted to a Dean-Stark apparatus and flushed with N_2. Under constant N_2 atmosphere, the flask was lowered into an oil bath set to 130 °C and allowed to stir overnight. The reaction mixture was then filtered through celite, and dried under reduced pressure to yield the product as a colourless powder. ^{1}H NMR (500MHz, $CDCl_3$, 292K, ppm): δ 1.82 – 1.39 (m, 32H), 1.29 – 1.05 (m, 12H), HRMS: Cal'd for $C_{24}H_{40}B_2O_4$ [M+H]+: 415.31855; found: 415.31873.

5.3.3 Expansion of Suzuki-like Chemistry

The following compounds were purchased commercially from Sigma-Aldrich: 1-methylvinyl acetate.

The following compounds were synthesized according to literature: 1-phenylvinyl acetate,[38] styryl acetate,[39] 1-acetyloxycyclohex-1-en-3-one,[39] 1-acetyloxycyclopent-1-en-3-one,[40] cyclohex-1-en-1-yl acetate.[41]

The following compounds were synthesized according to literature by David C. Leitch: ethyl 2-acetoxycyclohex-1-ene-1-carboxylate,[39] (*E*)-3-oxobut-1-en-1-yl pivalate.[42]

5.4 References

(1) Bursch, M.; Mewes, J.-M.; Hansen, A.; Grimme, S. Best-Practice DFT Protocols for Basic Molecular Computational Chemistry. *Angew. Chem. Int. Ed.* **2022**, *61* (42), e202205735. https://doi.org/10.1002/anie.202205735.

(2) A. Catlow, C. R. Concluding Remarks: Reaction Mechanisms in Catalysis: Perspectives and Prospects. *Faraday Discuss.* **2021**, *229* (0), 502–513. https://doi.org/10.1039/D1FD00027F.

(3) Hayashi, H.; Maeda, S.; Mita, T. Quantum Chemical Calculations for Reaction Prediction in the Development of Synthetic Methodologies. *Chem. Sci.* **2023**, *14* (42), 11601–11616. https://doi.org/10.1039/D3SC03319H.

(4) Chiacchio, M. A.; Legnani, L. Density Functional Theory Calculations: A Useful Tool to Investigate Mechanisms of 1,3-Dipolar Cycloaddition Reactions. *Int. J. Mol. Sci.* **2024**, *25* (2), 1298. https://doi.org/10.3390/ijms25021298.

(5) Lan, Y. Introduction of Computational Organometallic Chemistry. In *Computational Methods in Organometallic Catalysis*; John Wiley & Sons, Ltd, 2021; pp 1–18.

(6) Simmons, E. M.; Hartwig, J. F. On the Interpretation of Deuterium Kinetic Isotope Effects in C-H Bond Functionalizations by Transition-Metal Complexes. *Angew. Chem. Int. Ed.* **2012**, *51* (13), 3066–3072. https://doi.org/10.1002/anie.201107334.

(7) Atkins, P.; Paula, J. D.; Keeler, J. *Atkins' Physical Chemistry*, 12th ed.; Oxford University Press, 2022.

(8) MacQueen, P. M.; Holley, R.; Ghorai, S.; Colacot, T. J. Convenient One-Pot Synthesis of $L_2Pd(0)$ Complexes for Cross-Coupling Catalysis. *Organometallics* **2023**, acs.organomet.3c00059. https://doi.org/10.1021/acs.organomet.3c00059.

(9) Rio, J.; Liang, H.; Perrin, M.-E. L.; Perego, L. A.; Grimaud, L.; Payard, P.-A. We Already Know Everything about Oxidative Addition to Pd(0): Do We? *ACS Catal.* **2023**, *13* (17), 11399–11421. https://doi.org/10.1021/acscatal.3c01943.

(10) Labinger, J. A. Tutorial on Oxidative Addition. *Organometallics* **2015**, *34* (20), 4784–4795. https://doi.org/10.1021/acs.organomet.5b00565.

(11) Rasmussen, S. C. Transmetalation: A Fundamental Organometallic Reaction Critical to Synthesis and Catalysis. *ChemTexts* **2021**, *7* (1), 1. https://doi.org/10.1007/s40828-020-00124-9.

(12) Partyka, D. V. Transmetalation of Unsaturated Carbon Nucleophiles from Boron-Containing Species to the Mid to Late d-Block Metals of Relevance to Catalytic C−X Coupling Reactions (X = C, F, N, O, Pb, S, Se, Te). *Chem. Rev.* **2011**, *111* (3), 1529–1595. https://doi.org/10.1021/cr1002276.

(13) Jiang, T.; Zhang, H.; Ding, Y.; Zou, S.; Chang, R.; Huang, H. Transition-Metal-Catalyzed Reactions Involving Reductive Elimination between Dative Ligands and Covalent Ligands. *Chem. Soc. Rev.* **2020**, *49* (5), 1487–1516. https://doi.org/10.1039/C9CS00539K.

(14) Hartwig, J. F. Electronic Effects on Reductive Elimination To Form Carbon−Carbon and Carbon−Heteroatom Bonds from Palladium(II) Complexes. *Inorg. Chem.* **2007**, *46* (6), 1936–1947. https://doi.org/10.1021/ic061926w.

(15) Spessard, G. O.; Miessler, G. L. *Organometallic Chemistry*, Third Ed.; Oxford University Press: New York, New York, 2016.

(16) Pipaón Fernández, N.; Gaube, G.; Woelk, K. J.; Burns, M.; Hruszkewycz, D. P.; Leitch, D. C. Palladium-Catalyzed Direct C–H Alkenylation with Enol Pivalates Proceeds via Reversible C–O Oxidative Addition to Pd(0). *ACS Catal.* **2022**, *12* (12), 6997–7003. https://doi.org/10.1021/acscatal.2c01305.
(17) Gaube, G.; Pipaon Fernandez, N.; Leitch, D. C. An Evaluation of Palladium-Based Catalysts for the Base-Free Borylation of Alkenyl Carboxylates. *New J. Chem.* **2021**, *45* (43), 20095–20098. https://doi.org/10.1039/D1NJ04008A.
(18) Romanski, S.; Kraus, B.; Guttentag, M.; Schlundt, W.; Rücker, H.; Adler, A.; Neudörfl, J.-M.; Alberto, R.; Amslinger, S.; Schmalz, H.-G. Acyloxybutadiene Tricarbonyl Iron Complexes as Enzyme-Triggered CO-Releasing Molecules (ET-CORMs): A Structure–Activity Relationship Study. *Dalton Trans.* **2012**, *41* (45), 13862. https://doi.org/10.1039/c2dt30662j.
(19) Liu, Z.; Ma, Q.; Liu, Y.; Wang, Q. 4-(N,N-Dimethylamino)Pyridine Hydrochloride as a Recyclable Catalyst for Acylation of Inert Alcohols: Substrate Scope and Reaction Mechanism. *Org. Lett.* **2014**, *16* (1), 236–239. https://doi.org/10.1021/ol4030875.
(20) Oka, N.; Yamada, T.; Sajiki, H.; Akai, S.; Ikawa, T. Aryl Boronic Esters Are Stable on Silica Gel and Reactive under Suzuki–Miyaura Coupling Conditions. *Org. Lett.* **2022**, *24* (19), 3510–3514. https://doi.org/10.1021/acs.orglett.2c01174.
(21) Hu, Y.; Li, N.; Li, G.; Wang, A.; Cong, Y.; Wang, X.; Zhang, T. Solid Acid-Catalyzed Dehydration of Pinacol Derivatives in Ionic Liquid: Simple and Efficient Access to Branched 1,3-Dienes. *ACS Catal.* **2017**, *7* (4), 2576–2582. https://doi.org/10.1021/acscatal.7b00066.
(22) Yuan, J.; Jain, P.; Antilla, J. C. Bi(Cyclopentyl)Diol-Derived Boronates in Highly Enantioselective Chiral Phosphoric Acid-Catalyzed Allylation, Propargylation, and Crotylation of Aldehydes. *J. Org. Chem.* **2020**, *85* (20), 12988–13003. https://doi.org/10.1021/acs.joc.0c01646.
(23) Becica, J.; Heath, O. R. J.; Zheng, C. H. M.; Leitch, D. C. Palladium-Catalyzed Cross-Coupling of Alkenyl Carboxylates. *Angew. Chem. Int. Ed.* **2020**, *59* (39), 17277–17281. https://doi.org/10.1002/anie.202006586.
(24) Becica, J.; Gaube, G.; A. Sabbers, W.; C. Leitch, D. Oxidative Addition of Activated Aryl-Carboxylates to Pd(0): Divergent Reactivity Dependant on Temperature and Structure. *Dalton Trans.* **2020**, *49* (45), 16067–16071. https://doi.org/10.1039/D0DT01119C.
(25) Guchhait, S. K.; Priyadarshani, G. Synthesis of 2-Arylpyridopyrimidinones, 6-Aryluracils, and Tri- and Tetrasubstituted Conjugated Alkenes via Pd-Catalyzed Enolic C–O Bond Activation–Arylation. *J. Org. Chem.* **2015**, *80* (12), 6342–6349. https://doi.org/10.1021/acs.joc.5b00771.
(26) Moessner, C.; Hoffmann-Emery, F.; Adam, J.-M.; Fantasia, S.; Fishlock, D.; Meier, R.; Wuitschik, G.; Ratni, H. Development and Optimization of the Manufacturing Process for RNA-Splicing Modifier Risdiplam RG7916. In *Complete Accounts of Integrated Drug Discovery and Development: Recent Examples from the Pharmaceutical Industry. Volume 4*; ACS Symposium Series; American Chemical Society, 2022; Vol. 1423, pp 301–332.
(27) Andappan, M. M. S.; Nilsson, P.; Larhed, M. The First Ligand-Modulated Oxidative Heck Vinylation. Efficient Catalysis with Molecular Oxygen as Palladium(0) Oxidant. *Chem. Commun.* **2004**, No. 2, 218–219. https://doi.org/10.1039/B311492A.
(28) Enquist, P.-A.; Lindh, J.; Nilsson, P.; Larhed, M. Open-Air Oxidative Heck Reactions at Room Temperature. *Green Chem.* **2006**, *8* (4), 338–343. https://doi.org/10.1039/B517152K.

(29) Lindh, J.; Enquist, P.-A.; Pilotti, Å.; Nilsson, P.; Larhed, M. Efficient Palladium(II) Catalysis under Air. Base-Free Oxidative Heck Reactions at Room Temperature or with Microwave Heating. *J. Org. Chem.* **2007**, *72* (21), 7957–7962. https://doi.org/10.1021/jo701434s.
(30) Svennebring, A.; Sjöberg, P. J. R.; Larhed, M.; Nilsson, P. A Mechanistic Study on Modern Palladium Catalyst Precursors as New Gateways to Pd(0) in Cationic Heck Reactions. *Tetrahedron* **2008**, *64* (8), 1808–1812. https://doi.org/10.1016/j.tet.2007.11.111.
(31) Chinchilla, R.; Nájera, C. The Sonogashira Reaction: A Booming Methodology in Synthetic Organic Chemistry. *Chem. Rev.* **2007**, *107* (3), 874–922. https://doi.org/10.1021/cr050992x.
(32) Arundhathi, K. V.; Vaishnavi, P.; Aneeja, T.; Anilkumar, G. Copper-Catalyzed Sonogashira Reactions: Advances and Perspectives since 2014. *RSC Adv. 13* (7), 4823–4834. https://doi.org/10.1039/d2ra07685c.
(33) Mohajer, F.; Heravi, M. M.; Zadsirjan, V.; Poormohammad, N. Copper-Free Sonogashira Cross-Coupling Reactions: An Overview. *RSC Adv.* **2021**, *11* (12), 6885–6925. https://doi.org/10.1039/D0RA10575A.
(34) Gazvoda, M.; Virant, M.; Pinter, B.; Košmrlj, J. Mechanism of Copper-Free Sonogashira Reaction Operates through Palladium-Palladium Transmetallation. *Nat. Commun.* **2018**, *9* (1), 4814. https://doi.org/10.1038/s41467-018-07081-5.
(35) Tougerti, A.; Negri, S.; Jutand, A. Mechanism of the Copper-Free Palladium-Catalyzed Sonagashira Reactions: Multiple Role of Amines. *Chem. Eur. J.* **2007**, *13* (2), 666–676. https://doi.org/10.1002/chem.200600574.
(36) Lindh, J.; Sävmarker, J.; Nilsson, P.; Sjöberg, P. J. R.; Larhed, M. Synthesis of Styrenes by Palladium(II)-Catalyzed Vinylation of Arylboronic Acids and Aryltrifluoroborates by Using Vinyl Acetate. *Chem. Eur. J.* **2009**, *15* (18), 4630–4636. https://doi.org/10.1002/chem.200802744.
(37) Chen, C.; Chen, C. Reaction-Based and Single Fluorescent Emitter Decorated Ratiometric Nanoprobe to Detect Hydrogen Peroxide. *Chem. Eur. J.* **2013**, *19* (47), 16050–16057. https://doi.org/10.1002/chem.201302342.
(38) Eames, J.; Coumbarides, G. S.; Suggate, M. J.; Weerasooriya, N. Investigations into the Regioselective C-Deuteration of Acyclic and Exocyclic Enolates. *Eur. J. Org. Chem.* **2003**, *2003* (4), 634–641. https://doi.org/10.1002/ejoc.200390103.
(39) Gärtner, D.; Stein, A. L.; Grupe, S.; Arp, J.; Jacobi von Wangelin, A. Iron-Catalyzed Cross-Coupling of Alkenyl Acetates. *Angew. Chem. Int. Ed.* **2015**, *54* (36), 10545–10549. https://doi.org/10.1002/anie.201504524.
(40) Kim, T. H.; Oh, D. R.; Na, H. S.; Lee, H. C. Synthesis and Immunosuppressive Activity of Novel Succinylacetone Analogues. *Arch. Pharmacal Res.* **2003**, *26* (3), 192–196. https://doi.org/10.1007/BF02976828.
(41) de Souza, A. A. N.; Silva, N. S.; Müller, A. V.; Polo, A. S.; Brocksom, T. J.; de Oliveira, K. T. Porphyrins as Photoredox Catalysts in Csp^2 –H Arylations: Batch and Continuous Flow Approaches. *J. Org. Chem.* **2018**, *83* (24), 15077–15086. https://doi.org/10.1021/acs.joc.8b02355.
(42) Pan, W.-J.; Wang, Z.-X. Nickel-Catalyzed Cross-Coupling of β-Carbonyl Alkenyl Pivalates with Arylzinc Chlorides. *Org. Biomol. Chem.* **2018**, *16* (6), 1029–1036. https://doi.org/10.1039/C7OB02947K.

Appendix A: An experimental evaluation of an open to air, base-free, Pd-catalyzed reaction of enol carboxylates and aryl boronic acids.

A1 General Information

All solvents and common organic reagents were purchased from commercial suppliers and used without further purification. $Pd(OAc)_2$ and $Pd(PCy_3)_2$ was purchased from Strem Chemicals and used as received. PdPhBr(P(*o*-OMePh)$_3$) and [PdPh(μ-OAc)(P($_o$-OMePh)$_3$)]$_2$ were prepared according to literature.[1] $Pd_2dba_3 \bullet CHCl_3$ was prepared using the Zalesskiy and Ananikov method.[2] Phenyl trifluoromethanesulfonate was synthesized using literature procedures,[3] and characterized.[4] 5,5-dimethyl-3-oxocyclohex-1-en-1-yl acetate,[5] (4-Boronobenzyl)triphenylphosphonium hexafluorophosphate,[6] and 3'-bromo-5-oxo-1,2,5,6-tetrahydro-[1,1'-biphenyl]-3-yl acetate[7] were synthesized using literature procedures. All phosphine ligands were purchased from Strem Chemicals and used as received. Anhydrous solvents (SureSeal) were purchased from MilliporeSigma and used as received.

All air-free manipulations were performed under a dry nitrogen atmosphere using an MBraun glovebox.

All NMR spectra were acquired on either a Bruker AVANCE 300 MHz spectrometer or a Bruker AVANCE Neo 500 MHz spectrometer. All ^1H and ^{13}C NMR chemical shifts are calibrated to residual protio-solvents and all ^{31}P NMR chemical shifts are calibrated to external standards. All NMR spectroscopic data is processed using Bruker TopSpin 4.07.

Gas-Chromatography Mass-Spectrometry (GC-MS) analysis was conducted on a Finnigan Trace GC Ultra with DSQ mass spectrometer.

Electrospray-Ionization Mass-Spectrometry (ESI-MS) analysis was conducted on a Waters Acquity triple quadrupole detector. The capillary voltage was held at 3 kV, cone voltage at 13 V, extraction cone voltage at 2 V, and RF lens at 0.3 V. The desolvation gas flow rate 150 L/h, cone gas flow 150 L/h, source temperature 70 °C, desolvation temperature 150 °C. The mass range was set to *m/z* 50-1200; scan duration was 1 second; LM and HM resolution were set to 15.0. The mass range was narrowed and the LM and HM resolutions increased to 17.0 to obtain isotope pattern information.

A2 Preliminary Studies

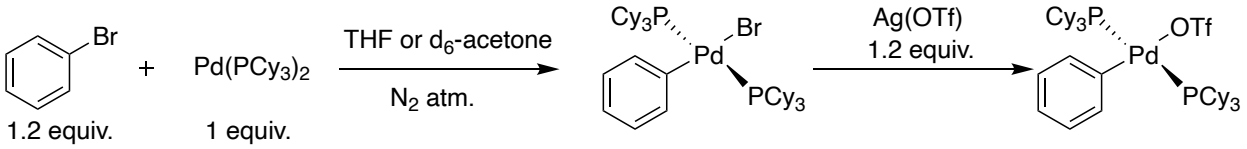

In an N_2 atmosphere, a 1-dram vial was charged with Pd(PCy3)2 (0.015 mmol, 10.0 mg) and bromobenzene (0.018 mmol, 1.88 µL). The solvent was dispensed into the 1-dram vial and transferred to a J-Young tube. The reaction was monitored overnight. After 18 h Ag(OTf) (0.018 mmol, 5.0 mg) was weighed into a 1-dram vial, and the contents of the J-young tube was transferred into the 1-dram vial, and transferred back into the J-Young tube, the reaction was analyzed using ^{1}H and ^{31}P NMR. Where the dominant ^{31}P NMR peak matched that of the product of phenyl triflate and $Pd(PCy_3)_2$ detailed in 2.6.2.

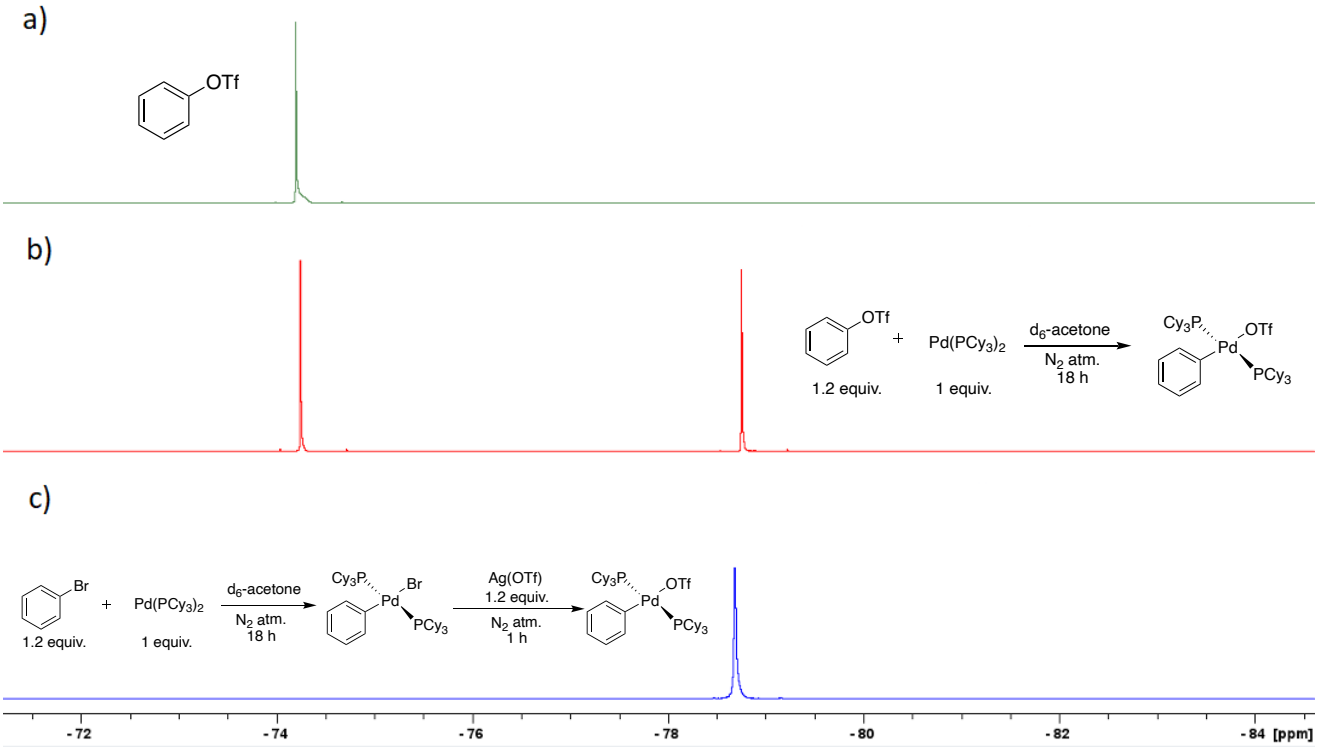

Figure A1: Comparison of Pd speciation by ^{31}P NMR spectroscopy: a) phenyl triflate in d_6-acetone, b) reaction of phenyl triflate with $Pd(PCy_3)_2$ in d_6-acetone, c) two-step reaction of bromobenzene and $Pd(PCy_3)_2$, followed by ligand exchange with Ag(OTf) in d_6-acetone.

A3 Analysis of Pd(II) vs Pd(0)/Pd(II) Mechanisms

A3.1 Additional GC MS data

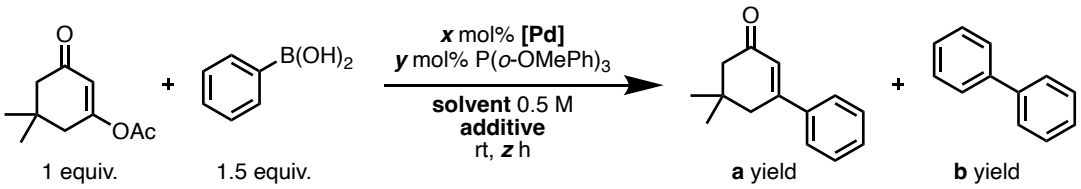

A 1-dram vial was charged with 5,5-dimethyl-3-oxocyclohex-1-en-1-yl acetate (50.0 mg, 0.27 mmol), phenyl boronic acid (50.2 mg, 0.41 mmol), [Palladium] (**x** mol%), P(*o*-OMePh)$_3$ (**y** mol%), **additive** and **solvent** (0.5 M). The vial was capped and allowed to stir for **z** h. At the appropriate time, an aliquot was taken for GC-MS analysis to determine the yield of **b** (shown as mol% relative to 1 equivalent of starting material) and the reaction was dried on a Genevac EZ-2

(Low BP, 30 °C) before yield of **a** was determined using ^{1}H-NMR in $CDCl_3$ with 1,3,5-trimethoxybenzene as an internal standard.

Entry	[Pd]	**x** mol% [Pd]	**y** mol% P(*o*-OMePh)$_3$	Solvent	**z** h	**a** yield / %	**b** yield / mol%
1	$Pd(OAc)_2$	4	6	10:1 Acetone/water (v/v)	1	29	2.8
2	$Pd(OAc)_2$	4	6	10:1 Acetone/water (v/v)	18	63	9.4
3[a]	$Pd(OAc)_2$	4	6	10:1 Acetone/water (v/v)	1	0	0.3
4[a]	$Pd(OAc)_2$	4	6	10:1 Acetone/water (v/v)	18	79	10.7
5[b]	Pd(P(*o*-OMePh)$_3$(Br)(Ph)	6.7	–	THF	18	0	0.3
6[b]	Pd(P(*o*-OMePh)$_3$(Br)(Ph)	6.7	–	d-acetone	18	0	0.1
7[b,c]	Pd(P(*o*-OMePh)$_3$(OTf)(Ph)	6.7	–	THF	18	0	0.4
8[b,c]	Pd(P(*o*-OMePh)$_3$(OTf)(Ph)	6.7	–	d-acetone	18	0	0.3
9	Pd_2(P(o-OMePh$_3$)$_2$(Ph)$_2$(μ-OAc)$_2$	2.5	–	10:1 Acetone/water (v/v)	18	87	6.1
10	Pd_2dba_3	4	6	10:1 Acetone/water (v/v)	18	66	12.8
11	$Pd(PCy_3)_2$	6	–	Acetone	1	67	3.4
12	$Pd(PCy_3)_2$	6	–	Acetone	18	90	3.1
13	$Pd(OAc)_2$	4	–	10:1 Acetone/water (v/v)	18	0	5.2
14	–	–	–	10:1 Acetone/water (v/v)	18	0	0
15[d]	$Pd(OAc)_2$	4	6	10:1 Acetone/water (v/v)	18	–	6.6
16[d]	–	–	–	10:1 Acetone/water (v/v)	18	–	0

Table A1: Yields of **a** and **b** determined using ^{1}H-NMR with 1,3,5-trimethoxybenzene as an internal standard and GCMS respectively. [a]1 equiv. phenyl triflate added, [b]NMR tube experiment, N_2 atmosphere, performed at 0.24 mmol (0.4 M), 1 equiv. phenyl boronic acid. [c][Pd] formed *in situ* using Ag(OTf). [d]no alkenyl carboxylate added.

A3.2 Additional ESI MS data

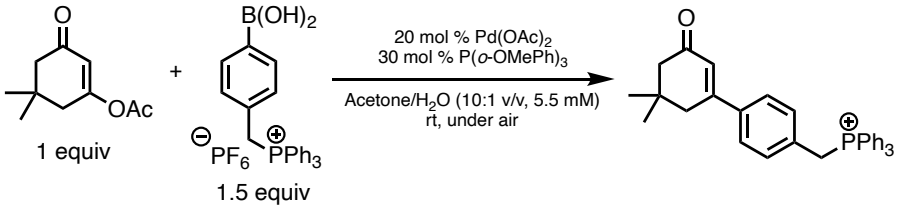

To a stirred solution of $Pd(OAc)_2$ (2.5 mg, 0.011 mmol) in 7.0 mL solvent (10:1 acetone/water (v/v)), sequentially the following was added: P(*o*-OMePh)$_3$ (5.8 mg, 0.017 mmol) in 1 mL solvent, (4-boronobenzyl)triphenylphosphonium hexafluorophosphate (44.6 mg, 0.082 mmol) in 1 mL solvent, and finally 5,5-dimethyl-3-oxocyclohex-1-en-1-yl acetate (10.0 mg, 0.055 mmol) in 1 mL solvent to obtain a final concentration of 5.5 mM in alkenyl carboxylate. Additions were only completed when new speciation formation had plateaued. Specific species (see Figure A3 for example) were subject to collision induced dissociation (CID) to aid in identification.

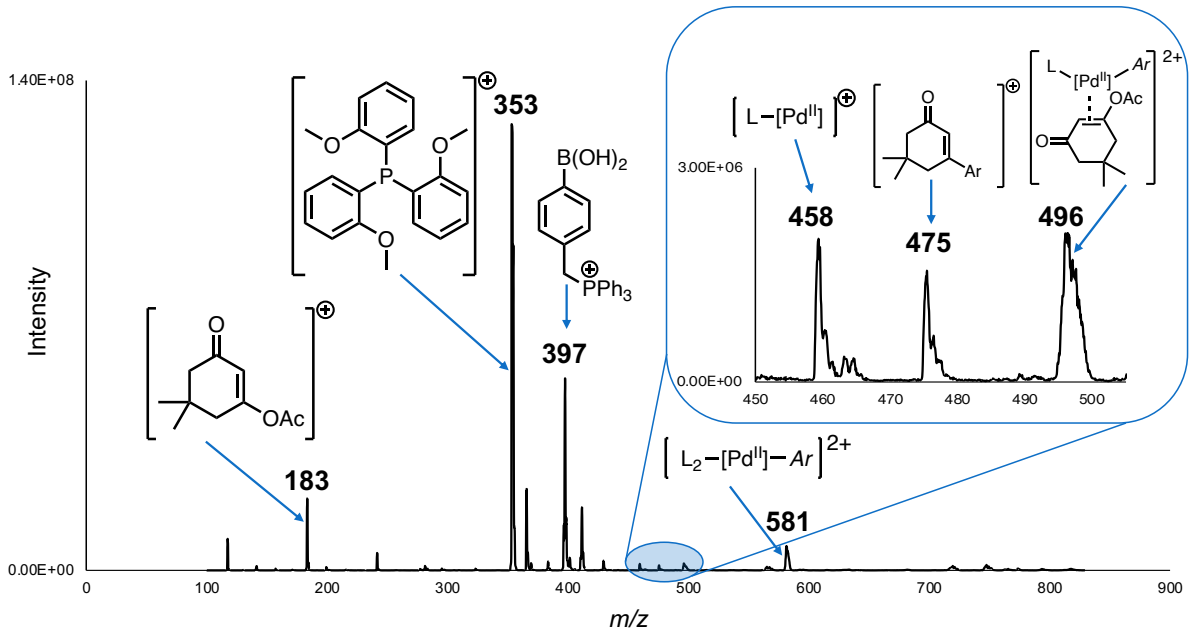

Figure A2: Mass spectrum of the reaction mixture after 24 h with relevant peaks identified. Inset: magnified portion of the spectrum (*m/z* 450-510).

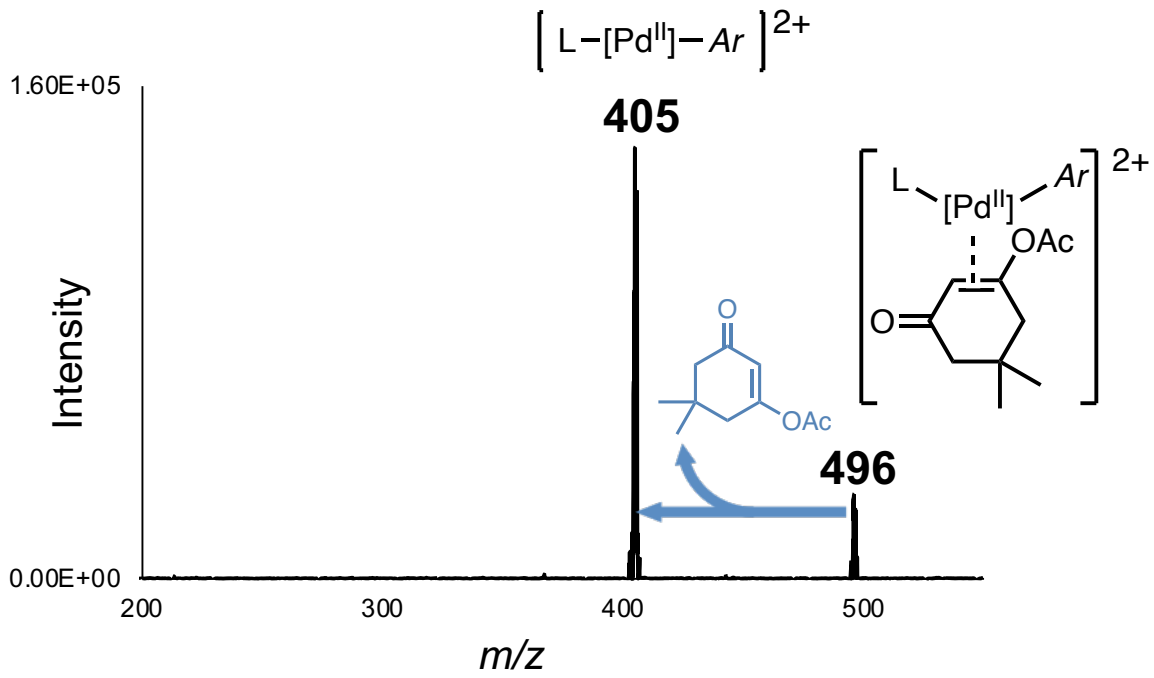

Figure A3: Collision-induced dissociation of *m/z* 496 results in observation of $[LPd(Ar)]^+$ species at a collision energy of 8 V.

A3.3 Simulated Spectra

Isotope patterns were simulated using ChemCalc free-to-use software (chemcalc.org),[8] and were overlayed with the experimental data (Figure A4).

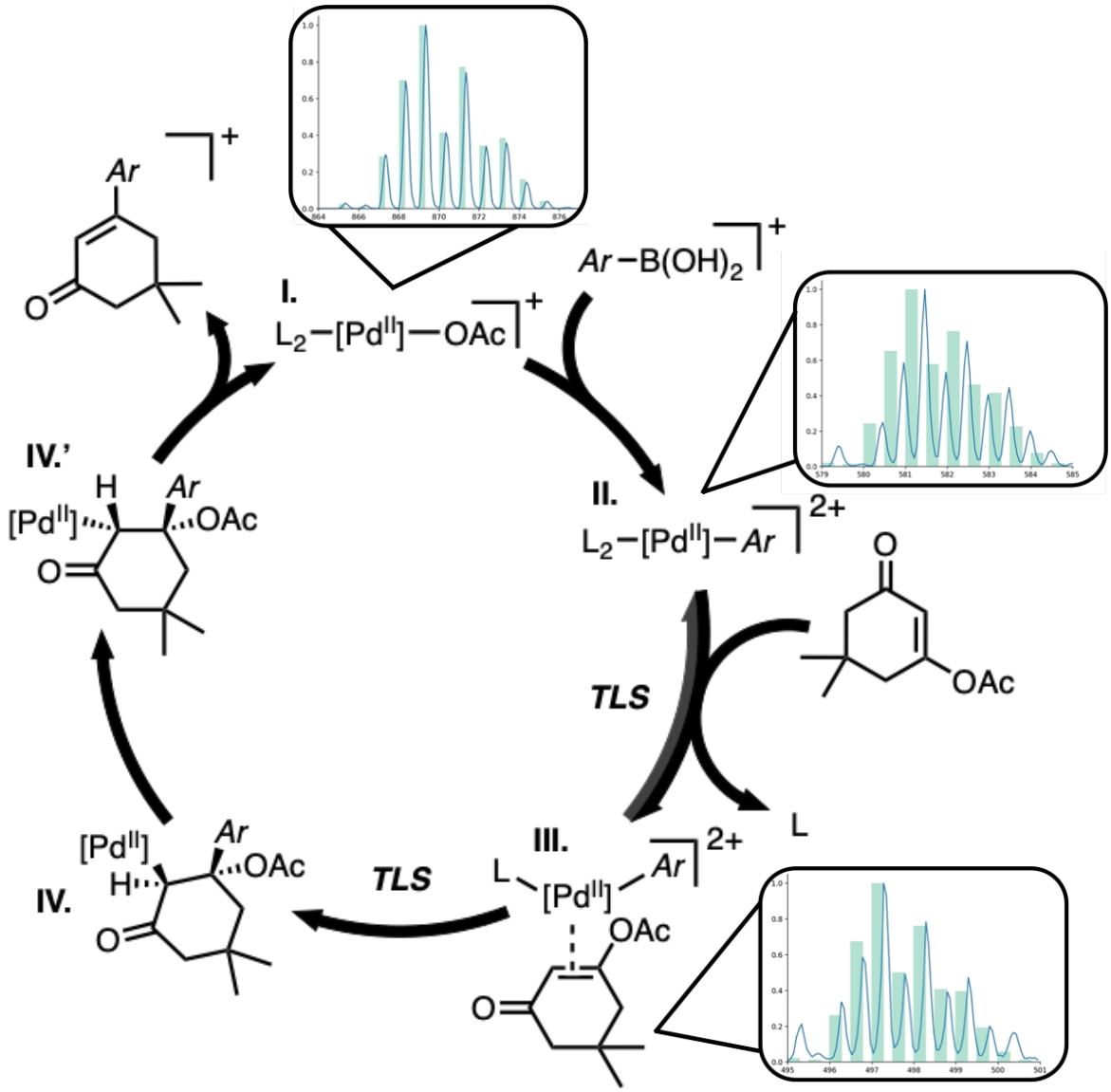

Figure A4: Proposed catalytic cycle displaying three overlay spectra of simulated (green) and collected isotope patterns (blue).

A4 Characterization Data

1-(4'-cyanophenyl)-5,5-dimethylcyclohex-1-en-3-one:

1-(4'-cyanophenyl)-5,5-dimethylcyclohex-1-en-3-one was synthesized as detailed in Section 2.6.2.

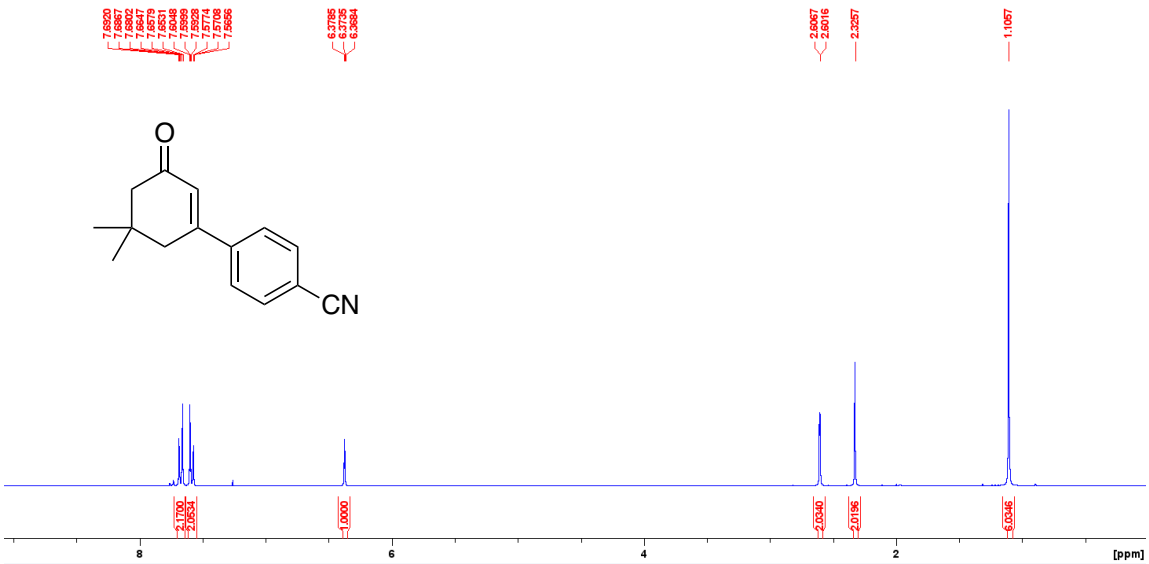

Figure A5: ^{1}H NMR spectrum (500 MHz, $CDCl_3$, 292 K) of **1-(4'-cyanophenyl)-5,5-dimethylcyclohex-1-en-3-one**

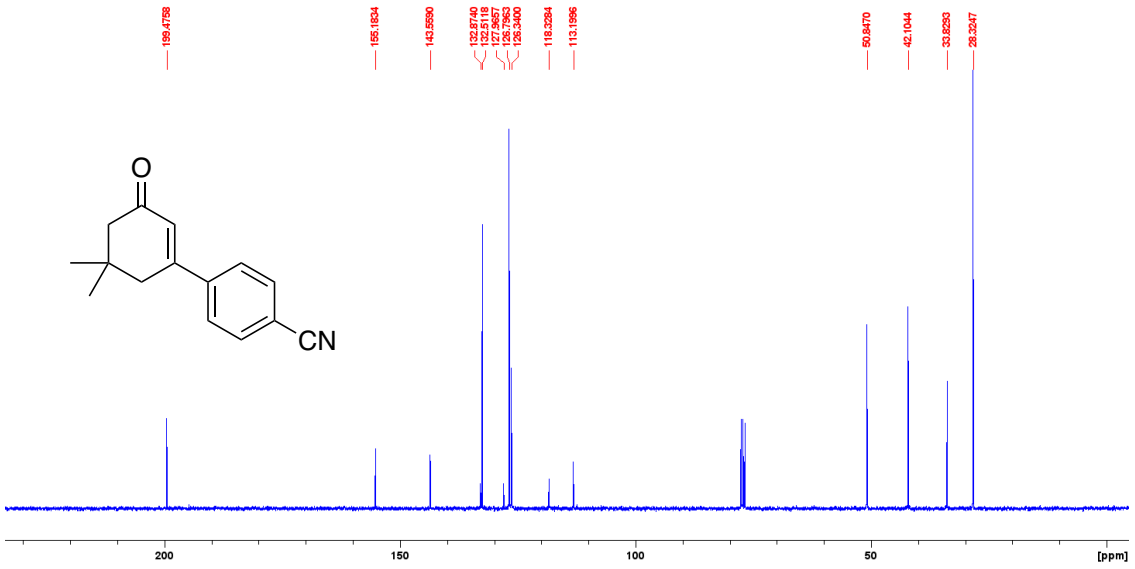

Figure A6: ^{13}C NMR spectrum (126 MHz, $CDCl_3$, 292 K) of **1-(4'-cyanophenyl)-5,5-dimethylcyclohex-1-en-3-one**

1-phenyl-5,5-dimethylcyclohex-1-en-3-one:

1-phenyl-5,5-dimethylcyclohex-1-en-3-one was synthesized and characterized in $CDCl_3$ according to literature.[7] ^{1}H NMR spectra are presented in both THF and acetone-d_6 below. Oxygen adjacent CH_2 of THF calibrated to 3.05 ppm.

^{1}H-NMR: (500 MHz, THF, 292 K, ppm): δ 6.94-6.90 ((dd, $^3J_{H-H}$ = 8.1, $^4J_{H-H}$ = 1.5), 2H), 6.74-6.69 (m, 3H), 5.66 (s, 1H), 2.00 (s, 2H), 1.58 (s, 2H), 0.43 (s, 6H).

^{1}H-NMR: (500 MHz, acetone-d_6, 292 K, ppm): δ 7.63-7.59 (m, 2H), 7.44-7.38 (m, 3H), 6.28 (s, 1H), 2.69 (s, 2H), 2.25 (s, 2H), 1.09 (s, 6H).

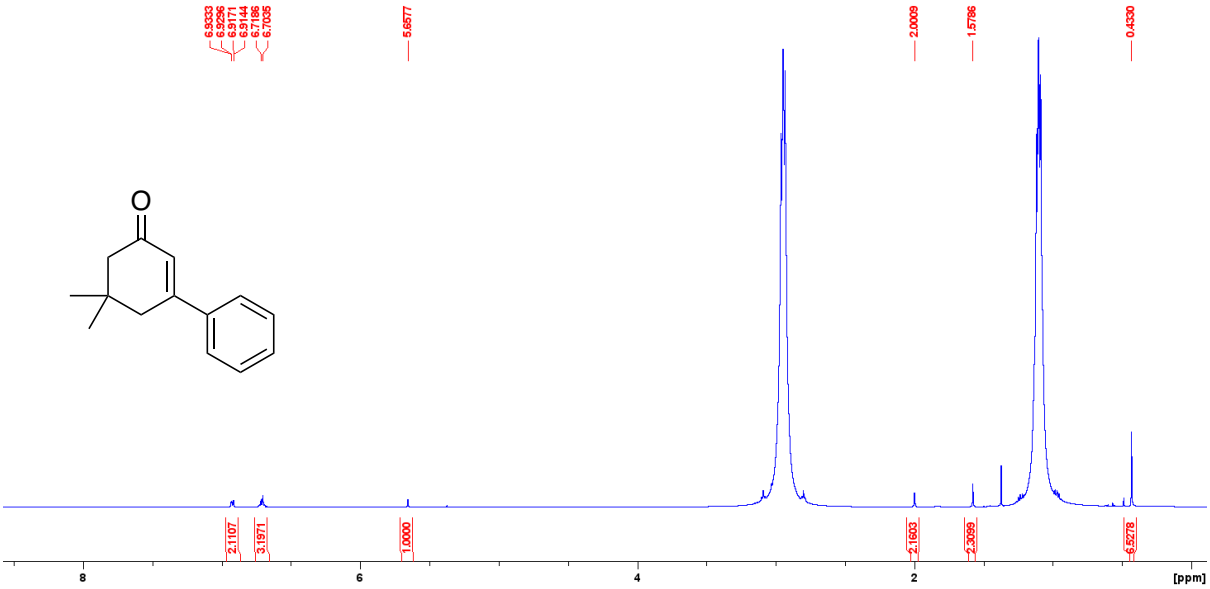

Figure A7: ^{1}H NMR spectrum of **1-phenyl-5,5-dimethylcyclohex-1-en-3-one** (500 MHz, THF, 292 K)

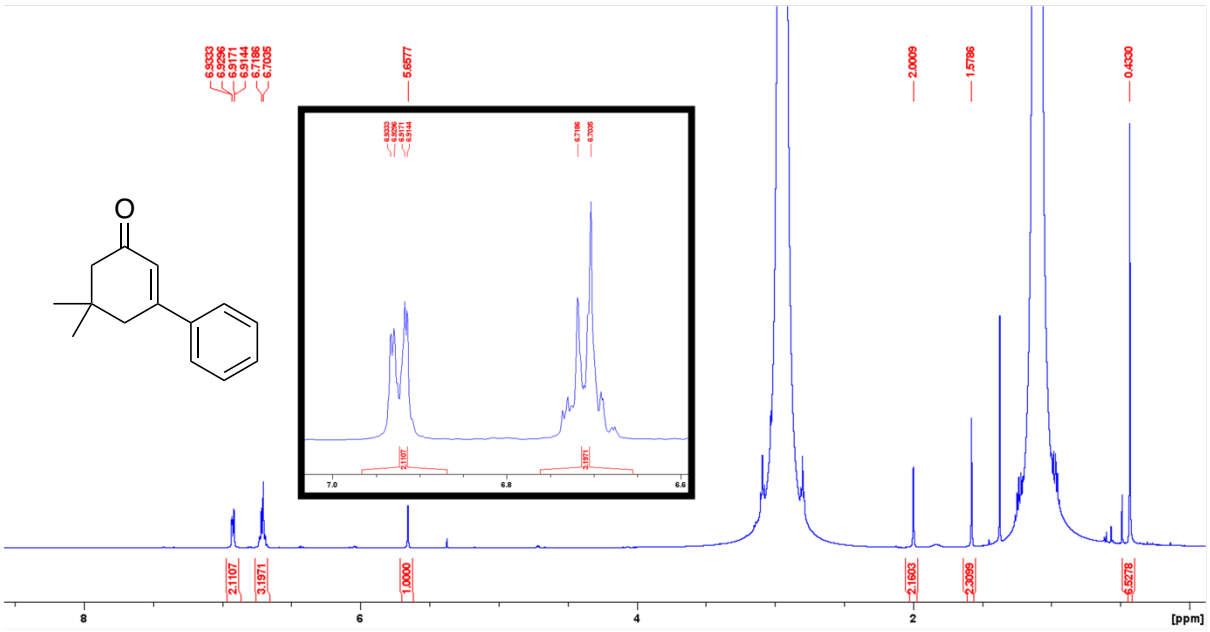

Figure A8: Enlarged ^{1}H NMR spectrum of **1-phenyl-5,5-dimethylcyclohex-1-en-3-one** (500 MHz, THF, 292 K)

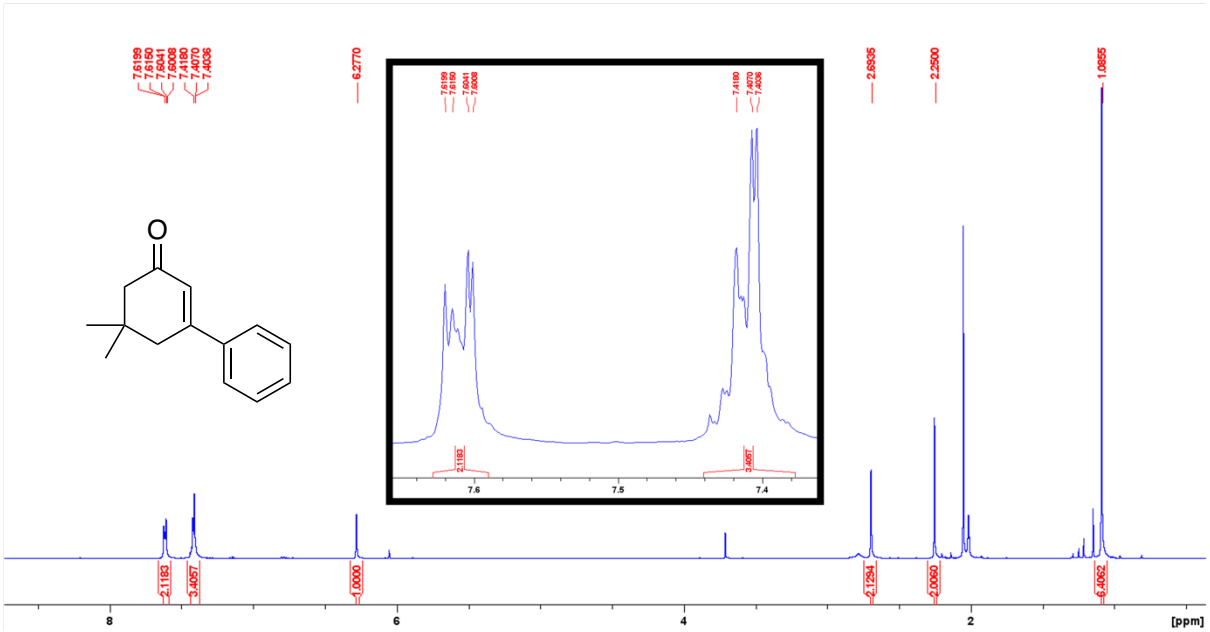

Figure A9: ^{1}H NMR spectrum of **1-phenyl-5,5-dimethylcyclohex-1-en-3-one** (500 MHz, acetone-d_6, 292 K)

A5 References

(1) Wakioka, M.; Nakamura, Y.; Montgomery, M.; Ozawa, F. Remarkable Ligand Effect of P(2-$MeOC_6H_4)_3$ on Palladium-Catalyzed Direct Arylation. *Organometallics* **2015**, *34* (1), 198–205. https://doi.org/10.1021/om501052g.

(2) Zalesskiy, S. S.; Ananikov, V. P. $Pd_2(Dba)_3$ as a Precursor of Soluble Metal Complexes and Nanoparticles: Determination of Palladium Active Species for Catalysis and Synthesis. *Organometallics* **2012**, *31* (6), 2302–2309. https://doi.org/10.1021/om201217r.

(3) Thompson, Ca. L. S.; Kabalka, G. W.; Akula, M. R.; Huffman, J. W. The Conversion of Phenols to the Corresponding Aryl Halides Under Mild Conditions. *New York* **2005**, No. 4.

(4) Gui, Y.-Y.; Liao, L.-L.; Sun, L.; Zhang, Z.; Ye, J.-H.; Shen, G.; Lu, Z.-P.; Zhou, W.-J.; Yu, D.-G. Coupling of $C(Sp^3)$–H Bonds with $C(Sp^2)$–O Electrophiles: Mild, General and Selective. *Chem. Commun.* **2017**, *53* (6), 1192–1195. https://doi.org/10.1039/C6CC09685A.

(5) Romanski, S.; Kraus, B.; Guttentag, M.; Schlundt, W.; Rücker, H.; Adler, A.; Neudörfl, J.-M.; Alberto, R.; Amslinger, S.; Schmalz, H.-G. Acyloxybutadiene Tricarbonyl Iron Complexes as Enzyme-Triggered CO-Releasing Molecules (ET-CORMs): A Structure–Activity Relationship Study. *Dalton Trans.* **2012**, *41* (45), 13862. https://doi.org/10.1039/c2dt30662j.

(6) Yunker, L. P. E.; Ahmadi, Z.; Logan, J. R.; Wu, W.; Li, T.; Martindale, A.; Oliver, A. G.; McIndoe, J. S. Real-Time Mass Spectrometric Investigations into the Mechanism of the Suzuki–Miyaura Reaction. *Organometallics* **2018**, *37* (22), 4297–4308. https://doi.org/10.1021/acs.organomet.8b00705.

(7) Becica, J.; Heath, O. R. J.; Zheng, C. H. M.; Leitch, D. C. Palladium-Catalyzed Cross-Coupling of Alkenyl Carboxylates. *Angew. Chem. Int. Ed.* **2020**, *59* (39), 17277–17281. https://doi.org/10.1002/anie.202006586.

(8) Patiny, L.; Borel, A. ChemCalc: A Building Block for Tomorrow's Chemical Infrastructure. *J. Chem. Inf. Model.* **2013**, *53* (5), 1223–1228. https://doi.org/10.1021/ci300563h.

Appendix B: Base-Free Palladium-Catalyzed Borylation of Enol Carboxylates and Further Reactivity Toward Deboronation and Cross-Coupling

B1 General Information

All solvents and chemicals were purchased from commercial suppliers and used without any further purification. All air-free manipulations were performed under a nitrogen atmosphere using an MBraun glovebox. Palladium (II) acetate, bis(tricyclohexylphosphine) palladium (0), Dichloro 1,1'-bis(diphenylphosphino)ferrocene palladium (II) dichloromethane, P(*o*-OMePh)$_3$, XPhos, SPhos, and dppf were purchased from Strem Chemicals and stored under inert atmosphere. B_2Pin_2 was purchased from AK Scientific and stored under inert atmosphere.

High-throughput screening experiments were performing using sealable aluminum reaction blocks obtained from Analytical Sales Inc. Heating/stirring was achieved using rare-earth magnetic tumble stirrers obtained from V&P Scientific.

All NMR spectra were acquired on either a Bruker AVANCE 300 MHz spectrometer or a Bruker AVANCE Neo 500 MHz spectrometer. All ^{1}H and ^{13}C chemical shifts are calibrated to residual protio-solvents. All data is processed using Bruker TopSpin 4.07. HRMS data was acquired on a Thermo Scientific Ultimate 3000 ESI-Orbitrap Exactive Plus.

B2 Additional Experimental Data

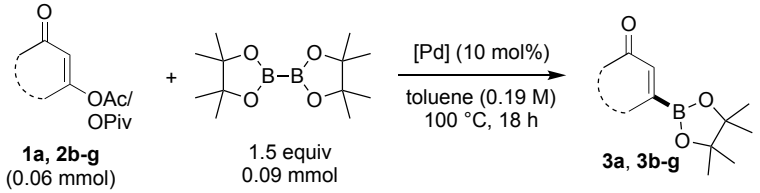

	1a	2b	2c	2d	2e	2f	2g
$Pd(PCy_3)_2$	62	49	87	>98	>98	31	75
No cat.	0	0	0	0	0	0	0

Figure B1: Additional data for $Pd(PCy_3)_2$ and no catalyst borylation experiments

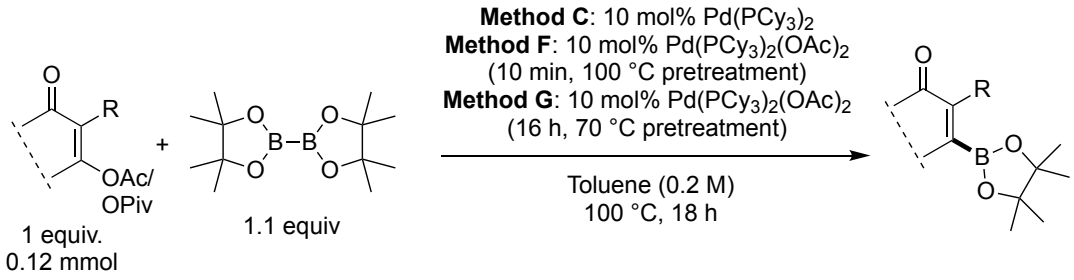

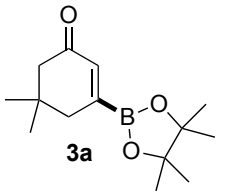

OAc: Method **C**: 33%
Method **F**: 51%
Method **G**: 17%

OPiv: Method **C**: 43%
Method **F**: 62%
Method **G**: 25%

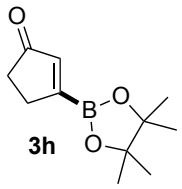

OPiv: Method **C**: 0%
Method **F**: 2%
Method **G**: 8%

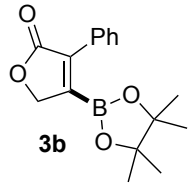

OPiv: Method **C**: 86%
Method **F**: 8%
Method **G**: 48%

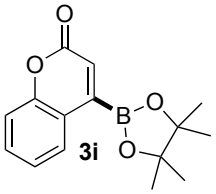

OPiv: Method **C**: 90%
Method **F**: 32%
Method **G**: 40%

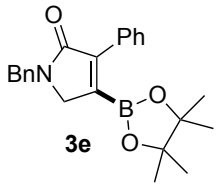

OPiv: Method **C**: 76%
Method **F**: 25%
Method **G**: 10%

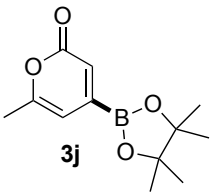

OPiv: Method **C**: 71%
Method **F**: 34%
Method **G**: 29%

Figure B2: **Methods F** and **G** using $Pd(PCy_3)_2(OAc)_2$. **Method C**: (10 mol% $Pd(PCy_3)_2$, toluene (0.2M), 18h, 100 °C) shown for reference)

B3 Purification Chromatograms

All column chromatography was conducted on Biotage Selekt instruments utilizing Biotage Sfär prepacked columns. Hexanes and ethyl acetate were used as the mobile phase.

B3.1 Deoxygenated Compounds

4b (3-phenyl-phenylfuran-2(5H)-one)

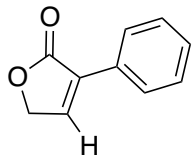

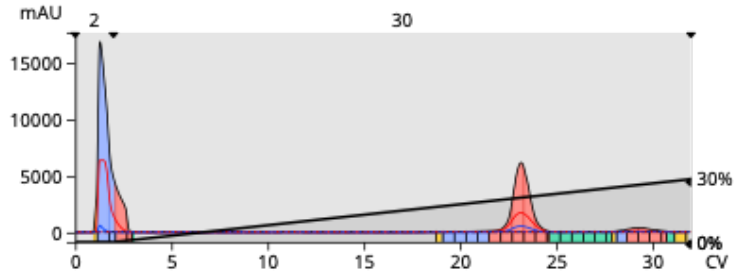

Signal	Wavelength	Threshold
λ-All (Collect)	200 - 400 nm	30 mAU
UV1 (Collect)	254 nm	30 mAU
UV2 (Collect)	280 nm	30 mAU

Gradient

Solvent A: n-Hexane **Solvent B:** Ethyl acetate

0-0%	Ethyl acetate in n-Hexane	2 CV
0-30%	Ethyl acetate in n-Hexane	30 CV

Run Parameters

Column Type: Biotage® Sfär 10g
Column ID: 2316011149
Flow Rate: 40 mL/min
Equilibration: On
Collect All: Off
Channel: 1
Comments: loaded with toluene

Sample Mass: 100

UV Baseline Correction: Standard

Figure B3: Column chromatography results for **4b**

4c (3-(4-trifluoromethyl)phenylfuran-2(5H)-one)

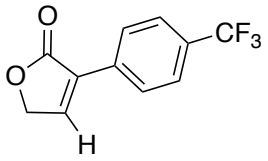

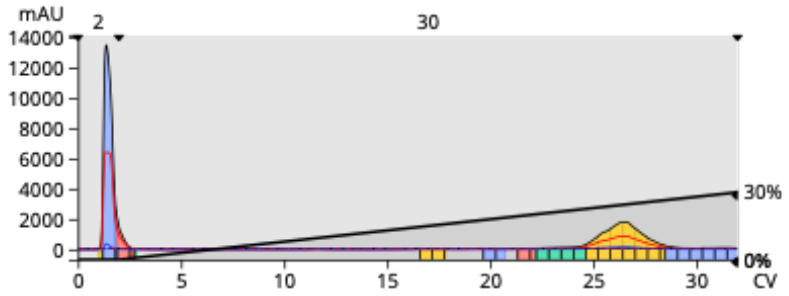

Signal	Wavelength	Threshold
λ-All (Collect)	220 - 400 nm	40 mAU
UV1 (Collect)	254 nm	40 mAU
UV2 (Collect)	280 nm	40 mAU

Gradient

Solvent A: n-Hexane **Solvent B:** Ethyl acetate

0-0%	Ethyl acetate in n-Hexane	2 CV
0-30%	Ethyl acetate in n-Hexane	30 CV

Run Parameters

Column Type: Biotage® Sfär 10g
Column ID: 2316011197
Flow Rate: 40 mL/min
Equilibration: On
Collect All: Off
Channel: 2
Comments: loaded with toluene

Sample Mass: 100

UV Baseline Correction: Standard

Figure B4: Column chromatography results for **4c**

4d (3-(4-methoxyphenyl)-phenylfuran-2(5H)-one)

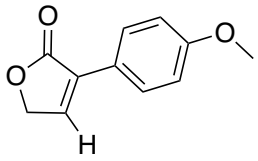

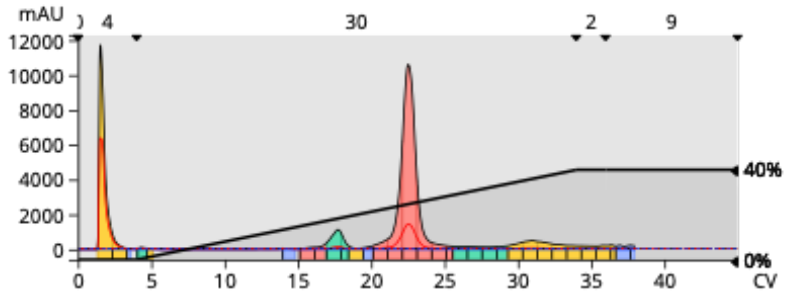

Signal	Wavelength	Threshold
λ-All (Collect)	220 - 400 nm	40 mAU
UV1 (Collect)	254 nm	40 mAU
UV2 (Collect)	400 nm	40 mAU

Gradient

Solvent A: n-Hexane **Solvent B:** Ethyl acetate

0-0%	Ethyl acetate in n-Hexane	0 CV	
0-0%	Ethyl acetate in n-Hexane	4 CV	
0-40%	Ethyl acetate in n-Hexane	30 CV	
40-40%	Ethyl acetate in n-Hexane	2 CV	
40-40%	Ethyl acetate in n-Hexane	9 CV	Auto extended

Figure B5: Column chromatography results for **4d**

4e (1-benzyl-3-phenyl-1,5-dihydro-2H-pyrrol-2-one)

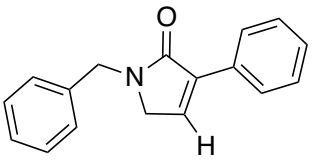

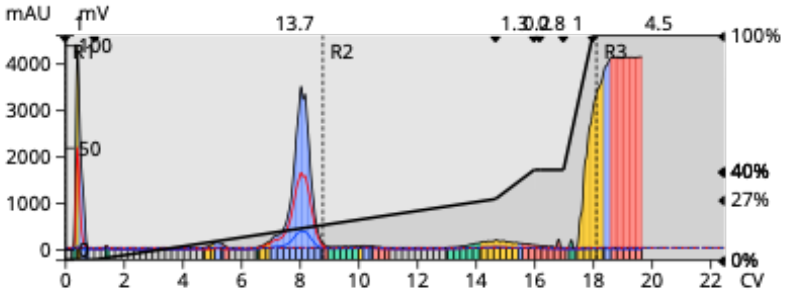

Signal	Wavelength	Threshold
λ-All (Collect)	200 - 400 nm	40 mAU
UV1 (Collect)	254 nm	40 mAU
UV2 (Collect)	280 nm	40 mAU

Gradient

Solvent A: n-Hexane **Solvent B:** Ethyl acetate

0-0%	Ethyl acetate in n-Hexane	1 CV	
0-27%	Ethyl acetate in n-Hexane	13.7 CV	
27-40%	Ethyl acetate in n-Hexane	1.3 CV	
40-40%	Ethyl acetate in n-Hexane	0.2 CV	
40-40%	Ethyl acetate in n-Hexane	0.8 CV	
40-100%	Ethyl acetate in n-Hexane	1 CV	
100-100%	Ethyl acetate in n-Hexane	4.5 CV	Auto extended

Figure B6: Column chromatography results for **4e**

4f (1-benzyl-3-(4-(trifluoromethyl)phenyl)-1,5-dihydro-2*H*-pyrrol-2-one)

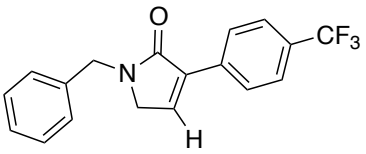

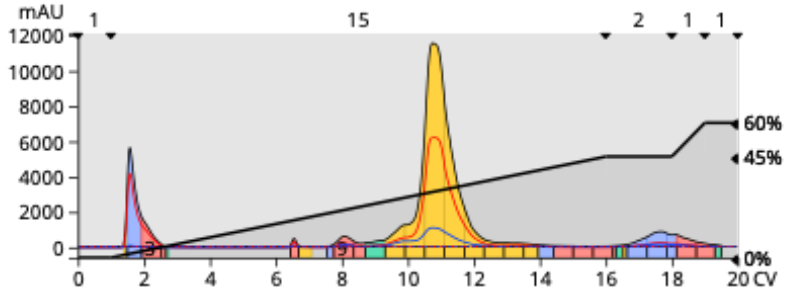

Signal	Wavelength	Threshold
λ-All (Collect)	200 - 400 nm	40 mAU
UV1 (Collect)	254 nm	40 mAU
UV2 (Collect)	280 nm	40 mAU

Gradient

Solvent A: n-Hexane **Solvent B:** Ethyl acetate

0-0%	Ethyl acetate in n-Hexane	1 CV
0-45%	Ethyl acetate in n-Hexane	15 CV
45-45%	Ethyl acetate in n-Hexane	2 CV
45-60%	Ethyl acetate in n-Hexane	1 CV
60-60%	Ethyl acetate in n-Hexane	1 CV

Figure B7: Column chromatography results for **4f**

4g (1-benzyl-3-(4-methoxyphenyl)-1,5-dihydro-2*H*-pyrrol-2-one)

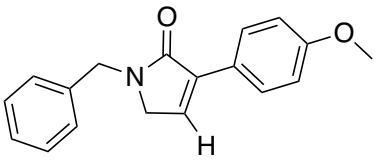

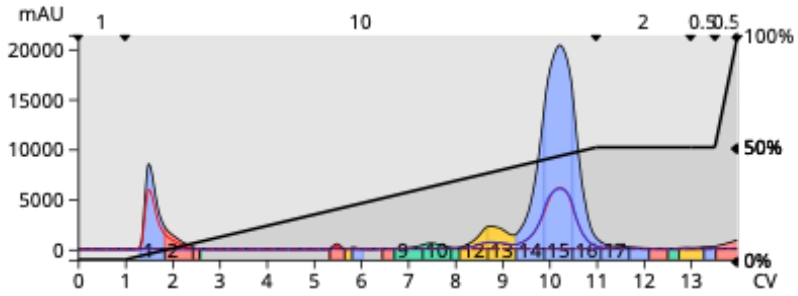

Signal	Wavelength	Threshold
λ-All (Collect)	200 - 400 nm	40 mAU
UV1 (Collect)	254 nm	40 mAU
UV2 (Collect)	280 nm	40 mAU

Gradient

Solvent A: n-Hexane **Solvent B:** Ethyl acetate

0-0%	Ethyl acetate in n-Hexane	1 CV	
0-50%	Ethyl acetate in n-Hexane	10 CV	
50-50%	Ethyl acetate in n-Hexane	2 CV	
50-50%	Ethyl acetate in n-Hexane	0.5 CV	
50-100%	Ethyl acetate in n-Hexane	0.5 CV	Auto extended

Figure B8: Column chromatography results for **4g**

B3.2 Ethylpinacol Borylated Compounds

6b (1-(4,4,5,5-tetraethyl-1,3,2- dioxaborolan-2-yl)-3-phenylpyran-3-en-2-one)

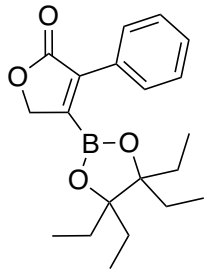

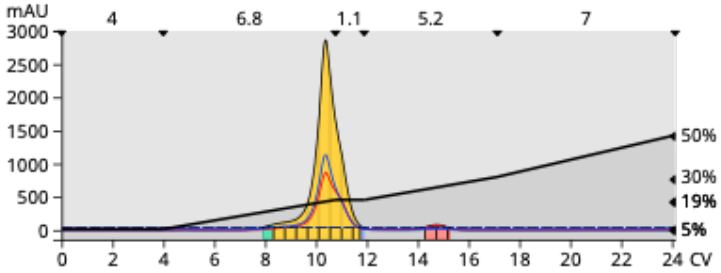

Signal	Wavelength	Threshold
λ-All (Collect)	200 - 400 nm	40 mAU
UV1	254 nm	
UV2 (Collect)	280 nm	40 mAU

Gradient

Solvent A: n-Hexane **Solvent B:** Ethyl acetate

5-5%	Ethyl acetate in n-Hexane	4 CV	
5-19%	Ethyl acetate in n-Hexane	6.8 CV	
19-19%	Ethyl acetate in n-Hexane	1.1 CV	Isocratic hold
19-30%	Ethyl acetate in n-Hexane	5.2 CV	
30-50%	Ethyl acetate in n-Hexane	7 CV	

Figure B9: Column chromatography results for **6b**

6c (1-(4,4,5,5-tetraethyl-1,3,2- dioxaborolan-2-yl) -3-(4-trifluoromethyl)phenylpyran-3-en-2-one)

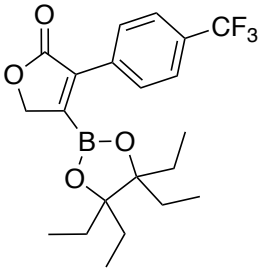

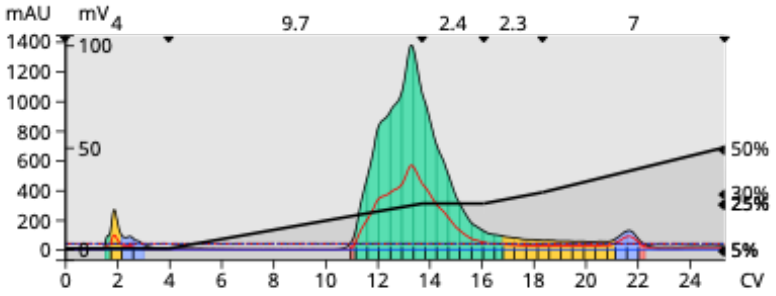

Signal	Wavelength	Threshold
λ-All (Collect)	220 - 400 nm	40 mAU
UV1 (Collect)	254 nm	40 mAU
UV2 (Collect)	400 nm	40 mAU

Gradient

Solvent A: n-Hexane **Solvent B:** Ethyl acetate

5-5%	Ethyl acetate in n-Hexane	4 CV	
5-25%	Ethyl acetate in n-Hexane	9.7 CV	
25-25%	Ethyl acetate in n-Hexane	2.4 CV	Isocratic hold
25-30%	Ethyl acetate in n-Hexane	2.3 CV	
30-50%	Ethyl acetate in n-Hexane	7 CV	

Figure B10: Column chromatography results for **6c**

6d (1-(4,4,5,5-tetraethyl-1,3,2- dioxaborolan-2-yl) -3-(4-methoxy)phenylpyran-3-en-2-one)

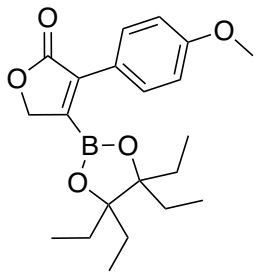

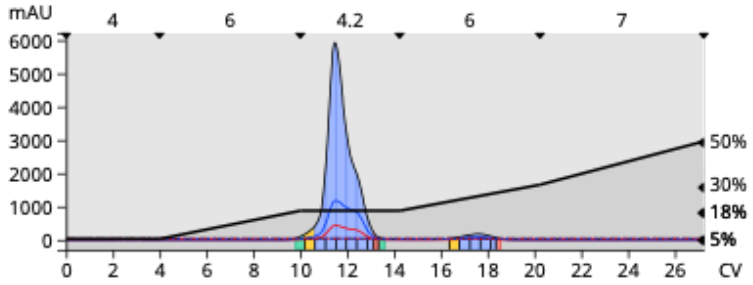

Signal	Wavelength	Threshold
λ-All (Collect)	200 - 400 nm	40 mAU
UV1 (Collect)	254 nm	40 mAU
UV2 (Collect)	280 nm	40 mAU

Gradient

Solvent A: n-Hexane **Solvent B:** Ethyl acetate

5-5%	Ethyl acetate in n-Hexane	4 CV	
5-18%	Ethyl acetate in n-Hexane	6 CV	
18-18%	Ethyl acetate in n-Hexane	4.2 CV	Isocratic hold
18-30%	Ethyl acetate in n-Hexane	6 CV	
30-50%	Ethyl acetate in n-Hexane	7 CV	

Figure B11: Column chromatography results for **6d**

6e (1-(4,4,5,5-tetraethyl-1,3,2- dioxaborolan-2-yl) -1-benzyl-3-phenylpyrrolidin-3-en-2-one)

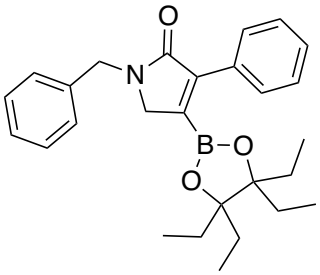

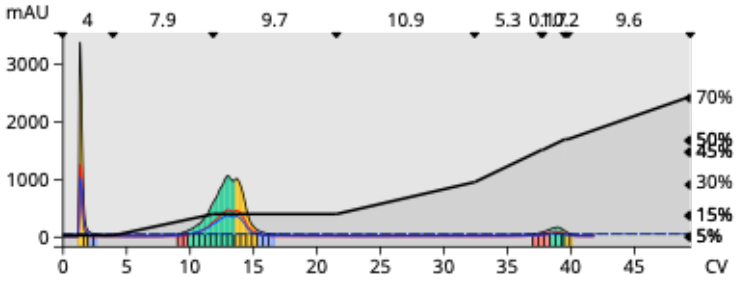

Signal	Wavelength	Threshold
λ-All (Collect)	200 - 400 nm	40 mAU
UV1	254 nm	
UV2 (Collect)	280 nm	40 mAU

Gradient

Solvent A: n-Hexane **Solvent B:** Ethyl acetate

5-5%	Ethyl acetate in n-Hexane	4 CV	
5-15%	Ethyl acetate in n-Hexane	7.9 CV	
15-15%	Ethyl acetate in n-Hexane	9.7 CV	Isocratic hold
15-30%	Ethyl acetate in n-Hexane	10.9 CV	
30-45%	Ethyl acetate in n-Hexane	5.3 CV	
45-45%	Ethyl acetate in n-Hexane	0.1 CV	Isocratic hold
45-50%	Ethyl acetate in n-Hexane	1.7 CV	
50-50%	Ethyl acetate in n-Hexane	0.2 CV	
50-70%	Ethyl acetate in n-Hexane	9.6 CV	Auto extended

Figure B12: Column chromatography results for **6e**

6f (1-(4,4,5,5-tetraethyl-1,3,2- dioxaborolan-2-yl) -1-benzyl-3-(4-trifluoromethyl)phenylpyrrolidin-3-en-2-one)

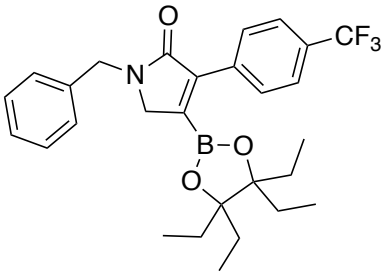

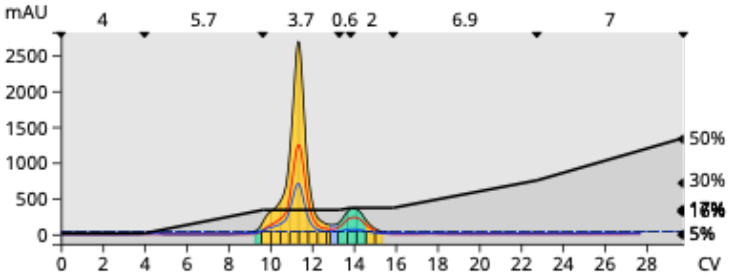

Signal	Wavelength	Threshold
λ-All (Collect)	200 - 400 nm	40 mAU
UV1	254 nm	
UV2 (Collect)	280 nm	40 mAU

Gradient

Solvent A: n-Hexane **Solvent B:** Ethyl acetate

5-5%	Ethyl acetate in n-Hexane	4 CV	
5-16%	Ethyl acetate in n-Hexane	5.7 CV	
16-16%	Ethyl acetate in n-Hexane	3.7 CV	Isocratic hold
16-17%	Ethyl acetate in n-Hexane	0.6 CV	
17-17%	Ethyl acetate in n-Hexane	2 CV	Isocratic hold
17-30%	Ethyl acetate in n-Hexane	6.9 CV	
30-50%	Ethyl acetate in n-Hexane	7 CV	

Figure B13: Column chromatography results for **6f**

6g (1-(4,4,5,5-tetraethyl-1,3,2- dioxaborolan-2-yl) -1-benzyl-3-(4-methoxy)phenylpyrrolidin-3-en-2-ones)

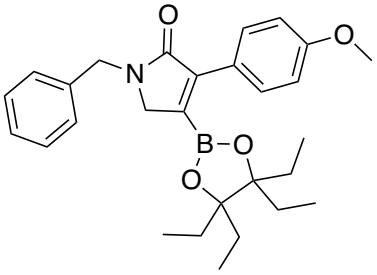

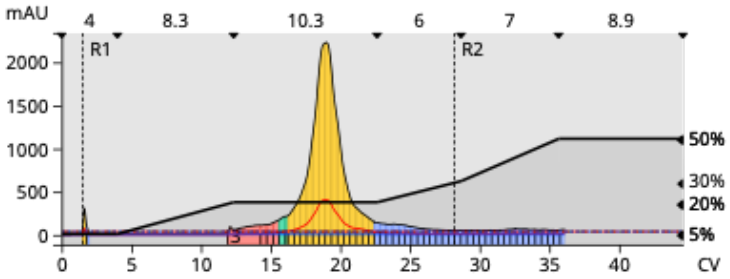

Signal	Wavelength	Threshold
λ-All (Collect)	220 - 400 nm	40 mAU
UV1 (Collect)	254 nm	40 mAU
UV2 (Collect)	400 nm	40 mAU

Gradient

Solvent A: n-Hexane **Solvent B:** Ethyl acetate

5-5%	Ethyl acetate in n-Hexane	4 CV	
5-20%	Ethyl acetate in n-Hexane	8.3 CV	
20-20%	Ethyl acetate in n-Hexane	10.3 CV	Isocratic hold
20-30%	Ethyl acetate in n-Hexane	6 CV	
30-50%	Ethyl acetate in n-Hexane	7 CV	
50-50%	Ethyl acetate in n-Hexane	8.9 CV	Auto extended

Figure B14: Column chromatography results for **6g**

B3.3 Arylated Compounds

5a 1-phenyl-5,5-dimethylcyclohex-1-en-3-one:

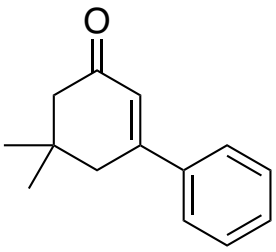

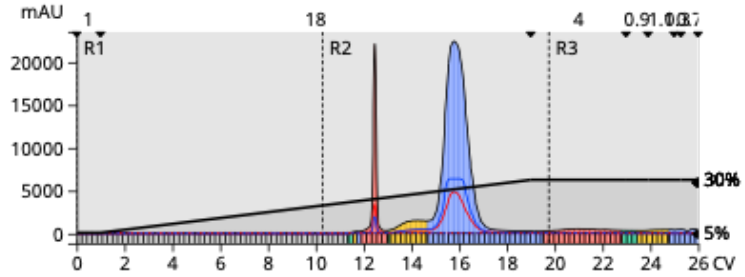

Signal	Wavelength	Threshold
λ-All (Collect)	200 - 400 nm	40 mAU
UV1 (Collect)	254 nm	40 mAU
UV2 (Collect)	280 nm	40 mAU

Gradient

Solvent A: n-Hexane **Solvent B:** Ethyl acetate

5-5%	Ethyl acetate in n-Hexane	1 CV	
5-30%	Ethyl acetate in n-Hexane	18 CV	
30-30%	Ethyl acetate in n-Hexane	4 CV	
30-30%	Ethyl acetate in n-Hexane	0.9 CV	
30-30%	Ethyl acetate in n-Hexane	1.1 CV	Auto extended
30-30%	Ethyl acetate in n-Hexane	0.3 CV	
30-30%	Ethyl acetate in n-Hexane	0.7 CV	

Figure B15: Column chromatography results for **5a**.

5h 1-phenylcyclopent-1-en-3-one:

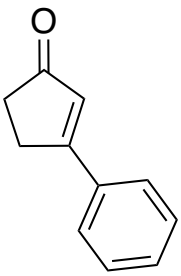

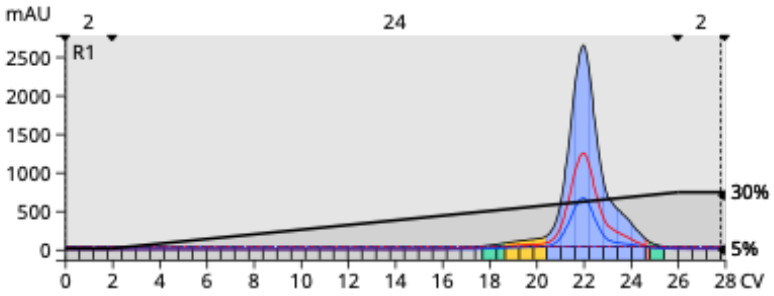

Signal	Wavelength	Threshold
λ-All (Collect)	200 - 400 nm	40 mAU
UV1 (Collect)	280 nm	40 mAU
UV2 (Collect)	254 nm	40 mAU

Gradient

Solvent A: n-Hexane **Solvent B:** Ethyl acetate

5-5%	Ethyl acetate in n-Hexane	2 CV
5-30%	Ethyl acetate in n-Hexane	24 CV
30-30%	Ethyl acetate in n-Hexane	2 CV

Figure B16: Column chromatography results for **5h**.

5i 4-phenylbenzopyran-2-one:

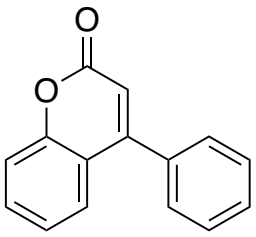

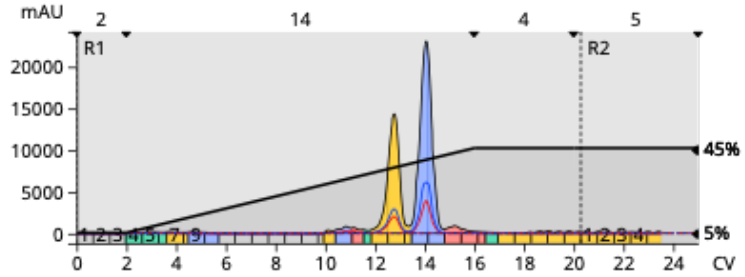

Signal	Wavelength	Threshold
λ-All (Collect)	200 - 400 nm	40 mAU
UV1 (Collect)	254 nm	40 mAU
UV2 (Collect)	280 nm	40 mAU

Gradient

Solvent A: n-Hexane **Solvent B:** Ethyl acetate

5-5%	Ethyl acetate in n-Hexane	2 CV	
5-45%	Ethyl acetate in n-Hexane	14 CV	
45-45%	Ethyl acetate in n-Hexane	4 CV	
45-45%	Ethyl acetate in n-Hexane	5 CV	Auto extended

Figure B17: Column chromatography results for **5i**.

5j 4-phenyl-6-methyl-2*H*-pyran-2-one:

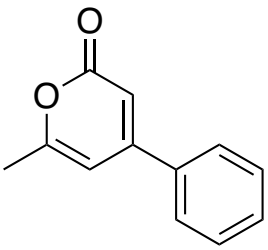

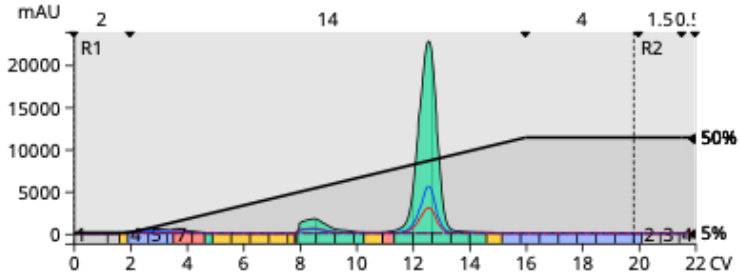

Signal	Wavelength	Threshold
λ-All (Collect)	200 - 400 nm	40 mAU
UV1 (Collect)	280 nm	40 mAU
UV2 (Collect)	254 nm	40 mAU

Gradient

Solvent A: n-Hexane **Solvent B:** Ethyl acetate

5-5%	Ethyl acetate in n-Hexane	2 CV	
5-50%	Ethyl acetate in n-Hexane	14 CV	
50-50%	Ethyl acetate in n-Hexane	4 CV	
50-50%	Ethyl acetate in n-Hexane	1.5 CV	
50-50%	Ethyl acetate in n-Hexane	0.5 CV	Auto extended

Figure B18: Column chromatography results for **5j**.

5e 4-phenyl-1-benzyl-3-phenylpyrrolidin-3-en-2-one co-elution with 1-benzyl-3-phenylpyrrolidin-3-en-2-one:

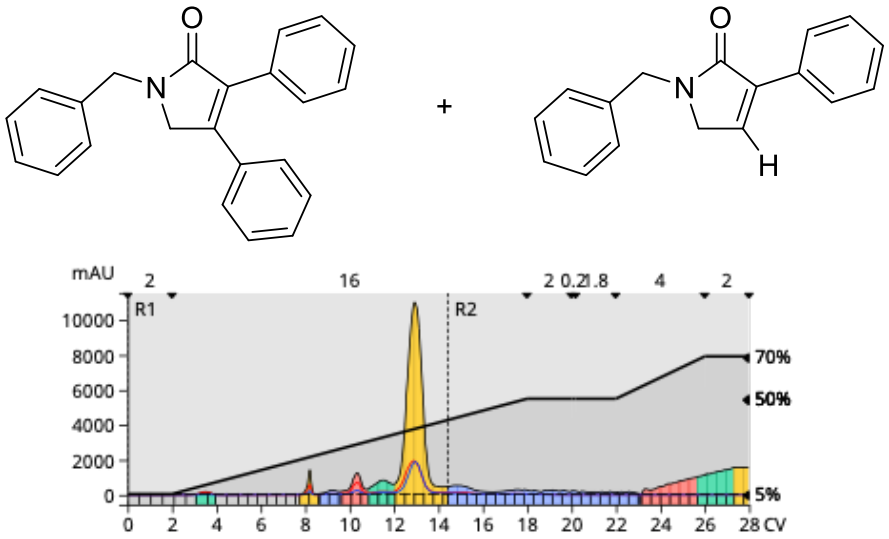

Signal	Wavelength	Threshold
λ-All (Collect)	200 - 400 nm	40 mAU
UV1	254 nm	
UV2	280 nm	

Gradient

Solvent A: n-Hexane **Solvent B:** Ethyl acetate

5-5%	Ethyl acetate in n-Hexane	2 CV	
5-50%	Ethyl acetate in n-Hexane	16 CV	
50-50%	Ethyl acetate in n-Hexane	2 CV	
50-50%	Ethyl acetate in n-Hexane	0.2 CV	
50-50%	Ethyl acetate in n-Hexane	1.8 CV	Auto extended
50-70%	Ethyl acetate in n-Hexane	4 CV	
70-70%	Ethyl acetate in n-Hexane	2 CV	

Figure B19: Column chromatography results for **5e**.

4b 3-phenylfuran-2(5H)-one:

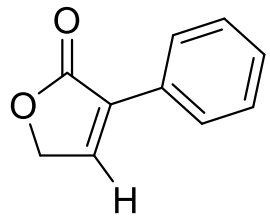

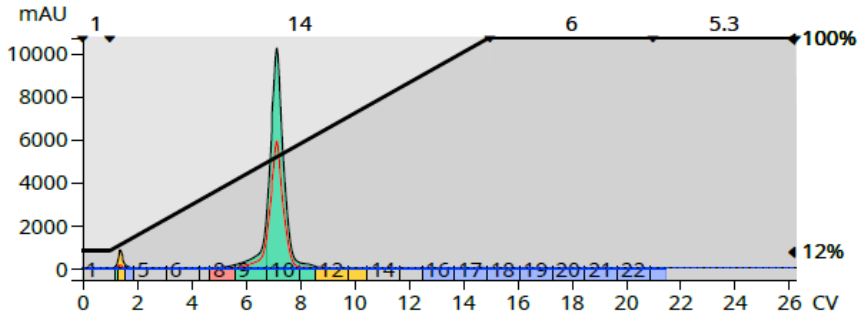

Signal	Wavelength	Threshold
λ-All (Collect)	200 - 400 nm	40 mAU
UV1 (Collect)	254 nm	40 mAU
UV2 (Collect)	220 nm	40 mAU

Gradient

Solvent A: n-Hexane **Solvent B:** Ethyl acetate

12-12%	Ethyl acetate in n-Hexane	1 CV	
12-100%	Ethyl acetate in n-Hexane	14 CV	
100-100%	Ethyl acetate in n-Hexane	6 CV	
100-100%	Ethyl acetate in n-Hexane	5.3 CV	Auto extended

Figure B20: Column chromatography results for **4b**.

4e 1-benzyl-3-phenylpyrrolidin-3-en-2-one:

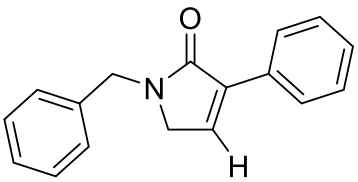

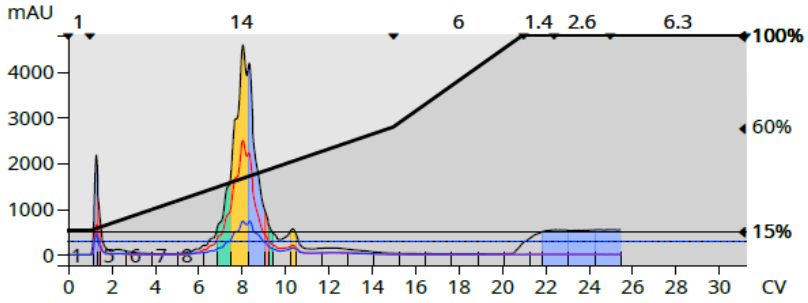

Signal	Wavelength	Threshold
λ-All (Collect)	200 - 400 nm	500 mAU
UV1 (Collect)	254 nm	300 mAU
UV2 (Collect)	280 nm	300 mAU

Gradient

Solvent A: n-Hexane **Solvent B:** Ethyl acetate

15-15%	Ethyl acetate in n-Hexane	1 CV	
15-60%	Ethyl acetate in n-Hexane	14 CV	
60-100%	Ethyl acetate in n-Hexane	6 CV	
100-100%	Ethyl acetate in n-Hexane	1.4 CV	
100-100%	Ethyl acetate in n-Hexane	2.6 CV	
100-100%	Ethyl acetate in n-Hexane	6.3 CV	Auto extended

Figure B21: Column chromatography results for **4e**.

5d (3-(4-methoxyphenyl)-4-phenylfuran-2(5*H*)-one)

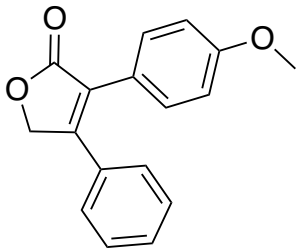

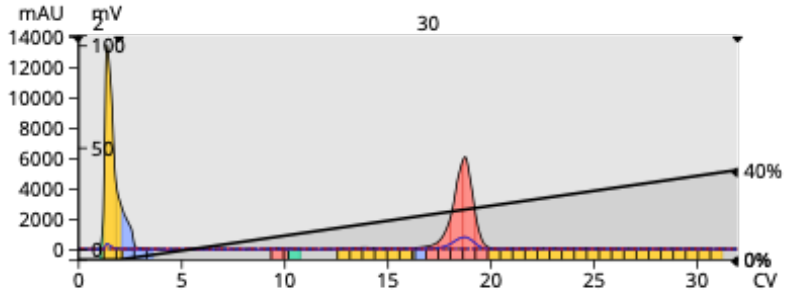

Signal	Wavelength	Threshold
λ-All (Collect)	200 - 400 nm	40 mAU
UV1 (Collect)	280 nm	40 mAU
UV2 (Collect)	280 nm	40 mAU

Gradient

Solvent A: n-Hexane **Solvent B:** Ethyl acetate

0-0%	Ethyl acetate in n-Hexane	2 CV
0-40%	Ethyl acetate in n-Hexane	30 CV

Figure B22: Column chromatography results for **5d**

B4 NMR Spectra

B4.1 Starting Materials

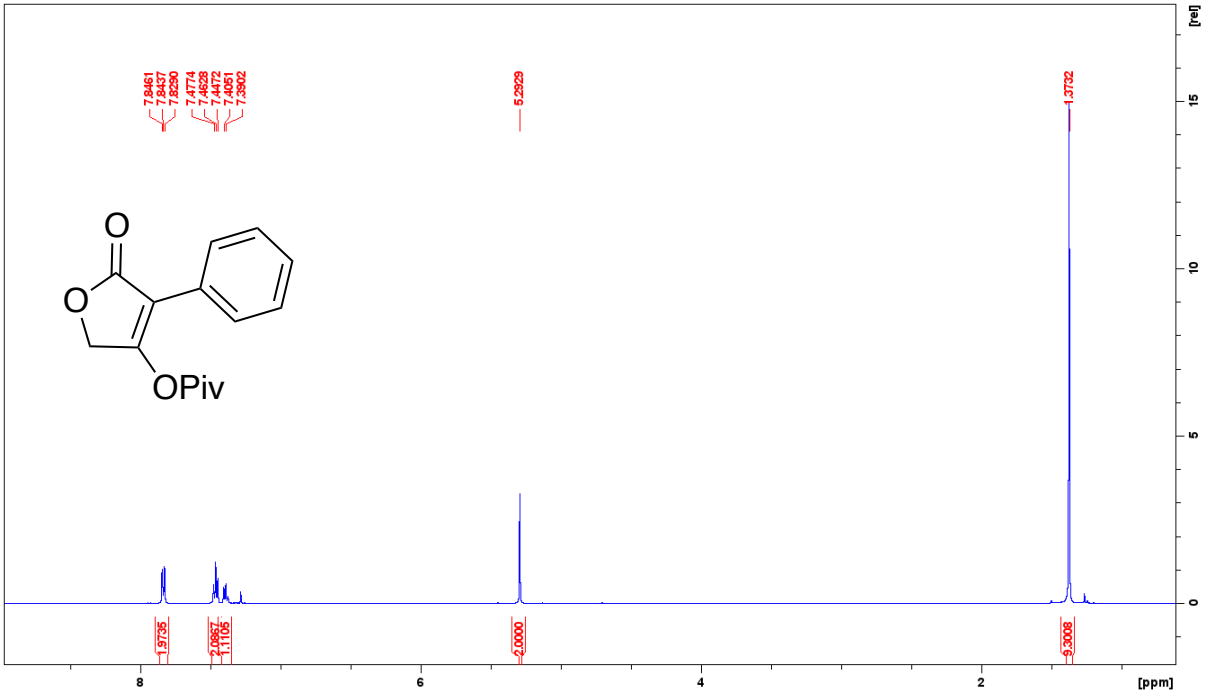

Figure B23: ^{1}H NMR spectrum (500 MHz, $CDCl_3$, 292 K) of **2b**

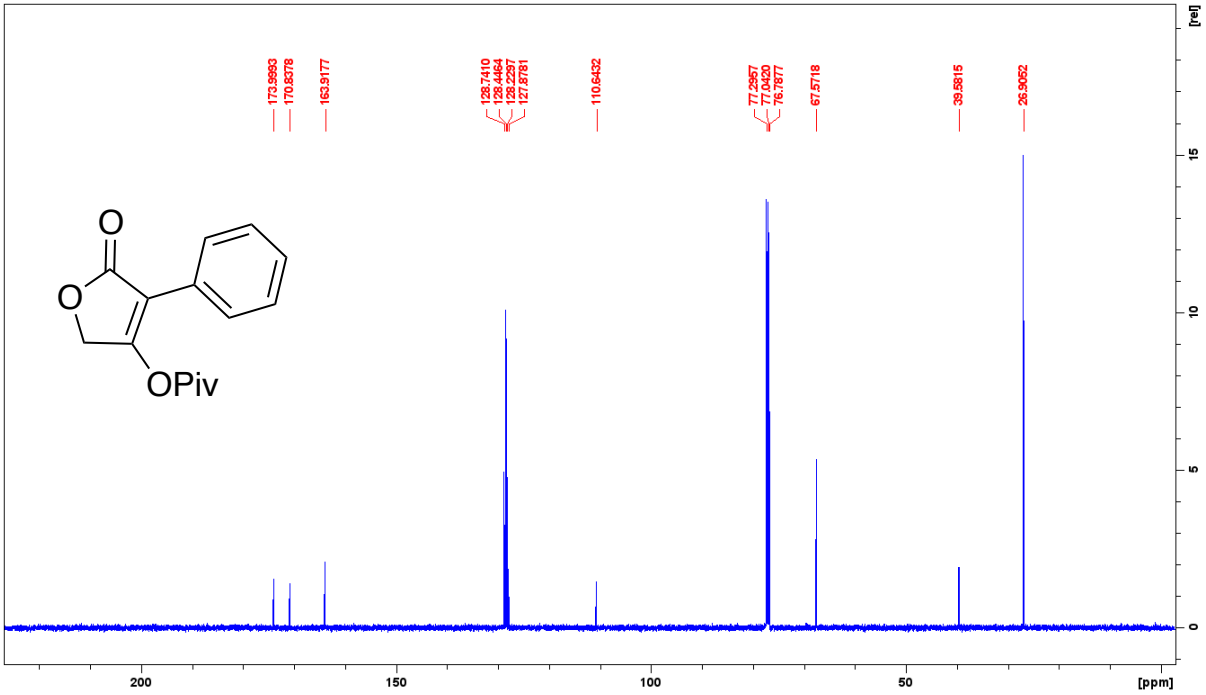

Figure B24: ^{13}C NMR spectrum (126 MHz, $CDCl_3$, 292 K) of **2b**

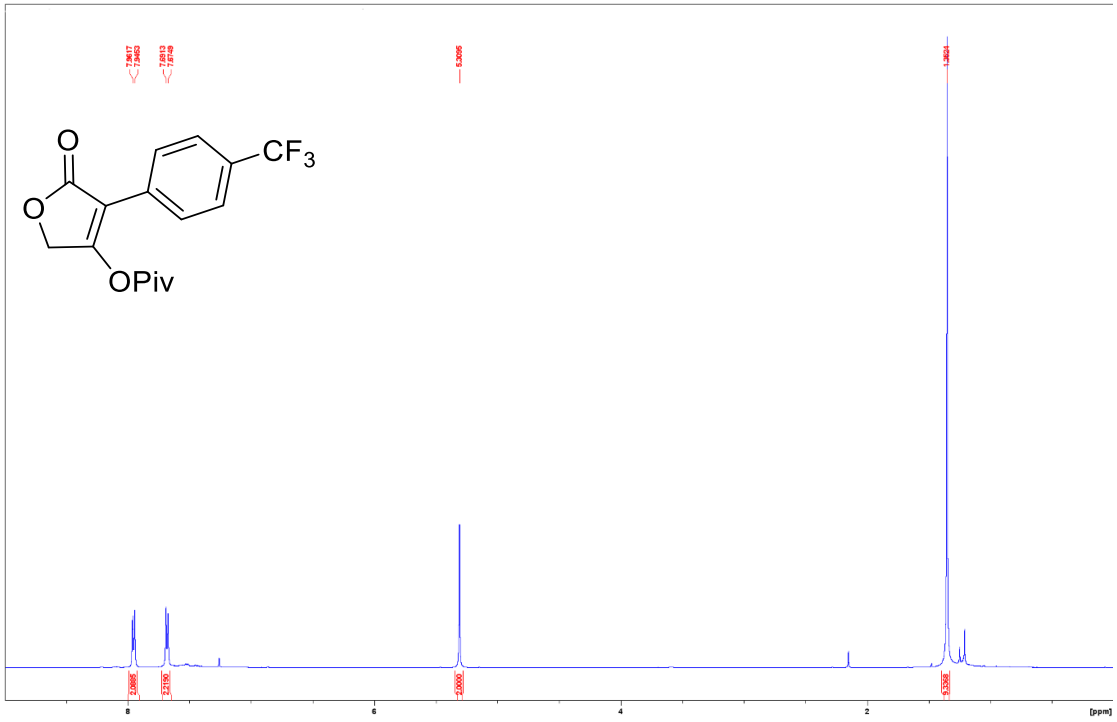

Figure B25: ^{1}H NMR spectrum (500 MHz, $CDCl_3$, 292 K) of **2c**

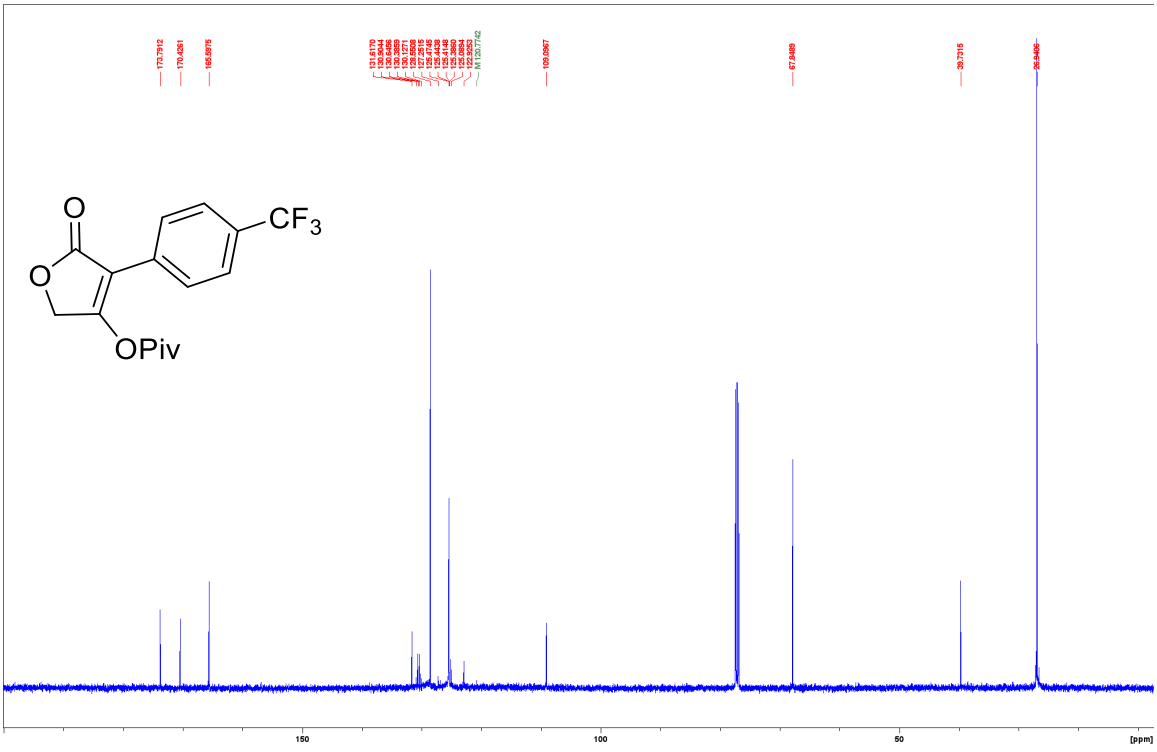

Figure B26: ^{13}C NMR spectrum (126 MHz, $CDCl_3$, 292 K) of **2c**

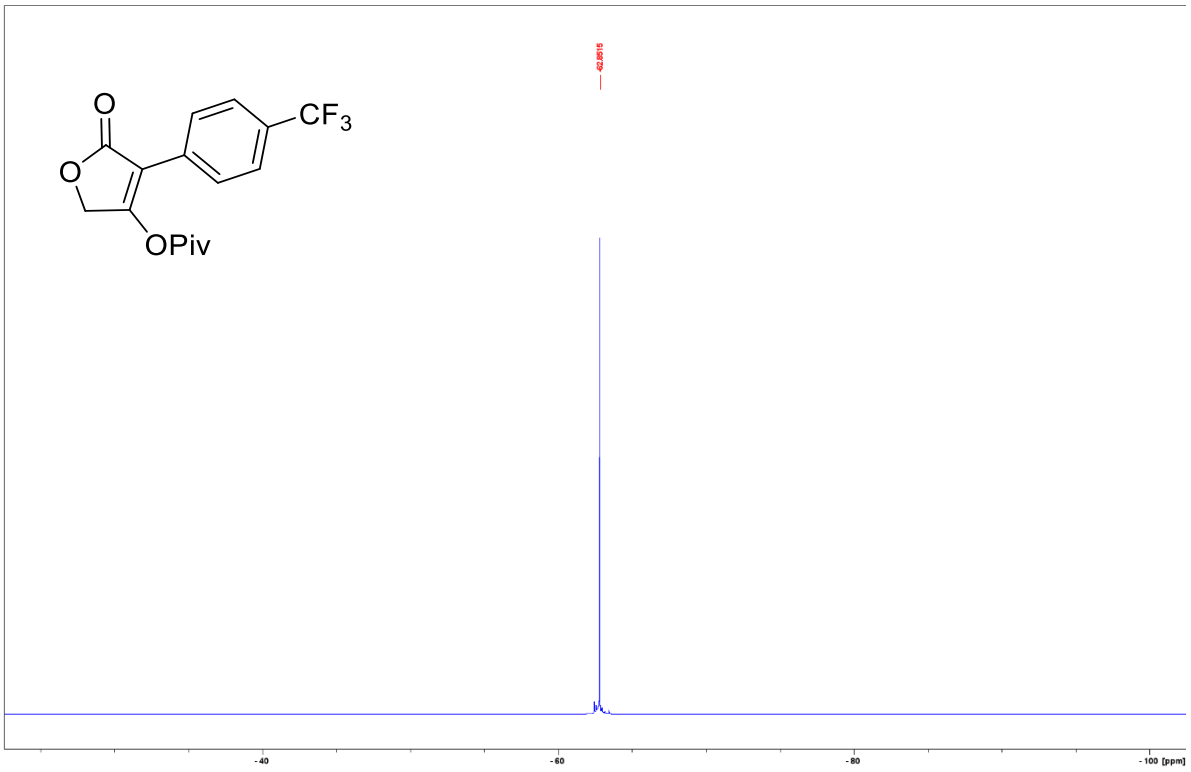

Figure B27: ^{19}F NMR spectrum (282 MHz, $CDCl_3$, 292 K) of **2c**

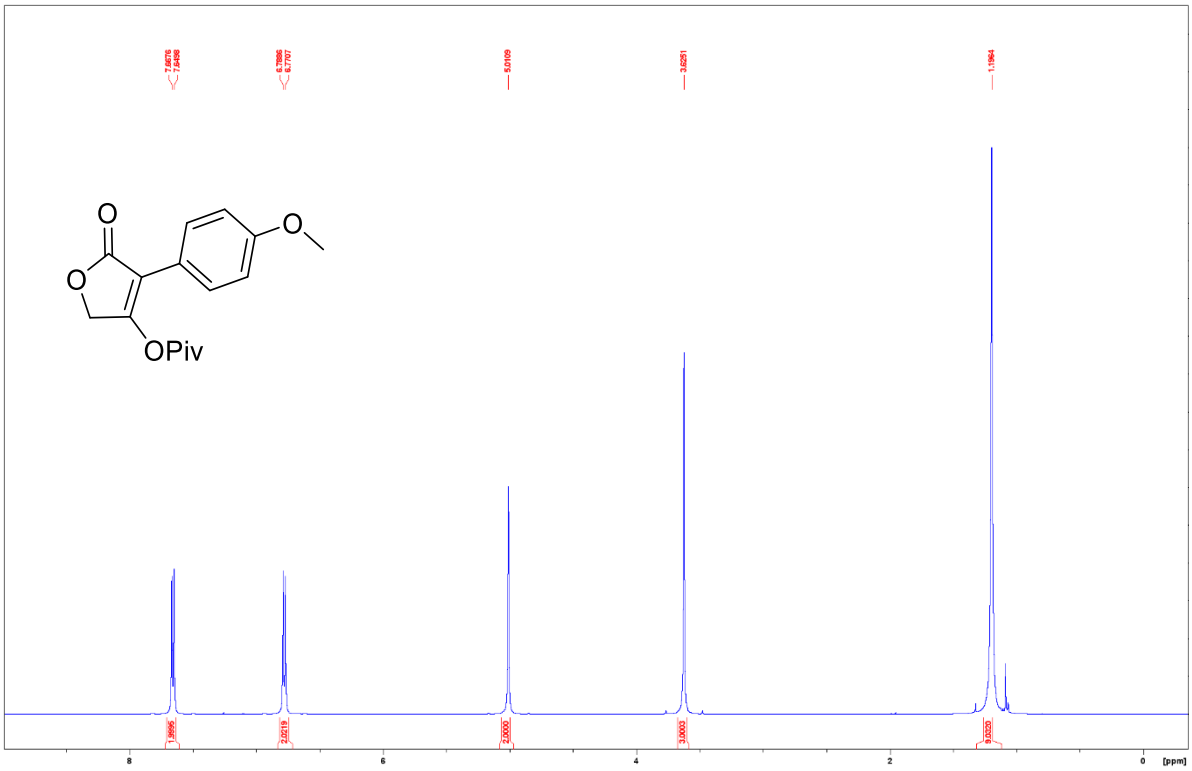

Figure B28: ^{1}H NMR spectrum (500 MHz, $CDCl_3$, 292 K) of **2d**

Figure B29: ^{13}C NMR spectrum (126 MHz, $CDCl_3$, 292 K) of **2d**

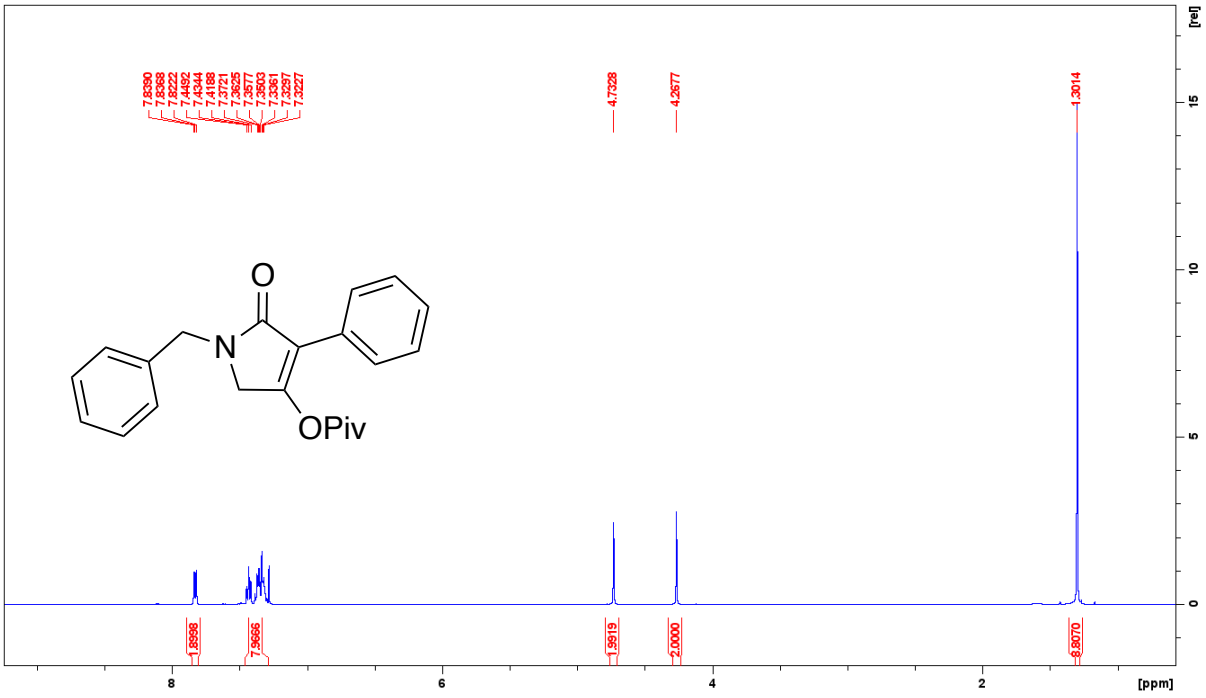

Figure B30: ^{1}H NMR spectrum (500 MHz, $CDCl_3$, 292 K) of **2e**

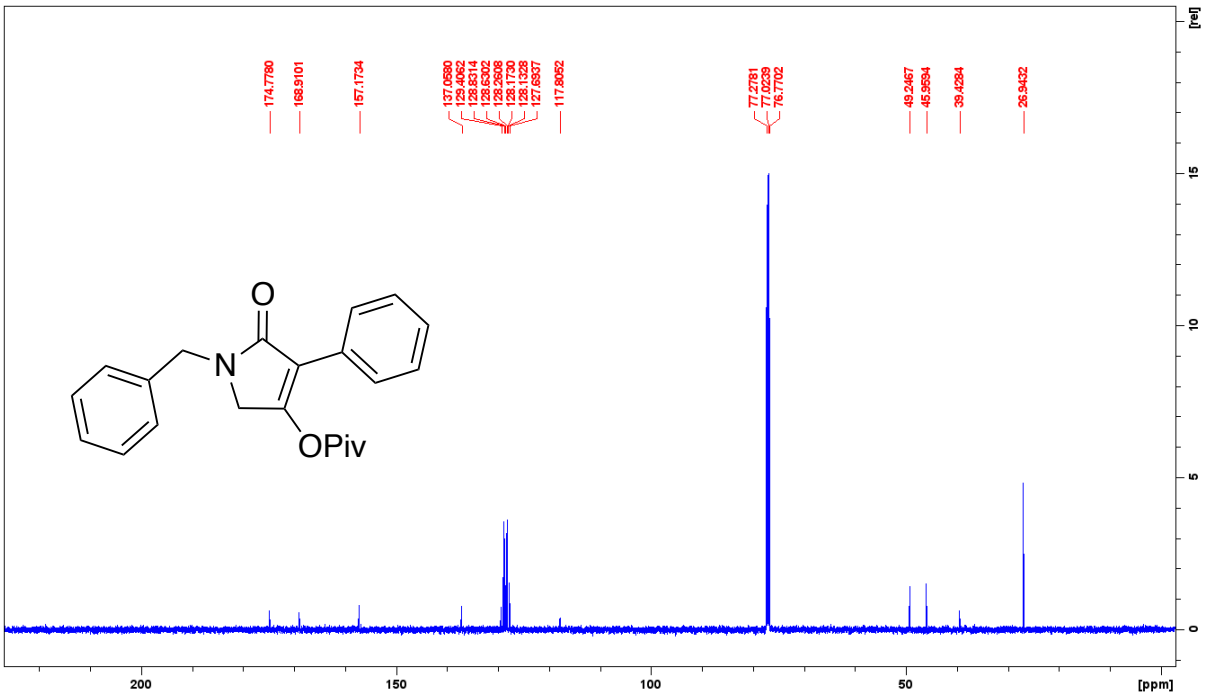

Figure B31: ^{13}C NMR spectrum (126 MHz, $CDCl_3$, 292 K) of **2e**

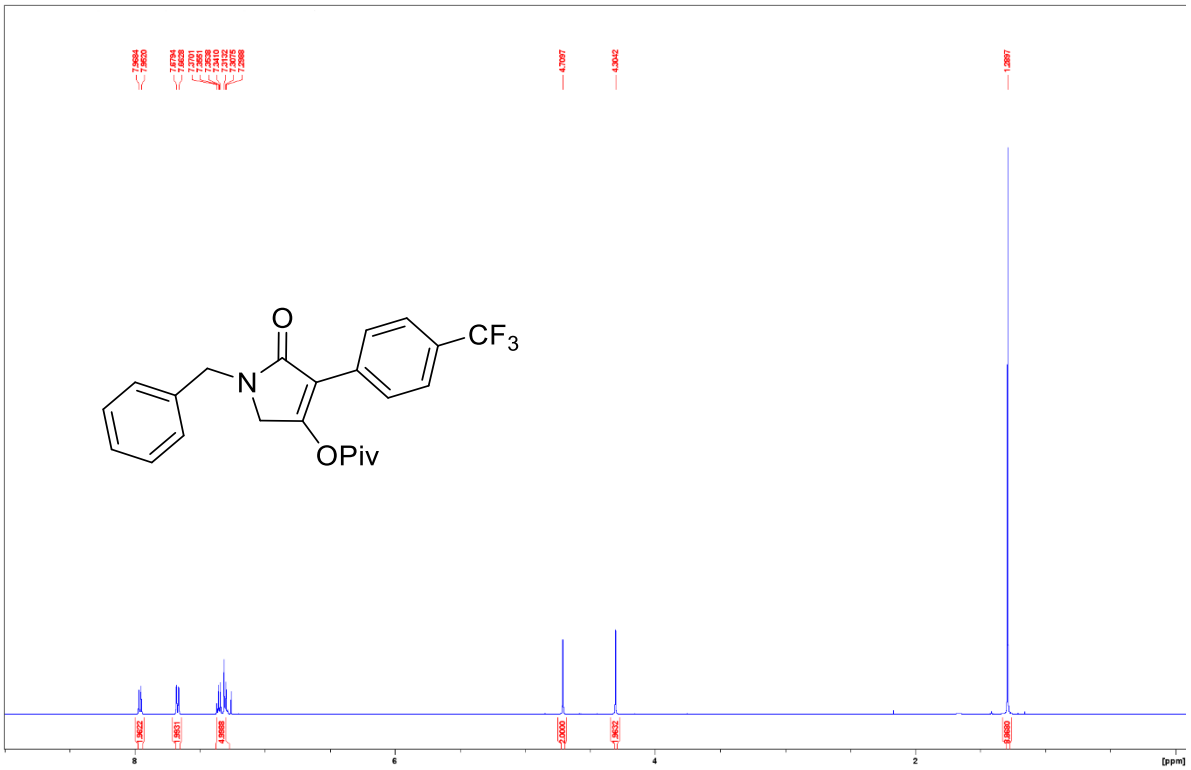

Figure B32: ^{1}H NMR spectrum (500 MHz, $CDCl_3$, 292 K) of **2f**

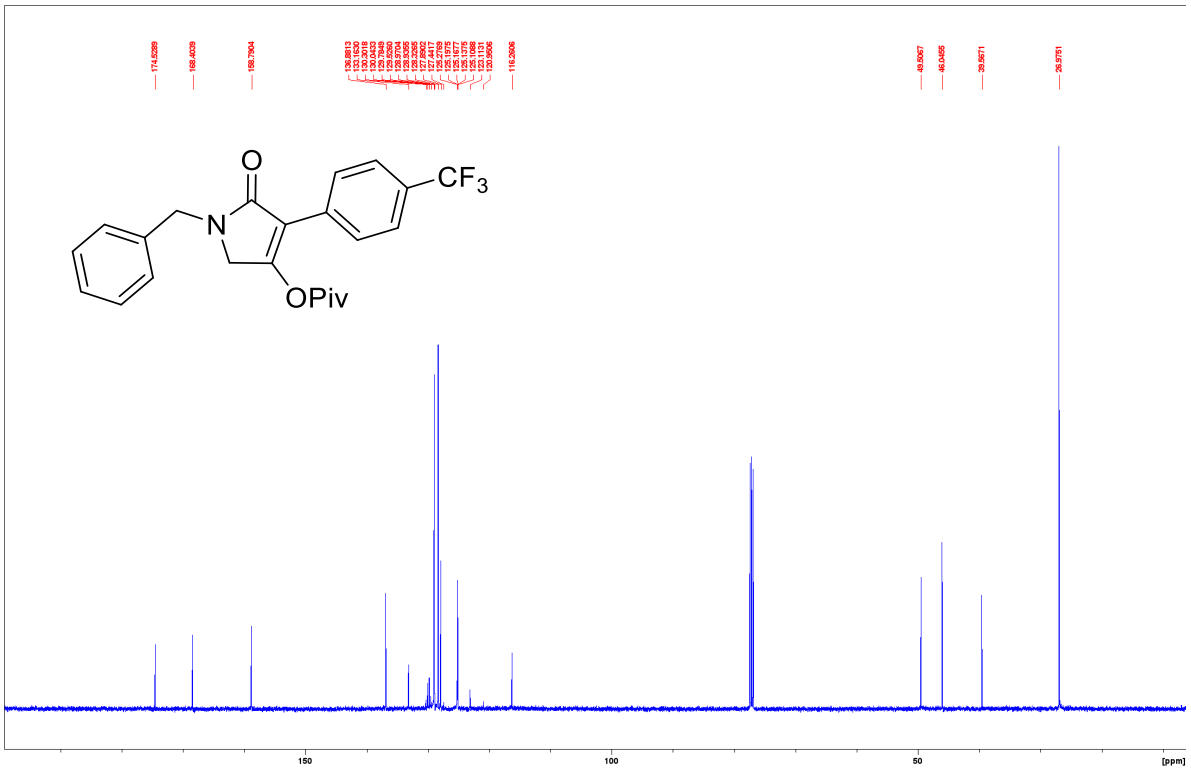

Figure B33: ^{13}C NMR spectrum (126 MHz, $CDCl_3$, 292 K) of **2f**

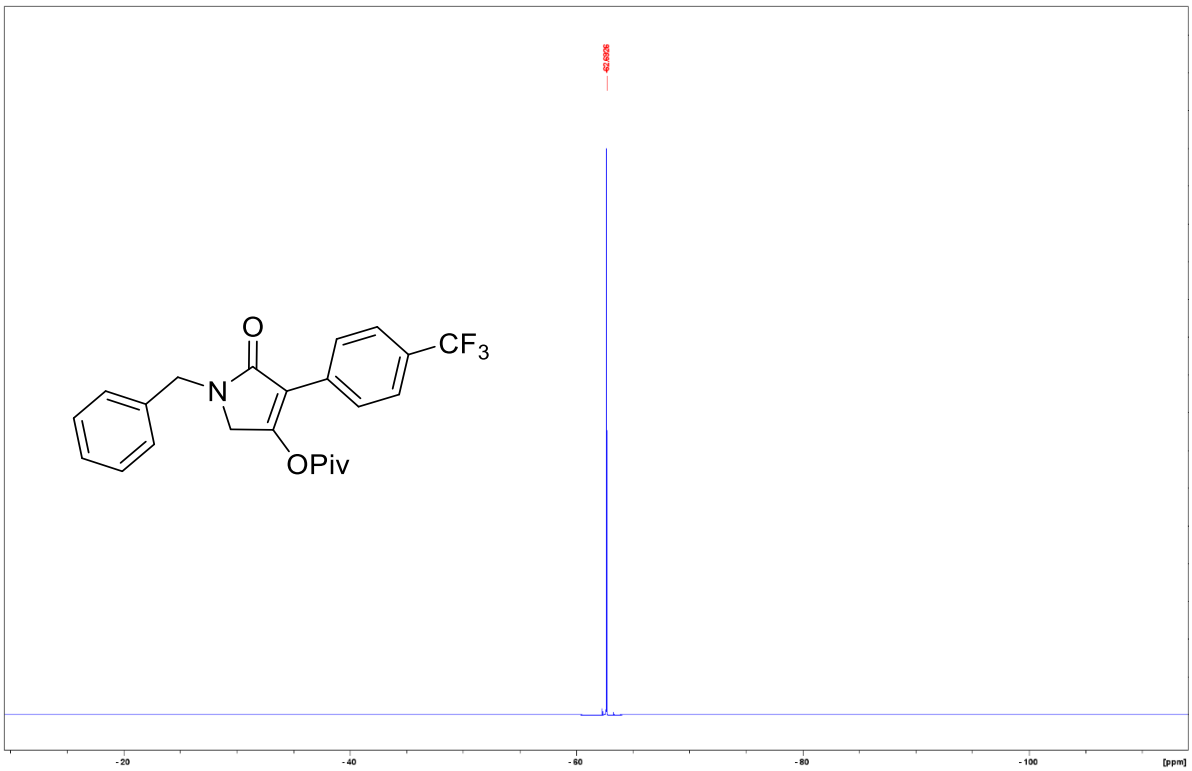

Figure B34: ^{19}F NMR spectrum (282 MHz, $CDCl_3$, 292 K) of **2f**

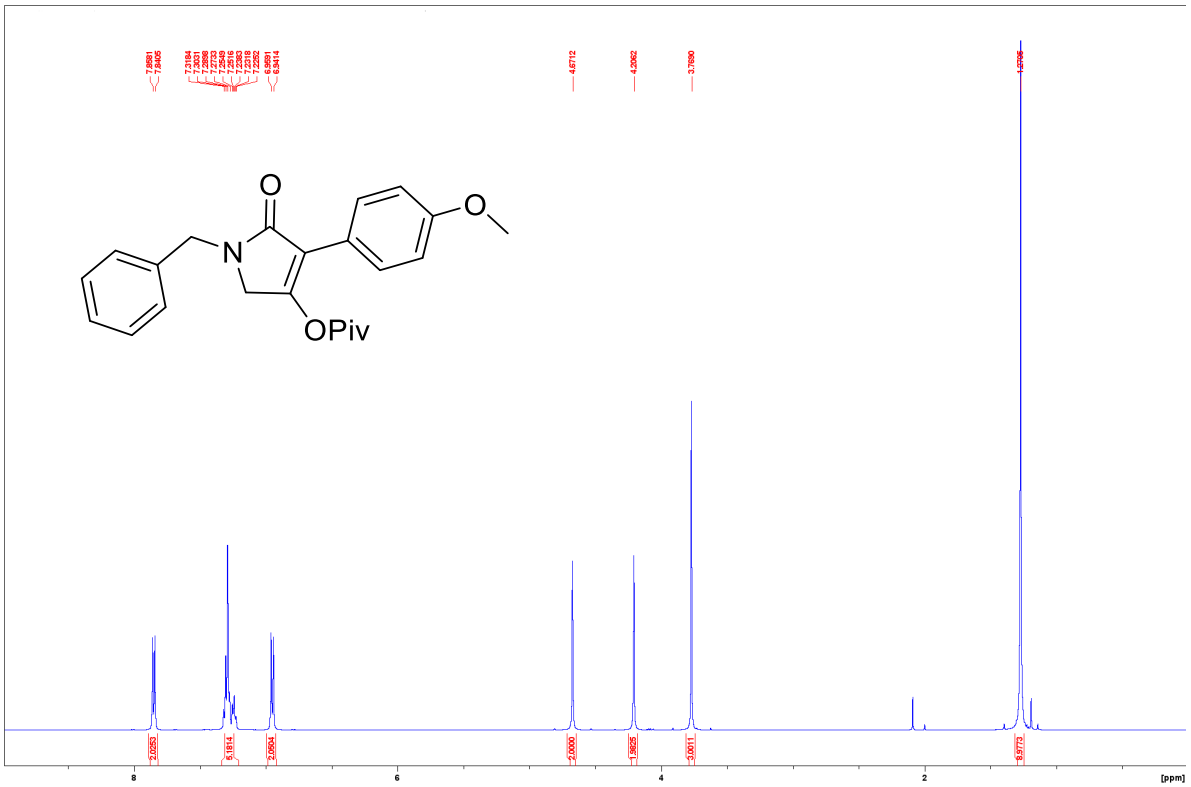

Figure B35: ^{1}H NMR spectrum (500 MHz, $CDCl_3$, 292 K) of **2g**

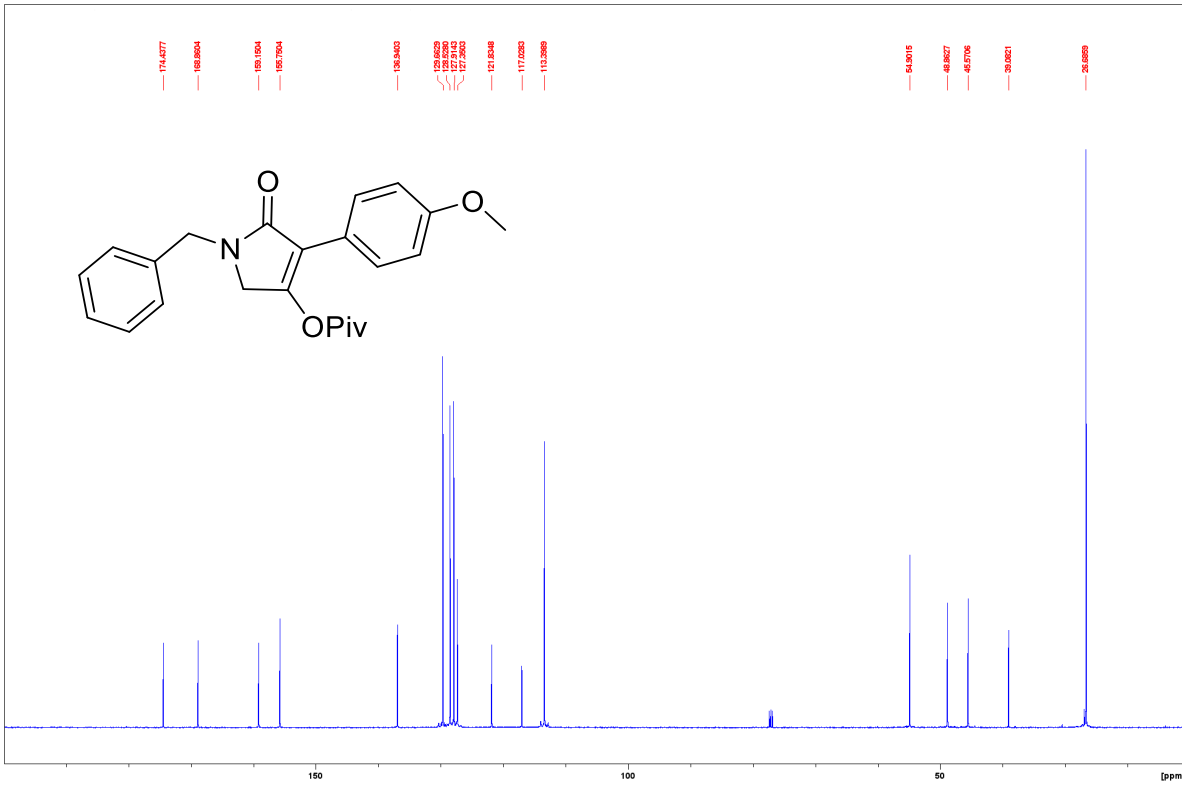

Figure B36: ^{13}C NMR spectrum (126 MHz, $CDCl_3$, 292 K) of **2g**

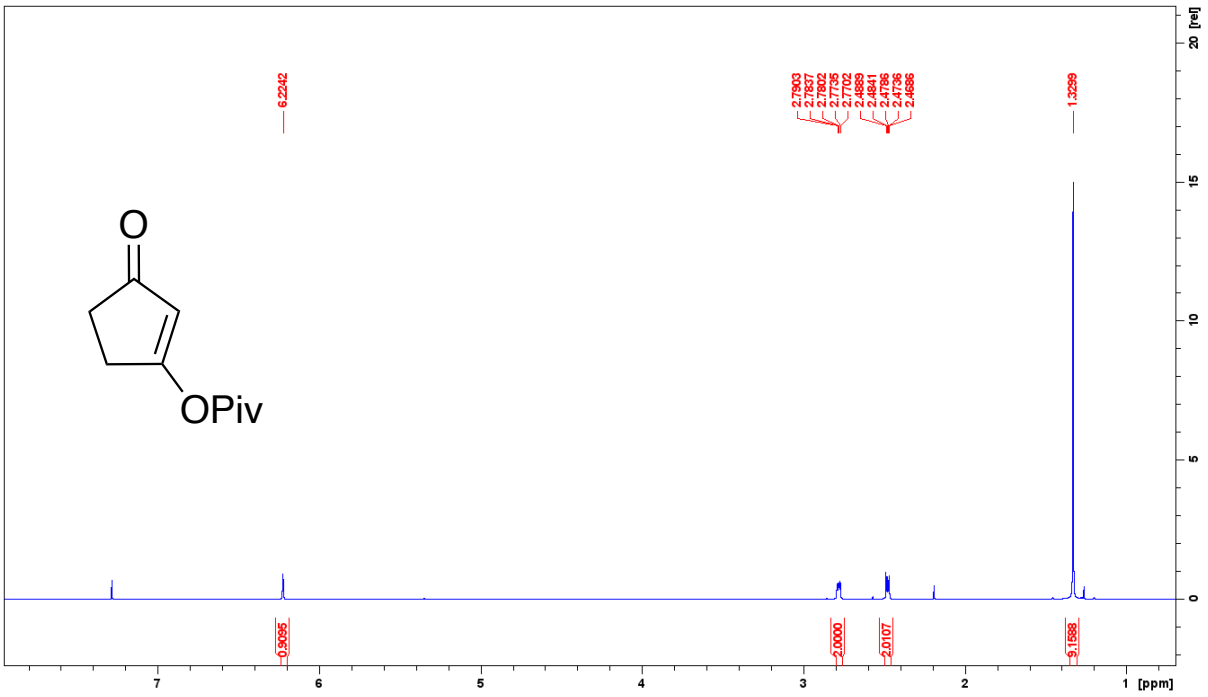

Figure B37: ^{1}H NMR spectrum (500 MHz, $CDCl_3$, 292 K) of **2h**

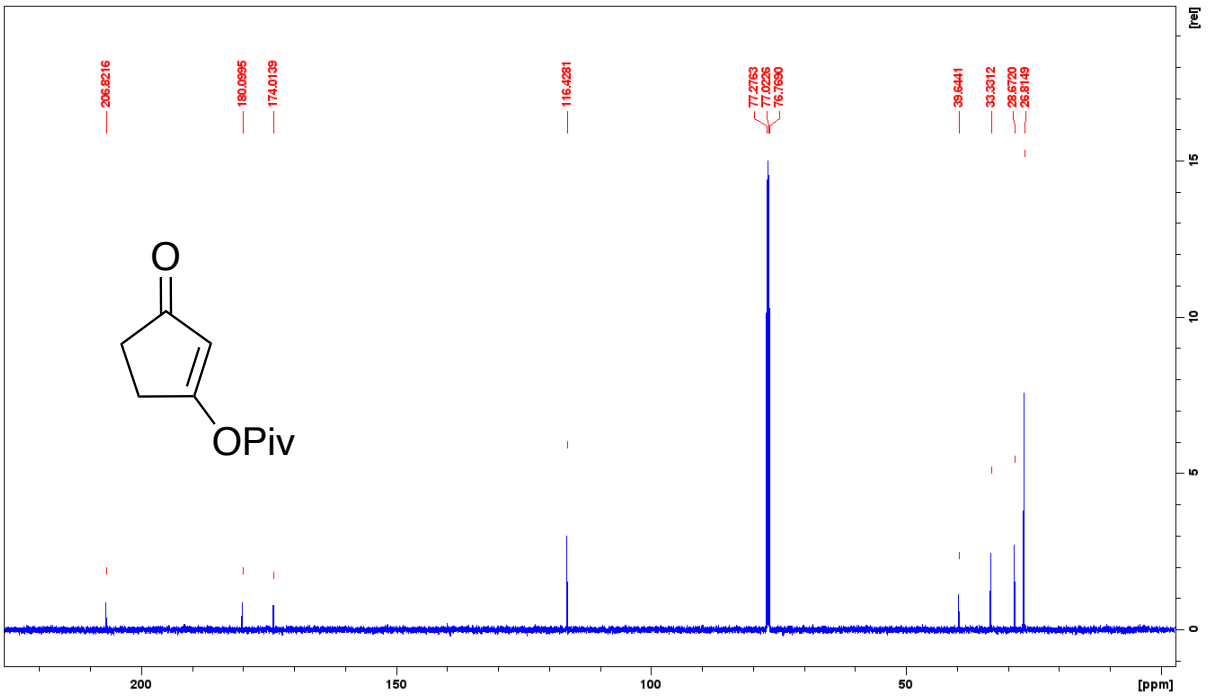

Figure B38: ^{13}C NMR spectrum (126 MHz, $CDCl_3$, 292 K) of **2h**

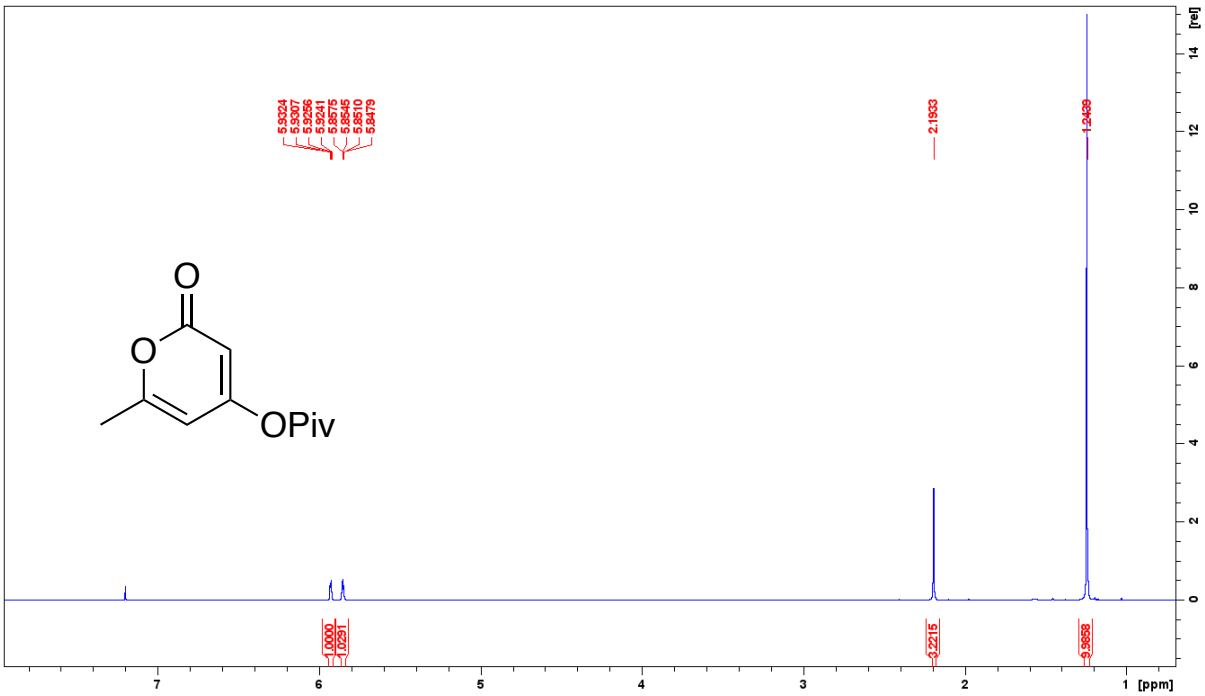

Figure B39: ^{1}H NMR spectrum (500 MHz, $CDCl_3$, 292 K) of **2i**

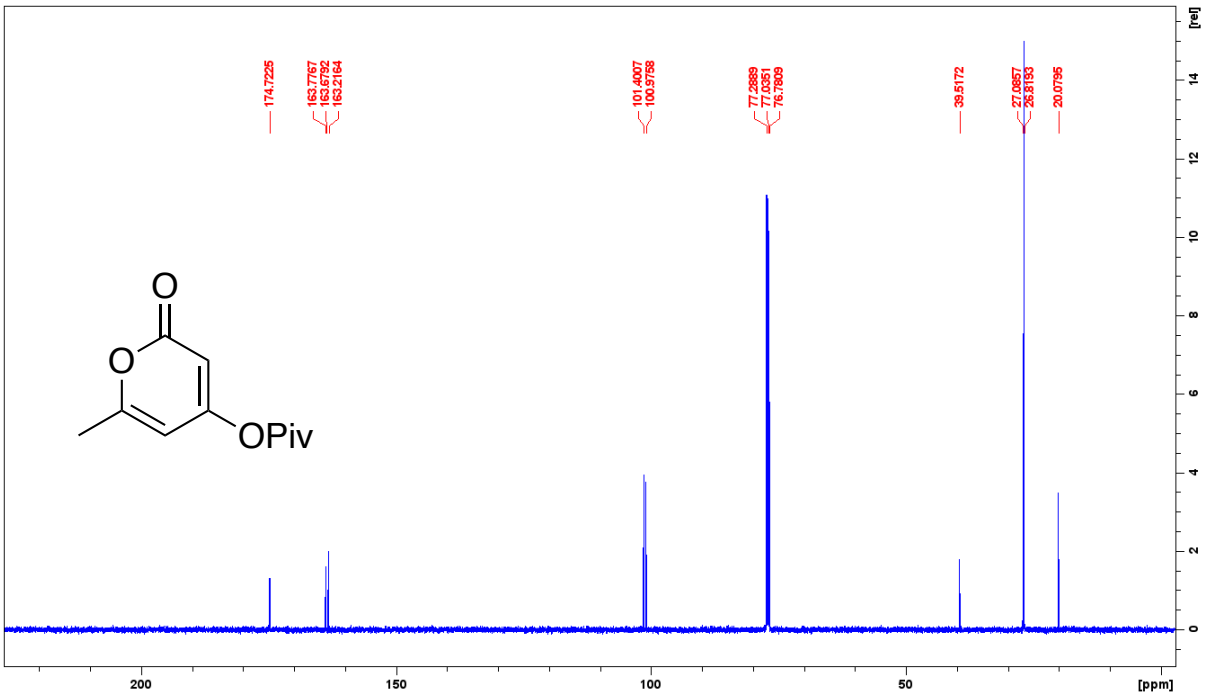

Figure B40: ^{13}C NMR spectrum (126 MHz, $CDCl_3$, 292 K) of **2i**

B4.2 Alkenyl Pinacol Boronates

All borylated compounds were characterized without undergoing work-up or purification.

All efforts to purify these compounds results in substantial deboronation.

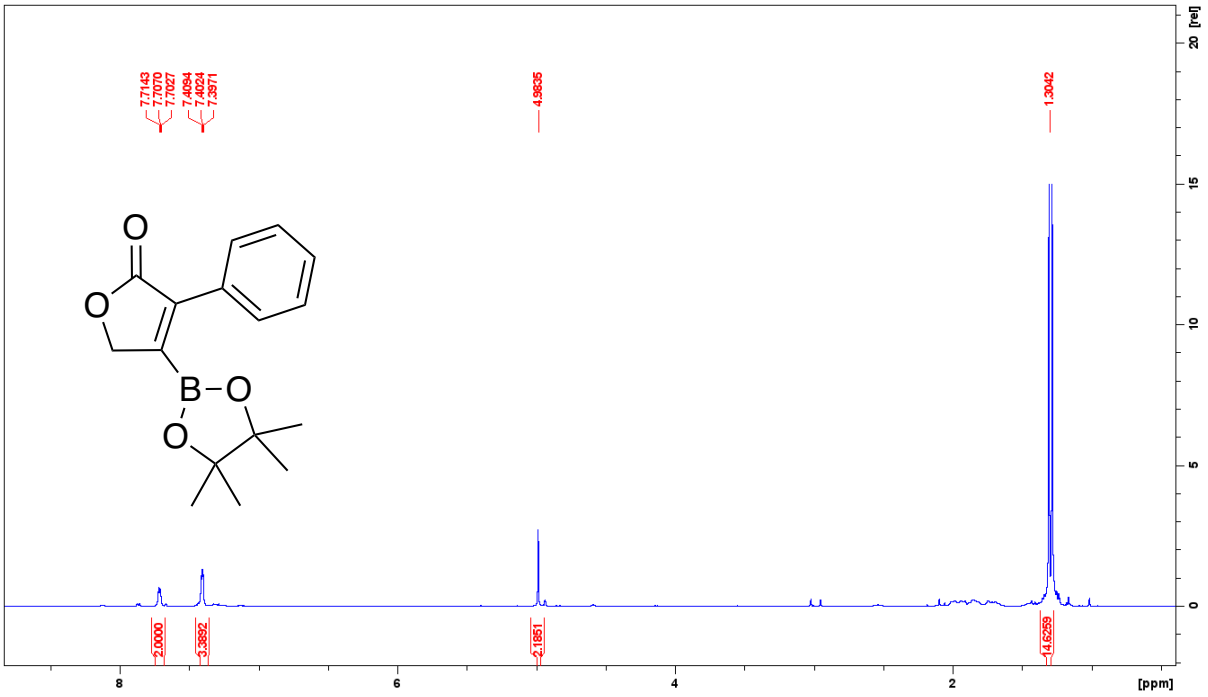

Figure B41: ^{1}H NMR spectrum (500 MHz, $CDCl_3$, 292 K) of **3b**

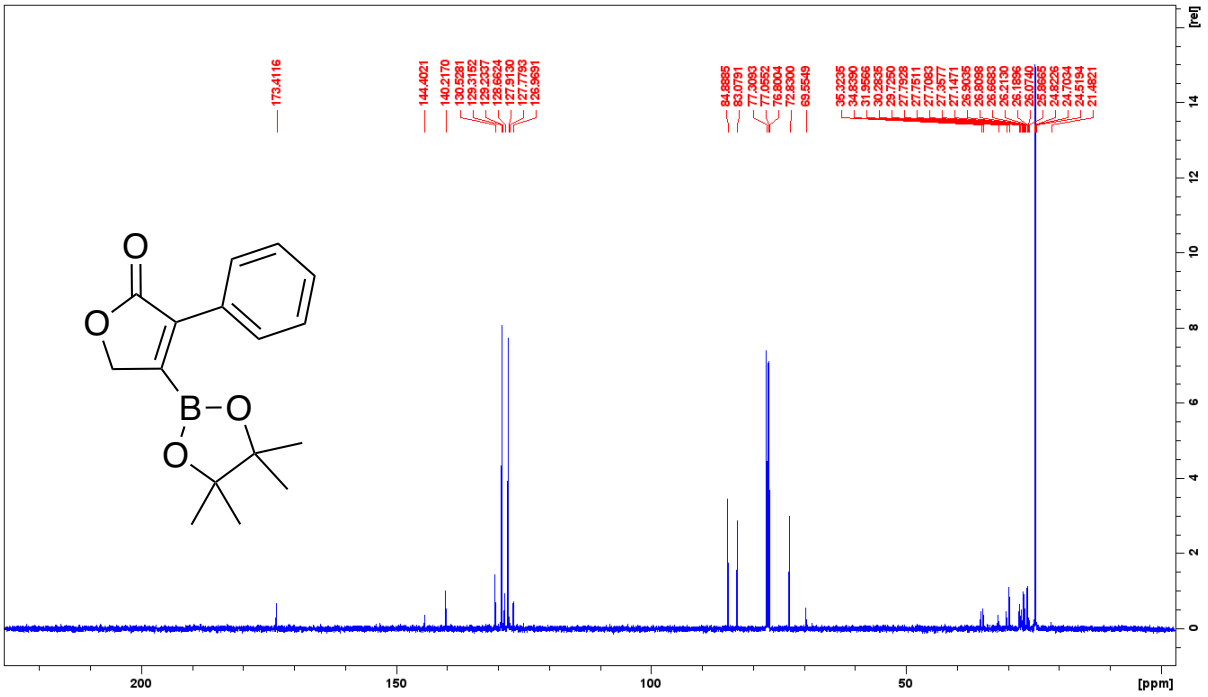

Figure B42: ^{13}C NMR spectrum (126 MHz, $CDCl_3$, 292 K) of **3b**

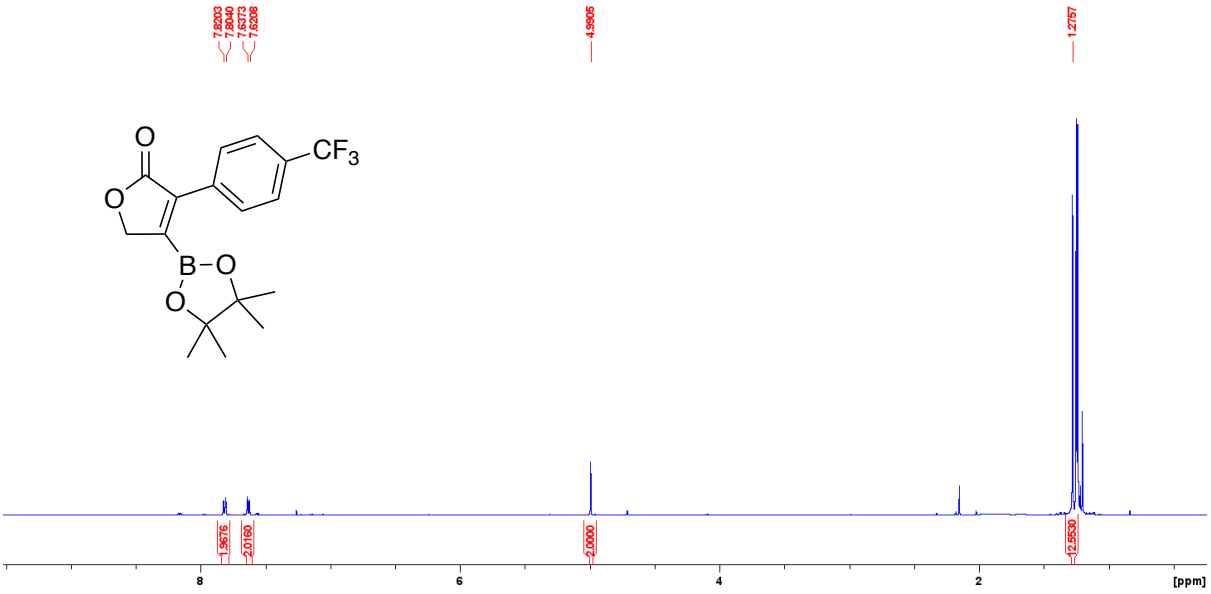

Figure B43: ^{1}H NMR spectrum (500 MHz, $CDCl_3$, 292 K) of **3c**

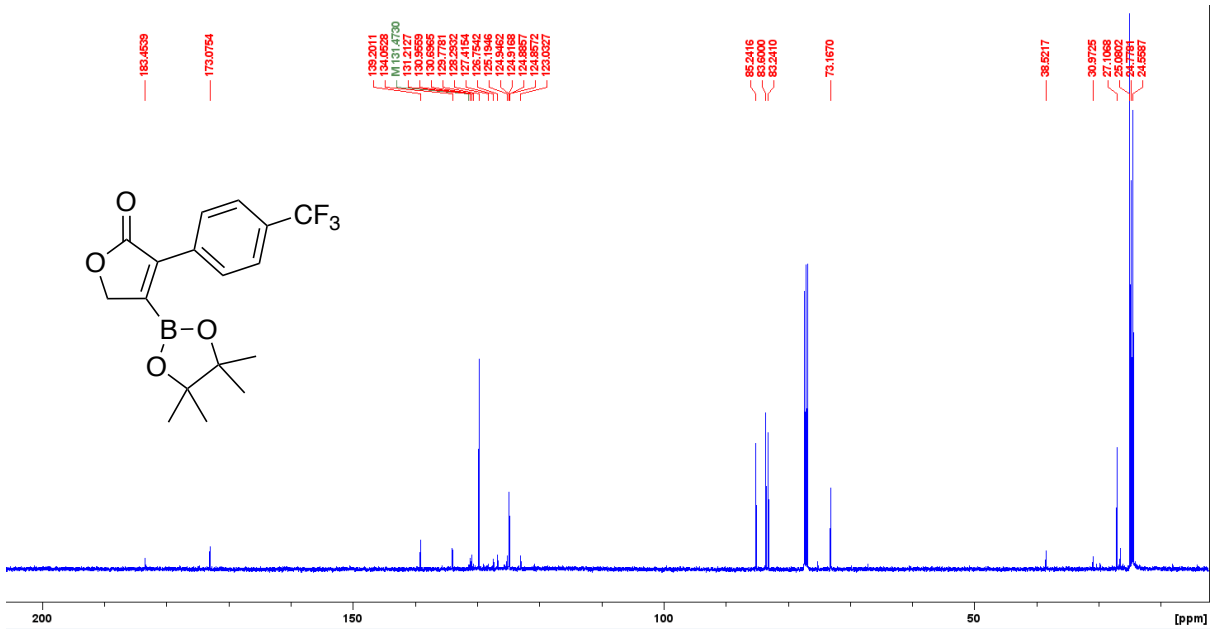

Figure B44: ^{13}C NMR spectrum (126 MHz, $CDCl_3$, 292 K) of **3c**

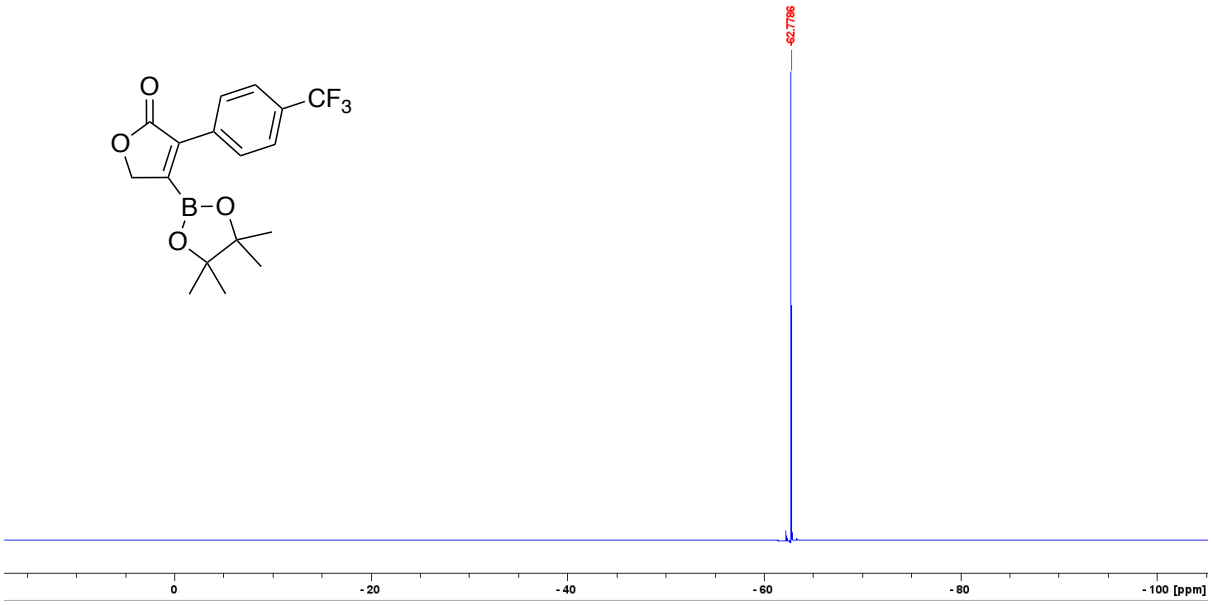

Figure B45: ^{19}F NMR spectrum of **3c** (282 MHz, $CDCl_3$, 292 K)

After borylation, **3d** is isolated as a mixture with **4d** in a 2.4 : 1 ratio. Efforts to purify further results in additional deboronation (increase in **4d**). **4d** characterization can be found in Section 3.6.7.

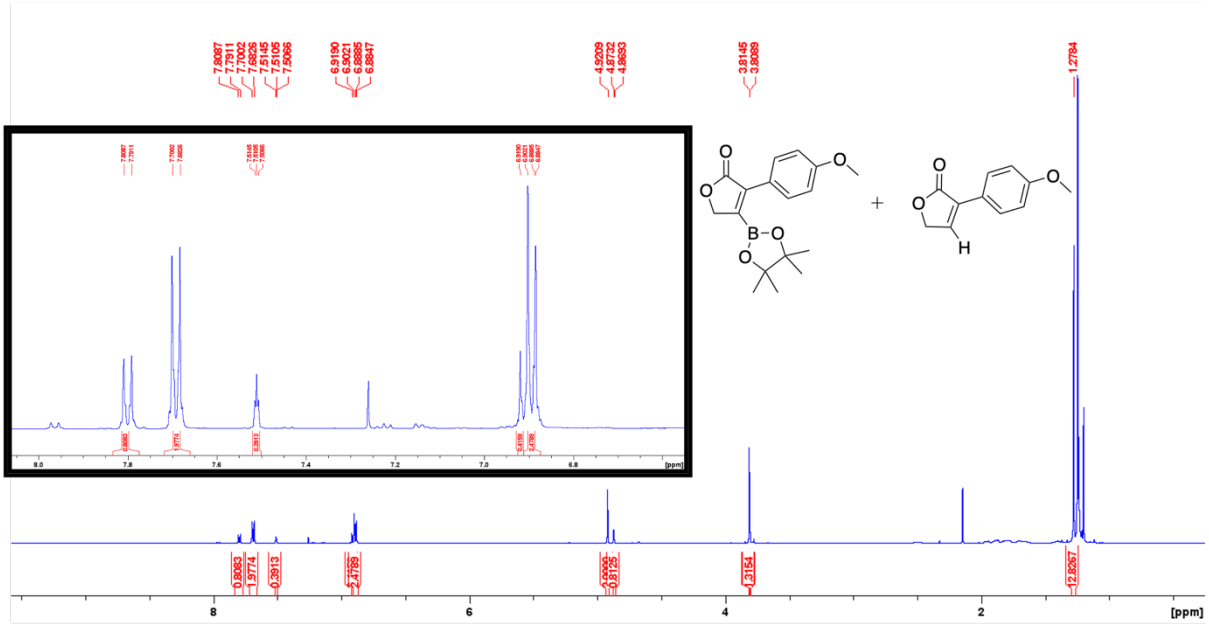

Figure B46: ^{1}H NMR spectrum of **3d : 4d** (2.4:1) (500 MHz, $CDCl_3$, 292 K)

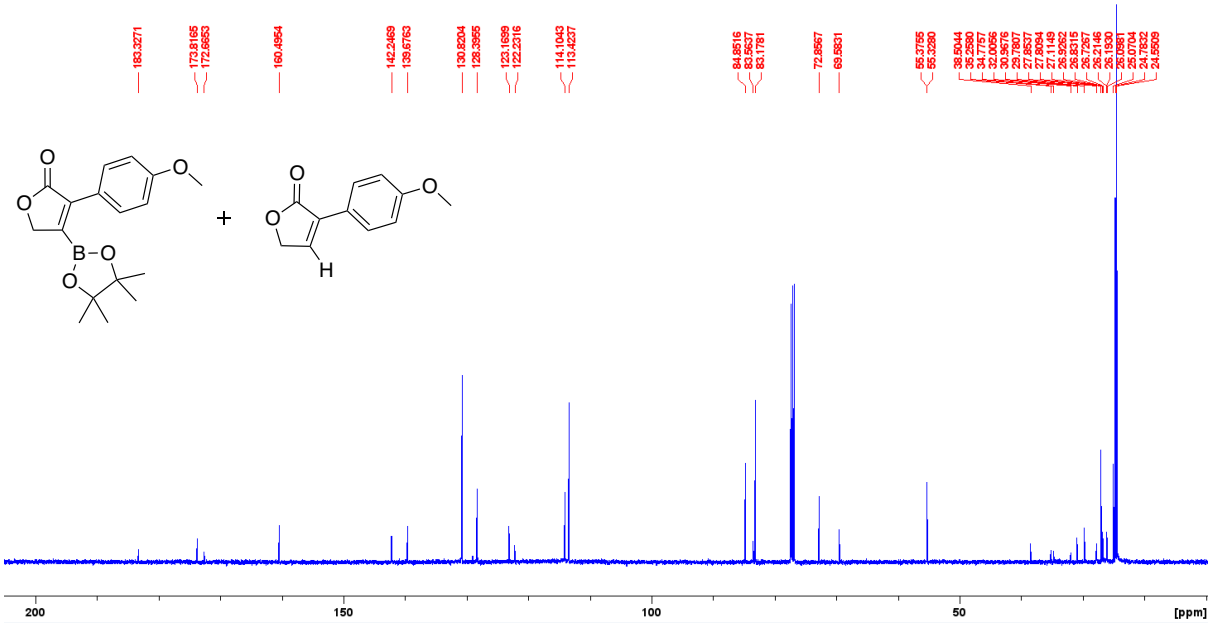

Figure B47: ^{13}C NMR spectrum (126 MHz, $CDCl_3$, 292 K) of **3d : 4d** (2.4:1)

After borylation, **3e** is isolated as a mixture with **4e** in a 3.33 : 1 ratio. Attempts to further purify **3e** resulted in additional protodeboronation (increase in **4e**). **4e** characterization can be found in Section 3.6.7.

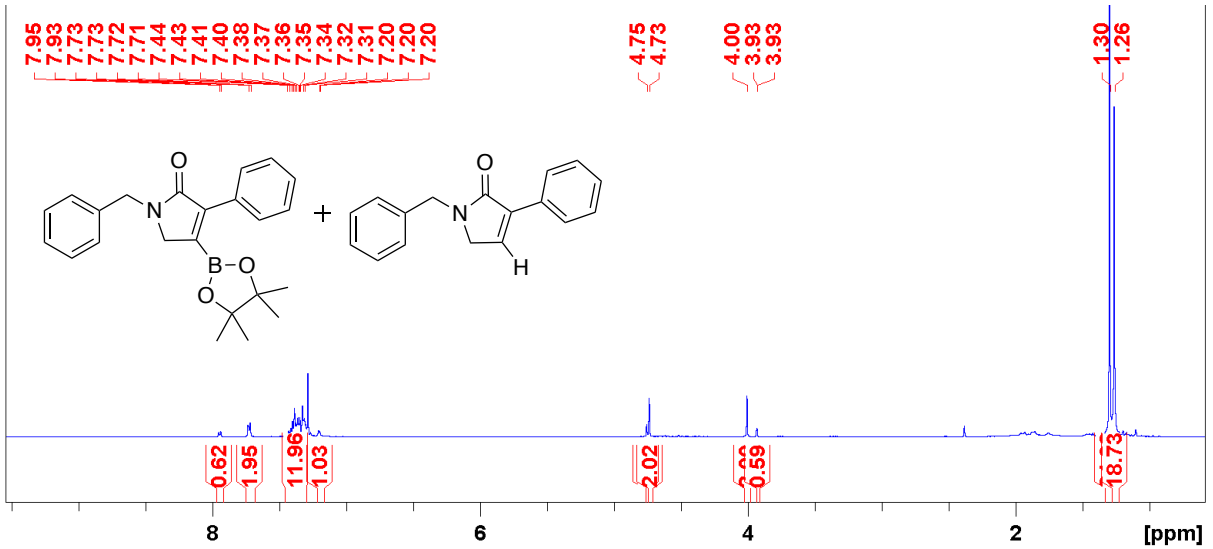

Figure B48: ^{1}H NMR spectrum (500 MHz, $CDCl_3$, 292 K) of **3e** : **4e** (3.33:1)

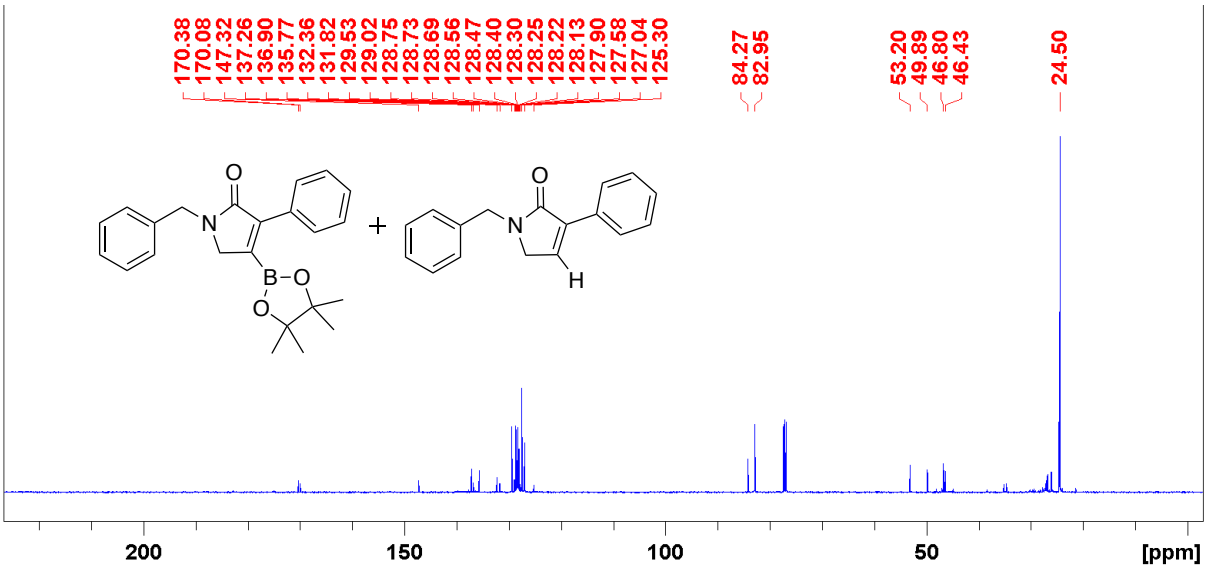

Figure B49: ^{13}C NMR spectrum (126 MHz, $CDCl_3$, 292 K) of **3e** : **4e** (3.33:1)

After borylation **3f** is isolated as a mixture with **4f** in a 2.5 : 1 ratio. Efforts to purify further results in additional deboronation (increase in **4f**). **4f** characterization can be found in Section 3.6.7.

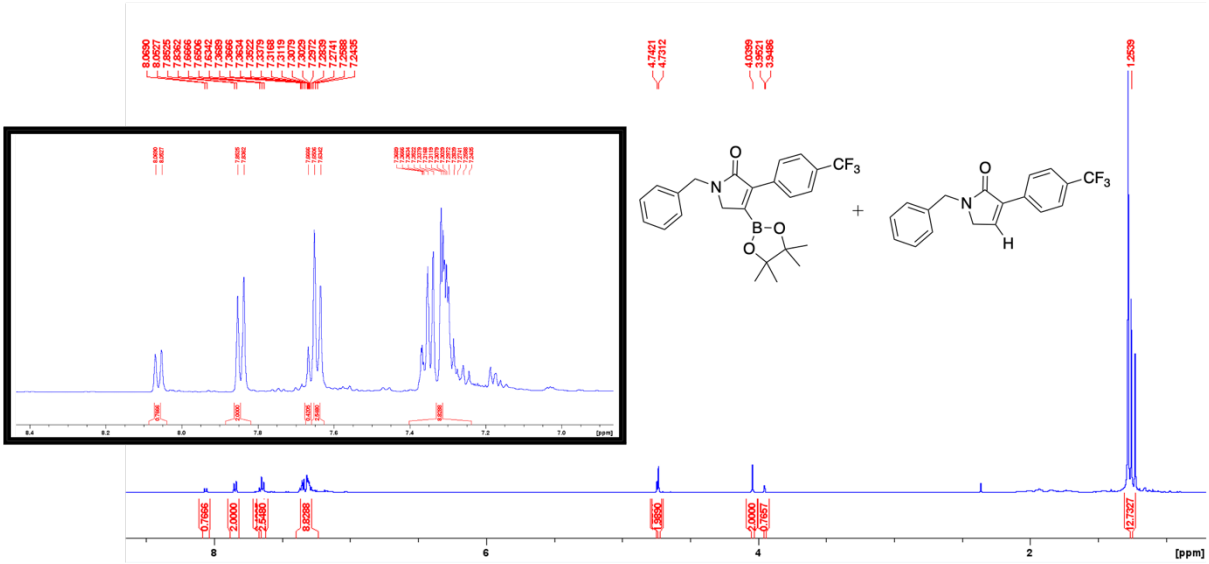

Figure B50: ^{1}H NMR spectrum (300 MHz, $CDCl_3$, 292 K) of **3f : 4f** (2.5:1)

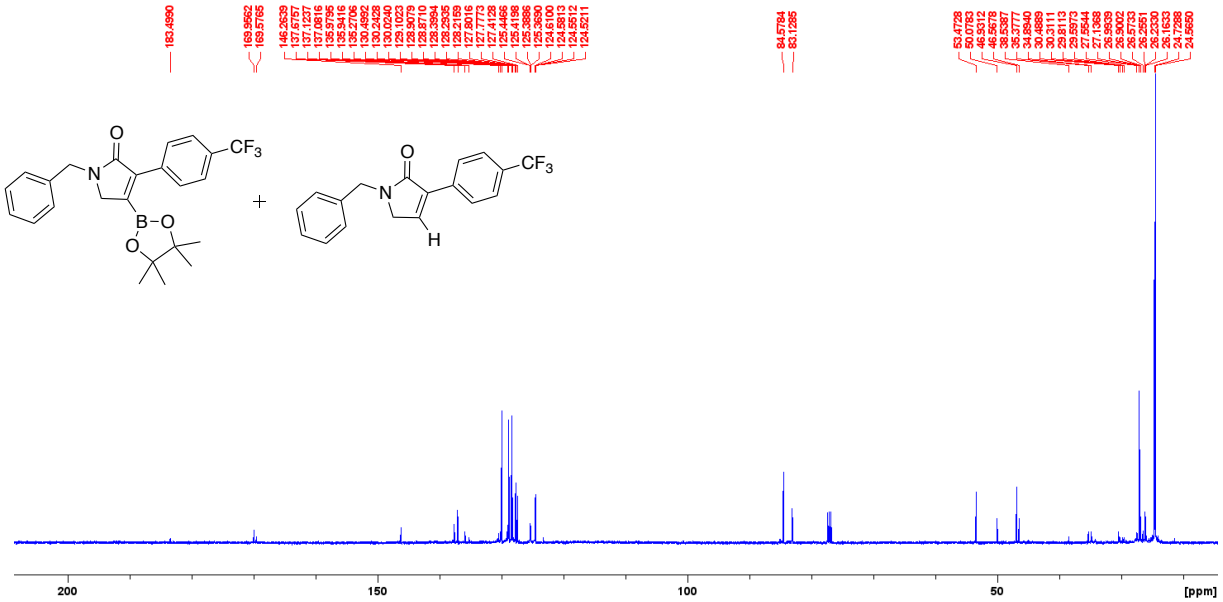

Figure B51: ^{13}C NMR spectrum (126 MHz, $CDCl_3$, 292 K) of **3f : 4f** (2.5:1)

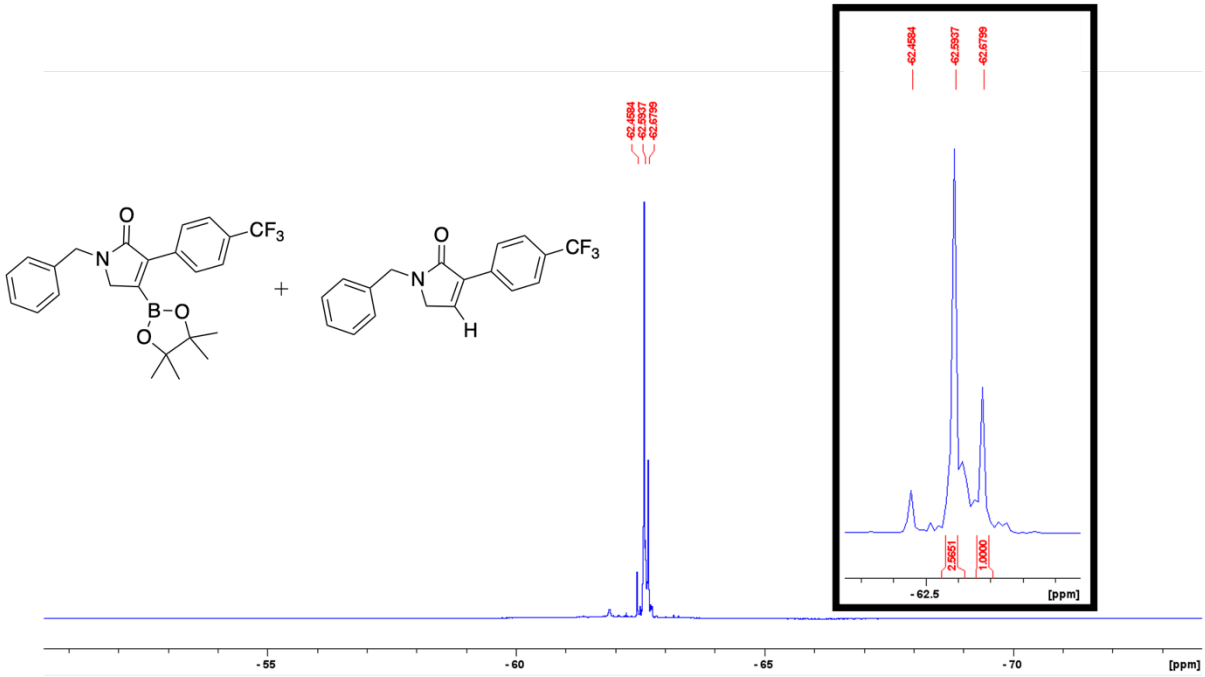

Figure B52: ^{19}F NMR spectrum (282 MHz, $CDCl_3$, 292 K) of **3f : 4f** (2.5:1)

After borylation, **3g** is isolated as a mixture with **4g** in a 4.7 : 1 ratio. Efforts to purify further results in additional deboronation (increase in **4g**). **4g** characterization can be found in Section 3.6.7.

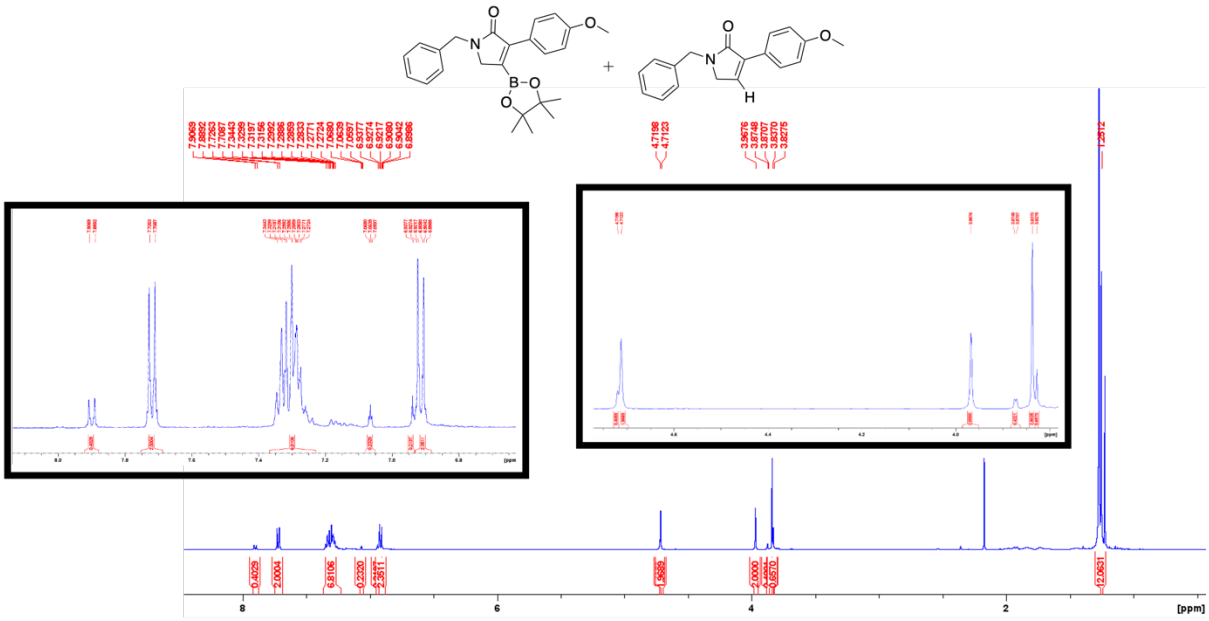

Figure B53: ^{1}H NMR spectrum (500 MHz, $CDCl_3$, 292 K) of **3g : 4g** (4.7:1)

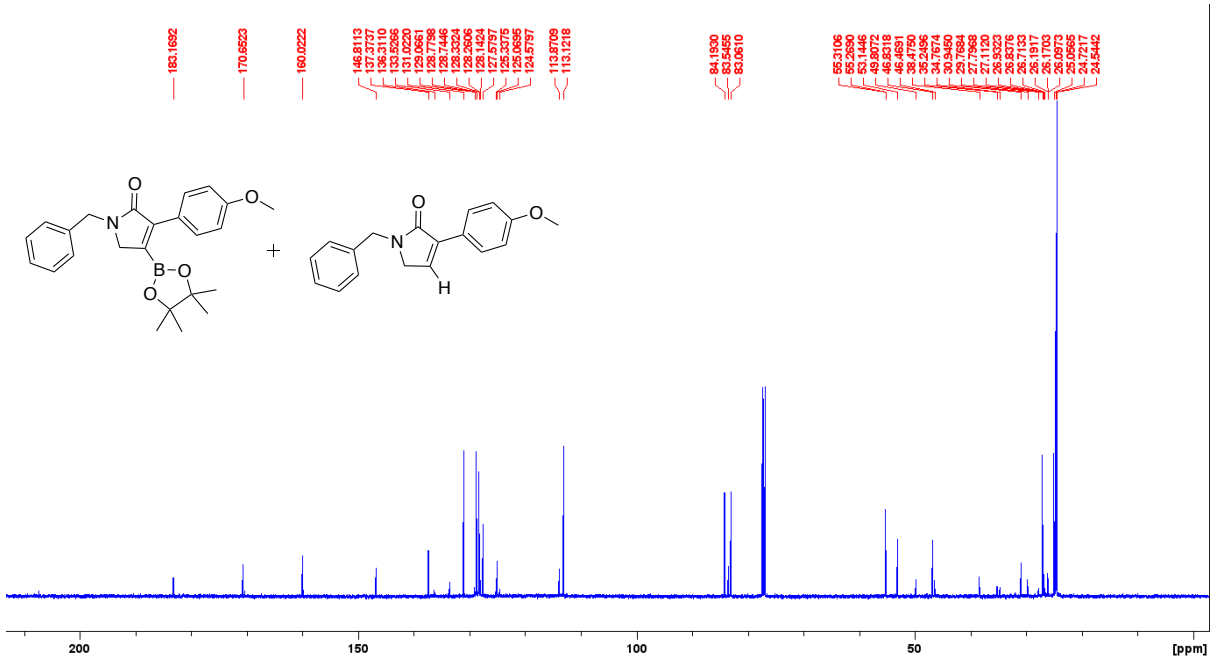

Figure B54: ^{13}C NMR spectrum (126 MHz, $CDCl_3$, 292 K) of **3g : 4g** (4.7:1)

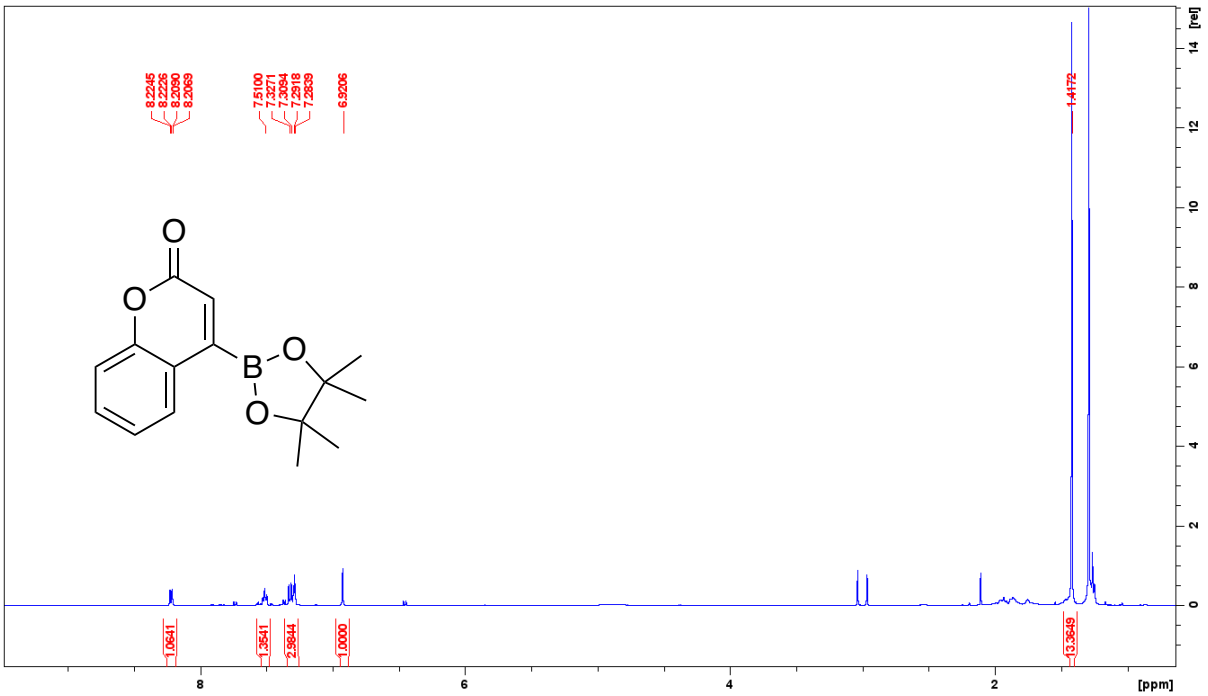

Figure B55: ^{1}H NMR spectrum (500 MHz, $CDCl_3$, 292 K) of **3i**

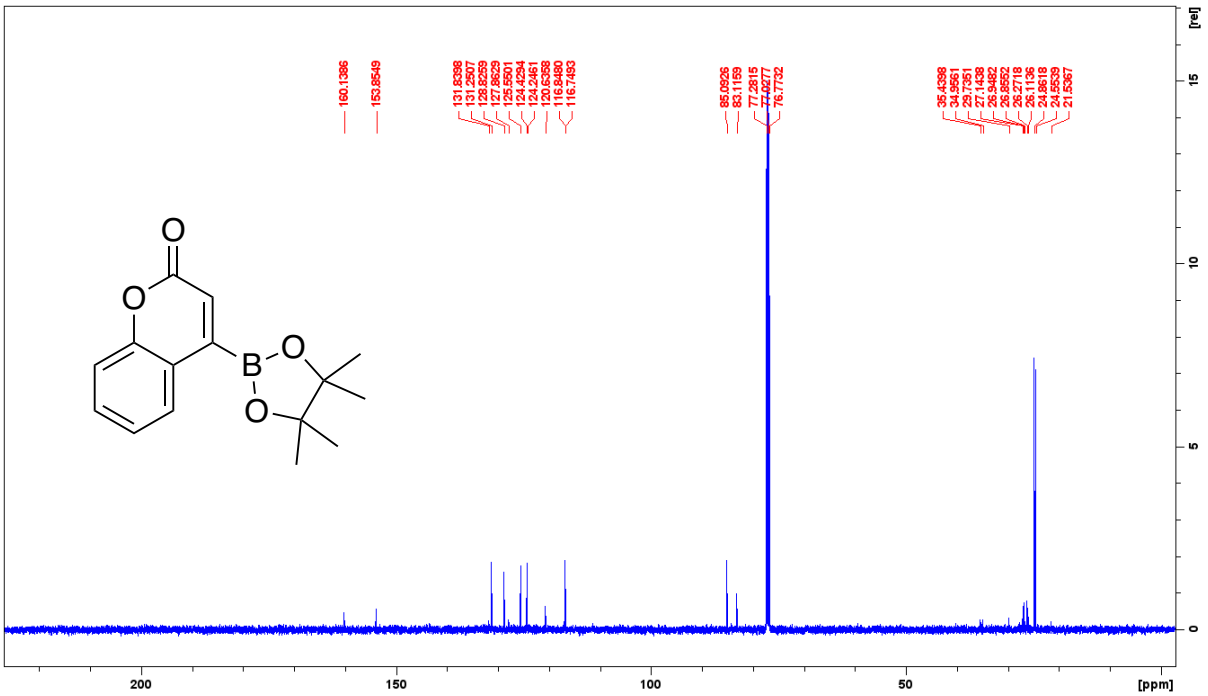

Figure B56: ^{13}C NMR spectrum (126 MHz, $CDCl_3$, 292 K) of **3i**

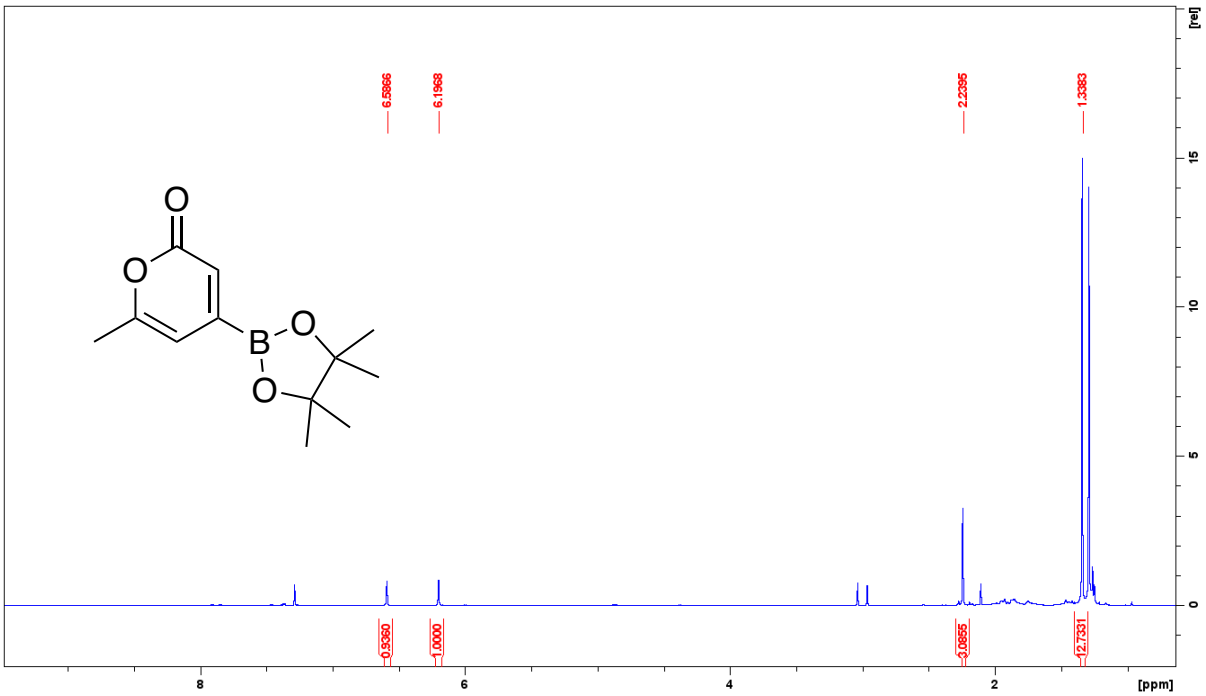

Figure B57: ^{1}H NMR spectrum (500 MHz, $CDCl_3$, 292 K) of **3j**

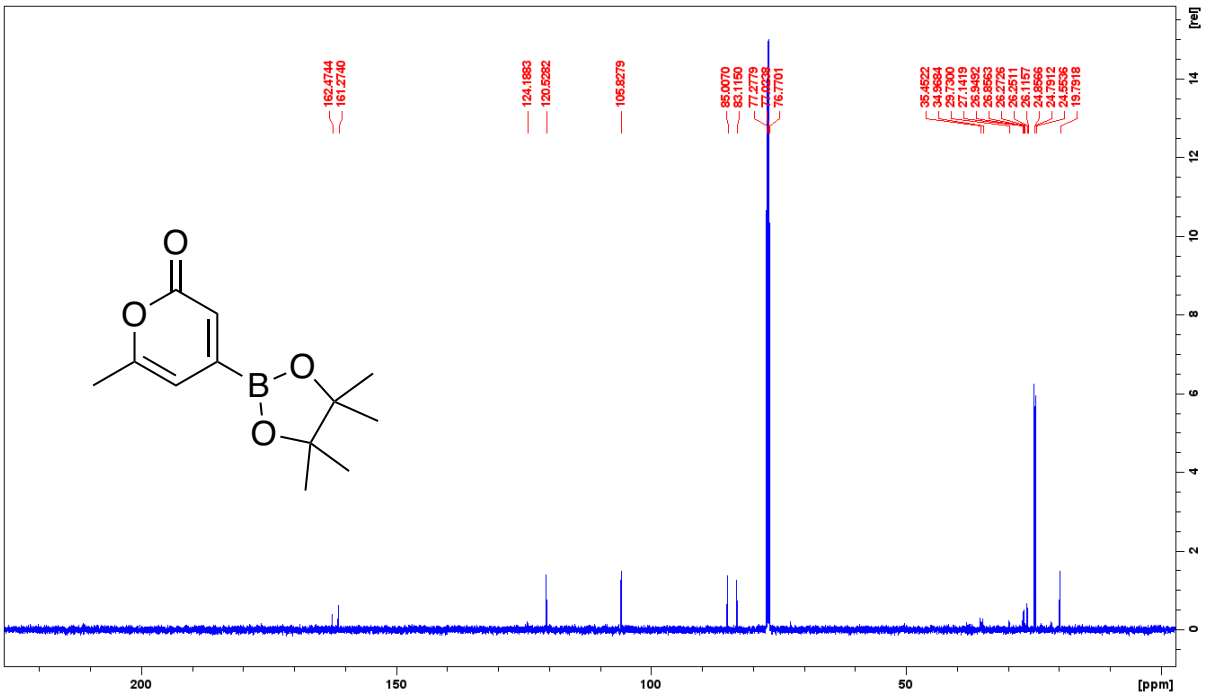

Figure B58: ^{13}C NMR spectrum (126 MHz, $CDCl_3$, 292 K) of **3j**

B4.3 Deboronated Compounds

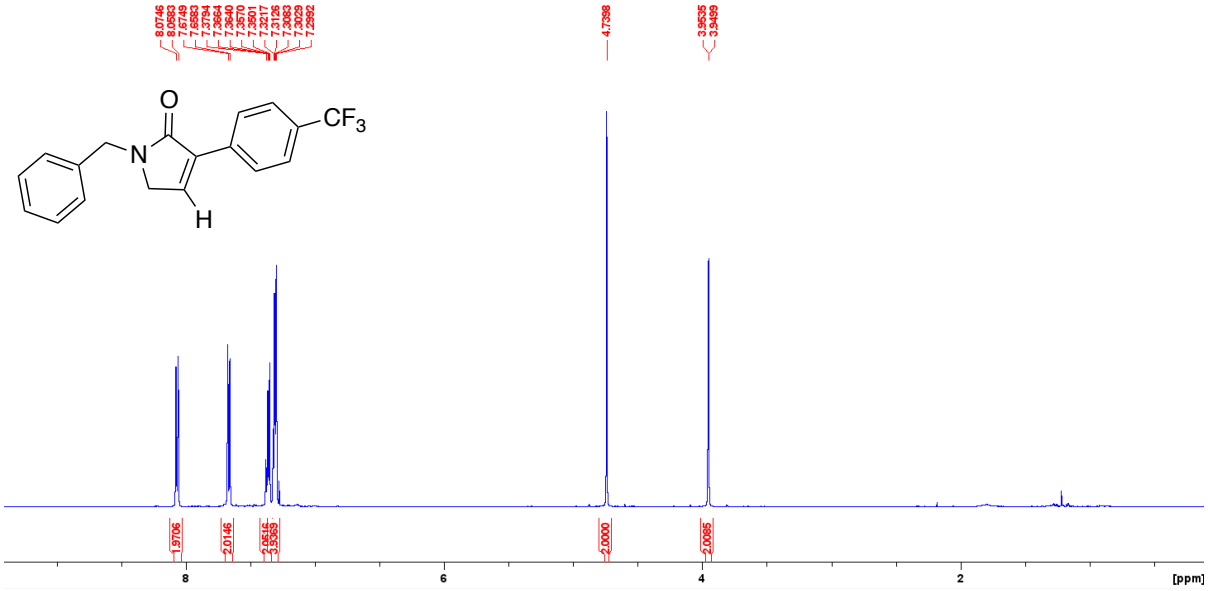

Figure B59: ^{1}H NMR spectrum (500 MHz, $CDCl_3$, 292 K) of **4f**

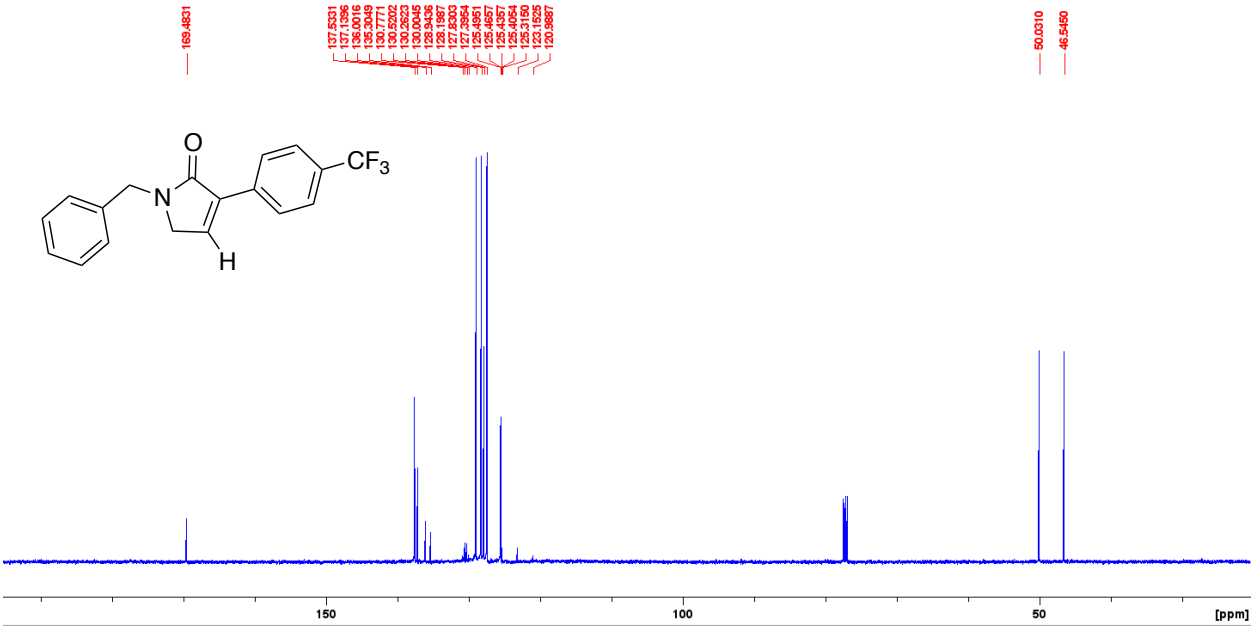

Figure B60: ^{13}C NMR spectrum (126 MHz, $CDCl_3$, 292 K) of **4f**

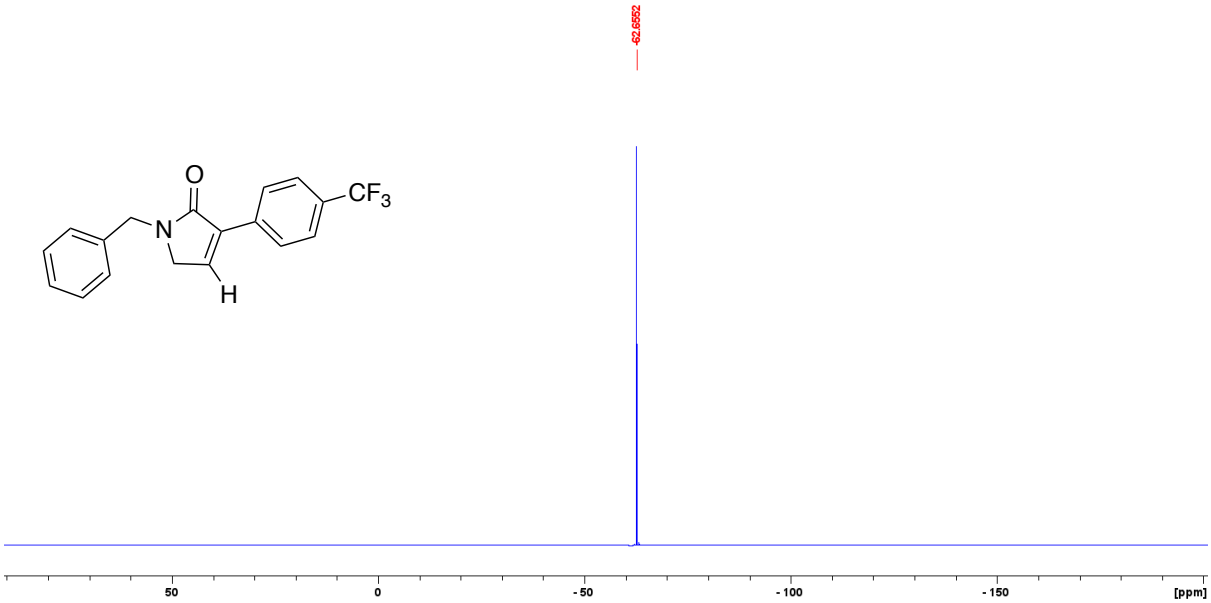

Figure B61: ^{19}F NMR spectrum (282 MHz, $CDCl_3$, 292 K) of **4f**

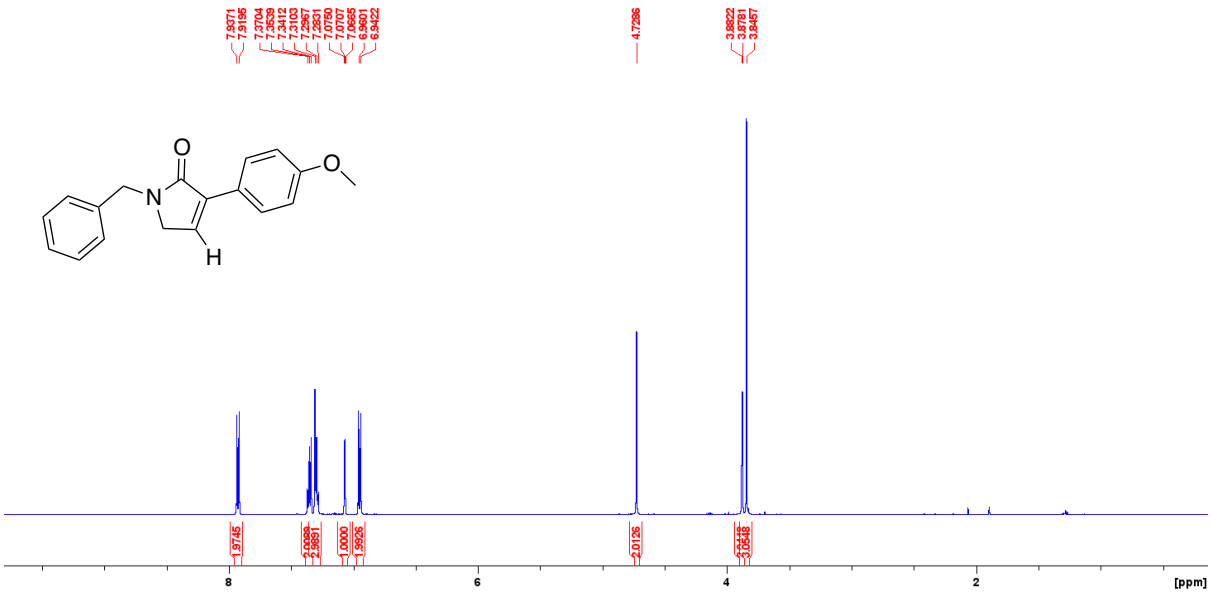

Figure B62: ^{1}H NMR spectrum (500 MHz, $CDCl_3$, 292 K) of **4g**

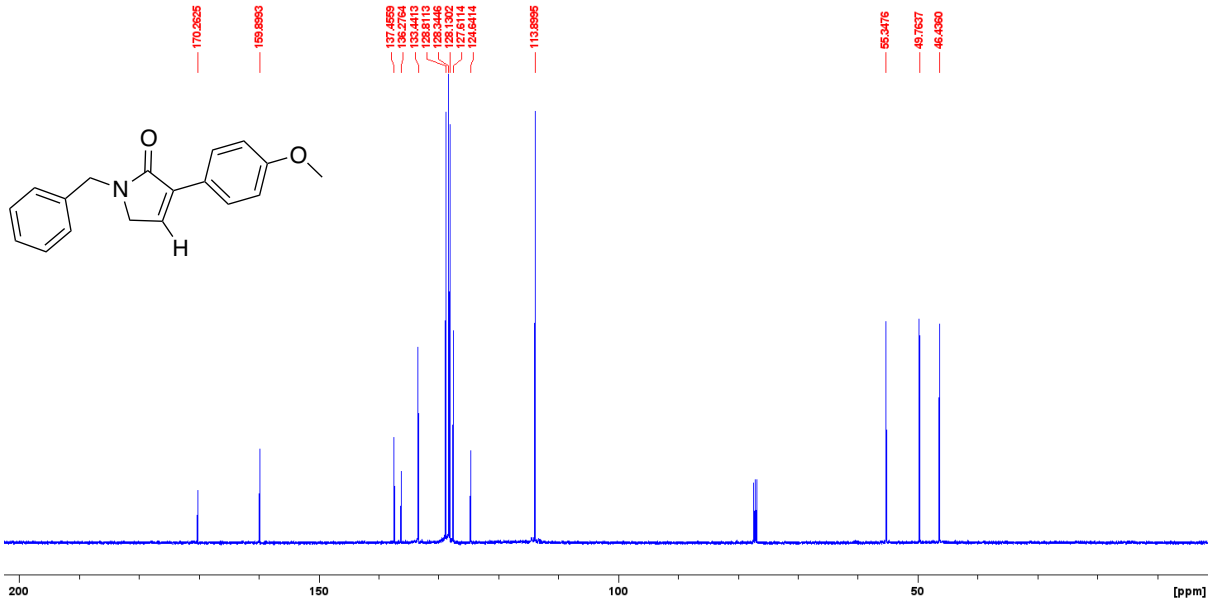

Figure B63: ^{13}C NMR spectrum (126 MHz, $CDCl_3$, 292 K) of **4g**

B4.4 Alkenyl Ethylpinacol Boronates

Alkenyl BEPin compounds were subject to column chromatography to obtain purified samples for characterization (Section B3).

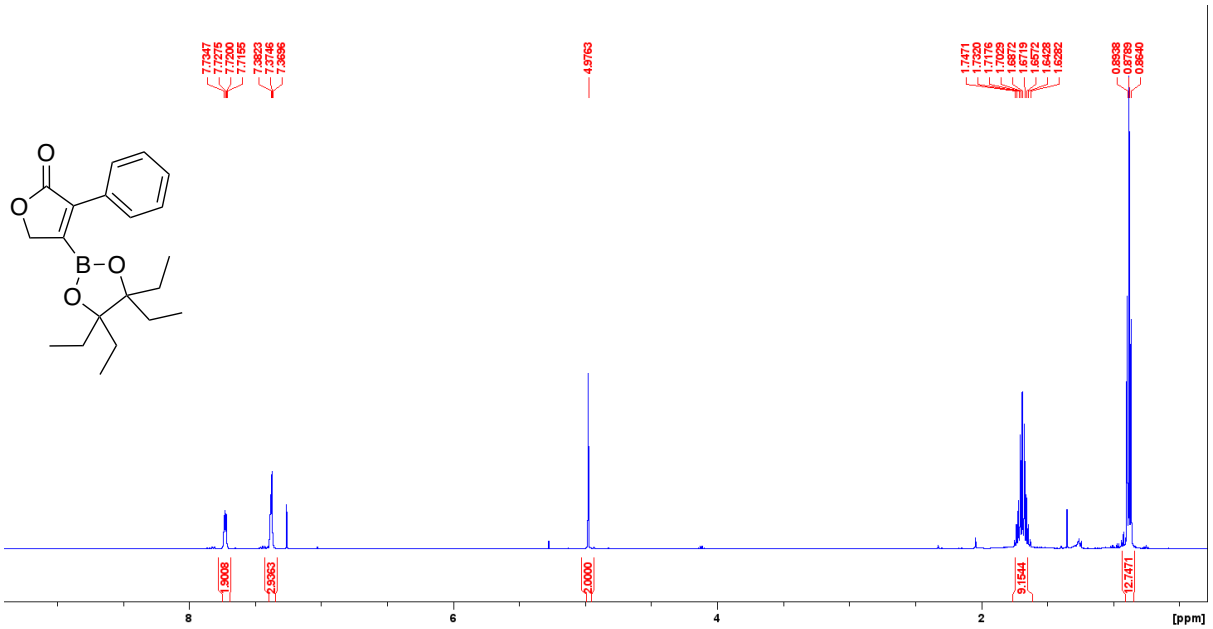

Figure B64: ^{1}H NMR spectrum (500 MHz, $CDCl_3$, 292 K) of **6b**

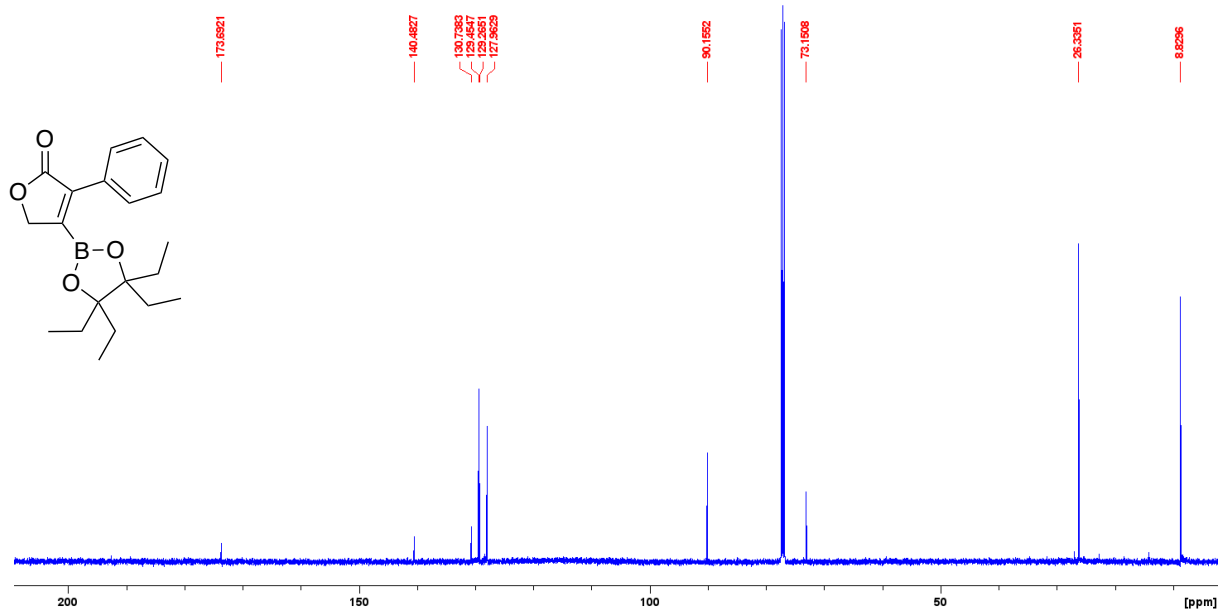

Figure B65: ^{13}C NMR spectrum (126 MHz, $CDCl_3$, 292 K) of **6b**

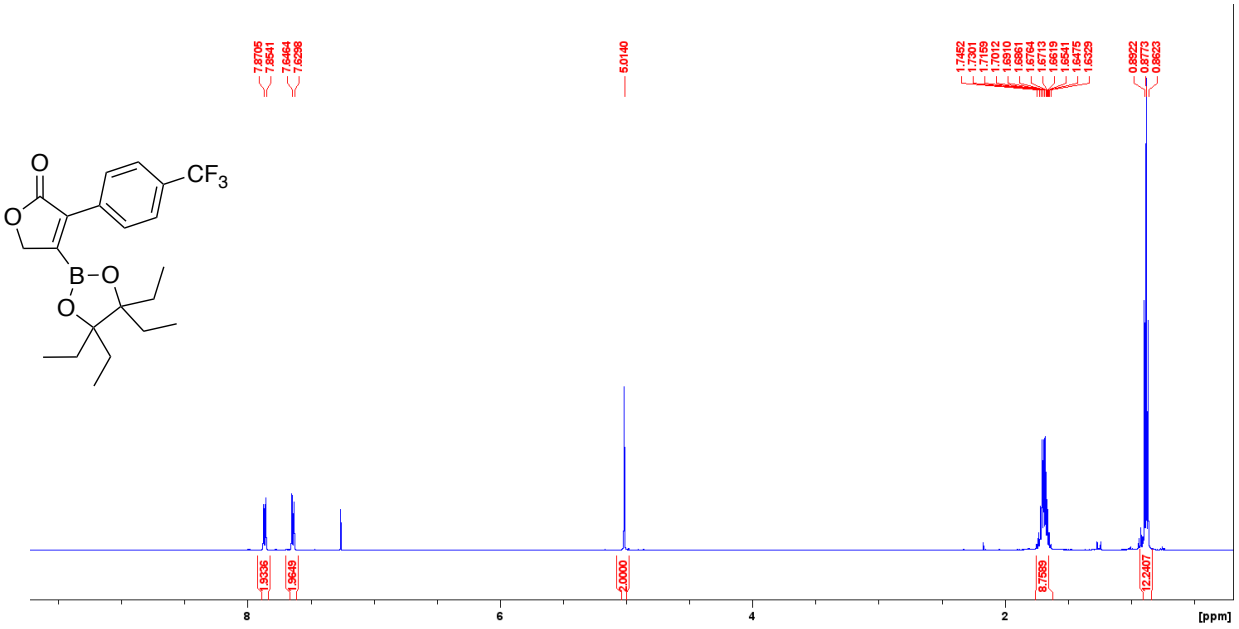

Figure B66: ^{1}H NMR spectrum (500 MHz, $CDCl_3$, 292 K) of **6c**

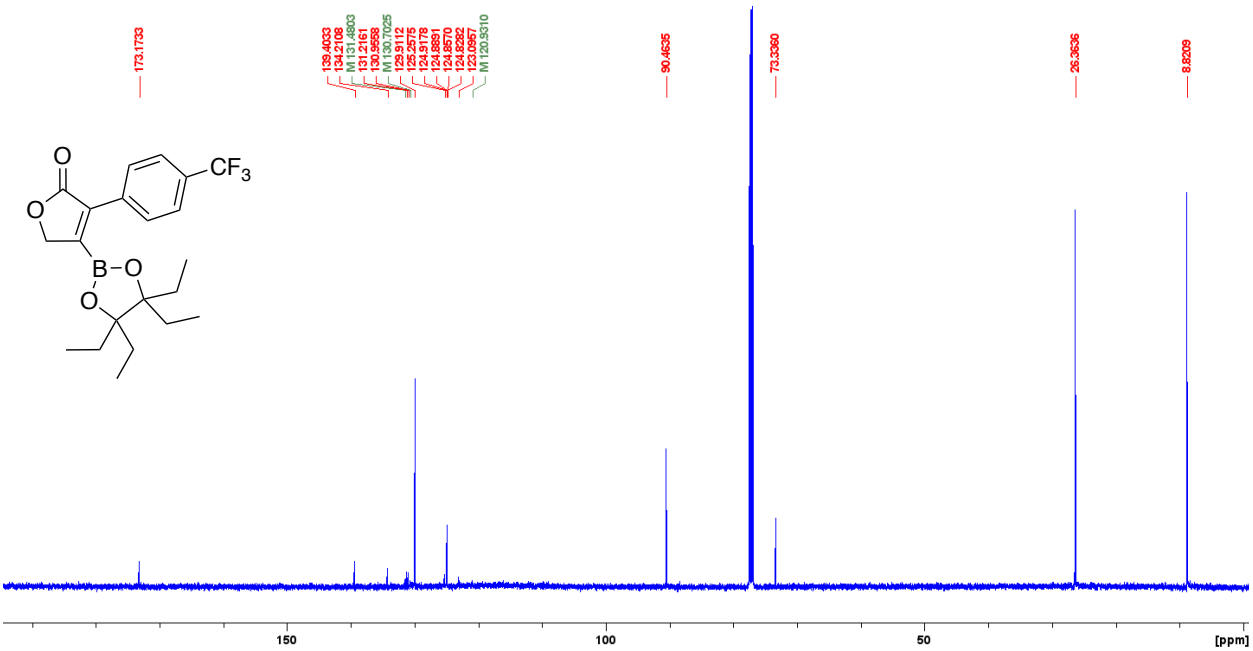

Figure B67: ^{13}C NMR spectrum (126 MHz, $CDCl_3$, 292 K) of **6c**

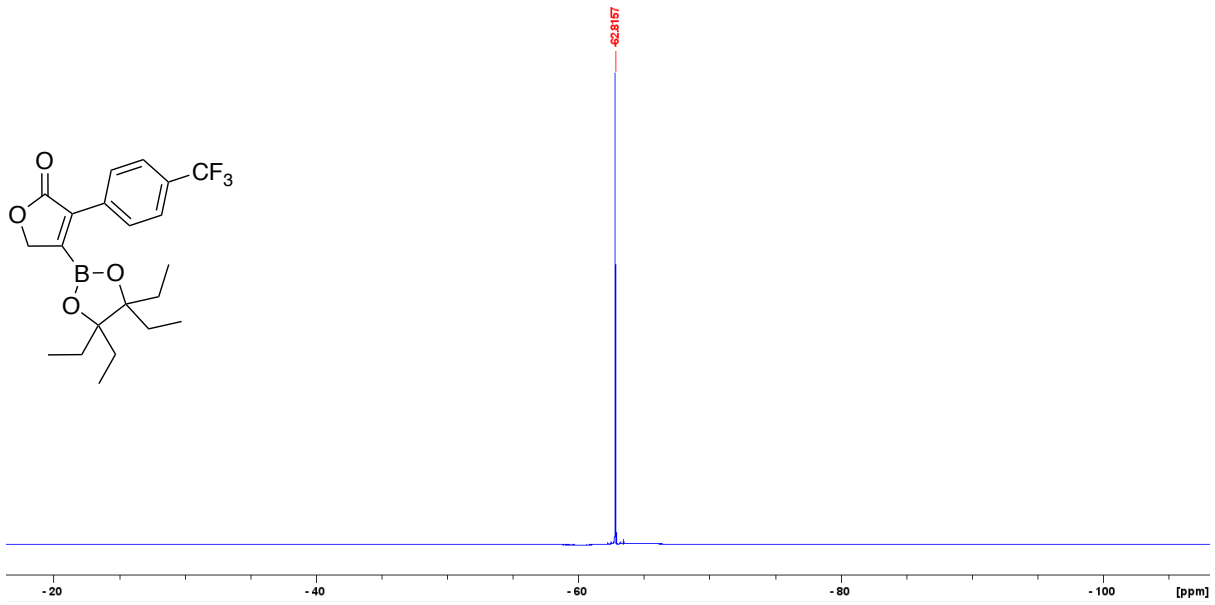

Figure B68: ^{19}F NMR spectrum (282 MHz, $CDCl_3$, 292 K) of **6c**

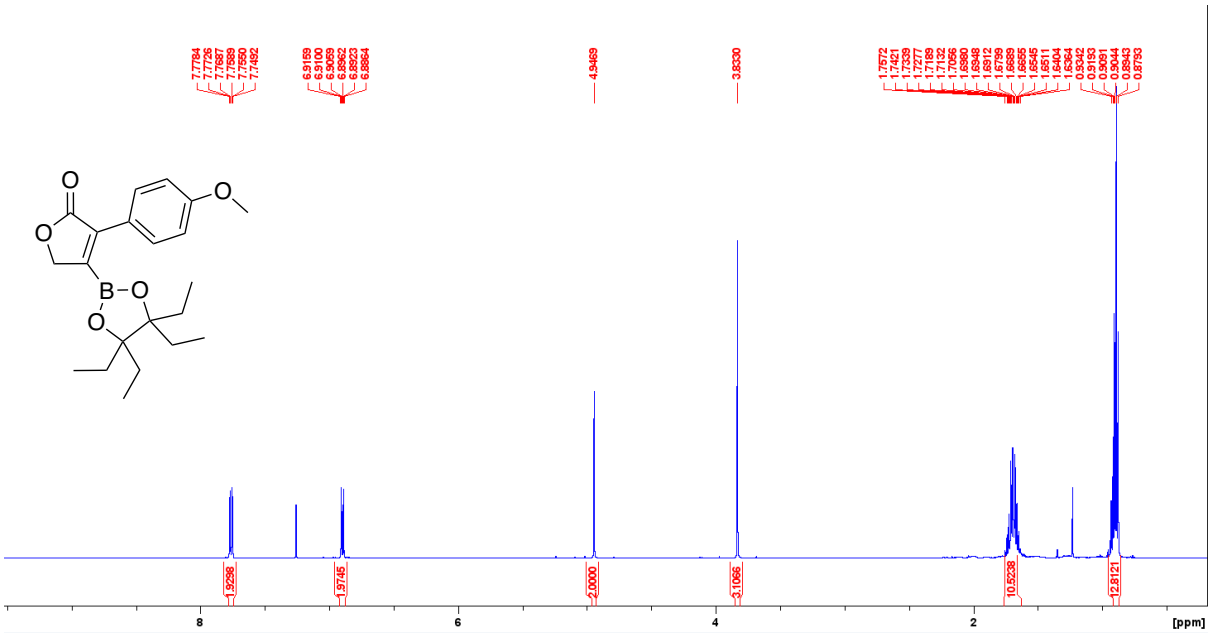

Figure B69: ^{1}H NMR spectrum (500 MHz, $CDCl_3$, 292 K) of **6d**

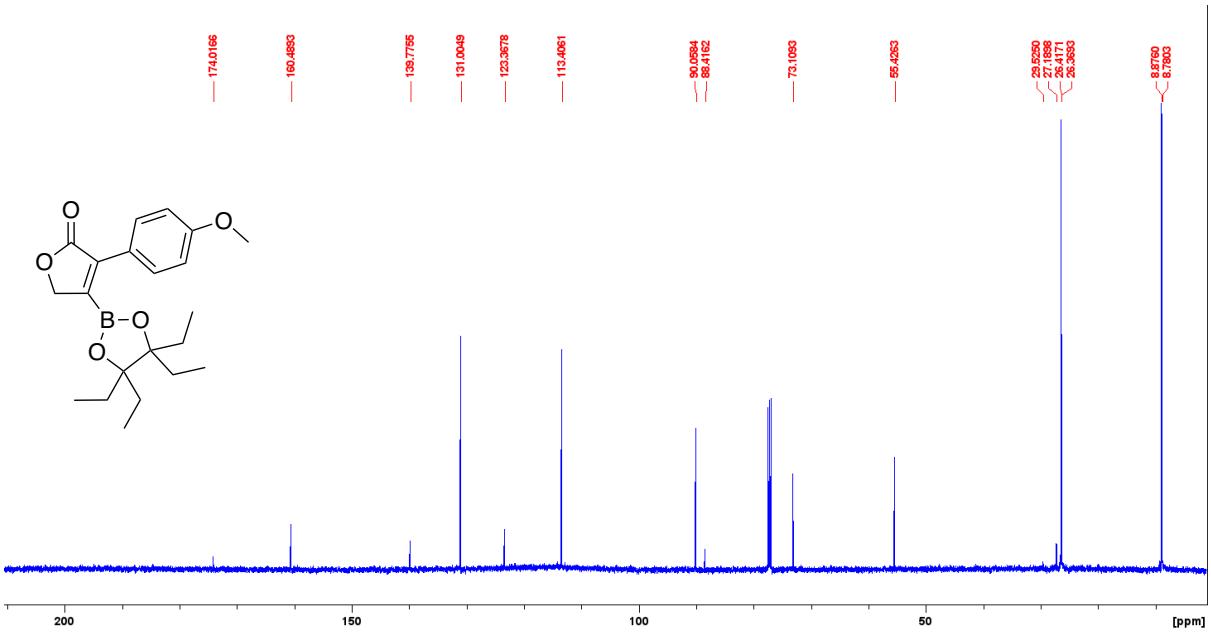

Figure B70: ^{13}C NMR spectrum (126 MHz, $CDCl_3$, 292 K) of **6d**

After borylation and column chromatography, **6e** is isolated as a mixture with **4e** in a 5.1 : 1 ratio (as well as co-eluting ethylpinacol). Efforts to purify further results in additional deboronation (increase in **4e**). **4e** characterization can be found in Section 3.6.7.

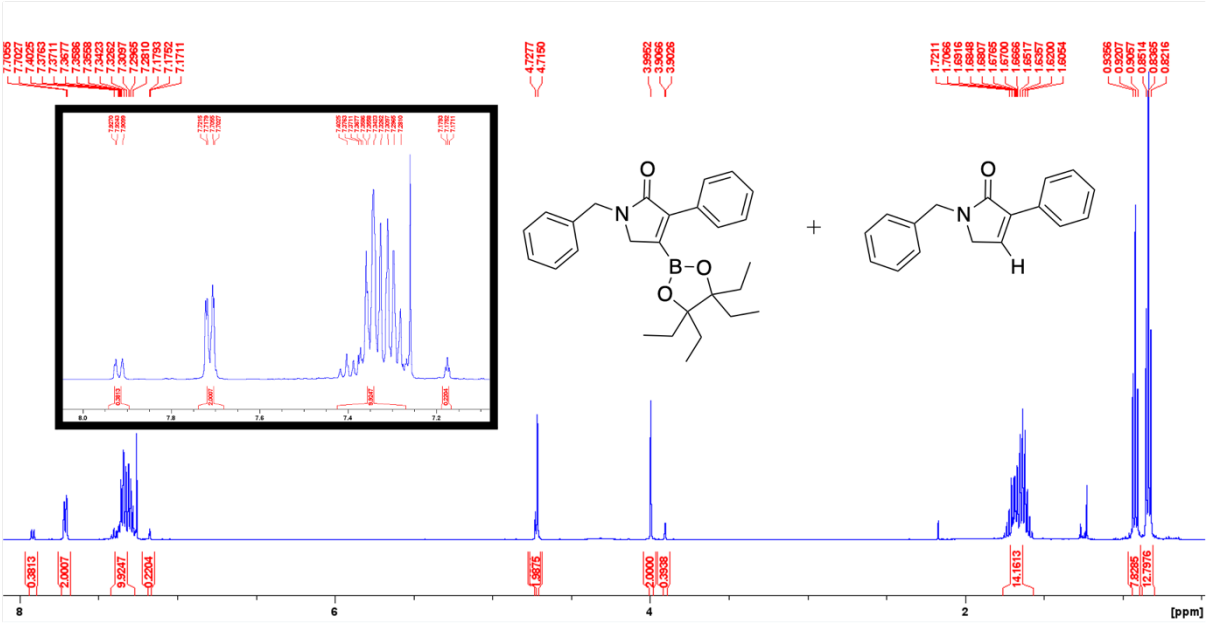

Figure B71: ^{1}H NMR spectrum (500 MHz, $CDCl_3$, 292 K) of **6e : 5e** (5.1:1)

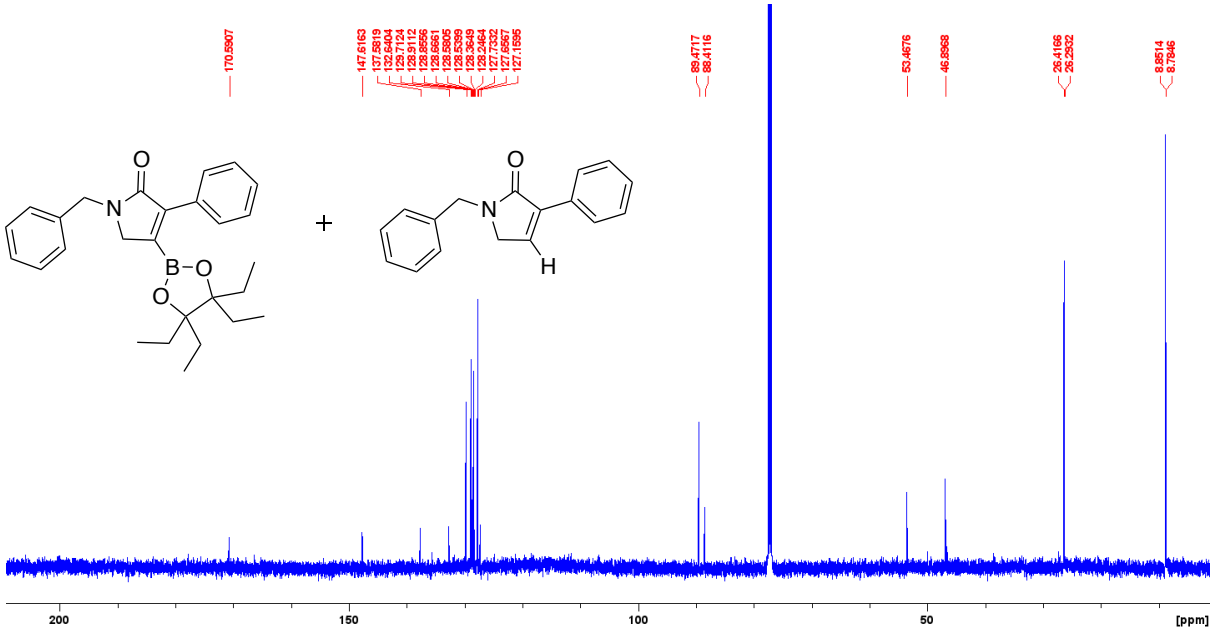

Figure B72: ^{13}C NMR spectrum (126 MHz, $CDCl_3$, 292 K) of **6e : 5e** (5.1:1)

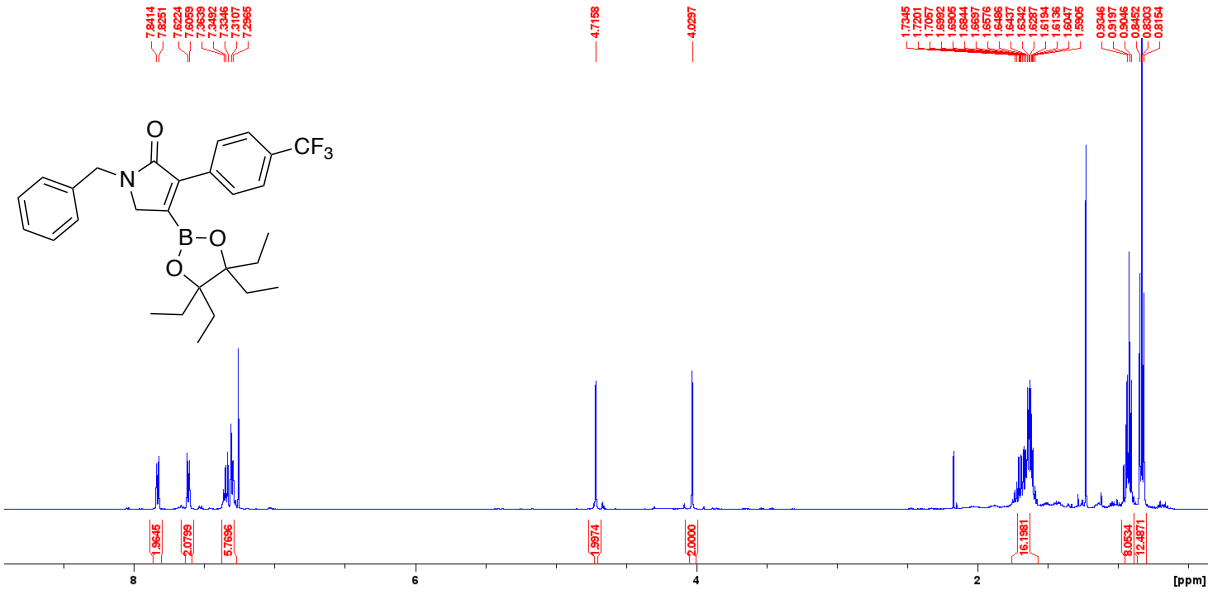

Figure B73: ^{1}H NMR spectrum (500 MHz, $CDCl_3$, 292 K) of **6f** (with co-eluting ethylpinacol)

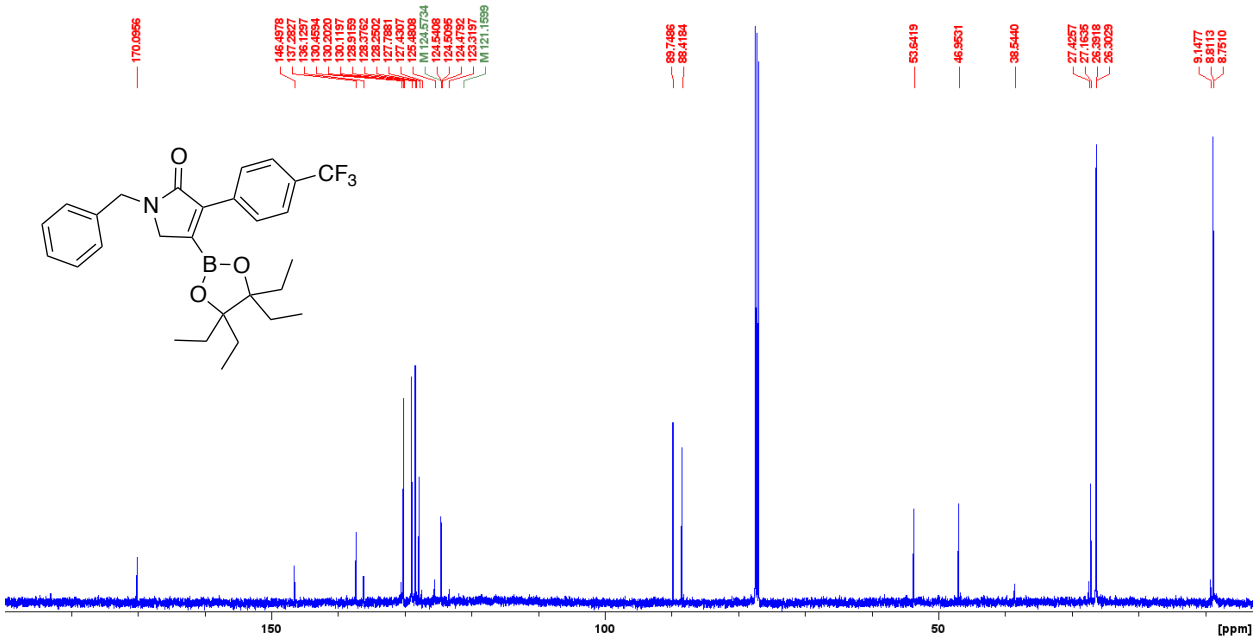

Figure B74: ^{13}C NMR spectrum (126 MHz, $CDCl_3$, 292 K) of **6f** (with co-eluting ethylpinacol)

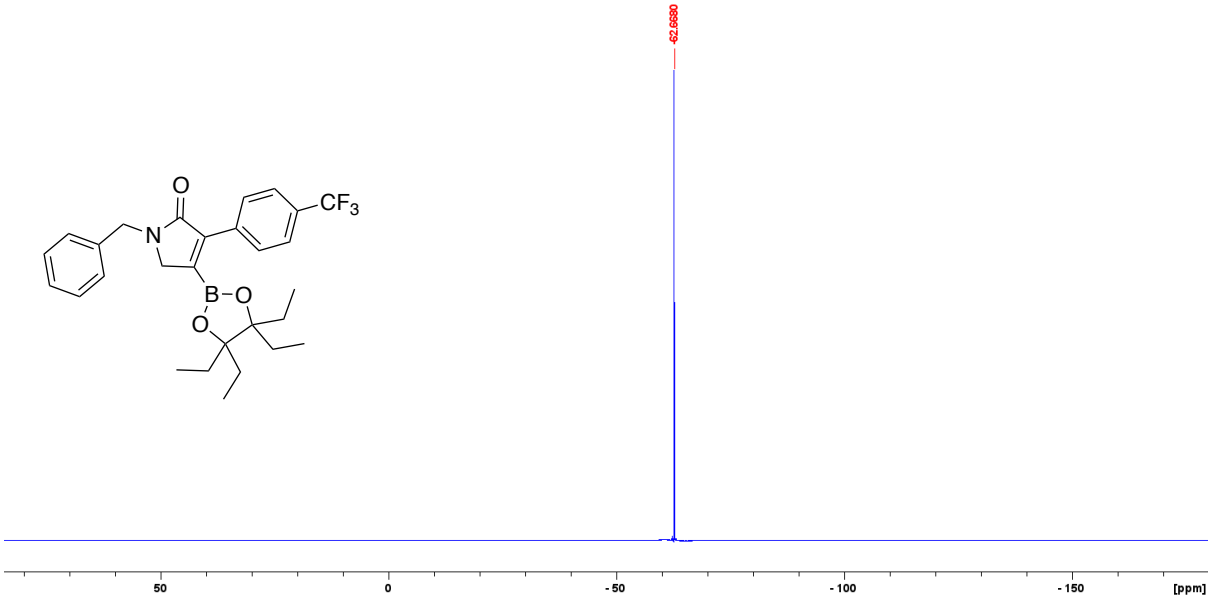

Figure B75: ^{19}F NMR spectrum of **6f** (282 MHz, $CDCl_3$, 292 K) of **6f**

After borylation and column chromatography, **6g** is isolated as a mixture with **2g** in a 7.7 : 1 ratio. Efforts to purify further results in deboronation to generate **4g**. **2g** characterization can be found in Section 3.6.3.

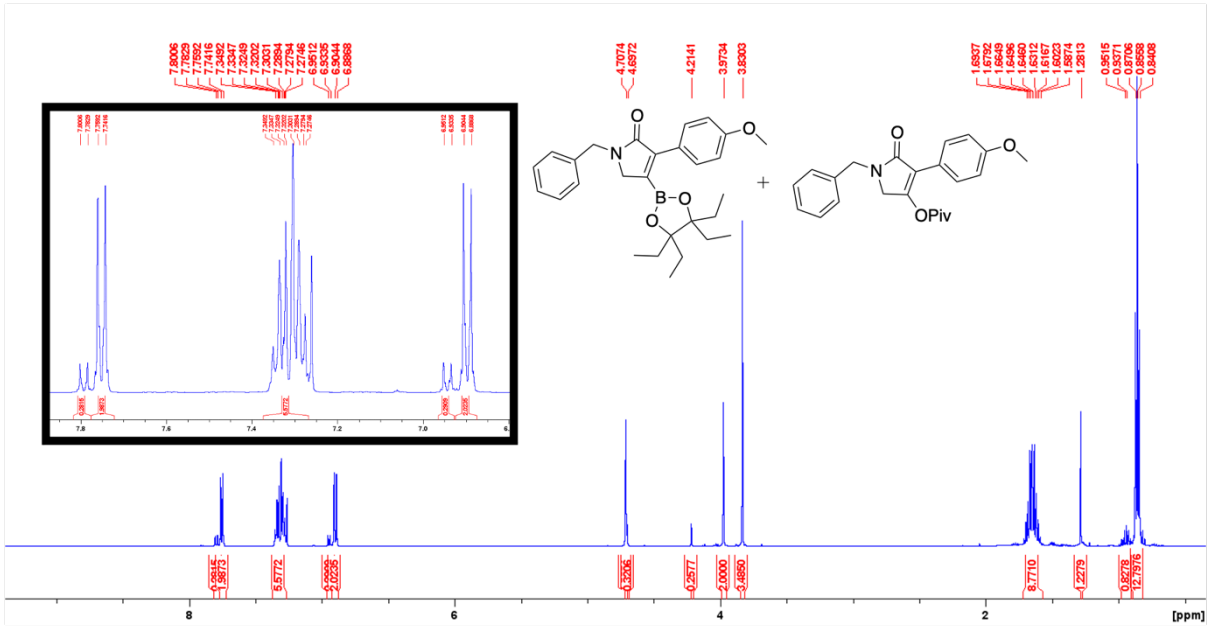

Figure B76: ^{1}H NMR spectrum (500 MHz, $CDCl_3$, 292 K) of **6g** (+ 10% **2g**)

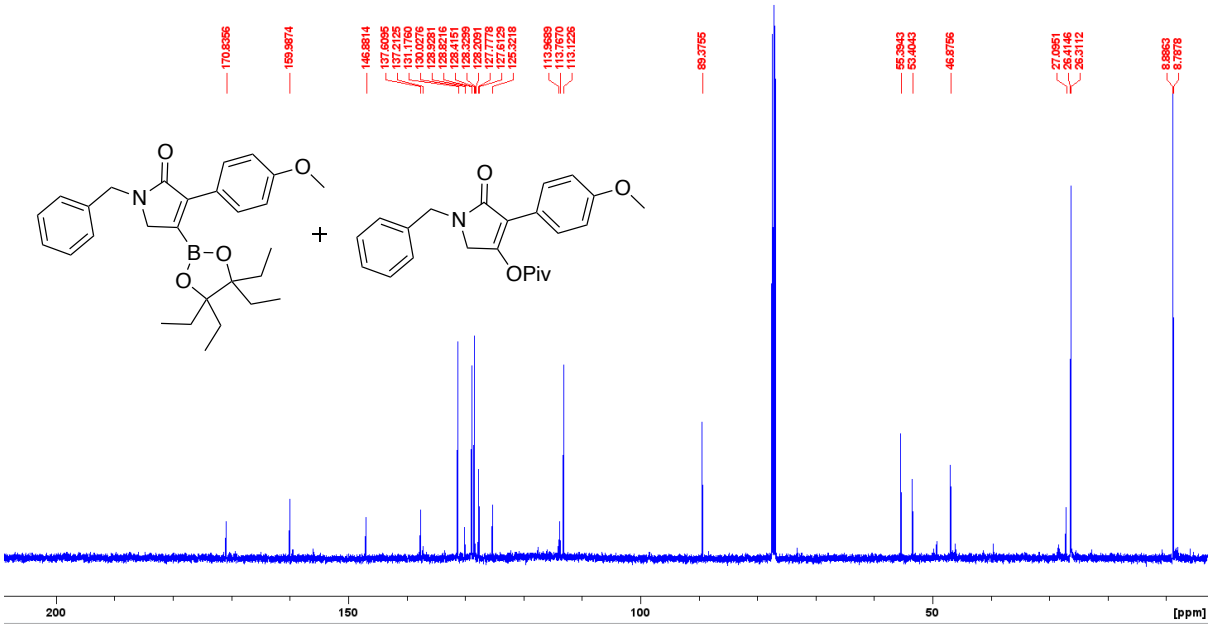

Figure B77: ^{13}C NMR spectrum (126 MHz, $CDCl_3$, 292 K) of **6g** (+ 10% **2g**)

B4.5 Suzuki Coupling Products

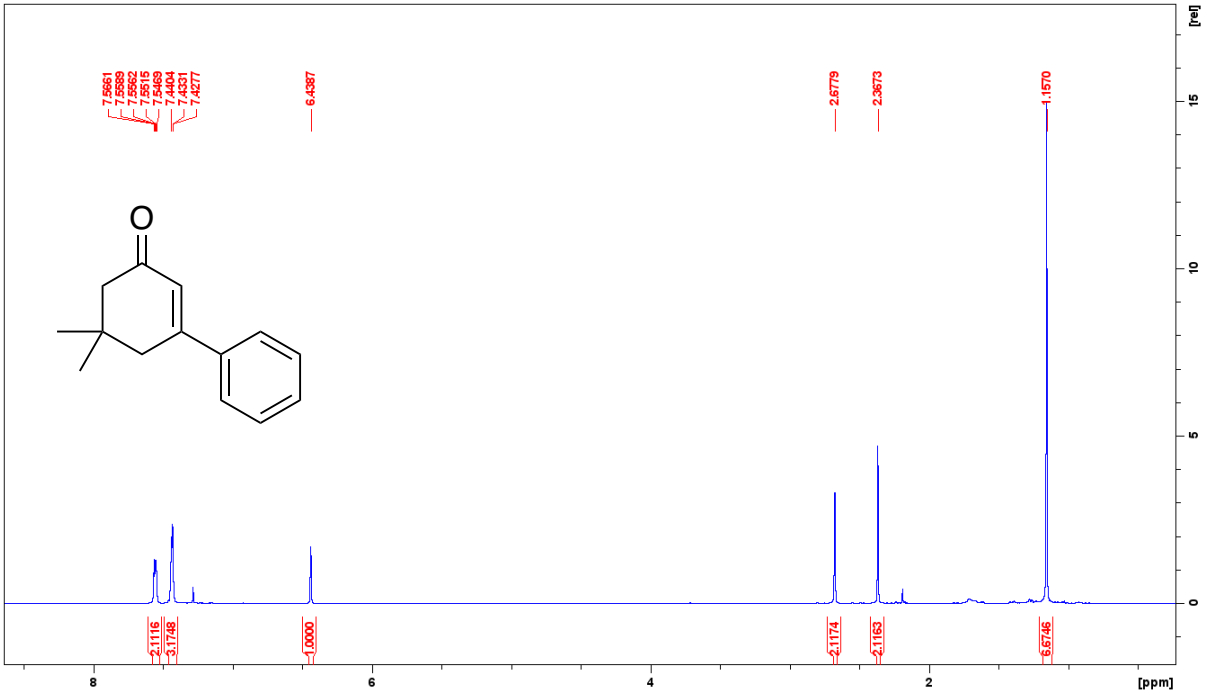

Figure B78: ^{1}H NMR spectrum (500 MHz, $CDCl_3$, 292 K) of **5a**[1]

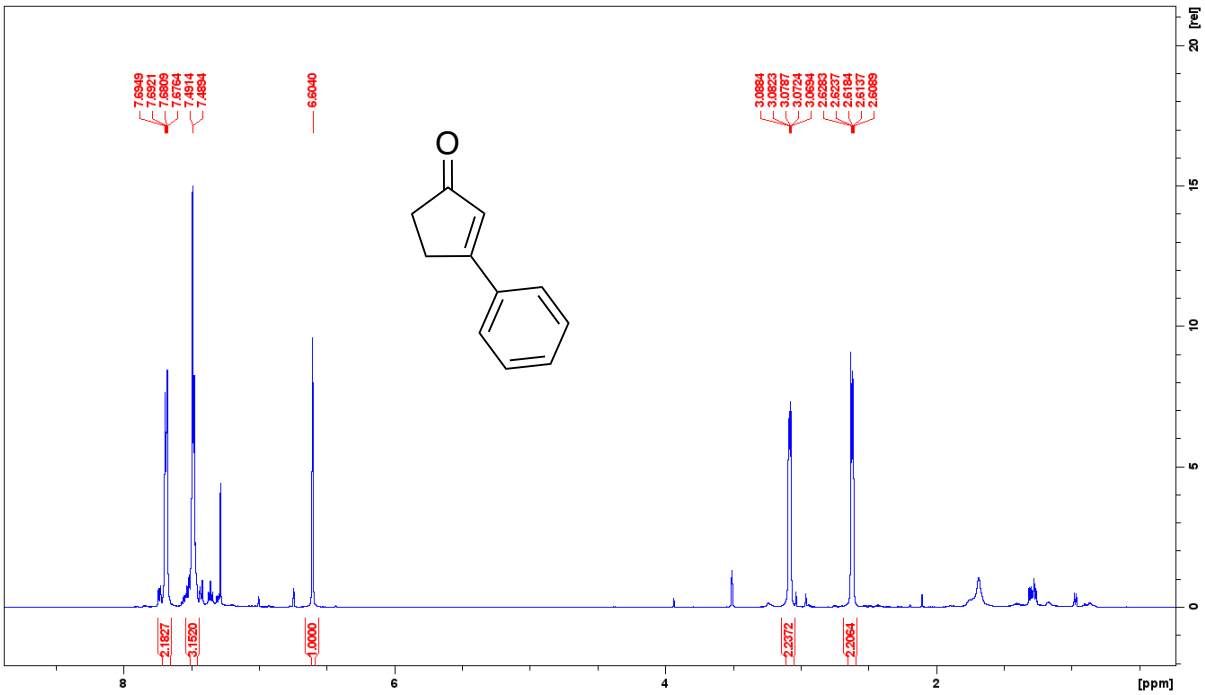

Figure B79: ^{1}H NMR spectrum (500 MHz, $CDCl_3$, 292 K) of **5h**[1]

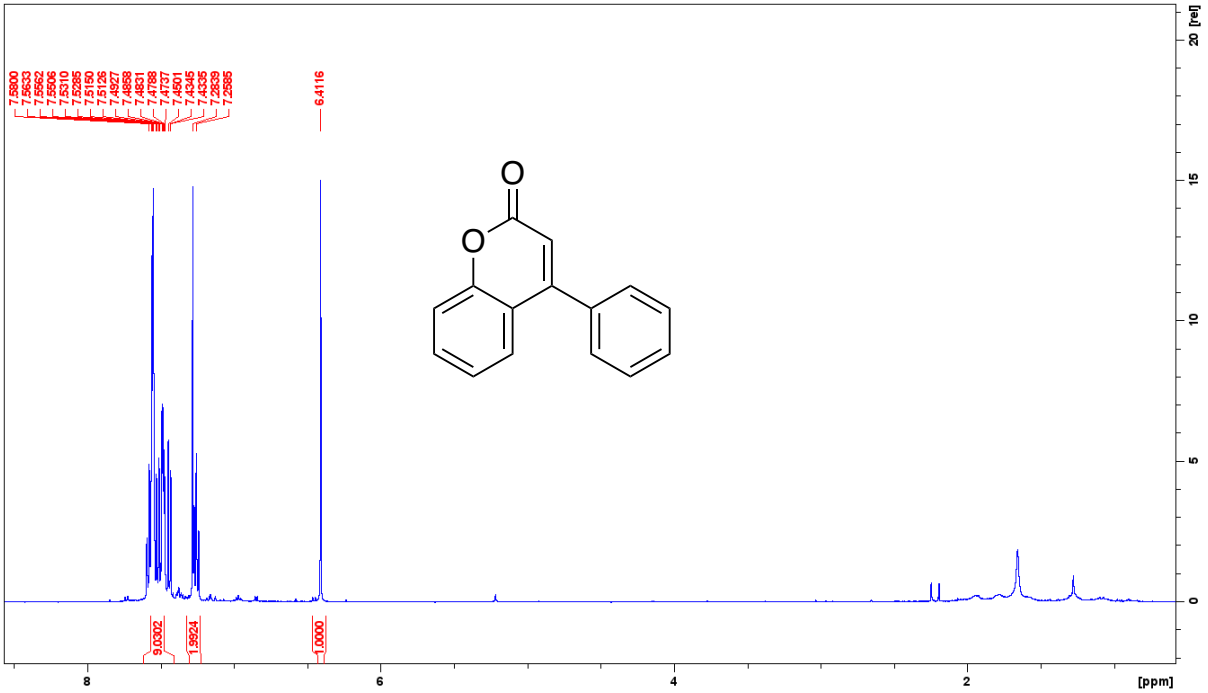

Figure B80: ^{1}H NMR spectrum (500 MHz, $CDCl_3$, 292 K) of **5i**[1]

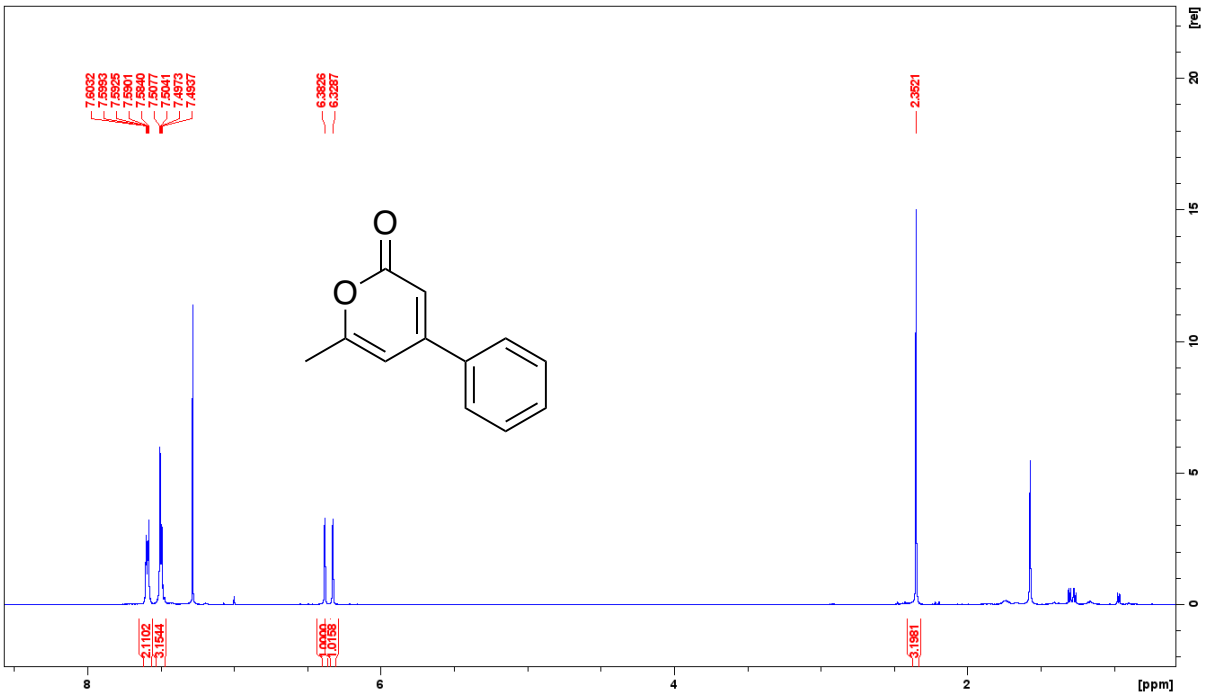

Figure B81: ^{1}H NMR spectrum (500 MHz, $CDCl_3$, 292 K) of **5j**[2]

Consistent with the ratio of **3e** to **4e** after borylation catalysis, we observe a 3.33 : 1 ratio of **5e** to **4e** after Suzuki coupling. **4e** characterization can be found in Section 3.6.7. These two compounds co-elute during column chromatography.

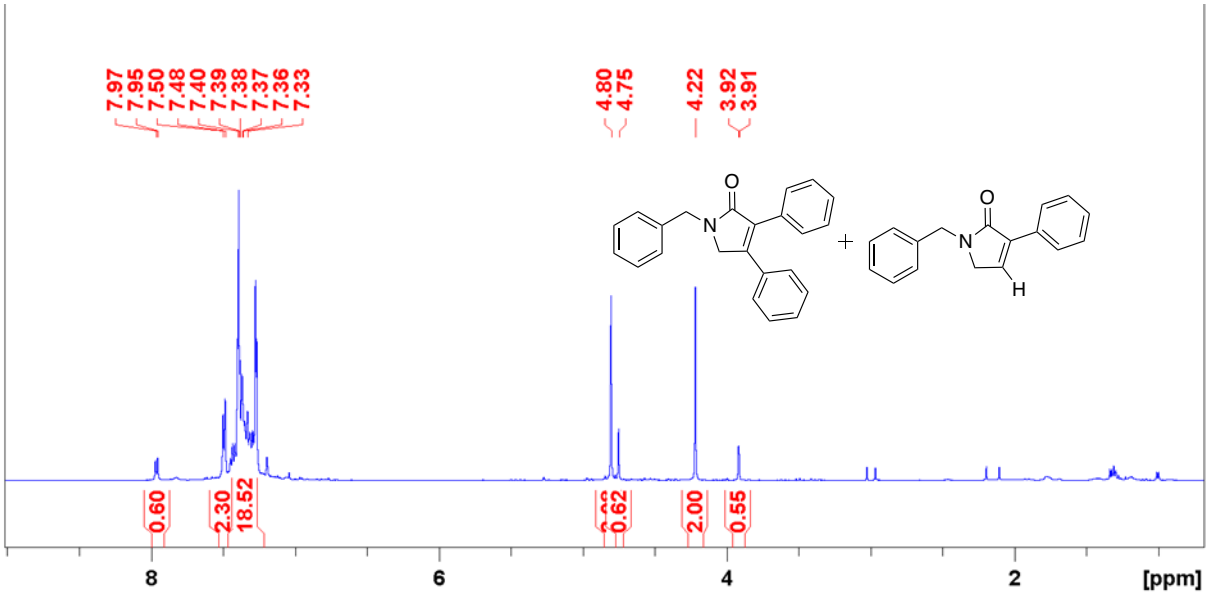

Figure B82: ^{1}H NMR spectrum (500 MHz, $CDCl_3$, 292 K) of **5e : 4e** (3.33:1)[1]

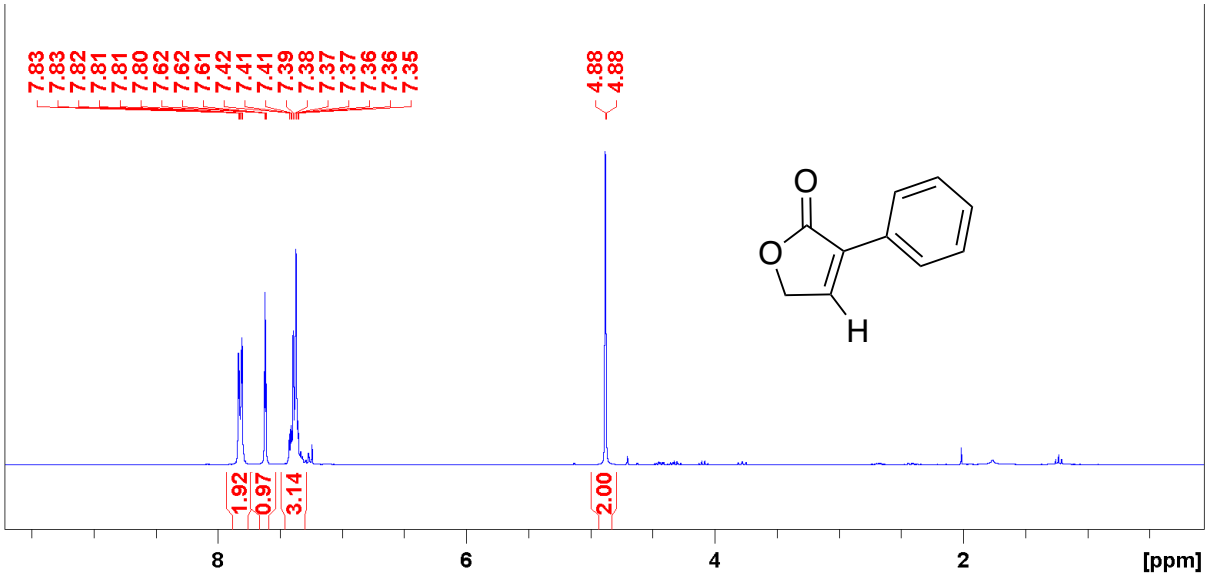

Figure B83: ^{1}H NMR spectrum (500 MHz, $CDCl_3$, 292 K) of **4b**[3]

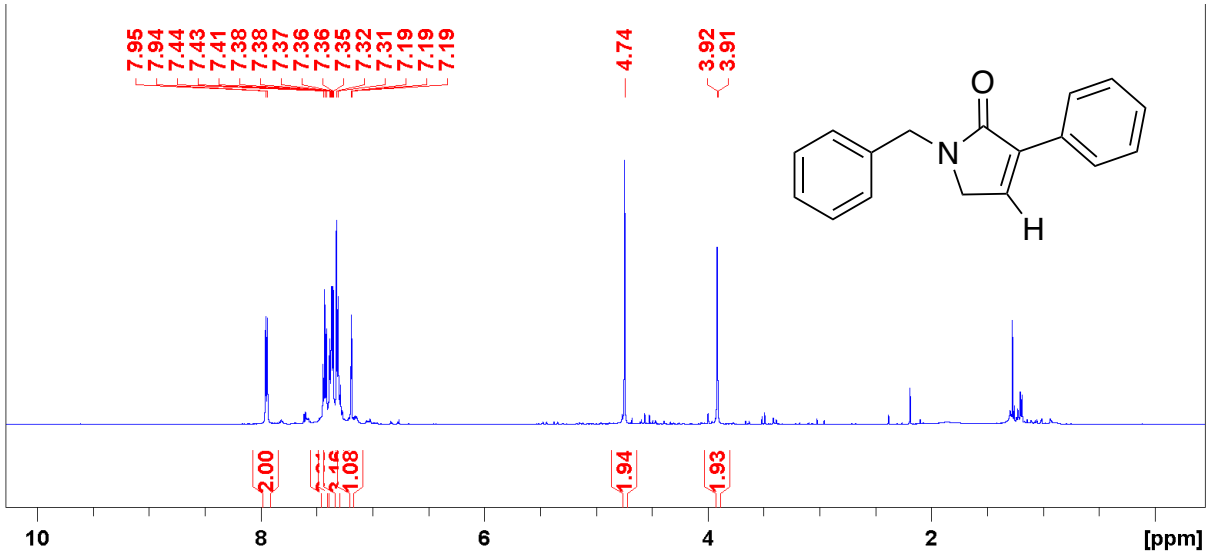

Figure B84: ^{1}H NMR spectrum (500 MHz, $CDCl_3$, 292 K) of **4e**[4]

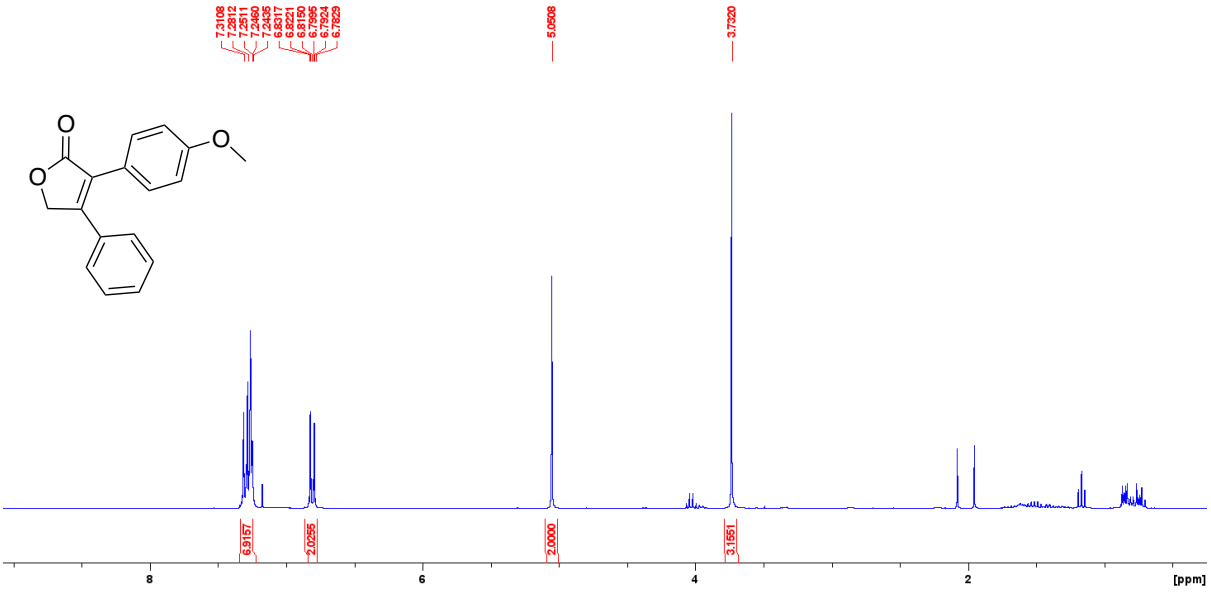

Figure B85: Representative ^{1}H NMR spectrum (500 MHz, $CDCl_3$, 292 K) of **5d**[5]

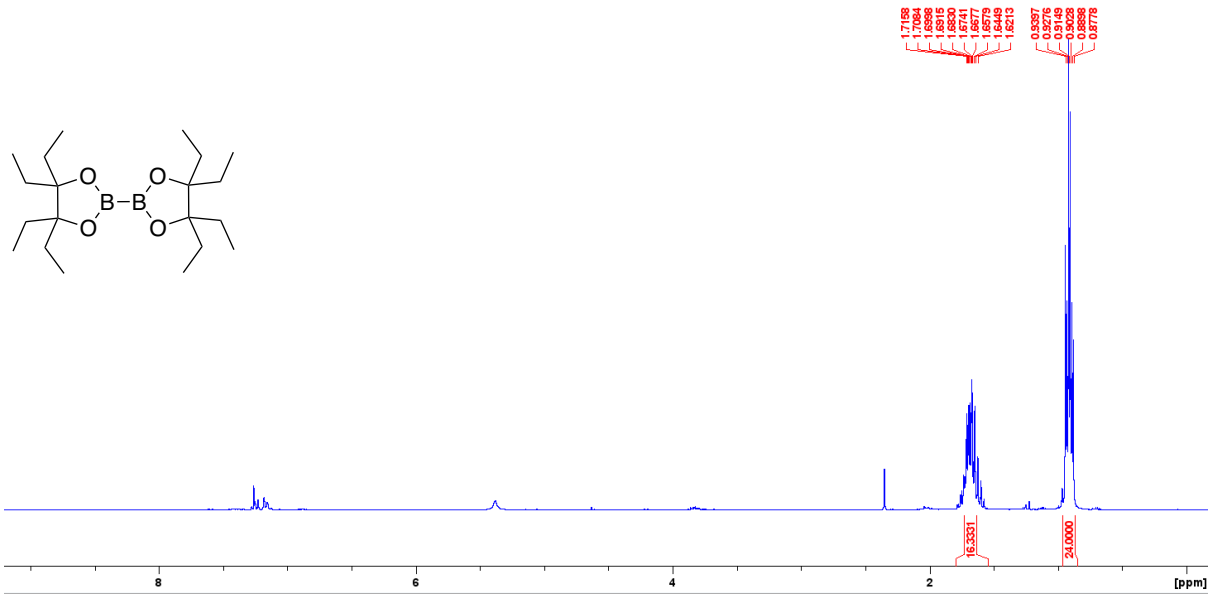

Figure B86: Representative ^{1}H NMR spectrum (500 MHz, $CDCl_3$, 292 K) of **recovered B_2EPin_2 post reaction**

B5 References

(1) Becica, J.; Heath, O. R. J.; Zheng, C. H. M.; Leitch, D. C. Palladium-Catalyzed Cross-Coupling of Alkenyl Carboxylates. *Angew. Chem. Int. Ed.* **2020**, *59* (39), 17277–17281. https://doi.org/10.1002/anie.202006586.

(2) Hu, Y.; Ding, Q.; Ye, S.; Peng, Y.; Wu, J. Rapid Access to 4-Substituted-Pyrones and 2(5H)-Furanones via a Palladium-Catalyzed C–OH Bond Activation. *Tetrahedron* **2011**, *67* (38), 7258–7262. https://doi.org/10.1016/j.tet.2011.07.048.

(3) Aubert, S.; Katsina, T.; Arseniyadis, S. A Sequential Pd-AAA/Cross-Metathesis/Cope Rearrangement Strategy for the Stereoselective Synthesis of Chiral Butenolides. *Org. Lett.* **2019**, *21* (7), 2231–2235. https://doi.org/10.1021/acs.orglett.9b00521.

(4) Xie, J.; Xue, S.; Escudero-Adán, E. C.; Kleij, A. W. Domino Synthesis of α,β-Unsaturated γ-Lactams by Stereoselective Amination of α-Tertiary Allylic Alcohols. *Angew. Chem. Int. Ed.* **2018**, *57* (51), 16727–16731. https://doi.org/10.1002/anie.201810160.

(5) Kang, Y.; Zhang, W.; Wang, T.; Liang, Y.; Zhang, Z. Two-Step Synthesis of π-Expanded Maleimides from 3,4-Diphenylfuran-2(5H)-Ones. *J. Org. Chem.* **2019**, *84* (19), 12387–12398. https://doi.org/10.1021/acs.joc.9b01792.

Appendix C: The Development of Novel Cross-Coupling Scaffolds for C–O Activation Chemistry – Supplementary Material

C1. General Information

Caution: This procedure requires very high temperatures, please refrain from using oil-based heating as the temperatures required for this reaction exceed the flash point of standard oil-based heating mediums.

All reactions were performed using standard Schlenk techniques under N_2. All starting materials were purchased from commercial suppliers and used without further purification. All NMR spectra were acquired on either a Bruker AVANCE 300 MHz spectrometer or a Bruker AVANCE Neo 500 MHz spectrometer. All ^{1}H and ^{13}C NMR chemical shifts are calibrated to residual protio-solvents. All NMR spectroscopic data is processed using Bruker TopSpin 4.10. High-resolution mass spectrometry (HRMS) were obtained using a Bruker maXis Impact Quadrupole Time-of-Flight LC/MS System, or Thermo Scientific Ultimate 3000 ESI-Orbitrap Exactive Plus.

C2. Reaction Optimization:

C2.1 Atmosphere Optimization:

In two separate round-bottom flasks, 2-aminopyridine (1 equiv) was suspended in diethyl malonate (5 equiv). One flask was exposed to air while the other was under inert N_2 atmosphere using standard Schlenk techniques. The solutions were brought up to reflux using an aluminum heat block (T_{block} = 230 °C) and left to stir for 18 h. Excess diethyl malonate was removed via distillation to obtain the crude solid which was suspended in hot hexanes, this was then filtered, and washed with diethyl ether to yield the cyclized product.

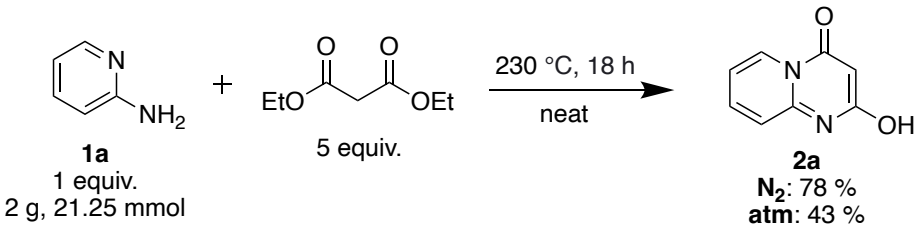

Figure C1: Reaction dependence on atmosphere

C2.2 Temperature Optimization with Method A:

A round-bottom flask (RBF) was charged with diethyl malonate (2.5 equiv) and a (substituted) 2-aminopyridine (1 equiv). The reaction was left to stir overnight at 140 °C for 24 h. The mixture was then cooled to room temperature and purified via flash chromatography. Diphenyl ether (0.5 M) was then charged into an RBF along with the intermediate product to stir at 160 °C for 24 h. In increments of 10 °C every 24 h, temperature was increased until product was formed. Yield was determined by ^{1}H-NMR in d-dmso.

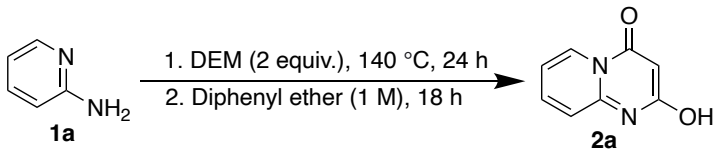

Temp / °C	Yield **2a**
160	0
170	0
180	0
190	0
200	31

Figure C2: Temperature optimization of Method A

C3. General Reaction and Diethyl Malonate

C3.1 General Reaction:

A round bottom flask is charged with diethyl malonate (5 equiv) and the desired 2-aminopyridine derivative (1 equiv – see Figure C6 for all attempted starting materials). A condenser fitted to an N_2 line was attached to the reaction flask. The reaction mixture was then brought to reflux using an aluminum heat block (T_{block} = 230 °C) and stirred for 3 h. At this point, the condenser was replaced with a distillation apparatus, and excess diethyl malonate was distilled from the flask at ambient pressure. The reaction mixture was then allowed to cool to room temperature before the residual solid was suspended in refluxing hexanes for 1-18 h.* The resulting solid was filtered, washed with diethyl ether, and dried *in vacuo*, giving the desired 2-hydroxy-PPD product as a solid. All NMR spectroscopy was conducted in d-DMSO.

**Reactions were refluxed in hexanes for 1 hour, except when the reaction mixture solidified into one solid mass. In these cases, the reaction was left to stir vigorously for up to 18 h until a suspension was obtained.*

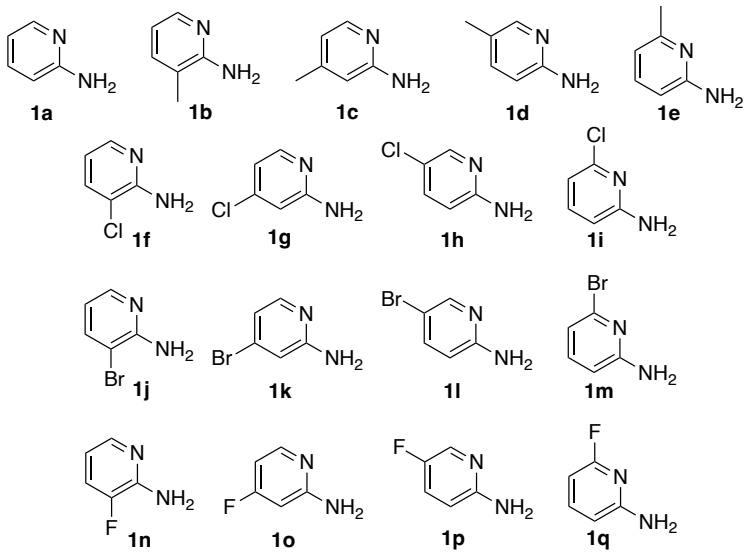

Figure C3: All attempted (substituted) 2-aminopyridines

Any successful reported ^{13}C spectra were obtained using a Bruker AVANCE Neo 500 MHz spectrometer. UDEFT experiments were used with number of scans (ns) exceeding 2000, and J-coupling between C and H (CNST2) set to 160.

C3.2 Recycling Diethyl Malonate:

Excess diethyl malonate is distilled during the above general reaction procedure. This diethyl malonate was collected and used instead of fresh starting material in the same general reaction procedure (see Figure C7).

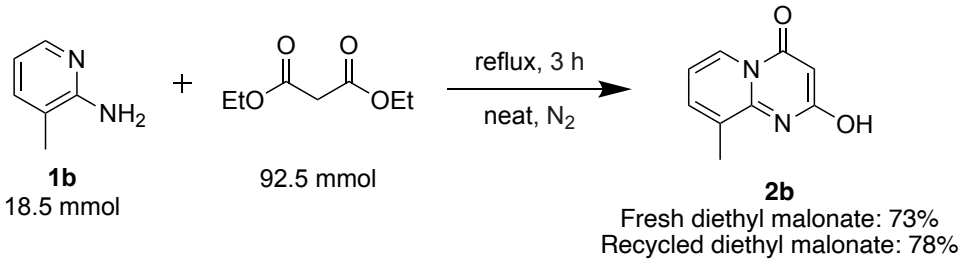

1b
18.5 mmol

92.5 mmol

2b
Fresh diethyl malonate: 73%
Recycled diethyl malonate: 78%

Figure C4: Reaction yield using fresh and recycled diethyl malonate

C4. PPD Characterization Data (^{1}H, ^{13}C, and ^{19}F NMR)

2a 2-hydroxy-4H-pyrido[1,2-a]pyrimidin-4-one

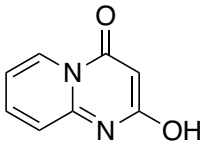

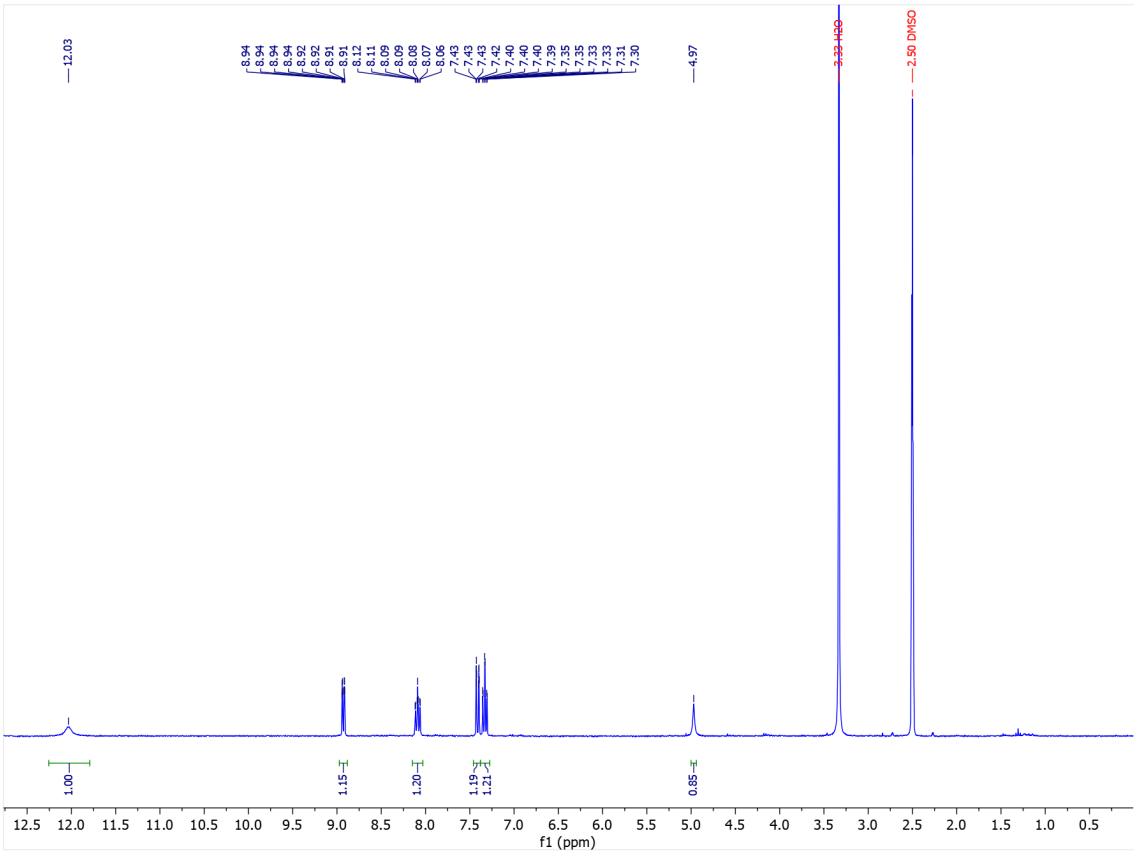

Figure C5: ^{1}H NMR spectrum (300 MHz, $(CD_3)_2SO$, 292 K) of **2a**: **2-hydroxy-4*H*-pyrido[1,2-*a*]pyrimidin-4-one**

2b 2-hydroxy-9-methyl-4H-pyrido[1,2-a]pyrimidin-4-one

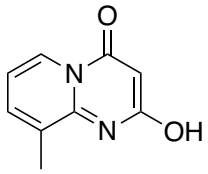

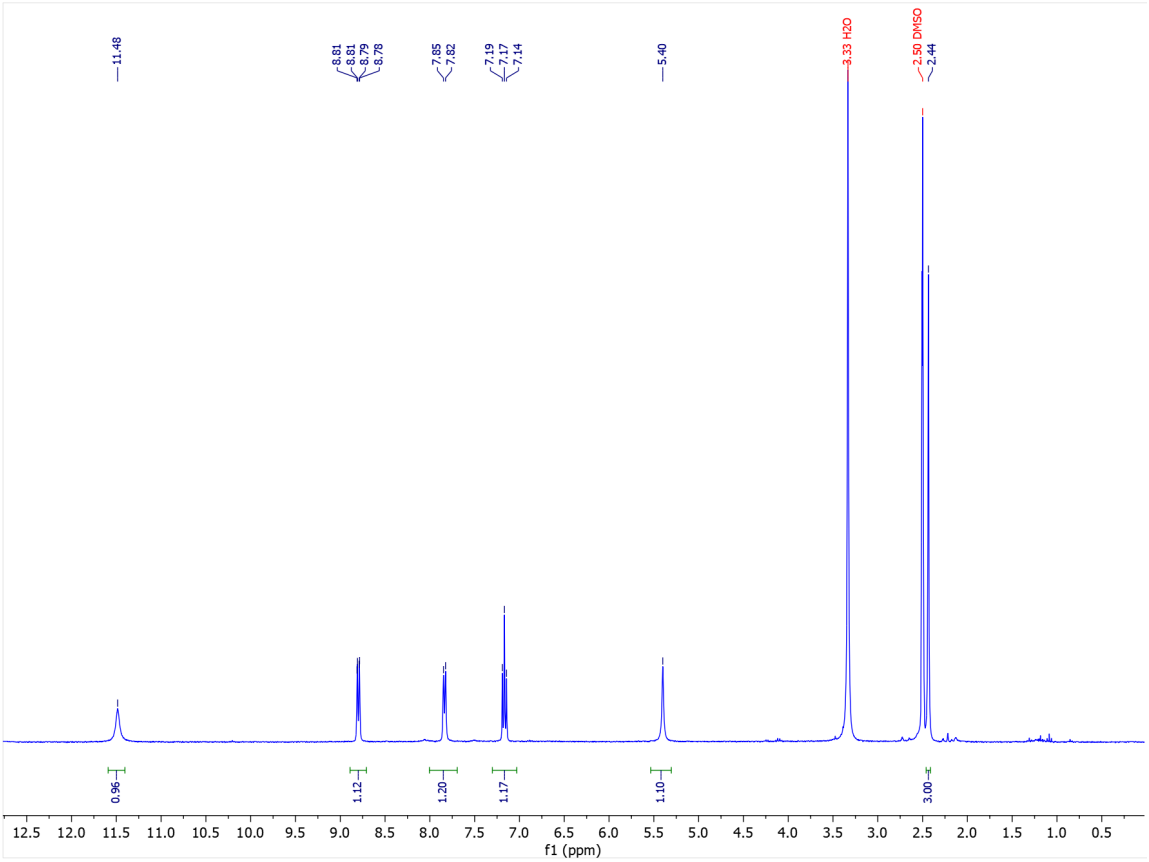

Figure C6: ^{1}H NMR spectrum (300 MHz, $(CD_3)_2SO$, 292 K) of **2b**: **2-hydroxy-9-methyl-4*H*-pyrido[1,2-*a*]pyrimidin-4-one**

2c 2-hydroxy-8-methyl-4H-pyrido[1,2-a]pyrimidin-4-one

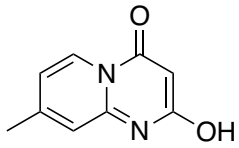

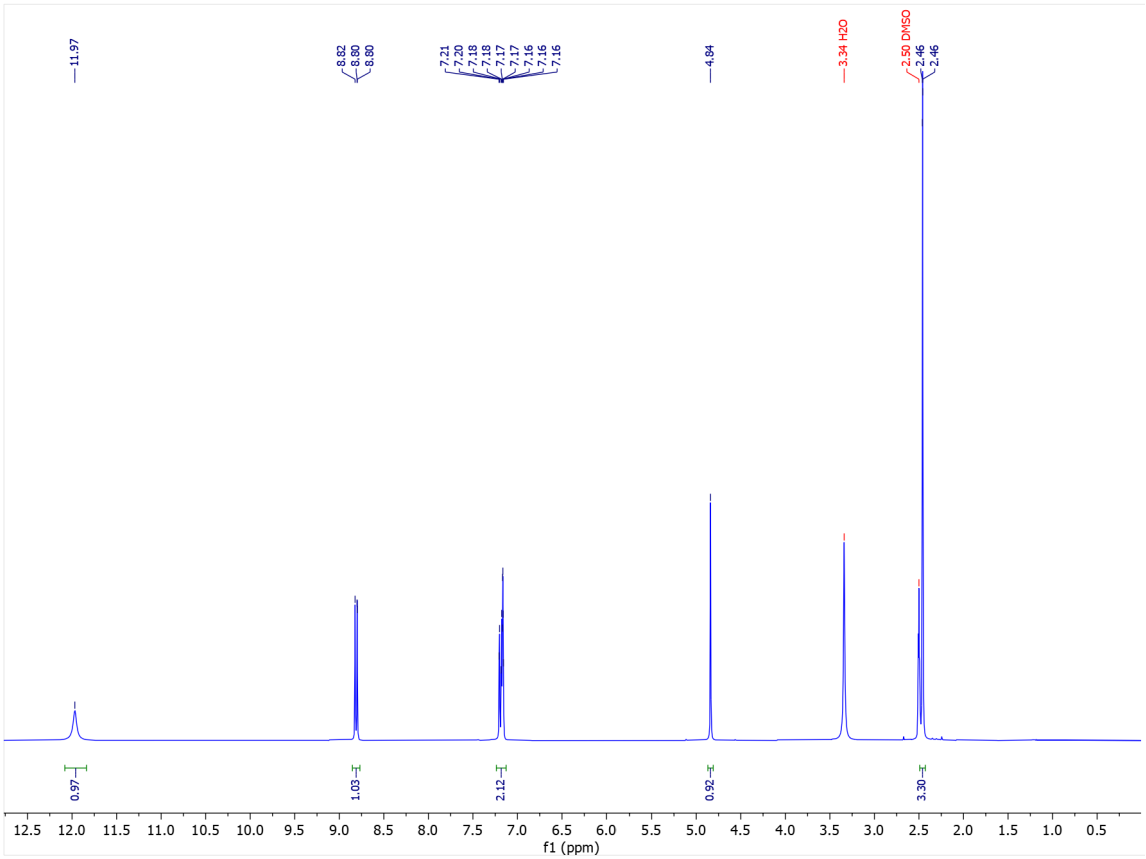

Figure C7: ^{1}H NMR spectrum (300 MHz, $(CD_3)_2SO$, 292 K) of **2c**: **2-hydroxy-8-methyl-4*H*-pyrido[1,2-*a*]pyrimidin-4-one**

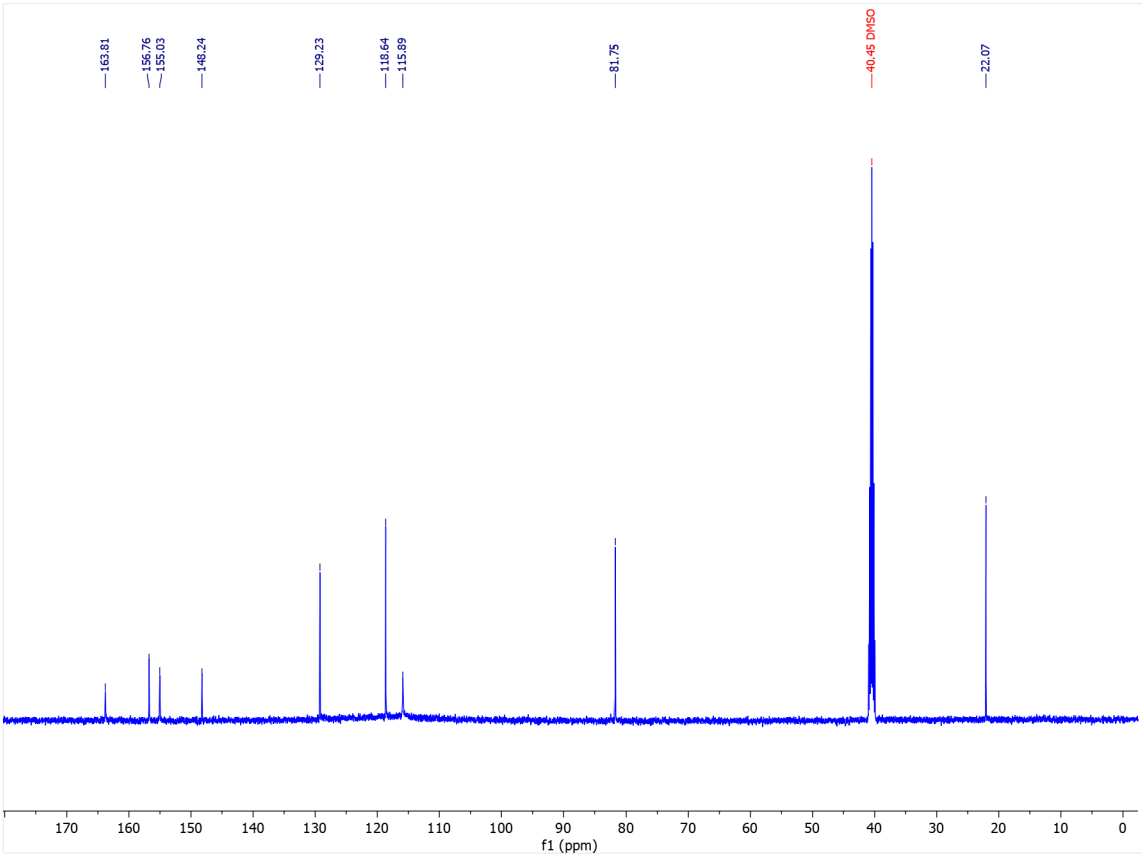

Figure C8: ^{13}C NMR spectrum (126 MHz, $(CD_3)_2SO$, 292 K) of **2c**: **2-hydroxy-8-methyl-4*H*-pyrido[1,2-*a*]pyrimidin-4-one**

2d 2-hydroxy-7-methyl-4H-pyrido[1,2-a]pyrimidin-4-one

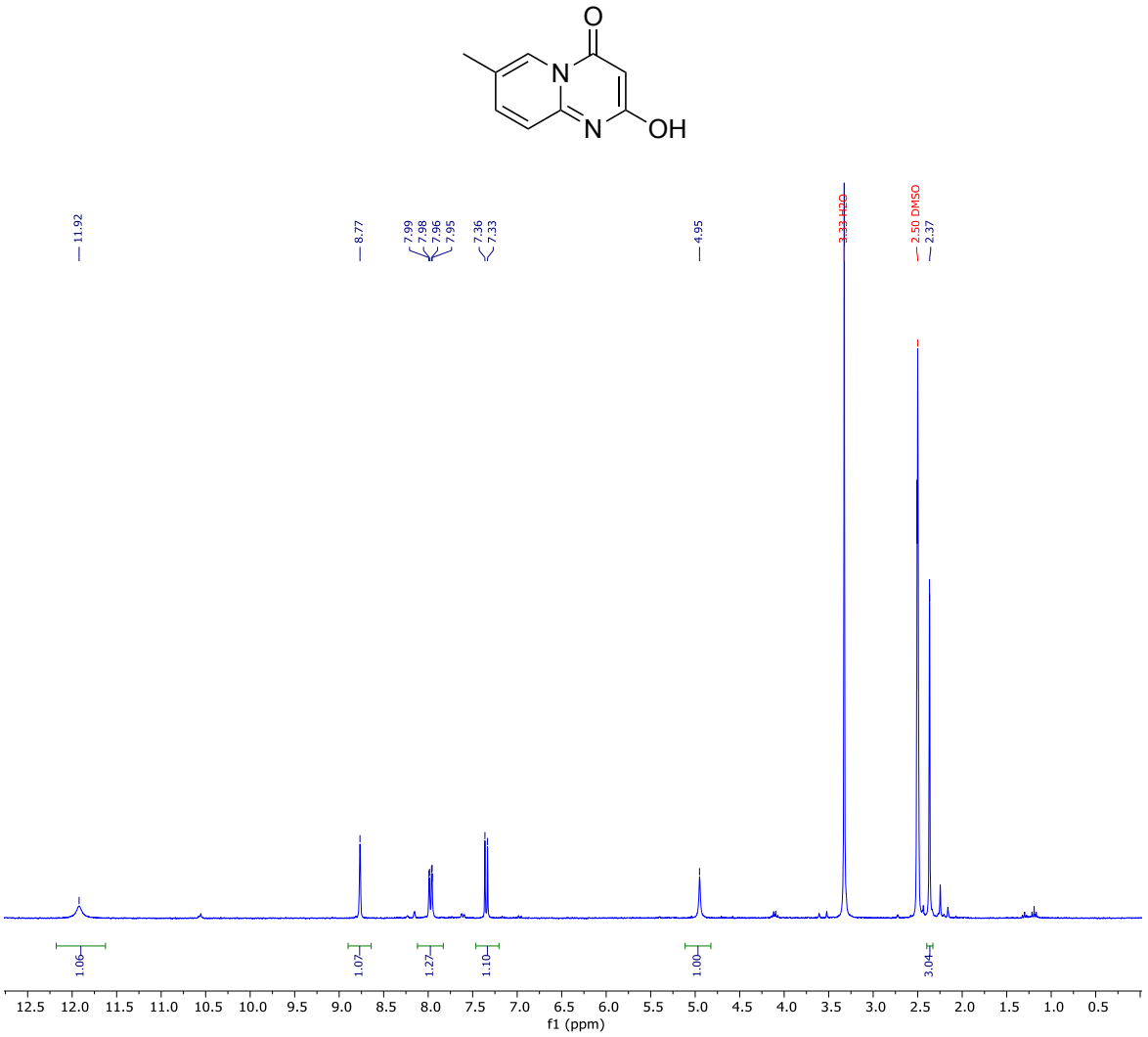

Figure C9: ^{1}H NMR spectrum (300 MHz, $(CD_3)_2SO$, 292 K) of **2c**: **2-hydroxy-7-methyl-4*H*-pyrido[1,2-*a*]pyrimidin-4-one**

2e 2-hydroxy-6-methyl-4H-pyrido[1,2-a]pyrimidin-4-one

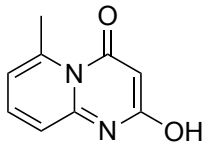

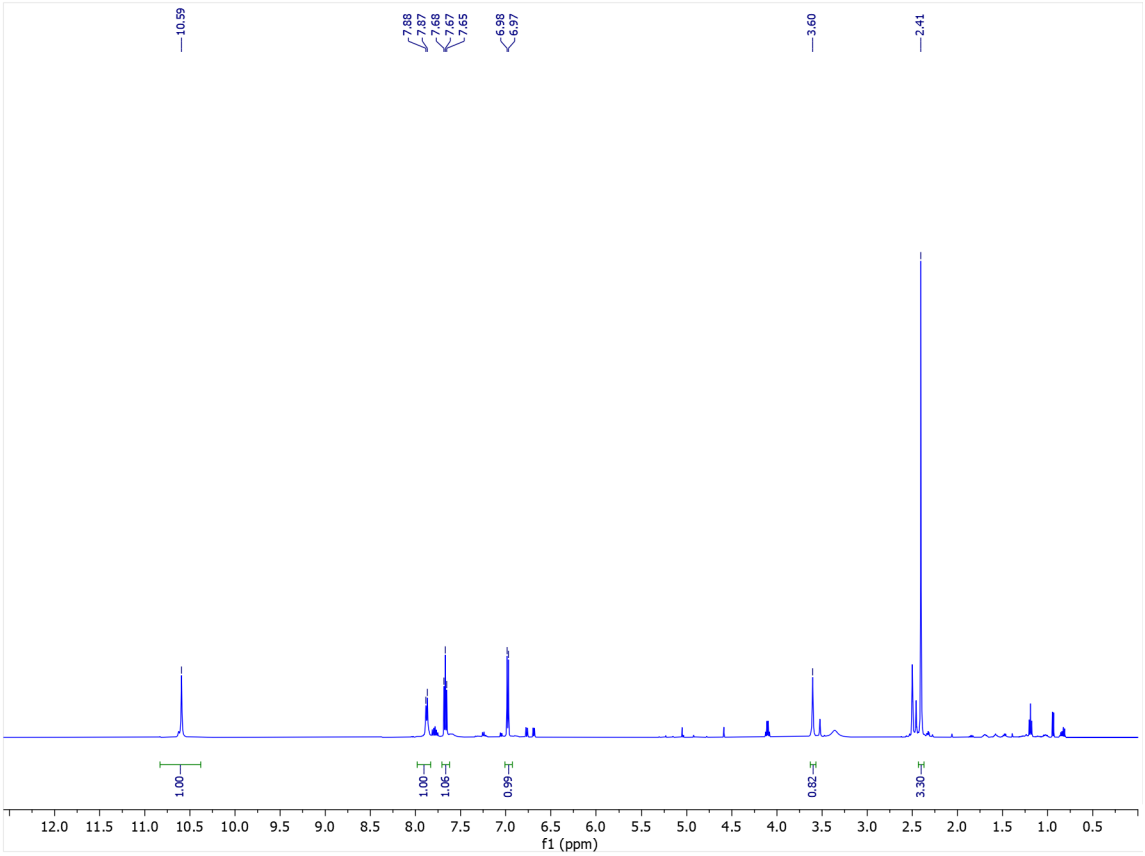

Figure C10: ^{1}H NMR spectrum (300 MHz, $(CD_3)_2SO$, 292 K) of **2e**: **6-methyl-2-hydroxy-4*H*-pyrido[1,2-*a*]pyrimidin-4-one**

2f 9-chloro-2-hydroxy-4H-pyrido[1,2-a]pyrimidin-4-one

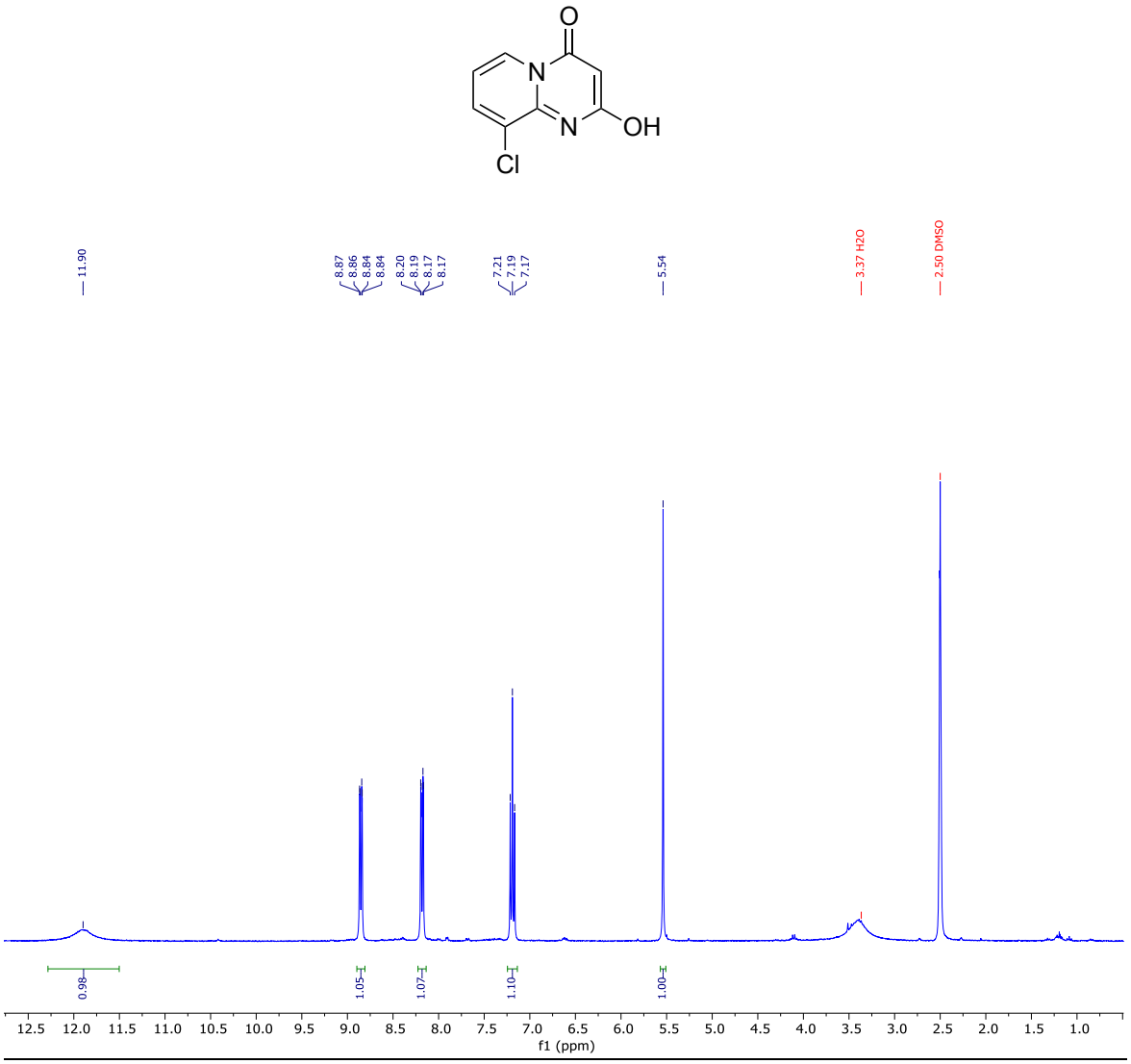

Figure C11: ^{1}H NMR spectrum (300 MHz, $(CD_3)_2SO$, 292 K) of **2f**: **9-chloro-2-hydroxy-4*H*-pyrido[1,2-*a*]pyrimidin-4-one**

2g 8-chloro-2-hydroxy-4H-pyrido[1,2-a]pyrimidin-4-one

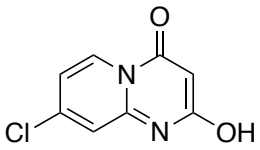

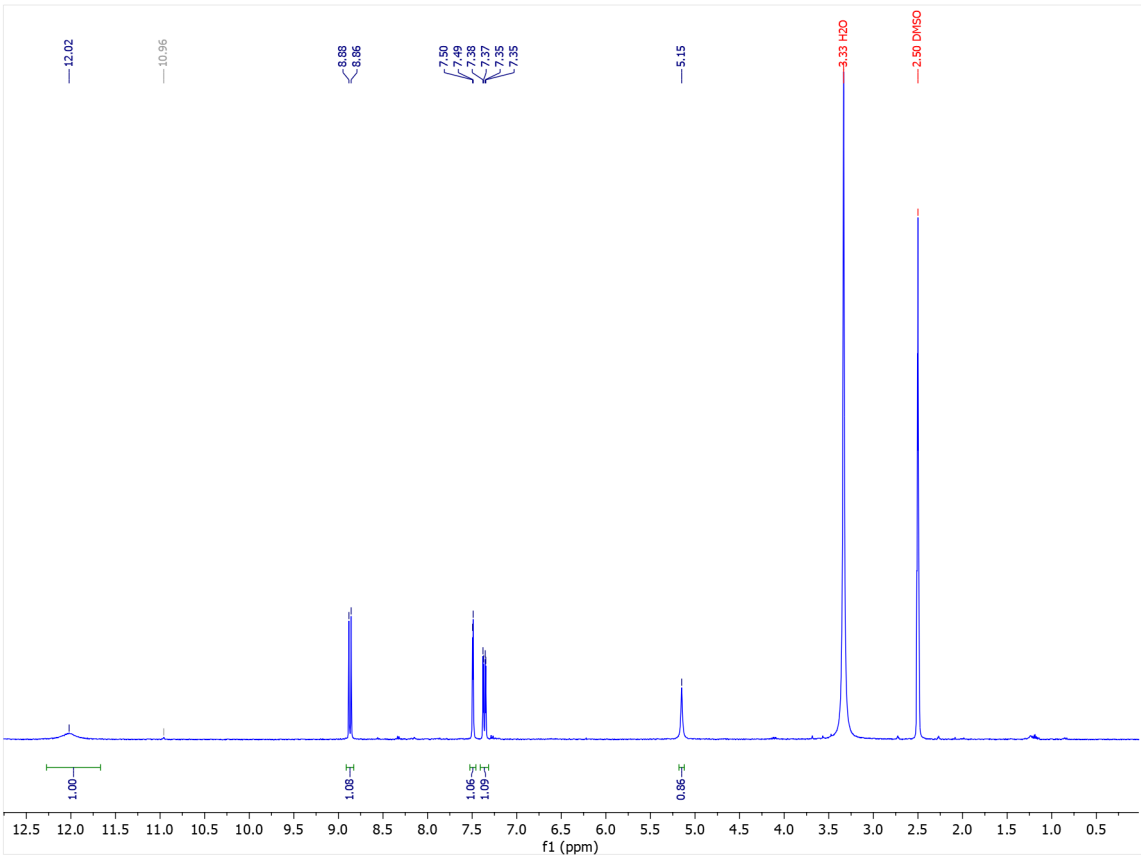

Figure C12: ^{1}H NMR spectrum (300 MHz, $(CD_3)_2SO$, 292 K) of **2g**: **8-chloro-2-hydroxy-4*H*-pyrido[1,2-*a*]pyrimidin-4-one**

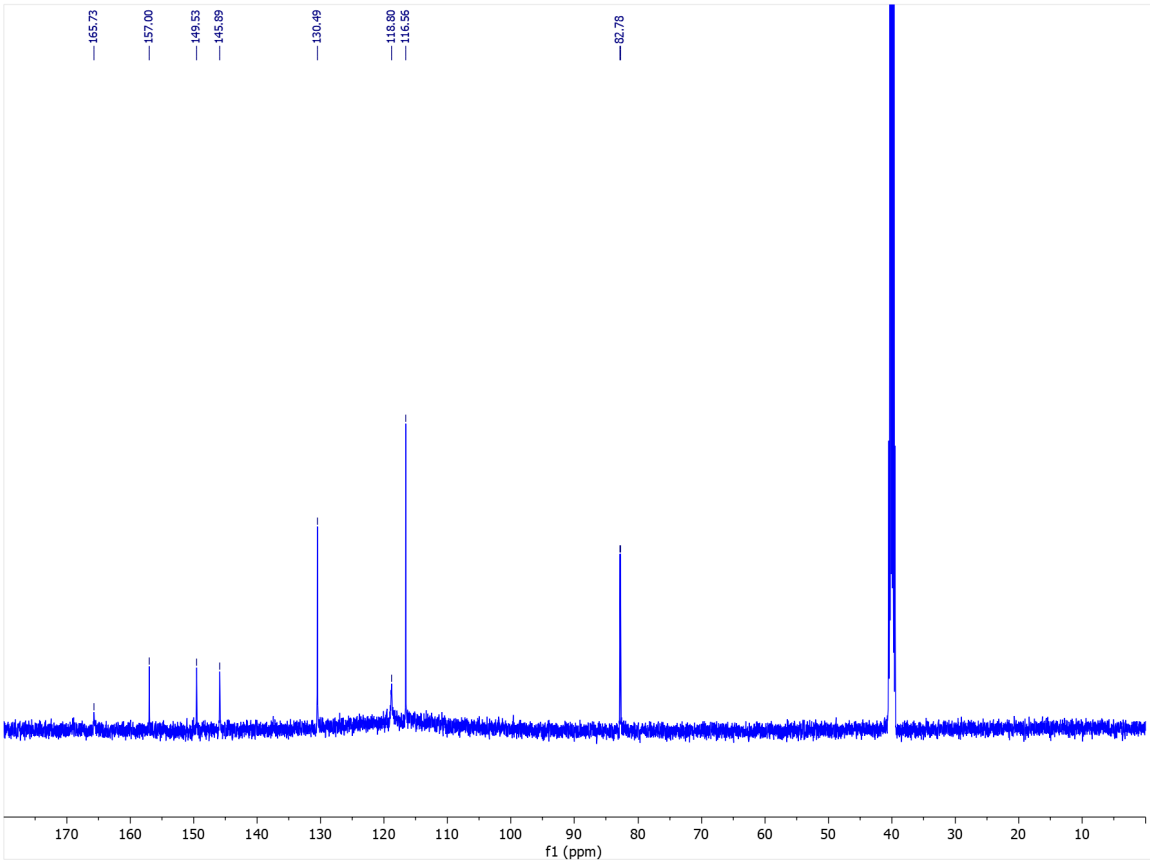

Figure C13: ^{13}C NMR spectrum (126 MHz, $(CD_3)_2SO$, 292 K) of **2g**: **8-chloro-2-hydroxy-4*H*-pyrido[1,2-*a*]pyrimidin-4-one**

2h 7-chloro-2-hydroxy-4H-pyrido[1,2-a]pyrimidin-4-one

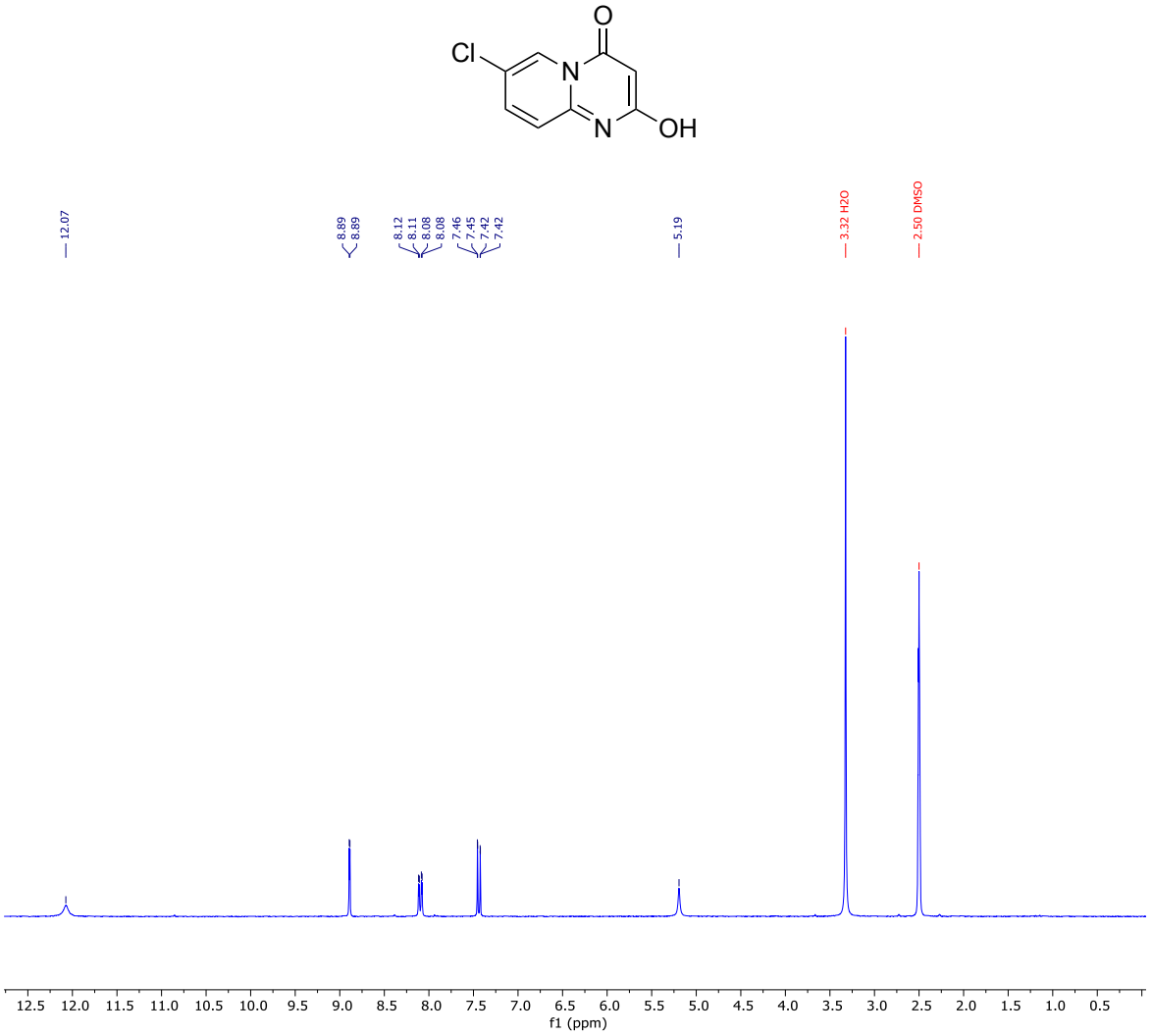

Figure C14: ^{1}H NMR spectrum (300 MHz, $(CD_3)_2SO$, 292 K) of **2h**: **7-chloro-2-hydroxy-4*H*-pyrido[1,2-*a*]pyrimidin-4-one**

2i 6-chloro-2-hydroxy-4H-pyrido[1,2-a]pyrimidin-4-one

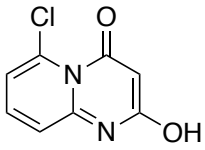

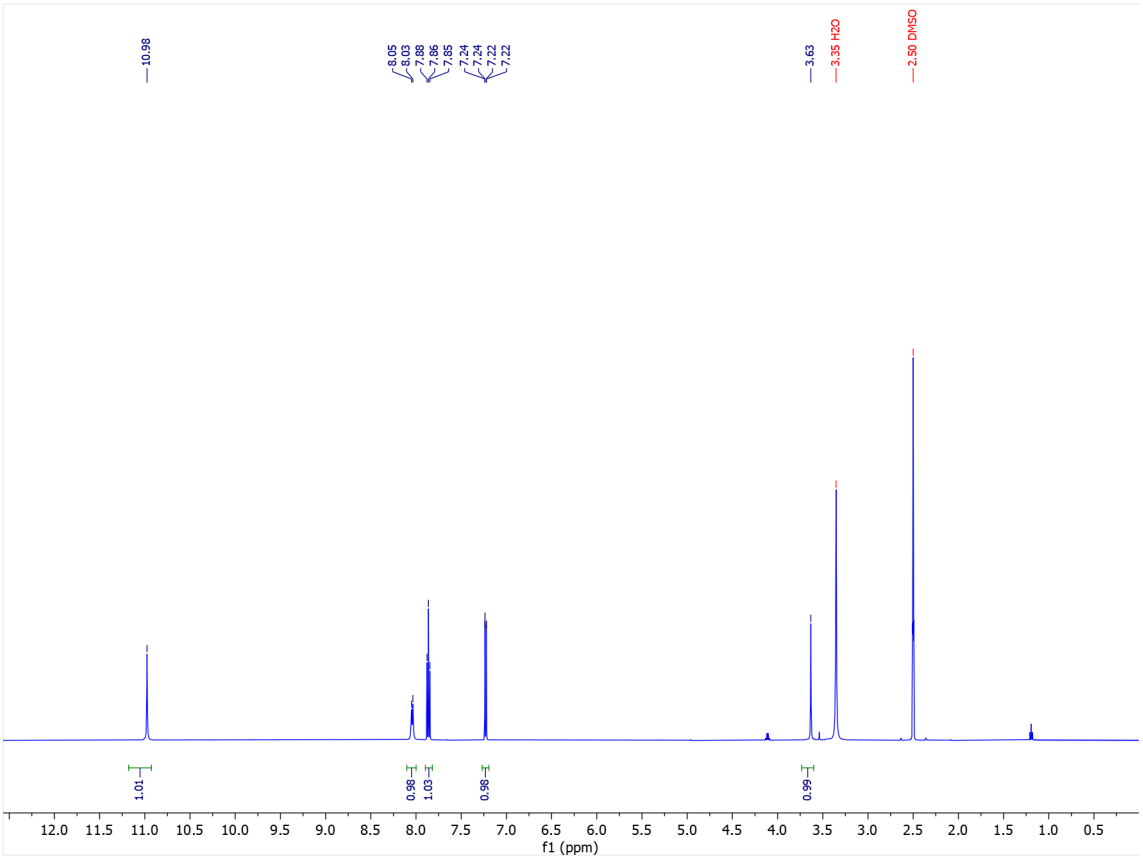

Figure C15: ^{1}H NMR spectrum (300 MHz, $(CD_3)_2SO$, 292 K) of **2i**: **6-chloro-2-hydroxy-4*H*-pyrido[1,2-*a*]pyrimidin-4-one**

2j 9-bromo-2-hydroxy-4H-pyrido[1,2-a]pyrimidin-4-one

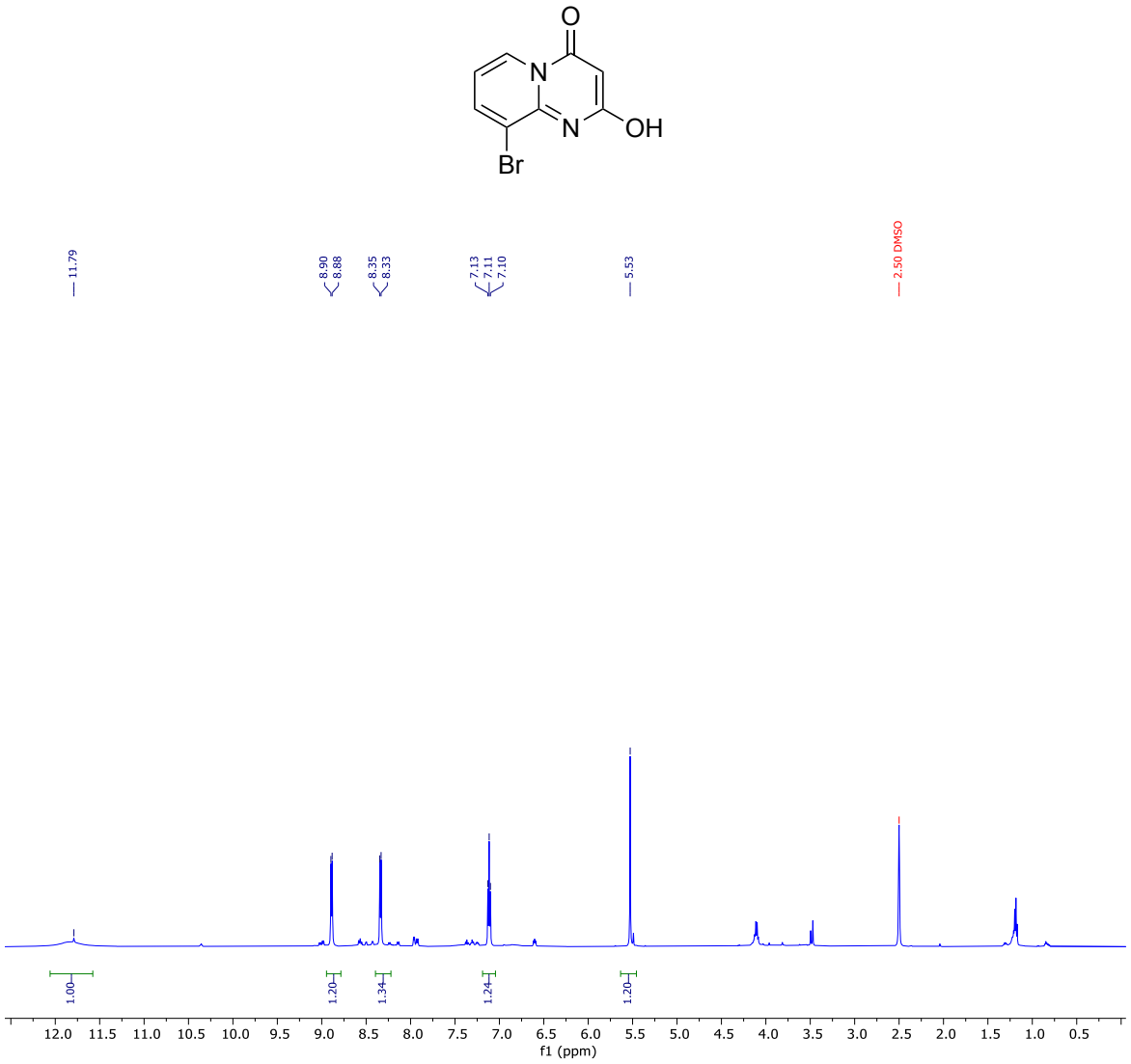

Figure C16: ^{1}H NMR spectrum (300 MHz, $(CD_3)_2SO$, 292 K) of **2j**: **9-bromo-2-hydroxy-4*H*-pyrido[1,2-*a*]pyrimidin-4-one**

2k 8-bromo-2-hydroxy-4H-pyrido[1,2-a]pyrimidin-4-one

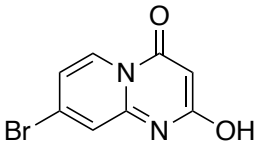

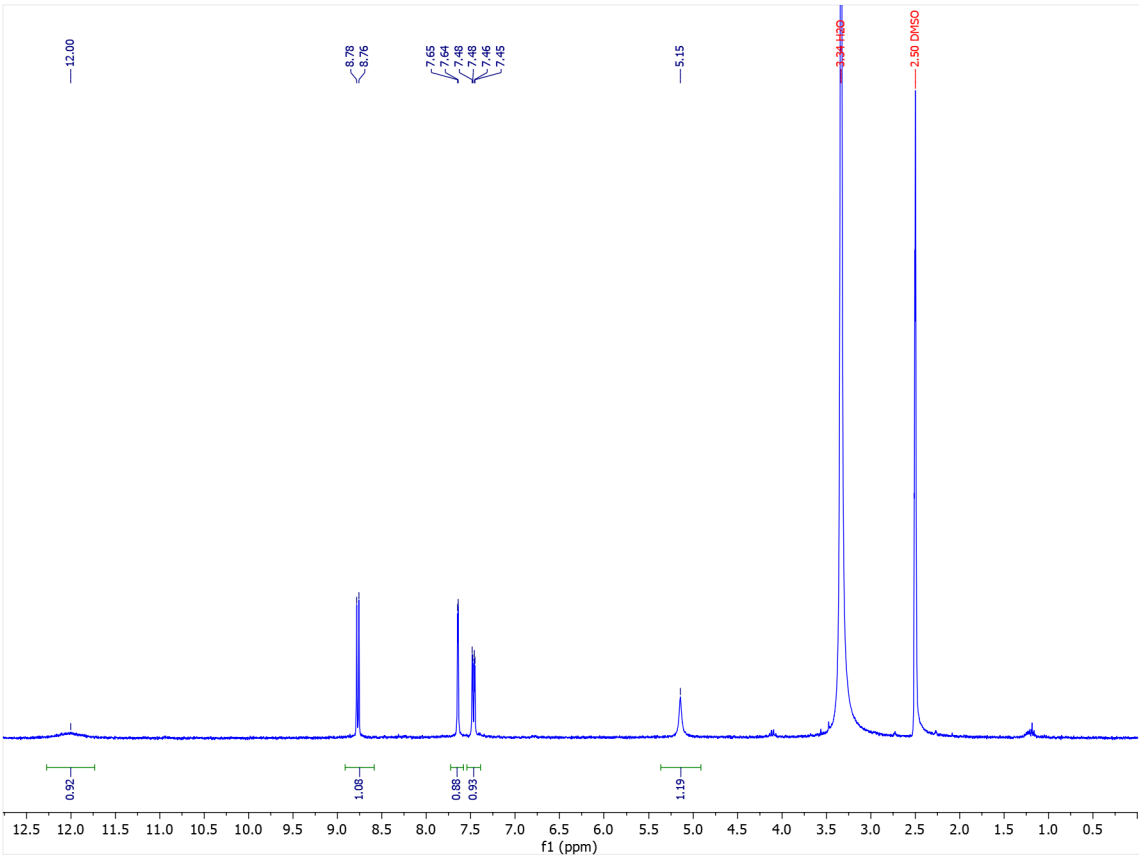

Figure C17: ^{1}H NMR spectrum (300 MHz, $(CD_3)_2SO$, 292 K) of **2k**: **8-bromo-2-hydroxy-4*H*-pyrido[1,2-*a*]pyrimidin-4-one**

2m 6-bromo-2-hydroxy-4H-pyrido[1,2-a]pyrimidin-4-one

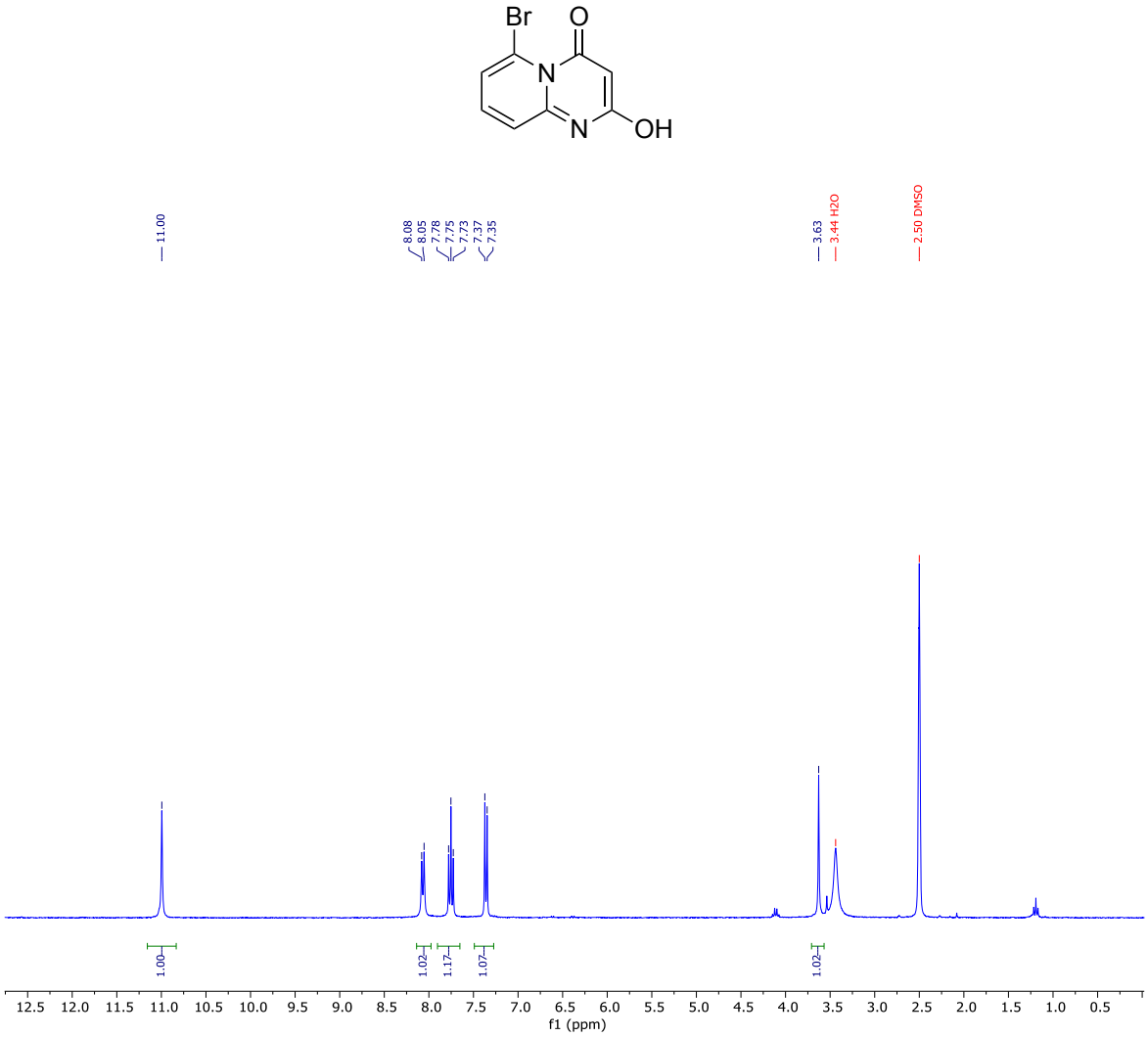

Figure C18: ^{1}H NMR spectrum (300 MHz, $(CD_3)_2SO$, 292 K) of **2m**: **6-bromo-2-hydroxy-4*H*-pyrido[1,2-*a*]pyrimidin-4-one**

2n 2-hydroxy-9-fluoro-4H-pyrido[1,2-a]pyrimidin-4-one

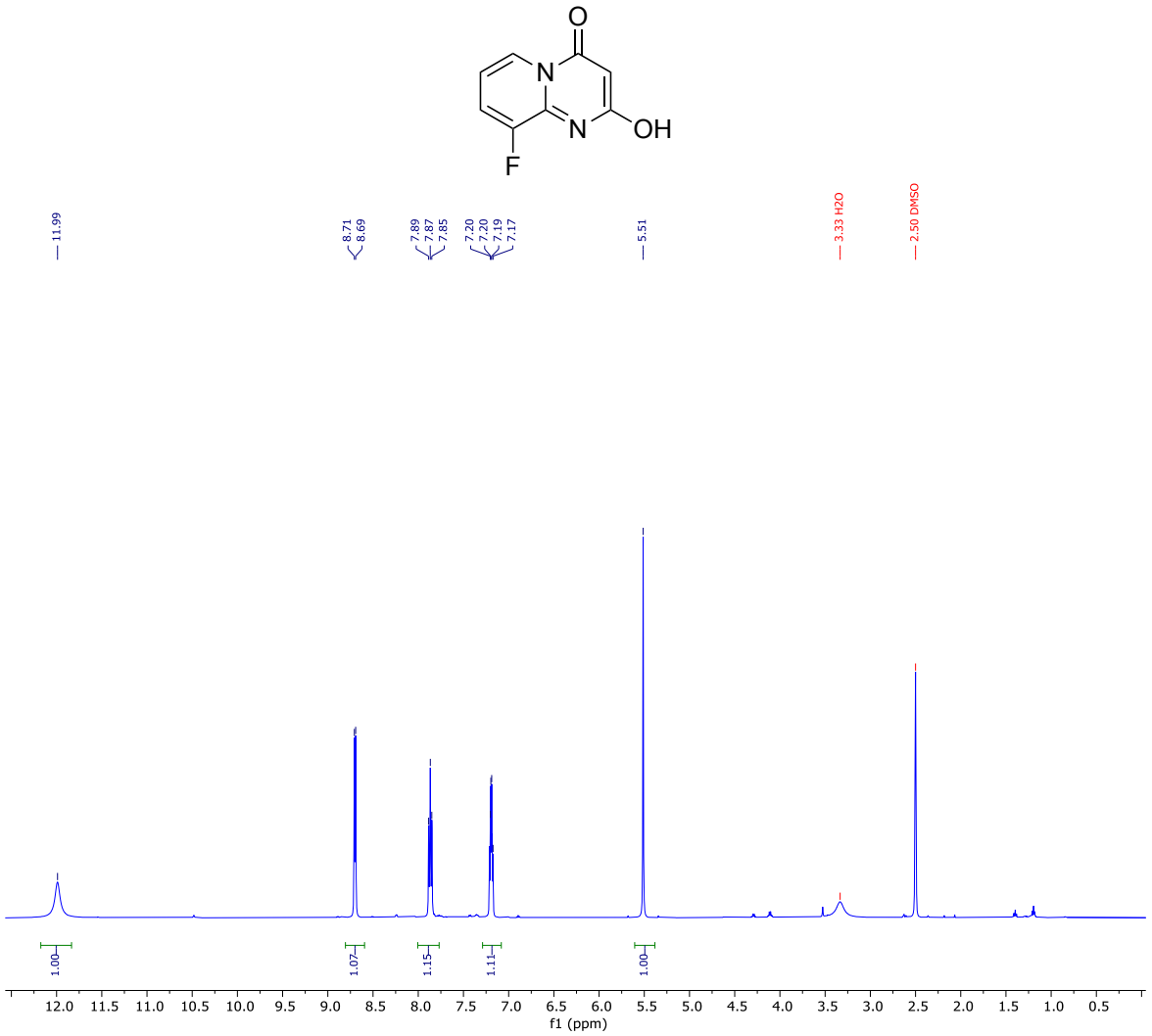

Figure C19: ^{1}H NMR spectrum (300 MHz, $(CD_3)_2SO$, 292 K) of **2n**: **9-fluoro-2-hydroxy-4*H*-pyrido[1,2-*a*]pyrimidin-4-one**

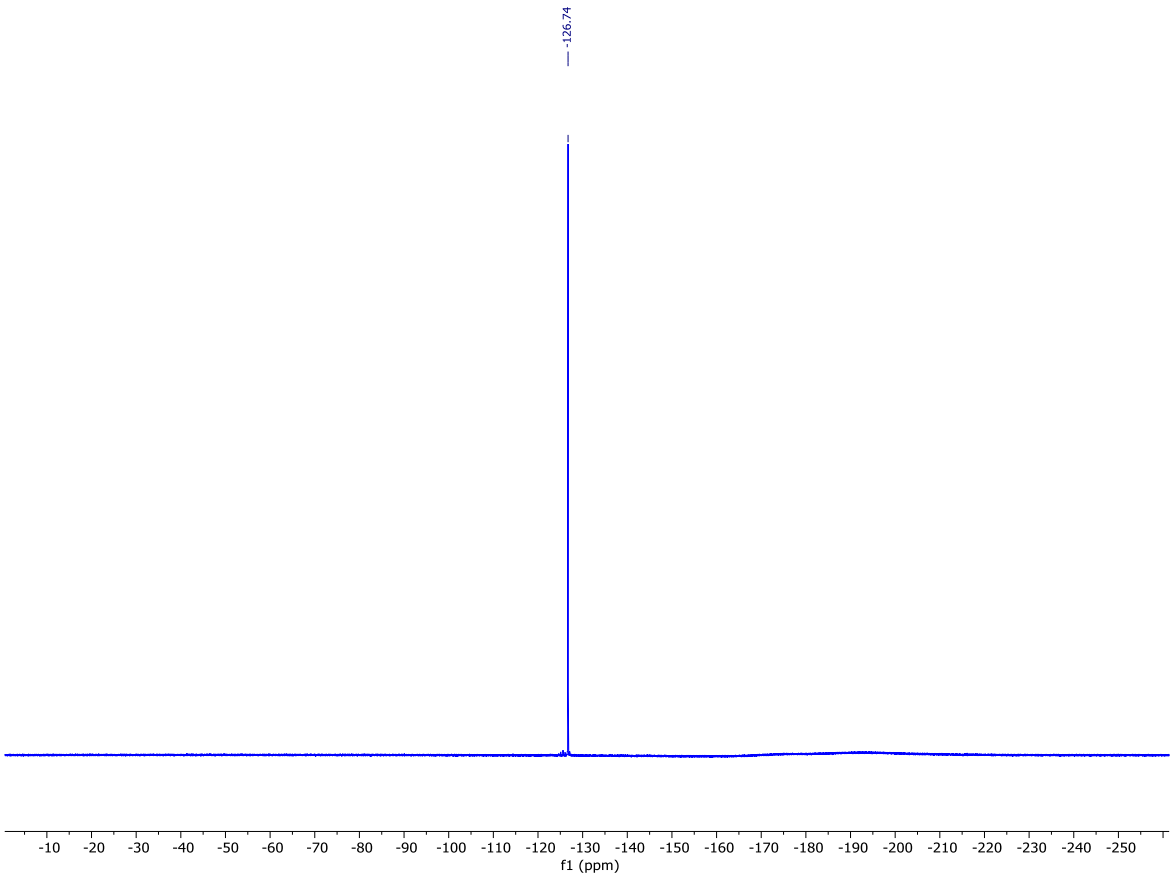

Figure C20: ^{19}F NMR spectrum (283 MHz, $(CD_3)_2SO$, 292 K) of **2n**: **9-fluoro-2-hydroxy-4*H*-pyrido[1,2-*a*]pyrimidin-4-one**

2p 2-hydroxy-7-fluoro-4H-pyrido[1,2-a]pyrimidin-4-one

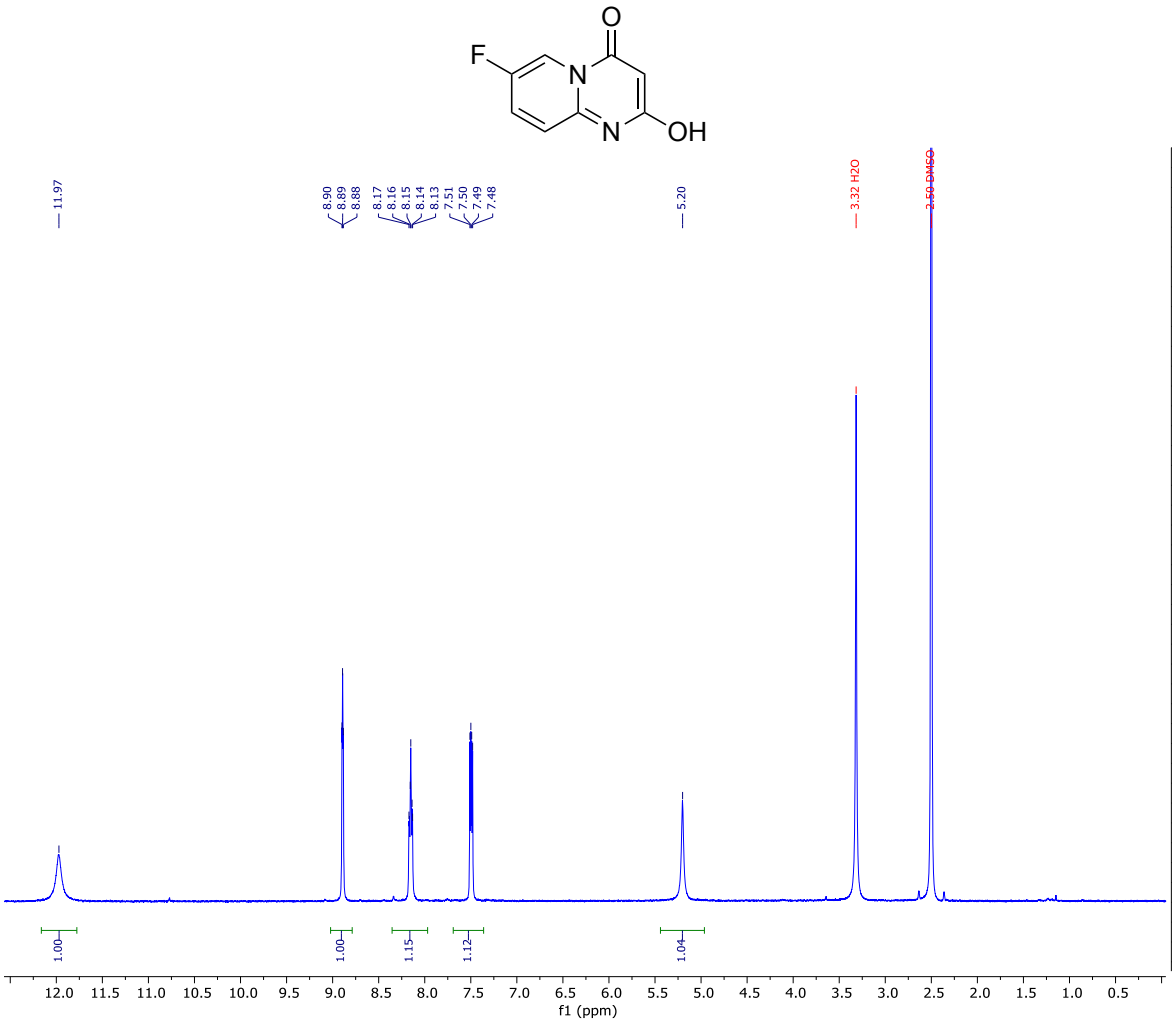

Figure C21: ^{1}H NMR spectrum (300 MHz, $(CD_3)_2SO$, 292 K) of **2p**: **7-fluoro-2-hydroxy-4*H*-pyrido[1,2-*a*]pyrimidin-4-one**

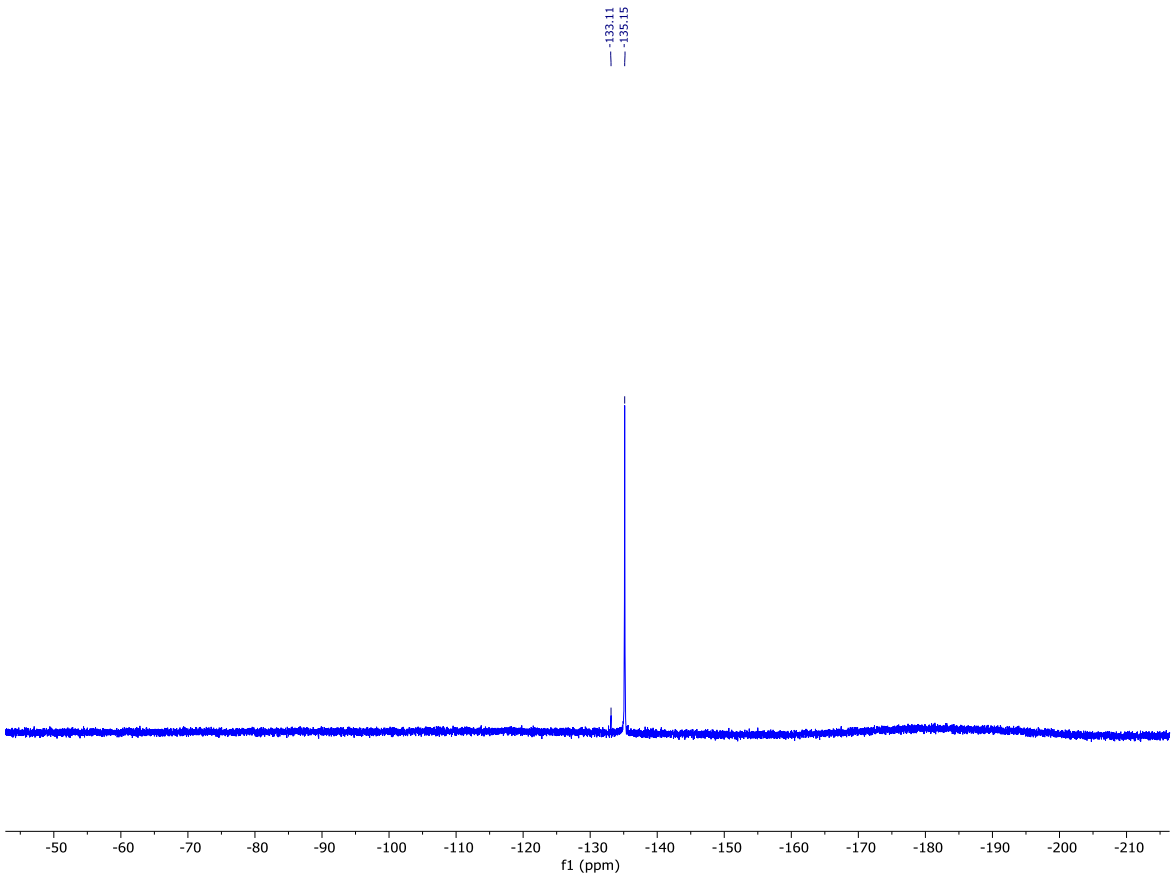

Figure C22: ^{19}F NMR spectrum (283 MHz, $(CD_3)_2SO$, 292 K) of **2p**: **7-fluoro-2-hydroxy-4*H*-pyrido[1,2-*a*]pyrimidin-4-one**

2q 2-hydroxy-6-fluoro-4H-pyrido[1,2-a]pyrimidin-4-one

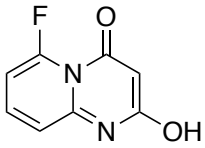

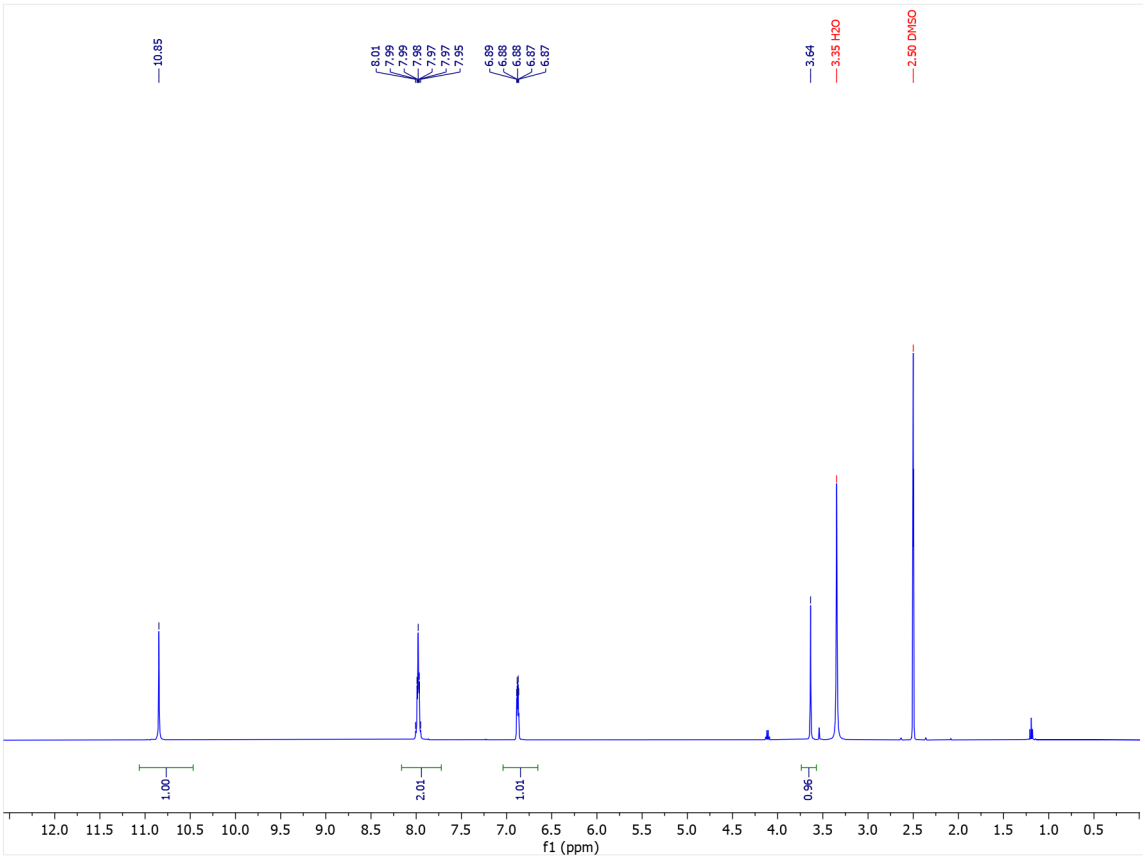

Figure C23: ^{1}H NMR spectrum (300 MHz, $(CD_3)_2SO$, 292 K) of **2q**: **6-fluoro-2-hydroxy-4*H*-pyrido[1,2-*a*]pyrimidin-4-one**

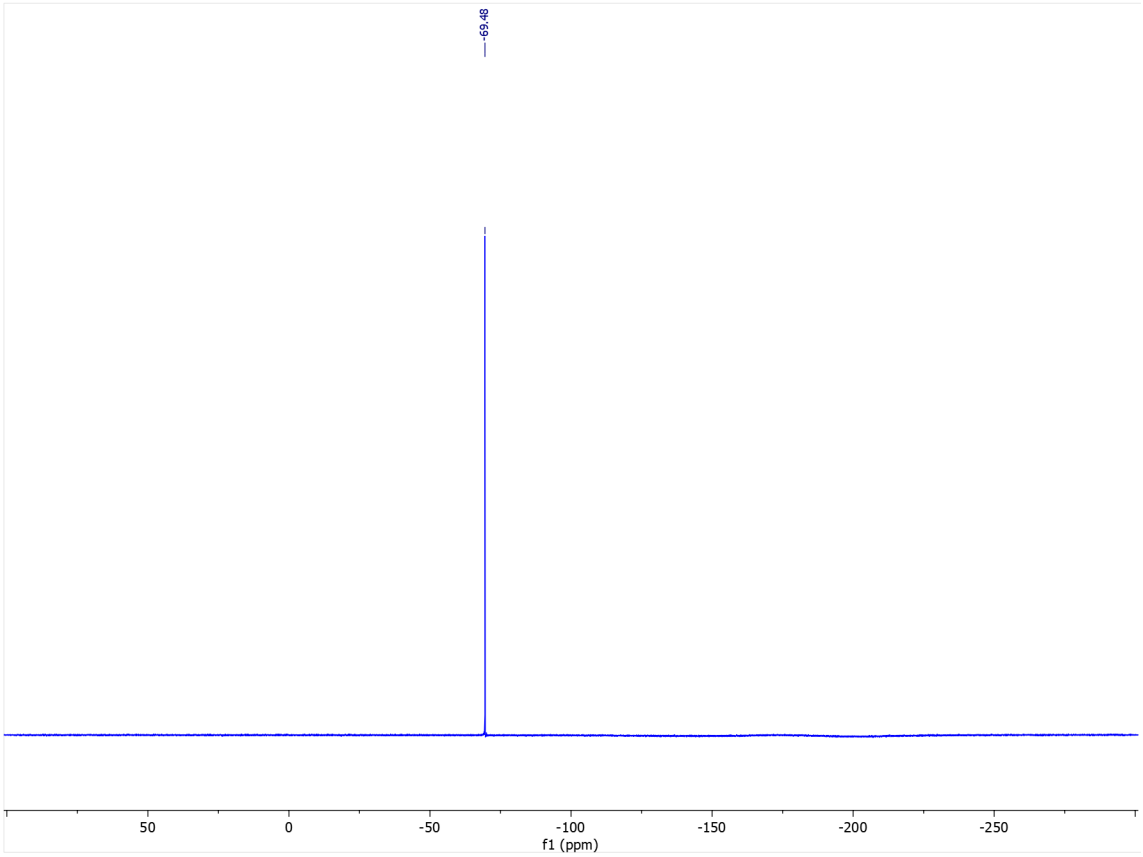

Figure C24: ^{19}F NMR spectrum (283 MHz, $(CD_3)_2SO$, 292 K) of **2h**: **6-fluoro-2-hydroxy-4*H*-pyrido[1,2-*a*]pyrimidin-4-one**

C5. Tosylation Characterization Data (^{1}H and C NMR)

3a 4-oxo-4H-pyrido[1,2-a]pyrimidin-2-yl 4-methylbenzenesulfonate

2-Hydroxy-4*H*-pyrido[1,2-*a*]pyrimidin-4-one (**2a**, 1g, 6.17 mmol) was charged in a round bottom flask with 30 mL DCM. Triethylamine (1.37 g, 1.89 mL, 13.57 mmol) was then added via syringe and the solution was allowed to stir. 4-Toluenesulfonyl chloride (1.29 g, 6.78 mmol) was dissolved in 10 mL DCM, and transferred to an addition funnel attached to the previously charged round bottom flask. The 4-toluenesulfonyl chloride solution was allowed to add dropwise, and the reaction was allowed to stir overnight at room temperature. The reaction was quenched with H_2O [20 mL], and the aqueous layer was extracted three time with DCM [20 mL]. The combined organic fractions were dried with $MgSO_4$ and filtered before evaporating to dryness. The resulting brown oil was then triturated with cold hexanes to yield a beige powder that was filtered and washed again with cold hexanes [40 mL] to yield the final product **3a** (1.90 g, 97% yield).

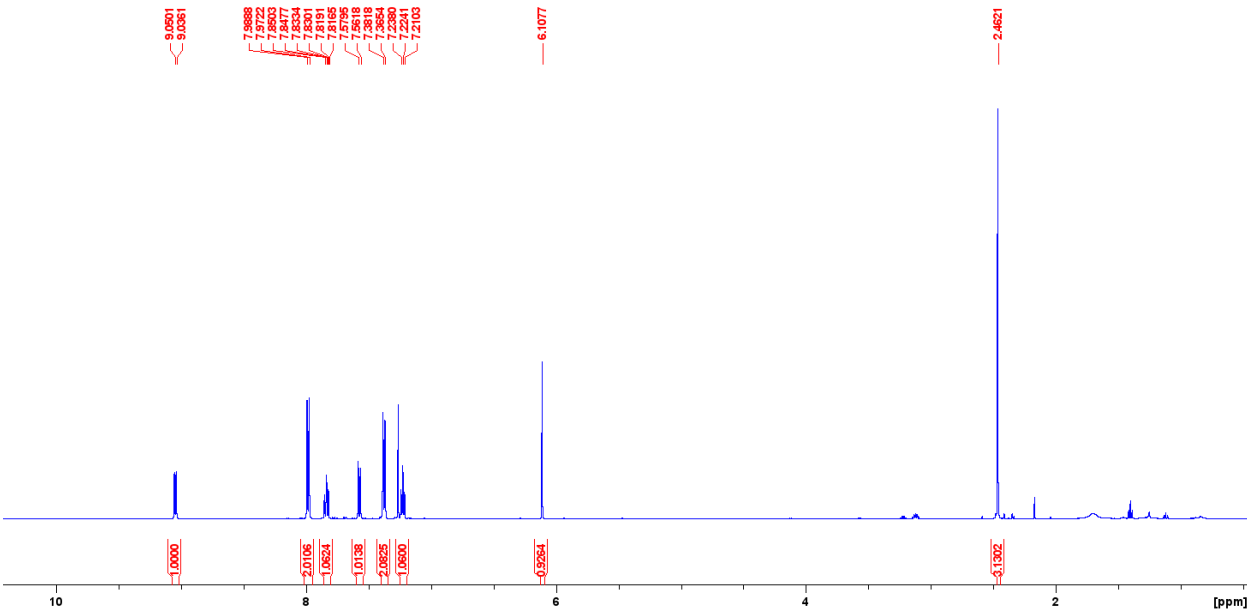

Figure C25: ^{1}H NMR spectrum (500 MHz, $CDCl_3$, 292 K) of **3a**: **4-oxo-4H-pyrido[1,2-a]pyrimidin-2-yl 4-methylbenzenesulfonate**

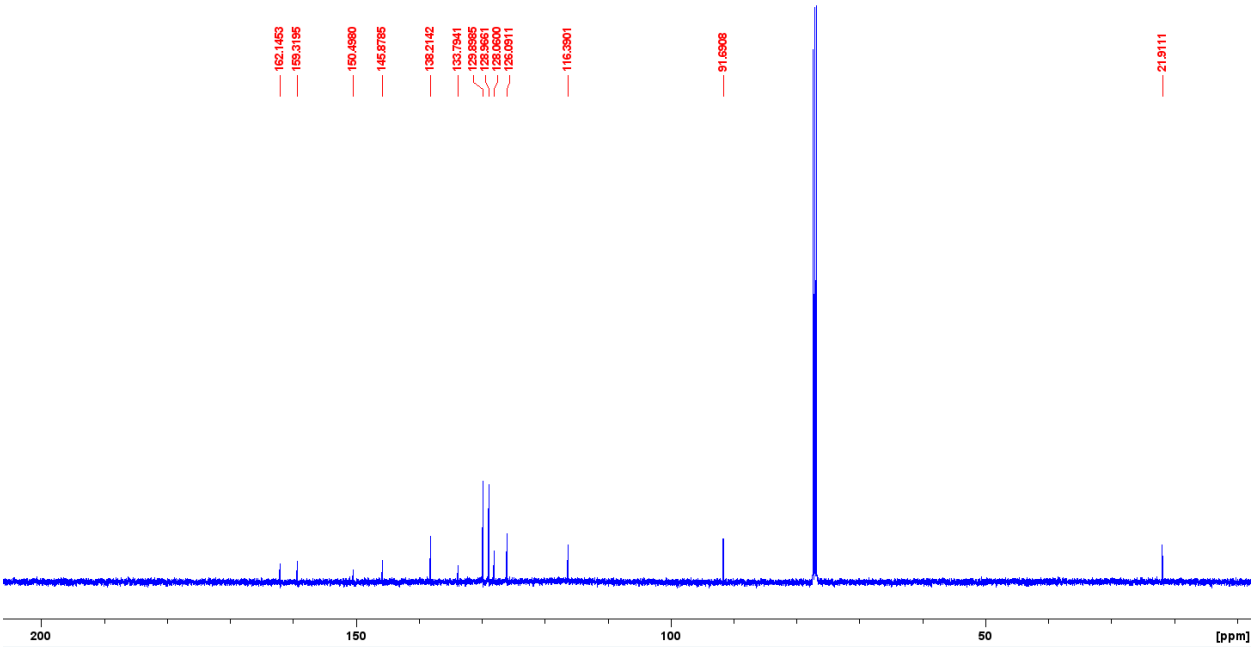

Figure C26: ^{13}C NMR spectrum (126 MHz, $(CD_3)_2SO$, 292 K) of **3a**: **4-oxo-4H-pyrido[1,2-a]pyrimidin-2-yl 4-methylbenzenesulfonate**

2l 7-bromo-2-hydroxy-4H-pyrido[1,2-a]pyrimidin-4-one

Using the above general procedure described in Section 4, 2-amino-5-bromopyridine **1l** (3.20 g, 18.5 mmol), was coupled with diethyl malonate (14.0 g, 92.5 mmol) to form a mixture containing **2l** (See Figure S28). The presence of the desired product **2l** was confirmed with HRMS: Cal'd for $C_8H_5BrN_2O_2$ [M+H]+: 240.96072; found: 240.96053.

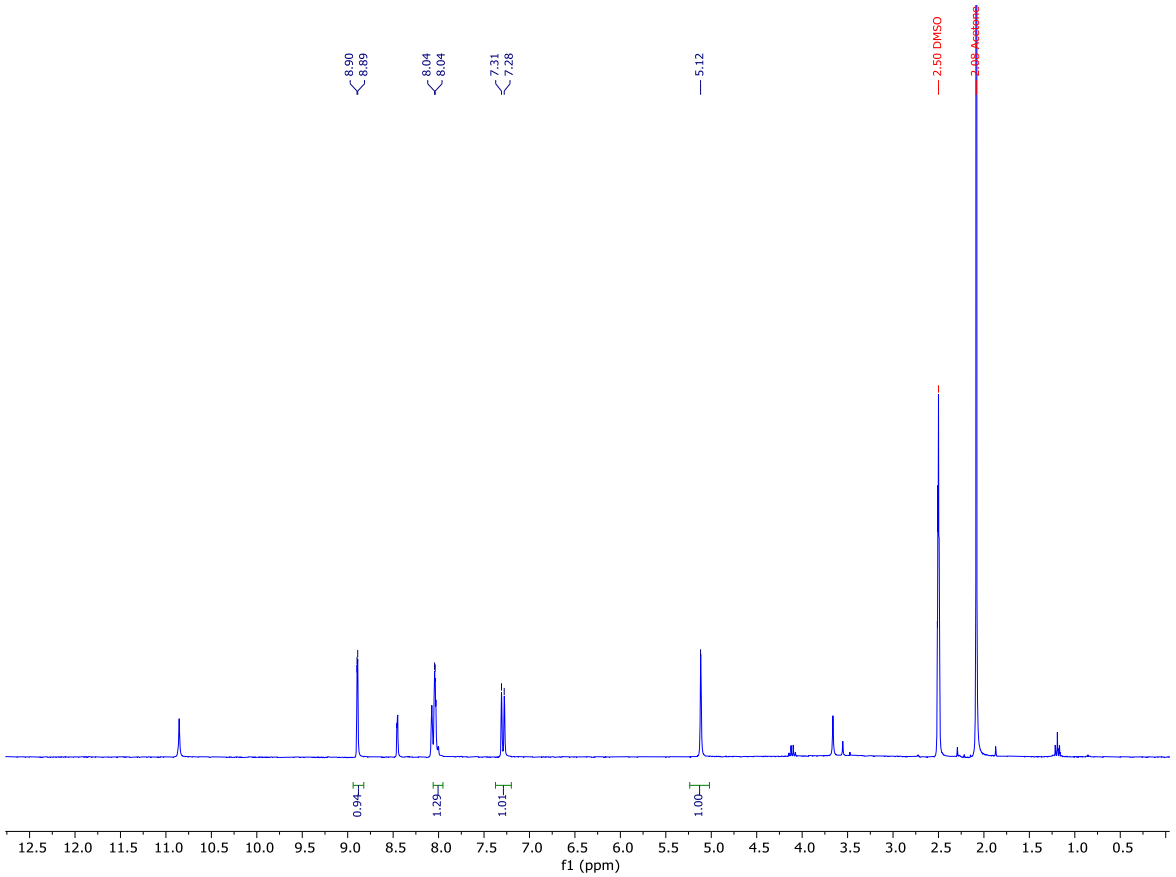

Figure C27: ^{1}H NMR spectrum (300 MHz, $(CD_3)_2SO$, 292 K) of **1l** and **2l**: (**7-bromo-2-hydroxy-4*H*-pyrido[1,2-*a*]pyrimidin-4-one)**

3l 7-bromo-4-oxo-4H-pyrido[1,2-a]pyrimidin-2-yl 4-methylbenzenesulfonate

The collected solid (2.58 g, see Figure S28 for ^{1}H-NMR) was charged into a round bottom flask with 53 ml DCM and triethylamine (2.2 equiv, 3.31 mL) was added dropwise. 4-Toluenesulfonyl chloride (1.0 equiv, 2.04 g) was added slowly to the stirred solution and allowed to stir overnight. The solution was washed with H_2O and subsequently dried with $MgSO_4$ and dried *in vacuo*. The resulting solid was resuspended in toluene, and dried on a Genevac EZ-2 to produce a light-brown solid **3l** (2.20 g, 30% yield over two steps).

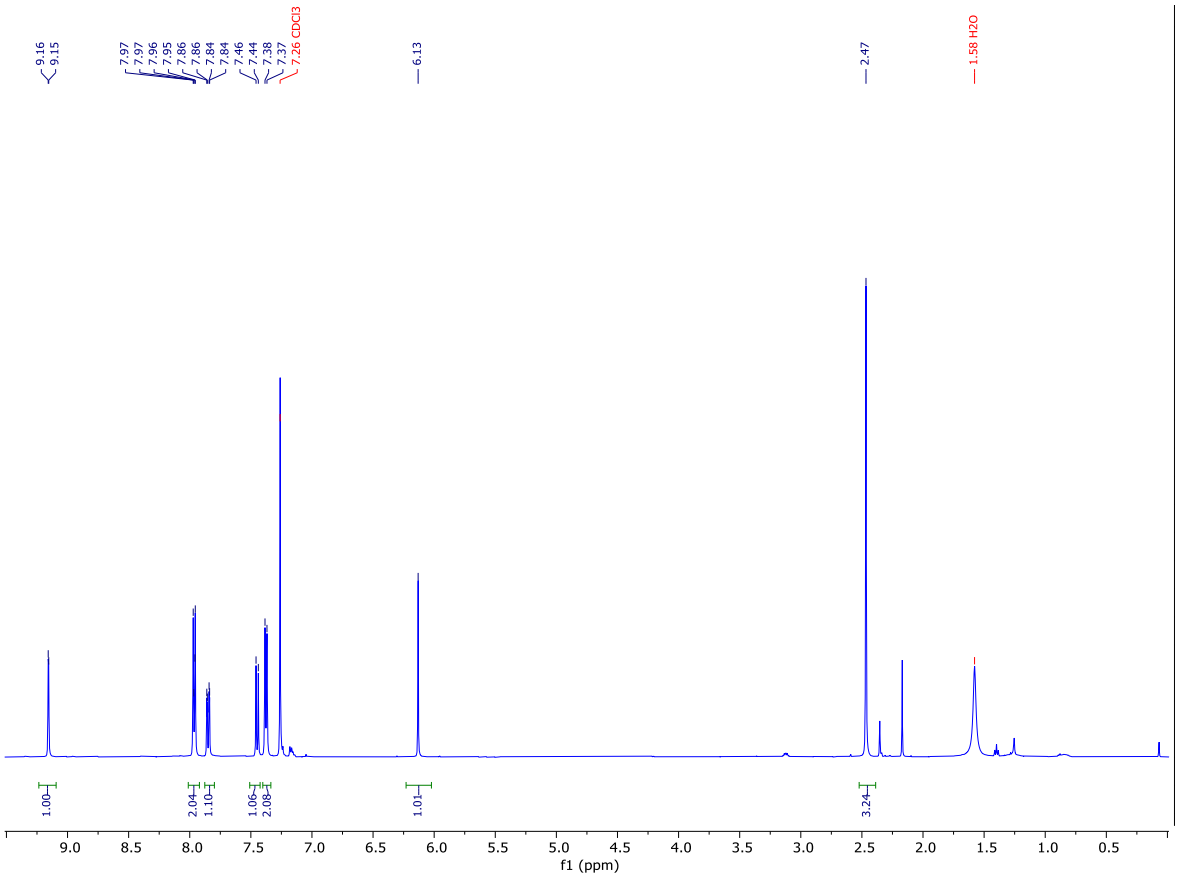

Figure C28: ^{1}H NMR spectrum (300 MHz, $(CD_3)_2SO$, 292 K) of **3l**: **7-bromo-4-oxo-4H-pyrido[1,2-a]pyrimidin-2-yl 4-methylbenzenesulfonate**

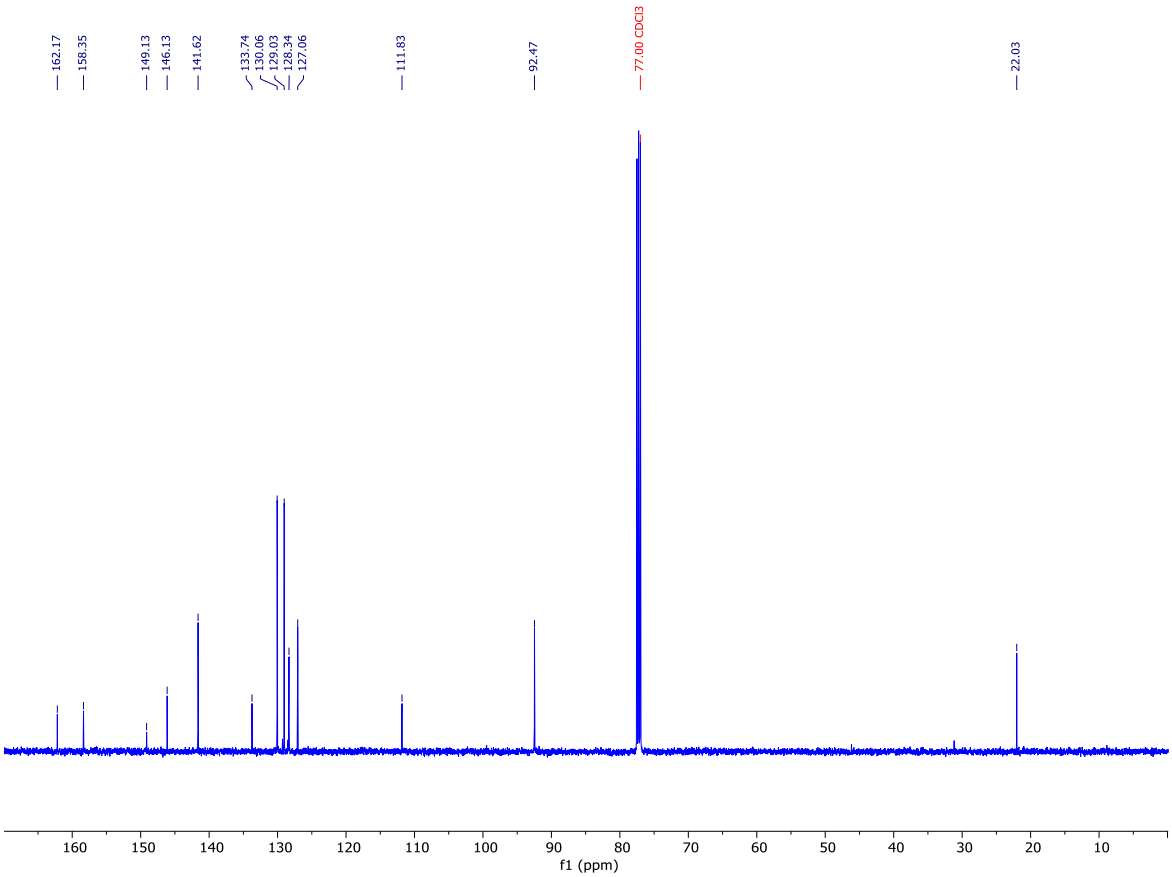

Figure C29: ^{13}C NMR spectrum (126 MHz, $(CD_3)_2SO$, 292 K) of **3l**: **7-bromo-4-oxo-4H-pyrido[1,2-a]pyrimidin-2-yl 4-methylbenzenesulfonate**

C6. Pivalation Characterization Data (^{1}H and ^{13}C NMR)

2-Hydroxy-4*H*-pyrido[1,2-*a*]pyrimidin-4-one (**2a**, 1.5 g, 9.25 mmol) was charged in a round bottom flask with 4-dimethylaminopyridine (113.0 mg, 0.925 mmol) and 70 mL DCM. Triethylamine (1.12 g, 1.55 mL, 11.1 mmol) was then added via syringe and the solution was allowed to stir. Pivaloyl chloride (1.34 g, 1.37 mL, 11.1 mmol) was then added slowly dropwise and the reaction was allowed to stir overnight at room temperature. The reaction was quenched with saturated sodium bisulfite [20 mL], washed with H_2O [40 mL], and the aqueous fractions were extracted three time with DCM [20 mL]. The combined organic fractions were

dried with $MgSO_4$ and filtered before evaporating to dryness. The resulting brown oil was then triturated with cold hexanes to yield a colourless powder that was filtered and washed again with cold hexanes [40 mL] to yield the final product **4a** (1.79 g, 61% yield).

4a 4-oxo-4H-pyrido[1,2-a]pyrimidin-2-yl pivalate

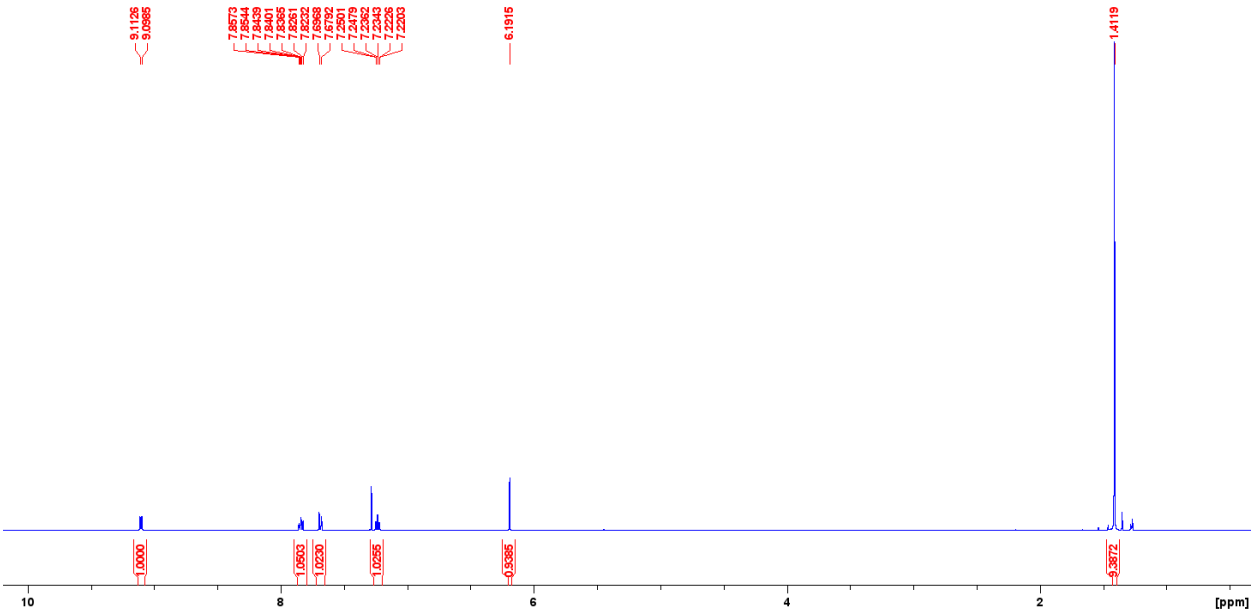

Figure C30: ^1H NMR spectrum (500 MHz, $(CD_3)_2SO$, 292 K) of **4a**: **4-oxo-4H-pyrido[1,2-a]pyrimidin-2-yl pivalate**

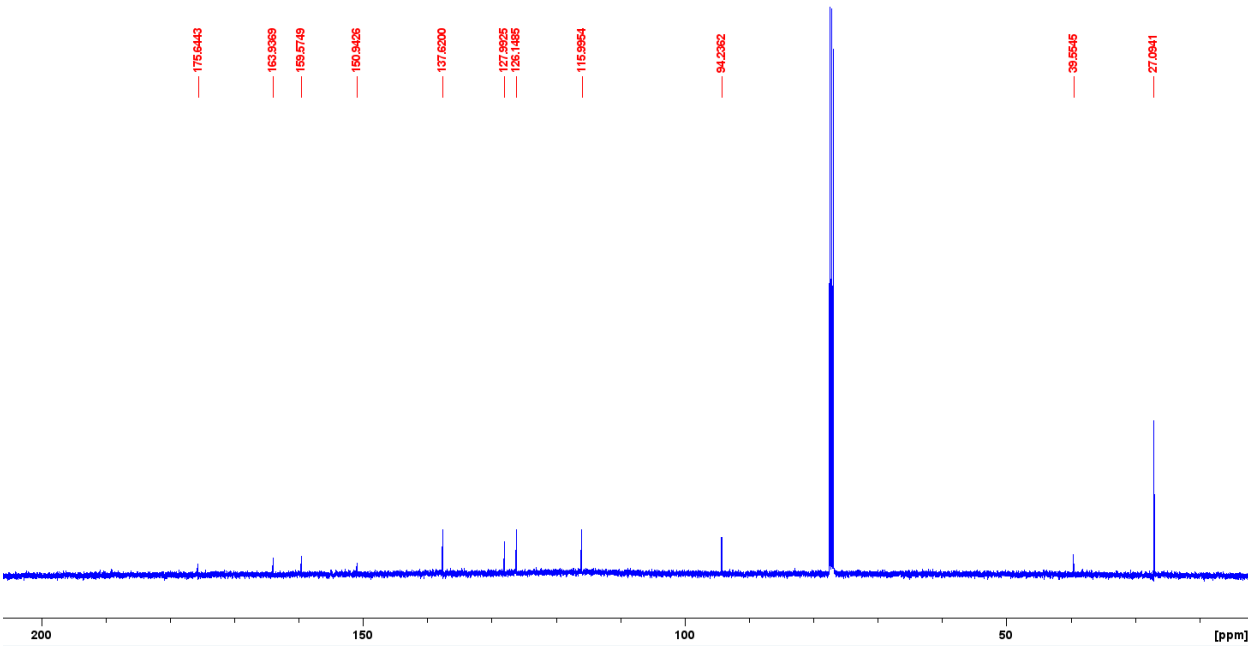

Figure C31: ^{13}C NMR spectrum (126 MHz, $(CD_3)_2SO$, 292 K) of **4a**: **4-oxo-4H-pyrido[1,2-a]pyrimidin-2-yl pivalate**

C7. References

(1) Roy, A.; Kundu, M.; Dhar, P.; Chakraborty, A.; Mukherjee, S.; Naskar, J.; Rarhi, C.; Barik, R.; Mondal, S. K.; Wani, M. A.; Gajbhiye, R.; Roy, K. K.; Maiti, A.; Manna, P.; Adhikari, S. Novel Pyrimidinone Derivatives Show Anticancer Activity and Induce Apoptosis: Synthesis, SAR and Putative Binding Mode. *ChemistrySelect* **2020**, *5* (15), 4559–4566. https://doi.org/10.1002/slct.202000208.

(2) Alwan, S. M. Synthesis and Preliminary Antimicrobial Activity of New Schiff Bases of Pyrido [1,2-A] Pyrimidine Derivatives with Certain Amino Acids. *Med. Chem.* **2014**, *4* (9). https://doi.org/10.4172/2161-0444.1000206.

(3) Characterization and Structure-Activity Relationship Study of Iminodipyridinopyrimidines as Novel Hepatitis C Virus Inhibitor. *Eur. J. Med. Chem.* **2017**, *140*, 65–73. https://doi.org/10.1016/j.ejmech.2017.09.010.

Appendix D: Conclusions and Future Work – Supplementary Material

D1. Oxidative Addition Monitoring of Alkenyl Carboxylates

General Procedure:

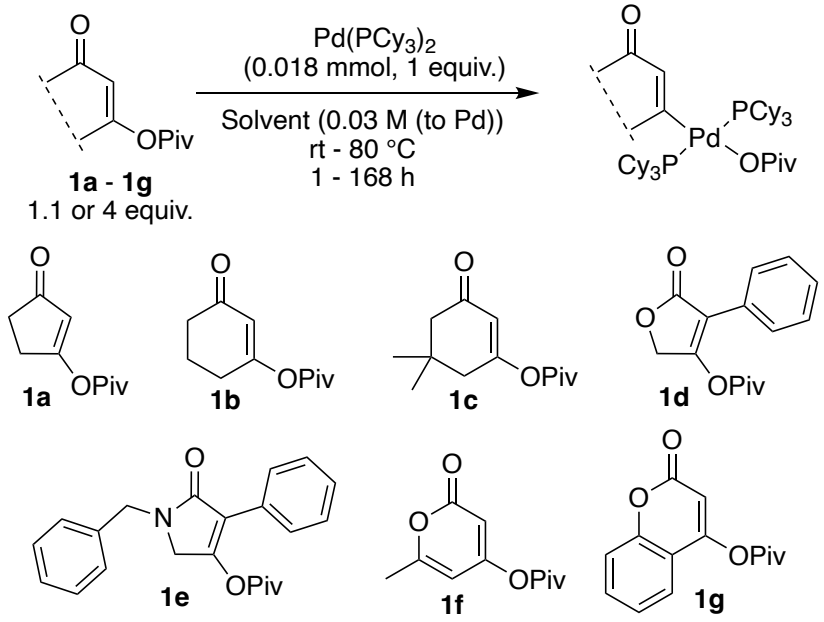

On the bench, an alkenyl carboxylate (0.020 mmol or 0.072 mmol – see Table D1 for specific masses) was weighed into a 1 dram vial and brought into the glovebox. The same vial was charged with $Pd(PCy_3)_2$ (12.0 mg, 0.018 mmol) and 0.6 mL (0.03 M) of either d_8-toluene or C_6D_6. The reaction mixture was transferred to a J-Young tube, sealed and brought out of the glovebox. A ^{1}H and ^{31}P NMR was acquired at time = 0, as well as every 24 hours for up to 7 days. Between analysis the J-Young tube was submerged in an oil bath set to the desired temperature.

Entry	Alkenyl carboxylate	Alkenyl Carboxylate /mmol	Alkenyl Carboxylate /mg	Solvent	Temperature	Experiment Duration /days
1	**1a**	0.072	13.1	d-Tol	rt - 80 °C	5
2	**1a**	0.020	3.3	d-Tol	rt - 80 °C	6
3	**1a**	0.072	13.1	d-Tol	rt	5
4	**1a**	0.072	13.1	C_6D_6	rt - 100 °C	7
5	**1a**	0.020	3.3	C_6D_6	rt - 100 °C	7
6	**1b**	0.072	14.1	d-Tol	rt - 80 °C	5
7	**1c**	0.072	16.1	d-Tol	rt - 80 °C	5
8	**1c**	0.020	4.0	d-Tol	rt - 80 °C	7
9	**1d**	0.072	18.7	d-Tol	rt - 80 °C	5
10	**1d**	0.020	5.1	d-Tol	rt - 80 °C	5
11	**1d**	0.072	18.7	d-Tol	rt	5
12	**1e**	0.072	26.1	d-Tol	rt - 80 °C	5
13	**1e**	0.020	7.2	d-Tol	rt - 80 °C	5
14	**1f**	0.072	15.1	d-Tol	rt - 80 °C	5
15	**1g**	0.072	17.7	d-Tol	rt - 80 °C	5
16	**1g**	0.020	4.4	d-Tol	rt - 80 °C	6
17	**1g**	0.072	17.7	d-Tol	rt	6

Table D1: Reaction conditions for oxidative addition monitoring experiments

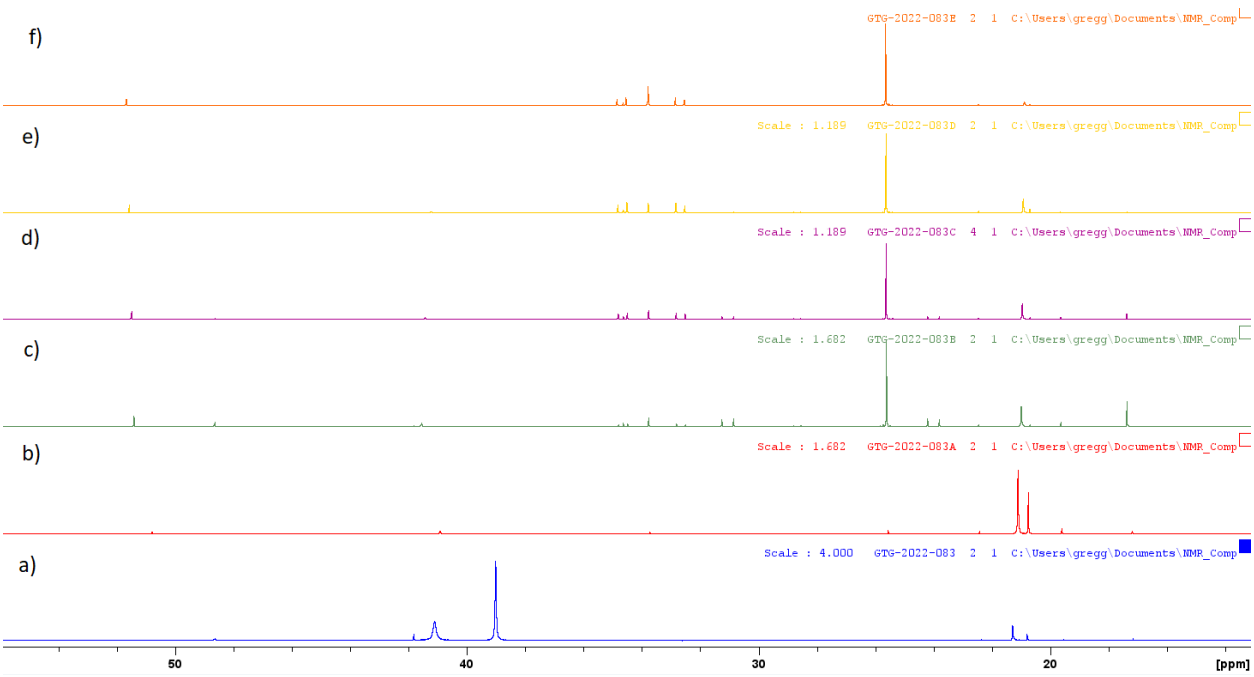

Figure D1: ^{31}P NMR monitoring of Entry 1 (4:1 **1a** : $Pd(PCy_3)_2$, d_8-toluene); a) t=0, b) 24 h at 50 °C, c) 48 h at 50 °C, d) 72 h at 50 °C, e) 72 h at 50 °C then 24 h at 60 °C, f) 72 h at 50 °C then 24 h at 60 °C then 24 h at 80 °C

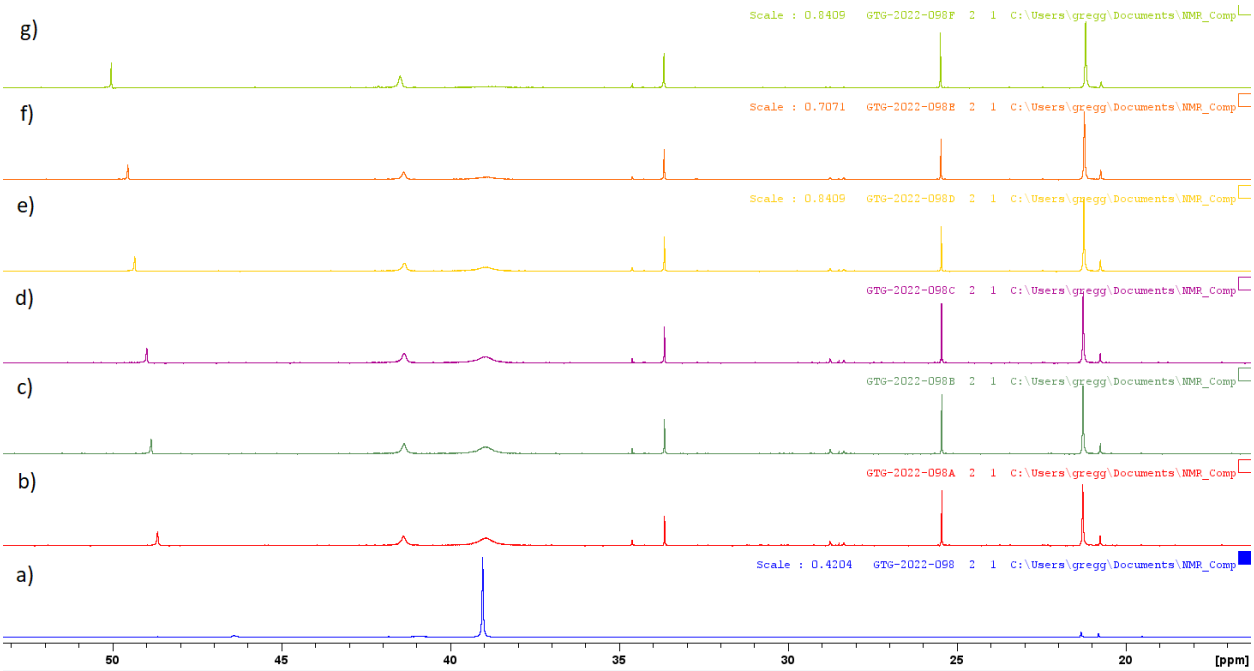

Figure D2: ^{31}P NMR monitoring of Entry 2 (1.1:1 **1a** : $Pd(PCy_3)_2$, d_8-toluene); a) t=0, b) 24 h at 50 °C, c) 48 h at 50 °C, d) 72 h at 50 °C, e) 72 h at 50 °C then 48 h at 60 °C, f) 72 h at 50 °C then 72 h at 60 °C, g) 72 h at 50 °C then 72 h at 60 °C then 24 h at 80 °C

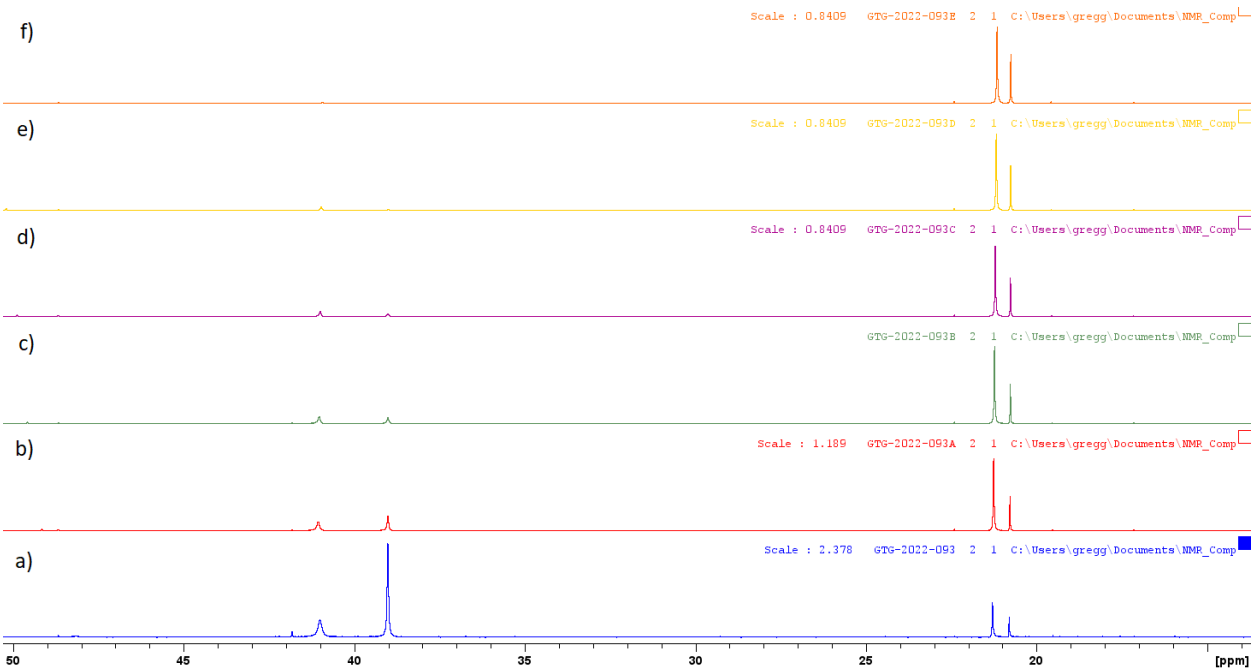

Figure D3: ^{31}P NMR monitoring of Entry 3 (4:1 **1a** : $Pd(PCy_3)_2$, d_8-toluene); a) t = 0, b) 24 h at rt, c) 48 h at rt, d) 72 h at rt, e) 96 h at rt, f) 120 h at rt

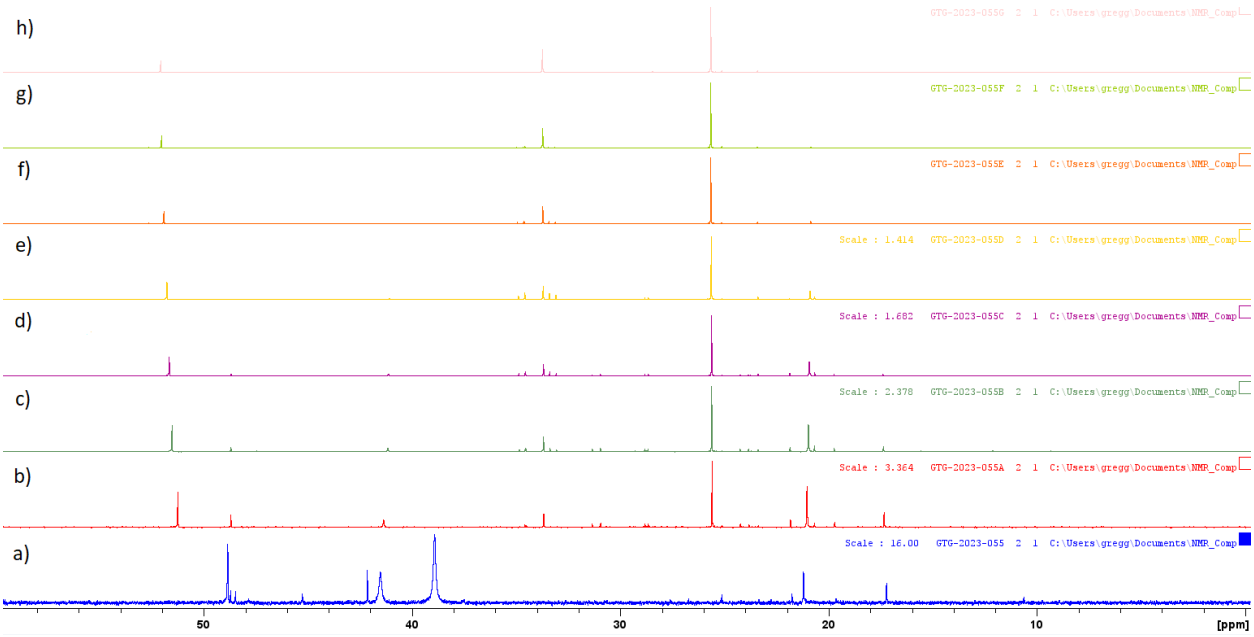

Figure D4: ^{31}P NMR monitoring of Entry 4 (4:1 **1a** : $Pd(PCy_3)_2$, C_6D_6)); a) t=0, b) 24 h at 50 °C, c) 48 h at 50 °C, d) 72 h at 50 °C, e) 72 h at 50 °C then 24 h at 60 °C, f) 72 h at 50 °C then 24 h at 60 °C then 24 h at 80 °C, g) 72 h at 50 °C then 24 h at 60 °C then 24 h at 80 °C then 24 h at 100 °C, h) 72 h at 50 °C then 24 h at 60 °C then 24 h at 80 °C then 48 h at 100 °C

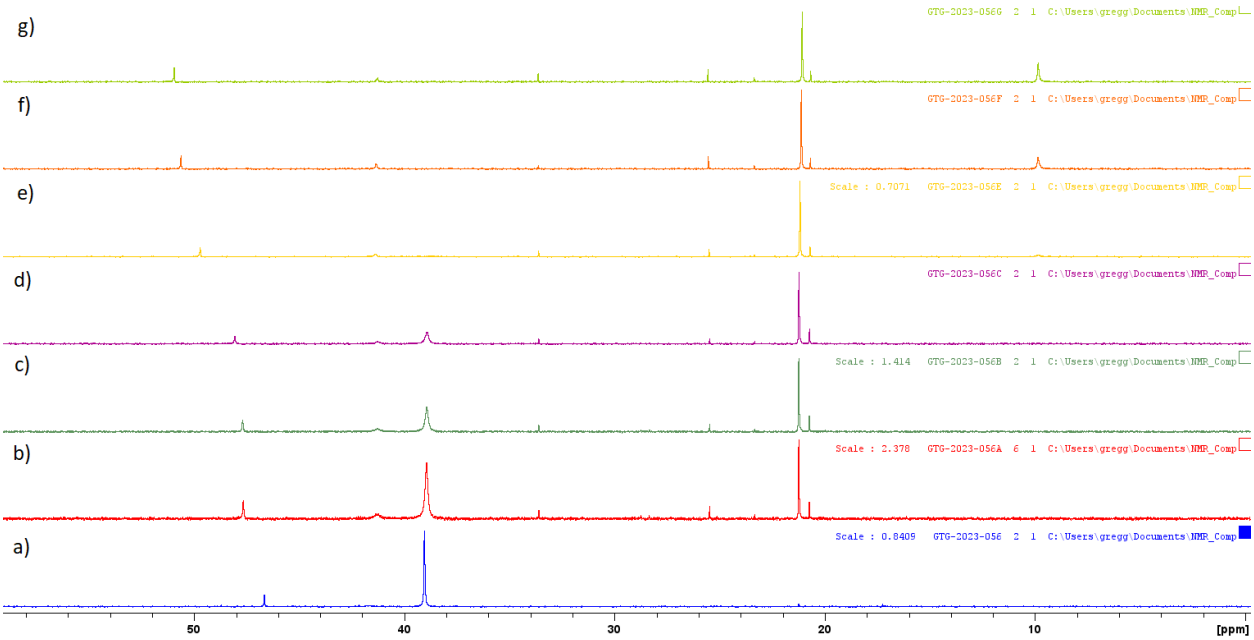

Figure D5: ^{31}P NMR monitoring of Entry 5 (1.1:1 **1a** : $Pd(PCy_3)_2$, C_6D_6)); a) t=0, b) 24 h at 50 °C, c) 48 h at 50 °C, d) 72 h at 50 °C, e) 72 h at 50 °C then 24 h at 60 °C then 24 h at 80 °C, f) 72 h at 50 °C then 24 h at 60 °C then 24 h at 80 °C then 24 h at 100 °C, g) h) 72 h at 50 °C then 24 h at 60 °C then 24 h at 80 °C then 48 h at 100 °C

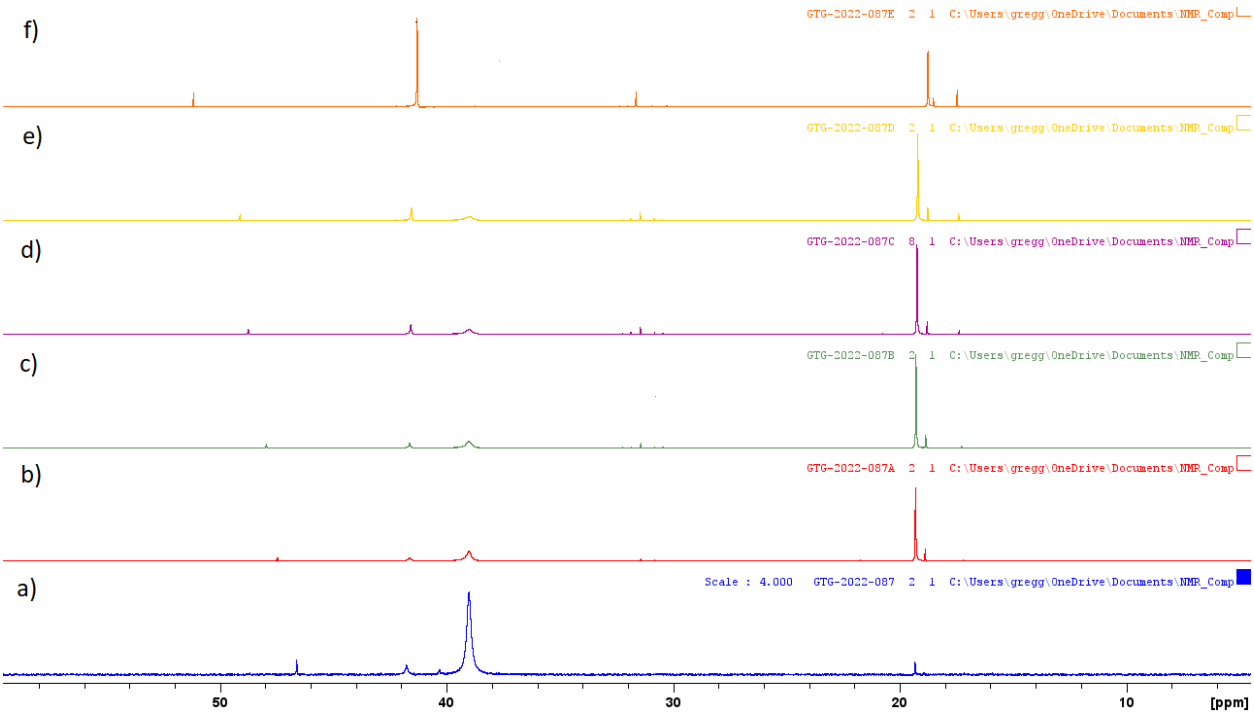

Figure D6: ^{31}P NMR monitoring of Entry 6 (4:1 **1b** : $Pd(PCy_3)_2$, d_8-toluene); a) t=0, b) 24 h at 50 °C, c) 48 h at 50 °C, d) 48 h at 50 °C then 24 h at 60 °C, e) 48 h at 50 °C then 48 h at 60 °C f) 48 h at 50 °C then 48 h at 60 °C then 24 h at 80 °C

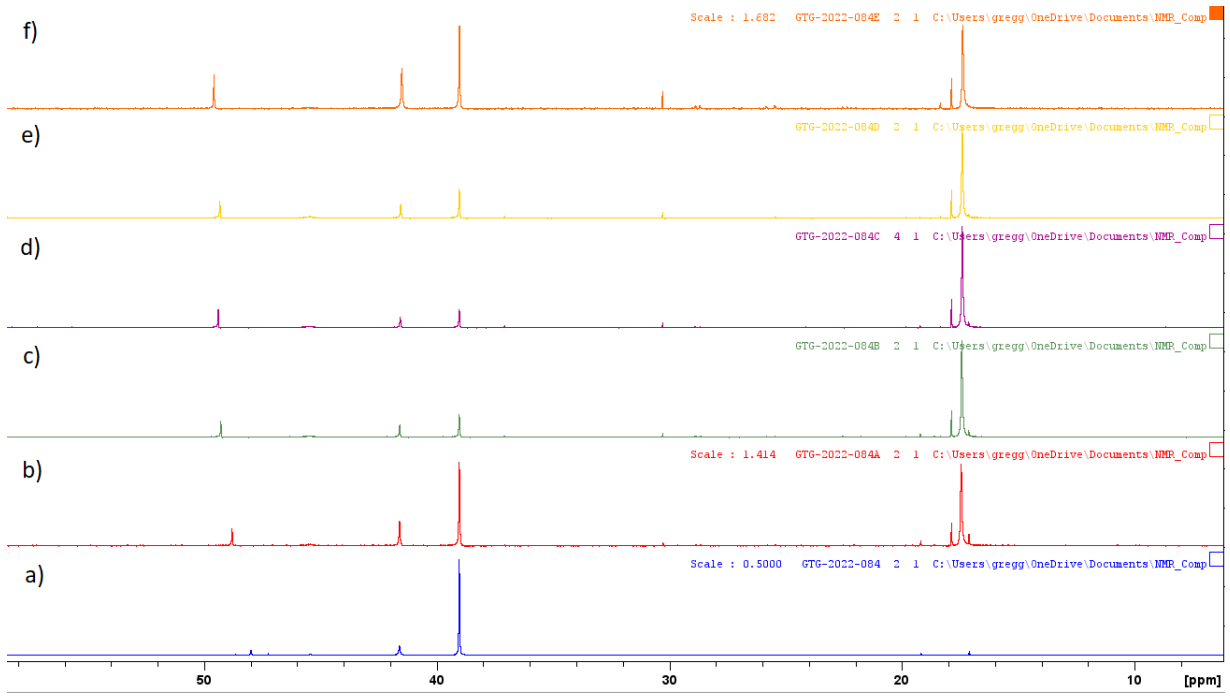

Figure D7: ^{31}P NMR monitoring of Entry 7 (4:1 **1c** : $Pd(PCy_3)_2$, d_8-toluene); a) t=0, b) 24 h at 50 °C, c) 48 h at 50 °C, d) 72 h at 50 °C, e) 72 h at 50 °C then 24 h at 60 °C, f) 72 h at 50 °C then 24 h at 60 °C then 24 h at 80 °C

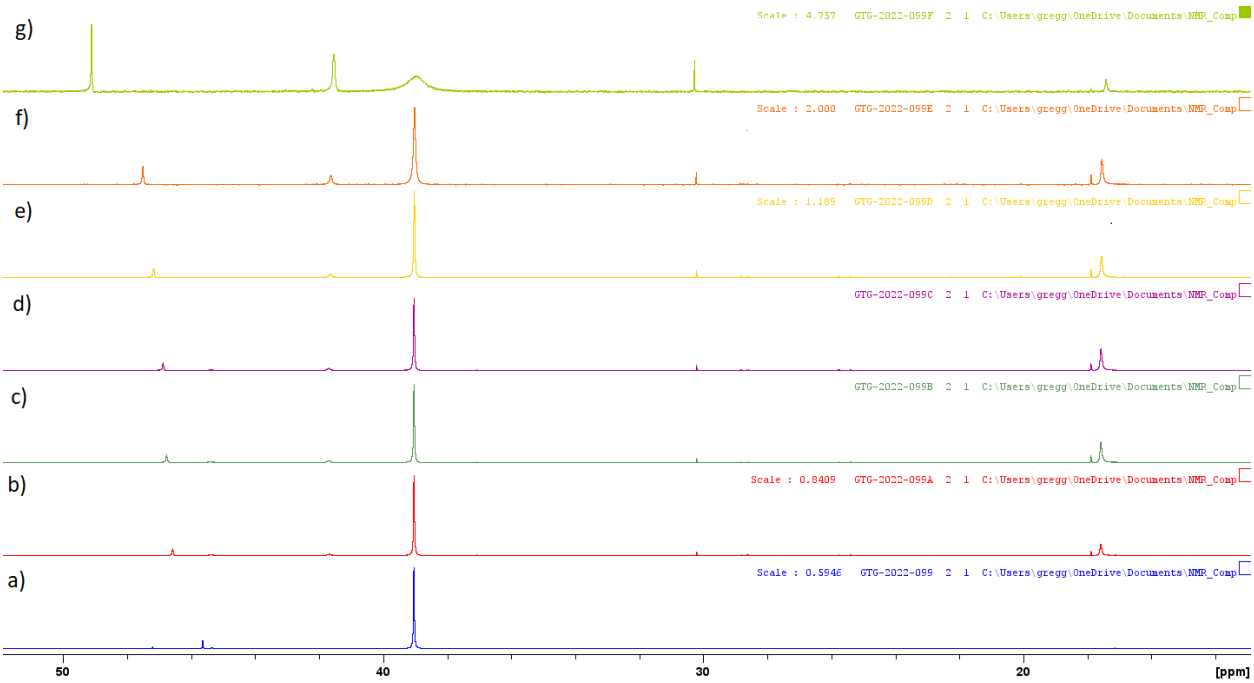

Figure D8: ^{31}P NMR monitoring of Entry 8 (1.1:1 **1c** : $Pd(PCy_3)_2$, d_8-toluene); a) t=0, b) 24 h at 50 °C, c) 48 h at 50 °C, d) 72 h at 50 °C, e) 72 h at 50 °C then 48 h at 60 °C, f) 72 h at 50 °C then 72 h at 60 °C, g) 72 h at 50 °C then 72 h at 60 °C then 24 h at 80 °C

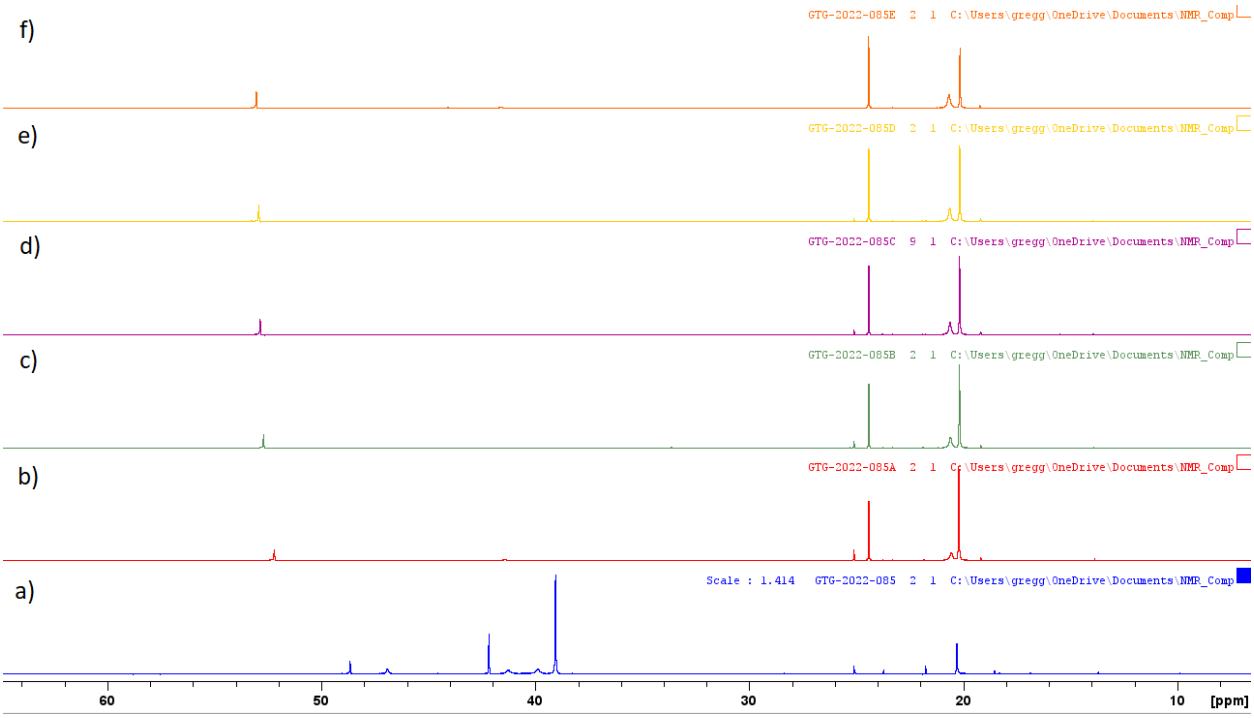

Figure D9: ^{31}P NMR monitoring of Entry 9 (4:1 **1d** : $Pd(PCy_3)_2$, d_8-toluene); a) t=0, b) 24 h at 50 °C, c) 48 h at 50 °C, d) 72 h at 50 °C, e) 72 h at 50 °C then 24 h at 60 °C, f) 72 h at 50 °C then 24 h at 60 °C then 24 h at 80 °C

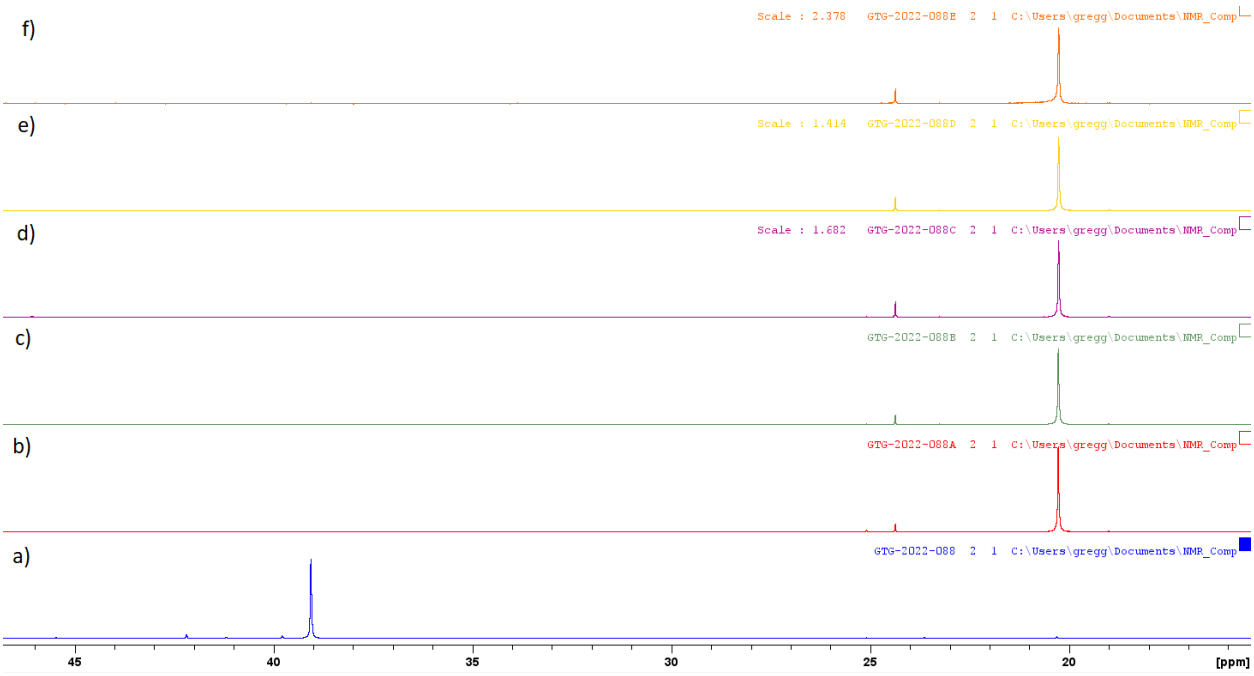

Figure D10: ^{31}P NMR monitoring of Entry 10(1.1:1 **1d** : $Pd(PCy_3)_2$, d_8-toluene); a) t=0, b) 24 h at 50 °C, c) 48 h at 50 °C, d) 72 h at 50 °C, e) 72 h at 50 °C then 24 h at 60 °C, f) 72 h at 50 °C then 48 h at 60 °C

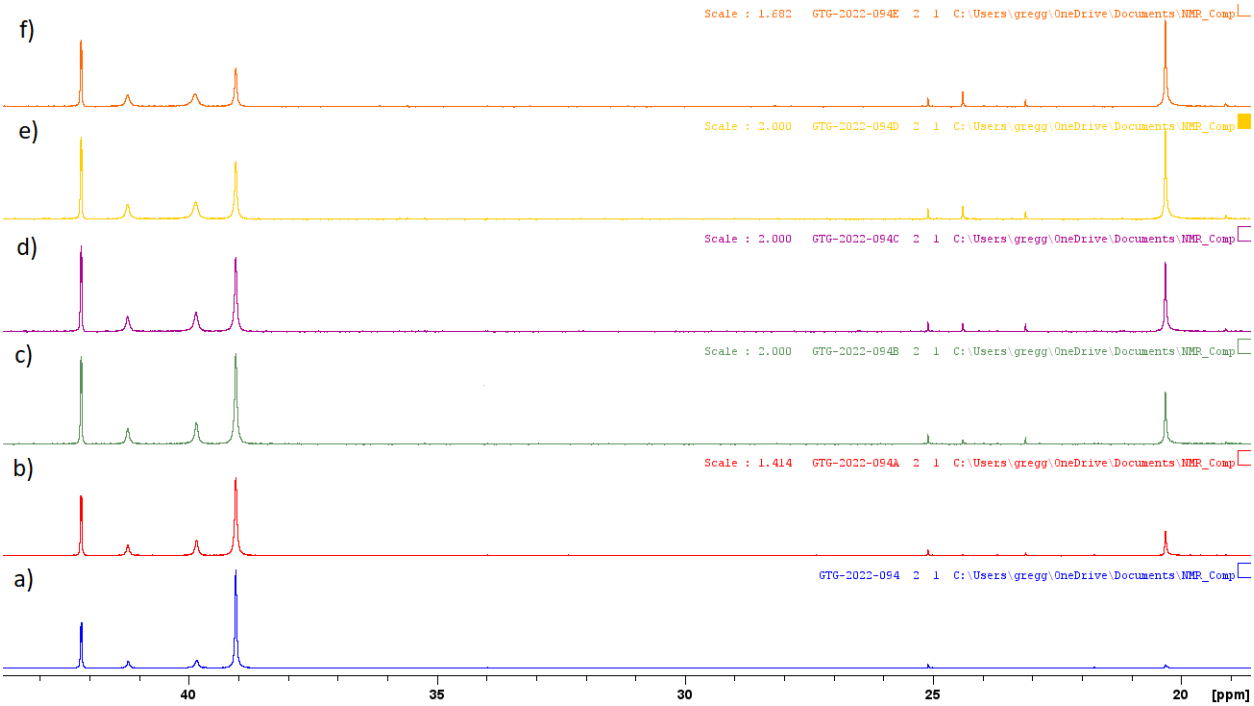

Figure D11: ^{31}P NMR monitoring of Entry 11 (4:1 **1d** : $Pd(PCy_3)_2$, d_8-toluene); a) t = 0, b) 24 h at rt, c) 48 h at rt, d) 72 h at rt, e) 96 h at rt, f) 120 h at rt

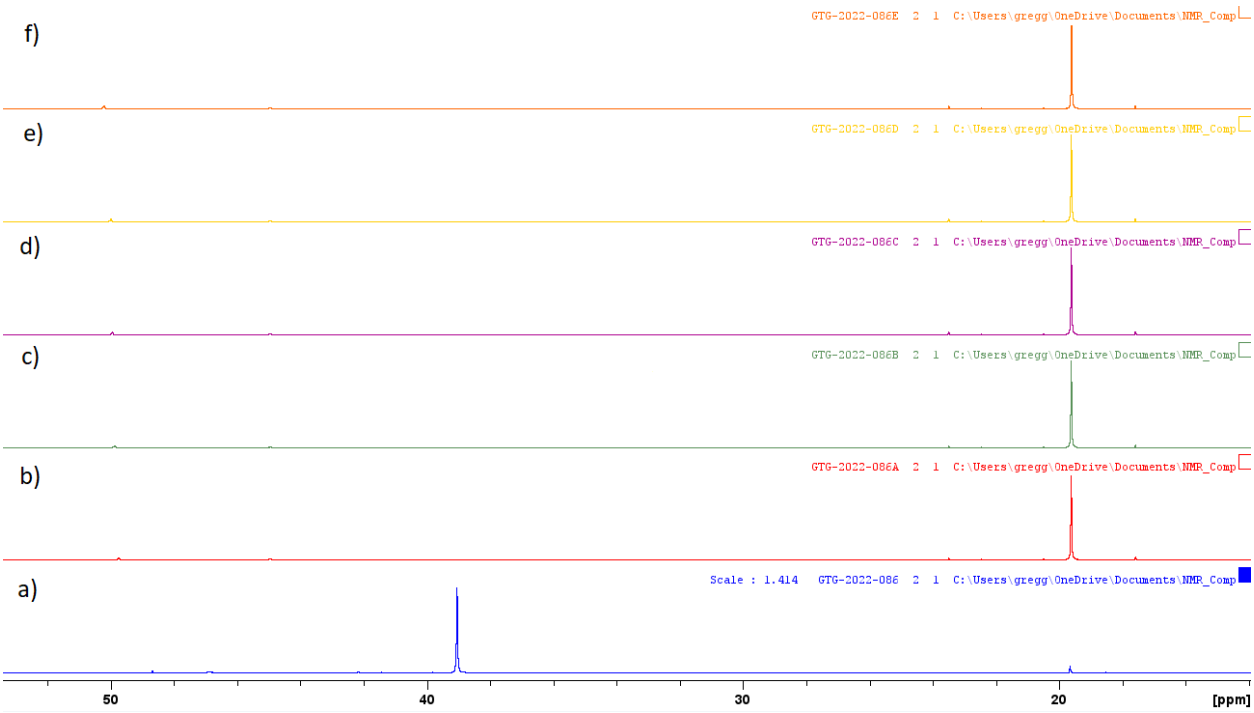

Figure D12: ^{31}P NMR monitoring of Entry 12 (4:1 **1e** : $Pd(PCy_3)_2$, d_8-toluene); a) t=0, b) 24 h at 50 °C, c) 48 h at 50 °C, d) 48 h at 50 °C then 24 h at 60 °C, e) 48 h at 50 °C then 48 h at 60 °C, f) 48 h at 50 °C then 48 h at 60 °C then 24 h at 80 °C

Figure D13: ^{31}P NMR monitoring of Entry 13 (1.1:1 **1e** : $Pd(PCy_3)_2$, d_8-toluene); a) t=0, b) 24 h at 50 °C, c) 48 h at 50 °C, d) 48 h at 50 °C then 24 h at 60 °C, e) 48 h at 50 °C then 48 h at 60 °C, f) 48 h at 50 °C then 48 h at 60 °C then 24 h at 80 °C

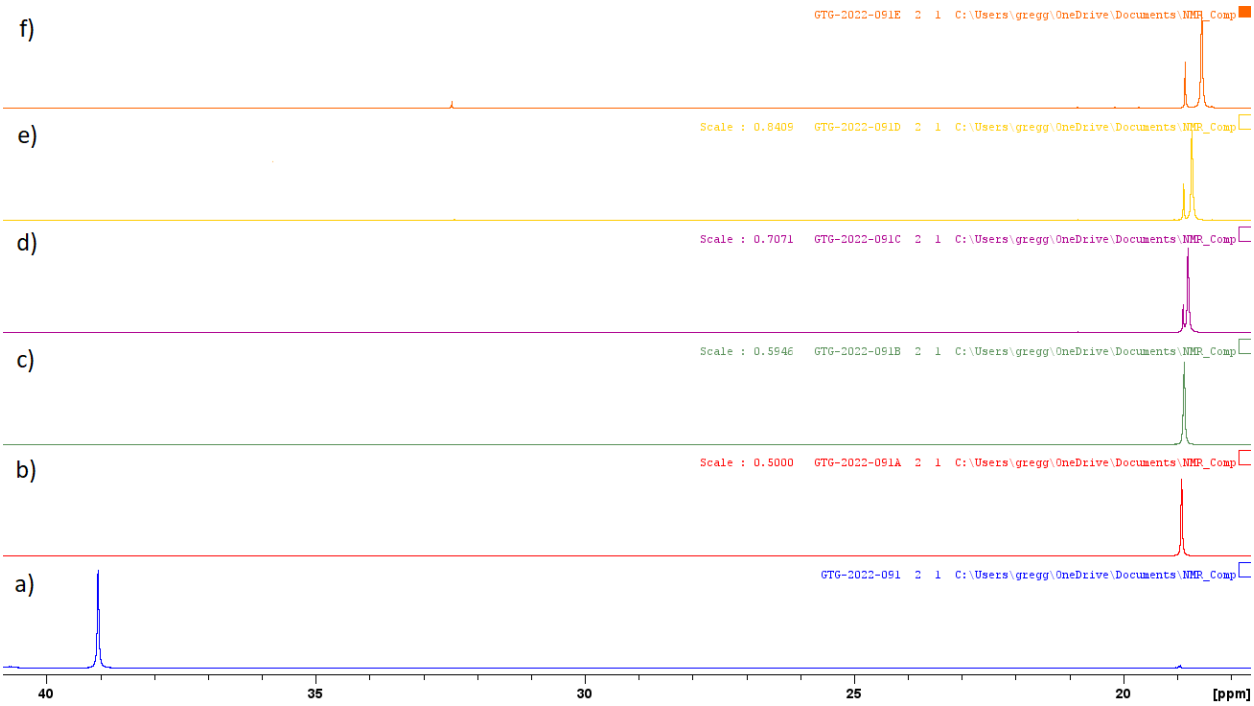

Figure D14: ^{31}P NMR monitoring of Entry 14 (4:1 **1f** : $Pd(PCy_3)_2$, d_8-toluene); a) t=0, b) 24 h at 50 °C, c) 48 h at 50 °C, d) 48 h at 50 °C then 24 h at 60 °C, e) 48 h at 50 °C then 48 h at 60 °C, f) 48 h at 50 °C then 48 h at 60 °C then 24 h at 80 °C

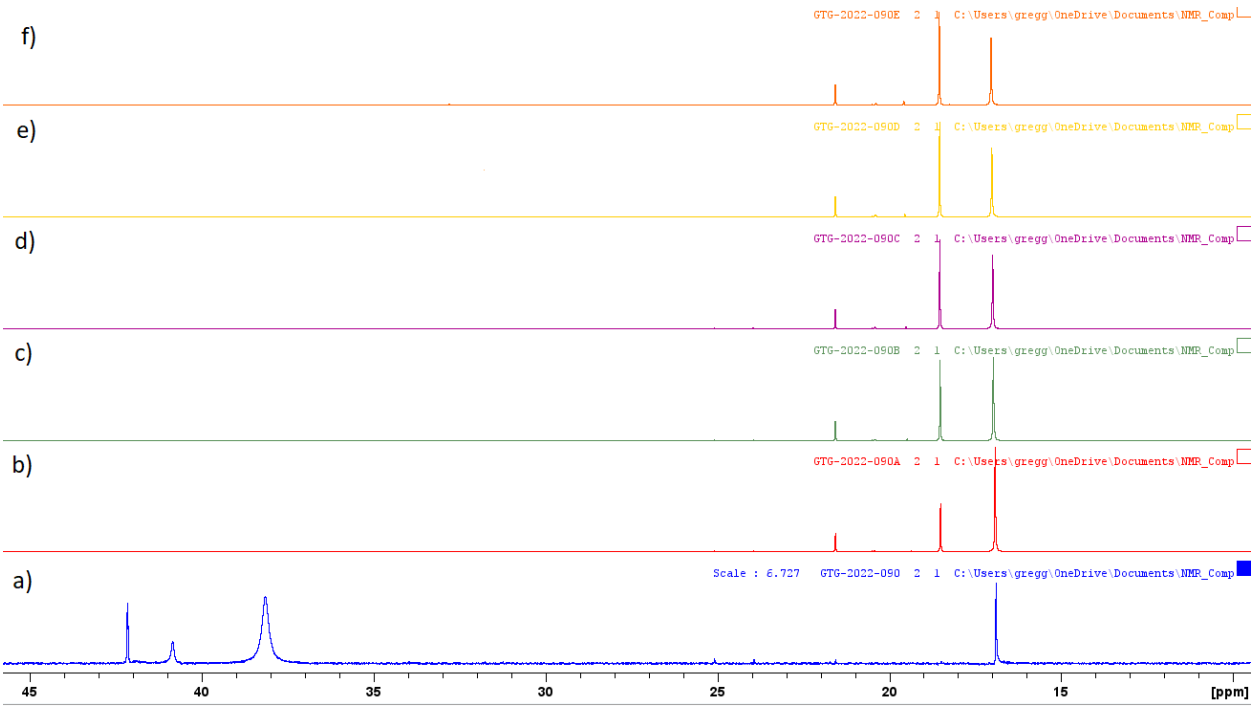

Figure D15: ^{31}P NMR monitoring of Entry 15 (4:1 **1g** : $Pd(PCy_3)_2$, d_8-toluene); a) t=0, b) 24 h at 50 °C, c) 48 h at 50 °C, d) 72 h at 50 °C, e) 72 h at 50 °C then 24 h at 60 °C, f) 72 h at 50 °C then 48 h at 60 °C

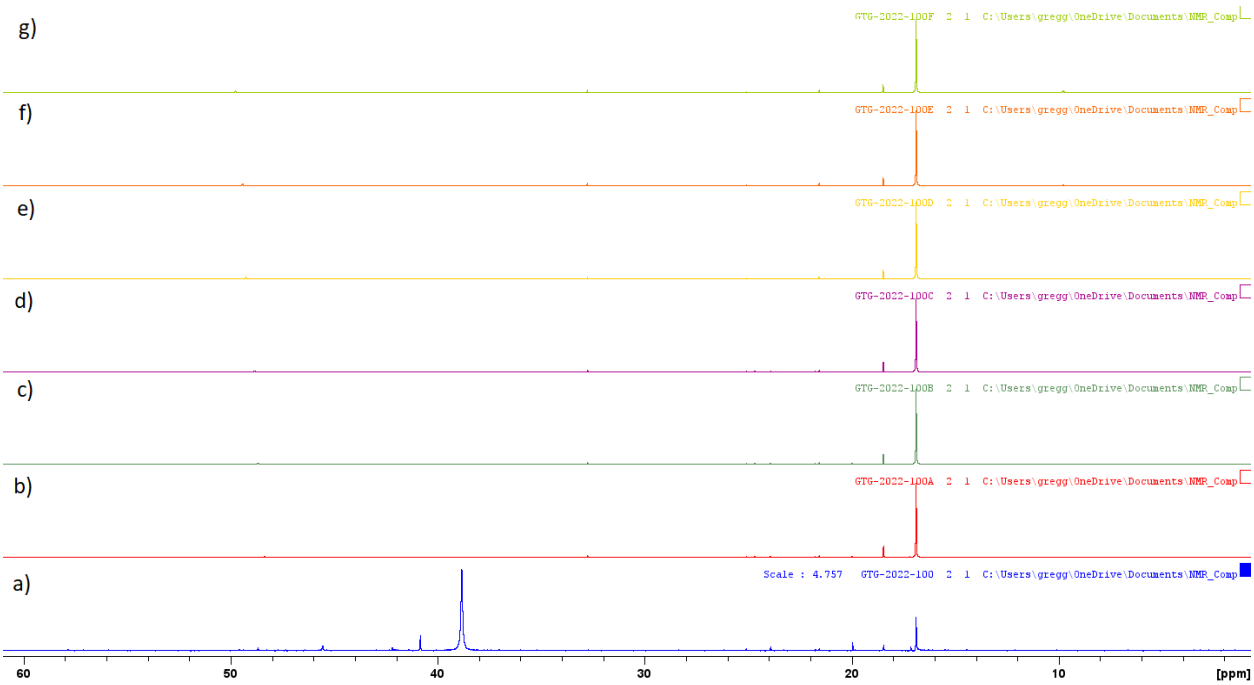

Figure D16: ^{31}P NMR monitoring of Entry 16 (1.1:1 **1g** : $Pd(PCy_3)_2$, d_8-toluene)); a) t=0, b) 24 h at 50 °C, c) 48 h at 50 °C, d) 72 h at 50 °C, e) 72 h at 50 °C then 48 h at 60 °C, f) 72 h at 50 °C then 72 h at 60 °C, g) 72 h at 50 °C then 72 h at 60 °C then 24 h at 80 °C

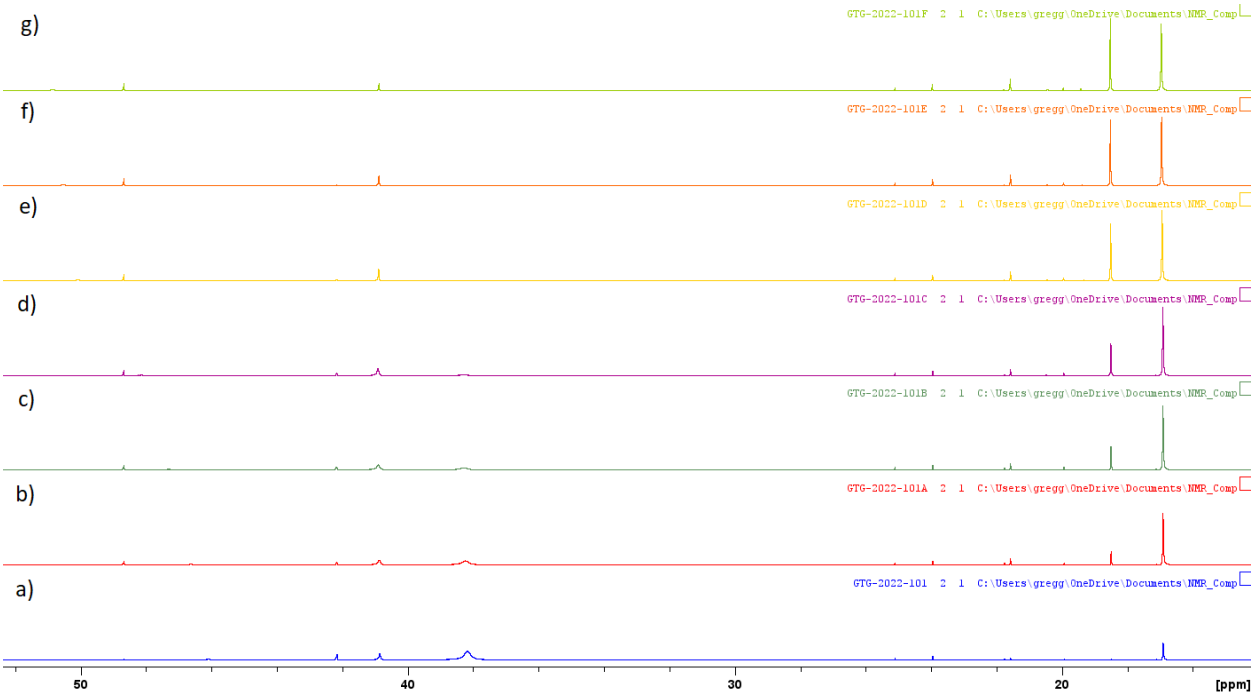

Figure D17: ^{31}P NMR monitoring of Entry 17 (4:1 **1g** : $Pd(PCy_3)_2$, d_8-toluene); a) t = 0, b) 24 h at rt, c) 48 h at rt, d) 72 h at rt, e) 120 h at rt, f) 144 h at rt, g) 168 h at rt

D2. Borylation of Alkenyl Carboxylates

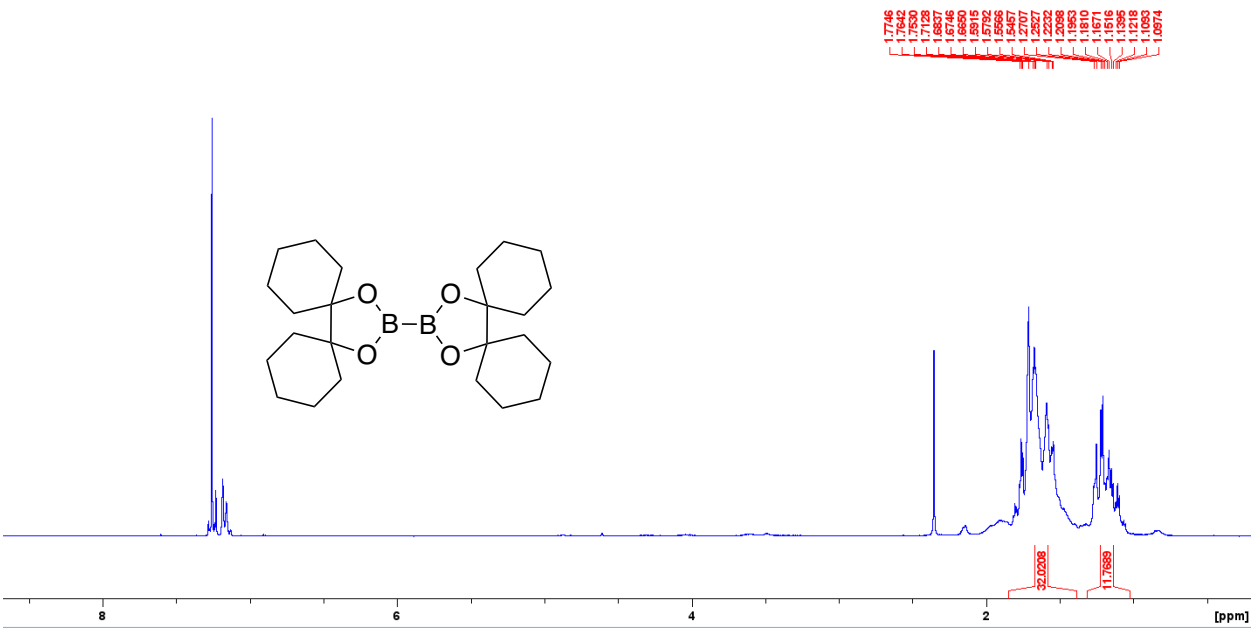

Figure D18: ^{1}H NMR spectrum (300 MHz, $CDCl_3$, (292 K) of B_2CHPin_2

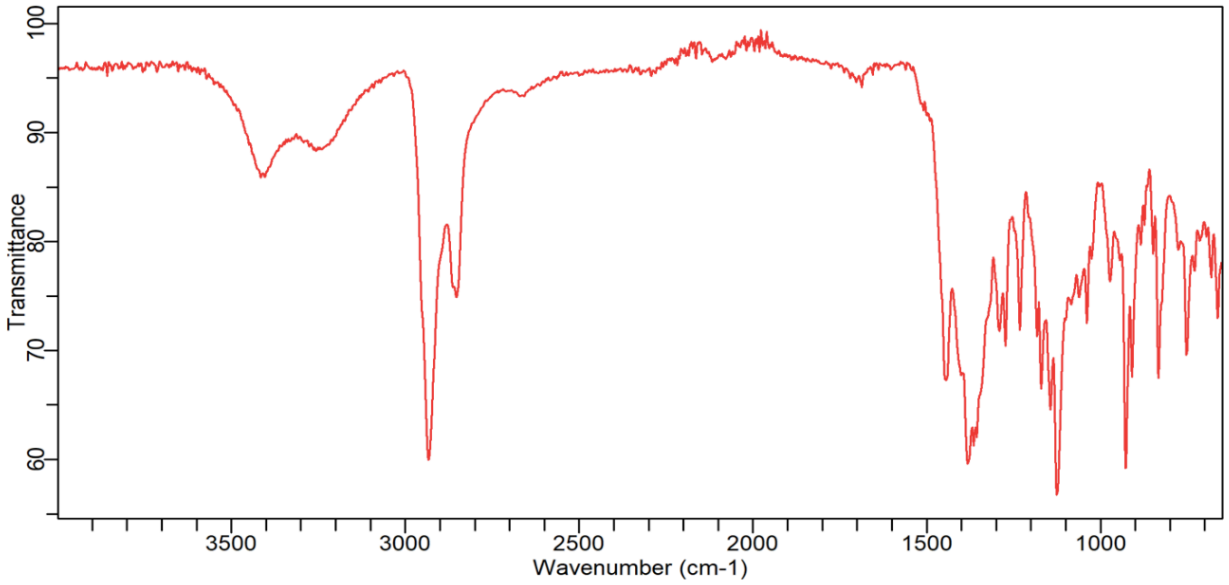

Figure D19: FT-IR spectrum of B_2CHPin_2

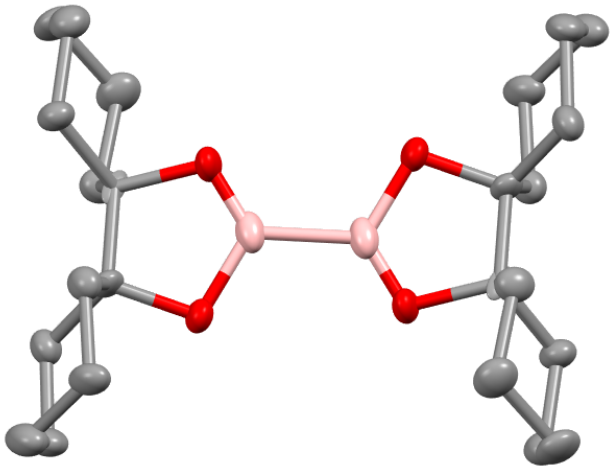

Figure D20: Solid-state molecular structure of B_2CHPin_2. Ellipsoids plotted at 50% probability.

One of two disordered rotational orientations shown. Hydrogens not shown for clarity.

So the chemistry's set

And I'm not the saddest cheerleader to forget the American word

For the gang in the head

That dwindles to no members when

The mystery's met

The sky looks threatened, heading home in the dust

Singing, "Life is for getting

Good enough for the frivolous"

-Gordon Edgar Downie, The Tragically Hip